CONTRACT AA851-CT1-25

SOUTH ATLANTIC OCS PHYSICAL OCEANOGRAPHY

FINAL PROGRESS REPORT
(Year Four)

Volume II: Technical Report

February 1983

Prepared for
MINERALS MANAGEMENT SERVICE
Washington, D.C.

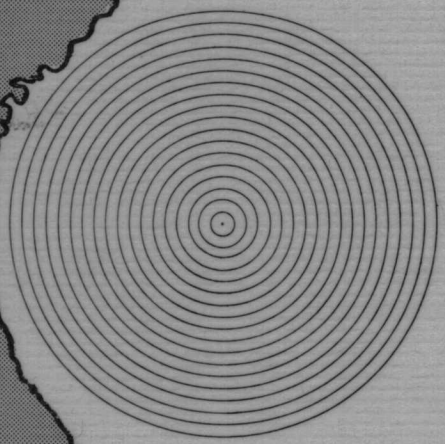

SCIENCE APPLICATIONS, INC.
4900 Water's Edge Drive, Suite 255
Raleigh, North Carolina 27606

This report has been reviewed by the Minerals Management Service and approved for publication. Approval does not signify that the contents necessarily reflect the views and policies of Minerals Management Service, nor does mention of trade names or commercial products constitute endorsement or recommendation for use.

SOUTH ATLANTIC OCS
PHYSICAL OCEANOGRAPHY
FINAL PROGRESS REPORT
(Year Four)

VOLUME II: TECHNICAL REPORT

February 1983

Contract No. AA851-CT1-25

Evans Waddell, Program Manager

TABLE OF CONTENTS

TABLE OF CONTENTS (Continued)

TABLE OF CONTENTS (Continued)

TABLE OF CONTENTS (Continued)

LIST OF FIGURES

LIST OF FIGURES (Continued)

LIST OF FIGURES (Continued)

LIST OF FIGURES (Continued)

LIST OF FIGURES (Continued)

LIST OF FIGURES (Continued)

LIST OF FIGURES (Continued)

LIST OF FIGURES (Continued)

LIST OF FIGURES (Continued)

LIST OF FIGURES (Continued)

LIST OF FIGURES (Continued)

LIST OF FIGURES (Continued)

LIST OF TABLES

LIST OF TABLES (Continued)

I. INTRODUCTION

1.1 INTRODUCTION

The South Atlantic Physical Oceanography Study[1] (SAPOS) is a Bureau of Land Management[2] program funded under contract with Science Applications, Inc. (SAI), to document major circulation producing processes and their impact on the South Atlantic Bight (SAB) and adjacent regions (Figure 1.1-1). The insights from the SAPOS will provide a basis for informed management decisions relating to outer continental shelf (OCS) oil and gas activities. Two key objectives of the SAPOS are:

(1) To examine and understand the influence of tide, wind, density, and the Gulf Stream (GS); i.e., all major forcing mechanisms producing observed SAB circulation patterns.

(2) To document and explain the spatial and temporal variability of SAB hydrographic conditions (temperature, salinity, density, dissolved oxygen, and selected nutrients).

In addition, the SAPOS is providing data for use in a coordinated MMS funded SAB numerical circulation model by Dynalysis, Inc.

To accomplish these overall SAPOS objectives, the following integrated data sets have been acquired over the past four years:

(1) Periodic (high and low frequency) synoptic determinations of the location of the Gulf Stream western boundary (cold wall) and associated features, using thermal imagery of sea surface temperature (SST). (Years 1-4).

(2) Regional winds measured at coastal and shelf meteorological stations and waterlevel fluctuations measured at coastal tide stations throughout the SAB. (Years 1-4).

(3) Periodic hydrographic cruises on the SAB shelf, North Carolina shelf and offshore waters, and the Blake Plateau (BP). (Years 1-4).

(4) Subsurface current measurements at various across- and along-shelf locations. (Years 1-4).

(5) Surface currents across the SAB shelf. (Year 2).

(6) Circulations and characteristics of coastal fronts, with emphasis on estuarine plumes. (Year 1).

---

[1] For Years 1-3 referred to as the South Atlantic Bight Physical Oceanography Study (SAB/POS).

[2] Effective May 1982, all former BLM leasing and resource management responsibilities and environmental study programs for the OCS were consolidated and placed within the Minerals Management Service (MMS).

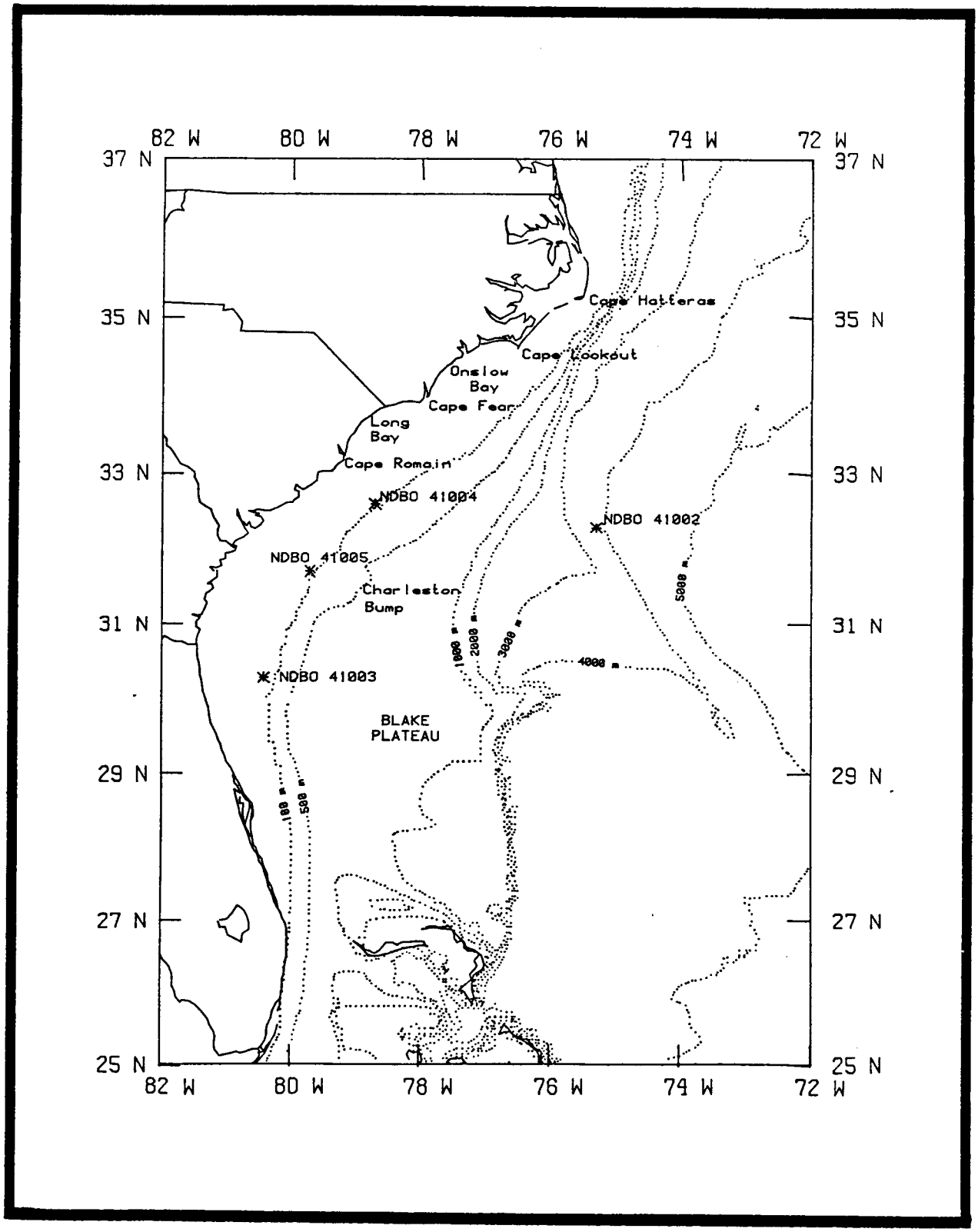

Figure 1.1-1. Study area for the South Atlantic Physical Oceanography Study.

Portions of these data sets are described in detail in the SAPOS Annual Progress Reports for Years 1-3, as well as the present Year 4 report (Chapter 2).

1.2 YEAR IV ACTIVITIES AND PARTICIPANTS

During Year 4, the data sets described above were either completed or utilized to develop insights supporting the overall program objectives. In general, the Year 4 efforts include:

(1) Statistical characterization of the GS western boundary position.

(2) Two cruises (winter and summer) to document hydrography of the North Carolina shelf and offshore waters.

(3) Examination of shelf forcing mechanisms, including regional winds and water levels.

(4) Evaluation of climatology of SAB physical oceanography.

(5) Identification of regions of persistent upwelling.

(6) Analytical characterization of wind and/or circulation processes which are related to shelf waves in the vicinity of the Charleston Bump.

(7) Multivariate synthesis of observations associated with GS western boundary events in the Georgia Embayment.

Principal Investigators (PI) and key personnel involved in Year 4 and their general area of effort are presented below. Multi-investigator efforts preclude associating a single PI with each task above; however, a lead role can be identified from the alphabetized listing below.

(1) Dr. L. Atkinson (Skidaway Institute of Oceanography): SAB hydrography.

(2) Dr. O. Brown (University of Miami): Satellite thermal imagery.

(3) Dr. T. Curtin (North Carolina State University): North Carolina hydrography.

(4) Dr. P. Hamilton (Science Applications, Inc.): Shelf forcing mechanisms emphasizing winds and water levels.

(5) Dr. T. Lee (University of Miami): Gulf Stream and shelf dynamics, emphasizing the Georgia Embayment.

(6) Dr. L. Pietrafesa (North Carolina State University): Analytical characterization of circulation patterns, emphasizing the Carolina Capes.

In addition to the above, J. Karpen (SAI) is program Data Manager and Dr. E. Waddell (SAI) is Program Manager (PM) for the SAPOS. An outline of the SAPOS Year 4 management structure is shown in Figure 1.2-1.

1.3 REPORT ORGANIZATION

This report has three volumes: Executive Summary (Vol. I); Technical Volume (Vol. II); and Data Products (Vol. III). The Executive Summary provides a nontechnical overview of the SAPOS, with emphasis on Year 4 activities and results. Vol. II presents a more in-depth description of Year 4 technical activities. Vol. III is a compendium of data products created as part of the Year 4.

The technical volume has a format similar to that used in previous reports. Chapter 2 describes data sources and acquisition; Chapter 3 describes data analysis; and Chapter 4 is a technical discussion of the results of Year 4 activities. This subdivision of material is used so that the technical discussion is unencumbered by nonessential support material.

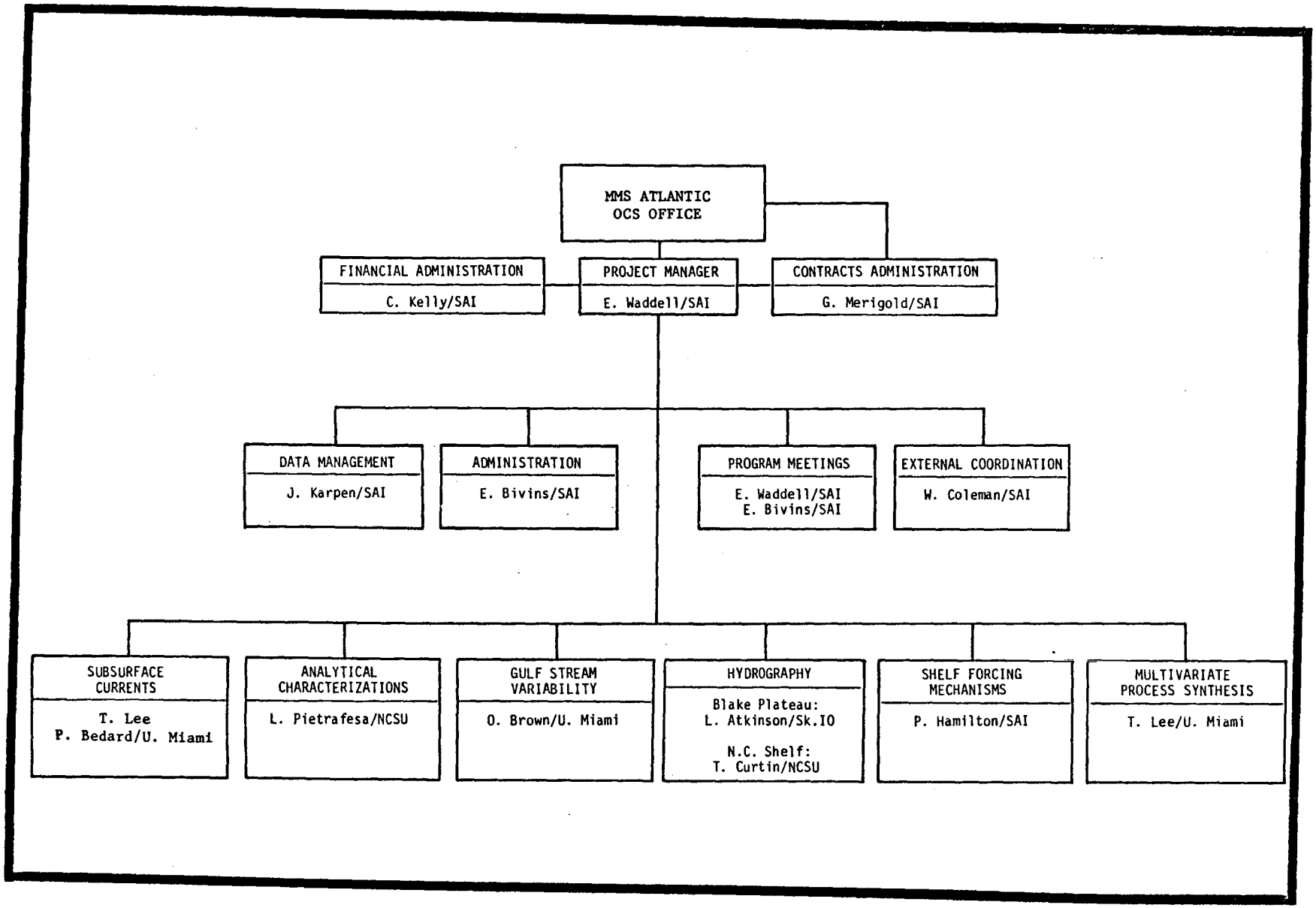

Figure 1.2-1. Program management structure.

II. DATA ACQUISITION

2.1 INTRODUCTION

Three major field data acquisition programs were undertaken during Year 4. These include:

(1) Two N.C. hydrographic cruises (winter, 1981; summer, 1981); and

(2) Subsurface current measurements on the Charleston Transect as part of the Georgia Bight Experiment (GABEX-II).

Data have been received from NOAA/NESS for examination of sea surface temperatures (SST). Wind data were obtained from the National Weather Service (NWS) for coastal, and the National Data Buoy Office (NDBO) for shelf buoy winds. Coastal sea level data were obtained from the National Ocean Survey (NOS).

2.2 THERMAL IMAGERY (Sea Surface Temperature)

Dr. Otis Brown (University of Miami) has been attempting to obtain AVHRR imagery from NOAA-6 or TIROS-N satellites. These two platforms sweep the study area at different times which should optimize the frequency of coverage. An effort has been and is presently being made to obtain: (1) complete GABEX I period coverage (Table 2.2-1); and (2) other coverage needed to support interpretation and synthesis for SAB physical oceanographic processes.

2.3 SHELF FORCING MECHANISMS

A summary of data sets used in evaluating shelf forcing mechanisms is presented in Figure 2.3-1. The buoy data was taken by NDBO environmental data buoys deployed at three mid-shelf locations (see Figure 1.1-1). Support for these buoys was provided to NDBO by BLM under an interagency agreement. BLM support ended 1 January 1982. All buoys were removed when 41004 (off Charleston) was retrieved on or about 27 July 1982.

All other data (coastal meteorological observations; i.e. wind velocity, atmospheric pressure and air temperature, and coastal waterlevels) are taken routinely by NWS and NOS, respectively. There is usually a substantial delay in receiving these data (as much as a year); however, the cost is small compared to at-sea observations.

2.4 NORTH CAROLINA HYDROGRAPHY

The objectives of the hydrographic sampling effort off North Carolina were to estimate the structure and variability of circulation features likely to occur over existing lease sites and to acquire northern boundary condition data for input to the large scale numerical circulation model being developed for the South Atlantic Bight. To achieve these objectives, two hydrographic cruises were successfully completed in 1981, providing additional information on both winter and summer conditions. The R/V Cape Henlopen, equipped with a Neil Brown CTD system and associated hardware (Table 2.4-1), was contracted for the cruises. As a cost-effective measure, the NOAA facility at Norfolk

TABLE 2.2-1

South Atlantic Bight imagery

Satellite	Orbit	Date	Time
TN	1699	08 Feb 79	039:19:32:1
TN	1679	09 Feb 79	040:07:55:54
TN	2593	15 Apr 79	105:08:26:01
TN	2600	15 Apr 79	105:19:49:30
TN	2601	16 Apr 79	106:08:19:03
TN	2621	17 Apr 79	107:08:05:31
TN	2628	17 Apr 79	107:19:30:31
TN	2635	17 Apr 79	---
TN	2649	19 Apr 79	---
TN	2650	19 Apr 79	---
TN	2656	19 Apr 79	---
TN	2664	20 Apr 79	---
TN	2678	21 Apr 79	111:09:05:52
TN	2692	22 Apr 79	112:08:55:26
TN	2755	26 Apr 79	116:19:37:41
TN	2783	28 Apr 79	---
TN	2791	29 Apr 79	---
TN	2798	29 Apr 79	---
TN	3658	29 Jun 79	180:20:06:00
TN	3665	30 Jun 79	181:08:36:03
TN	3672	30 Jun 79	181:19:55:30
TN	3693	02 Jul 79	183:08:14:29
TN	3700	02 Jul 79	183:19:37:01
TN	3714	03 Jul 79	184:19:25:03

24 Scenes Total

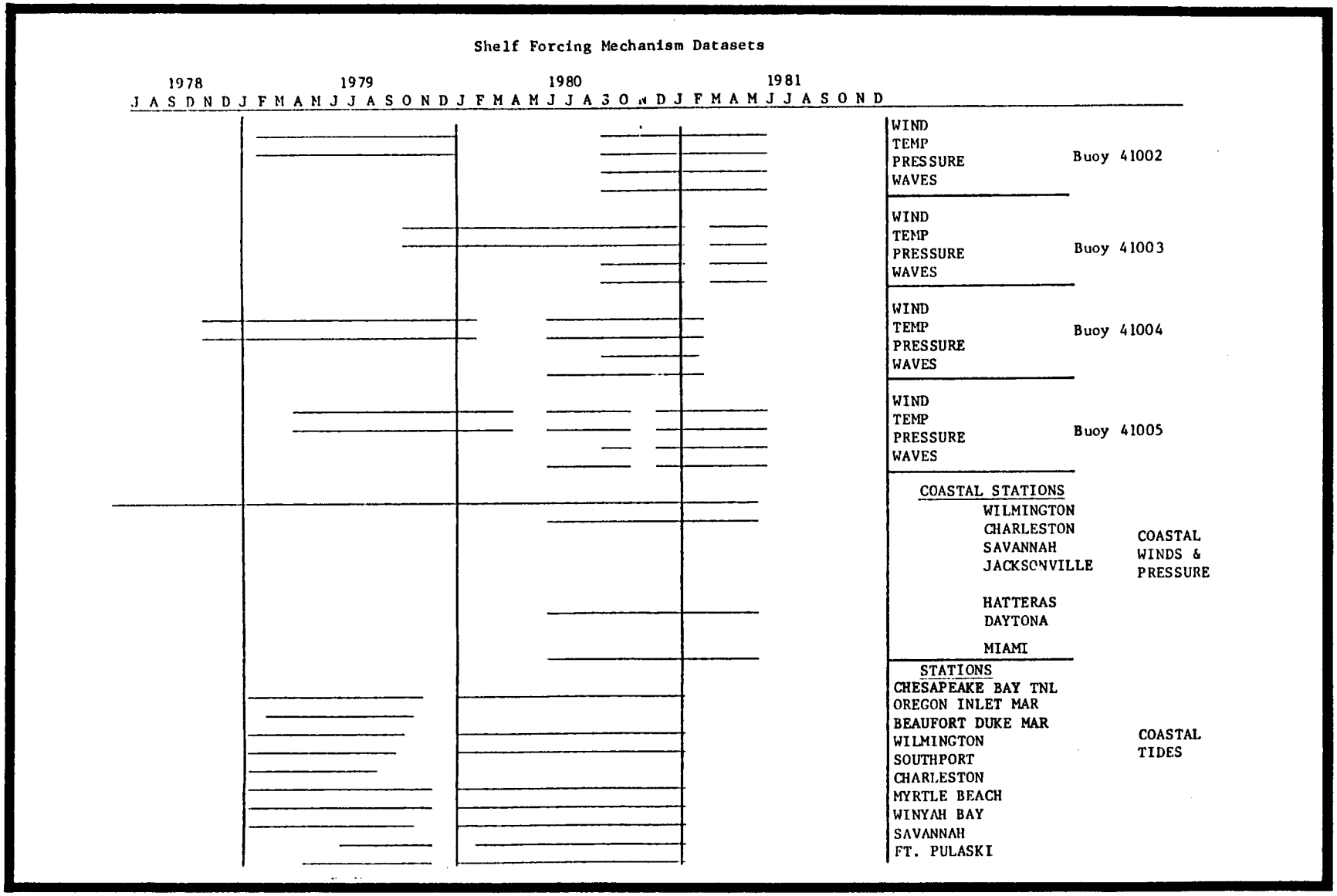

Figure 2.3-1. Shelf forcing mechanism data sets.

Table 2.4-1. Specifications for Neil Brown CTD system

Range	Accuracy	Resolution
Pressure 0-1600 decibar	0.1% of FS	0.0015% FS
Temperature (—3 to +32°C)	0.005°C (—3 to +32°C)	0.0005°C
Conductivity 1 to 65mmhos	0.005mmhos	0.001mmhos
Oxygen Sensor Current 0-2uA	2nA	0.5nA

was used as the point of embarkation and debarkation. The tracklines and associated station arrays were run as planned, with approximately one day total sampling time per cruise lost to adverse weather conditions. The procedure and methods reviewed below are described in detail in previous SAPOS Final Progress Reports (e.g., Years I and II).

2.4.1 Winter 1981

From 1 to 8 February 1981, 107 hydrographic stations (Figure 2.4-1; Table 2.4-2) were occupied on a hydrographic survey cruise in the shelf/slope/Gulf Stream region centered on Cape Hatteras. Completed were two cross-shelf, cross-Gulf Stream transects, a transect along the eastern edge of the Stream, and a high resolution mapping of the Gulf Stream frontal zone spanning Cape Hatteras. Conductivity-temperature-depth (CTD) data were obtained at each station to within 5 m of the bottom for depths less than 1600 m. For depths greater than 1600 m, the deepest samples were obtained at the 1600-m level. Temperature, conductivity, pressure, and dissolved oxygen were measured with the CTD unit. The data (down cast only) with vertical resolution between 10 and 25 cm were recorded on magnetic tape and hard copy listed as well as plotted. Five to six 10-liter Nisken bottle samples were obtained (via remotely actuated Rosette) during each upcast at selected points determined by the structure observed in the down cast profile. Surface and cast extremity samples were always taken. These samples were frozen for later inorganic nutrient (nitrate, phosphate, and silicate) and salinity analyses onshore. Two reversing thermometers were used on the surface Nisken bottle to provide independent surface temperature values. These thermometers were read and recorded by two readers at the end of each cast.

Beginning and ending station position coordinates (LORAN-C) and other associated station variables (e.g., depth) were recorded by the scientific watch from standard shipboard instrumentation.

2.4.2 Summer 1981

From 29 August to 5 September 1981, 114 hydrographic stations (Figure 2.4-2; Table 2.4-3) were occupied on a hydrographic survey cruise in the shelf/slope/Gulf Stream region centered on Cape Hatteras. Completed were two cross-shelf/cross-Gulf Stream transects, a transect along the eastern edge of the stream, and a high resolution mapping of the Gulf Stream frontal zone spanning Cape Hatteras. CTD data were obtained at each station to within five meters of the bottom in depths less than 1600 m, and to 1600 m in depths greater than 1600 m. Temperature, conductivity, pressure, and dissolved oxygen were measured with the CTD unit. The data (down cast only) with vertical resolution between 10 and 25 cm were recorded on magnetic tape (analog, digital cassette, and digital 9-track) and hard copy listed as well as plotted. Typically, three Nisken bottle samples were obtained (via remotely actuated Rosette) during each cast retrieval, at selected points determined by the observed structure in the down profile. Surface samples were always taken. Drawn from the Nisken bottles, 200 ml (approx.) samples were frozen for later inorganic nutrient (nitrate, phosphate, and silicate) and salinity analyses onshore.

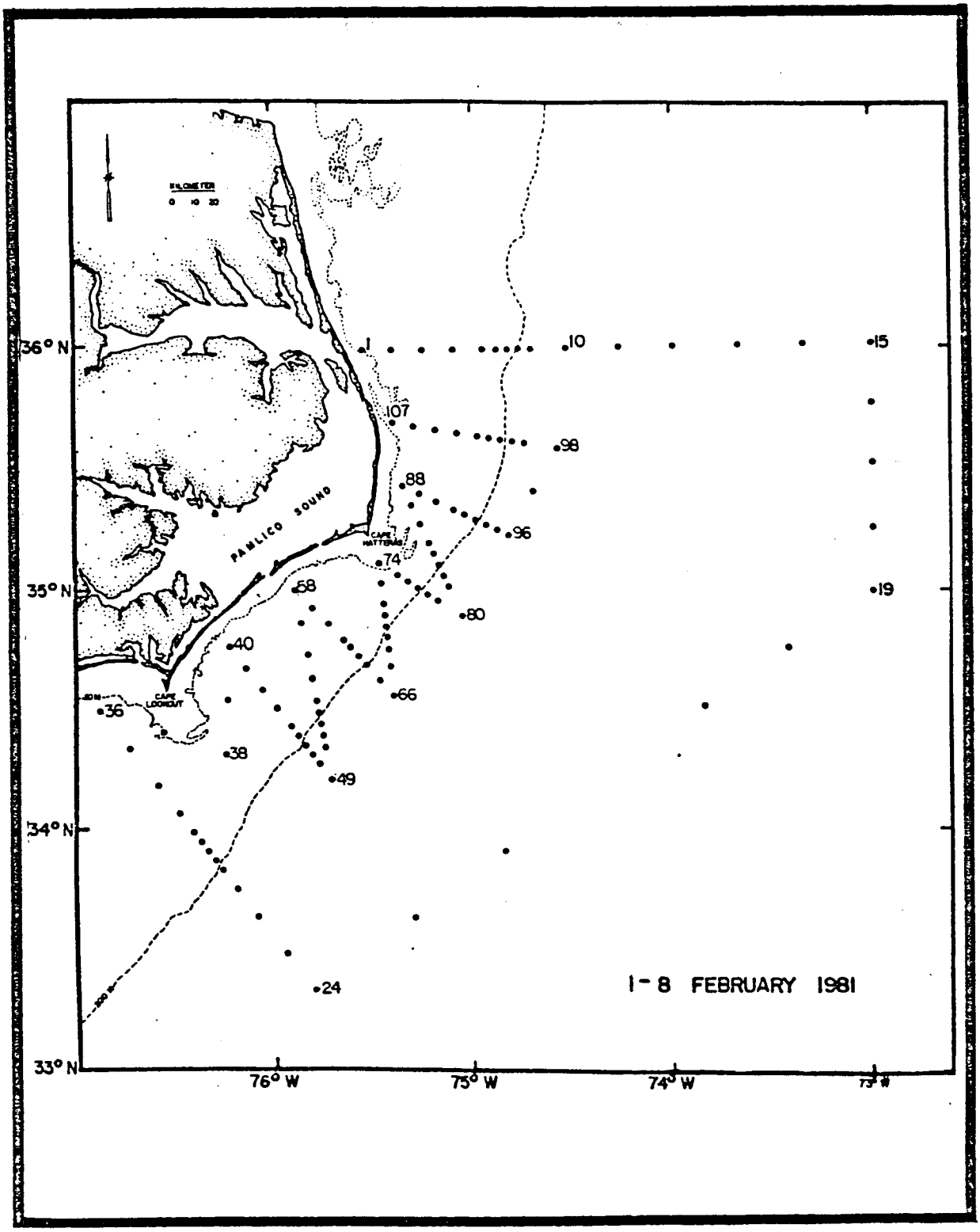

Figure 2.4-1. Station locations, 1 to 8 February 1981.

Table 2.4-2. Station coordinates, 1 to 8 February 1981.

STA. NO.	DATE (FEB. 1981)	TIME (EDT) ARRIVE	TIME (EDT) LEAVE	POSITION ARRIVE LAT.	POSITION ARRIVE LON.	POSITION LEAVE LAT.	POSITION LEAVE LON.	DEPTH (M)
1	1	1650	1725	35 594	75 353	35 595	75 352	20
2		2254	2306	35 598	75 258	35 598	75 258	22
3		2038		35 594	75 172			26
4		2219	2239	35 597	75 075	35 599	75 075	33
5		2341		35 596	74 583			45
6	2	1601	1640	35 596	74 554	36 013	74 564	73
7		1748	1807	35 596	74 511	35 598	74 507	92
8		1841		35 594	74 472			215
9		1949		35 595	74 432			875
10		2130	2216	35 592	74 326	35 586	74 322	1830
11	3	0105	0206	35 596	74 165	35 598	74 155	2169
12		0332	0420	36 013	74 052	36 013	74 042	3129
13		0630	0734	35 594	73 396	36 018	73 362	3100
14		0900		35 598	73 198			3294
15		1115	1151	35 596	72 593	35 598	72 586	3477
16		1349	1446	35 447	72 596	35 442	72 578	4026
17		1631	1723	35 294	72 593	35 259	72 527	4209
18		1850		35 143	72 594			4209
19		2050	2130	34 593	72 594	34 582	72 590	4209
20	4	0028		34 446	73 254			4026
21		0447	0536	34 292	73 513	34 293	73 500	4026
22		1255	1344	33 471	74 544	33 471	74 530	3522
23		1640	1732	33 298	75 222	33 300	75 207	3275
24		2048	2127	33 131	75 513	33 137	75 502	2397
25	5	0008	0133	33 264	76 023	33 284	75 572	1380
26		0349	0421	33 365	76 110	33 370	76 091	624
27		0538		33 442	76 177			455
28		0701	0720	33 492	76 218	33 491	76 219	300
29		0746	0759	33 518	76 240	33 517	76 236	200
30		0823	0845	33 538	76 259	33 539	76 259	70

Table 2.4-2. Continued.

STA. NO.	DATE (FEB. 1981)	TIME (EDT) ARRIVE	TIME (EDT) LEAVE	POSITION ARRIVE LAT.	POSITION ARRIVE LON.	POSITION LEAVE LAT.	POSITION LEAVE LON.	DEPTH (M)
31	5	0918	0930	33 561	76 279	33 565	76 279	45
32		1016	1029	33 587	76 299	33 586	76 297	43
33		1121	1133	34 038	76 341	34 036	76 341	40
34		1238		34 111	76 404			33
35		1420		34 208	76 486			25
36		1612		34 305	76 574			21
37		1800	1815	34 245	76 381	34 246	76 384	25
38		1942	1952	34 184	76 191	34 184	76 194	32
39		2105	2115	34 326	76 185	34 325	76 187	27
40		2226	2235	34 465	76 173	34 464	76 174	23
41		2317	2328	34 402	76 121	34 401	76 124	28
42	6	0002	0020	34 348	76 074	34 342	76 075	36
43		0047		34 299	76 033			42
44		0133	0148	34 254	75 592			55
45		0208	0222	34 227	75 568	34 228	75 570	91
46		0242		34 202	75 548			150
47		0319	0341	34 175	75 527	34 175	75 528	272
48		0355	0422	34 151	75 510	34 170	75 512	385
49		0453	0520	34 112	75 474	34 117	75 468	560
50		0605		34 196	75 491			330
51		0646	0706	34 224	75 491	34 230	75 492	250
52		0722	0739	34 257	75 502	34 263	75 502	145
53		0802	0822	34 286	75 505	34 299	75 506	106
54		0841	0859	34 315	75 511	34 317	75 509	66
55		0935	0946	34 376	75 524	34 378	75 521	46
56		1014	1026	34 438	75 533	34 438	75 532	38
57		1109	1121	34 518	75 562	34 520	75 550	29
58		1208		35 006	75 568			25
59		1302		34 559	75 516			26
60		1341	1352	34 513	75 471	34 512	75 472	27

Table 2.4-2. Continued.

STA. NO.	(FEB. 1981)	TIME (EDT) ARRIVE	LEAVE	POSITION ARRIVE LAT.	LON.	LEAVE LAT.	LON.	DEPTH (M)
61	6	1420	1432	34 467	75 422			43
62		1445		34 445	75 402			46
63		1514		34 419	75 374			90
64		1547	1606	34 395	75 350	34 404	75 351	226
65		1632	1707	34 355	75 312	34 356	75 310	1030
66		1755	1835	34 316	75 266	34 318	75 262	1830
67		1925	1958	34 394	75 285	34 398	75 274	960
68		2023	2041	34 438	75 282	34 439	75 281	385
69		2103	2119	34 469	75 285	34 472	75 283	208
70		2139	2201	34 500	75 293	34 504	75 285	105
71		2214	2224	34 528	75 293	34 530	75 292	73
72		2246	2254	34 561	75 299	34 562	75 298	54
73		2324	2331	35 013	75 304	35 012	75 304	36
74	7	2359	0007	35 064	75 307	35 062	75 307	20
75		0032		35 032	75 253			30
76		0058		35 015	75 221			65
77		0131		34 598	75 192			92
78		0158	0218	34 582	75 163	34 582	75 161	204
79		0234	0258	34 564	75 129	34 565	75 128	516
80		0334		34 523	75 056			1830
81		0949	1017	35 001	75 099	35 002	75 095	614
82		1033	1050	35 032	75 113	35 032	75 112	195
83		1105	1114	35 058	75 130	35 060	75 129	82
84		1128	1142	35 086	75 142	35 089	75 141	37
85		1156	1205	35 113	75 158	35 114	75 157	18
86		1231	1241	35 162	75 185	35 162	75 184	25
87		1307		35 209	75 211			25
88		1344	1356	35 259	75 234	35 257	75 235	22
89		1425		35 233	75 170			27
90		1503		35 216	75 128			29

Table 2.4-2. Continued.

STA. NO.	DATE (FEB. 1981)	TIME (EDT) ARRIVE	LEAVE	POSITION LAT.	LON.	LAT.	LON.	DEPTH (M)
91	7	1540		35 195	75 078			27
92		1610	1627	35 185	75 045	35 190	75 049	31
93		1643	1702	35 170	75 008	35 172	75 007	77
94		1624	1744	35 156	74 581			205
95		1801	1840	35 143	74 541	35 147	74 544	1115
96		1913	2000	35 131	74 510	35 137	74 514	1830
98	8	0949		35 346	74 355			1830
99		1126	1153	35 362	74 459	35 366	74 457	800
100		1214	1241	35 366	74 496	35 367	74 492	183
101		1306	1325	35 368	74 534	35 370	74 530	70
102		1355	1410	35 374	74 568	35 375	74 566	51
103		1432	1448	35 380	75 003	35 382	75 002	45
104		1528	1544	35 387	75 070	35 390	75 069	33
105		1619	1634	35 398	75 134			34
106		1717	1730	35 407	75 205	35 407	75 201	26
107		1810		35 416	75 267			21

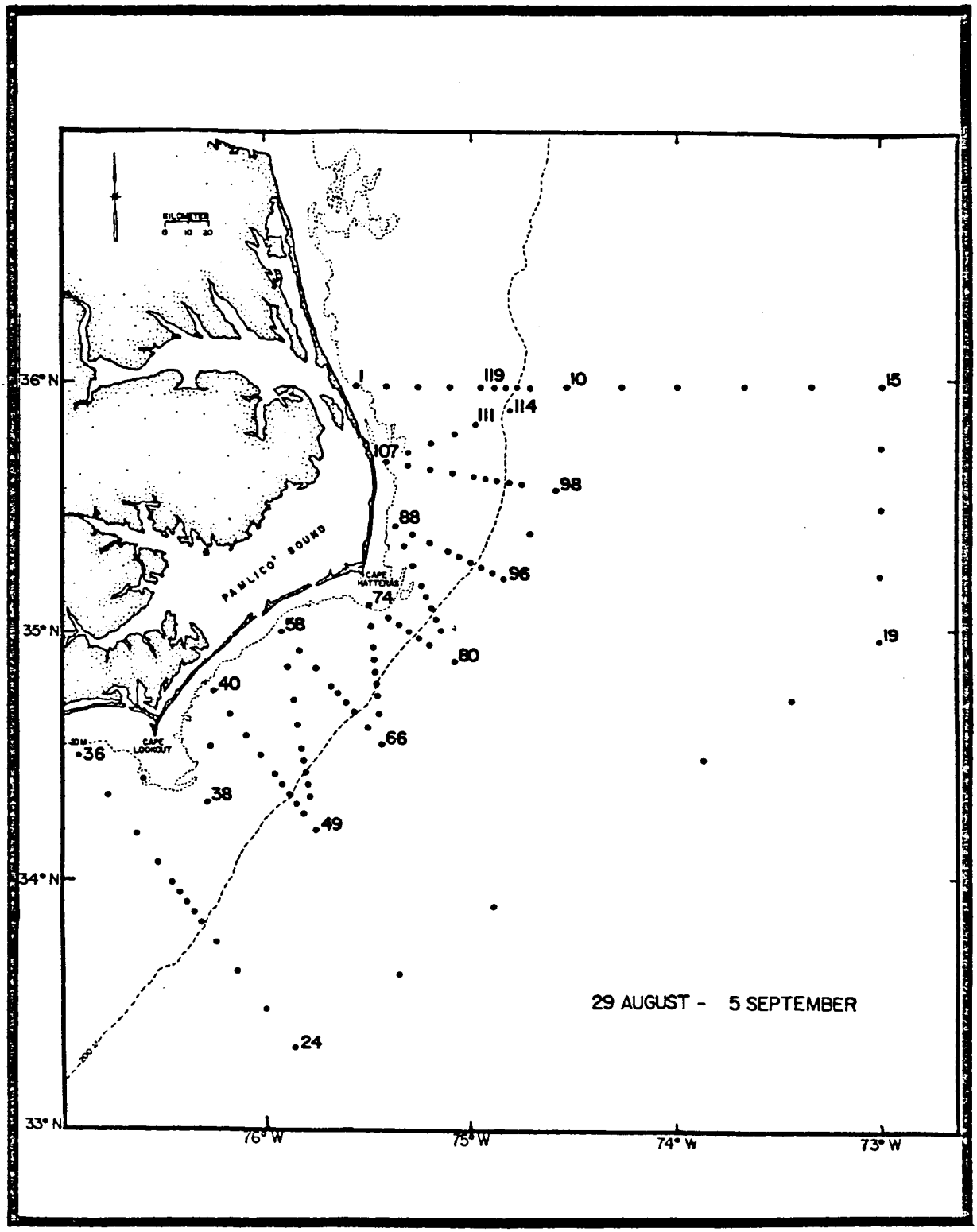

Figure 2.4-2. Station locations, 29 August to 5 September 1981. (Note: 114 total stations).

Table 2.4-3. Station coordinates, 29 August to 5 September 1981

STA. NO.	DATE (AUG. 1981)	TIME (EDT) ARRIVE	TIME (EDT) LEAVE	POSITION ARRIVE LAT.	POSITION ARRIVE LON.	POSITION LEAVE LAT.	POSITION LEAVE LON.	DEPTH (M)
1	29	1924	1933	35 599	75 361	35 599	75 361	22
2		2039	2049	36 000	75 269	36 000	75 269	26
3		2143	2151	35 599	75 177	35 599	75 177	27
4		2252	2302	36 000	75 082	36 001	75 082	34
5		2358	0012	36 000	74 589	36 001	74 589	50
6	30	0049	0104	36 000	74 555	36 000	74 555	76
7		0135	0150	36 000	74 527	36 000	74 527	95
8		0250	0309	36 000	74 481	36 000	74 482	175
9		0352	0428	36 000	74 434	35 599	74 437	855
10		0555	0709	36 000	74 335	36 006	74 337	1830
11		0844	0940	36 000	74 169	36 015	74 169	2169
12		1116	1231	36 000	74 002	36 030	73 598	3129
13		1636	1703	36 010	73 400	36 018	73 400	3100
14		1853	1953	36 000	73 204	36 002	73 207	3294
15		2143	2249	36 000	73 000	36 004	73 005	3477
16	31	0146	0223	35 447	73 000	35 445	73 026	4026
17		0409	0459	35 299	73 001	35 297	73 006	4209
18		0636	0736	35 149	73 001	35 146	73 009	4209
19		0917	1015	35 000	73 001	35 000	73 007	4209
20		1245	1342	34 447	73 266			4206
21		1535	1630	34 298	73 523	34 283	73 533	4206
22		2204	2318	33 482	74 550	33 486	74 547	3522
23	01	0258	0347	33 316	75 234	33 322	75 227	3275
24		0716	0812	33 150	75 520	33 156	75 515	2397
25		0937	1022	33 280	76 031	33 290	76 020	1342
26		1208	1236	33 383	76 107	33 389	76 098	627
27		1450	1507	33 453	76 180	33 454	76 170	451
28		1601	1616	33 502	76 222	33 503	76 217	265
29		1642	1653	33 526	76 244	33 526	76 242	175
30		1723	1732	33 550	76 266	33 549	76 266	67

Table 2.4-3. Continued.

STA. NO.	DATE (SEPT. 1981)	TIME (EDT) ARRIVE	TIME (EDT) LEAVE	POSITION ARRIVE LAT.	POSITION ARRIVE LON.	POSITION LEAVE LAT.	POSITION LEAVE LON.	DEPTH (M)
31	01	1757	1806	33 576	76 287	33 574	76 288	45
32		1833	1841	34 001	76 309	34 000	76 310	42
33		1919	1927	34 048	76 350	34 047	76 351	40
34		2027	2036	34 120	76 414	34 119	76 414	34
35		2155	2203	34 217	76 498	34 217	76 499	27
36		2318	2327	34 315	76 580	34 314	76 581	20
37	02	0105	0112	34 254	76 391	34 253	76 392	28
38		0249	0256	34 195	76 203	34 192	76 204	33
39		0422	0428	34 335	76 193	34 333	76 194	28
40		0557	0603	34 471	76 181	34 469	76 183	20
41		0645	0653	34 412	76 135	34 411	76 137	25
42		0735	0744	34 358	76 086	34 351	76 087	37
43		0818	0826	34 308	76 042	34 307	76 043	42
44		0901	0911	34 261	75 599	34 259	75 599	57
45		0931	0942	34 236	75 578	34 234	75 573	77
46		0958	1011	34 212	75 557	34 211	75 556	152
47		1031	1052	34 187	75 536	34 181	75 535	274
48		1109	1128	34 163	75 514	34 160	75 510	408
49		1157	1223	34 126	75 480	34 125	75 469	575
50		1330	1347	34 205	75 497	34 201	75 495	352
51		1417	1431	34 235	75 504	34 231	75 502	237
52		1506	1517	34 265	75 509	34 262	75 509	150
53		1549	1559	34 296	75 516	34 292	75 516	102
54		1630	1638	34 324	75 521	34 322	75 522	65
55		1727	1733	34 383	75 533	34 382	75 534	44
56		1824	1832	34 443	75 543	34 441	75 548	35
57		1929	1939	34 528	75 573	34 523	75 573	29
58		2036	2049	35 015	75 579	35 013	75 580	20
59		2131	2141	34 565	75 526	34 564	75 528	25
60		2220	2234	34 519	75 479	34 514	75 479	28

Table 2.4-3. Continued.

STA. NO.	DATE (SEPT. 1981)	TIME (EDT) ARRIVE	TIME (EDT) LEAVE	POSITION ARRIVE LAT.	POSITION ARRIVE LON.	POSITION LEAVE LAT.	POSITION LEAVE LON.	DEPTH (M)
61	02	2309	2316	34 473	75 432	34 472	75 433	43
62		2342	2356	34 451	75 408	34 446	75 403	48
63	03	0041	0102	34 428	75 384	34 423	75 338	217
63A		0132	0145	34 428	75 385	34 425	75 388	80
64		0211	0228	34 405	75 359	34 402	75 363	201
65		0306	0348	34 364	75 318	34 360	75 318	1026
66		0422	0523	34 324	75 277	34 323	75 269	1830
67		0624	0711	34 400	75 285	34 397	75 283	978
68		0744	0805	34 444	75 291	34 440	75 291	383
69		0829	0843	34 474	75 295	34 471	75 296	203
70		0929	0940	34 504	75 297	34 502	75 301	108
71		1009	1020	34 535	75 302	34 533	75 304	69
72		1045	1055	34 566	75 306	34 564	75 308	53
73		1132	1140	35 018	75 312	35 016	75 312	37
74		1219	1226	35 070	75 319	35 068	75 319	22
75		1300	1306	35 039	75 260	35 038	75 261	29
76		1329	1339	35 021	75 230	35 018	75 232	65
77		1404	1414	35 004	75 200	35 002	75 202	87
78		1440	1454	34 589	75 160	34 585	75 163	252
79		1512	1532	34 570	75 140	34 567	75 143	465
80		1623	1715	34 531	75 063	34 531	75 060	1830
81		2247	2317	35 007	75 105	35 000	75 110	575
82		2354	0010	35 034	75 120	35 029	75 123	214
83	04	0049	0058	35 062	75 134	35 059	75 135	85
84		0134	0140	35 090	75 148	35 088	75 148	40
85		0217	0221	35 118	75 165	35 116	75 165	27
86		0305	0310	35 167	75 191	35 165	75 191	21
87		0354	0359	35 215	75 217	35 213	75 217	24
88		0440	0444	35 263	75 244	35 261	75 244	21
89		0519	0523	35 242	75 191	35 241	75 191	26

Table 2.4-3. Continued.

STA. NO.	DATE (SEPT. 1981)	TIME (EDT) ARRIVE	TIME (EDT) LEAVE	POSITION ARRIVE LAT.	POSITION ARRIVE LON.	POSITION LEAVE LAT.	POSITION LEAVE LON.	DEPTH (M)
90	04	0559	0603	35 221	75 138	35 220	75 138	29
91		0636	0642	35 200	75 086	35 198	75 087	24
92		0703	0710	35 188	75 053	35 186	75 055	31
93		0732	0741	35 175	75 019	35 174	75 020	71
94		0803	0818	35 163	74 584	35 160	74 585	218
95		0843	0939	35 151	74 551	35 158	74 541	1216
96		1013	1112	35 137	74 516	35 147	74 509	1830
97		1228	1336	35 248	74 440	35 264	74 436	1830
98		1445	1545	35 356	74 364	35 373	74 356	1830
99		1700	1727	35 366	74 467	35 366	74 465	684
100		1803	1814	35 370	74 504	35 367	74 504	79
101		1837	1846	35 375	74 539	35 373	74 539	57
102		1911	1920	35 380	75 575	35 378	74 574	51
103		1944	1954	35 385	75 012	35 383	75 013	47
104		2034	2041	35 394	75 076	35 393	75 076	35
105		2116	2123	35 402	75 141	35 400	75 141	31
106		2156	2202	35 410	75 207	35 408	75 207	26
107		2235	2241	35 418	75 275	35 417	75 274	21
108		2321	2328	35 443	75 204	35 442	75 205	20
109	05	0007	0013	35 464	75 136	35 463	75 136	38
110		0054	0059	35 488	75 077	35 487	75 077	34
111		0148	0154	35 510	74 599	35 509	75 000	50
112		0223	0229	35 522	74 564	35 520	74 564	68
114		0311	0322	35 545	74 499	35 543	74 500	175
119		0407	0414	36 000	74 555	35 598	74 555	77

Two reversing thermometers were used on the surface Nisken bottle to provide independent surface temperature values. These thermometers were read and recorded by two readers at the end of each cast.

Beginning and ending station position coordinates (LORAN-C) and associated station variables (e.g., depth) were recorded and displayed automatically through a computer interface connected to shipboard instrumentation.

Between stations, near-surface ($\sim$ 2 m deep) temperature and conductivity were monitored, using the CTD unit attached to a system designed to pump near-surface water past the sensors. These data were recorded on a dual channel analog strip chart recorder.

2.5 SUBSURFACE CURRENTS - GABEX-II

The GABEX-II moored current meter array was deployed on the southeast U.S. shelf for a 4-month period from June to October 1981. The locations of the moorings are shown in Figure 2.5-1, and the instrument configuration is given in Table 2.5-1. The current meter array consisted of 21 subsurface, taut-wire current meter moorings oriented along isobaths in 10- to 75-m water depths, and contained 50 current meters, 4 thermistor strings, 8 bottom pressure recorders, and an instrumented tower (Savannah Light tower). The eight outer-shelf moorings on the 40- and 75-m isobaths were the responsibility of the University of Miami (T. Lee). North Carolina State University (Dr. L. Pietrafesa) had the primary responsibility for the 10 mid- and inner-shelf moorings on the 10- to 28-meter isobaths. BLM/SAI contributed three moorings on the 30-, 40- and 75-meter isobaths off Cape Romain (Moorings 22, 23, and 24). A list of the equipment provided by the University of Miami, North Carolina State University, and BLM/SAI is given in Table 2.5-2. The nearshore zone in the vicinity of tidal inlets was also studied simultaneously by Skidaway Institute of Oceanography (J. Blanton). Shipboard observations involved two ships working simultaneously during the upwelling period, June-August. One ship made detailed hydrographic, nutrient, and phytoplankton measurements through stranded intrusions and across the shelf at 30°N, while the second ship conducted zooplankton and microbiological measurements within the event.

The GABEX-II array design was essentially the same as the GABEX-I array (Lee and Atkinson in press), except that the outer-shelf moorings (Moorings 5, 6, 11, and 12) were omitted, since the experimental design of GABEX-II was to investigate effects of summer upwelling and stranded intrusions in the mid-shelf area where along-shelf coherence was found to be on the order or 400 km. Therefore, an along-shelf spacing of about 100 km should be sufficient when combined with the hydrographic measurements to resolve movements of events at mid-shelf. The moorings were recovered 3-15 October 1981. Current meters on the outer-shelf moorings were all in working order on recovery, and the data are now being processed. However, Moorings 16 and 25 were not recovered, for reasons unknown. The moorings were equipped with two acoustic releases each, and neither release would respond or release thus indicating the moorings were probably no longer there. A circular dragging operation was also unsuccessful at each site. In addition, the lower current meter on Mooring 22 was lost when it became entangled with the ship's propellers. Additional data sources available during GABEX-II are listed in Table 2.5-3.

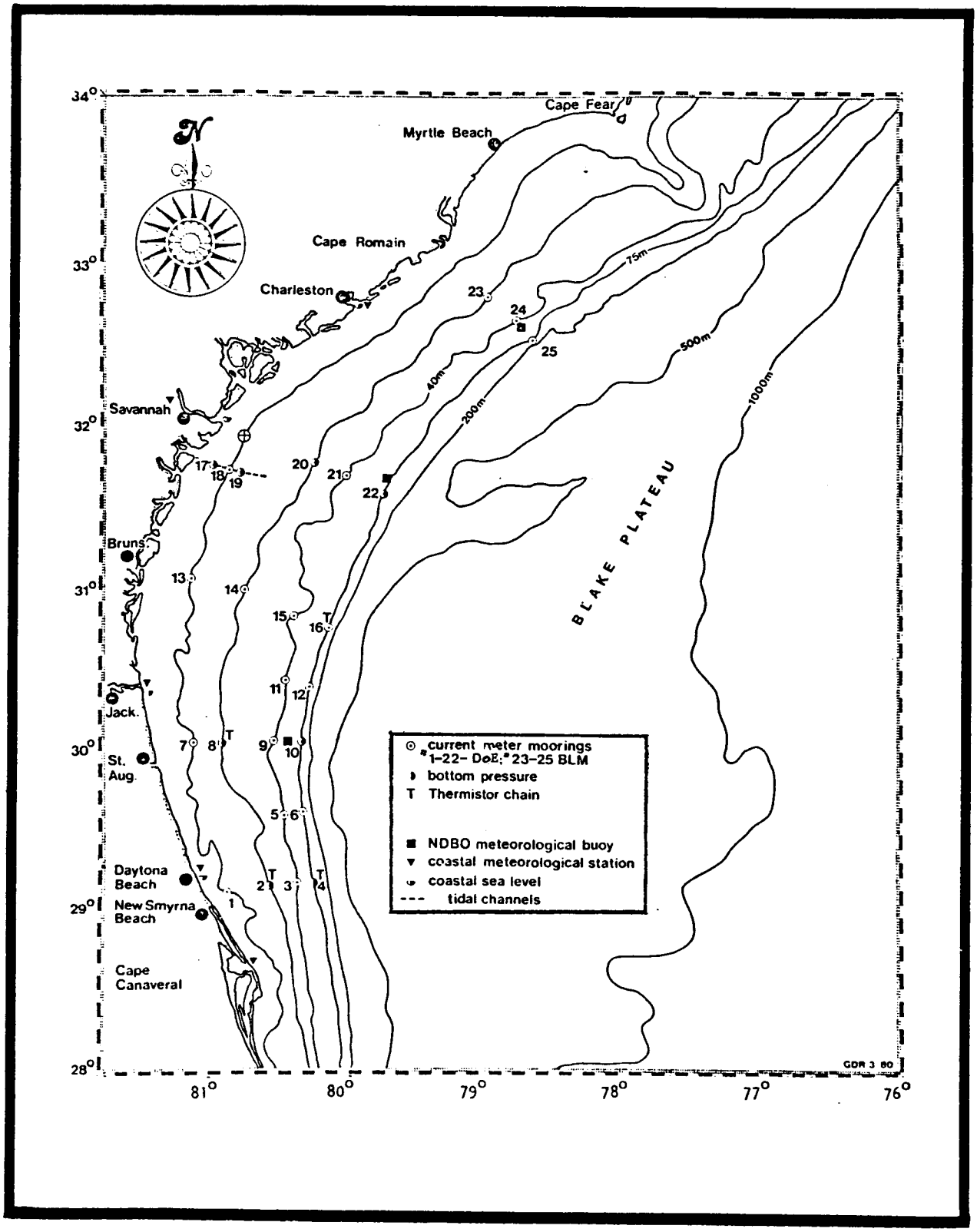

Figure 2.5-1. GABEX-I subsurface current meter array, 17 February to 26 June 1980.

Table 2.5-1. GABEX-II instrument configuration

Mooring No.	Latitude	Longitude	Water Depth (m)	Current Meter Depth (m)	Current Meter Type	Thermistor Chain Depth (m)	Thermistor Chain Type	Conductivity Depth (m)	Conductivity Type	Pressure Depth (m)	Pressure Type
1	29°05.7'	80°47.4'	15	5	EN					14	GOP
				12	EN						
2	29°08.9'	80°28.2'	28	17	AA	6-25	AA			27	AP
				25	AA	(Separate mooring)					
3	29°10.2'	80°19.4'	40	17	AA						
				37	AA						
4	29°11.8'	80°09.6'	75	17	AA	22-72	AA			74	AP
				45	AA	(Separate mooring)					
				72	AA						
7	30°03.0'	81°09.4'	15	5	EN						
				12	EN						
8	30°03.0'	80°46.8'	28	7	AA	6-25	AA			28	AP
				17	AA	(Separate mooring)					
				25	AA						
9	30°03.0'	80°27.6'	40	6	VACM						
				7	SAA						
				17	AA						
				27	AA						
				37	AA						
10	30°03.0'	80°15.0'	75	7	GO	22-72	AA	17	AA	74	AP
				17	AA	(Separate mooring)					
				27	AA						
				45	AA						
				60	AA						
				72	AA						
13	31°02.5'	81°02.8'	15	5	EN						
				12	AA						
14	30°56.2'	80°39.2'	28	17	AA						
				25	AA						
15	30°50.7'	80°19.4'	40	17	AA						
				37	AA						
16	30°46.5'	80°03.5'	75	17	AA						
				45	AA						
				72	AA						
17	31°46.2'	80°53.8'	10	5	EN					9	GOP

(continued on second page)

(continued) Table 2.5-1. GABEX-II instrument configuration

Mooring No.	Latitude	Longitude	Water Depth (m)	Current Meter Depth (m)	Current Meter Type	Thermistor Chain Depth (m)	Thermistor Chain Type	Conductivity Depth (m)	Conductivity Type	Pressure Depth (m)	Pressure Type
18	31°43.6'	80°47.3'	13	5	EN						
19	31°43.2'	80°42.2'	15	5	EN					14	GOP
20	31°46.9'	80°11.8'	28	17	AA					19	GOP
				25	AA						
21	31°41.2'	79°54.2'	40	17	AA						
				37	AA						
22	31°35.9'	79°39.9'	75	17	AA						
				72	AA						
23	32°48.5'	78°55.3'	30	17	VACM						
				27	VACM						
24	32°39.8'	78°43.7'	40	17	VACM						
				37	VACM						
25	32°32.4'	78°36.1'	75	17	VACM						
				45	VACM						
				72	VACM						

SYMBOLS:
- AA - Aanderaa Current Meter
- SAA - Modified Shallow Water Aanderaa Current Meter
- EN - Endeco Current Meter
- GO - General Oceanics Current Meter
- T - Thermistor String
- AP - Aanderaa Bottom Pressure
- GOP - General Oceanics Bottom Pressure
- VACM - Vector Averaging Current Meter

Table 2.5.2. GABEX-11 mooring array equipment list (13 May - 15 October 1981)

Equipment Totals: 21 moorings
50 current meters
31 acoustic releases

University of Miami contribution (DOE):
8 moorings on 40 and 75 m isobaths
Current meters - 25: 22 AA, 1 SAA, 1 GOCM, 1 VACM
Releases - 19 total: 2/mooring for U. Miami plus 3 for NCSU

NCSU contribution (DOE)
10 moorings on 10, 28 m and inlets
Current meters - 18: 8 AA, 8 Endecos, 2 Endecos, 2 GOCM (from U. Miami)
Releases - 6
Thermistor strings - 4 AA (2 - 20 m, 2 - 50 m)
Bottom Pressure: 8: 4 AA, 4 GOP

SAI/BLM contribution:
3 moorings on 30, 40 and 75 m isobaths
Current meters - 7 VACM's
Releases - 6 (2/mooring)

BLM supported NDBO meteorological buoys on the shelf off Charleston, SC, (near Mooring 24, Figure 2.5-1), Savannah, GA (near Mooring 22), and St. Augustine, FL (between Moorings 9 and 10). These buoys record wind speed and direction, air temperature, water temperature, and atmospheric pressure. Additional meteorological and sea level data is available from the coastal stations shown on Figure 2.5-1 and Table 2.5-3. Together, this network of coastal and offshore meteorological stations provides an excellent data base of meteorological forcing from which estimates of wind curl and divergence can be derived.

Table 2.5-3. GABEX-II additional data sources

Data Type	Location	Source
Coastal subsurface pressure:	Daytona Beach, FL	NOS
	Jacksonville, FL	NOS
	Savannah, GA	NOS
	Charleston, SC	NOS
Coastal Meteorological stations:	Cape Canaveral, FL	Nat. Wea. Svs.
	Jacksonville, FL	Nat. Wea. Svs.
	Savannah, GA	Nat. Wea. Svs.
	Charleston, SC	Nat. Wea. Svs
Offshore wind measurements:	Savannah Lighthouse	Skidaway
	NDBO buoy off Charleston	BLM/SAI
	NDBO buoy off Savannah	BLM/SAI
	NDBO buoy off St. Augustine	BLM/SAI

III. DATA ANALYSIS

3.1 INTRODUCTION

This section describes analyses used during the course of this study. Few new procedures have been used during Year 4. Tidal analysis (amplitude and phase of tidal constituents) was conducted using techniques as described in Section 3.3. Many other techniques employed have been described in detail in Volume 2 of the final Progress Reports for Years 1-3 (SAI 1979, 1981, and 1982).

3.2 SEA SURFACE TEMPERATURES/GULF STREAM VARIABILITY

Procedures used in evaluating weekly Experimental Ocean Frontal Analysis (EOFA) and satellite imagery have been described in detail in the Year 3 Final Progress Report - Section 3.1.

3.3 SHELF FORCING MECHANISMS

All analysis procedures used have been described previously with the exception of the tidal analysis described briefly below.

3.3.1 Tidal Analysis

Tidal analysis was performed on the hourly water level records from the SAB for the years 1979 and 1980. The tidal analysis uses the harmonic method originally developed by Doodson (Doodson and Warburg 1941), further refined by Cartwright (Cartwright and Taylor 1971), and Godin (1972). The computer program is based in Godin's 1972 treatise and was developed by Foreman (1977). The reader is referred to the latter two references for details of the analysis program.

The method involves a least squares fit of observed time series of tidal heights to a time series generated from astronomical tidal potential. The unknowns to be fitted are the amplitude and phase of the harmonic, astronomically calculated constituents.

The method of choosing the harmonic constituents is fairly complicated and is based on Godin's studies. There is a maximum of 146 constituents, of which 45 are astronomical in origin. The remaining 101 are shallow water constituents which are generally multiples of the astronomical constituents (M4, M6, etc.) or derived from the interaction of the main constituents. The basic analysis program used for SAB data includes all the main and 24 of the shallow water constituents. The criteria for inclusion of a constituent depends upon the length of the series and its resolution (using the Rayleigh criterion) from nearby major constituents.

The major constituents often occur in closely related bands (e.g. the diurnal band) and thus a group of constituents are clustered by their Doodson numbers as main and satellite. The initial least squares fit is calculated for the frequency of the main constituents and the apparent amplitude and phase of the cluster is then corrected for the influence of the satellite constituents. This is called a nodal modulation correction to the amplitude and phase of the main constitutents.

In order to make the nodal modulation correction to the main constituent's amplitude and phase, it is necessary to know the relative amplitudes and phases of the satellites. As is commonly done, it is assumed that the same relationship found with the equilibrium tide holds for the actual tide. That is, the tidal potential amplitude ratio of a satellite to its main constituent is assumed to be equal to the corresponding tidal heights amplitude ratio, and the difference in tidal potential phase equals the difference in tidal height phase.

The phase differences calculated by the least squares fit are related to the start time of the measurements. In tidal analysis, phase of the constitutent is related to the tidal potential, so that phase can be calculated without regard to the time origin of the observations.

Instead of regarding each tidal constituent as the result of some particular component of the tidal potential, an artificial causal agent can be attributed to each constituent in the form of a fictitious star which travels around the equator with an angular speed equal to that of its corresponding constituent. Making use of this conceptual aid, the astronomical argument, V(L,t), of a tidal constituent can then be viewed as the angular position of this fictitious star relative to longitude (L), and at time (t). Although the longitudinal dependence is easily calculated, for historical reasons L is generally assumed to be the Greenwich meridian, and V is reduced to a function of one variable.

The Greenwich phase lag, g, is the difference between this astronomical argument for Greenwich and the phase of the observed constituent signal. Its value is dependent upon the time zone in which the hourly heights of the record were taken. This means that when phases at various stations, not necessarily in the same time zone, are compared, they must be reduced to a common zone in order to avoid spurious differences due to different relative times. Specifically, if σ is the constituent frequency and $g(j+\Delta_j)$ and $g(j)$ are the Greenwich phase lags evaluated for time zones $j+\Delta_j$ and j, respectively (e.g. Eastern Standard Time is +5), then

$$g(j+\Delta_j) = g(j) - (\Delta_j)\sigma.$$

The Greenwich Phase Lag for SAB calculations is referred to Eastern Standard Time (EST).

One of the major advantages of the harmonic method is that gaps in the data can be easily handled, as the least squares method ignores gaps where no data are available. The calculations for SAB stations were performed for the data exactly as it was received from NOS. The analysis was performed for two separate years, noting that Godin suggests that errors will be introduced if time series longer than a year are used.

3.4 NORTH CAROLINA HYDROGRAPHY

Initial CTD data analysis included edit checks for data point validity, calculation of first order derived variables, and appropriate interval averaging, as well as validating and integrating the associated horizontal and vertical coordinate data (positions and depths).

Editing criteria were defined on the basis of physically realistic ranges for each variable observed. The CTD temperature sensor was calibrated against the 1968 International Practical Temperature Scale (Comite International des Poids et Mesures, 1969). Salinity was calculated from in situ temperature, conductivity, and pressure, using an algorithm (Figure 3.4-1) based on the data of Bradshaw and Schleicher (1965) and Brown and Allentroft (1966). Dissolved oxygen was calculated from in situ temperature (an average of ambient and inter-membrane) and salinity, according to the algorithm given in Figure 3.4-2. A comparison of directly derived dissolved oxygen values with those determined from Winkler titration showed that in situ observed dissolved oxygen profiles were repeatable (i.e., precise) minimally only to within an arbitrary constant. For an internally consistent data set, the procedure adopted was to normalize each profile to a surface saturation value based on the locally measured temperature and salinity.

Nutrient analyses were made using Technicon Auto-Analyzer procedures based on the manual methods of Murphy and Riley (1962) for reactive phosphate and of Armstrong et al. (1967) for dissolved silicate, and nitrate. The automated methods have been described in detail by Friederich and Whitledge (1972).

All station data were averaged over 1-meter intervals and plotted in vertical profile, vertical cross section field, and selected horizontal surface field formats by techniques described in previous Final Progress Reports. The complete graphical data set thus generated is contained in Vol. III of this report. Data were hard-copy listed and stored on magnetic tape for further analysis. Finalized data sets were also transmitted to NODC for archiving.

3.5 SUBSURFACE CURRENTS- GABEX-II

The GABEX-II experiment generated a considerable amount of data from the various sources previously discussed. In order to avoid duplication of efforts and conserve manpower, the responsibilities associated with data collection, processing, and analysis divided among the appropriate investigators. Table 3.5-1 shows that responsibilities associated with the current meter array were split between Karpen (SAI), for data products and Bedard (U. Miami), for instrumentation for the BLM data and Drs. T. Lee (U. Miami) and L. Pietrafesa (NCSU) for the DoE data. These responsibilities included providing mooring hardware and instrumentation; mooring construction, deployment and recovery; data transcription and processing; and routine analyses. The standard products listed in Table 3.5-1 are generated with each current meter record as part of the routine analyses, thus making data intercomparison and interpretation easier. Investigators responsible for additional data sources are listed in Table 3.5-2. Analysis of the physical processes that have been identified from our previous studies in the SAB to be of significance are also grouped according to the individuals that are primarily responsible for their investigation (Table 3.5-3). This approach is the same as taken in the DoE study and allows the investigators to concentrate on particular processes by having available and utilizing standard data products from the total data inventory. These are stored at, and made available through SAI in Raleigh, upon request.

```
REM*****CALCULATE SALINTIY*************************************
T1=T+4.4E-6*T*(100-T)
I4=1.5192-T1*(0.045302-T1*(8.3089E-4-T1*7.9E-6))
I5=P*(0.001042-P*(3.3913E-8-P*3.3E-13))
I6=4.0E-4+P*(2.577E-5-P*2.492E-9)
I7=1-T1*(0.1535-T1*(0.008276-T1*1.657E-4))
J4=0.00695-7.6E-5*T1
J5=35-S
I9=1+0.01*(I4*I5+I6*I7)*(1+J4*J5)
K=6.7249142E-9
J0=T1*(0.020131661+T1*(9.9886585E-5-T1*(1.9426015E-7+T1*K)))
J0=J0+0.67652453
J1=C/(42.909*J0*I9)
J2=J1+(J1-1)*J1*(0.0175-J1*0.0045)*(-1+T1*(0.08-T1*8.9E-4))
S=-0.73469+J2*(32.28071+J2*(3.4775-J2*0.02395))
RETURN
```

Figure 3.4-1. Algorithm for CTD salinity computation.

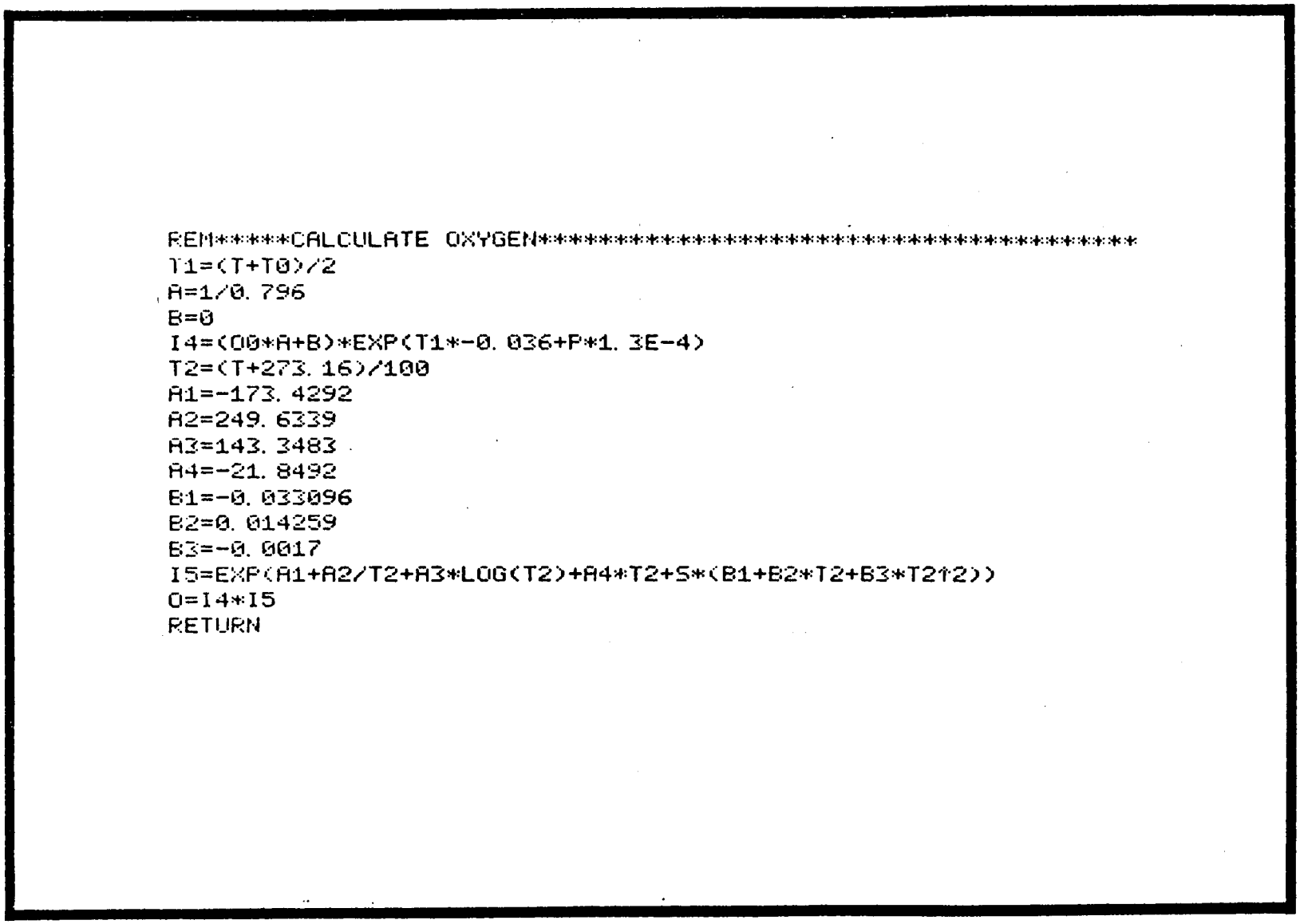

```
REM*****CALCULATE OXYGEN*************************************
T1=(T+T0)/2
A=1/0.796
B=0
I4=(O0*A+B)*EXP(T1*-0.036+P*1.3E-4)
T2=(T+273.16)/100
A1=-173.4292
A2=249.6339
A3=143.3483
A4=-21.8492
B1=-0.033096
B2=0.014259
B3=-0.0017
I5=EXP(A1+A2/T2+A3*LOG(T2)+A4*T2+S*(B1+B2*T2+B3*T2↑2))
O=I4*I5
RETURN
```

Figure 3.4-2. Algorithm for CTD dissolved oxygen computation.

Table 3.5-1. GABEX-II. Current meter array - responsibilities.

ACTIVITY	PRIMARY RESPONSIBILITY		
	DOE Outer-shelf moorings 40 and 75 m isobaths	DOE inner- and mid-shelf moorings 15 and 28 m isobaths	BLM Cape Romain cross-shelf array
Mooring hardware/construction	T. Lee (T.L.)	L. Pietrafesa (L.P.)	P. Bedard (P.B.) and T.L.
Mooring deployment/recovery	T.L. & L.P.	L.P. & T.L.	P.B. & T.L.
Data transcription	T.L.	L.P.	P.B.
Data editing	T.L.	L.P.	P.B. and J. Karpen (J.K.)
Data processing: 3 & 40 HLP filtered, rotated u,v,T	T.L.	L.P.	J.K.
First order statistics: means, S.D., Var., Max., Min., of 3 & 40 HLP data	T.L.	L.P.	J.K.
Flux calculations: $\overline{u'v'}$, $\overline{u'T'}$, $\overline{v'T'}$ of 3 & 40 HLP data	T.L.	L.P.	J.K.
Spectra: u-v of 3 & 40 HLP u-T and v-T of 40 HLP data	T.L.	L.P.	J.K.
Interstation horizontal and vertical coherence and phase: 40 HLP data	T.L.	L.P.	J.K.
Weekly cumulative averages: $\bar{u}$, $\bar{v}$, $\bar{T}$, $u'v'$, $u'T'$, $v'T'$, of 40 HLP data	T.L.	L.P.	J.K.
Monthly averages: $\bar{u}$, $\bar{v}$, $\bar{T}$, of 40 HLP data	T.L.	L.P.	J.K.

Table 3.5-2. GABEX-II. Additional data sources to be included with current meter data responsibilities

DATA	INDIVIDUAL RESPONSIBLE
Coastal wind	P. Hamilton (SAI)
Coastal sea level	P. Hamilton (SAI)
BLM meteorological buoys	P. Hamilton (SAI)
Savannah River tower	J. Blanton (Skidaway)
Thermistor strings	L. Pietrafesa (NCSU)
Satellite IR	O. Brown (U. Miami)
Hydrography	L. Atkinson (Skidaway)
River discharge	J. Blanton (Skidaway)

Table 3.5-3. Responsibility for physical processes to be investigated

PHYSICAL PROCESS	PRIMARY RESPONSIBILITY
Gulf Stream spin-off eddies	T. Lee
Gulf Stream meanders	T. Lee
Wind-driven shelf circulation	T. Lee
Trapped wave response	L. Pietrafesa
Topographic influences	L. Pietrafesa
Density induced circulation	L. Pietrafesa
Tidal/Inertial motions	L. Pietrafesa
Gulf Stream-shelf water mass interactions	L. Atkinson
Surface water response	P. Hamilton/ V. Waddell

The investigations of Gulf Stream meander and eddy processes require the joint analysis of the current, temperature, wind, hydrographic, and satellite VHRR data sets. The studies are geared toward understanding shelf/Gulf Stream interactions, developing reliable statistics, and determining the effect on shelf physical and biological processes. The investigations of wind-driven shelf circulation involved the joint spectral analysis of BLM and DoE supported shelf current meter records with wind and coastal sea level records. The response of shelf waters to wind forcing was evaluated in both the Savannah, Ga, and Cape Romain, S.C., shelf areas for winter and summer conditions.

3.6 OBSERVATIONAL METHODS

Seven cross-shelf pairs of subsurface, taut-wire, current meter moorings were deployed on the 40- and 75-m (shelf break) isobaths between Cape Canaveral, Fla. and Cape Romain, S.C. for a 4-month period from 16 February to 2 July 1980 (Figure 2.5-1). The array was designed to investigate the effects of propagating Gulf Stream frontal disturbances on shelf processes over a wide range of spatial scales. Standard Aanderaa current meters were deployed at depths of 17, 45, and 72 m on most of the shelf-break moorings, and 17 and 37 m on the moorings at the 40-m isobath, with upper flotation at 15 m. Vertical resolution was enhanced at the 30°N transect with 6 current meters at the 75-m isobath at depths of 7, 17, 27, 45, 60, and 72 m (Mooring 10), and 4 current meters at the 40-m isobath at depths of 7, 17, 27, and 37 m (Mooring 9). The upper current meter at Mooring 10 was a General Oceanics winged device set to burst sample over surface wave periods. The top instrument on Mooring 9 was an experimental Aanderaa modified at the University of Miami for use in shallow water by replacing the Savonius rotor with a Wellor propeller. (Leaman et al. in press) The BLM supported current meters at the Cape Romain transects (Moorings 23, 24, and 25) were all VACM's. Local shelf wind data were obtained from a BLM supported NDBO buoy stationed between Moorings 9 and 10. Additional wind and sea level data were obtained from coastal stations. Low-frequency (subtidal) time series of all data sets were obtained by filtering with a 40-HLP Lanczos filter kernal to remove variance associated with tidal and inertial motions. Semidiurnal tides are attenuated by more than 10^5 by the filter, which results in a 4-day truncation at the start and end of the records. The filtered data were subsampled every 6 hours and current and wind vectors were rotated to the local topography, such that the velocity components (u, v) are positive in the offshore and northward along-shelf directions, respectively.

IV. TECHNICAL DISCUSSIONS

4.1 INTRODUCTION

The following are a series of technical discussions of analysis or interpretation during Year 4. All Principal Investigators contributed to this chapter, however, it is not possible to associate a single author with each section. With the report organization used, certain PI's are responsible for parts of several sections. Section 1.2 provides a summary of general areas of each PI's emphasis.

Section 4.2 (Gulf Stream Variability) is of limited extent, since Dr. Otis Brown had little additional interpretive responsiblity in Year 4. However, the presented material represents a more detailed presentation of GS western boundary (GSWB) positions than was available in the Year 3 Final Progress Report (SAI 1982).

Section 4.3 (Winds and Waterlevels) documents several important topics including a summary of major tidal constituents in the SAB. This information was created by using some of the most up-to-date tidal analysis routines presently available. Section 4.4 is the result of a very preliminary look at data obtained on two hydrographic cruises on the N.C. shelf and offshore waters. Sections 4.5, 4.6, and 4.7 are the major interpretive activities supported during Year 4. These should be considered as intermediate results in a synthesis effort to continue through Year 5 of this program.

4.2 GULF STREAM VARIABILITY

Analysis has continued in evaluating the statistical character of the GSWB positions. As an extension of the more standard statistics presented in the Final Progress Report, Year 3, the present material provides a density function (relative frequency histogram) of the GS boundary position on each of several representative transects.

In developing this distribution, transects were established normal to the mean GSWB, then in each thermal image, the location of the GSWB on that transect was determined. These were then summarized by showing the percent (number of times) the GSWB was located in a given interval of the transect. The results as shown in Figure 4.2-1 are plots of relative frequency as a function of across-shelf location. Since all the basic data have been digitized, similar information could be developed for other transects of interest.

The distribution of GSWB positions as shown in the inserts in Figure 4.2-1, illustrates several key SAB processes. The southern transect (Transect 1) shows very low variability with a single dominant preferred location. This is an area where GSWB perturbations form and then migrate northward. These features are discussed in detail in Section 4.6 of this report. The location variability increases northward and seems to be fairly similar on the two Georgia Embayment transects (2 & 3).

Transect 3 is south of the Charleston Bump (CB) and Transect 4 is north of the CB. The GSWB has a bimodal distribution on Transect 4, which is to say the GSWB has two preferred locations separated by approximately 50 km. It can

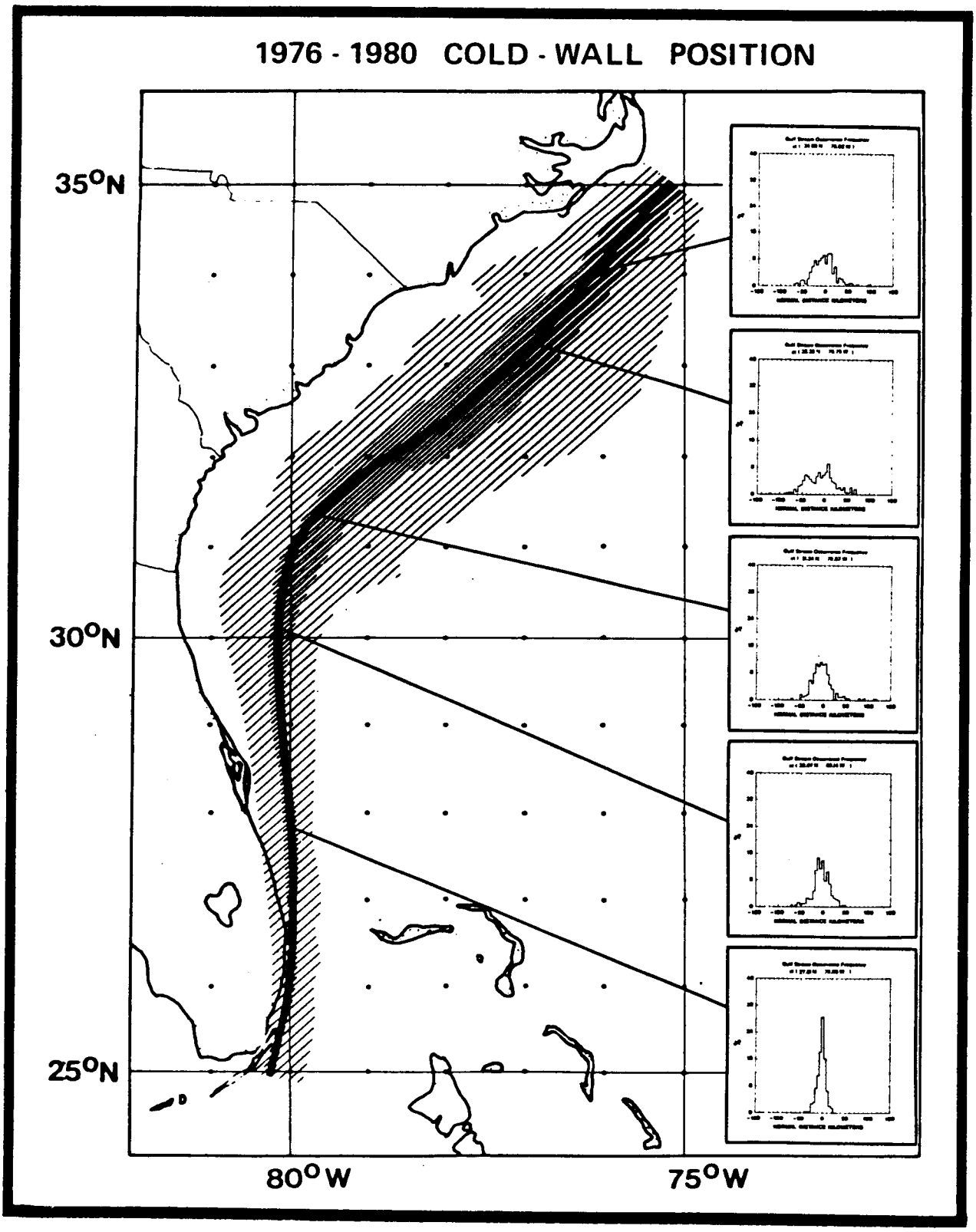

Figure 4.2-1. Stochastic characterization of GS western boundary (cold wall). The dark solid line is the mean position. The dark hatched area is one standard deviation; the light hatched area represents the range of extreme positions. The five panels to the right show the position histogram for shelf normal transects at indicated locations.

be surmised that the transition between these two locations is relatively rapid, compared to the residence times at the preferred positions. This condition is generally consistent with the notion that interaction of the GS and the Charleston Bump creates a semi-permanent meander in the GS. Some evidence suggests that this same interaction causes waves to form and propagate downstream. The form of the northern histogram on (Transect 5) is similar to that for Transect 3 in the Georgia Embayment.

4.3 WINDS AND WATER LEVELS

4.3.1 Hurricane David

Hurricane David was one of the major extra-tropical cyclones to cross U.S. waters in 1979. Between 3 and 5 September 1979, the low pressure center of David moved along the east Florida coast, eventually crossing the coastline a little north of Savannah before moving inland. The data from National Weather Service (NWS) coastal stations, offshore National Data Buoy Office (NDBO) buoys, and National Ocean Survey (NOS) coastal sea level stations are used to describe the large-scale response of the SAB to strong local (hurricane) wind forcing.

Hurricanes are usually thought of as compact storms. This is true if the region of hurricane force winds is considered. However, examination of surface atmospheric pressure maps shows that the hurricane wind regime may extend considerable distances from the center. In Hurricane David, winds up to about 1000 km from the center would be expected to be related to winds close to the low pressure (storm) center.

Sea-level records are available for the period during which Hurricane David occurred from the following coastal gauges: Fort Pulaski (867-0870), Charleston (866-5530), Winyah Bay (866-2746), Myrtle Beach (866-1070), and Oregon Inlet (865-2587). Figure 4.3-1 shows the original sea-level records, low-pass filtered, and the records corrected for the inverse barometer effect (1 cm mb^{-1}). Sea level tends to rise with decreasing atmospheric pressure so as to maintain a constant pressure beneath the sea surface. To resolve wind effects on sea level, this atmospheric pressure effect is removed. Figure 4.3-1 shows that the coastal sea level rise due to the hurricane is largely the result of wind, although close to the the storm center approximately 20 cm of the 80 cm sea level increase at Fort Pulaski (mouth of the Savannah River) is due to lower atmospheric pressure. Note that atmospheric pressure decreases away from the hurricane center. Also note the apparent northwards propagation of the sea-level peak due to the hurricane. This is opposite to the direction of free shelf wave propagation (Gill and Schumann 1974) and suggests a forced wave mode.

The winds (low-pass filtered) in north and east coordinates are shown in Figure 4.3-2 for the coastal stations, and buoys 41004 (off Charleston) and 41005 (off Savannah). North of Charleston as far as Cape Hatteras the winds are similar at the buoys and coastal stations. The closest approach of the low pressure center to the Cape Hatteras wind station was approximately 500 km. Wind stations at Savannah and Jacksonville show a different wind pattern during the storm (days 246-251, Figure 4.3-2), since these two stations were to the west of the hurricane track, while the other stations were north and east. The center of low pressure actually passed about midway between

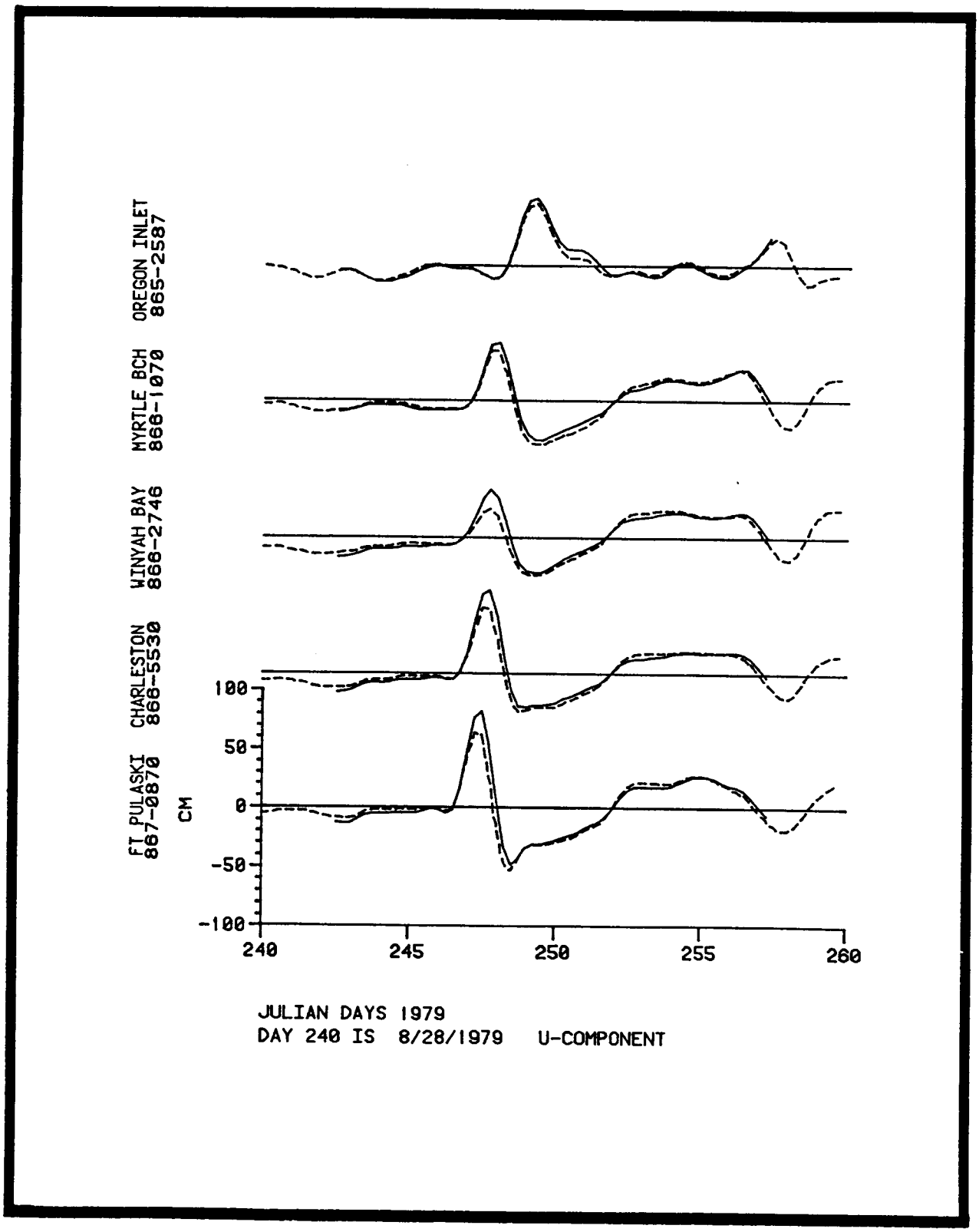

Figure 4.3-1. Low-passed filtered water levels for the indicated stations during passage of Hurricane David. Solid line = observed levels; dashed line = observed levels corrected for the inverse barometer effects.

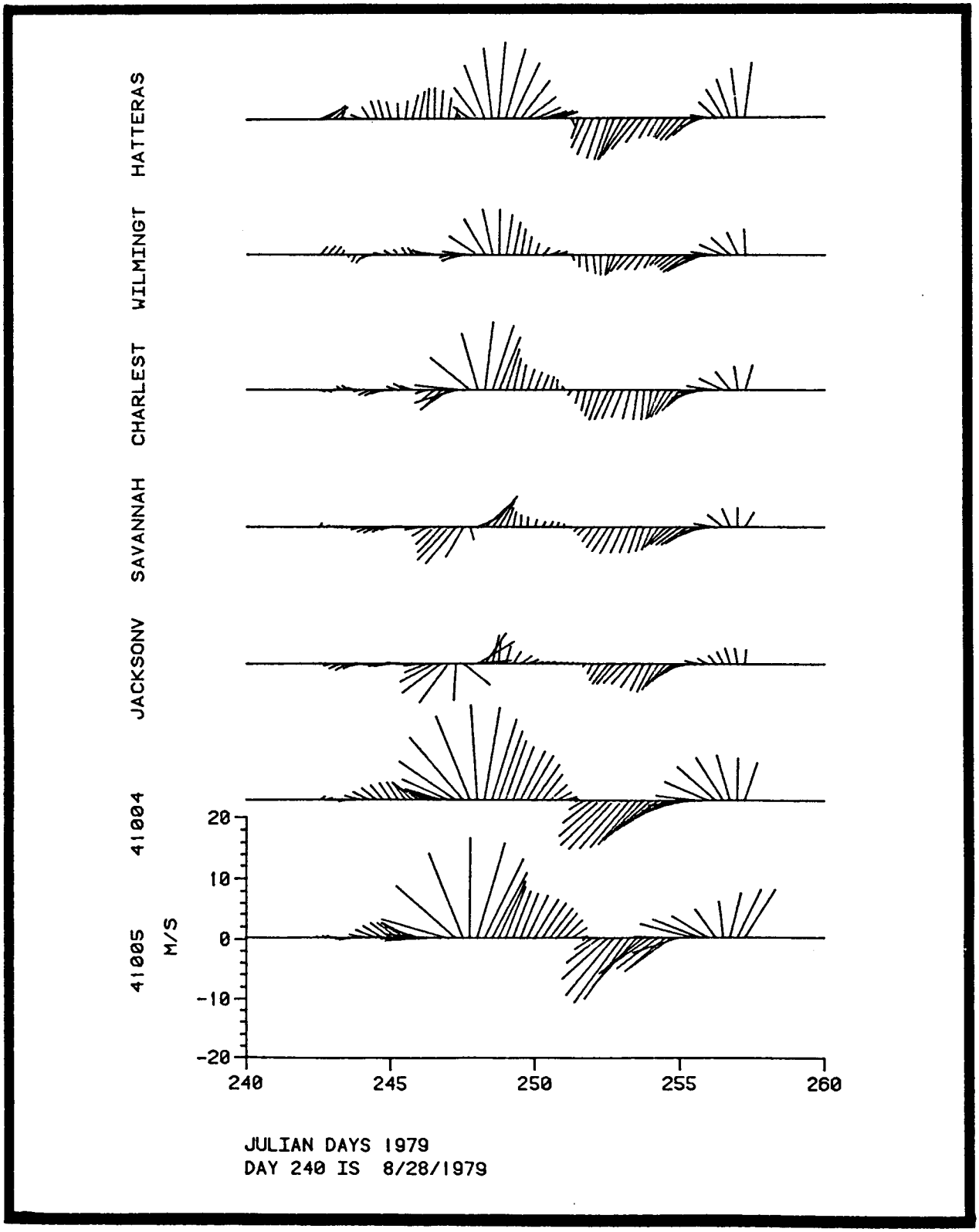

Figure 4.3-2 Stick diagram of NDBO buoy and coastal station low-passed winds during passage of Hurricane David.

Savannah and offshore buoy 41005; therefore (on day 246), the winds at these two stations are in approximately opposite directions. If sea level at Fort Pulaski is primarily forced by local winds, then it is expected that the sea-level peak due to hurricane winds is more closely related to buoy 41005 winds than Savannah winds, because buoy 41005 winds would be more representative of winds over the continental shelf.

The alongshore wind drives set-up and set-down of coastal sea level. Therefore, coastal winds at Savannah, Charleston, and Wilmington and winds at Buoys 41004 and 41005 have had the coordinate system rotated clockwise by 50°, so that the u component of velocity is parallel to the predominant trend of the isobaths and coastline in this region. The along-shelf and cross-shelf wind components are shown in Figures 4.3-3 and 4.3-4, respectively. In this coordinate system, the longshore winds have a similar pattern at all stations (from Daytona to Hatteras), though with differing magnitudes of the positive maximum at about days 247-248. The apparent northward propagation of the peak is also in evidence north of Savannah. The cross-shore wind component does show a difference between the coastal stations south of, and including Savannah, and the buoys and remaining coastal stations in South, and North Carolina. Notice the strong onshore peak for these latter stations which precedes the strong positive alongshore peak by about half a day.

Tables 4.3-1 and 4.3-2 show normalized correlation coefficients between sea level and alongshore winds versus alongshore winds for selected pairs of stations. Sea level versus local alongshore wind (Table 4.3-1) shows that the fluctuations in water level are strongly inversely correlated with the longshore wind with a 12 to 18 hour lag. (A positive lag in Table 4.3-1 and 4.3-2 indicates that the first series lags the second series by the indicated number of hours). In contrast, there is little consistent pattern in correlations between cross-shelf component (u) and the wind and water level. The water level at Oregon Inlet is correlated moderately and directly with both components of the wind, with lags of less than 6 hours. This is in contrast with the southern stations, but may be explained from the position of Oregon Inlet tide gauge, on the Pamlico Sound side of the Outer Banks barrier Island. Water-level variations at the Oregon Inlet tide station are due more to the wind over the shallow Pamlico Sound and are essentially out of phase with the set-up on the ocean-side of the inlet. However, for our purposes the Oregon Inlet record indicates that there is a response related to the winds of Hurricane David.

Table 4.3-2 shows high correlations between pairs of sea-level stations and corresponding pairs of wind stations. It is noteworthy that Fort Pulaski leads Myrtle Beach sea level by 12 hours, and buoy 41005 longshore wind leads Wilmington longshore wind by 12 hours; indicating that for the Georgia and South Carolina coasts, water level response apparently travels northward at approximately the same speed as the longshore component of the wind, so that water level response to the large impulse provided by a northward moving hurricane is essentially due to the wind local to the tide station. The anomalous behavior of Oregon Inlet tide gauge is also noted in this table, showing large apparent lags between Oregon Inlet and the Georgia Bight which are not reflected in the winds.

The NDBO buoys also measure sea-surface temperature, and Figure 4.3-5 shows the alongshore and cross-shore winds from the buoys as well as sea-

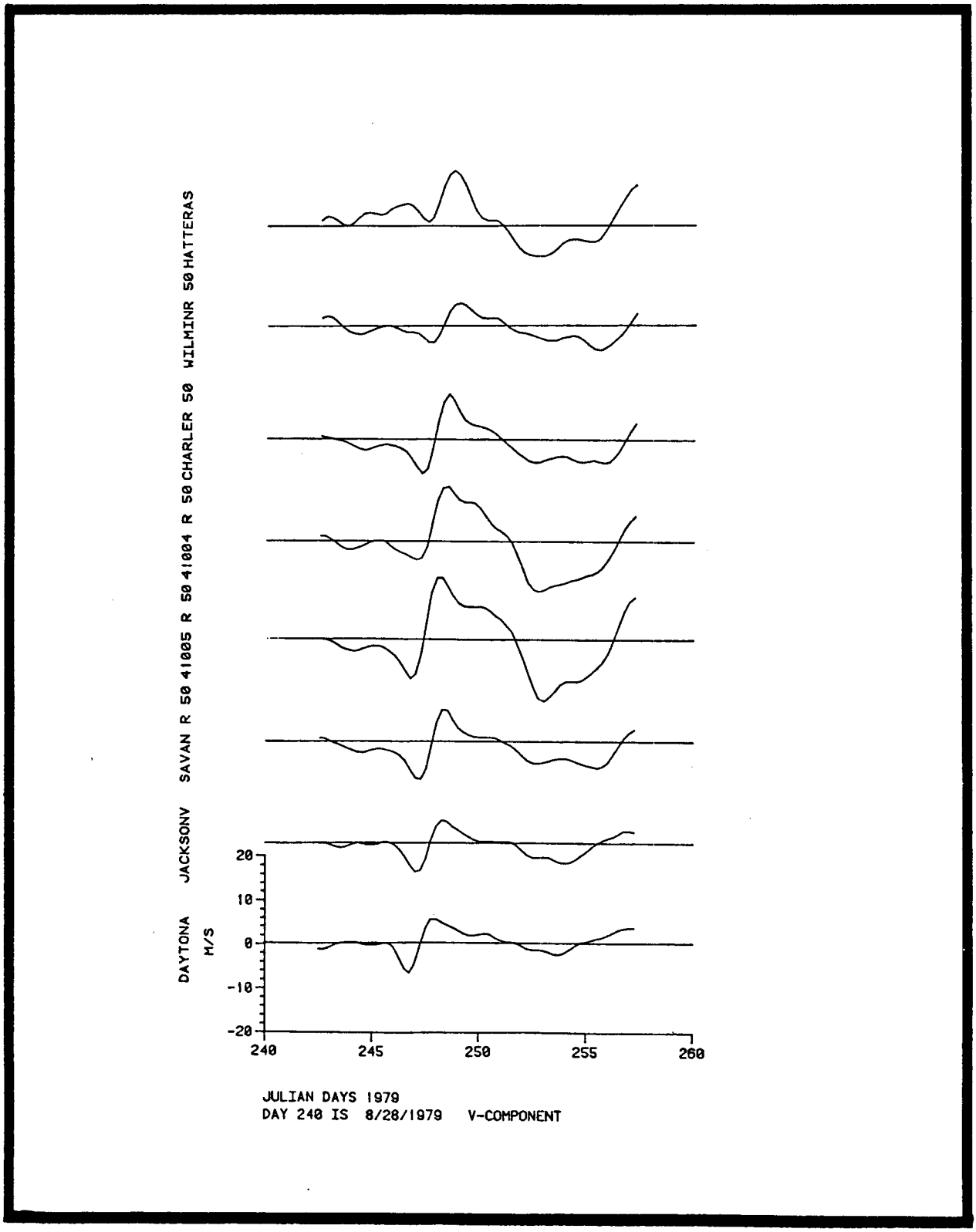

Figure 4.3-3. Longshore component of the low-passed wind records for the indicated coastal stations and NDBO buoys during passage of Hurricane David.

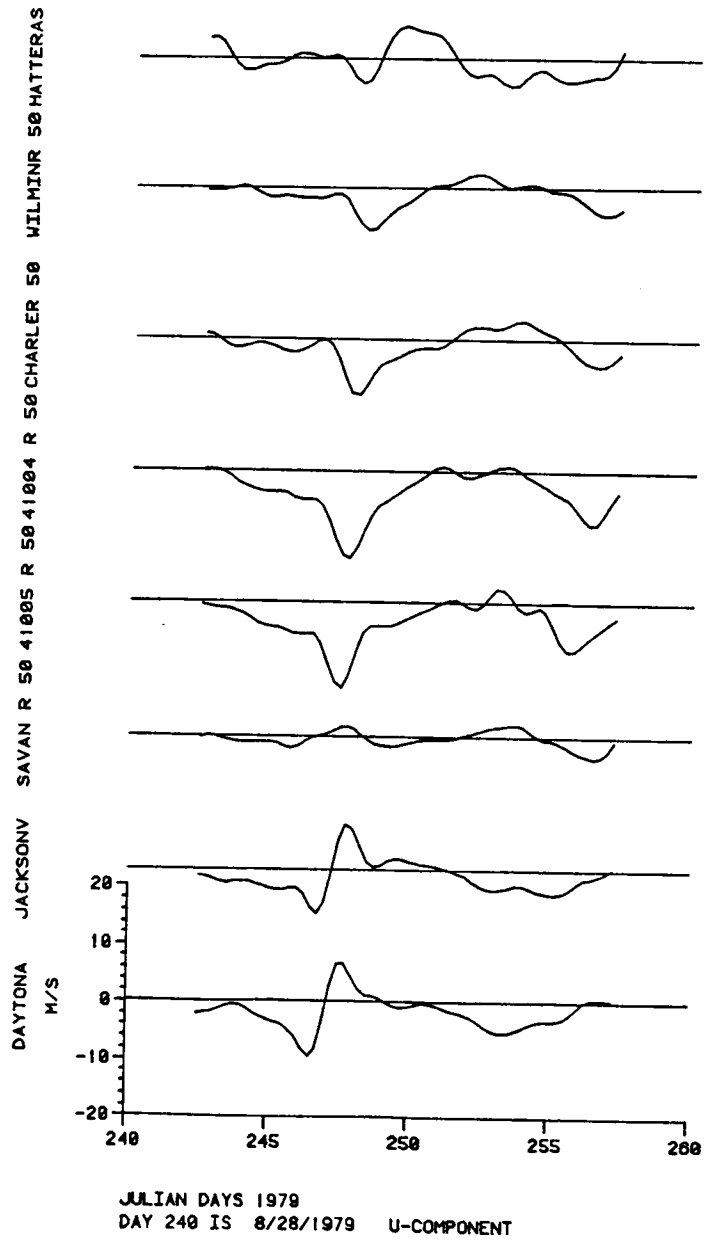

Figure 4.3-4 Cross-shore component of low-passed wind records for the indicated coastal stations and NDBO buoys during passage of Hurricane David.

Table 4.3-1. Sea-level cross-correlation coefficients

Sea Level	vs	Sea Level (V)	C_o	C_m	Lag	Sea Level	vs	Cross Shore Wind (U)	C_o	C_m	Lag (Hours)
Ft. Pulaski 867-0870		41005	-0.675	-0.864	12	Ft. Pulaski 867-0870		41005	-0.370	-0.370	-6
Charleston 866-5530		41004	-0.598	-0.804	12	Charleston 866-5530		41004	-0.069	-0.516	-6
Charleston 866-5530		Charleston	-0.711	-0.874	12	Charleston 866-5530		Charleston	-0.069	0.691	24
Mrytle Beach 866-1070		41004	-0.501	-0.852	18	Myrtle Beach 866-1070		41004	-0.431	-0.431	0
Myrtle Beach 866-1070		Charleston	-0.516	-0.894	18	Myrtle Beach 866-1070		Charleston	-0.135	0.722	36
Oregon Inlet 865-2587		Hatteras	0.615	0.694	6	Oregon Inlet 865-2587		Hatteras	0.621	0.710	-6

Table 4.3-2. Sea-level cross-correlation coefficients

Sea Level	vs	Sea Level	C_o	C_m	Lag	Longshore Wind	vs	Longshore Wind	C_o	C_m	Lag
Ft. Paluski		Myrtle Beach	0.674	0.938	-12	41005		Wilmington	0.667	0.824	-12
Charleston		Myrtle Beach	0.903	0.960	-6	Savannah		Wilmington	0.788	0.882	-6
Ft. Paluski		Oregon Inlet	-0.558	0.517	-48	Charleston		Wilmington	0.840	0.890	-6
Charleston		Oregon Inlet	-0.595	0.588	-42	Charleston		Hatteras	0.753	0.753	0
Myrtle Beach		Oregon Inlet	-0.603	0.488	-36	41004		Hatteras	0.847	0.847	0

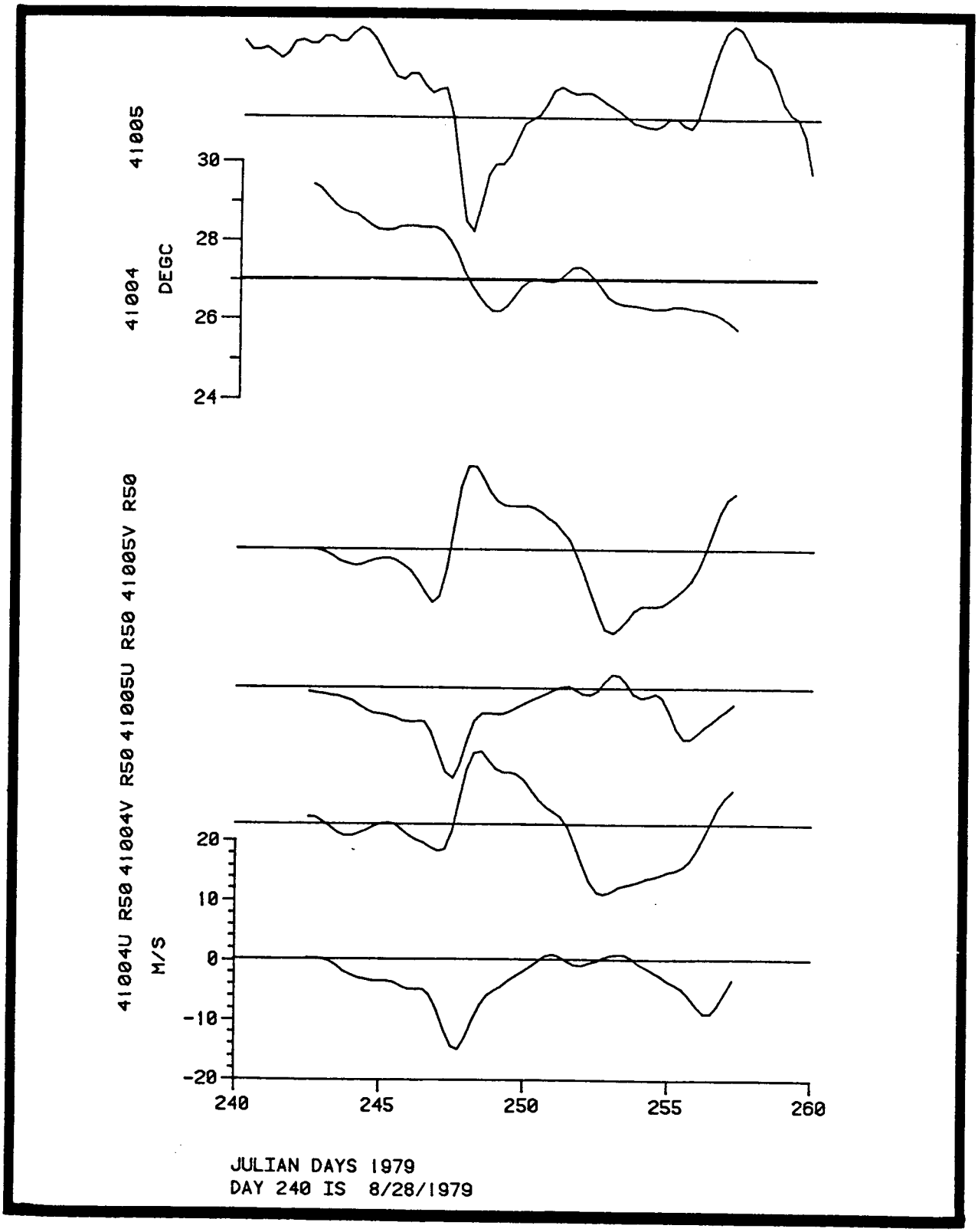

Figure 4.3-5. Cross-shore and longshore low-passed components of the wind and sea surface temperature records from NDBO buoys during passage of Hurricane David.

surface temperature. Buoy 41005 shows a large 3°C drop followed by a slower rise during the period when the hurricane was closest to the buoy. The buoy (41004) further north shows a less precipitous drop, with little recovery, which occurs later than the cooling at buoy 41005. The drop at buoy 41005 may be due to intensive mixing with cooler bottom water, and the subsequent recovery due to restratification or intrusion of Gulf Stream water on the shelf.

The conclusions for this section are that sea level changes during Hurricane David along the Georgia and South Carolina Coasts are best explained as a response to local longshore wind fields. Near the center of the hurricane, inverse barometer effects will substantially contribute to sea level rise.

4.3.2 Regional Wind Forcing of Water Levels in the SAB

4.3.2.1 Introduction

The greatest north-south coverage of water-level data in the SAB is in 1979, where the southern station is Tiger Island (32°42.3'N, 81°28.2'W), a platform off the coast near Jacksonville, and the northern station is the Chesapeake Bay Bridge Tunnel. Two periods of 64 days were chosen for analysis, beginning on 16 February 1979 and 4 April 1979, respectively. A period of 64 days was used for the analysis so that signals with periods of 10- to 12- days and shorter are resolved, but there is little contamination of the low frequency spectra from seasonal trends in the data. A 64-day time series when decimated to 6-hourly intervals produces a series which is an exact power of two in length which makes for efficient fast fourier tranforms. The first period uses data from the following stations: Chesapeake Bay Bridge Tunnel; Beaufort Marine Lab, N.C.; Southport, N.C.; Myrtle Beach, S.C.; Winyah Bay, S.C.; Charleston, S.C.; and Tiger Island, Ga. The second period excludes Beaufort because the station was not operating, but includes Fort Pulaski, Ga., which was operating.

In the Mid-Atlantic Bight, the sharp bend in the coastline at the mouth of the New York Bight divides the sea-level response into regions. A locally wind-forced response dominates from Cape Cod to Cape May, while a southward propagation of 600 km day^{-1} was not correlated with the local wind (Wang 1979). In the South Atlantic Bight, the coastline also bends in the region of the Georgia Bight, and previous BLM studies for the South Carolina and North Carolina coasts (SAPOS Year 3 Final Progress Report) and Chao and Pietrafesa (1980) for North Carolina, have indicated that the water-level response is locally forced. The previous section, on the response to an impulsive wind, (Hurricane David) also shows that sea-level response between Savannah and Cape Hatteras is best described as locally forced by the longshore component of the wind.

However, some important questions remain. They are: How much of the southward traveling wave in the Mid-Atlantic Bight propagates around Cape Hatteras and contributes to sea-level response in the South Atlantic Bight? Additionally, does sea-level response south of Savannah differ from the locally forced regime in the Georgia Bight? There is some evidence from Florida tide gauges (Brooks and Mooers 1977) that southward propagation of sea level along the Florida coast contributes to the sea-level response.

The methods used to investigate these questions are to predict the locally wind-driven component of sea level, using transfer functions in the frequency domain and investigating the relationships of residual sea level, obtained by subtracting the predicted from the original time series. The technique used for the prediction is described in detail in the SAPOS Year 3 Final Report. A brief review is given below.

4.3.2.2 Analysis

Wind and tide data were processed as follows. The tide data were corrected for the inverse barometer effect and filtered by a 40-HLP filter and then decimated to 6-hour intervals. Since wind stress is the forcing function for shelf waters, wind velocities (u,v) were converted to wind stress components (τ_x,τ_y) by the relations:

$$\tau_x = c\rho_a\, u|u|$$

$$\tau_y = c\rho_a\, v|v|$$

where the coefficient of friction, c , was taken to be 0.0013 and ρ_a is air density. The wind stress components were subsequently 40-HLP filtered and then decimated to 6-hour intervals similar to the water-level time series. The main wind stress component of interest is the alongshore component, so coordinate axis rotation of 50° clockwise from true north are used for the Savannah, Charleston, and Wilmington wind records, as in the previous section. The alongshore component for Hatteras and Jacksonville is taken to be in the north direction. The sets of data beginning 16 February 1979 and 4 April 1979 will be designated by February and April respectively. Though data from buoys 41004 and 41005 were available for these periods, they did not correlate with nearby water-level data significantly better than data from the coastal weather stations. Therefore, for consistency, only the coastal weather station winds are used.

Figures 4.3-6 through 4.3-12 show low-frequency water-level spectra and spectra of the alongshore wind stress of the nearest coastal weather station. Also shown are coherence squared and phase difference between the two series for the February period. A general feature of most records is the decreased energy for frequencies higher than 0.4 cpd in both wind and tide records, which is usually accompanied by a drop in the coherence level. Therefore, processing of these spectra was performed for the frequency band 0-0.4 cpd. Except for Tiger Island (872-0008) and Chesapeake Bay Bridge Tunnel (867-8863), the records show high coherence between alongshore wind stress and water-level records. Comparing Figures 4.3-6 and 4.3-7 shows that Tiger Island is less coherent with alongshore wind stress from the closest weather station at Jacksonville than with wind stress from Savannah further to the north. Recall that there is a 50° shift in the v axis between Jacksonville and Savannah, and these alongshore components of wind are less well correlated than components in the N and E coordinate system. This indicates that sea level at Tiger Island is closely related to the locally forced sea level in the Georgia Bight, and this locally forced signal in the Bight is propagating southward towards the east Florida shelf. Therefore, for the wind-forced prediction, Savannah wind data will be used for Tiger Island.

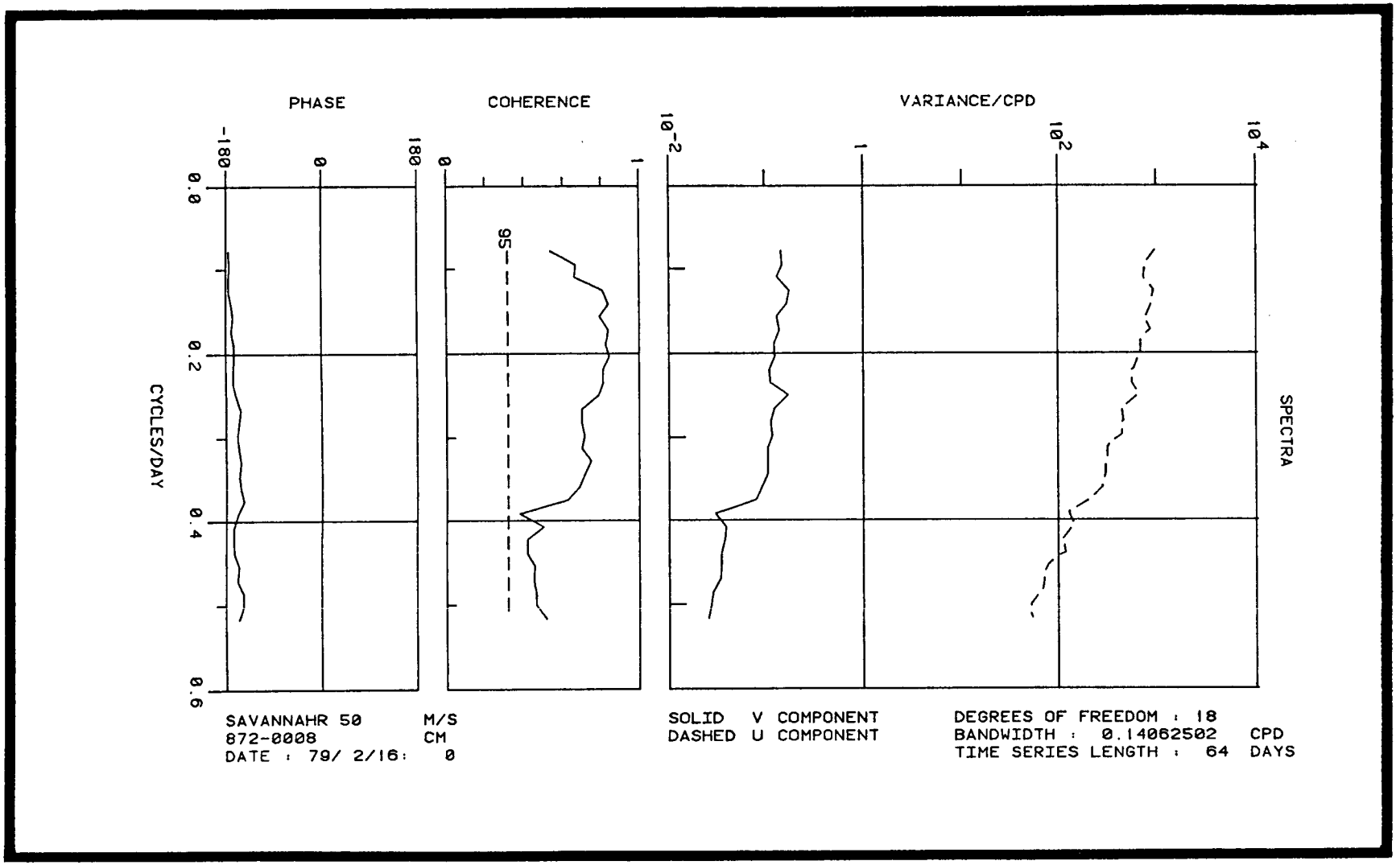

Figure 4.3-6 Spectra, coherence squared, and phase difference for Savannah longshore wind stress and water level from 872-0008 (Tiger Island, Fla.).

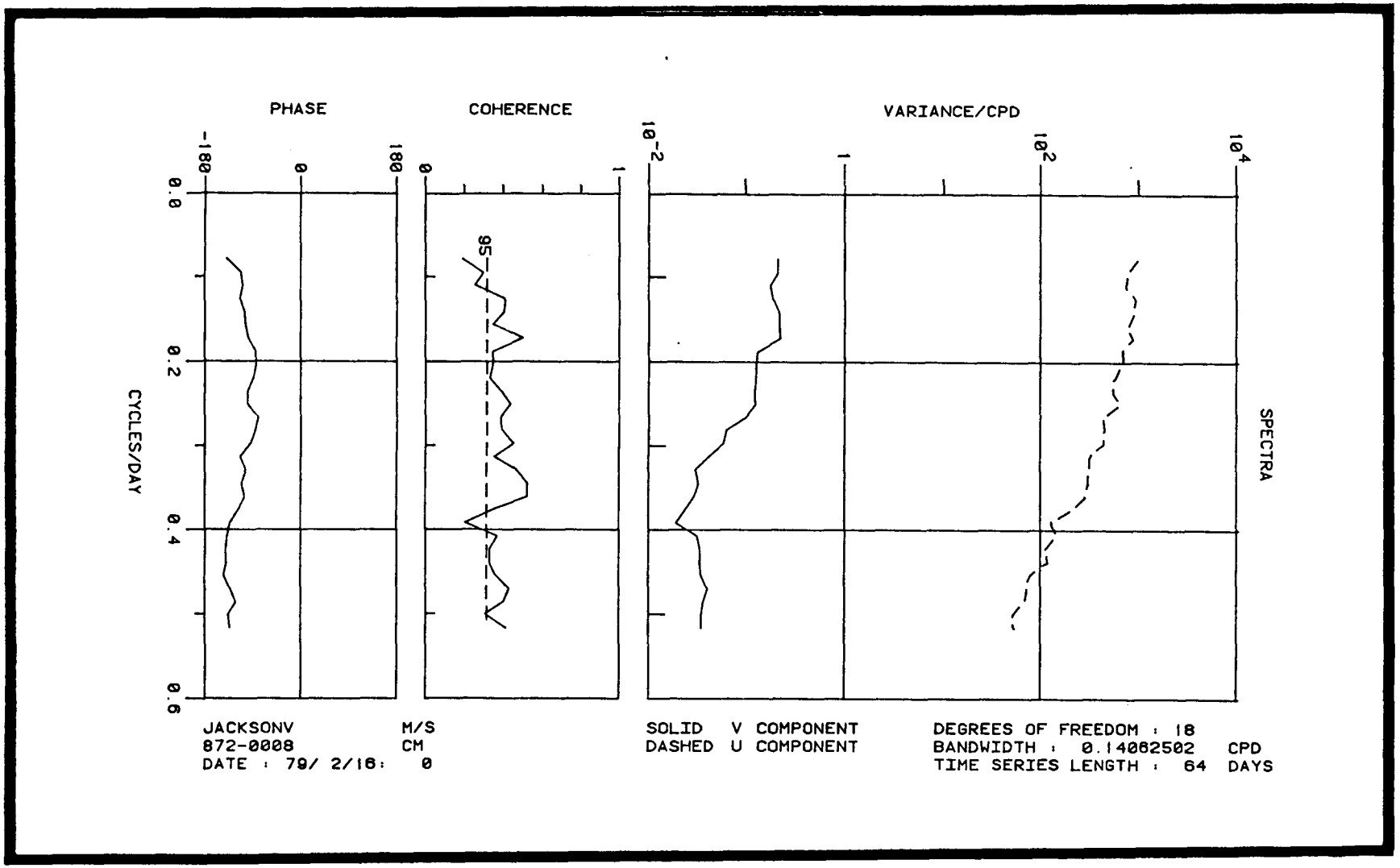

Figure 4.3-7 Spectra, coherence squared, and phase difference for Jacksonville longshore wind stress and water level from 872-0008 (Tiger Island, Fla.).

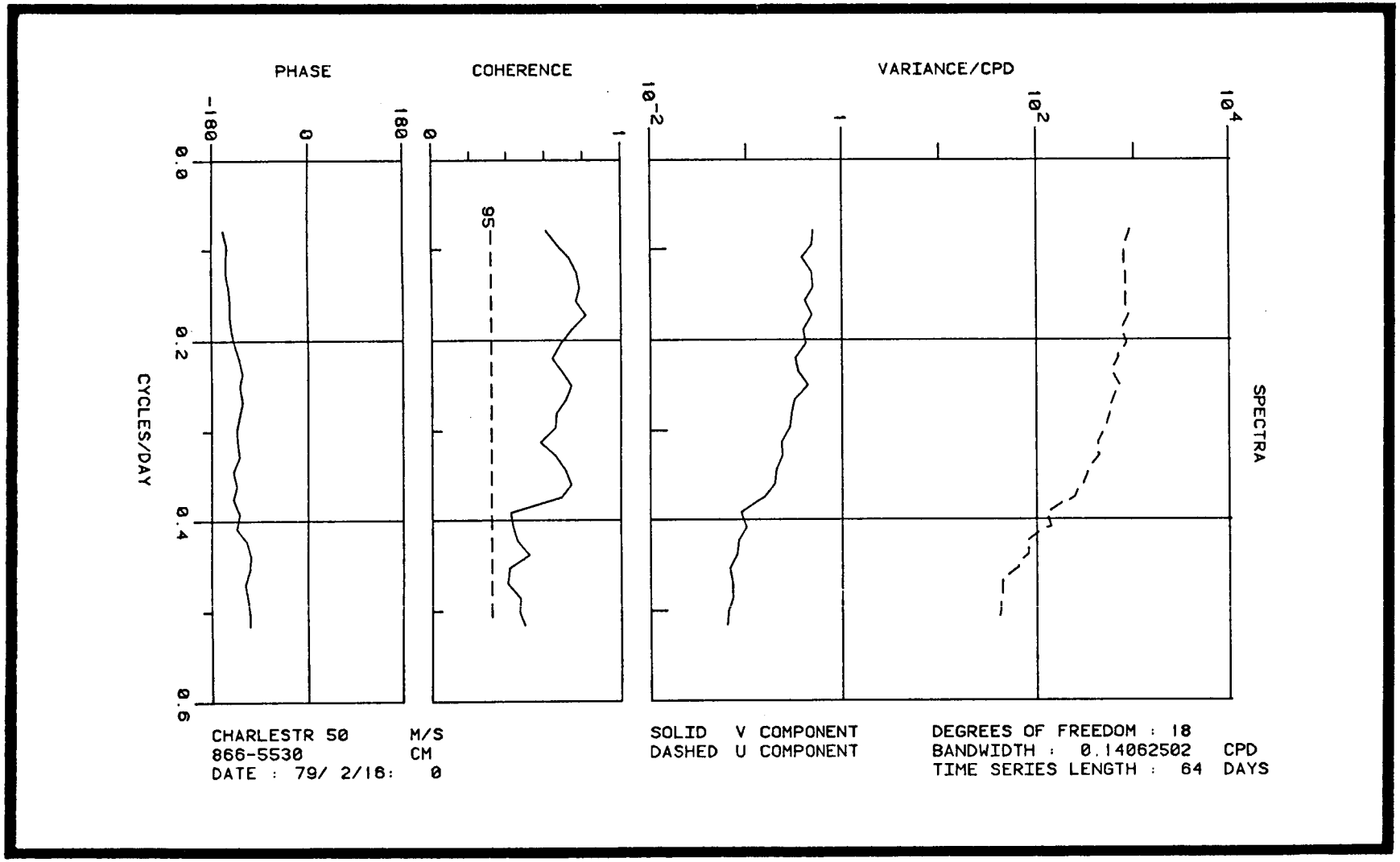

Figure 4.3-8 Spectra, coherence squared, and phase difference for Charleston longshore wind stress and water level from 866-5530 (Charleston, S.C.).

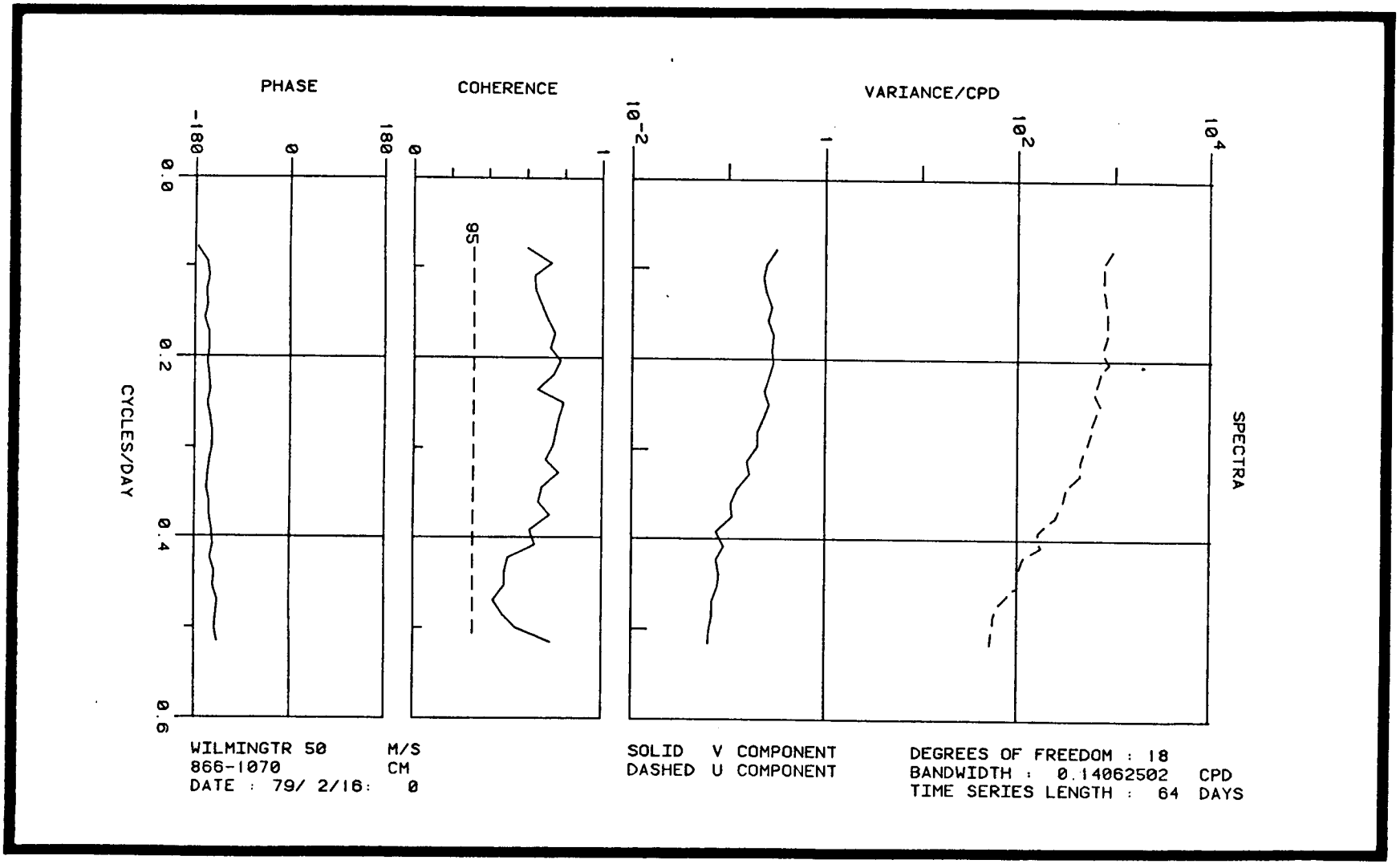

Figure 4.3-9 Spectra, coherence squared, and phase difference for Wilmington longshore wind stress and water level from 866-1070 (Myrtle Beach, S.C.).

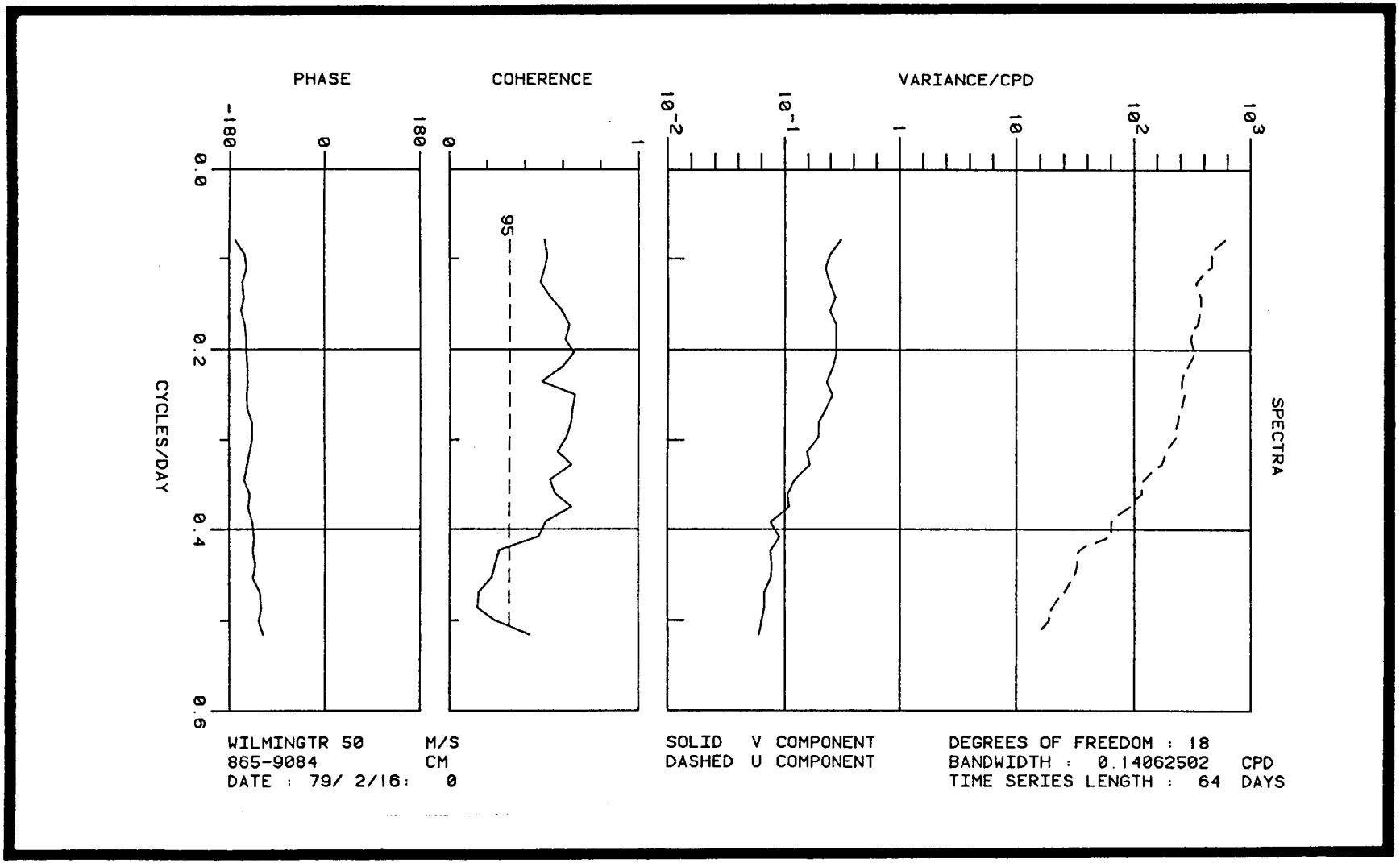

Figure 4.3-10 Spectra, coherence squared, and phase difference for Wilmington longshore wind stress and water level from 865-9084 (Southport, N.C.)

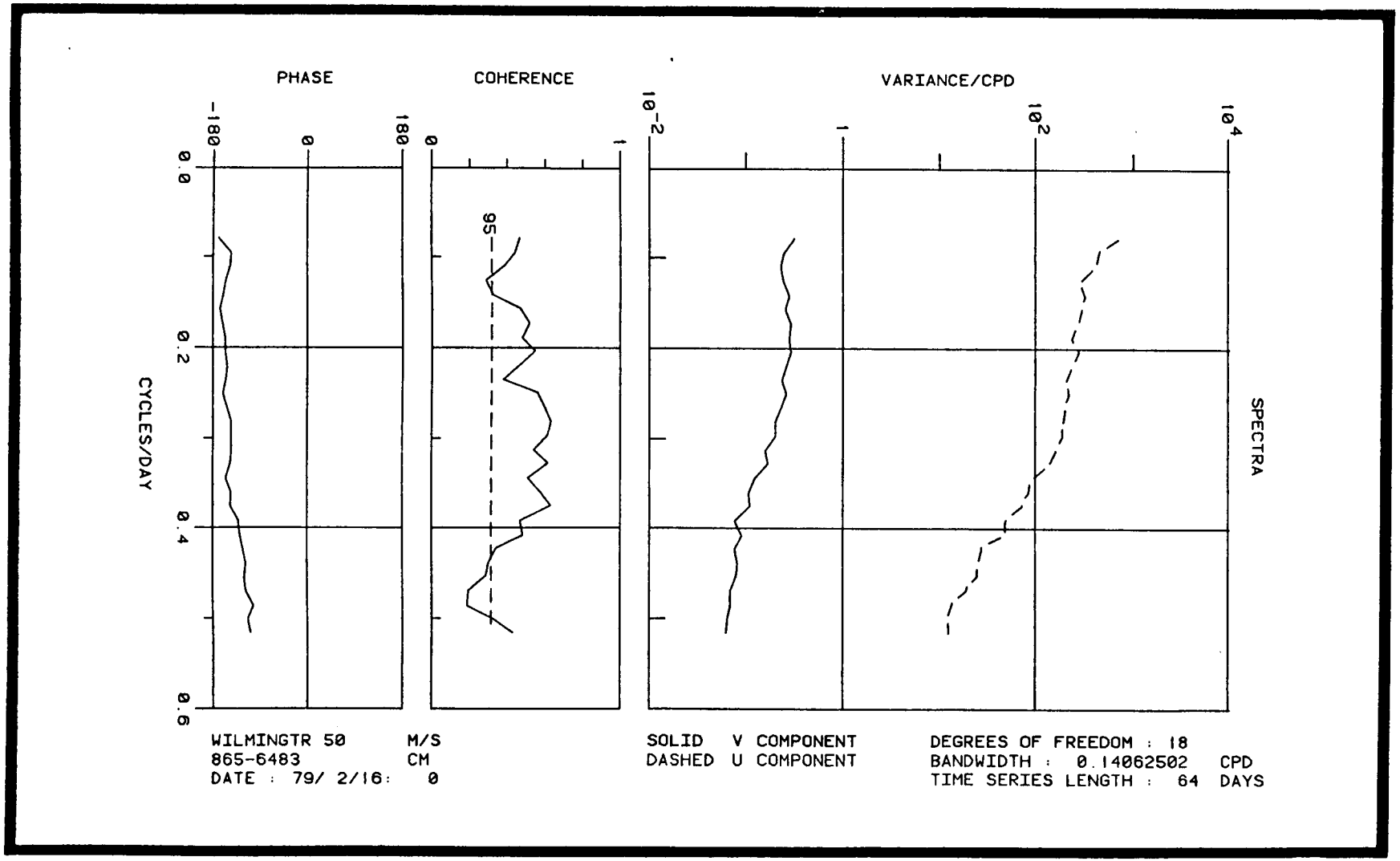

Figure 4.3-11. Spectra, coherence squared and phase difference for Wilmington longshore wind stress and water level from 865-6483 (Beaufort, N.C.)

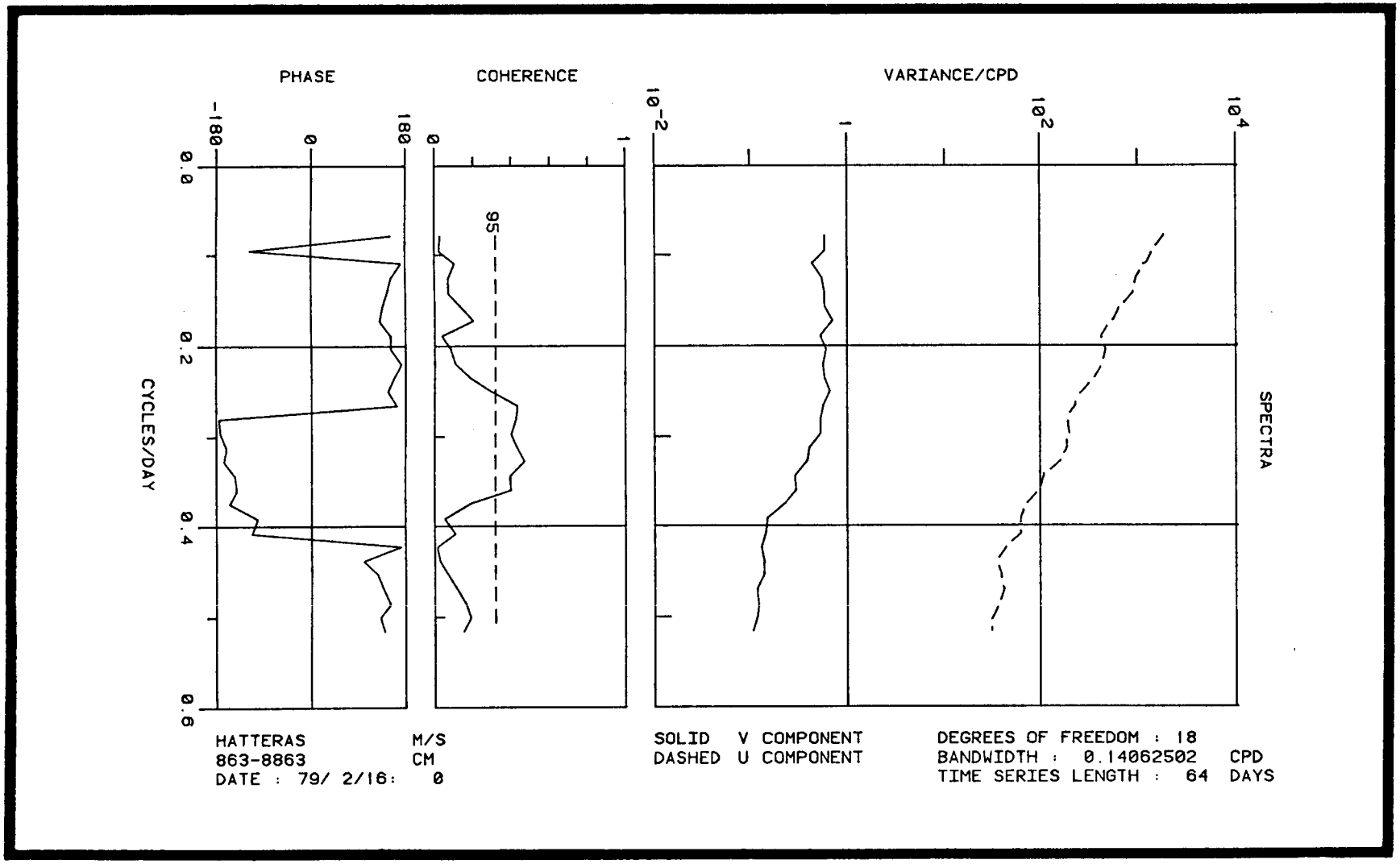

Figure 4.3-12. Spectra, coherence squared, and phase difference for Hatteras longshore wind stress and water level from 863-8863 (Chesapeake Bay Bridge Tunnel).

Chesapeake Bay Bridge Tunnel water levels show little or no correlation with Cape Hatteras alongshore wind stress, except around 0.3 cpd. The coherence levels increase between alongshore wind stress and water levels moving south from Cape Hatteras.

A similar sequence of figures (Figures 4.3-13 through 4.3-20) shows similar results for the April period, with Tiger Island being more coherent with Savannah alongshore wind stress than with Jacksonville. Chesapeake Bay Bridge Tunnel sea level is barely coherent with Hatteras winds. Coherence levels are generally a little higher in April than in February for the center of the SAB, with the lack of energy and coherence above 0.4 cpd being more marked for the later period.

Transfer functions between predictor (alongshore wind stress) and sea-level time series are given in Table 4.3-3. Both April and February data sets show the same structure. Myrtle Beach sea level is the best prediction, and the phase relationships are consistent with wind-forced flow, with sea level being approximately out of phase with, and lagging the wind. The April data set shows a general increase in transfer-function amplitude from north to south. February shows approximately the same trend with the exception of Charleston and Winyah Bay, which are less well predicted than in April.

The transfer functions are used to predict sea-level time series at each station. This predicted time series is subtracted from the original water-level time series to produce nonwind-driven residual time series. These residual time series and the original time series are shown in Figures 4.3-21 and 4.3-22. Of course, if the sea-level record is perfectly predicted then the residual would be zero. If the sea-level time series are not related to the alongshore wind stress, then the residual time series would be identical to the original sea-level series. Note that because of the 10% cosine taper applied before the spectra is calculated, the beginning and end of the residual series are forced close to zero, and so the predictions appear to be enhanced at these times. Generally the larger wind-driven peaks are well predicted, but some of the longer period fluctuations are not. For example, Figure 4.3-22, between days 130 and 136, shows a fluctuation in the residual which is close to the original at all stations and appears to propagate southwards through all the stations.

Since sea level at Tiger Island is not well related to local wind, but is related to the alongshore wind at Savannah, it is of interest to see how much of residual sea level is related to the alongshore wind stress at Jacksonville. During the February period there is no relation between local Jacksonville winds and residual sea level (Figure 4.3-23), but for April there is moderate coherence at low frequencies (0.1 cpd) (Figure 4.3-24). Thus sea-level fluctuations at Tiger Island are dominated by southward leakage of the wind-driven mode in the Georgia Bight. The mechanism has been recently modeled by Chao (1981) and is basically due to the tendency of sea-level fluctuations to propagate southwards in the form of barotropic shelf waves. The "leakage" is primarily due to the change in spatial structure of the alongshore wind stress, as the orientation of the coast lines changes even though the total wind field (i.e. the vector) is highly spatially coherent in this region.

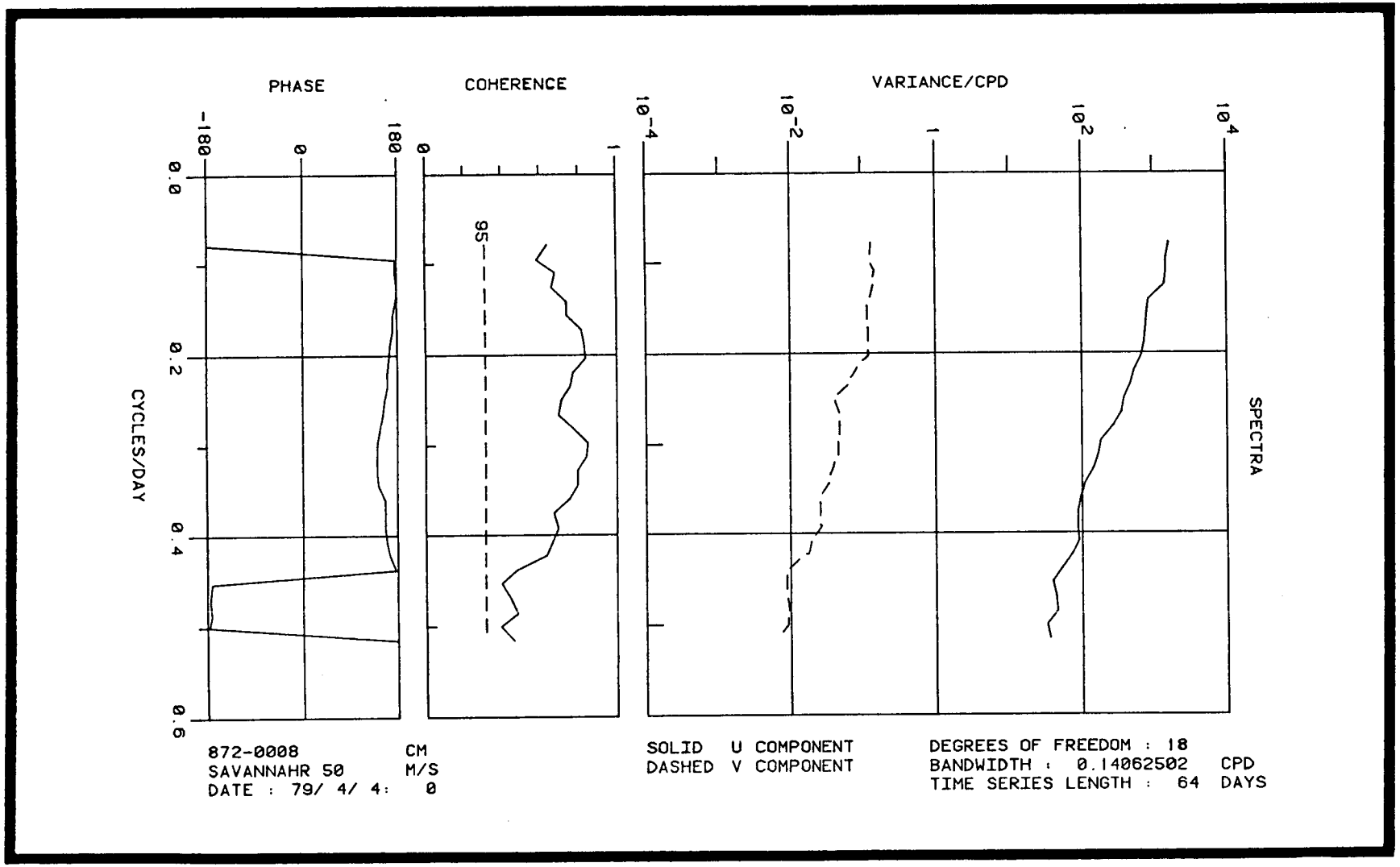

Figure 4.3-13. Spectra, coherence squared, and phase difference for Savannah longshore wind stress and water level from 872-0008 (Tiger Island, Fla.) for April-May 1979.

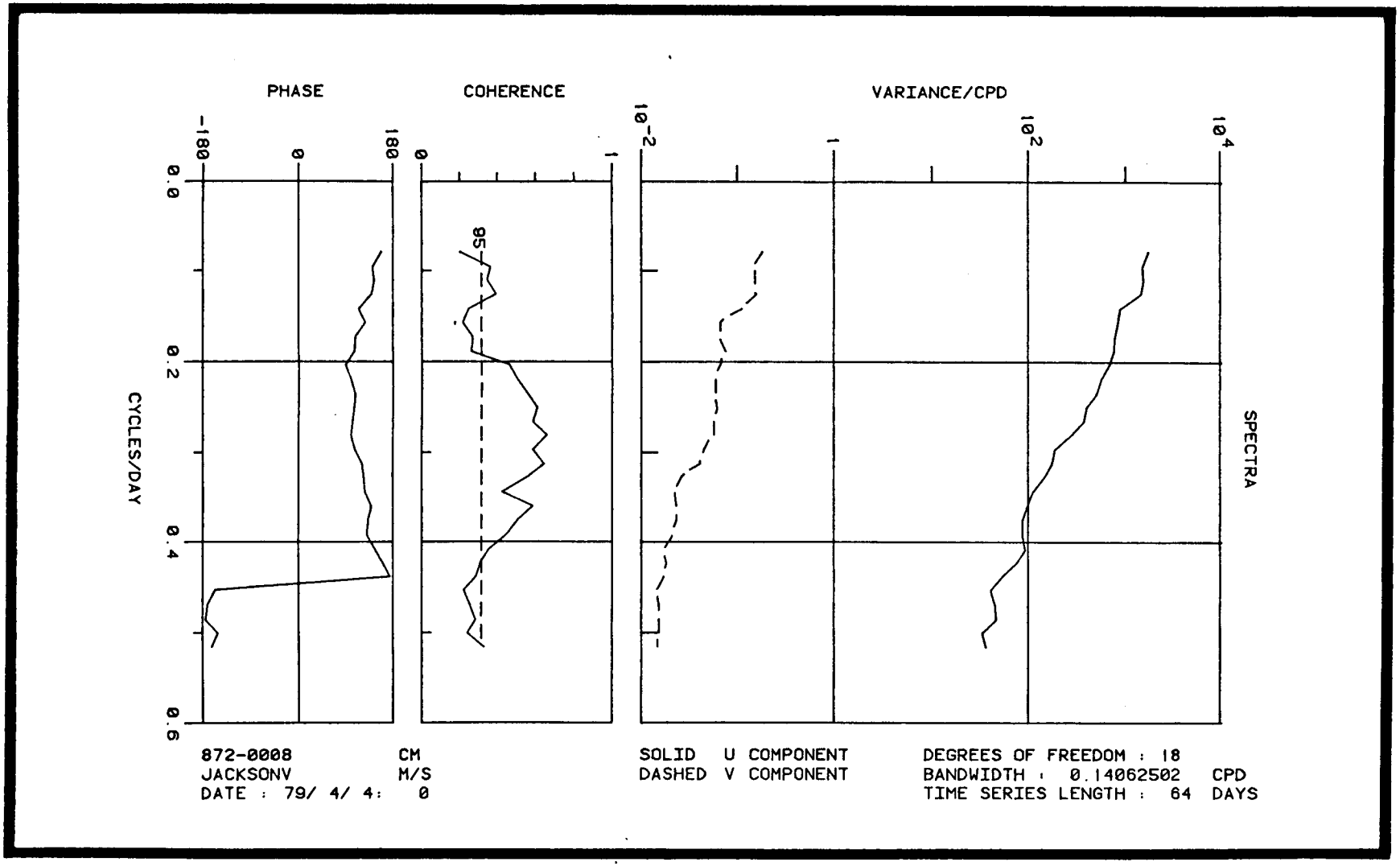

Figure 4.3-14. Spectra, coherence squared, and phase difference for Jacksonville longshore wind stress and water level from 872-0008 (Tiger Island, Fla.) for April-May 1979.

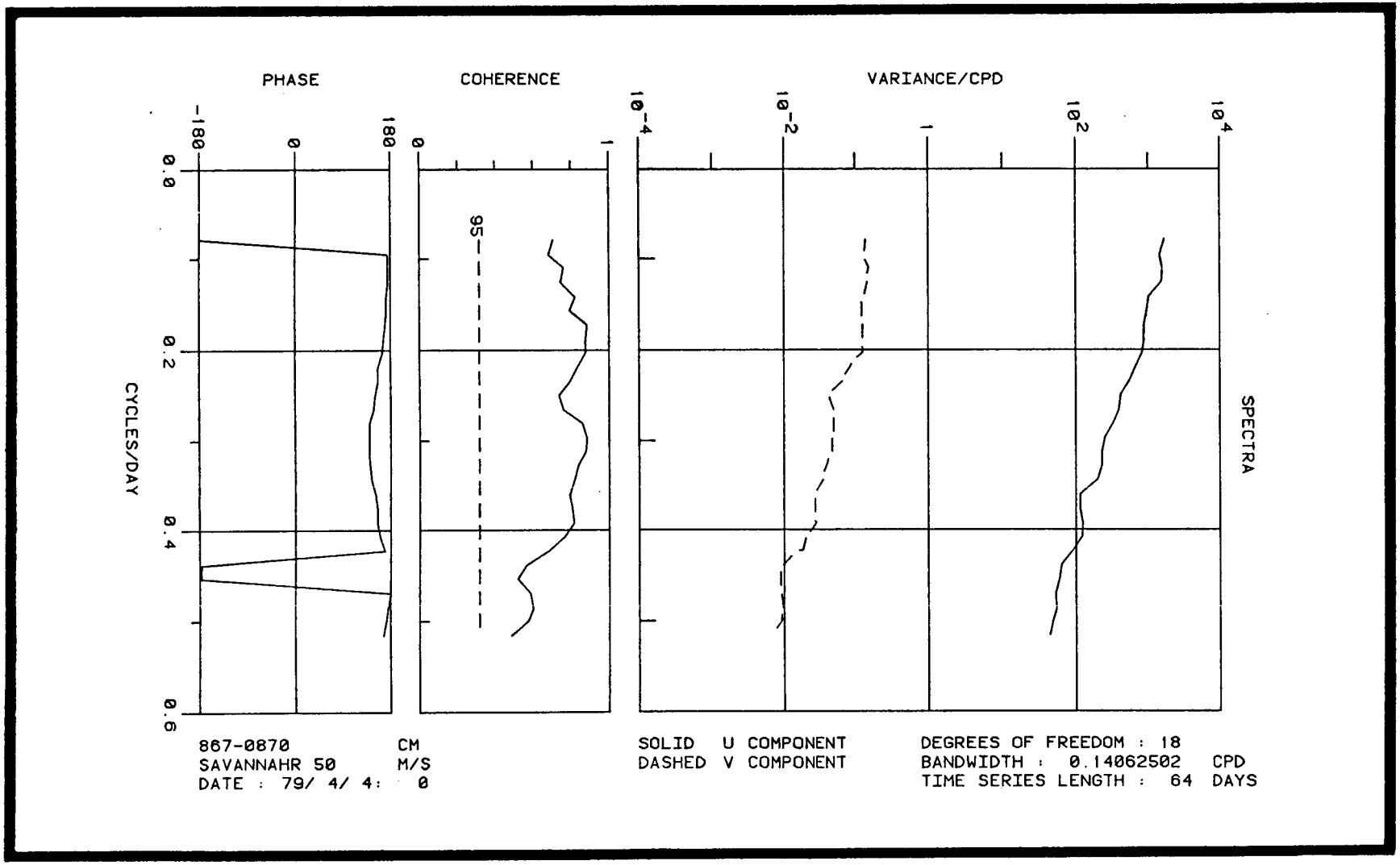

Figure 4.3-15. Spectra, coherence squared and phase difference for Savannah longshore wind stress and water level from 867-0870 (Fort Pulaski, Ga.) for April-May 1979.

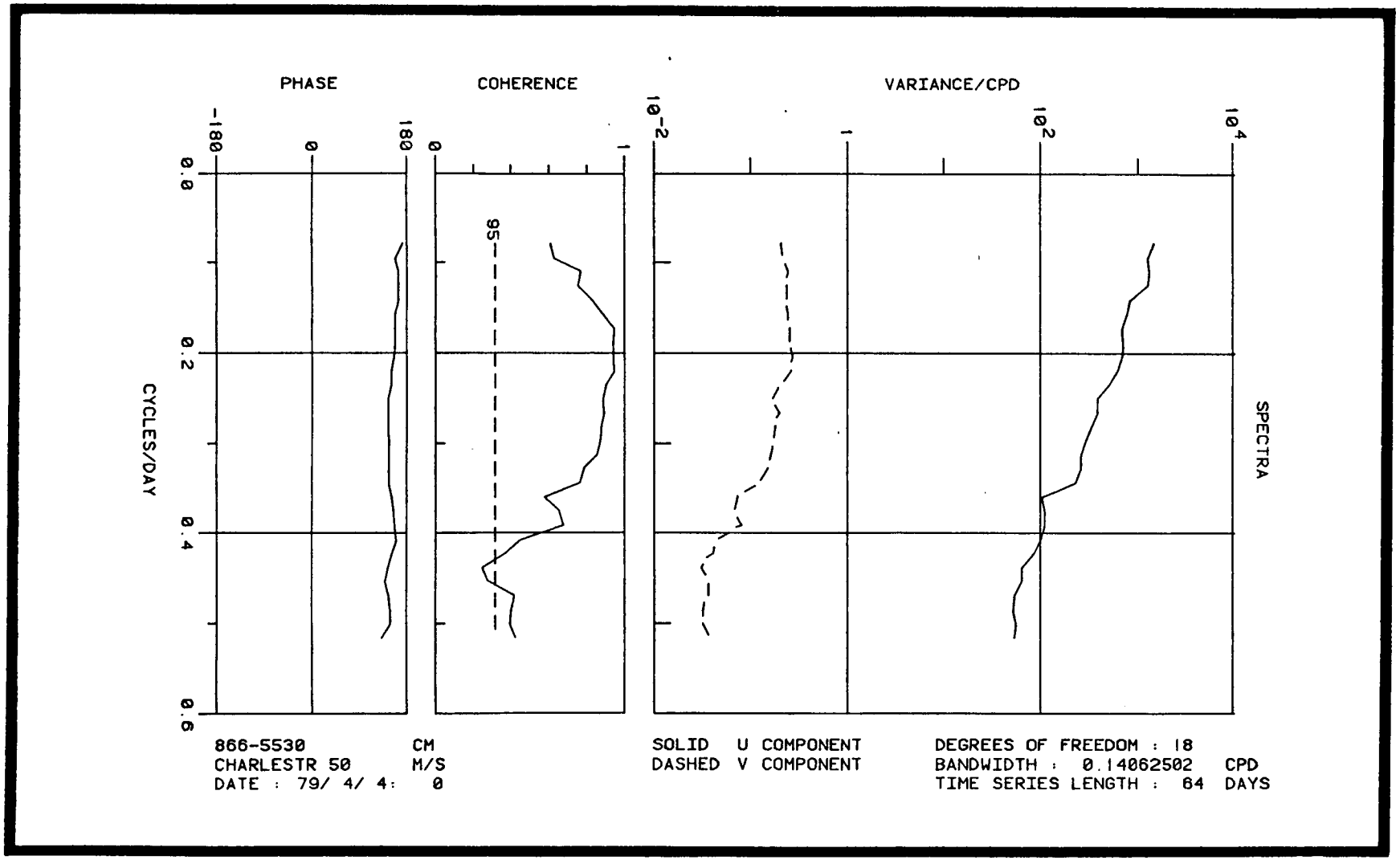

Figure 4.3-16. Spectra, coherence squared, and phase difference for Charleston longshore wind stress and water level from 866-5530 (Charleston, S.C.) for April-May 1979.

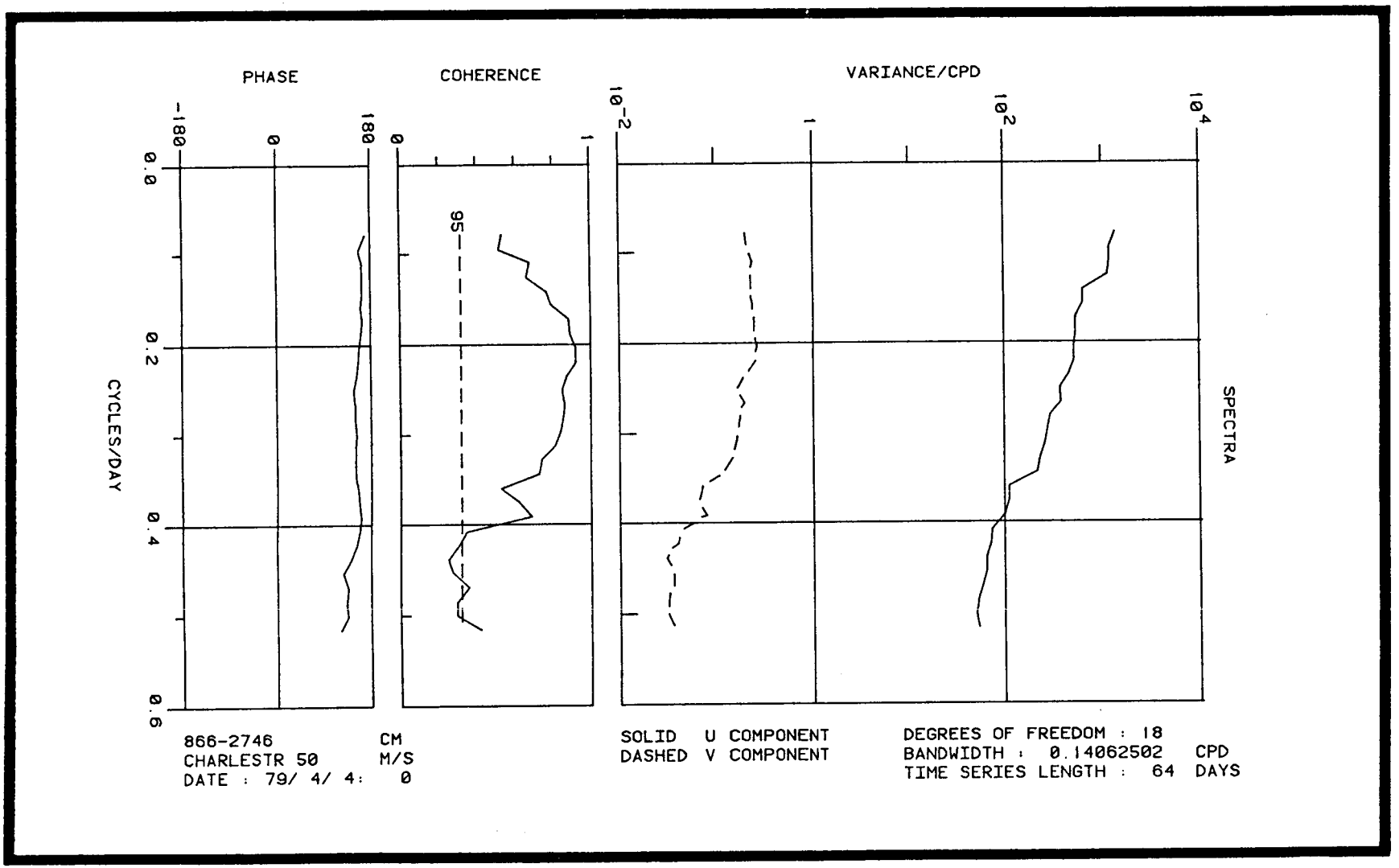

Figure 4.3-17. Spectra, coherence squared, and phase difference for Charleston longshore wind stress and water level from 866-2746 (Winyah Bay, S.C.) for April-May 1979.

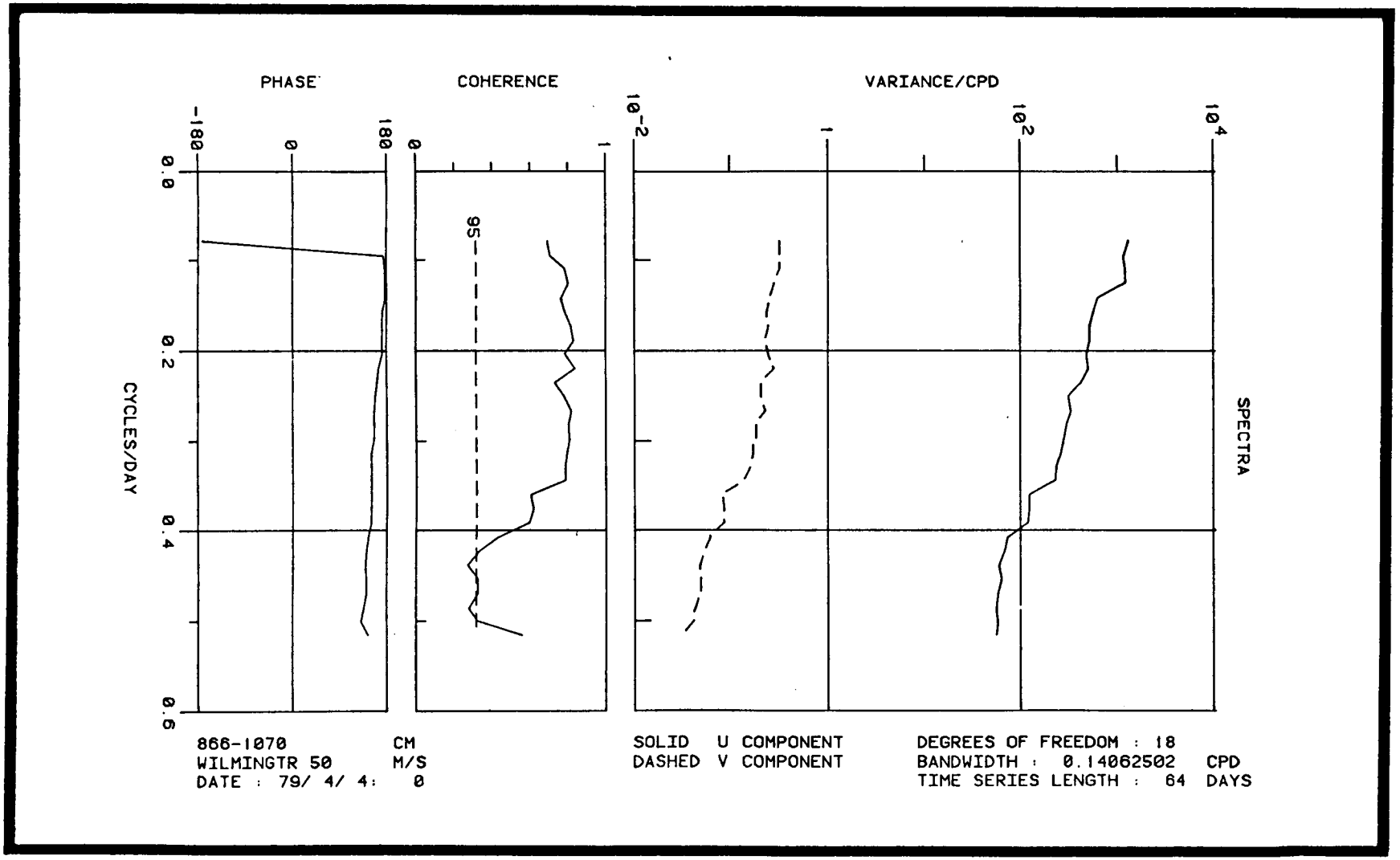

Figure 4.3-18. Spectra, coherence squared, and phase difference for Wilminton longshore wind stress and water level from 866-1070 (Myrtle Beach, S.C.) for April-May 1979.

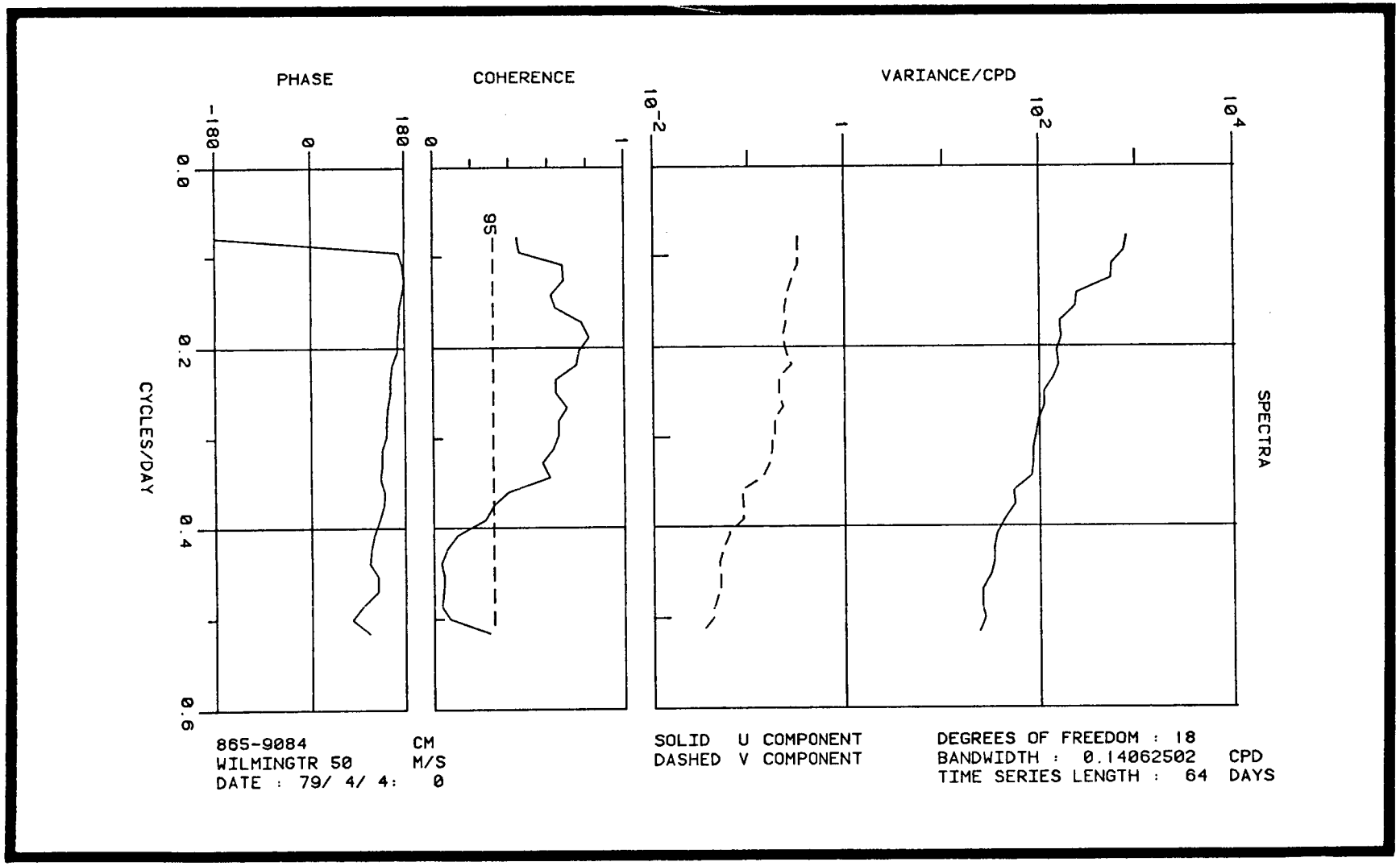

Figure 4.3-19. Spectra, coherence squared, and phase difference for Wilmington longshore wind stress and water level from 865-9084 (Southport, N.C.) for April-May 1979.

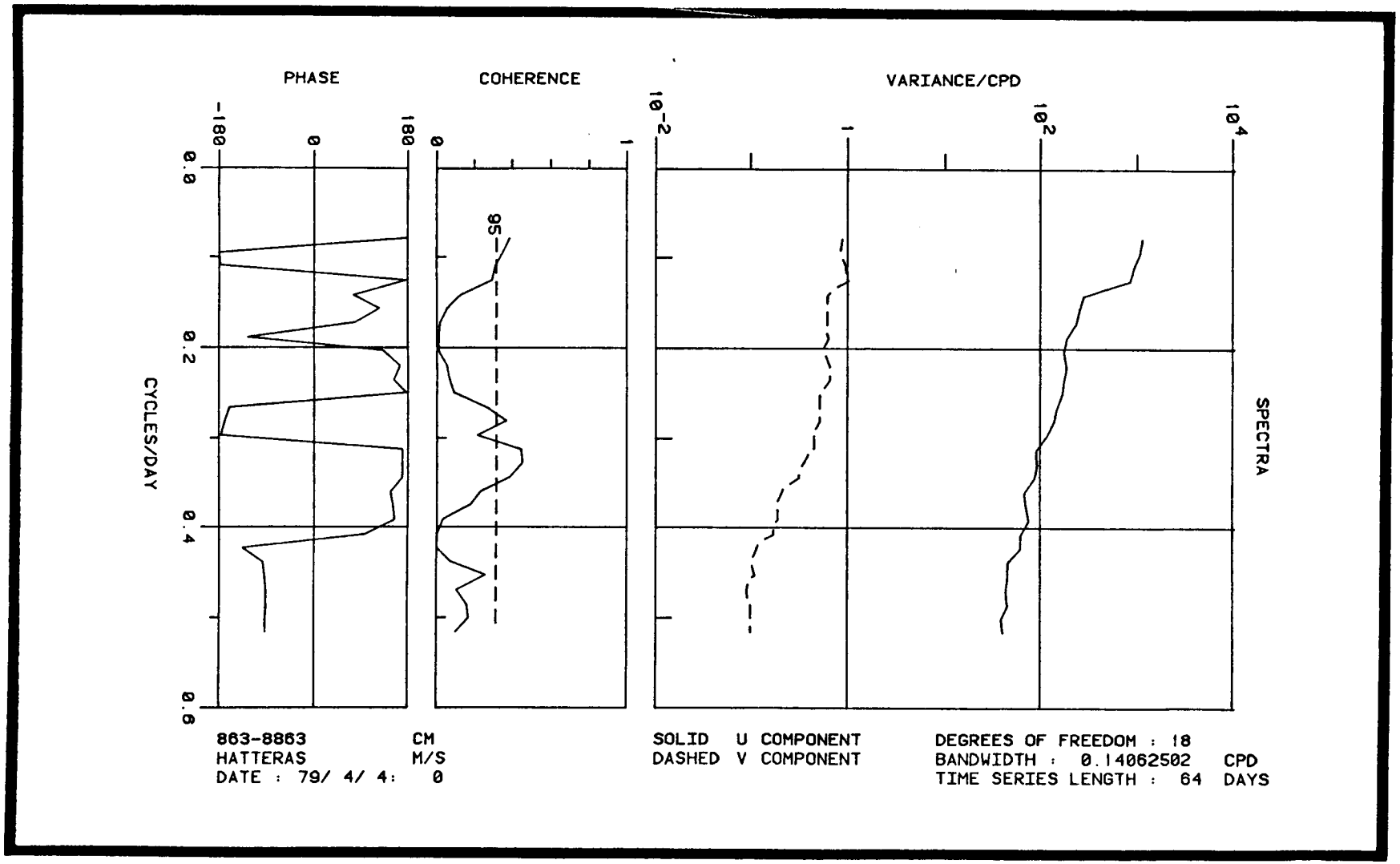

Figure 4.3-20. Spectra, coherence squared, and phase difference for Hatteras longshore wind stress and water level from 863-8863 (Chesapeake Bay Bridge Tunnel) for April-May 1979.

Sea Level Series to be Predicted	Longshore Wind stress Predictor	Transfer Functions February 1979 Amptitude Phase	Coherence Squared	Transfer Functions April 1979 Amptitude Phase	Coherence Squared
Tiger Island	Savannah	56.80-192.8	0.620	77.97-187.7	0.638
Fort Pulaski	Savannah	--- ---	---	83.68-188.8	0.693
Charleston	Charleston	33.92-217.9	0.604	51.18-199.5	0.642
Winyah Bay	Charleston	32.21-211.48	0.542	46.88-198.4	0.591
Myrtle Beach	Wilmington	42.46-198.1	0.642	43.33-184.6	0.661
Southport	Wilmington	27.59-203.9	0.510	25.07-189.7	0.419
Beaufort	Wilmington	26.04-199.1	0.442	--- ---	---
Chesapeake	Hatteras	9.20-172.7	0.05	13.57-186.7	0.230

Table 4.3-3. Transfer functions between sea level and longshore wind stress.

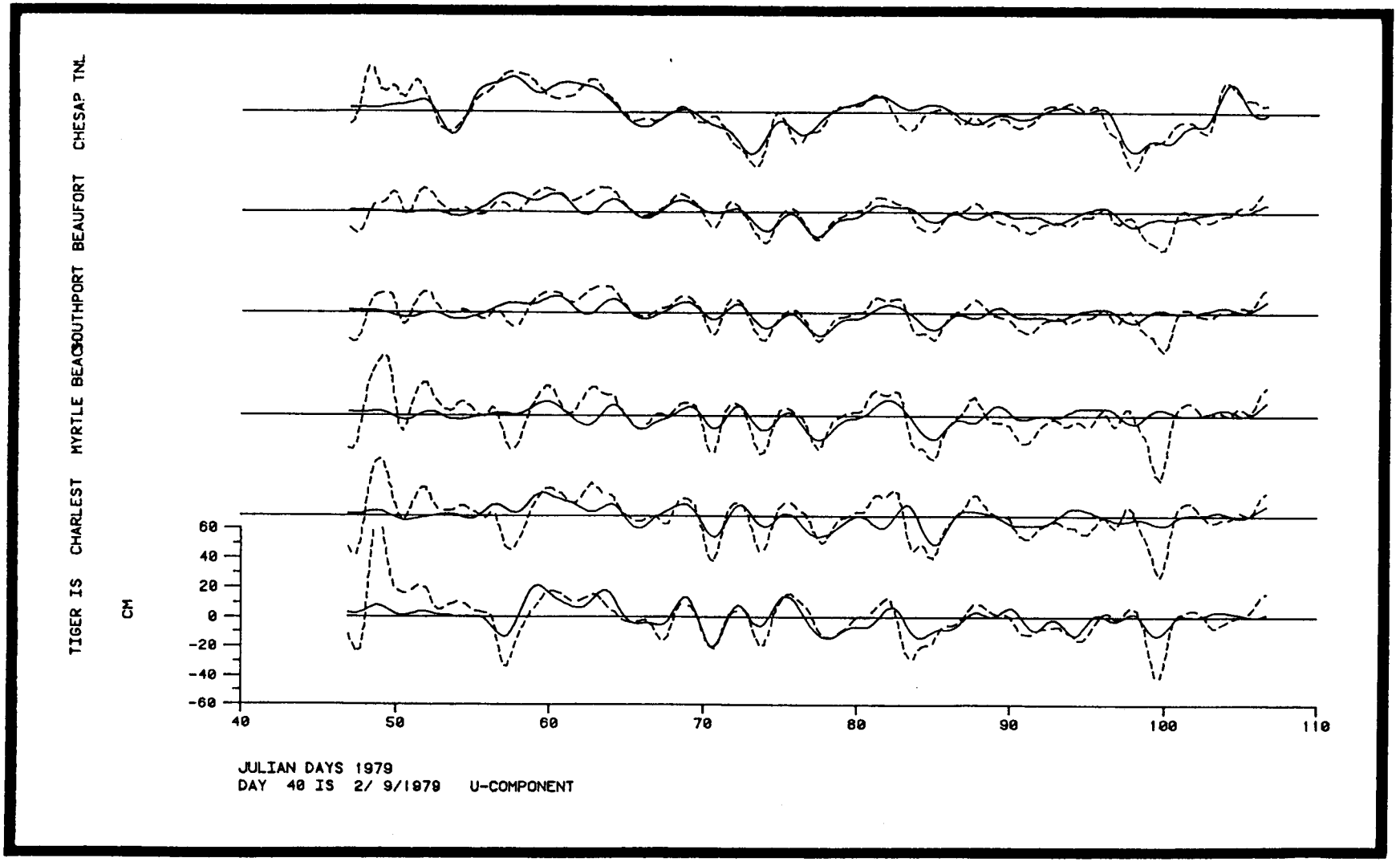

Figure 4.3-21. Nonwind-driven residual water-level time series (solid) and original water-level time series (dashed) for February and March 1979.

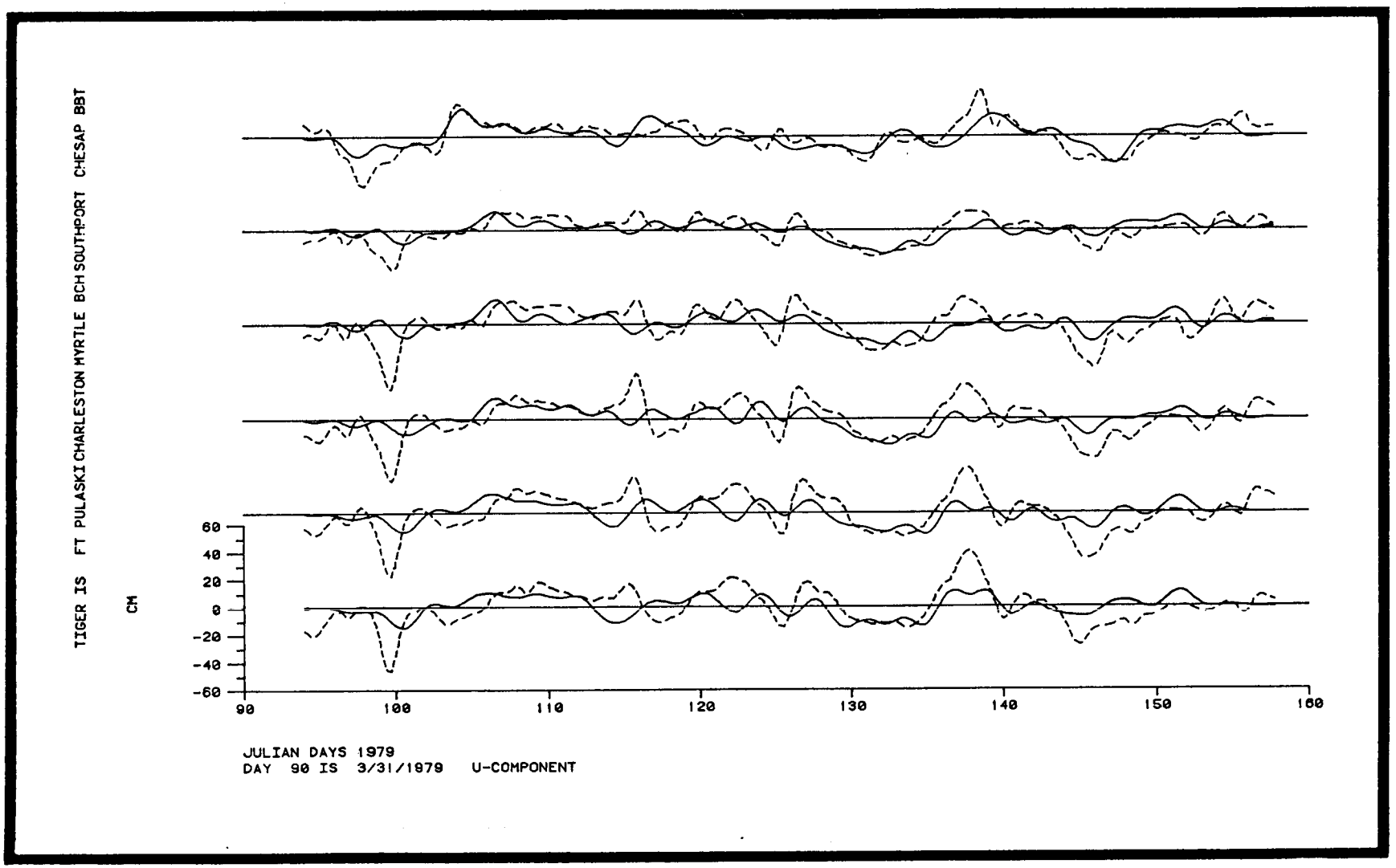

Figure 4.3-22. Nonwind-driven residual water-level time series (solid) and original water-level time series (dashed) for April and May 1979.

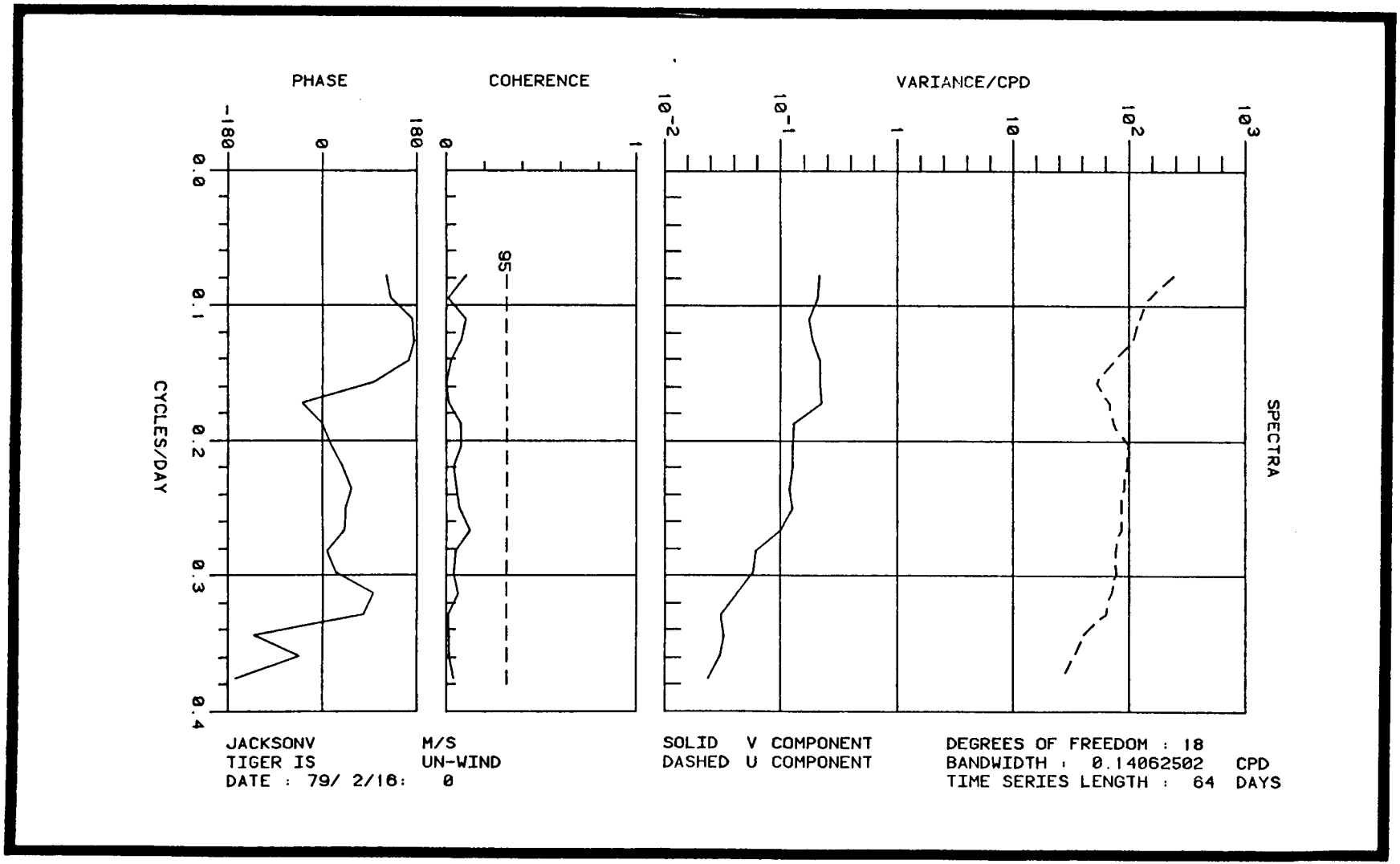

Figure 4.3-23. Spectra, coherence squared, and phase difference for Jacksonville longshore wind stress and the residual nonwind-driven water levels from Tiger Island for February-March 1979.

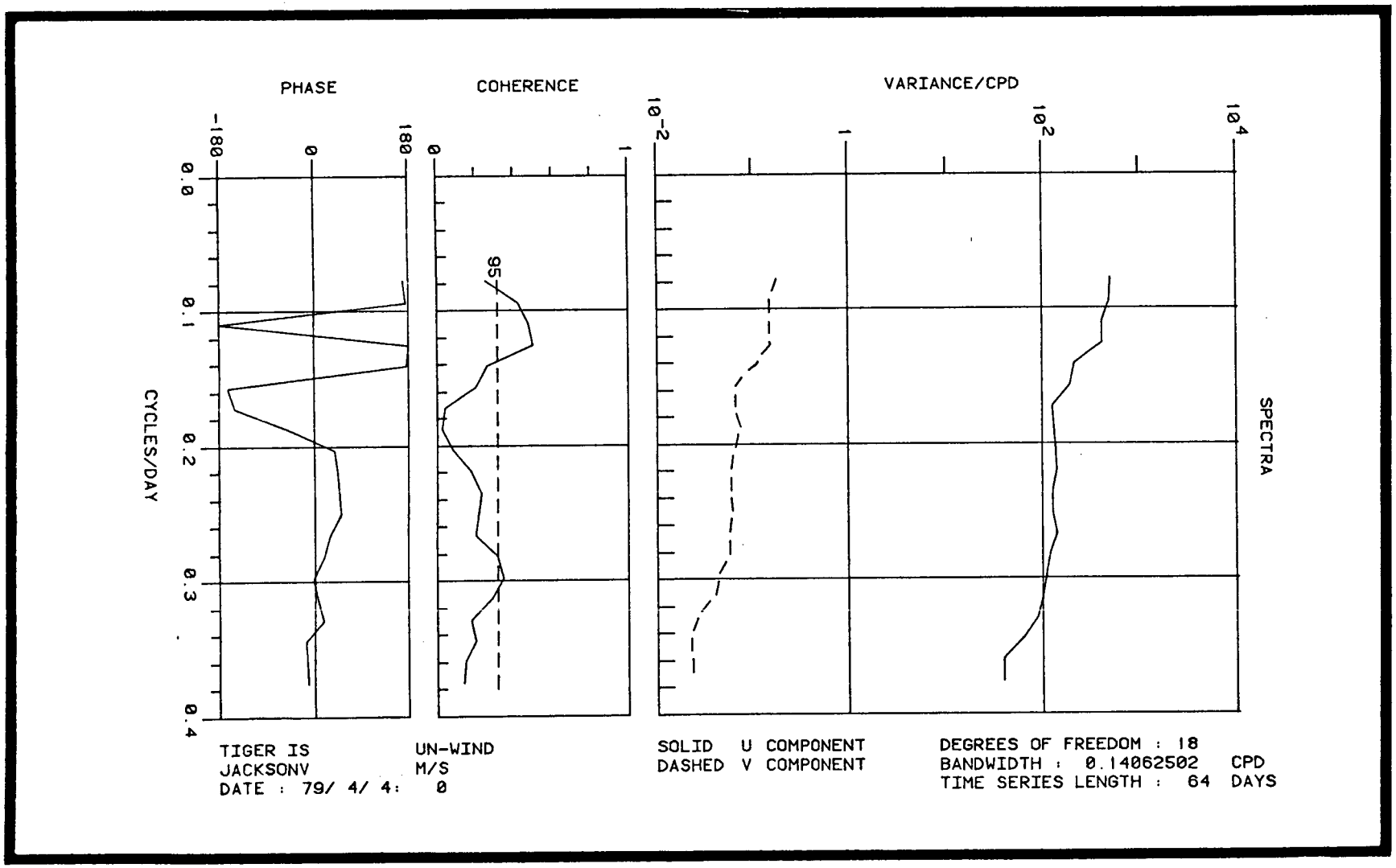

Figure 4.3-24. Spectra, coherence squared, and phase difference for Jacksonville longshore wind stress and the residual nonwind-driven water levels from Tiger Island for April-May 1979.

The relationships between nonwind-driven residual water levels are analyzed using empirical orthogonal function (EOF) analysis in the frequency domain. The frequency band 0-0.4 cpd is again used, and the resulting EOF's have 52 degrees-of-freedom, with the center frequency of the band being 0.2109 cpd. The dominant first mode is given in Table 4.3-4. The February results show a southward propagation of the nonwind-driven signal between Chesapeake Bay Bridge Tunnel and Southport, accompanied by decay in amplitude. South of Myrtle Beach, phases do not seem consistent with any preferred direction of propagation. The phase difference between Chesapeake Bay and Southport gives a propagation time of about 8.5 hours, hence a speed of approximately 1000 km day^{-1}. The first mode of the April data seems to be dominated by the southern stations, but there is some evidence of southward propagation between Chesapeake Bay and Southport, with about half the propagation speed of February.

Performing EOF analysis with residual water levels and wind-predicted water levels for both data sets shows that residual water levels are virtually orthogonal to the predicted set and so represent a different phenomena. The EOF analysis also helps to eliminate noise for the data sets.

The conclusions of this section are that there is evidence of leakage southwards by the dominant wind-driven water levels in the SAB. Thus Tiger Island is closely related to Savannah winds, but not local winds. There is also evidence that the shelf waves in the Mid-Atlantic Bight penetrate around Cape Hatteras into the Carolina Bays with the same order of magnitude phase speeds, but probably decay before they reach the center of the SAB.

4.3.3 Sea Breeze

Previous studies, which hindcast offshore-wind time series from coastal station winds, concentrated on low-frequency motions (i.e, periods greater than one day). This was because these motions have the most energy and show the highest coherence between stations. However, it has been noted that the diurnal sea breeze in late spring and summer is present at all offshore and coastal wind stations, with amplitudes ranging from 1-3 m s^{-1}.

Sea-breeze systems are important for their effects on oil spills, because the onshore/offshore component of the sea breeze may blow the spill towards or away from the shoreline, depending on the phase of the sea-breeze cycle. It is therefore useful to investigate how far the sea-breeze system extends over and across the shelf and to calculate the amplitudes at the shelf break.

The July-August period of 1980 is suitable for the analysis in that all three shelf-edge Buoys 41003, 41004, and 41005 as well as the offshore Buoy 41002 were recording data. Figures 4.3-25 and 4.3-26 show spectrum for u and v components (east and north components, respectively) for buoy 41004 and its nearest coastal station (Charleston), respectively. They are plotted on a linear frequency axis so as to show high-frequency motion in more detail. Buoy 41004 shows a substantial peak at 1 cpd (also a harmonic at 2 cpd), where u and v components are moderately coherent with v leading u by approximately 90°, indicating clockwise rotary motion. However, Charleston shows more energy in the v than u component at 1 cpd and there is only marginal coherence between the two.

	February 1979			April 1979		
	February 1979			April 1979		
	Amplitude	Phase	Coherence Squared	Amplitude	Phase	Coherence Squared
Tiger Is.	0.200	-34.4	0.326	0.393	-4.9	0.808
Ft. Pulaski	---	---	---	0.399	-15.0	0.853
Charleston	0.336	-23.5	0.631	0.420	-25.6	0.933
Winyah Beach	0.392	-41.7	0.677	0.427	-17.5	0.941
Myrtle Beach	0.251	-14.7	0.430	0.353	-21.9	0.787
Southport	0.289	-27.3	0.705	0.353	-13.1	0.856
Beaufort	0.347	-23.8	0.842	---	---	---
Chesapeake	0.653	0.0	0.686	0.280	0.0	0.323
% of total variance = 64.2				% of total variance = 76.9		

Table 4.3-4. Mode 1 EOF analysis, 0 - 0.4 cpd, nonwind-driven residual water levels.

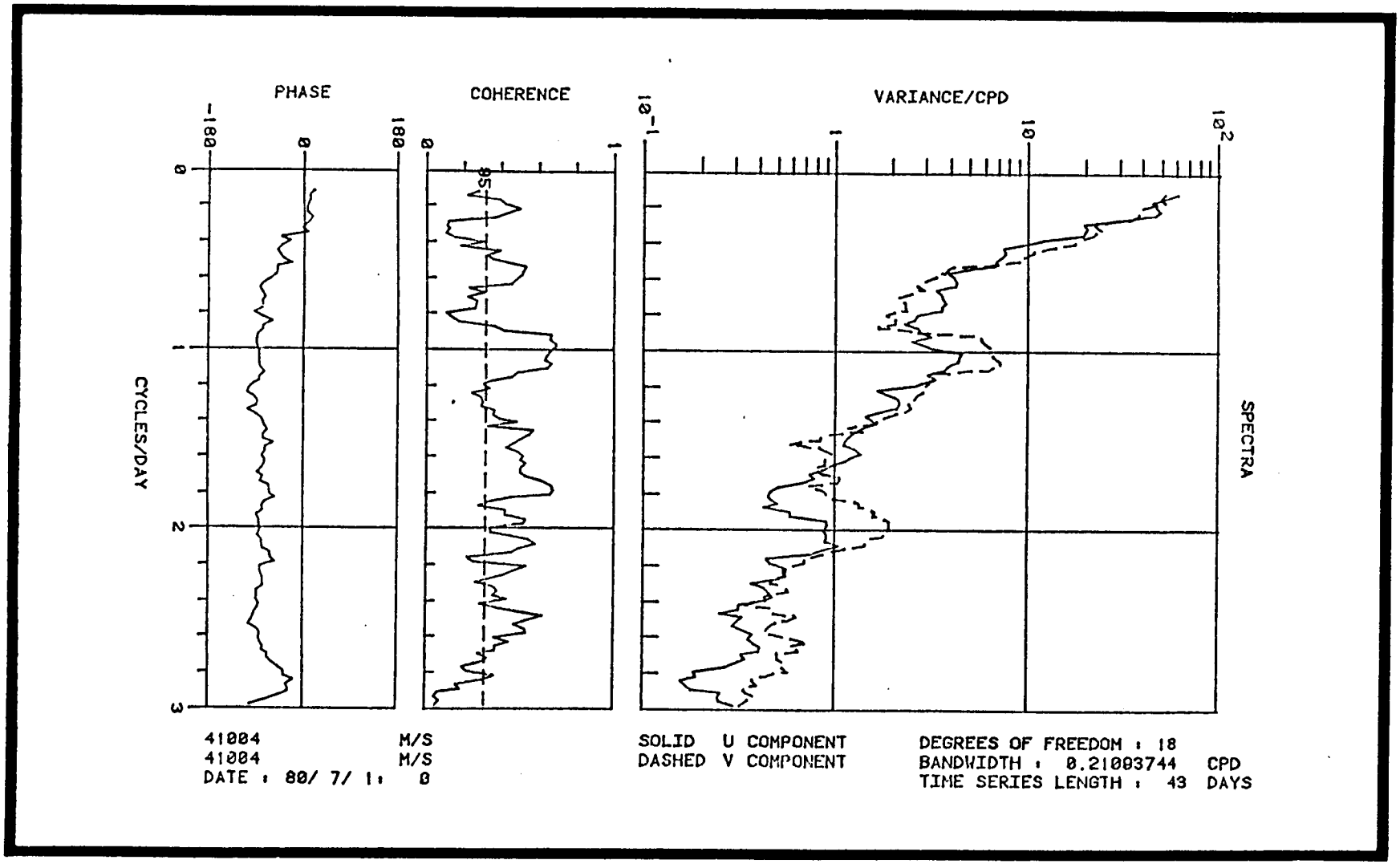

Figure 4.3-25. Spectra, coherence squared, and phase differences for U and V components of wind at 41004.

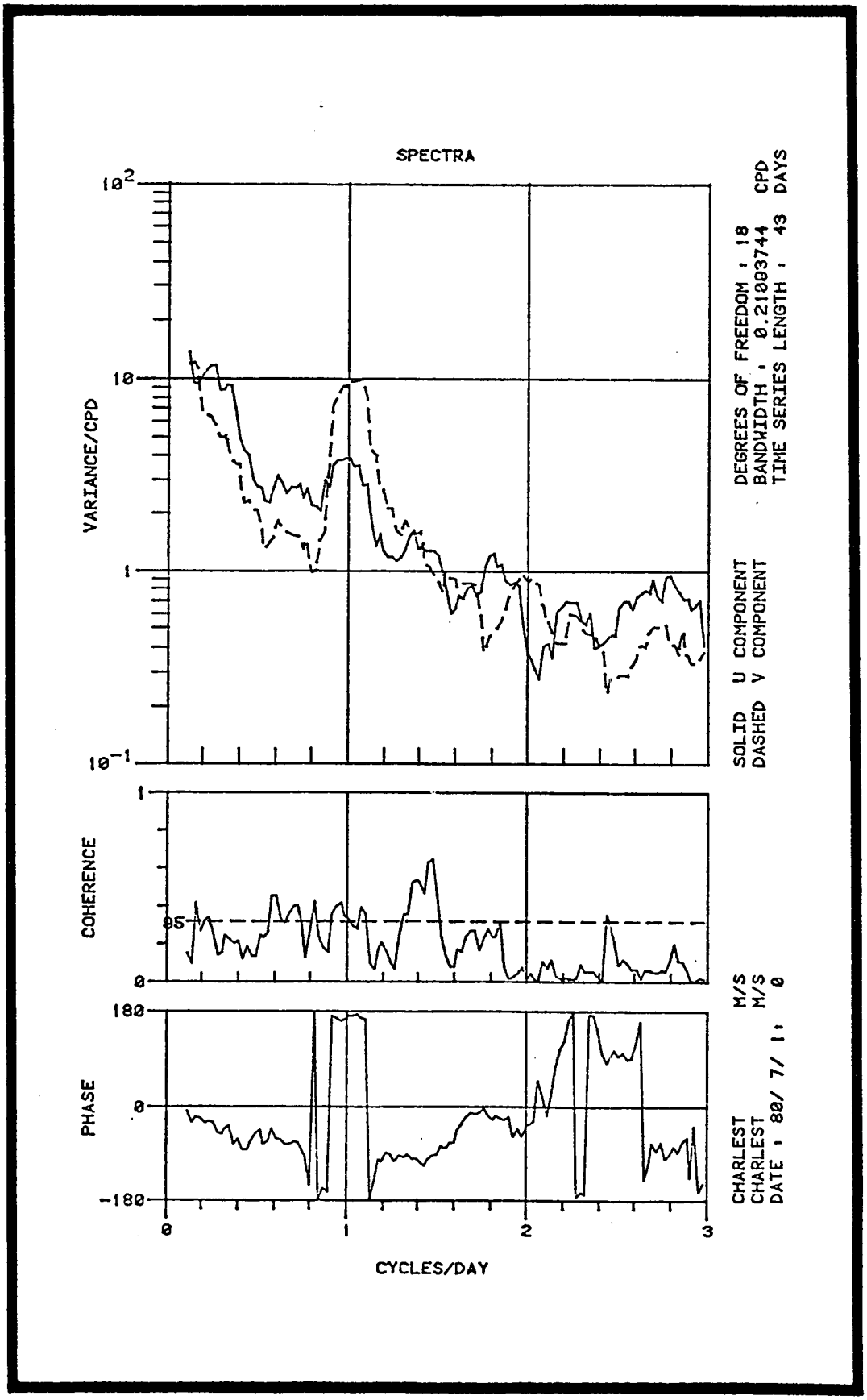

Figure 4.3.26. Spectra, coherence squared, and phase differences for U and V components of wind at Charleston.

An example of alongshore coherence is shown (Figure 4.3-27) for the v components of Buoy 41003 and 41004 (off of Jacksonville and Charleston, respectively). The energy at 1 cpd at both buoys is similar, with moderate coherence of about 0.6. There is virtually no phase lag, but in the onshore/offshore direction there is a consistent phase lag for the v component of between 60 to 80° for various buoy coastal station pairs, indicating that the sea-breeze system acts like a wave with a wave front parallel to the shoreline and a propagation time of about 5 to 6 hours between the coast and the shelf edge.

The coherence of the sea-breeze signals was investigated, using EOF spectral analysis for a band of width 0.1 cpd centered on .1 cpd. The results are shown in the form of ellipses in Figure 4.3-28. Coastal stations Hatteras, Charleston, Savannah, and Jacksonville and records from buoys 41004, 41005, and 41003 were used in the analysis.

The signal is coherent between Jacksonville and Hatteras on the coast and also at the shelf edge. Except for Hatteras, the coastal stations show a minor axis approximately parallel to the coastline, and energy increases moving northwards along the coast. At the shelf break, amplitudes are more nearly constant with less difference between the major and minor axis. The buoys also show higher energy than at the coast, though coastal weather stations are usually a few miles inland from the beach, thus are not representative of beach winds (Hatteras is again an exception).

4.3.4 Tidal Analysis

The results of the analysis described in Section 3.3 for 1979 and 1980 are given for all SAB water level stations in Table 4.3-5 through 4.3-9 and are probably the most accurate available to date and should be generally superior to the 29-day analyses found in the NOAA/NOS Tide Tables. The semidiurnal band is dominated by M2, but the N2 and S2 periods have similar spacial relationships for amplitude and phase. The largest amplitude is seen at the mouth of the Savannah River at Fort Pulaski, with a steady decrease northwards. Greenwich phases are similar at all ocean stations, with Myrtle Beach tending to lead all the other stations both north towards North Carolina and south towards Georgia. Consistency in the calculation between years is generally better than 1 cm for amplitude, and 1° in phase. Note that the Oregon Inlet tide is different in amplitude and phase with its closest neighbor because of its position inside the barrier island. Thus the ocean tidal signal is attenuated through Oregon Inlet and influenced by the shallow sounds. The diurnal tides are much weaker than the the semidiurnal tides, being comparable in amplitude to the N2. Otherwise the amplitude and phase relationship between stations is similar to the semidiurnal tides.

4.4 NORTH CAROLINA HYDROGRAPHY

A thorough analysis and synthesis of the data from both of the Year 4, North Carolina hydrographic surveys is scheduled for the upcoming year (Year 5). At the present time, samples and data from the winter survey are further along in processing. Subsequently, an initial characterization of the principal features observed during the winter will follow. Additions and refinements, as well as synthesis of other data, will be the focus of the upcoming year's effort.

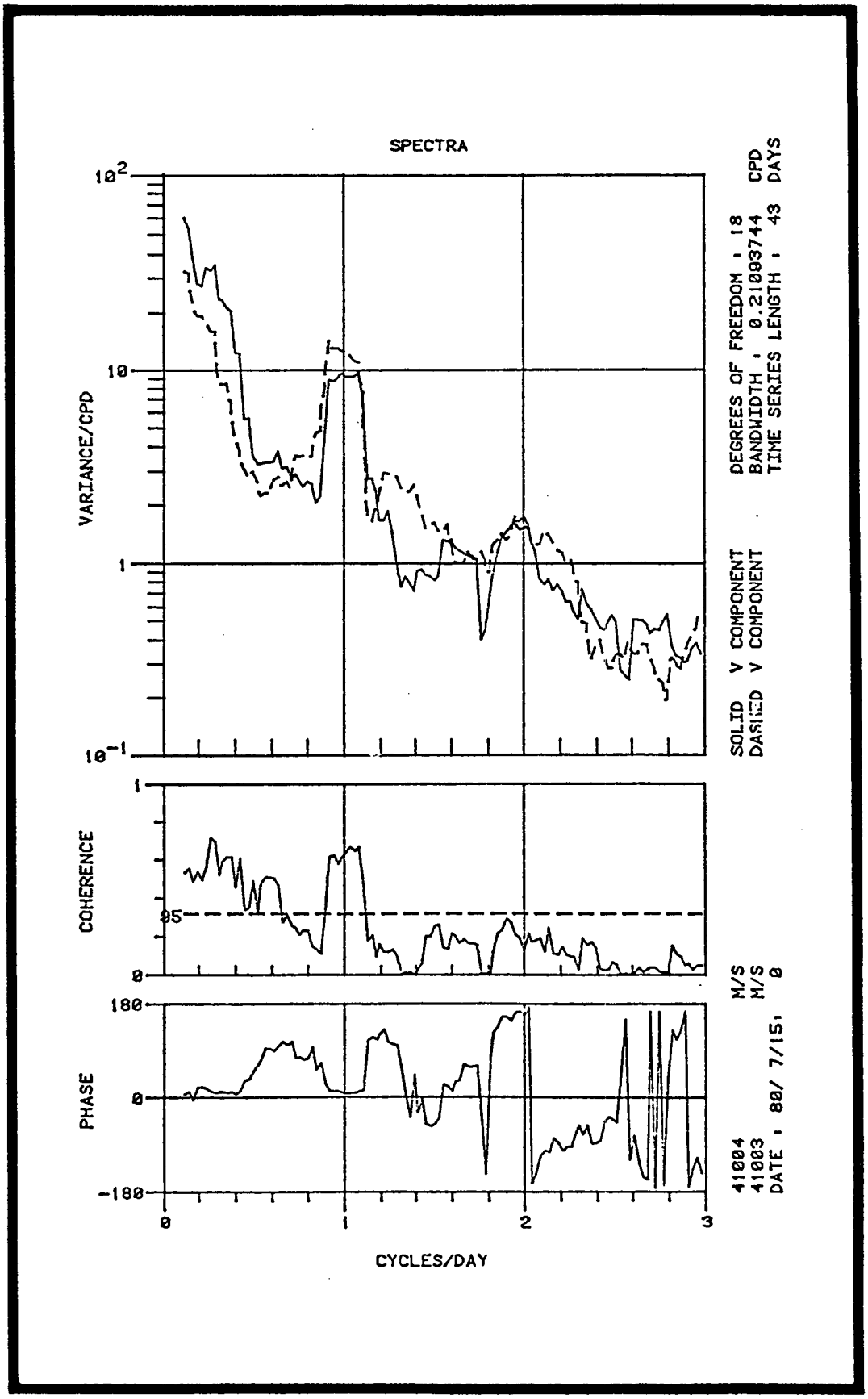

Figure 4.3-27. Spectra, coherence squared, and phase differences for V components of wind at 41004 and 41003.

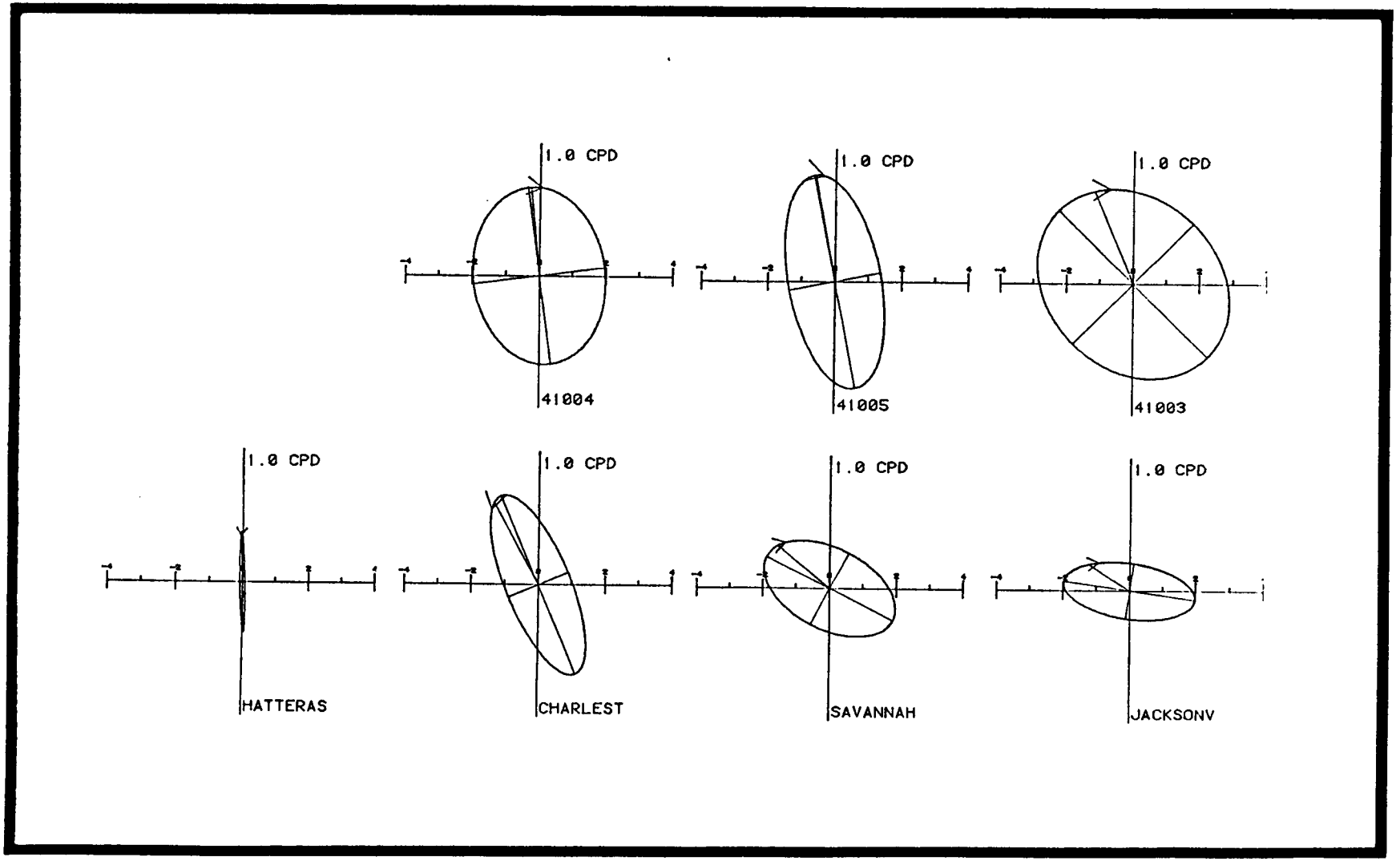

Figure 4.3-28. Hodographs of 1cpd motion computed from Mode 1 EOF analysis for indicated wind stations.

M 2

STATION	1979		1980	
	A(cm)	Ø	A(cm)	Ø
Chesapeake	38	236.25	38	235.20
Oregon Inlet	07	264.62	---	---
Beaufort	41	225.58	42	224.24
Southport	63	224.78	---	---
Myrtle Beach	74	215.00	74	214.66
Winyah Bay	56	239.49	55	241.22
Charleston	78	223.35	78	223.78
Ft. Pulaski	102	231.83	101	230.47
Tiger Island	89	244.32	---	---

Table 4.3-5. Amplitude (A) in cm and phase (θ) for M2 tide for indicated stations and years.

N 2

STATION	1979		1980	
	A(cm)	∅	A(cm)	∅
Chesapeake	08	220.94	09	218.35
Oregon Inlet	01	254.13	---	---
Beaufort	10	211.92	09	210.76
Southport	13	213.29	---	---
Myrtle Beach	17	201.33	17	198.54
Winyah Bay	11	226.05	11	226.47
Charleston	17	213.17	17	214.04
Ft. Pulaski	22	221.57	22	217.67
Tiger Island	18	224.99	---	---

Table 4.3-6. Amplitude (A) in cm and phase (Θ) for N2 tide for indicated stations and years.

S 2

STATION	1979		1980	
	A(cm)	∅	A(cm)	∅
Chesapeake	07	258.57	07	256.00
Oregon Inlet	01	274.11	---	---
Beaufort	06	247.14	07	242.62
Southport	11	246.99	---	---
Myrtle Beach	13	231.74	13	232.50
Winyah Bay	09	261.39	08	260.08
Charleston	13	245.01	13	244.47
Ft. Pulaski	17	254.77	17	254.99
Tiger Island	17	267.32	---	---

Table 4.3-7. Amplitude (a) in cm and phase (Θ) for S2 tide for indicated stations and years.

K 1

STATION	1979		1980	
	A(cm)	Ø	A(cm)	Ø
Chesapeake	06	107.22	06	109.15
Oregon Inlet	02	149.21±±	---	---
Beaufort	08	126.12	08	126.04
Southport	09	119.27	---	---
Myrtle Beach	10	114.00	10	114.33
Winyah Bay	09	135.12	09	135.43
Charleston	11	124.61	10	124.51
Ft. Pulaski	12	124.83	11	124.01
Tiger Island	09	113.49	---	---

Table 4.3-8. Amplitude (A) and phase (Θ) for K1 tide for indicated stations and years.

O 1

STATION	1979		1980	
	A(cm)	ø	A(cm)	ø
Chesapeake	04	140.26	04	136.28
Oregon Inlet	01	158.31	---	---
Beaufort	06	142.44	06	134.57
Southport	07	132.28	---	---
Myrtle Beach	08	123.51	08	120.32
Winyah Bay	07	142.70	06	141.35
Charleston	08	130.36	07	130.75
Ft. Pulaski	08	128.67	07	133.83
Tiger Island	08	140.52	---	---

Table 4.3-9. Amplitude (A) and phase (Θ) for O1 tide for indicated stations and years.

A synoptic view of the structure of the Gulf Stream system in the survey region is provided by a sea-surface temperature analysis based on radiometric satellite imagery for 4-5 February 1981. (Figure 4.4-1). Several filament-type features are evident along the western Gulf Stream frontal zone, both north and south of Cape Hatteras. On the eastern side of the Stream, one large, bifurcated, filament-type feature was present offshore of Cape Lookout. Nearshore, the shelf water ranged from 5 to 9°C alongshore, with the maximum alongshore gradient occurring at Cape Hatteras.

The northernmost transect along 36°N (Figure 4.4-2) crossed over the shelf and then sliced through the southernmost extremity of a large inshore filament before penetrating into the main Gulf Stream frontal zone, thus transiting three distinct regimes. In this situation, the shelf regime north of Hatteras was both horizontally and vertically stratified with relatively warm, salty water of Gulf Stream origin penetrating beneath an overriding layer of fresh, cool water originating from the nearshore shoal regions and Chesapeake Bay. The interaction of these two water masses over the shelf often results in the formation of sharp thermal and saline frontal zones, with the frontal layer inclined such that surface fronts are displaced laterally 5 to 10 km cross-shelf from bottom fronts (Figure 4.4-3). The compensating effects of temperature and salinity on density tends to produce a less intense density structure, often dominated by vertical stratification. In winter, this mechanism for generating vertical stratification is opposed by vertical mixing, driven by wind-induced surface turbulence.

The structure of the large inshore filament (Figure 4.4-2) indicates that such a feature extended to at least 600 m depth. On the seaward side, the relatively cool band (viewed along a level surface) between the filament and the main Gulf Stream frontal zone was about 10 km wide. On the shoreward side, relatively warm water (greater than 12°C in the upper 100 m) extended all the way to the shelf break, a distance of 100 km from the filament core. The observed velocity structure reflects a state of geostrophic balance; flow in the upper layers being northward seaward of the shelf break, except for a southerly flowing countercurrent between stations 13 and 14.

In contrast to this broad, deep, inshore filament north of Hatteras, filaments observed inshore and south of Hatteras were relatively shallow (100 to 200 m) features and located over the shelf break (Figures 4.4-4 and 4.4-5). The intervening cool band was barely discernable in the subsurface structure, resulting in a much weaker main GS front south of Hatteras, at least in regions offshore of well-defined filaments. The shelf waters south of Hatteras, when vertically stratified due to Gulf Stream events, are generally characterized by warm, saline water from offshore, above much cooler, somewhat less saline water which has acquired its properties from nearshore surface waters.

The vertical extent of the large filament observed on the seaward side of the Stream (Figure 4.4-6) was about 300 m, intermediate between the two inshore types observed. Core salinity values in the filament were similar to those of the main stream, indicating that not much mixing had occurred since this filament was formed. Satellite images from the weeks before and after the sampling period show no evidence of this feature at the surface, suggesting that the time scale for formation and dissipation may be about one week. Ship drift observations indicate that significant (1 knot or greater)

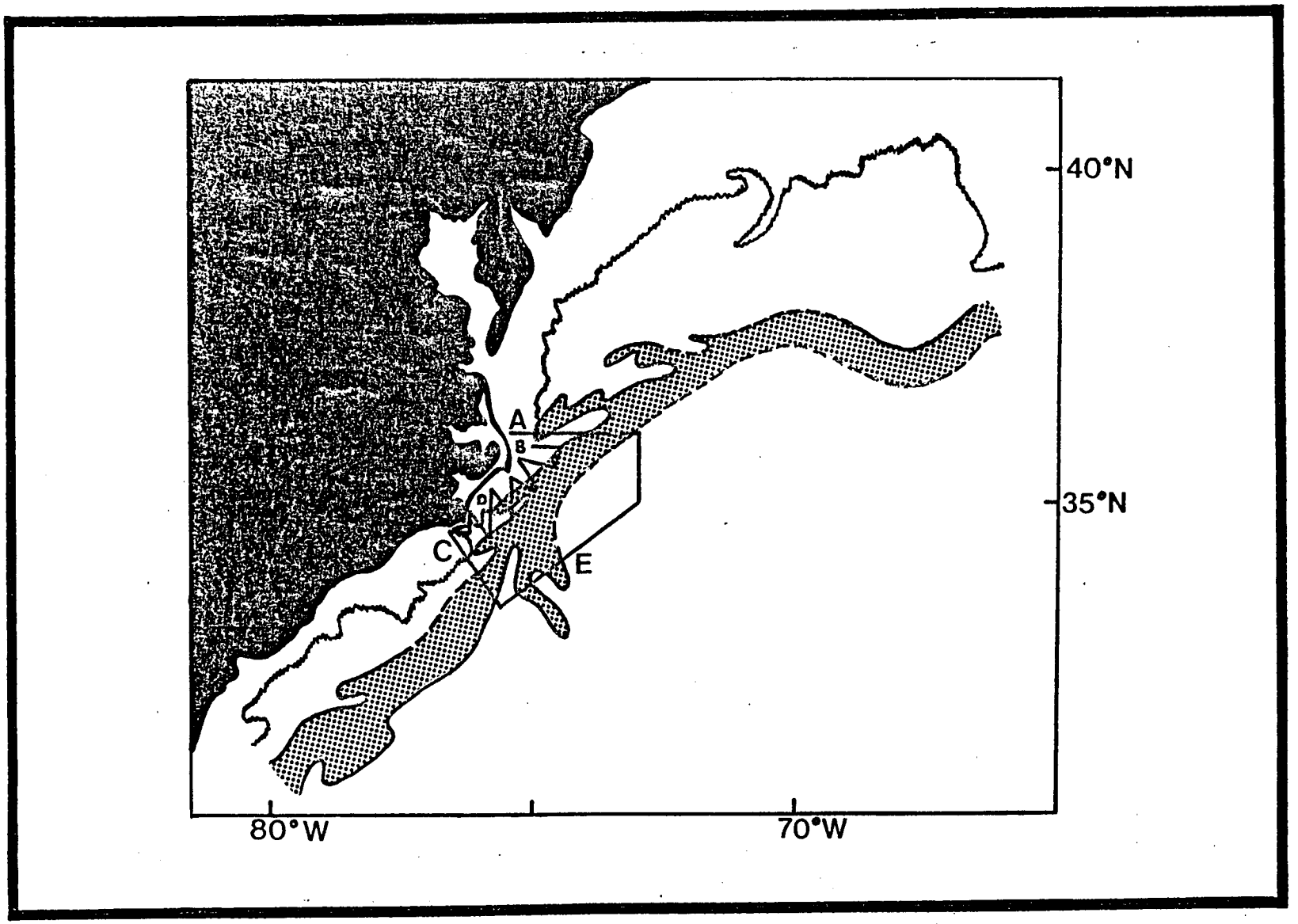

Figure 4.4-1. Surface oceanographic analysis, 4-5 February 1981. (Product provided regularly by the National Weather Service and the National Environmental Satellite Service.) Cruise track-lines have been added.

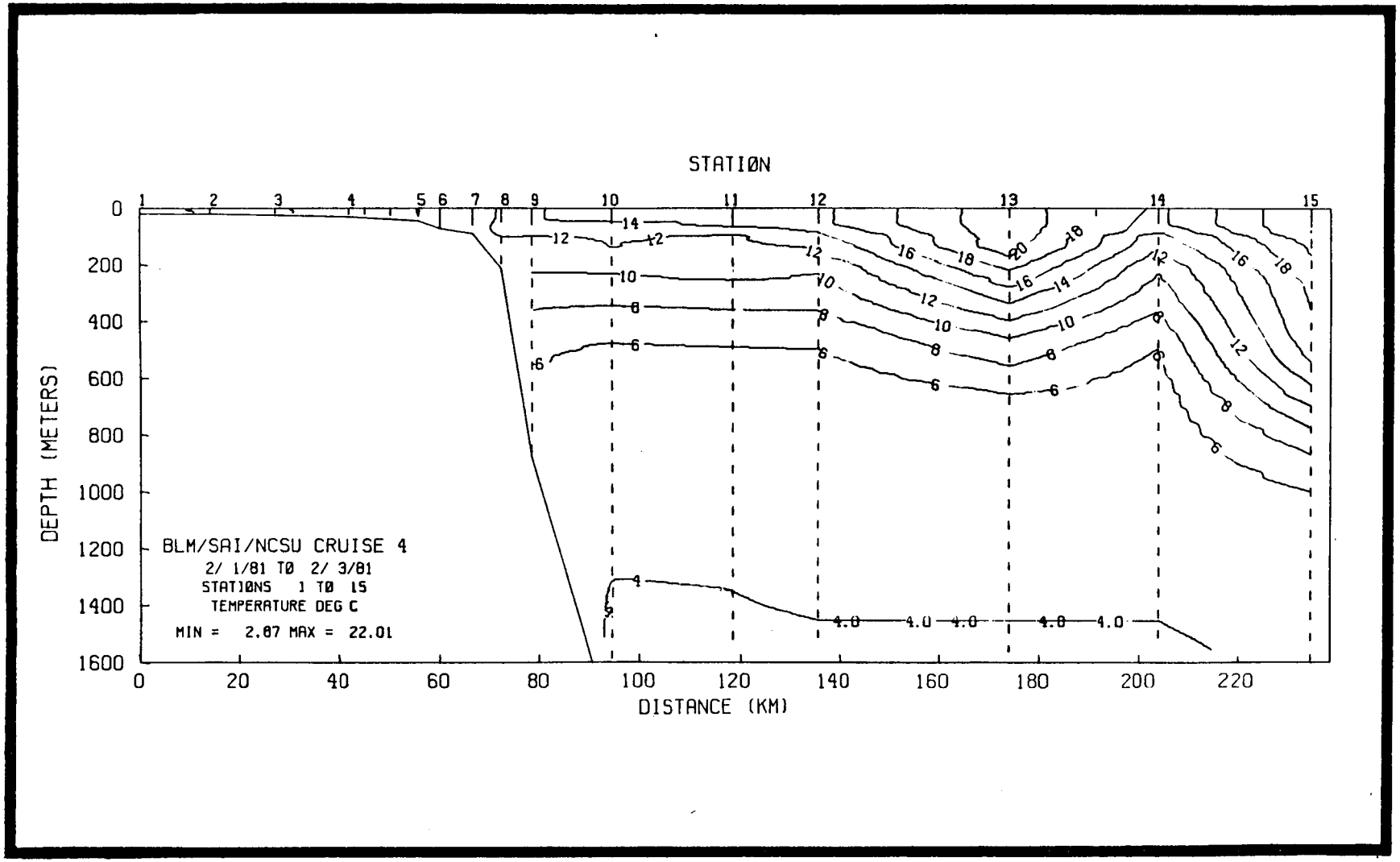

Figure 4.4-2a. Temperature for transect A (Stations 1-15) February 1981.

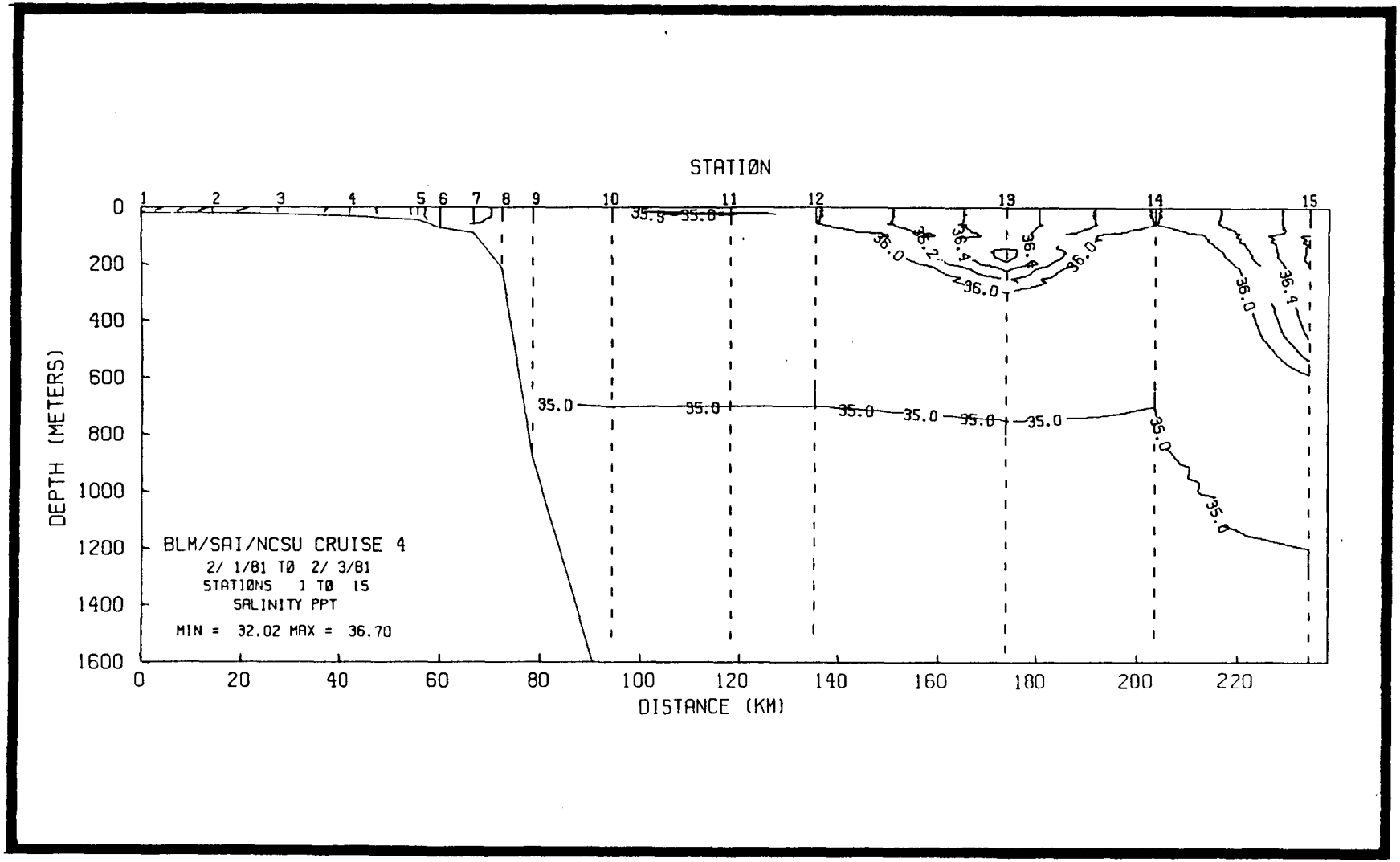

Figure 4.4-2b. Salinity for transect A (Stations 1-15) February 1981.

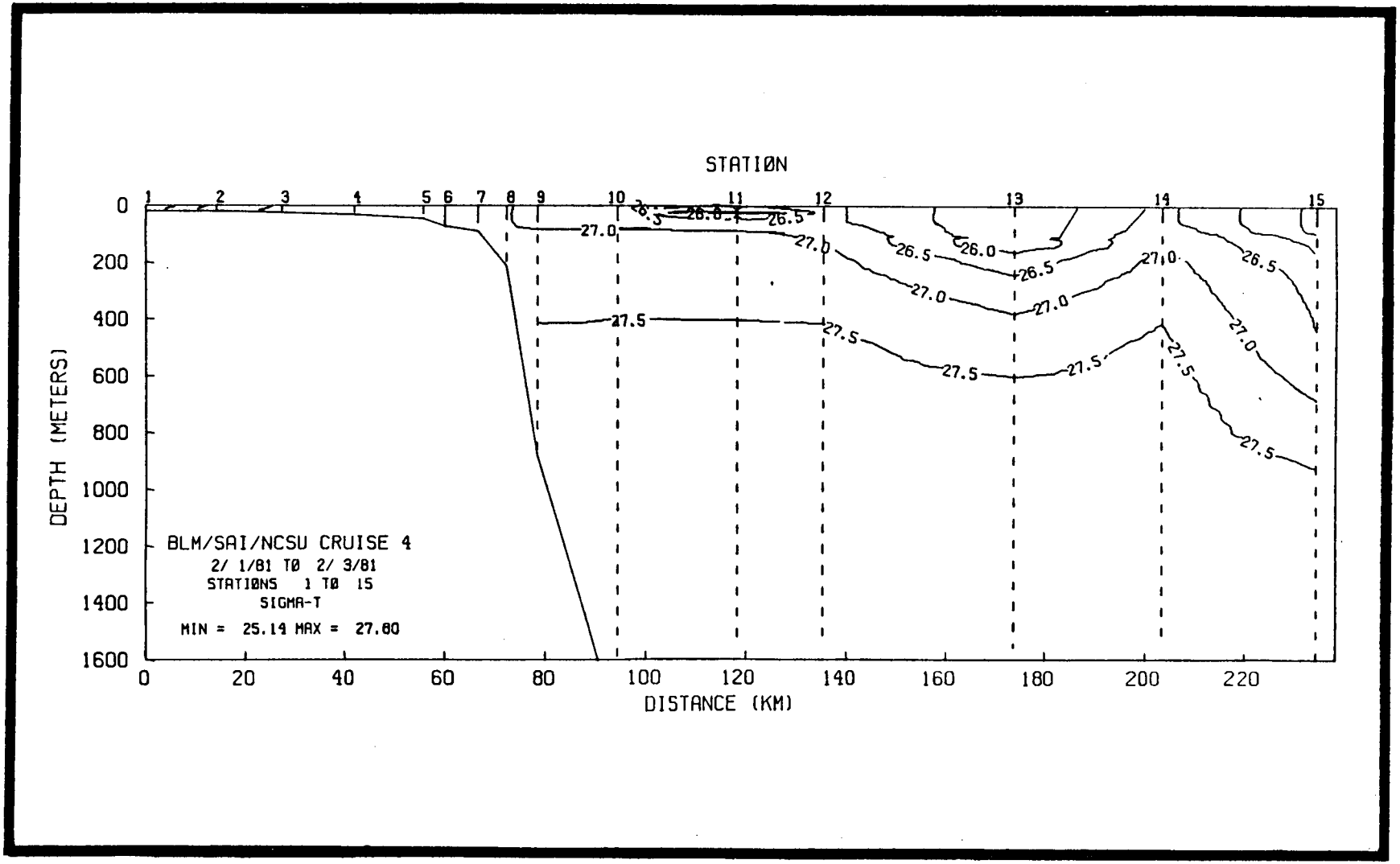

Figure 4.4-2c. Density for transect A (Stations 1-15) February 1981.

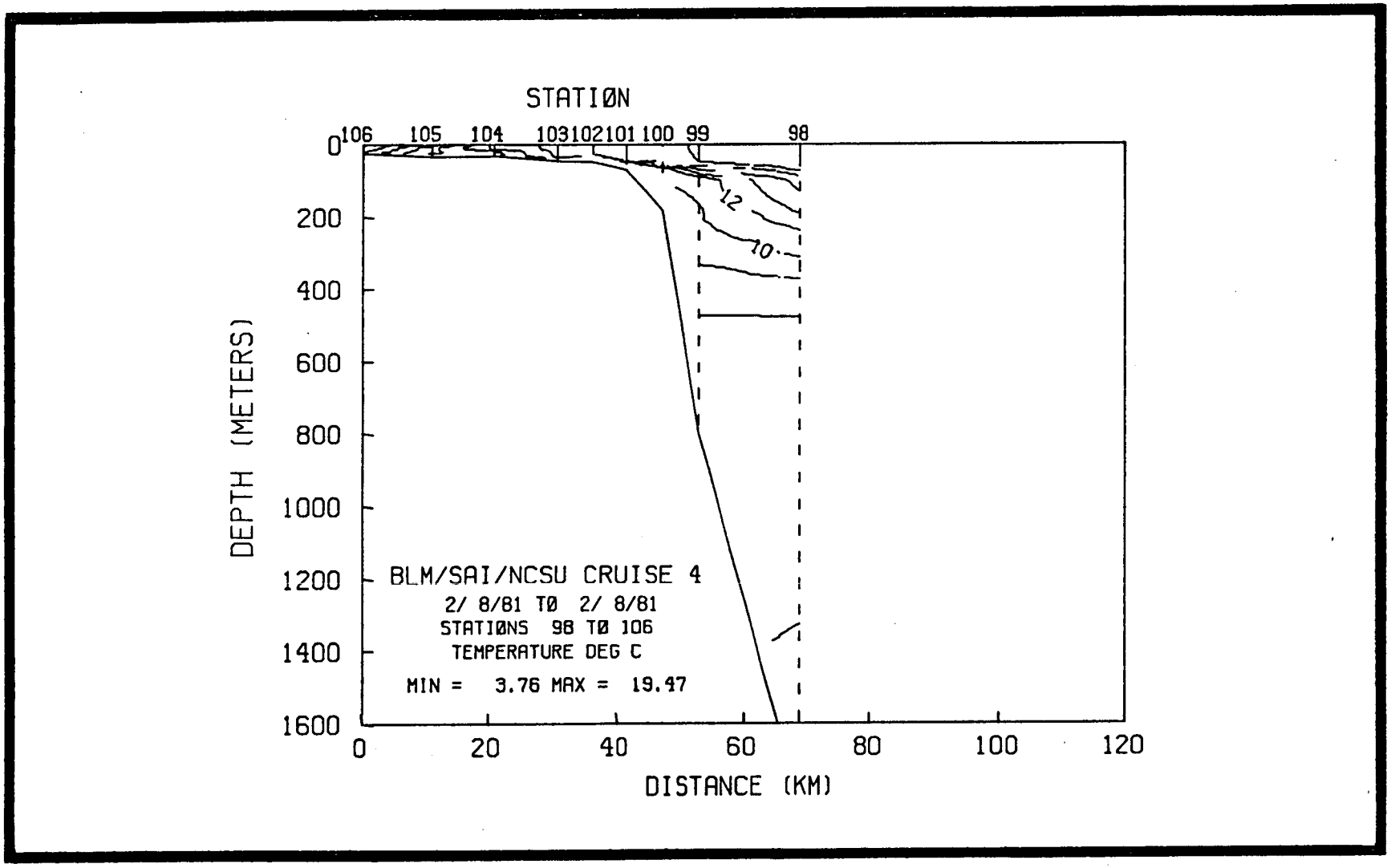

Figure 4.4-3a. Temperature for transect B (Stations 98-106) February 1981.

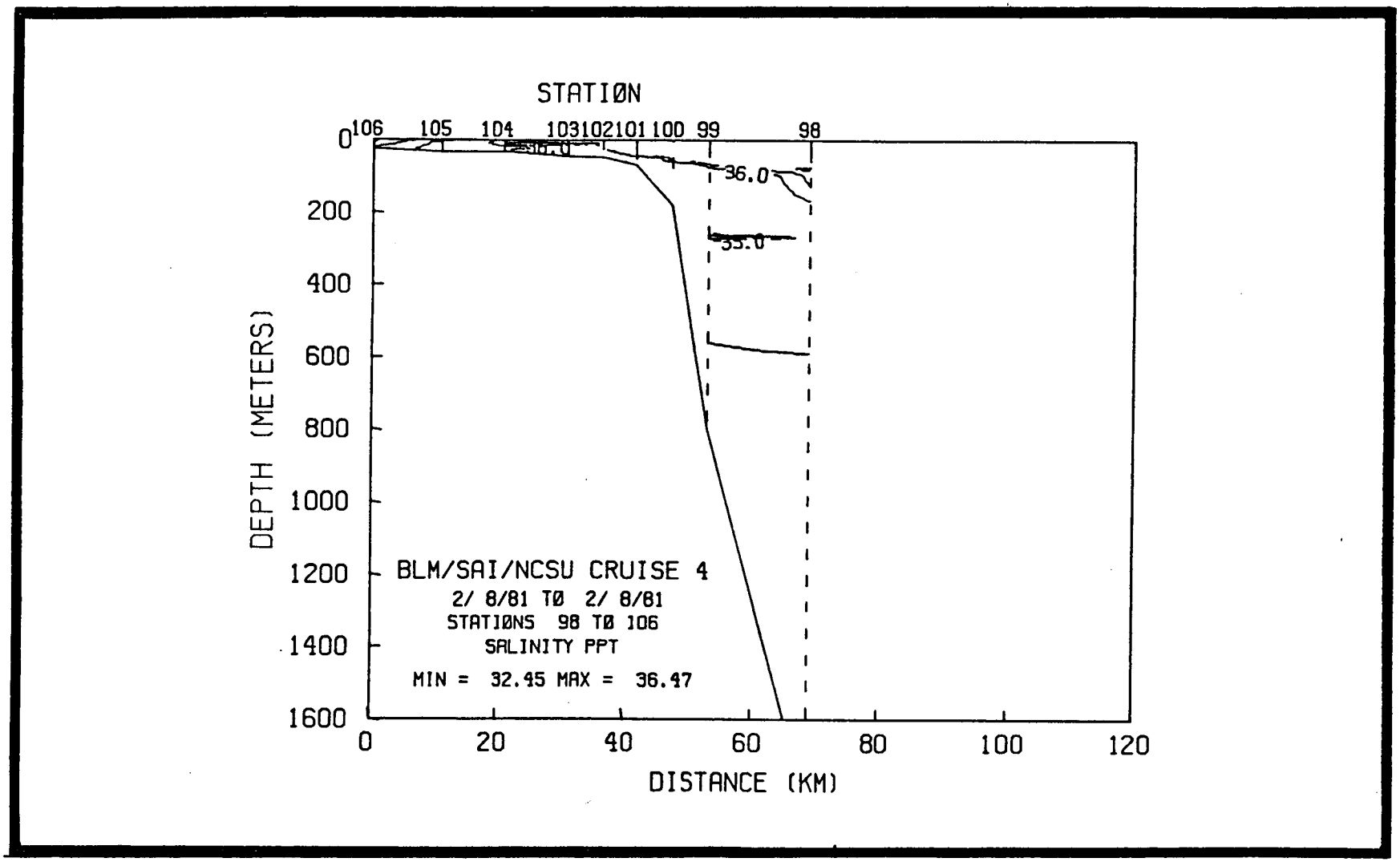

Figure 4.4-3b. Salinity for transect B (Stations 98-106) February 1981.

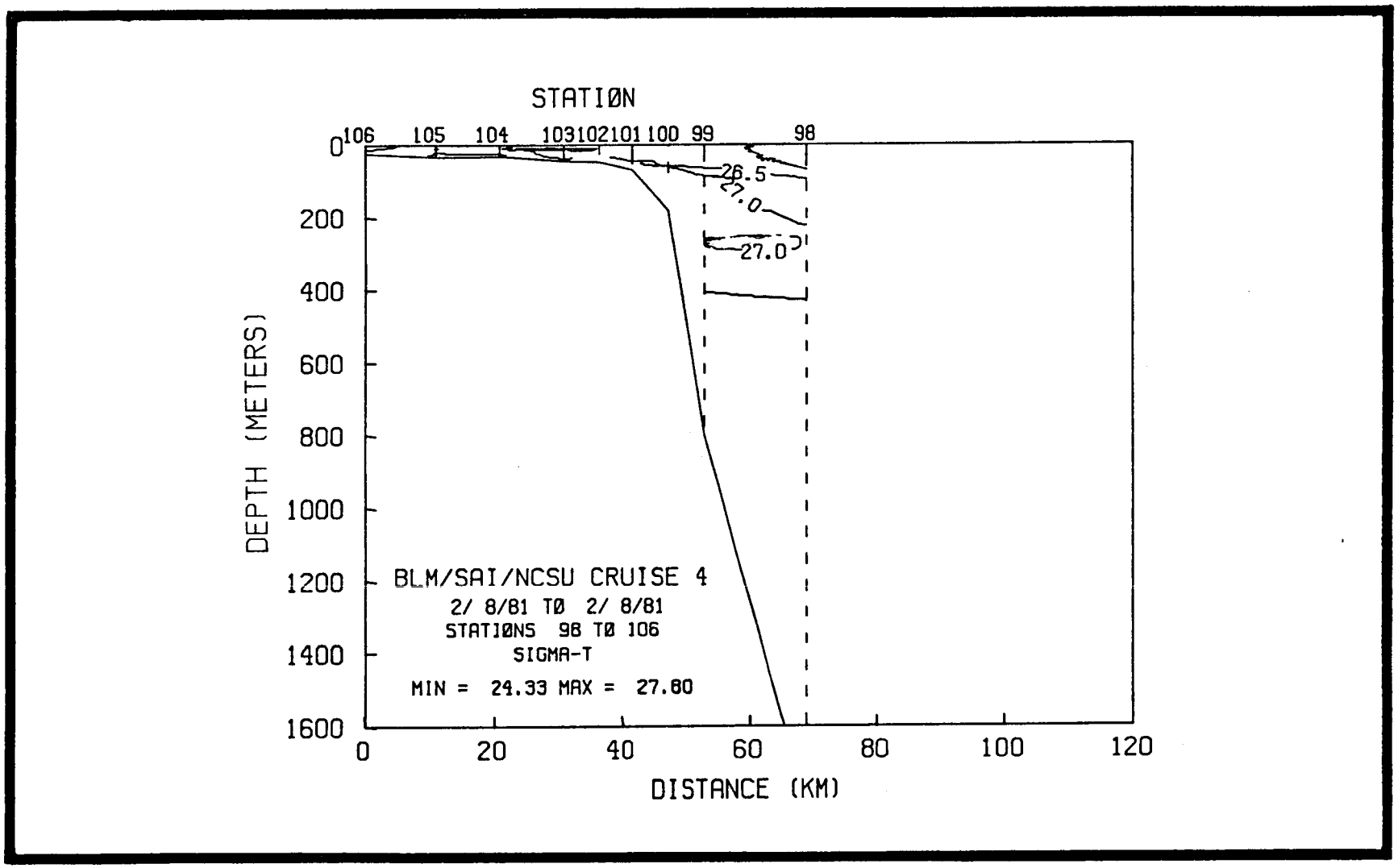

Figure 4.4-3c. Density for transect B (Stations 98-106) February 1981.

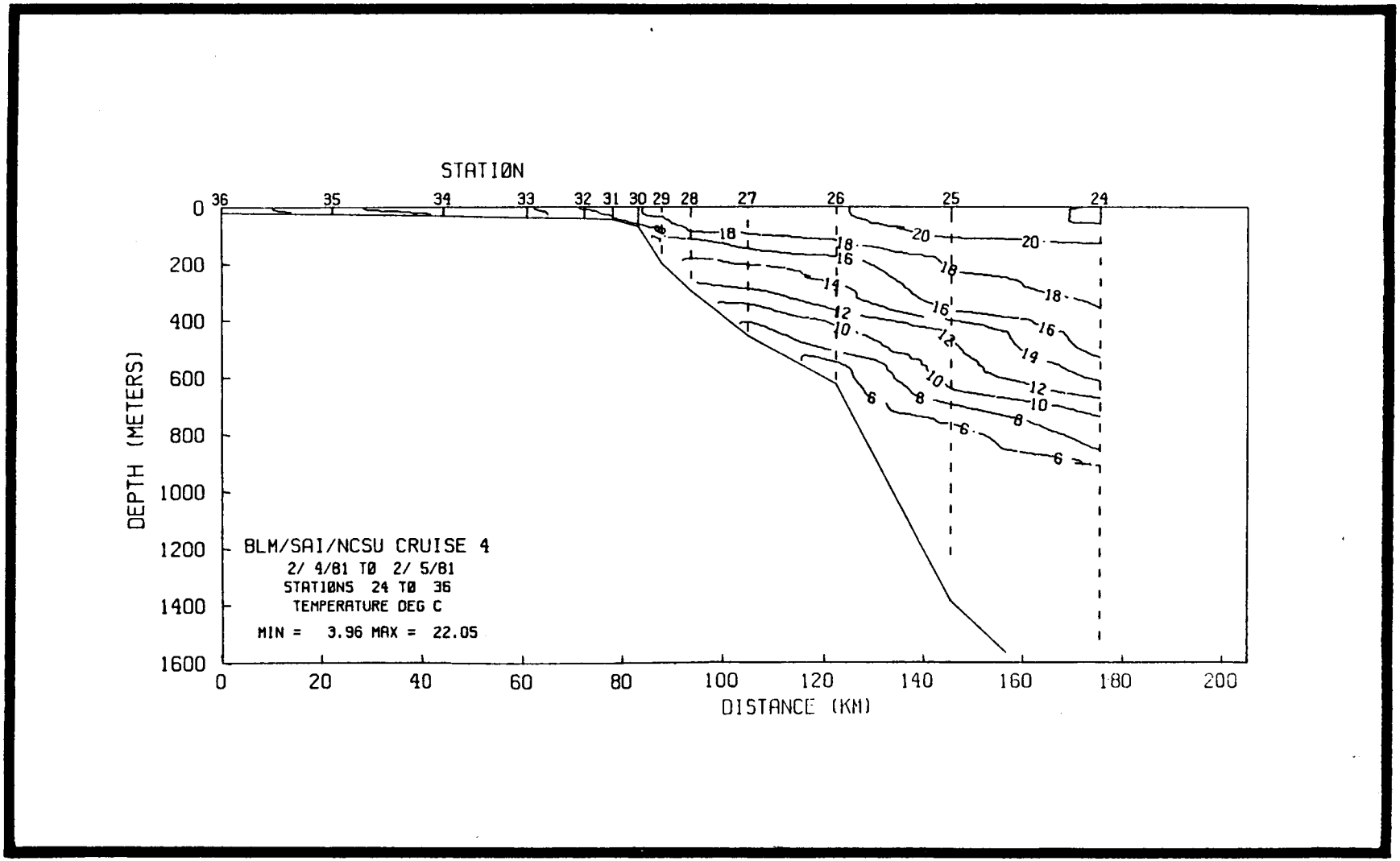

Figure 4.4-4a. Temperature for transect C (Stations 24-36) February 1981.

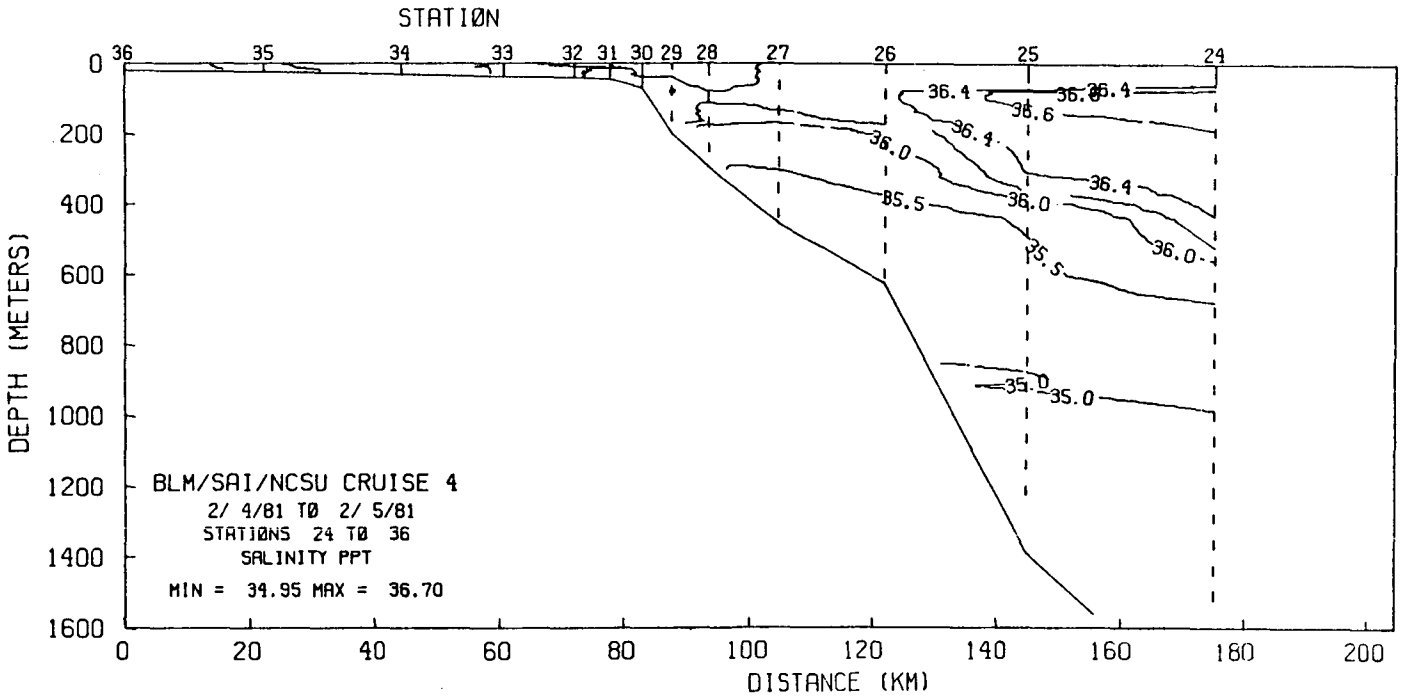

Figure 4.4-4b. Salinity for transect C (Stations 24-36) February 1981.

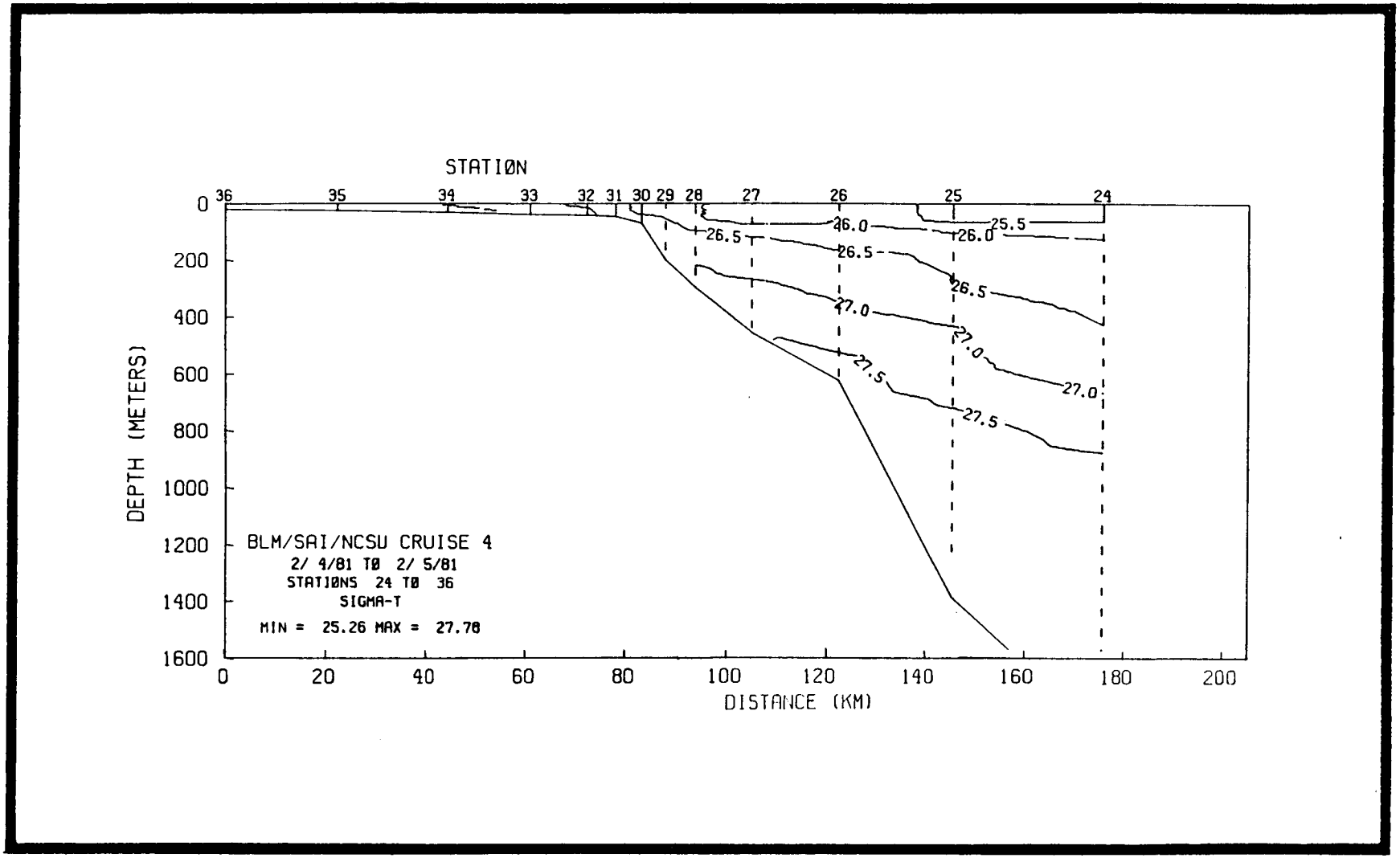

Figure 4.4-4c. Density for transect C (Stations 24-36) February 1981.

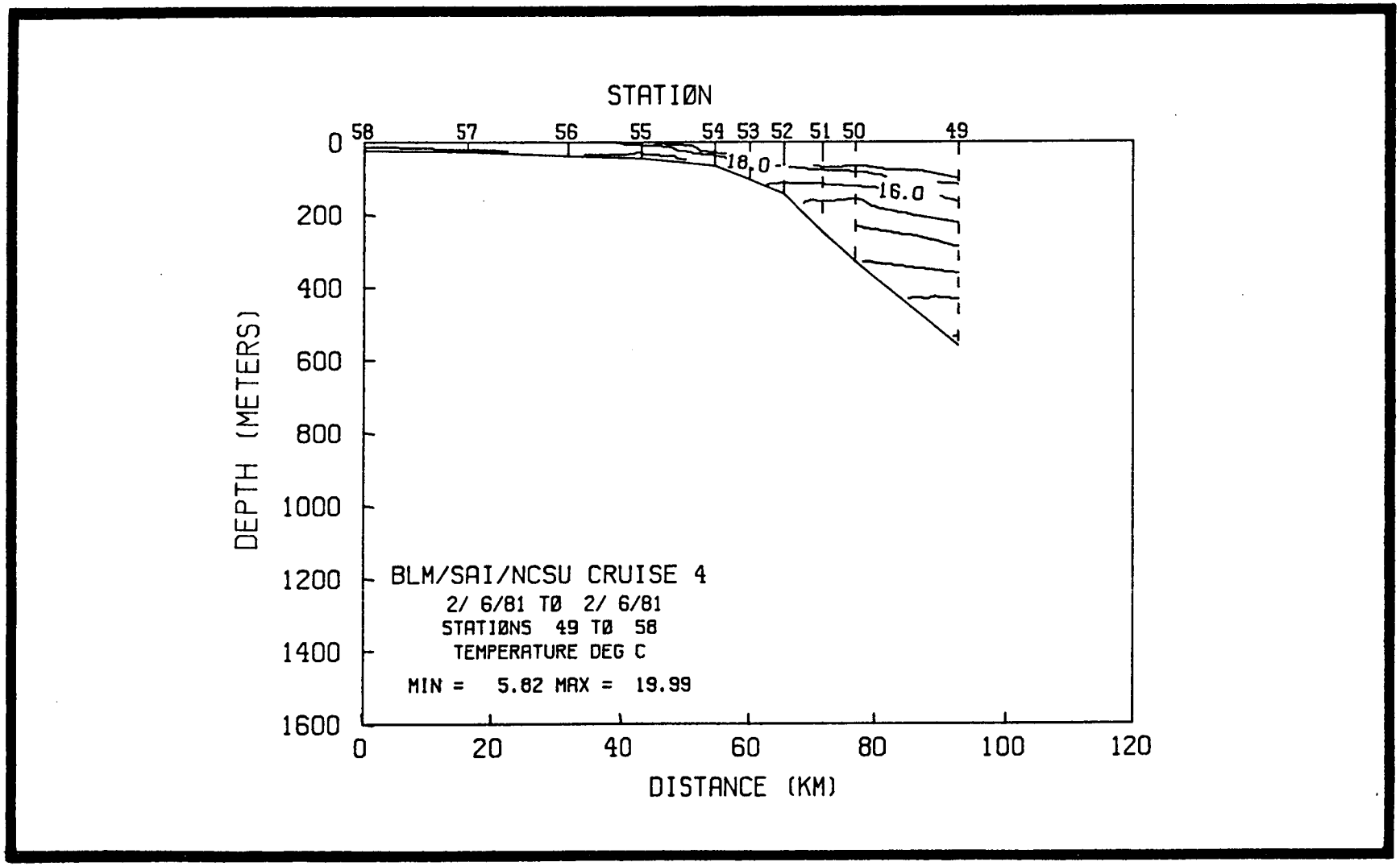

Figure 4.4-5a. Temperature for transect D (Stations 49-58) February 1981.

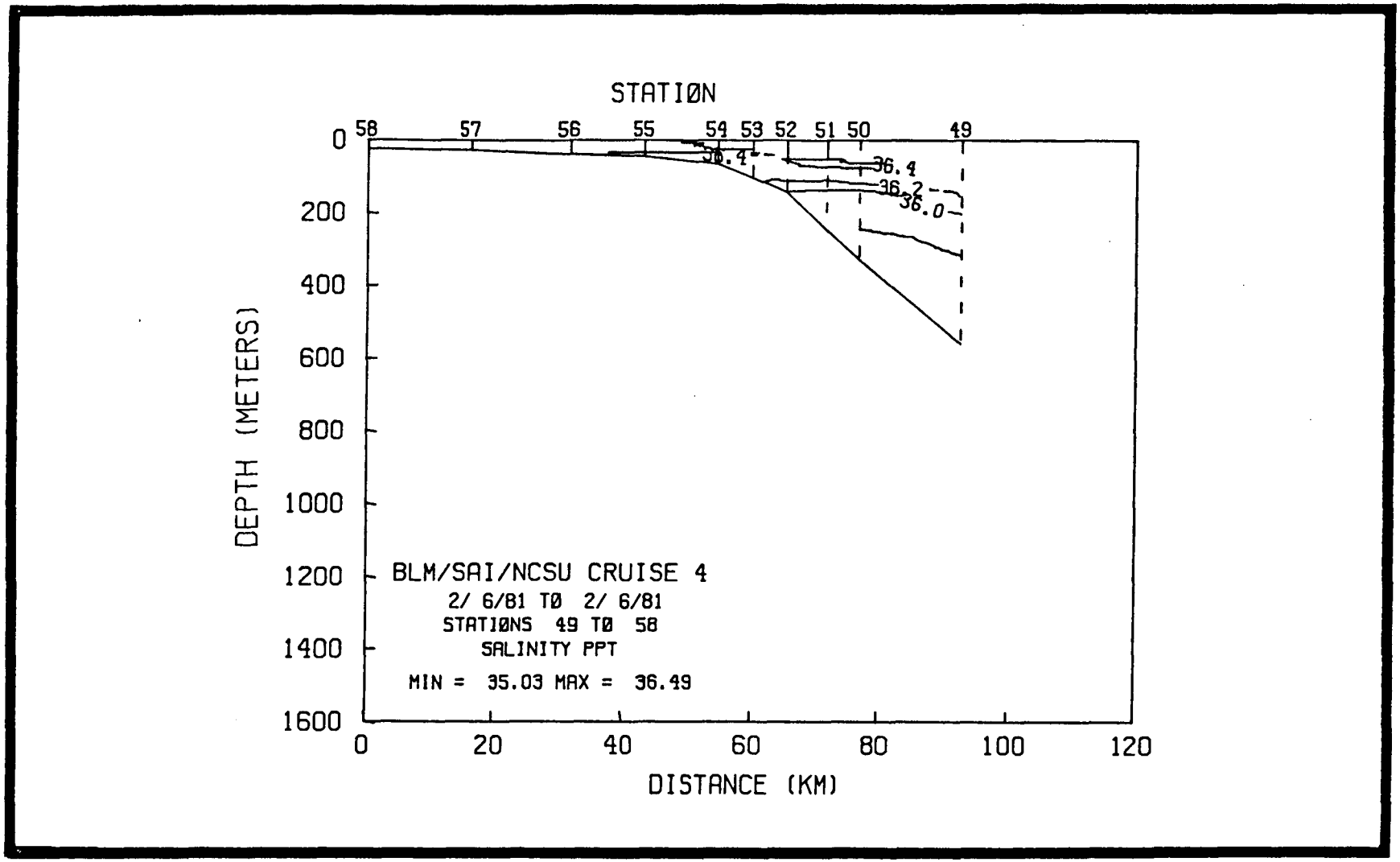

Figure 4.4-5b. Salinity for transect D (Stations 49-58) February 1981.

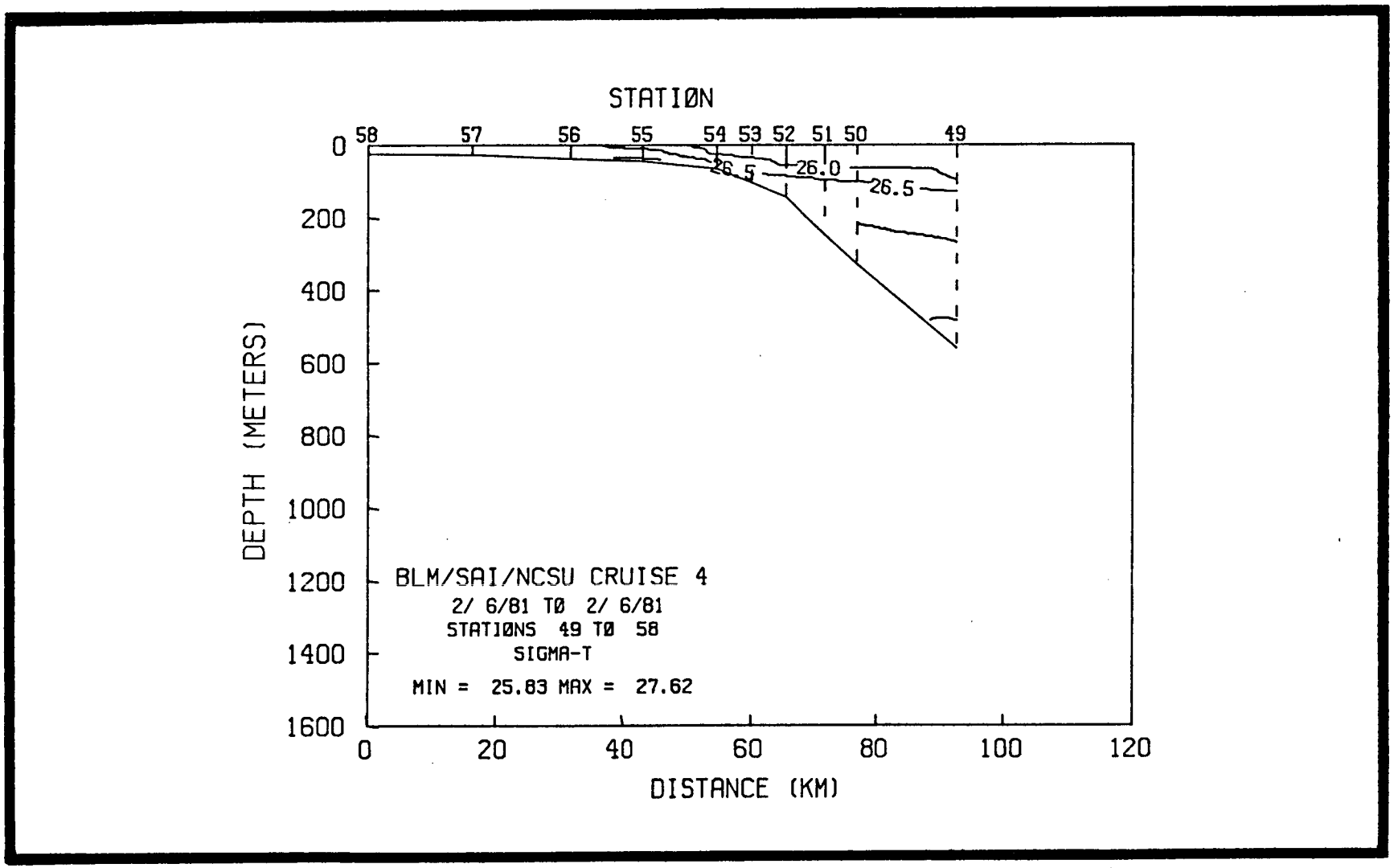

Figure 4.4-5c. Density for transect D (Stations 49-58) February 1981.

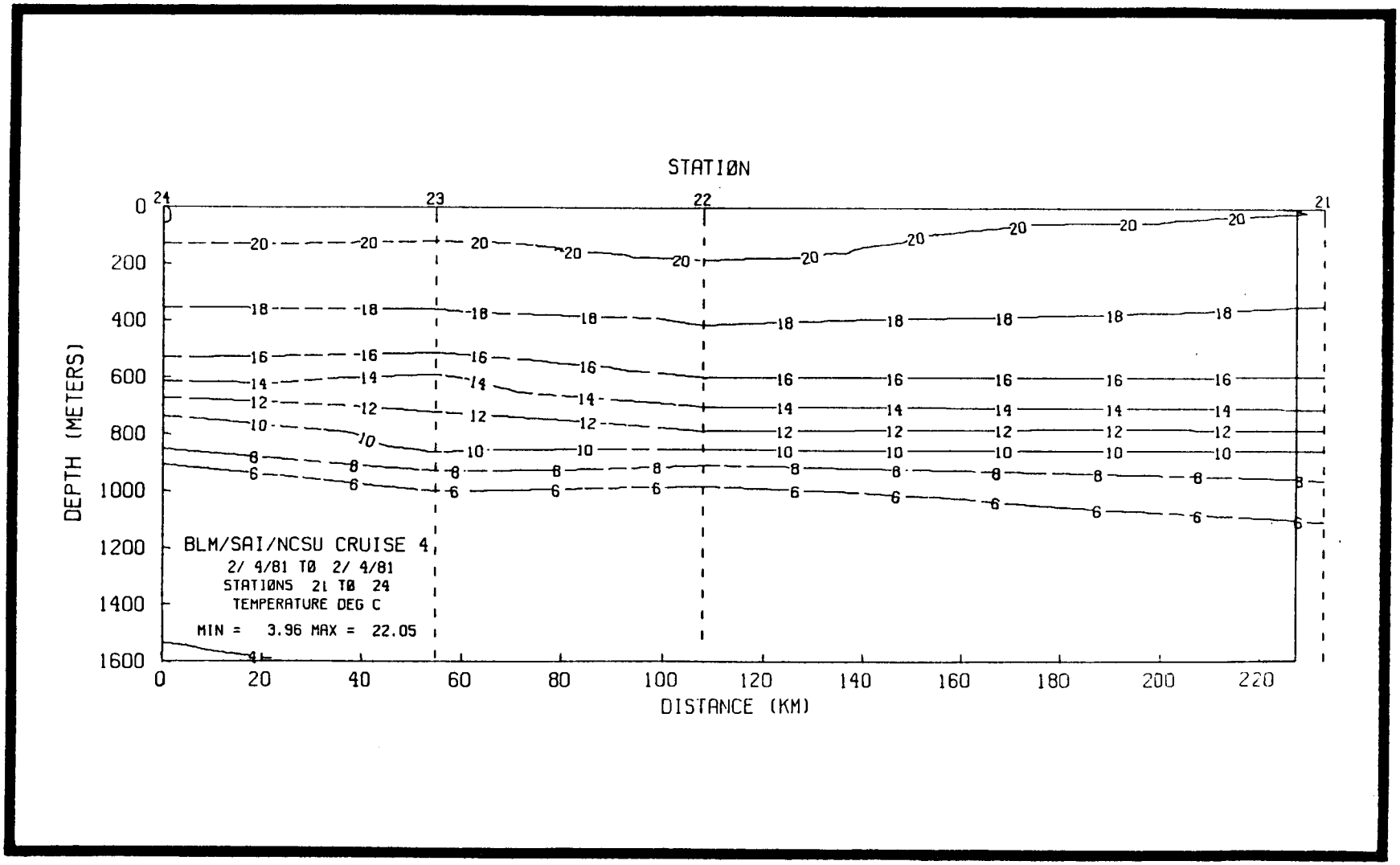

Figure 4.4-6a. Temperature for transect E (Stations 21-24) February 1981.

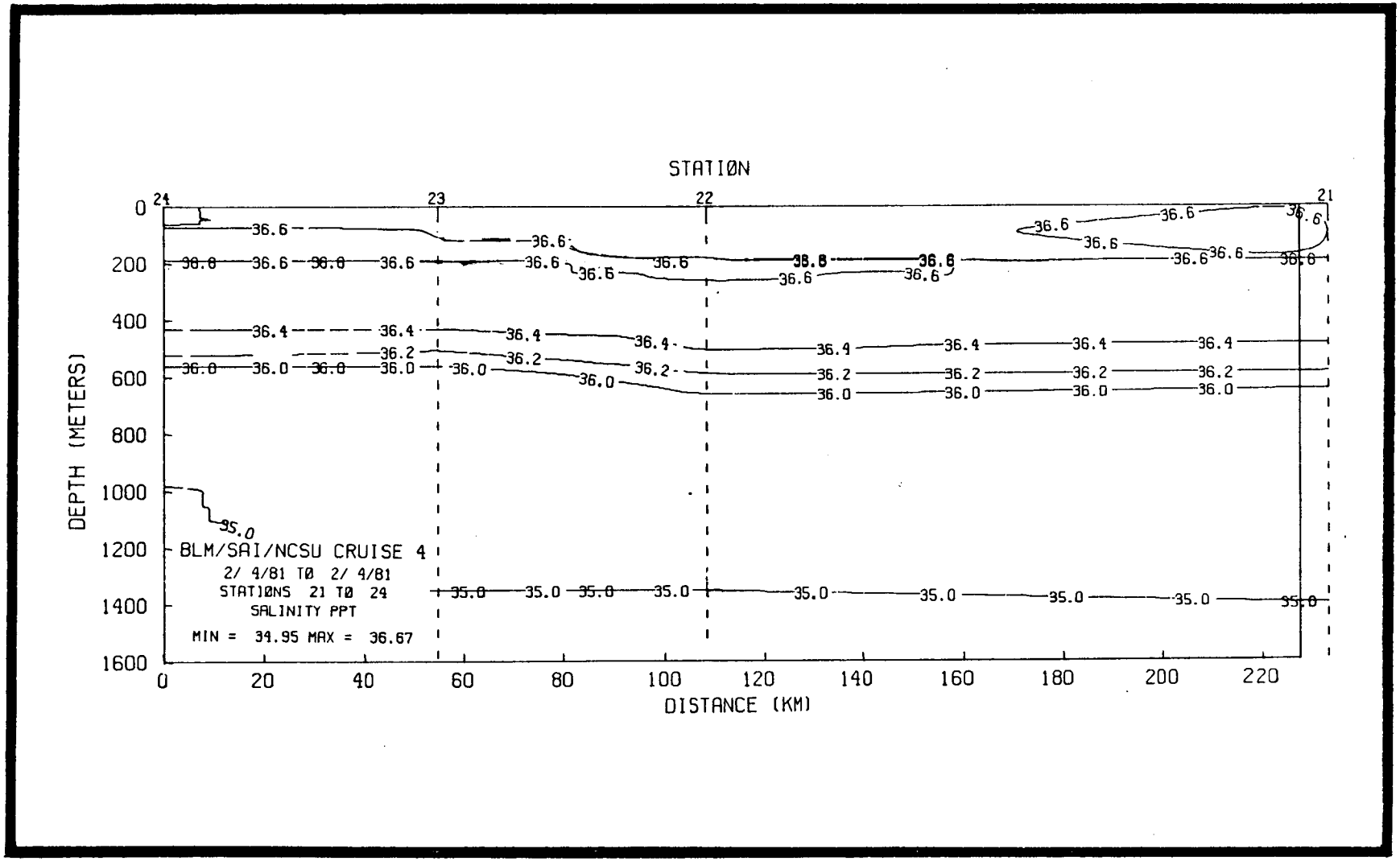

Figure 4.4-6b. Salinity for transect E (Stations 21-24) February 1981.

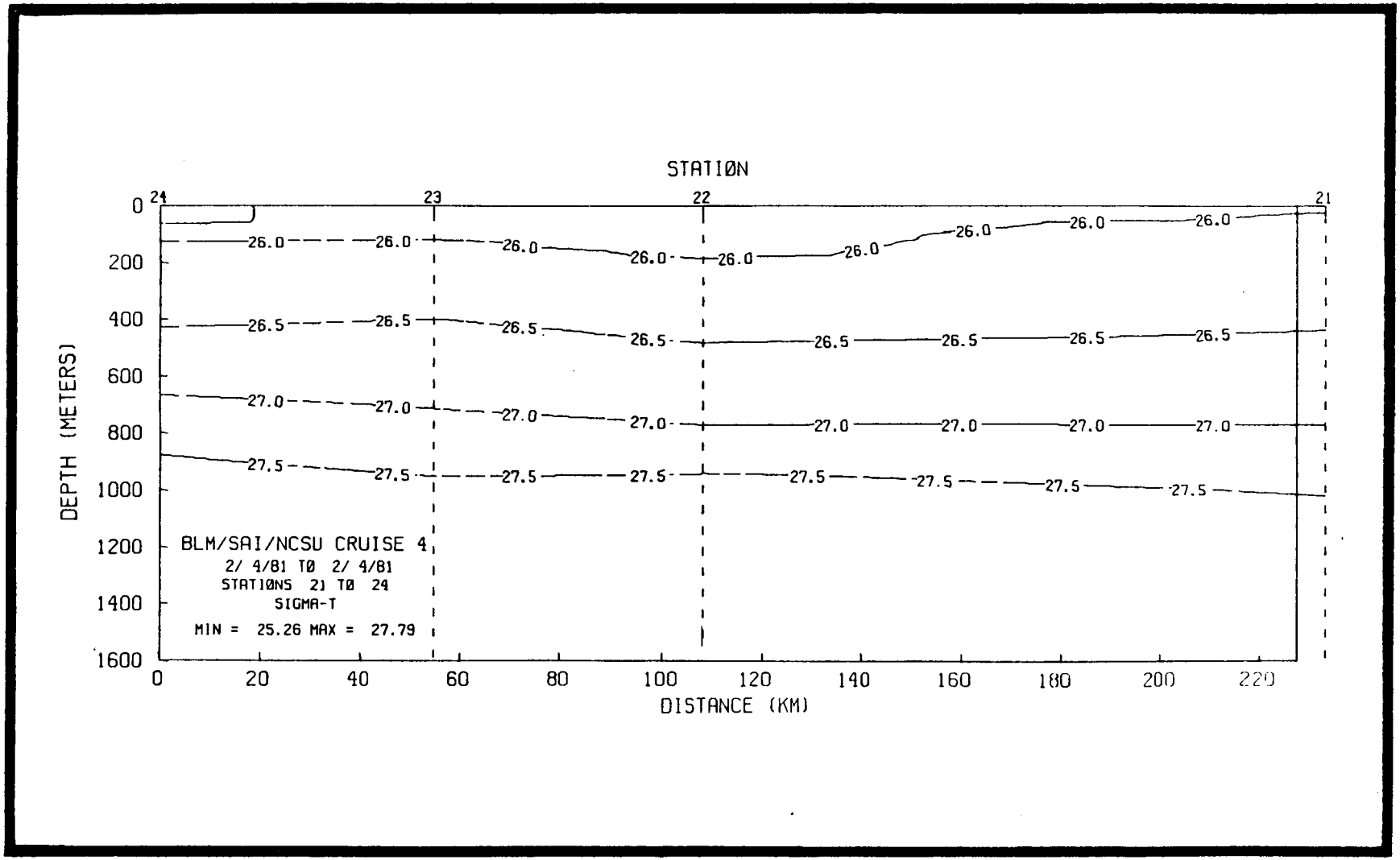

Figure 4.4-6c. Density for transect E (Stations 21-24) February 1981.

surface countercurrents are often associated with these features, making their occurrence of practical importance for vessel or marine operations.

4.5 SOUTH ATLANTIC BIGHT HYDROGRAPHY

4.5.1 Introduction

Below are presented results of two major investigations of SAB hydrographic conditions. One study evaluates oceanographic climatology of the SAB and the second analyzes hydrography in the vicinity of the Charleston Bump.

4.5.2 Climatology of the Southeastern United States Continental Shelf Waters

4.5.2.1. Introduction

Recent studies of the southeastern U.S. continental shelf waters have increased significantly the spatial and temporal coverage of hydrographic and current meter observations. Combining these data with historic data sets allows examination of the oceanographic climatology of the SAB in terms of monthly mean hydrographic properties and seasonal mean flows.

The general atmospheric climatology of SAB region, has been described by Jacobson (1974) and Ruzeki (1974). The monthly wind regime was described recently based on an analysis of the surface wind field of the SAB from a large set of ship observations (Weber and Blanton 1980). Several papers have discussed some aspects of the nearshore oceanographic climatology using lightship data (Parr 1933; Bumpus and Chase 1965; Chase 1969; and Chase 1971). Another series of papers (Church 1937; Fuglister 1947; and Schroeder 1963) discussed temperature variations in the open ocean, using data from either thermographs or hydrographic stations. However, these papers do not discuss shelf waters in detail. Studies of the SAB shelf oceanographic climatology have been limited because of the sparcity of the data base (Kantha et al. 1981); so as part of a coordinated study of the southeastern U.S. continental shelf, a large amount of new hydrographic and time series data have been gathered that, when combined with the older, historic data set, permits an examination of the climatology in terms of monthly mean conditions throughout the SAB area.

Before continuing, it is necessary to discuss the time scale of events in this area and the relationship of monthly mean statistics to both longer and shorter time scales. The broad shallow SAB responds quickly to atmospheric conditions, especially the inner-shelf area. The inner-shelf water temperature responds to air temperature cycles, ranging from daily to seasonal to interannual. The heat capacity of water acts as a low-pass filter and insures a highly damped response to daily air temperature cycles, while cycles at seasonal and interannual time scales have a large effect. Similar arguments apply to the inner-shelf salinity field, which is controlled by seasonal and interannual cycles of river discharge.

The outer shelf has a seasonal response to atmospheric conditions, but response is damped, owing to the proximity of the deep ocean. The dominant variablility there is due to Gulf Stream effects which occur on a period of

two days to two weeks (Lee et al. 1981). Niiler and Richardson (1973) demonstrated that variations in Gulf Stream transport at the two-day to two-week time scale are as large as seasonal variations. Thus outer-shelf statistics must be viewed with particular caution, especially when biological implications are considered. Because of sampling limitations of the monthly mean statistics, we will present selected examples of variability at periodicities below and above the monthly time scale.

4.5.2.2 Methods

A considerable amount of hydrographic and current meter data have been collected in the SAB over the past five years as part of a coordinated interdisciplinary study of shelf processes. A master file of this recent and historical information was created which included all data between 28° and 35°N, in water depths less than 60 m. The file contained 2872 stations for the years from 1942 to 1980. To perform the analysis, the SAB was divided into eight regions by each degree of latitude, then each region was divided into three depth zones (1-20 m, 21-40 m, and 41-60 m) representing inner, middle, and outer shelf (Figure 4.5-1). The area and volume of each depth range in each region was determined, and the results are shown in Table 4.5-1. The data were then sorted by this criteria, and surface and near bottom (within 5 m of the reported bottom depth) data were extracted for statistical analysis. Monthly means, ranges, variances, and the total number of data points of temperature, salinity, and density were computed for surface and bottom waters over the 24 sub-regions of the SAB.

4.5.2.3 Background Information

4.5.2.3.1 Physical Setting

The continental shelf of the southeast U.S. varies in width from 50 km off Cape Hatteras (Figure 4.5-1) to 150 km off of Savannah. Shelf-break water depths vary from 50 to 75 m and tend to be shallower in the southern portion. South of Cape Fear the shelf-break bathymetry is quite uniform, generally following the coastline. Extending seaward from Cape Fear, Cape Lookout, and Cape Hatteras are extensive shoals that form a series of cuspate shaped bays (Long Bay, Onslow Bay, and Raleigh Bay). A series of small rivers discharge along the western boundary between Cape Fear and Jacksonville, Fla. Along the seaward edge, the shelf is bordered by the northward flowing Gulf Stream. The Gulf Stream western edge generally lies with ± 15 km of the shelf break south of 32°N latitude (Bane and Brooks 1979). Between 32 and 33°N, a topographic feature known as the "Charleston Bump", forces an offshore meander of the Gulf Stream (Brooks and Bane 1978; Pietrafesa et al. 1978; Legeckis 1979). Downstream of the "Bump" enlarged east-west meanders displace the Gulf Stream front up to 100 km from the shelf break (Legeckis 1979; Bane and Brooks 1979).

The shelf was divided into three depth zones, which roughly correspond to zones of different flow and exchange properties. Low-frequency flow variability and water exchange in the outer shelf (41-60 m) is primarily produced by Gulf Stream events, such as northward propagating, wave-like frontal meanders and cyclonic frontal eddies, which occur on time scales of two days to two weeks (Lee and Brooks 1979; Lee et al. 1981). In the mid-shelf zone (21-40 m), low-frequency variability is mainly dependent on local wind forcing in the two-day to two-week period band (Lee and Brooks

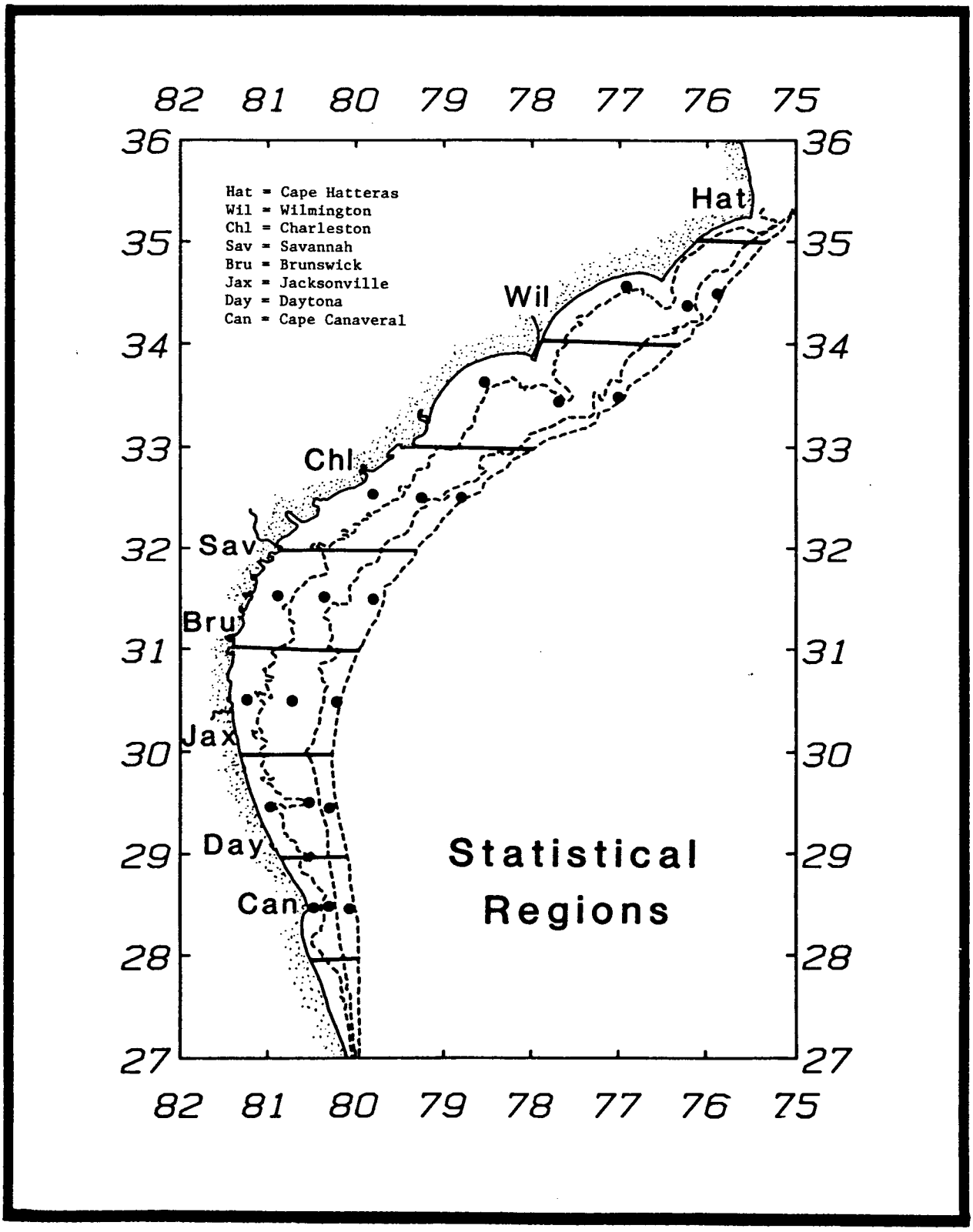

Figure 4.5-1. The South Atlantic Bight. Statistic sampling areas and central points of those areas are indicated.

Table 4.5-1 Area (km^2) and volume (km^3) of the SAB sub-regions (rounded to two significant figures).

Region	Depth	Area (km^2)	Volume (km^3)
28-29°N	0-20 m	2100	21
	20-40 m	2400	72
	40-60 m	1400	69
29-30°N	0-20 m	2800	28
	20-40 m	4900	150
	40-60 m	1400	72
30-31°N	0-20 m	4000	40
	20-40 m	7100	210
	40-60 m	2100	110
31-32°N	0-20 m	6300	63
	20-40 m	5500	170
	40-60 m	3300	160
32-33°N	0-20 m	6600	66
	20-40 m	6400	190
	40-60 m	2300	120
33-34°N	0-20 m	7000	70
	20-40 m	9800	290
	40-60 m	2200	110
34-35°N	0-20 m	3800	38
	20-40 m	7600	230
	40-60 m	1600	81
Totals	0-20 m	32,600	326
	20-40 m	43,700	1312
	40-60 m	14,300	722
	0-60 m	90,600 km^2	2,360 km^3

1979; Lee et al. 1981). Gulf Stream events can occasionally penetrate into this zone, and seasonal changes can occur due to variations in wind forcing and buoyancy flux. Waters in the inner-shelf zone (1-20 m) are strongly influenced by density effects from river run-off in addition to forcing by local winds and seasonal atmospheric changes (Blanton 1981).

4.5.2.3.2 Atmospheric Climatology and Runoff

Monthly mean air temperatures are available from coastal stations (Figure 4.5-1). Seasonal variations of monthly mean air temperature at Daytona, Savannah, and Cape Hatteras are shown in Figure 4.5-2. Minimum temperatures range from 6°C at Cape Hatteras in February to 14°C at Daytona. Maximums reach 25-28°C in July at Daytona and Savannah. The amplitude of the annual temperature cycle increases with latitude, whereas the annual mean temperature decreases with latitude. The interannual variability of the annual means have cycles at each station of 1-2°C at periods of 10-20 years. Air temperature will have greater influence on ocean temperature in the inner shelf than the outer shelf due to shallower depths.

The climatology of wind forcing in the SAB has been described by Saunders (1977), and Weber and Blanton (1980). The latter authors used marine weather observations for the period 1945-1973 to compute monthly mean winds over the SAB in a ½° x ½° grid. These data were spatially averaged across the shelf at the 29°, 31°, 33°and 35°N latitudes and are plotted as monthly mean wind-stress vectors in Figure 4.5-3. The five seasonal mean wind regimes discussed by Weber and Blanton are clearly present: winter (November through February) mean winds are northwesterly; spring (March through May) is a transition period; summer (June and July) mean winds are southeasterly off southern Florida, southerly off northern Florida and Georgia, and southeasterly off the Carolinas; fall (August) is another transitional period; and mariners' fall (September and October), mean winds are strong northeasterly.

4.5.2.3.3 Runoff Distribution

Runoff into the SAB is not concentrated in one particular area, but rather, is almost a line source between the St. John's River at 30°N and the Cape Fear River at 34°N. Figure 4.5-4 shows the distribution of runoff per km of coastline. Most of the runoff appears between 31 and 33°N. The monthly runoff pattern (Figure 4.5-5) shows a peak in February through March and a minimum in September to November. Monthly total flow varies from 30 km^3 to 100 km^3 (1-4% of the SAB volume). The total yearly flow is in the 600 km^3 range (25% of the SAB volume).

4.5.2.4 Oceanographic Climatology

4.5.2.4.1 Surface Temperature (Figure 4.5-6)

In the summer (June and July), solar insolation and shelf-water temperatures are at maximum. By July, surface temperatures greater than 28°C are found in inner-, middle-, and outer-shelf waters of the central SAB and in the outer-shelf waters off Florida. North of 32°N, surface temperatures are high but less than 28°C. In August this pattern persists with temperatures greater than 28°C throughout the central SAB, the offshore waters of Florida, and the Carolinas. The lower surface temperatures over the inner shelf from

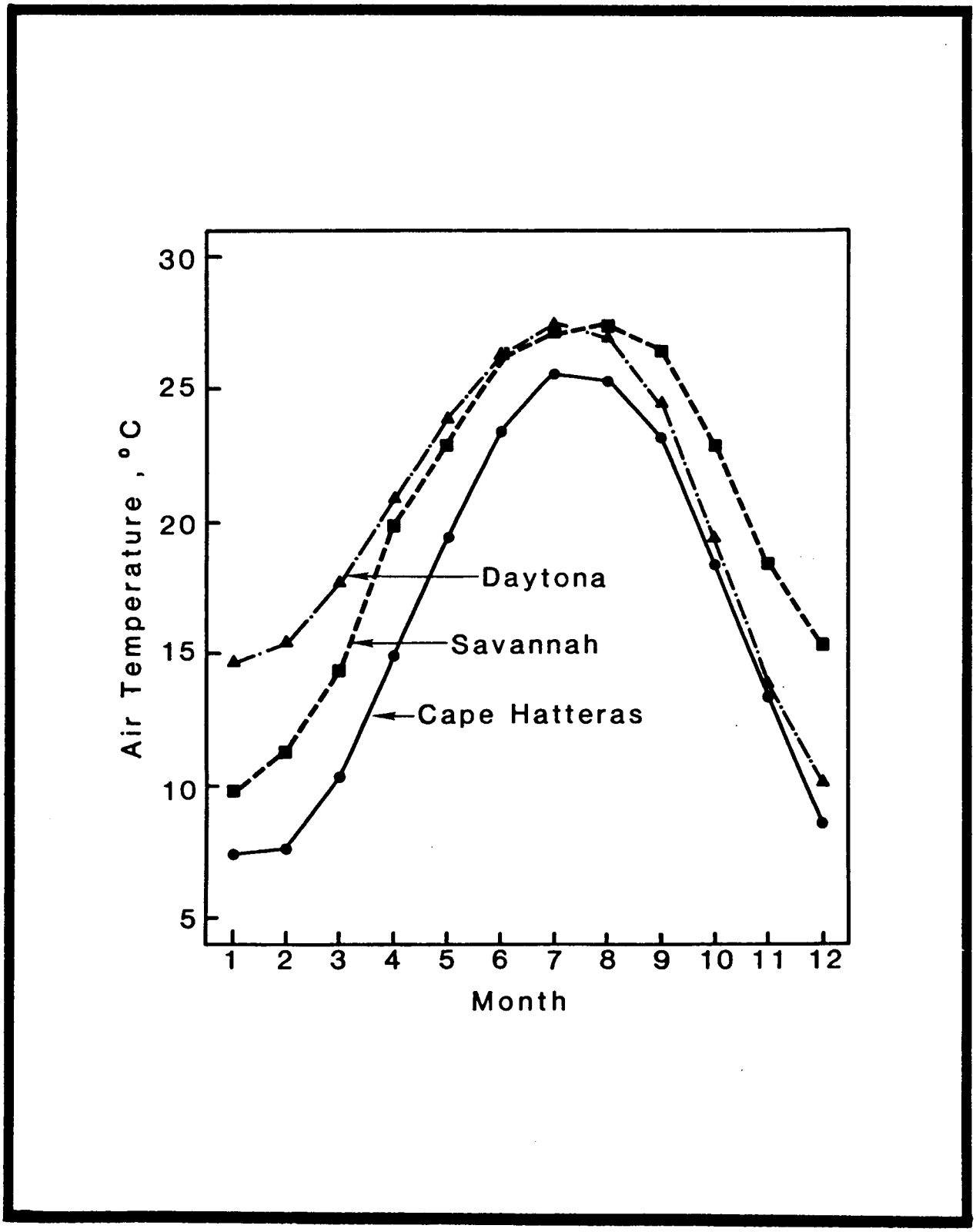

Figure 4.5-2. Monthly mean air temperature at various coastal locations.

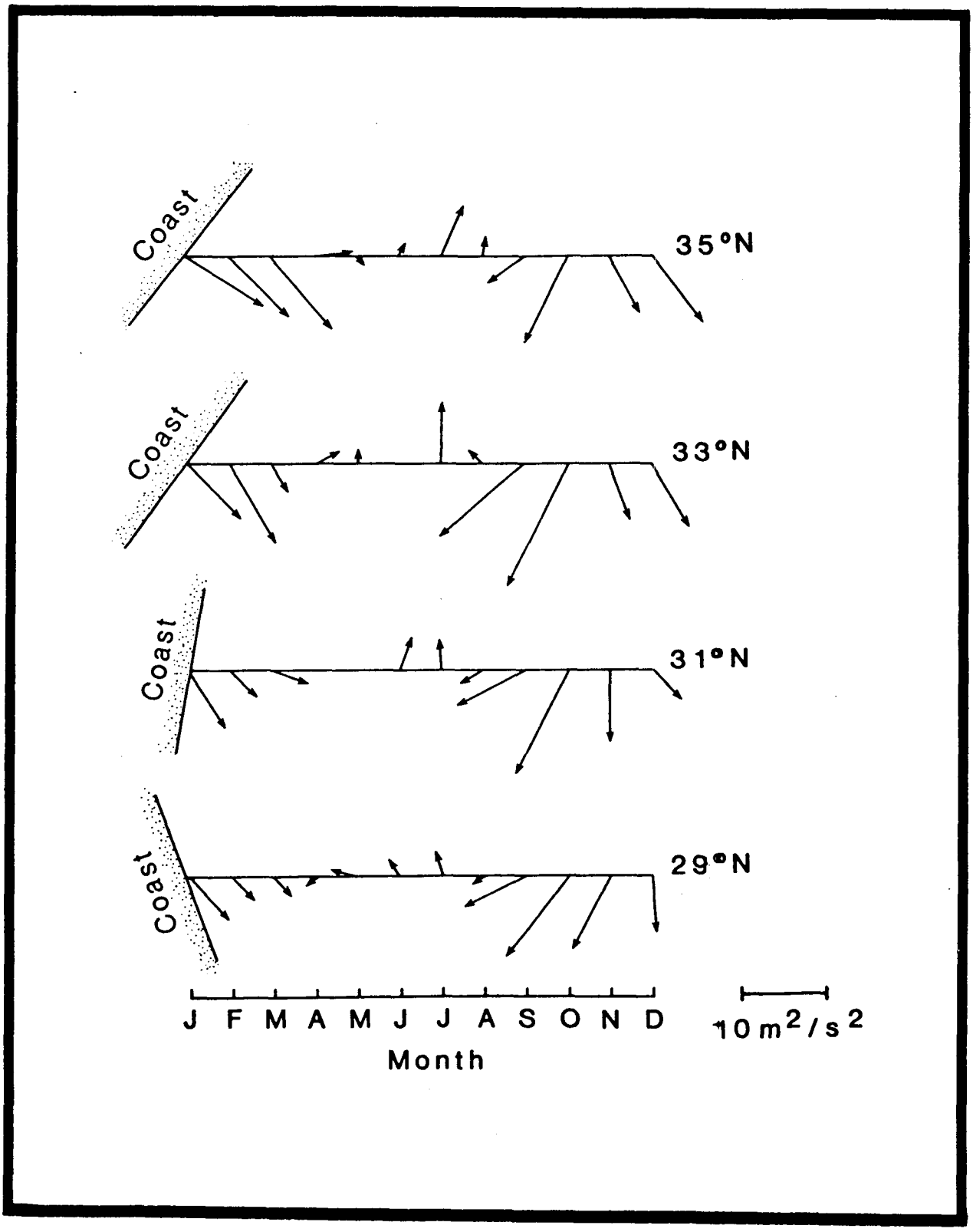

Figure 4.5-3. Monthly wind stress at various coastal locations.

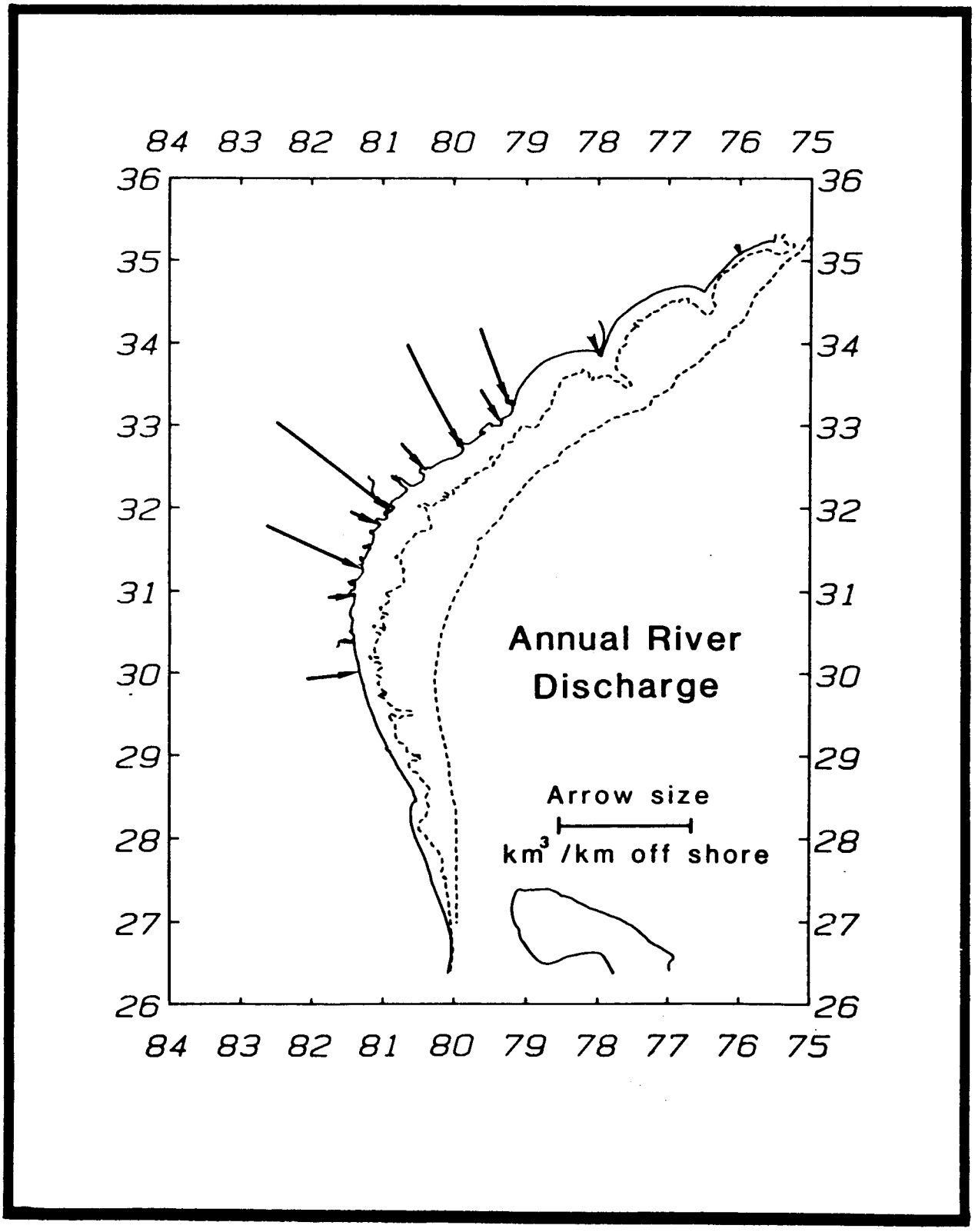

Figure 4.5-4. Distribution of runoff along the coast. Arrows indicate annual discharge in km^3 per km of coast line.

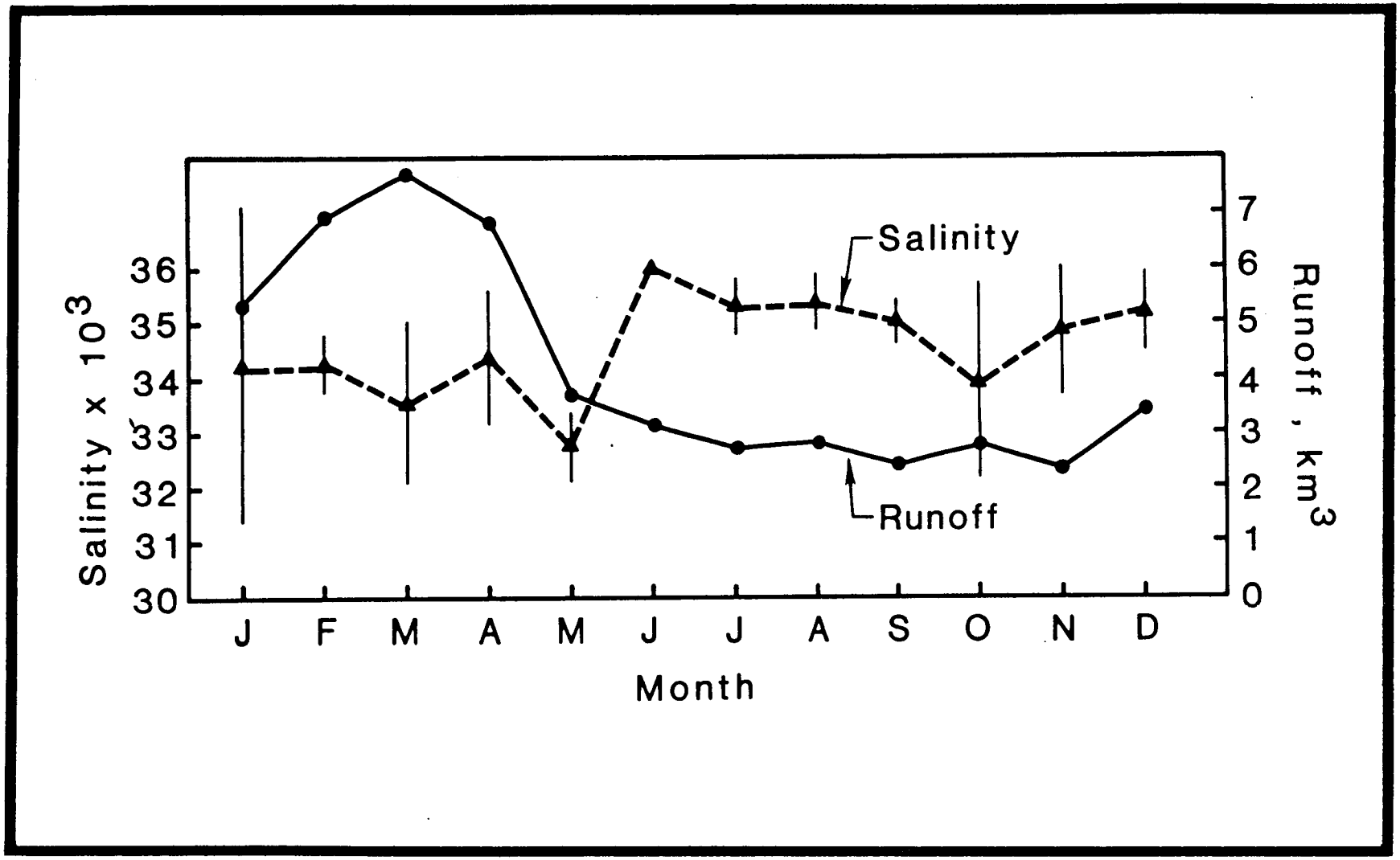

Figure 4.5-5. Monthly runoff averaged over 20 years and mean monthly inner shelf salinity.

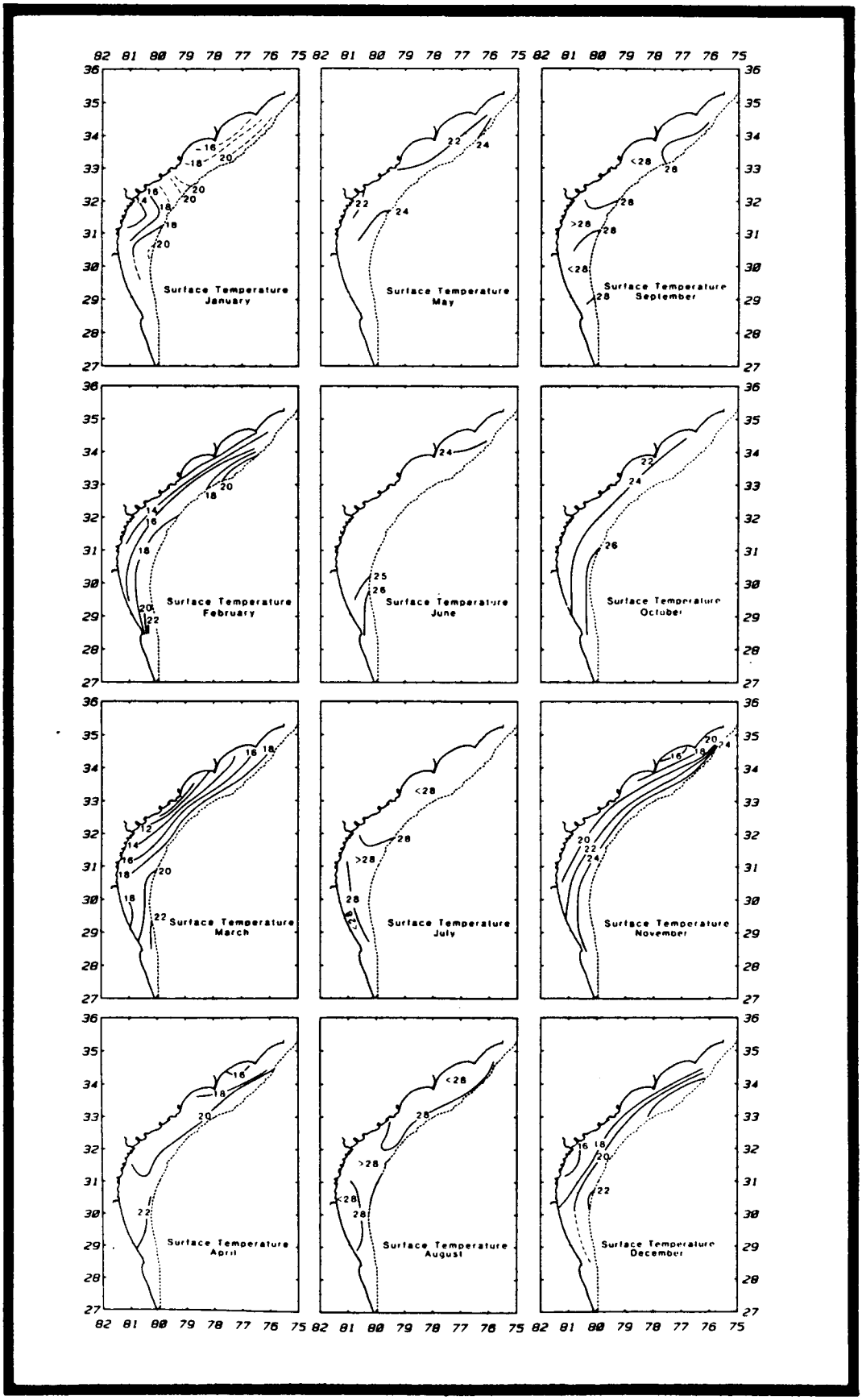

Figure 4.5-6. Monthly mean surface temperature.

29° to 31°N is no doubt related to shelf-scale upwelling induced by the upwelling favorable southwest to southeast winds during the summer (Weber and Blanton 1980; Taylor and Stewart 1959; Green 1944). In September, northern SAB waters have cooled slightly and the area less than 28°C has expanded, as has the region less than 28°C off north Florida. The region with waters greater than 28°C in the central SAB has decreased correspondingly in area.

In October, transistion into "mariners fall" (Weber and Blanton 1980) is complete. Winds are strong out of the northeast, and cooling occurs. The inner-shelf waters throughout the SAB cool uniformly, as do mid-shelf waters. Lowest temperatures are found in Long Bay (33.5°N), and warmest surface waters are over the outer shelf between 29 and 31°N. Shelf-wide cooling continues into fall, with minimum temperatures of 16°C in Onslow Bay (34°N) in November. In December maximum temperatures are found off Georgia (31-32°N). This pattern persists into January, when minimum temperatures of 14°C are observed off Georgia (31-32°N), and a second area of minimum temperatures is found off southern North Carolina (33.5-34.5°N). Surface temperatures in February are further lowered when inshore waters off North Carolina are less than 12°C, and waters off Georgia are between 12 and 14°C. The annual low temperatures are observed in March, when inshore waters off South Carolina are less than 10°C. To the north and south, inner-shelf waters are beginning to warm. In April, shelf waters are heating uniformly from south to north, a pattern which persists through June.

4.5.2.4.2 Surface Salinity (Figure 4.5-7)

Runoff should significantly affect shelf salinites, and indeed the lowest salinities are observed in April and May during the periods of highest runoff, offshore of the Georgia and South Carolina coasts. Curiously, during October, very low salinities are found off Florida. Fall runoff is one-third the spring runoff, so either the monthly mean is biased or, as we believe, the strong northerly winds of October are restricting low salinity water to the coastal zone, inhibiting horizontal exchange processes and advecting these waters to the south.

In summer, shelf salinities vary from 34 to 36°/oo. Lowest salinities are found on the inner shelf off South Carolina. Highest salinities are found over the north Florida and Georgia outer shelf. A region of lower salinity appears over the north Florida shelf. This may be related to upwelling in that area. The position of low salinity water off South Carolina may be related to southerly winds advecting the low salinity coastal waters to the north.

4.5.2.4.3 Bottom Temperature Distribution (Figure 4.5-8)

Near-shore bottom temperatures are similar to surface waters, with a winter minimum in the central SAB and off North Carolina, with temperatures decreasing from offshore to onshore. By April, the situation reverses in the southern SAB where the heated shelf waters are warmer than upwelled Gulf Stream waters. In May, the only area of contrast is the outer shelf in the middle SAB. In June, July, and especially August, middle- and outer-shelf waters of the southern SAB are clearly affected by upwelled Gulf Stream water. With fall cooling, the situation again reverses to the winter situation of increasing temperatures offshore.

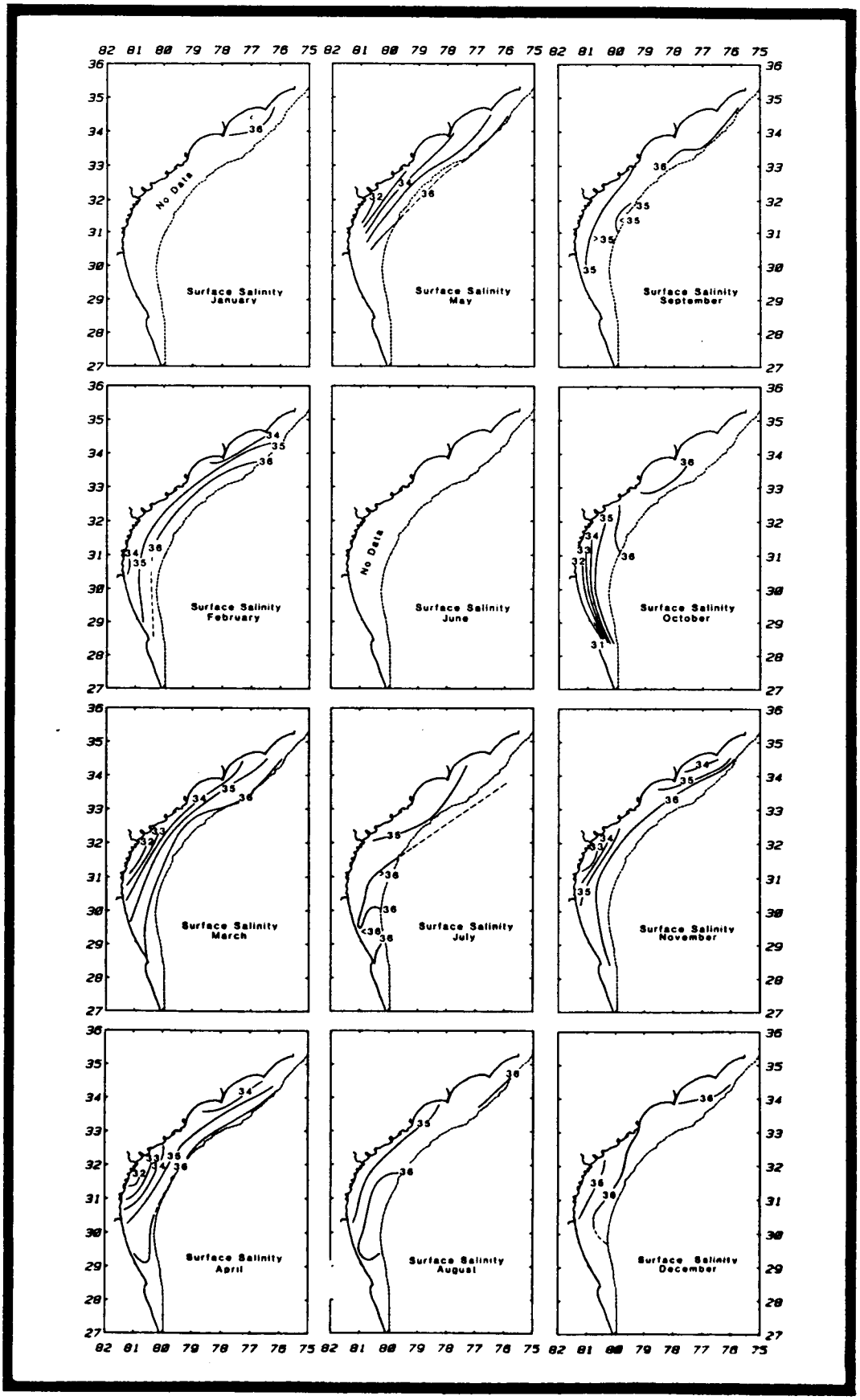

Figure 4.5-7. Monthly mean surface salinity.

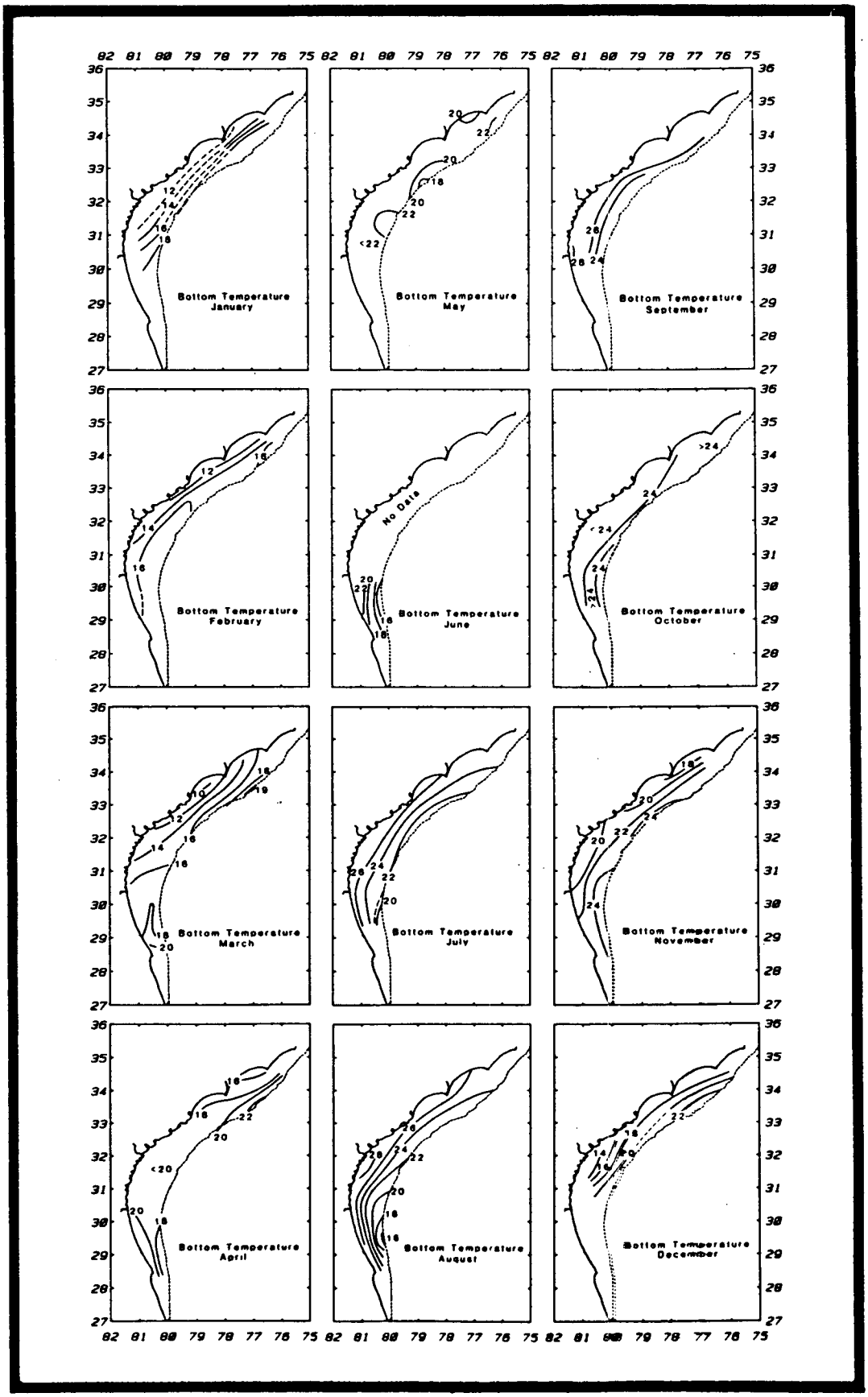

Figure 4.5-8. Monthly mean bottom temperature.

4.5.2.4.4 Currents

The climatology of SAB mean flow conditions is not as well defined as for atmospheric and hydrographic variables. Early estimates of mean flows were derived from hydrographic data and drifter trajectories. Bumpus (1973) presented results of drifter studies that showed surface flow generally northward from January through July, switching to southward in August through October, with an indication of continued southward flow in November and December. Surface flows showed a strong tendency to follow the prevailing winds. There was also evidence of a more persistent southward flow in a narrow band near the coast. Bottom flows were generally onshore throughout the year with either a north or south component that was not consistent with the surface flow except in August and September. Weber and Blanton (1980) found that if one takes into account a time lag of about one month between drifter release and recovery, then Bumpus' (1973) surface drifter data were consistent with the mean wind patterns; i.e., northwesterly in winter (November through February), southeasterly in summer (June and July), and northeasterly during mariner's fall (September and October).

Current measurements using moored current meters are relatively new to the SAB and cover only a small portion of the overall area. Winter and summer mean flow patterns on the Georgia shelf were determined from averaged current meter data for the periods 10 December 1976 to 10 April 1977 and 2 July to 4 November 1977 (Figures 4.5-9a-b). Analysis of cumulative weekly averages indicates that mean flows begin to stabilize for averaging periods of three months or greater. Therefore, mean values based on averaging periods less than three months should be viewed cautiously.

The mean flows are surprisingly similar for the winter and summer periods. A strong Gulf Stream influence in the outer shelf is clearly visible. Mean upper layer flow at the shelf break (75-m isobath) was toward the north at about 65 cm s^{-1} in the winter and 54 cm s^{-1} in the summer, with onshore components of 1 and 6 cm s^{-1} in the winter and summer, respectively. The standard deviation of subtidal along-shelf flow was ± 44 cm s^{-1} in winter and ± 56 cm s^{-1} in summer. In the near-bottom layer at the shelf break, mean flow was to the north at 8 cm s^{-1}, with an offshore component of 3 cm s^{-1} in winter. In summer, flow was toward the north at about 3 cm s^{-1}, with an onshore component of 1 cm s^{-1}. Standard deviations were about ± 13 cm s^{-1} for the subtidal along shelf flow during winter and summer.

At the 45-m isobath, a significant Gulf Stream influence is still evident. In the upper layer, the winter mean flow was northward at 17 cm s^{-1}, with an offshore component of 6 cm s^{-1}. Summer mean flow was southward at 5 cm s^{-1} and onshore at 3 cm s^{-1}. In the lower layer, the mean flow was northward at 4 cm s^{-1} and offshore at 2 cm s^{-1} in the winter, and onshore at 1 cm s^{-1} and zero along-shelf component in the summer. Subtidal standard deviations were several times the means during both seasons. At mid-shelf (30-m isobath) the summer mean was weakly to the north at 1 cm s^{-1} in both layers, with an offshore component of 1 cm s^{-1} in the upper layer, and onshore at 1 cm s^{-1} in the lower layer. The standard deviations were approximately ± 9 cm s^{-1} for the upper and lower layers during both seasons.

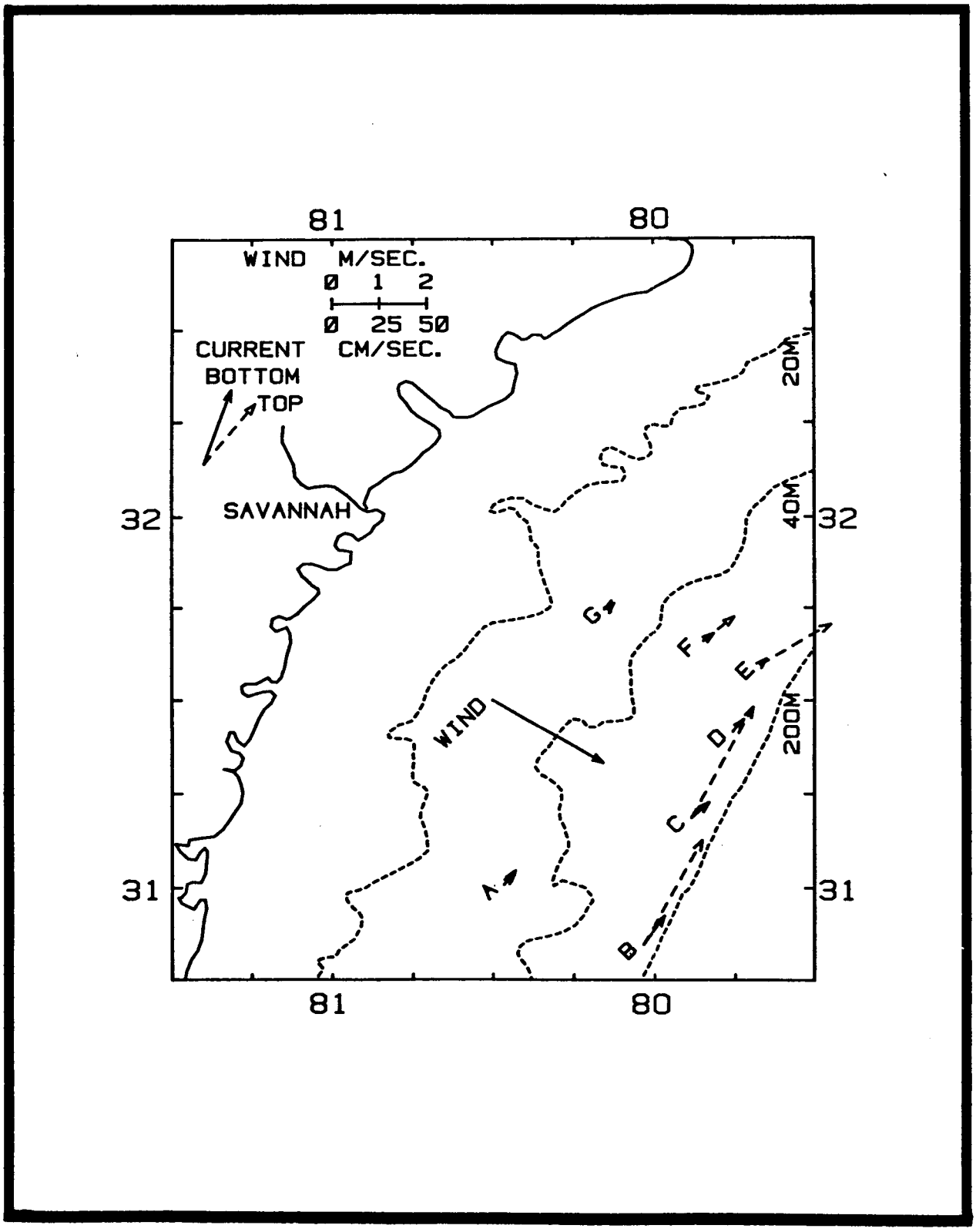

Figure 4.5-9a. Mean circulation during winter 1977.

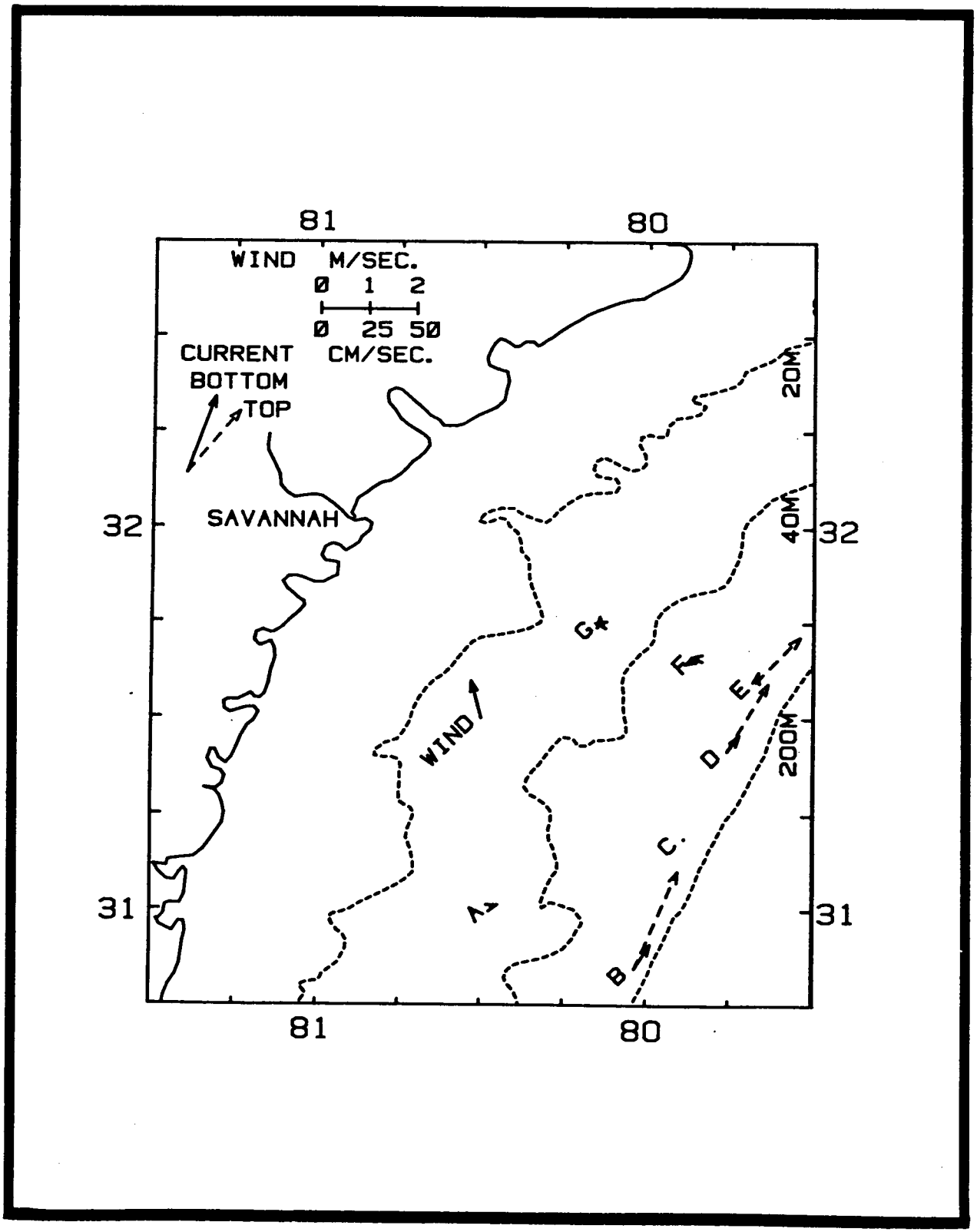

Figure 4.5-9b. Mean circulation during summer 1977.

4.5.2.5 Discussion

4.5.2.5.1 Heat Flux in Inner-shelf Waters

Heat exchange between shelf waters and the atmosphere can be calculated for the inner shelf by assuming that advective heat flux is relatively small. This is believed to be a reasonable assumption, since the inner-shelf waters on this broad, shallow shelf respond quickly to atmospheric thermal forcing, and the frequency of atmospheric events is higher than hydrospheric advection. The net heat exchange, Q_n, was calculated by determing the monthly change in the heat content of the inner-shelf statistical areas:

$$Q_n = (\Delta T)(Z)(\alpha) \quad (1)$$

where ΔT = change in monthly mean temperature (C°)

Z = mean depth of inner shelf (10 m)

α = heat capacity (1 cal g^{-1}).

Data were smoothed by spatially averaging over the southern (29 and 30°N), middle (31 and 32°N), and northern (33 and 34°N) parts of the SAB (Figure 4.5-10a). Heat exchange estimates were converted into units of watts m^{-2} by using the conversion factor 1 Kcal cm^{-2} $(30 \text{ days})^{-1}$ = 16.15 watts m^{-2}.

The heat flux estimates indicate heating in March through July with maximum rates of 100 W m^{-2} (6.3 Kcal cm^{-2} $month^{-1}$) corresponding to a 6.3°C rise in the inner-shelf mean water temperature. Cooling occurs in October through February, with maximum exchange rates of about -80 W m^{-2} (4.9 kcal cm^{-2} $month^{-1}$). These rates are slighly less than those for the Mid-Atlantic Bight (Bunker 1976, as cited in Beardsley and Boicourt 1981).

The annual net heat exchange, Q_T, for the three areas (Figure 4.5-10b) shows a calculated net heat loss of 2.6 Kcal cm^{-2} $month^{-1}$ over the year. This is about 10% of the total yearly heat flux (absolute value of the monthly flux) and probably within our error margin. This agrees with other annual average heat gain calculations (Bunker 1976). The mean shelf-water temperature, T, clearly lags the accumulated heat input during the spring, reflecting losses due to sensible heat flux and evaporation. Back radiation is in the range of 200-250 cal cm^{-2} day^{-1} which would cause a temperature decrease of 7.5°C per month in the 10-m average depth inner-shelf waters. The additional heat loss due to latent heat associated with evaporation would cause an additional 12.1°C temperature decrease (assuming evaporation = 0.7 cm day^{-1}; mean water temperature = 20°C).

The rapid response of the inner-shelf waters is well illustrated in time series from a bottom temperature recorder located about 12 km off the coast at 31°N in 12 m of water (Figure 4.5-11). Water temperature was recorded at the bottom of a normally-mixed water volume, and air temperatures are the average of those recorded at the Savannah and Jacksonsville airports. Since cooling events are associated with northerly winds, these air temperatures are no doubt representative of air temperature at the offshore site. In the fall, sea temperatures decrease with the arrival of each cold front and there appears to be less than a 30° phase lag. During spring, warming water responds more slowly to atmospheric changes, due to smaller air-sea

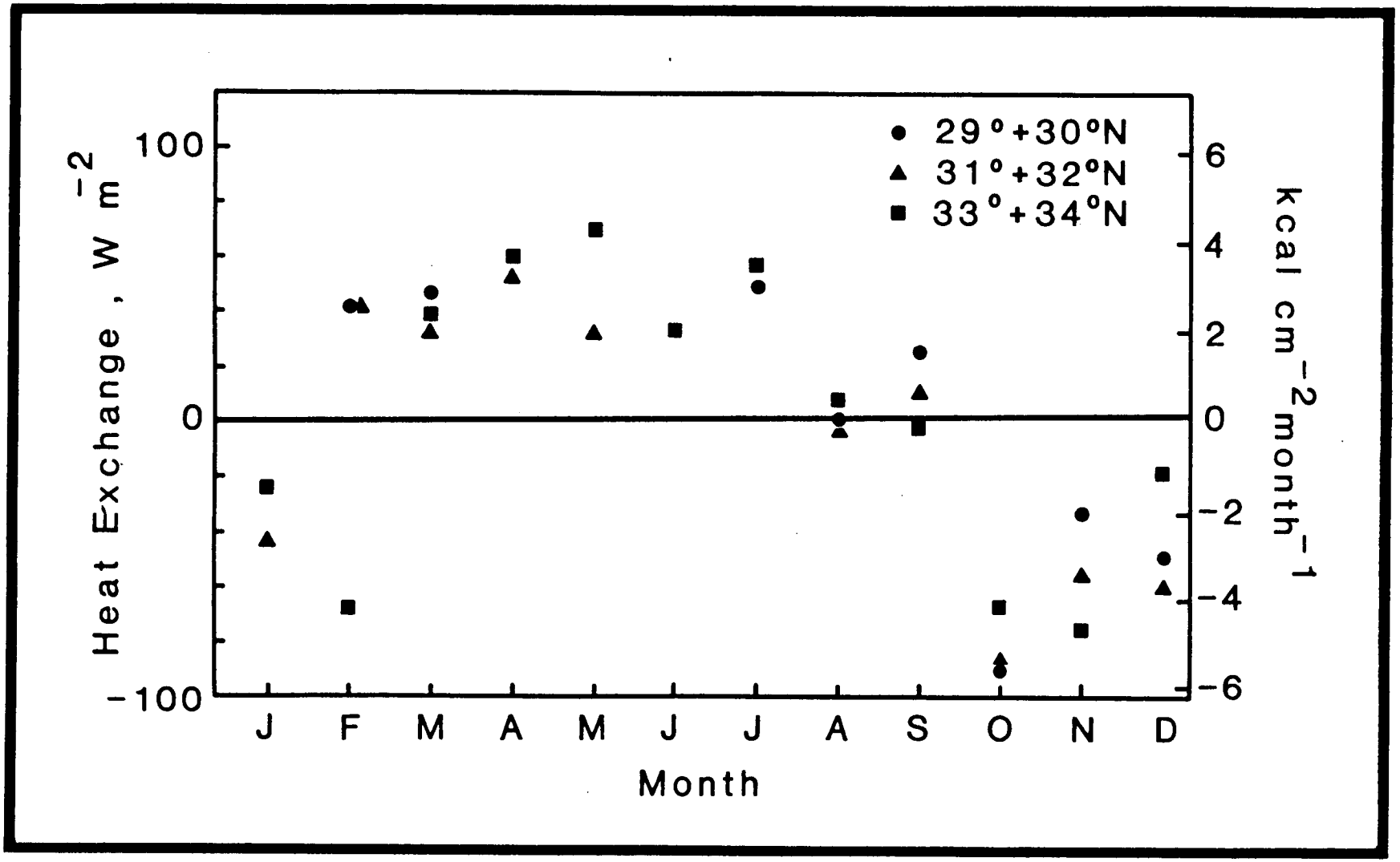

Figure 4.5-10a. Mean monthly heat flux for the southern, middle, and northern inshore SAB.

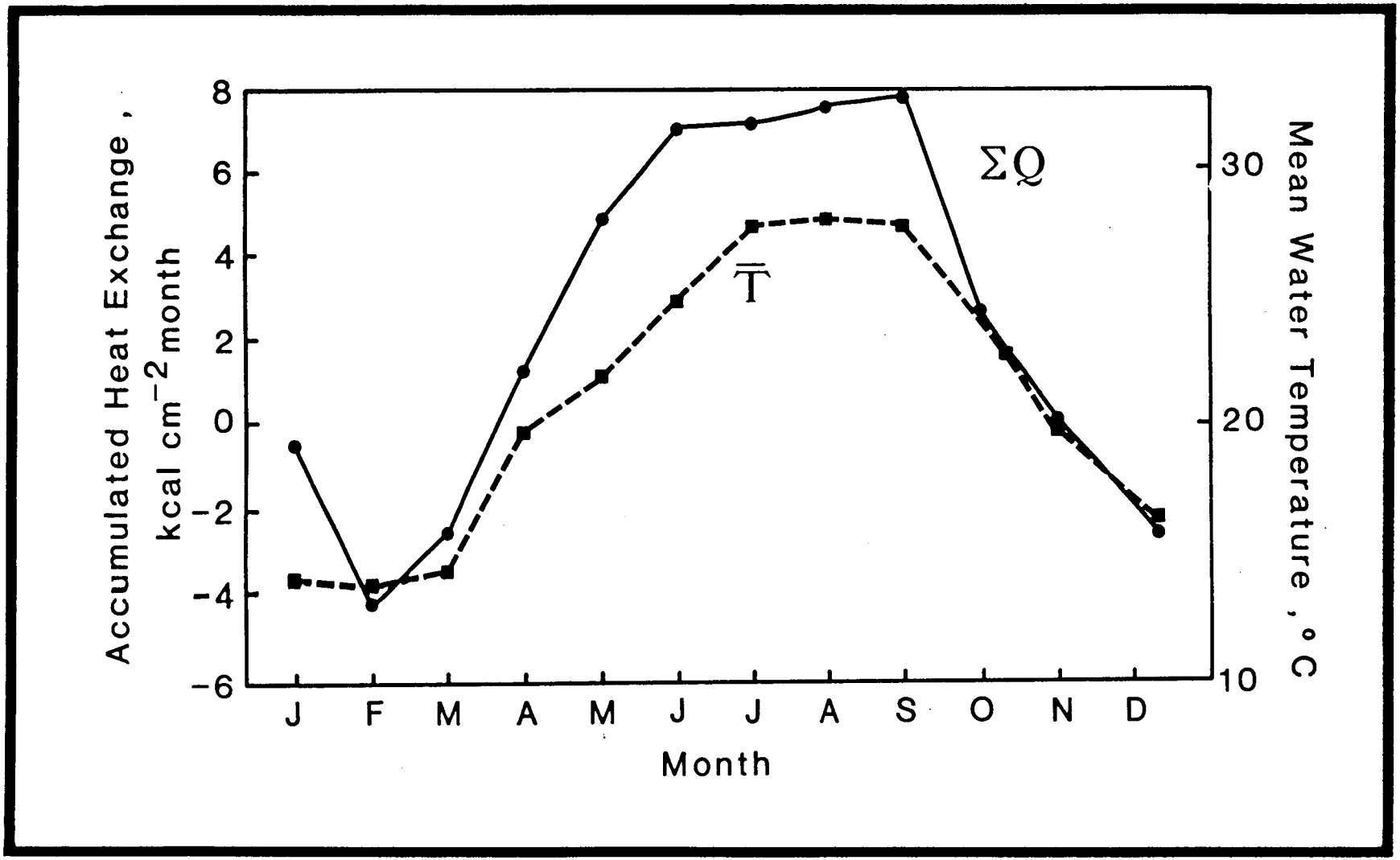

Figure 4.5-10b. Accumulated heat flux and mean inner-shelf temperature.

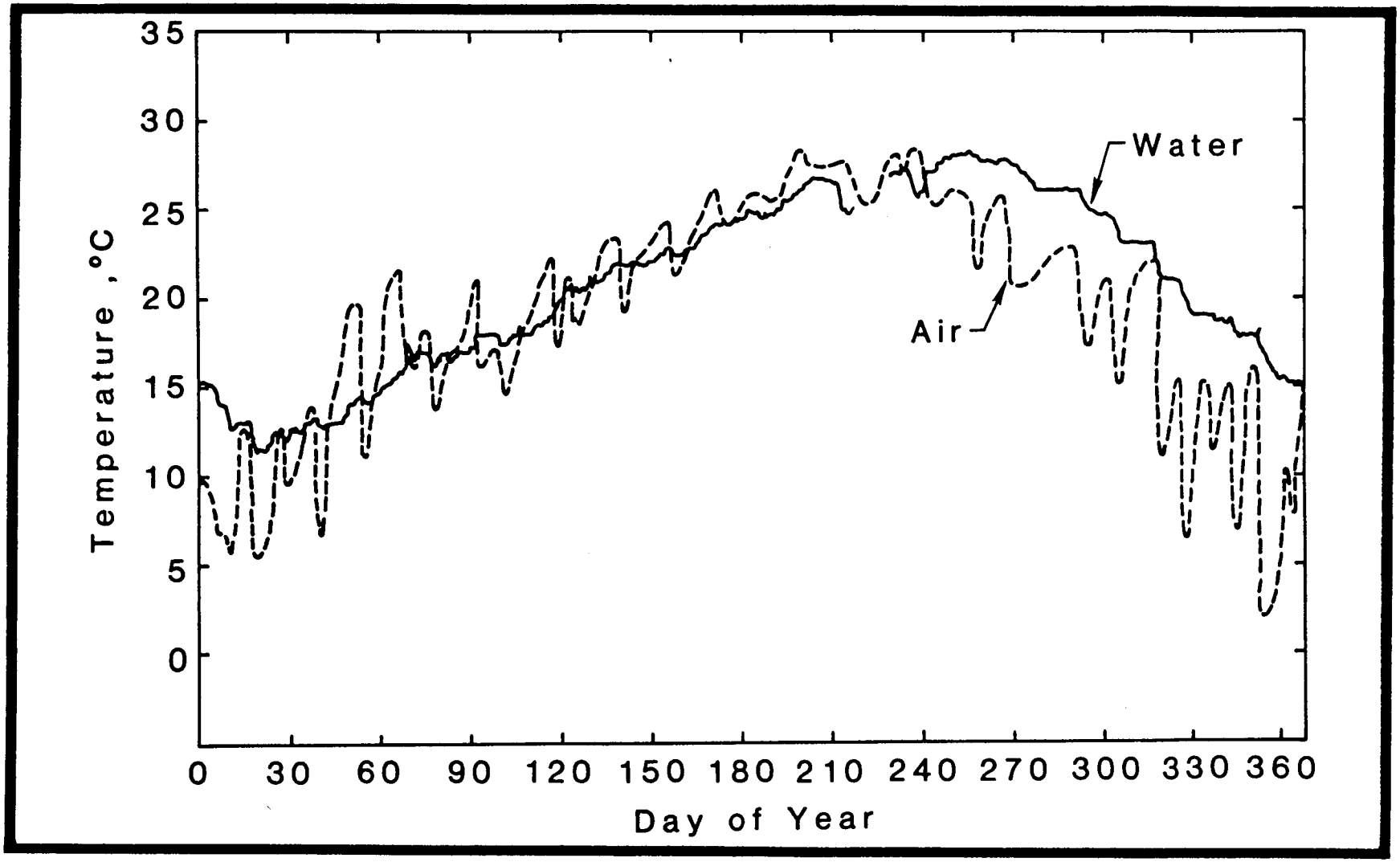

Figure 4.5-11. Bottom temperature (—) at 12 m of water at 31°N, and average of air temperature at Jacksonville and Savannah airports (---).

temperature differences and weaker winds. Thus, heat is quickly removed from inner-shelf waters in the fall, but added more slowly in the spring.

4.5.2.5.2 Mean Inshore Salinities

The mean salinity for all inshore stations (0-20 m) is plotted by month in Figure 4.5-5, along with the 20-year mean monthly runoff. Clearly, inshore salinities are higher during periods of low runoff and lower for periods of high runoff. The point scatter makes any interpretation questionable, but it is notable that October again appears as a slight anomaly, with lower salinities associated with slightly higher runoff.

A monthly mean flushing rate can be calculated from the monthly runoff rate, mean salinity, and an assumed base salinity of 36°/oo (Atkinson et al. 1978). The mean annual flushing rate calculated this way is 3 months, with a range of 1.7 to 6.5 months (Table 4.5-2). The monthly flushing rate values are scattered, but tend to be higher in the spring and fall. Summer stratification and weaker winds may restrict cross-shelf circulation.

4.5.2.5.3 Volumetric Analysis

Volumetric T-S diagrams for each month (Figure 4.5-12) show the volume of water in km^3 in each bivariate class. Because of the large variations in T and S, we chose a bivariate increment of 1°/oo for salinity and 3°C for temperature. A finer scale could be used, but the salient points are readily discernable at present increments. For each month we have indicated the volume of the shelf represented in that data set. In January, for example, we had data representing only 43% of the volume of the shelf, which would be too small a sample for reasonable interpretation. However, in most months over 80% of the shelf volume was in our sample, thus mean conditions on the shelf are represented.

In February, as in all months, a substantial amount of shelf water is in the 36°/oo salinity class. However, because of increasing runoff, about 23% of the shelf volume exhibits salinities less than 36°/oo. In March, runoff increased, and the associated higher salinity is obvious. Waters less than 36°/oo salinity account for 29% of the shelf volume. In April, waters with salinity less than 36°/oo have shifted to the 18-24°C range from the 15-24°C range; the cooler outer-shelf waters in the northern part of the SAB are warming. By May, high salinity waters are warming. June data are sparse and will not be discussed. In July, no shelf waters are less than 24°C, and 52% are less than 36 °/oo salinity. This same situation holds in August, when 32% of the shelf water is less than 36°/oo salinity. We believe that the increased volume of water with salinity less than 36°/oo during the summer months is related to upwelling at the shelf break rather than river input of freshwater. This hypothesis is partly confirmed by the lack of significant amounts of water with salinity lower than 35°/oo, and that in July the lower salinity water has a cooler component (less than 27°C).

In September the percentage of waters with less than 36 °/oo salinity drops to 14% of the shelf volume. October, which features strong southerly wind stress, has anomalously low salinity water. Waters less than 36°/oo salinity occupy 22% of the shelf volume, while runoff is at its lowest. In November, the situation is similar, with 23% of the shelf volume in the less

Table 4.5-2. Mean salinity, runoff, and flushing rate

Month	Mean Salinity (S m%)	Runoff (km^3)	Flushing Rate (Month)
January	34.20*	5.3	2.5
February	34.27	6.9	1.9
March	33.51	7.7	2.4
April	34.40	6.8	1.8
May	32.75	3.7	6.5
June	36.0*	3.1	-
July	35.31	2.7	1.9
August	35.38	2.8	1.6
September	35.05	2.4	2.9
October	33.91	2.8	5.5
November	34.88	2.3	3.6
December	35.20	3.4	1.8
			X = 3.0

(Note: * = limited data.)

Flushing rate calculated using base salinity of 36.00 °/₀₀ and inner-shelf volume of 267 km^3.

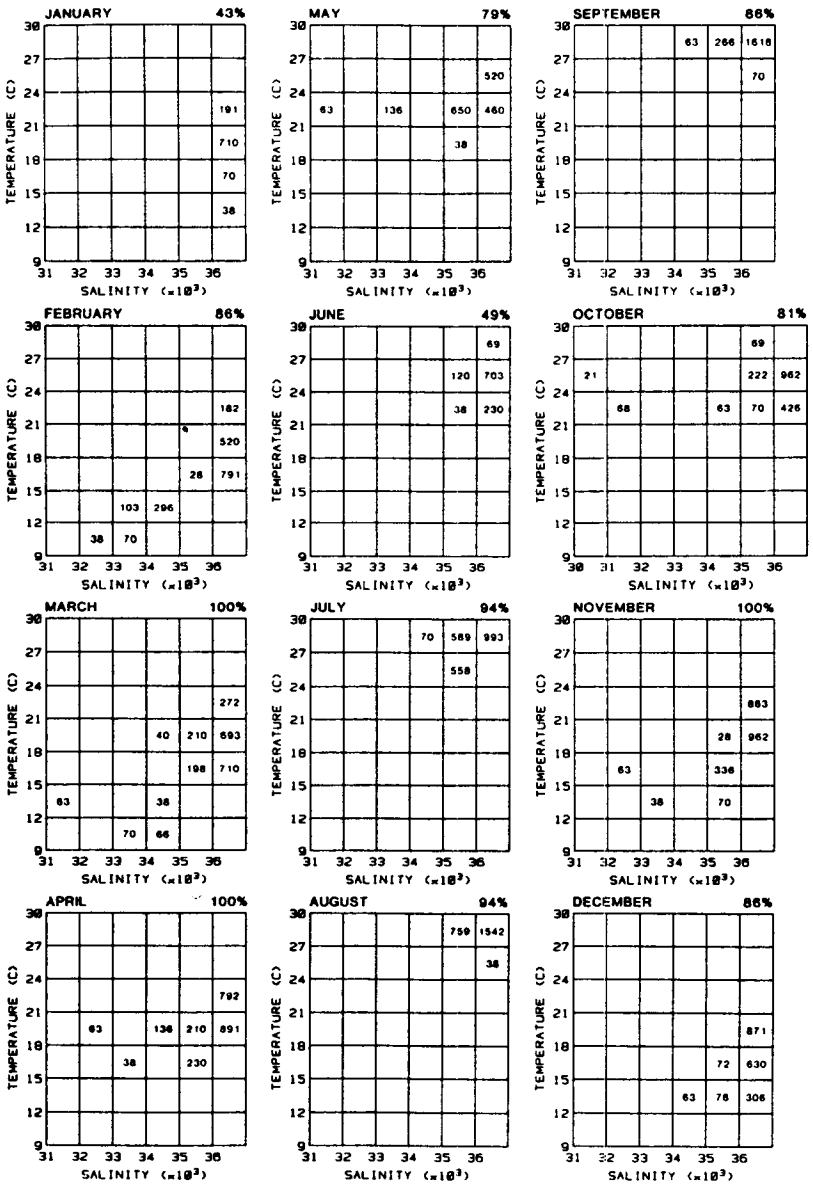

Figure 4.5-12. Analysis of shelf waters by month. The number in each bivariate class = volume in km^3. Percent shown in upper right of each figure = percentage of shelf volume for data available.

than 36^{o}/oo category. We believe this implies that movement of water across the shelf is restricted, probably by increased wind stress.

4.5.2.5.4 Bulk Stratification

Stratification of shelf waters is caused by seasonal processes such as heating/cooling, runoff, and wind mixing. Thus, bulk stratification calculated from monthly differences in surface and bottom density will be a reasonable estimate of annual variations in stratification for different parts of the SAB. In Figure 4.5-13 we show the regional distribution of the bulk stratification parameter.

In February, stratification is weak throughout the SAB. The inner shelf at 34-35°N is slightly stratified, possibly because of lower salinity Virginian coastal water flowing south around Cape Hatteras (Stefansson et al. 1971). Slight stratification is also found off Florida (29-30°N).

Bulk stratification is higher throughout the SAB in April, reflecting increased heat flux, freshwater runoff, and decreased winds. Stratification is highest off Georgia (30-33°N), where runoff is greatest. Stratification off Florida is relatively high, but lower than February values.

By August, surface heating and slackened winds increase stratification throughout the SAB. Stratification is lowest over the inner shelf on the central SAB and highest to the south and north. The enhanced stratification off Florida is believed to be caused by localized, topographically enhanced summer upwelling that significantly decreases bottom temperature in that area (Blanton et al. 1981). Stratification in November is similar to that of February, presumably due to increased wind stress and reduced runoff, during those periods.

Clearly stratification is most intense in the inshore waters of the central SAB during spring runoff. Other times of the year, stratification is most intense off Florida, with moderate stratification off North Carolina.

4.5.2.5.5 Salt Balance

Monthly mean surface and bottom salinities are used to estimate mean shelf exchange rates and residence times, using a salt balance method (Pritchard 1960). The topographically similar region south of the Carolina Capes from 28 to 34°N, which receives most of the river runoff, is considered. Volume-averaged salinities in each depth zone are plotted with total monthly runoff in Figure 4.5-14. Also shown is the volume-averaged salinity of the combined inner- and mid-shelf regions, between the 0- and 40-m isobaths (S). Monthly mean salinites in the outer shelf (S_{os}) are relatively constant, due to rapid exchange with the Gulf Stream. Lee et al. (1981) estimated an average two-week residence time for the outer shelf resulting from enhanced exchange during passage of Gulf Stream frontal eddies. In fact, shelf water (salinity < 36^{o}/oo) is rarely found in the outer shelf, due to this rapid renewal. Annual average outer-shelf salinity is 36.08^{o}/oo. Monthly mean inner-shelf salinities (S_{is}) show the largest variations and tend to follow the river runoff cycle. Maximum runoff occurred in March, and minimum inner-shelf salinities occurred two months later in May. Runoff decreased

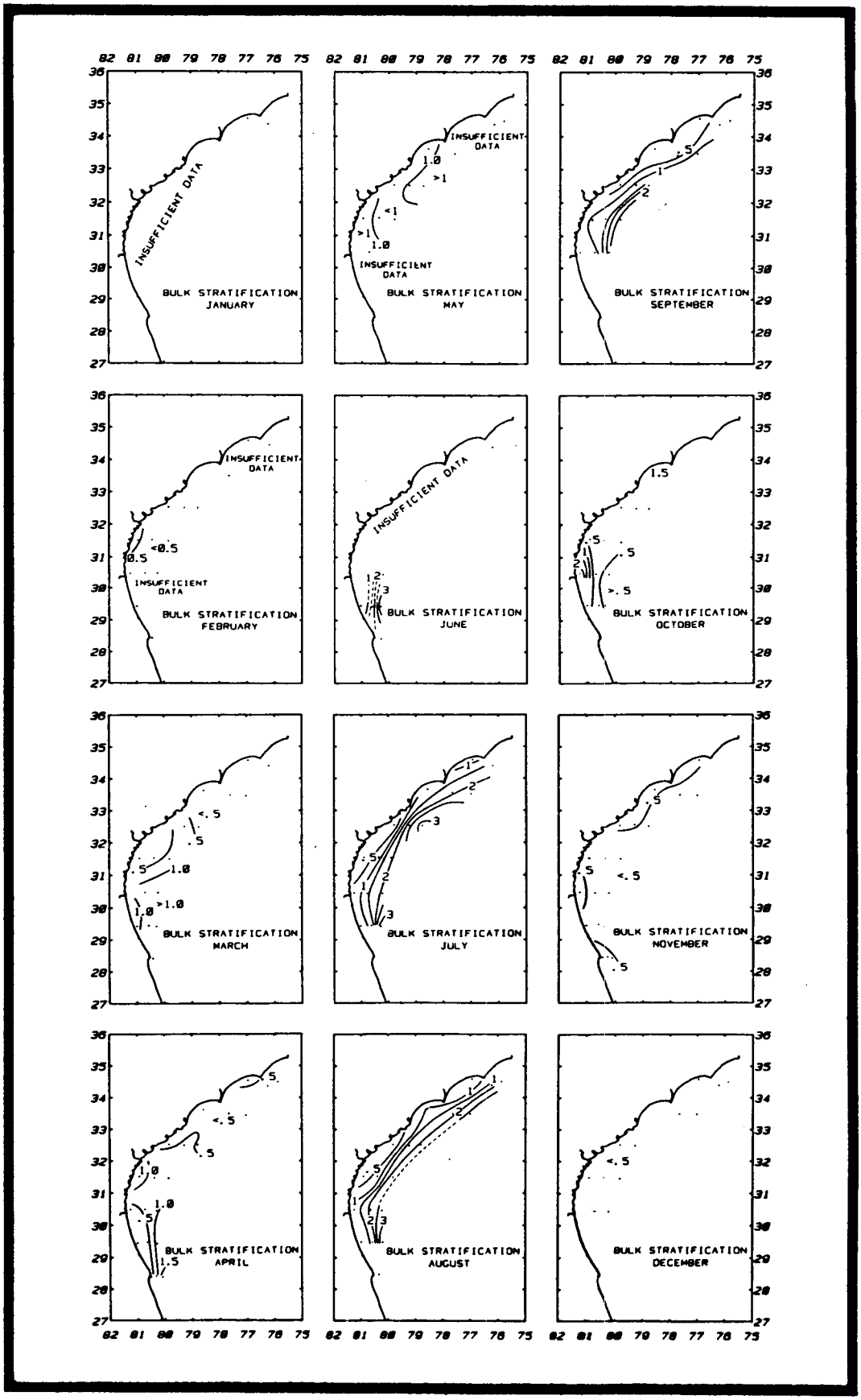

Figure 4.5-13. Distribution of bulk stratification.

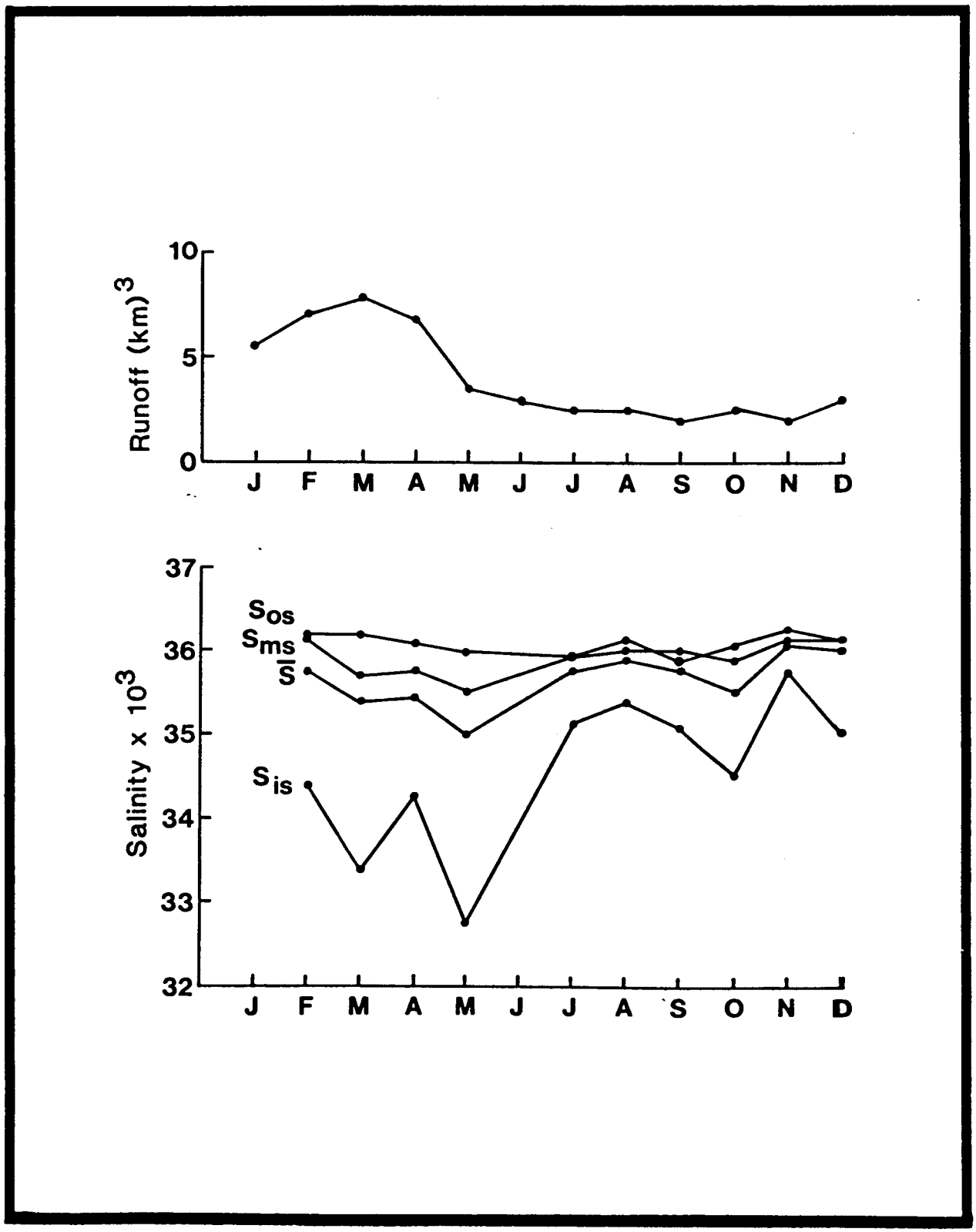

Figure 4.5-14. Time series of mean salinities for the entire shelf ($\bar{S}$), inner shelf (S_{is}), mid-shelf (S_{ms}) and outer shelf (S_{os}). The upper time series gives monthly average total SAB runoff.

after March then remained relatively constant from May to December. The inner-shelf salinity increased rapidly from May to July, then showed smaller variations. These data indicate that exchange is occurring between outer-, mid-, and inner-shelf waters in order to produce the rapid increase of mean inner-shelf salinity which levels out below mid-shelf (S_{ms}) and outer-shelf (S_{os}) values. The data also suggest that shelf precipitation must be approximately equal to evaporation in order for shelf salinities to remain below Gulf Stream values, and for near-surface Gulf Stream salinities to be nearly constant.

The mean rate of exchange of shelf waters within the 0- to 40-m zone with waters of the outer shelf, between Cape Canaveral, Fla. and Cape Fear, N.C., can be estimated from conservation of volume and salt concepts. Conservation of volume simply states that if the mean sea level is constant, then the volume transport of the shelf (Q_o) must equal the volume transport into the region from the outer shelf (Q_{os}) and river runoff (r):

$$Q_o = Q_{os} + r. \tag{2}$$

This assumes that along-shelf flow around Cape Canaveral and Cape Fear is either small and neglected, or that the flows are approximately equal and in the same direction, so that their effects cancel. We also assume that precipitation is approximately equal to evaporation for the reasons previously stated. Conservation of salt states that the net transport of salt into or out of the shelf must equal the local time rate of change of the shelf volume average salt content:

$$\frac{\partial}{\partial t} \iiint_V S \, dV = Q_{os} S_{os} - Q_o S_o. \tag{3}$$

Where V is the mean volume of the shelf between the 0- to 40-m isobaths and 28 to 34°N latitudes, V equals 1370 m^3 from Table 4.5-1; S_o is the volume mean salinity of the water transported out of the shelf, averaged over the time period of interest, and is assumed to be equal to S, the volume average shelf salinity.

Using eq. (2) and the above, eq. (3) can be written:

$$V \, \partial S/\partial t = Q_{os} S_{os} - (Q_{os} + r) S. \tag{4}$$

Equation (4) is solved for the fraction rate-of-exchange of outer shelf with shelf water:

$$Q_{os}/V = \partial S/\partial t \; 1/S_{os} - S + S/S_{os} - S \; r/V. \tag{5}$$

The steady-state exchange rate can be found by assuming that on the annual average the volume-averaged shelf salinity does not change with time $\partial S/\partial t = 0$; and taking the annual average of the values shown in Figure 4.5-13 from Eq (5), we find that $Q_{os}/V - 0.2$ or 20% of the shelf volume is exchanged with the outer shelf each month on an annual average. The steady-state exchange rate can be used to find the time needed to exchange any fractional amount of shelf water from the following recurrence formula:

$$C_n = C_{n-1} \; 1 - Q_{os}/V \tag{6}$$

where C_n is the percent of original shelf water (C_o - 100%) remaining after n months. If we define shelf residence time (T_r) as the time necessary to renew 95% of the original shelf volume, then from eq. (6) the shelf residence time is estimated at approximately one year.

During spring (February through May), runoff is high and shelf-mean salinity decreases $\partial S/\partial t = -0.26$. From Eq. (5), $Q_{os}/V = 0.14$ or 14% of the shelf volume is renewed each month, primarily because of increased runoff. Shelf residence time in this case is about 15 months. During summer (May through September), runoff is low and the shelf-mean salinity increased $\partial S/\partial t = +0.20$. Using Eq. (5), we find that $Q_{os}/V = + 0.56$ or 56% of the shelf's volume is replaced each month, which gives a shelf residence time of approximately 2.5 months for this period.

4.5.2.5.6 Mean Shelf Circulation

Outer-shelf mean flows off Florida and Georgia are obviously influenced by the strong northward flowing Gulf Stream, which tends to follow the shelf break in this region. At mid-shelf, mean flows are the result of: (1) transient Gulf Stream and wind-forced events occurring on two-day to two-week time scales, and (2) changes in the shelf density distribution which occur on a seasonal time scale. However, northward mean flows in the upper and lower layers were nearly equal in magnitude for both seasons, suggesting a barotropic flow.

The depth-integrated form of the equations of motion for mean flow at mid-shelf (neglecting along-shelf changes in density in comparison to larger cross-shelf gradients) can be written:

$$\rho fhv = g\rho_o h\, \partial\zeta/\partial x + g \int_{-d}^{o} \partial\alpha/\partial x\, dz - \tau_x = rv_b \qquad (7)$$

$$\rho fhu = g\rho_o h\, \partial\zeta/\partial y + \tau_y - rv_b. \qquad (8)$$

Where u, and v are depth-averaged velocities in the x (cross-shelf) and y (along-shelf) directions defined by $v = h^{-1} \int_{-d}^{\zeta} v dz$, z is the vertical coordinate, positive upwards; τ_x and τ_y are the wind-stress components in the x and y directions; h is the total water depth $h = \zeta + d$, where ζ is the free surface elevation above the undisturbed surface $z = o$; ρ is seawater density; and $\alpha = \int_{-d} \rho dz$ is the integrated density. A linear form of bottom friction is used(ru_b, rv_b) where r is the friction coefficient and u_b, v_b are near-bottom velocities.

For flow near a coast, we assume zero net cross-shelf flow ($u = 0$), so the essential balance in the along-shelf directions is:

$$\tau_y = g\rho_o h\, \partial\zeta/\partial y + rv_b. \qquad (9)$$

The mean along-shelf stress was almost zero for the four-month winter and summer averaging periods, indicating from Eq. (9) that the mean along-shelf slope in sea level was approximately balanced by bottom friction. Estimates of near-bottom velocities from Eq.(9), using data from the winter and summer periods, are + 5.4 cm s^{-1} compared to + 5.0 cm s^{-1} observed during winter and +2.0 cm s^{-1} compared to +1.0 cm s^{-1} observed in summer. The along-shelf slope

in sea level and friction coefficient is estimated by least-squares fitting Eq. (9) to the along-shelf stress and bottom-current data grouped into 16 different wind categories, with r taken as the slope of the line and $g\rho_o h\, \partial\zeta/\partial$ as a constant offset, where $\zeta = 1.67 \times 10^{-7}$, r = 0.1 for winter and $\zeta = 0.67 \times 10^{-7}$, r = 0.1 for summer. The friction coefficient is close to the 0.16 value found by Scott and Csanady (1976) in the Mid-Atlantic Bight, and the sea-level slope is quite close to the 2 cm decrease per degree of latitude found by Sturges (1964), using steric anomalies offshore of the SAB.

The terms in the cross-shelf momentum balance are more difficult to estimate. However, if we ignore the baroclinic term, then a mean cross-shelf sea-level slope of only a few centimeters will produce geostrophic (barotropic) flows equivalent to those observed. Lee et al. (1981) used the summer 1977 current records with hydrographic data taken in July of 1977 in the region of the current meter array (Atkinson et at. 1979) to estimate the summer mean transport with a steady-state finite-element diagnostic model developed by Galt (1975). They also found that the baroclinic transport was insignificant compared to the barotropic. Thus, it appears that a significant fraction of the mean along-shelf flow at mid-shelf is barotropic during both winter and summer and results primarily from cross- and along-shelf sea-level slopes, which can result from wind-induced set-up of coastal sea level. However, longer time series of currents, bottom pressure, and hydrography are needed to substantiate these findings.

4.5.2.6 Conclusion

The above results confirm that the climatology of oceanographic properties on the shelf in the SAB can be separated into three depth zones, according to the controlling physical processes. These processes regulate the degree of circulation and exchange within each zone.

Mean hydrographic and flow properties in the outer shelf (41- to 60-m isobaths) are the result of the combined effects of transient Gulf Stream events occurring on time scales of two days to two weeks, and to a lesser extent on wind forcing. Off the Florida and Georgia shelves, proximity to the Gulf Stream produces strong northward mean flows. Rapid exchange with Gulf Stream frontal disturbances results in residence times on the order of two weeks, which maintain salinities in the outer shelf of Gulf Stream origin ($\geq 36^{o}/oo$) throughout the year.

Mean flow and hydrographic properties at the mid-shelf (21- to 40-m isobaths) are a mixed response to wind, Gulf Stream, and density forcing. Mean flows appear to result from barotropic current responses to transient local wind forcing. Wind forcing causes the coastal sea level to set-up (or set-down) and thus produce cross-shelf and along-shelf slopes in sea level that drive the barotropic flows. On the Georgia shelf, mean wind during the winter (December through March) was offshore, and mean flow was northward along the isobaths. In summer (June through August), mean winds were northward as were mean currents. In fall, mean winds shifted to southward, and the mean flow was also southward. Mid-shelf salinities appear to be a mixture of Gulf Stream and inner-shelf waters. Mean monthly, volume-averaged salinities were always between Gulf Stream and inner-shelf values, and tended to be closer to Gulf Stream salinity. Stratification undergoes a pronounced seasonal cycle in the mid-shelf zone. During November through March,

atmospheric cooling over the variable depths results in cross-shelf gradients in density, with denser water in shallower depths. However, the combination of wind and tidal mixing with low river runoff is sufficient to maintain vertically homogeneous conditions over most of the mid-shelf region. Topographically enhanced stratification appears to occur in the lee of Capes and regions of diverging isobaths such as in the vicinity of Cape Canaveral and the Carolina Capes. April appears to be a transition period with decreasing wind speeds, increasing runoff, and atmospheric heating, which results in a positive cross-shelf density gradient and the onset of stratification at mid-shelf. During June through August, stratification is widespread, and the shelf becomes essentially a two-layered system. The fall transition occurs in September and October with the onset of southward wind events which increase vertical mixing and break up the summer stratification.

In the inner shelf (0 to 20-m isobaths), flow and hydrographic properties are strongly influenced by river runoff and atmospheric forcing. Runoff tends to form an along-shelf band of low salinity water in the inner shelf which results in some degree of stratifications year-round. The salinity in the band is less, and stratification greatest, during spring when runoff is highest. The shallow, stratified waters of the inner shelf are very responsive to wind forcing. During June and July, mean winds are toward the north, and low salinity waters are observed off the Carolinas. In September and October, southward winds appear to be related to the occurrence of low salinity water in the inner shelf off Florida and Georgia.

The exchange of mid- and inner-shelf waters with the outer shelf appears to be related to wind forcing. The smallest exchange rate was found in the spring when mean winds are weakest. Only 14% per month of the mid- and inner-shelf volume was exchanged with the outer shelf during this period. Maximum exchange of 58% per month was found during the summer, when northward mean winds occur. Presumably, offshore Ekman transport associated with northward flow enhances water exchange and decreases the shelf residence time to approximately 2.5 months for this season. The development of summer stratification will also encourage salt transport by decreasing vertical mixing and the associated short circuiting effect on transport.

4.5.3 Cape Romain and the Charleston Bump: Historical and Recent Hydrographic Observations

4.5.3.1 Introduction

Recently there has been a growing interest in the study of the seaward deflection of the Gulf Stream off Charleston, South Carolina. This interest has been fueled significantly by the advent of satellite infrared imagery. Rao et al. (1971) and DeRycke and Rao (1973) presented the first data of this type for the region, noting the recurring meander and eddy features. Earlier, however, many periodic observations had been made of the excursions of the Gulf Stream in the area. Bartlett (1883) and Pillsbury (1891) both noted an easterward flow of the Gulf Stream from surface drift measurements. Fuglister and Worthington (1951) showed an easterward trend of the 100-m cross-current temperature gradient near 33°N, and Von Arx et al. (1955) observed an east to northeast trend in the surface frontal outcrop near 32°N. Pratt (1963) observed easterward flow in the bottom current. Fuglister and Voorhis (1965) and Pratt (1966) showed the deflection in the 200-m contour of the 15°C

isotherm, and Ewing et al. (1966) found that "a major erosion channel cut(s) across the southward extension of the Cape Fear arch at about 32°N 78°W...". Busby (1969) reported the entrainment of a deep-sea submersible in an eddy, and Knauss (1969) noted the apparent occurrence of a large meander. Richardson et al. (1969) showed the Gulf Stream's high velocity core well offshore of the 200-m isobath just north of this area, and Pashinski and Maul (1973) stated that on one occasion the Gulf Stream had been observed to flow east as far as 76.5°W before turning northward.

More recently the "quasi-permanence" of the deflection of the Gulf Stream surface thermal front has been documented with very high resolution radiometry (VHRR) and radar altimeter (RA) satellite data (Brooks and Bane 1978, Pietrafesa et al. 1978, and Legeckis 1979). In addition, two models have been applied to the region, examining bottom topography as an explanation for the feature (Rooney et al. 1978, Chao and Janowitz 1979). Topographically influenced models have been projected for a similar meander periodically observed in the Kuroshio at approximately the same latitude (Robinson and Taft 1972, McCreary and White 1979, Matsukawa 1979).

Bane and Brooks (1979) obtained a mean position for the Gulf Stream surface thermal front in the South Atlantic Bight (SAB) along 14 sections between 28 and 35°N. These data suggest a departure of the Gulf Stream from a position parallel to the 200-m isobath, beginning near 32°N and returning near 34.5°N. Airborne expendable bathythermograph (AXBT) observations by Bane et al. (1980b,c and 1981) and Bane and Brooks (1981) suggest a region of influence extending from approximately 31.5 to 34°N. Nearly the same extent of influence is shown by the 15°C isotherm at 200 m by Pratt (1966), Fuglister and Voorhis (1965), and Schroeder (1963). These south-north, offshore-onshore limits roughly parallel the east-west movement of the 400-m isobath in this region (Figure 4.5-15).

One should be cautioned that the regional bathymetry has been mislabeled (meters for fathoms) in several papers: Pietrafesa et al. 1978, Rooney et al. 1978, and Chao and Janowitz 1979. However, these authors have indicated (personal communication) that this error was not made in modeling calculations and their results are unaffected. In addition, it is pointed out that satellite infrared (IR) imagery is presently incapable of monitoring this region year-round because of its susceptibility to periodic cloud cover and poor resolution during the summer (Maul et al. 1978, Pietrafesa et al. 1978, and Legeckis 1979). This is further emphasized by Strack's (1953) observation that June through October are the worst months for using sea surface temperature gradients as Gulf Stream indicators.

Vertically, hydrographic data for the region are often characterized by doming of the isopleths in the area between the shelf break and the Gulf Stream. This is similar to the doming observed between Sombrero Key and Cay Sol Bank in the Bahamas (Schroeder 1963 and Chew 1974), as the Gulf Stream turns cyclonically out of the Gulf of Mexico and begins to move north through the Florida Straits. It is also similar to the much discussed "cold water region" of the "Kuroshio meander" (e.g., Nan-niti 1958, Moriyasu 1961, and Uda 1964).

Bane et al. (1980c and 1981) present a vertical section of temperature off Onslow Bay, North Carolina, for February 1979, that characterizes the

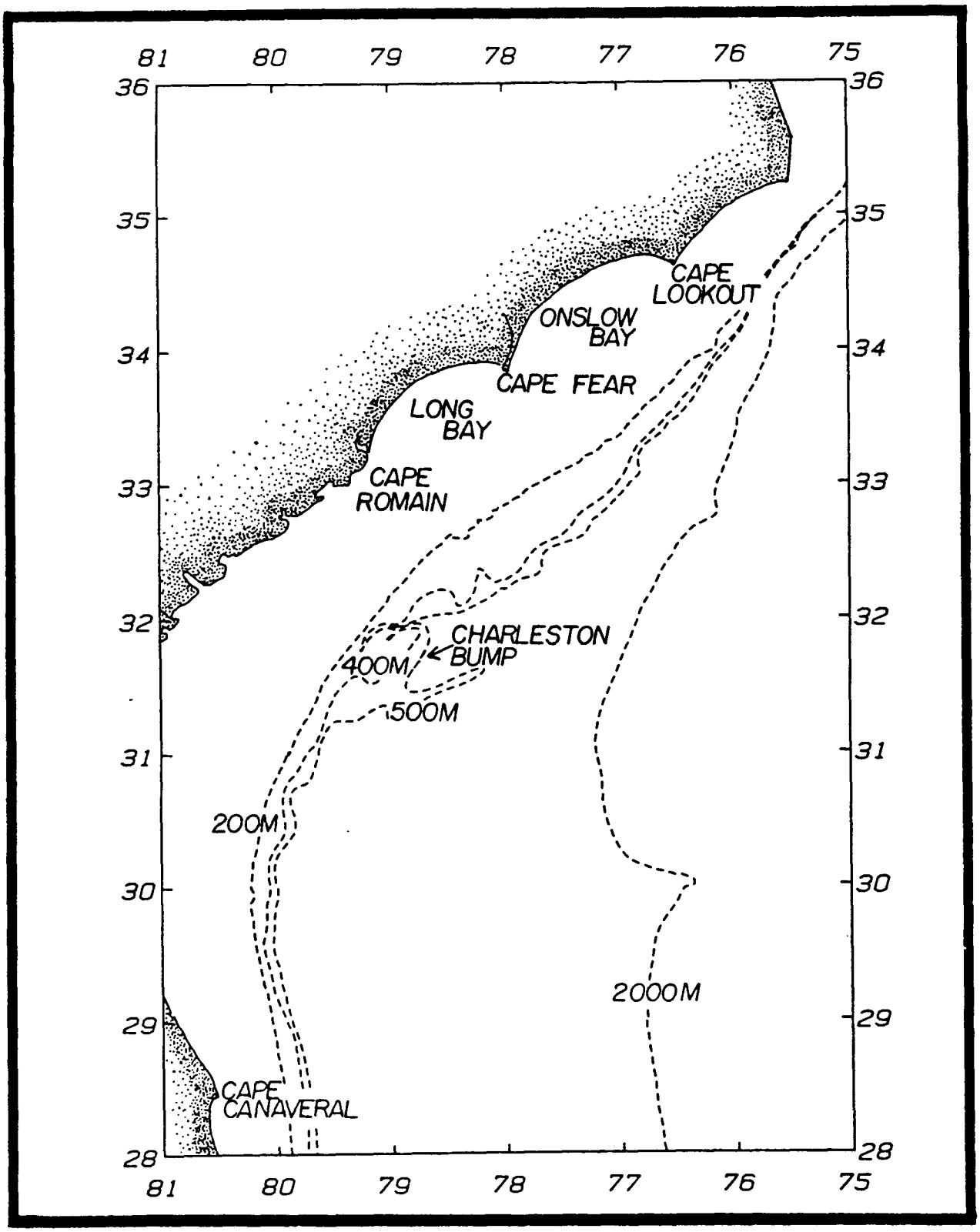

Figure 4.5-15. Bathymetry of the South Atlantic Bight (SAB) (from American Association of Petroleum Geologists, 1970).

doming in the region. Other recent hydrographic work includes Vuckovich and Crissman (1980) who presented temperature, salinity, and sigma-t (density) data collected along three hydrographic sections in May 1977 and reported their observations discussing the doming. Earlier, work by Matthews and Pashuk (1977) presented temperature, salinity, sigma-t, oxygen, and phosphate data for February through March, May and November 1973, clearly showing doming in all parameters. However, the longest and most exhaustive efforts are those reported by Hazelworth (1976) where one section was repeated 25 times, approximately once every two weeks from August 1965 through July 1966. Vertical sections of temperature, salinity, sigma-t, and oxygen are presented in this report. This data set also documents the year-round persistence of the seaward deflection of the Gulf Stream from the 200-m isobath.

The M/V Gill cruises of 1953 and 1954 also sampled this region. These data are presented in reports with vertical plots of temperature, salinity and sigma-t (Anderson et al. 1956a,b and Anderson and Gehringer 1957a,b, 1958, 1959a,b,c,). Once again, the doming feature is apparent. Other hydrographic works which reveal doming, or are otherwise indicative of Gulf Stream deflection in the region, include Pierce (1953), Swallow and Worthington (1961), Costin (1969), Stefánsson et al. (1971) and Atkinson (1978).

The purpose here is to review and examine these and other historical hydrographic data and to present new data for the "Bump" region. This should serve as a foundation for future work in the area. A region of doming will be identified, and the seasonal characteristics of the region will be discussed. Onshore-offshore sections of temperature, salinity, sigma-t, nitrate and total chlorophyll will be presented as will a discussion of the characteristics of Gulf Stream deflection off Long Bay, N.C.

4.5.3.2 Methods

The historical data discussed herein are taken from technical publications which describe the respective sampling techniques and analytical methods. Data from NOAA's R/V Peirce (Hazelworth 1976) and the R/V Dolphin (Mathews and Pashuk 1977) cruises were obtained from NODC on magnetic tape and were processed at Skidaway Institute of Oceanography (SKIO).

For more recent data, a Grundy Model 9400 conductivity, temperature, depth (CTD) recorder, a General Oceanics Model 1015 Rosette with 1.7 liter Niskin bottles, and an expendable bathythermograph (XBT) were used. The CTD data were processed according to Chandler et al. (1978) and the XBT data were manually digitized. Nutrient samples were frozen in 125 ml polyethylene bottles and stored in the dark until thawed and analyzed. Standard Technicon Autoanalyzer methods were used (Glibert and Loder 1977). Duplicate chlorophyll samples were filtered and frozen and stored in the dark. Total chlorophyll was determined by the method of Yentsch and Menzel (1963), as described by Strickland and Parsons (1972).

4.5.3.3 The Doming Region

For the purpose of this discussion, doming (probably associated with a cyclonic flow pattern) is defined as an upward and then downward sloping of the 15°C isotherm in the surface layer (0-200 m) offshore of the 200-m isobath

(Figure 4.5-16a). This definition distinguishes the phenomenon from upwelling at the shelf-break (Figure 4.5-16b) and most frontal eddies (Lee et al. 1981) observed south of 31.5°N. The 15°C dome of these latter features is generally shoreward of the 200-m isobath and much less broad.

In examining the available data (Tables 4.5-3, -4 and -5), it was noted that in some instances only an upward slope was observed, as the sampling did not extend far enough offshore to detect the eastern extent of the dome. In such cases, the furthest extent offshore was considered the maximum dome (inflection or center) position. In most instances, at least two stations offshore of the 200-m isobath were necessary for consideration. When two such stations were not available, a careful examination of contours at shallower depths eliminated some sections which otherwise appeared applicable.

4.5.3.3.1 Doming Statistics

A region of maximum doming was identified between 31.5 and 34.5°N (Figure 4.5-17). Nearly 75% of all observations occurred in the area between the 200- and 400-m isobath. However, doming was also observed offshore of the 500-m isobath, particularly north of 33°N, where the continental slope steepens. South of 31.5°N, a few doming events were observed. These were related to frontal eddies, with the exception of the event at 30.8°N, where a Gulf Stream meander was identified. The average depth at the center dome position was 360 meters for all data and 310 meters for the observations occurring between the 200- and 400-m isobaths.

4.5.3.3.2 Relative Frequency

The relative frequency of doming off Cape Romain, Long Bay, Cape Fear, and Onslow Bay was inferred from the M/V Gill cruises (2 in each season) run along these sections (Figure 4.5-18; transects B, D, F, and G; Table 4.5-6). The M/V Gill cruises constitute the largest data set of seasonal repetitions of identical sections available. Doming occurred most frequently off Long Bay (86%). and to a lesser extent off Cape Romain (25%) and Cape Fear (43%). No doming observations were made on nine sections (not shown) that extended south to 27°N, and only Onslow Bay (17%) exhibited any doming on two northerly sections to Cape Lookout. These observations are summarized in Figure 4.5-19.

The high incidence of doming off Long Bay tends to support the view of Pietrafesa and Janowitz (1980) that there is a cyclonic circulation pattern persisting throughout much of the year. Such a circulation would be independent of the passage of frontal eddies, though perhaps enhanced by their appearance and/or the occurrence of NE winds. Variation in the north-south and offshore-onshore extent would explain the lesser occurrence of doming off the two Capes.

4.5.3.4 Seasonal Variation in Temperature, Salinity, and Sigma-t in the Doming Region

Twenty-five NOAA crusies in 1965 and 1966 (Hazelworth 1976) present an excellent opportunity to examine seasonal characteristics of the doming region. The cruise track for this work is shown in Figure 4.5-18, section A. This section occurs rather close to and traverses southeasterly across 32°N 79°W, the latitude and longitude at which Pietrafesa et al. (1978) reported

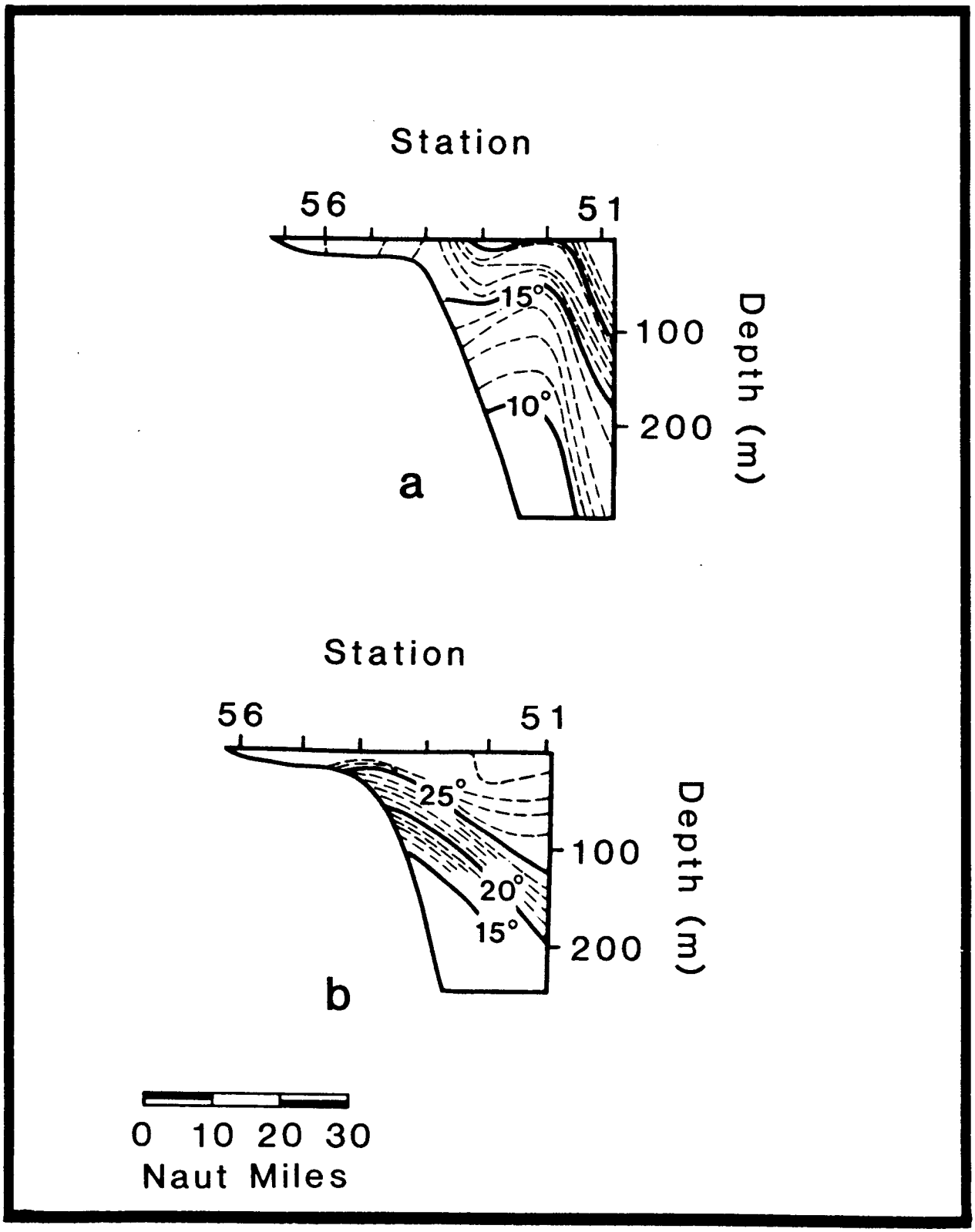

Figure 4.5-16. (a) Doming and (b) upwelling at the shelf break off Long Bay, North Carolina (from Anderson, Gehringer, and Cohen 1956a and Anderson and Gehringer 1957a).

Table 4.5-3 Published data sources examined in compiling the region of maximum doming.

Ship	Year	Vertical Plots of Temperature Presented In:
Caryn & Atlantis	1953-1954	Bumpus and Pierce (1955)
Gill	1953-1954	Anderson et al. (1956, 1957, 1958, 1959)
Atlantis	1955	Swallow and Worthington (1961)
Peirce	1965-1966	Hazelworth (1976)
Eastward	1966-1967	Stefansson et al. (1971)
Dolphin	1973	Mathews and Pashuk (1977)
Eastward	1973-1974	Atkinson (1978)
Iselin	1976	Deschamps et al. (1979)
Iselin	1977	Atkinson et al. (1979)
Advance II and Blue Fin	1977	O'Malley et al. (1978)
Northstar	1977	Vukovich and Crissman (1980)
Blue Fin and Iselin	1977-1978	Singer et al. (1980)
AXBT's*	1979	Bane et al. (1980b)
AXBT'*	1979	Bane and Brooks (1981)
Endeavor	1979	Bane et al. (1980a)
Endeavor	1979	Brooks, et al. (1980)
Gillis	1979	Lasley et al. (1981)

* Airborne XBT's dropped.

Table 4.5-4 Recent seasonal cruises (data presented in unpublished reports).

Ship	NODC I.D.	Dates
Pierce (Tracor)	PP-001-78	6-12 March 1978
Iselin	IC-004-78	12-23 April 1978
Iselin	IC-006-78	26-30 July 1978
Iselin	IC=008-78	9-14 November 1978
Pierce (Tracor)	PP-001-79	14-19 March 1979
Pierce (Tracor)	PP-002-79	28 May - 2 June 1979
Pierce (Tracor)	PP-003-79	22-27 August 1979
Iselin	IC-002-79	27 Oct - 2 Nov 1979
Eastward*	EZ-002-80	10-27 April 1980
Iselin*	IC-003-80	10-26 April 1980
Pierce (Tracor)	PP-001-80	3-14 September 1980

* Cruise did not extend into the shelf break region north of 31.5°N.

Table 4.5-5 NODC Ship of Opportunity XBT data and plots examined in compiling the region of maximum doming.*

NODC I.D.	Originator's I.D.	Ship
50203	7611	Lash Turkiye
51303	7703	Lash Turkiye
51390	7704	Mormac Argo
52342	7712	Marmac Argo
52990	7810	Lash Atlantico
52994	7811	Lash Atlantico

* An attempt was made to include Naval XBT data, however, these efforts were unsuccessful as the data were not made available in a useable format.

Table 4.5-6 Hydrographic sections selected for seasonal observations (see Figure 4.5-18).

Section	End Point Locations	Years	Comments
A	32°21'N 79°13'W to 30°8'N 77°42'W	1965-1966	Peirce Cruise
B	32°51'N 79°18'W to 31°57'N 78°9'W	1953-1954	Gill Cruise 1-5 and 7-9
C	33°2'N 79°16'W to 32°7'N 78°10'W	1978-1980	Present Authors
D	33°31'N 78°56'W to 32°19'N 77°34'W	1953-1954	Gill Cruises 1, 3-5 and 7-9
E	33°42'N 77°58'W to 32°51'N 77°19'W	1978-1980	Present Authors
F	33°36'N 77°56'W to 32°40'N 76°46'W	1953-1954	Gill Cruises 1-5 and 7-9
G	34°11'N 77°29'W to 33°12'N 76°24'W	1953-1954	Gill Cruises 2-5 and 7-9

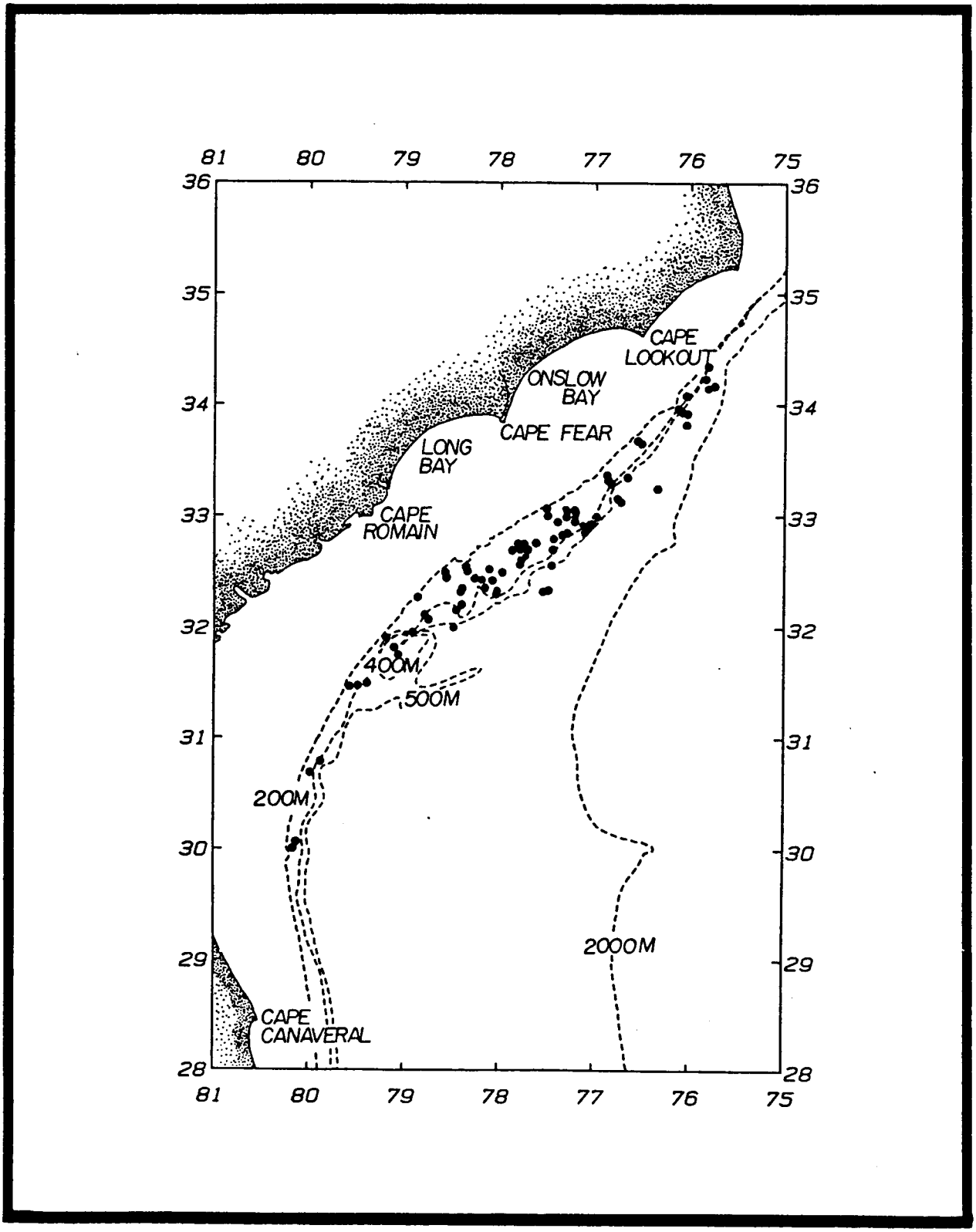

Figure 4.5-17. Region of maximum doming.

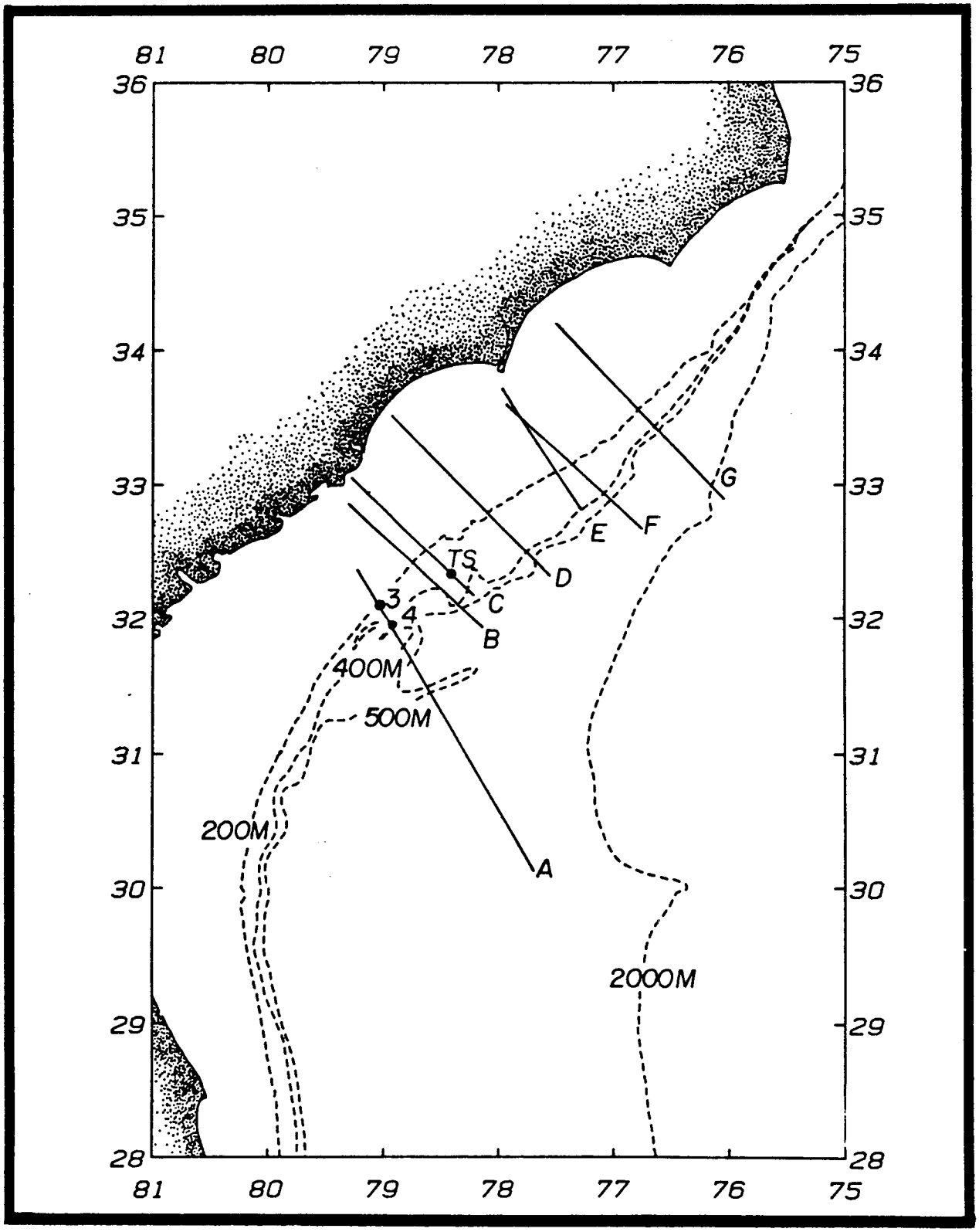

Figure 4.5-18. Selected hydrographic sections (see Table 4. 5-6).

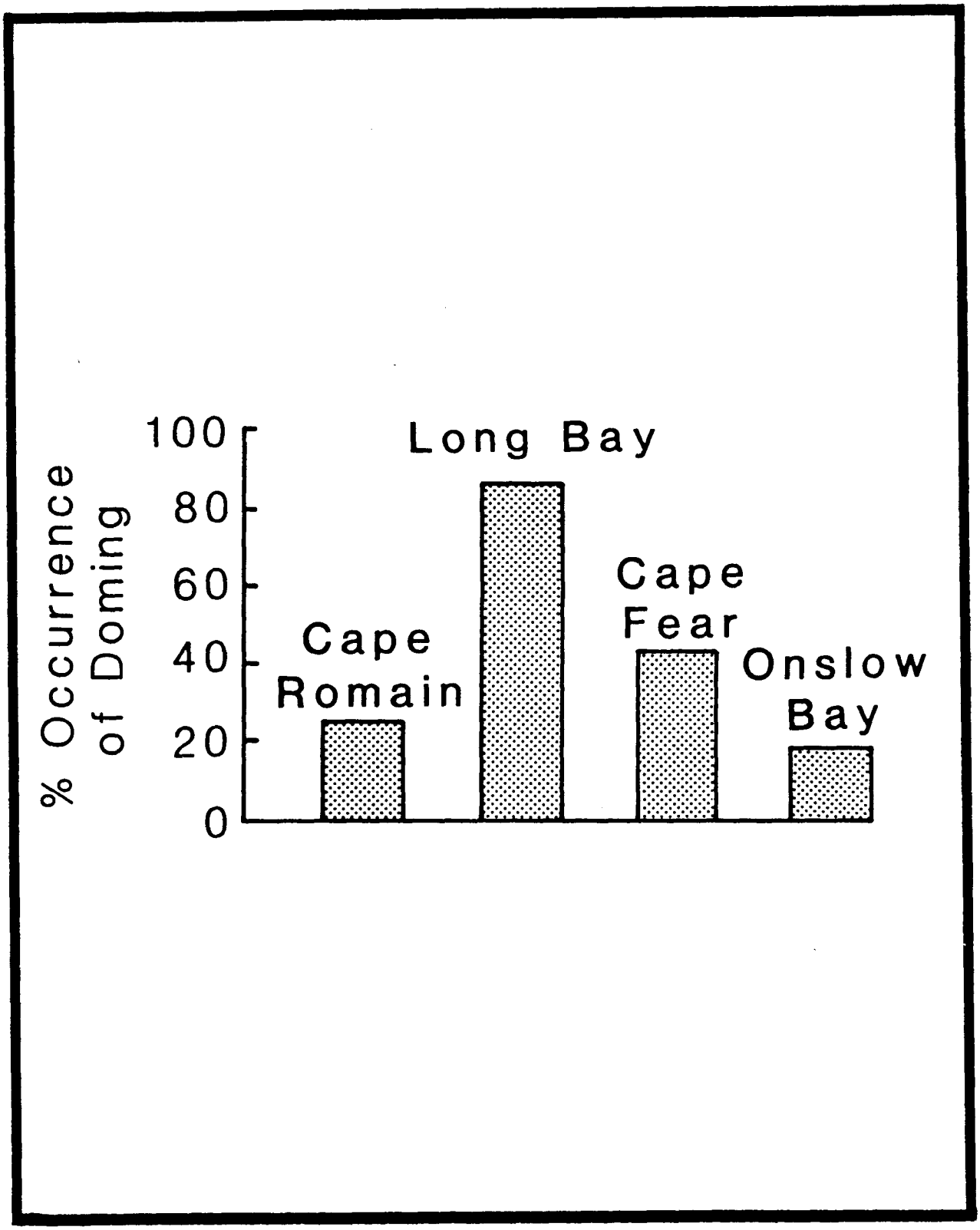

Figure 4.5-19. Percent occurrence of doming north of 32°N (from M/V Gill cruises of 1953 and 1954).

repeated seaward deflection of the surface thermal front from the 200-m isobath. Station spacing was approximately 10 nautical miles (18.5 km). These data reveal that the Gulf Stream was always east of station 4, and that the lowest temperatures at 200 m occurred at stations 3 or 4 of the data set (Table 4.5-7 and Figure 4.5-18). The lower station temperatures at this depth and corresponding salinities and densities are plotted versus time in Figure 4.5-20. Also presented are corresponding surface and 100-m observations.

4.5.3.4.1 Surface Observations

In the surface layer, temperature and sigma-t were inversely related with no set relation to salinity. Highest temperatures occurred in late August and early September and lowest in early February. The lowest surface salinities occurred primarily between late June and early August (during a period of extended southwesterly winds), with a secondary low in mid-May. The highest surface salinities were observed in December through February, and April. Observational extremes are presented in Table 4.5-8.

The temperature and sigma-t observations are readily explained as responses to seasonal warming and cooling, and compare favorably in trend with Chase (1971) for Frying Pan Shoals Light Station off Cape Fear. In addition, Chase (1969) showed that historically the lowest mean surface salinities off Cape Fear occur in July.

Atkinson and Targett (in press) reported surface shelf-break (60-m isobath) salinities lower than $36^{o}/oo$ in late June 1980 between 31° and 32°40'N. They suggested an offshore flow of waters in the region. The occurrence of extended periods of southwesterly winds (which occurred) would favor such observations, causing low salinity shelf waters to move into the frictional drag of the Gulf Stream, as suggested by Bumpus (1955). Here, however, the shelf waters would first move off-shelf into the doming region and then into the frictional drag of the Gulf Stream. Interestingly, Weber and Blanton (1980) have found that southerly to southwesterly winds occur primarily in July in this area. This suggests that for the annual cycle the largest quantities of low salinity shelf water are moved off-shelf en masse in the 'Bump' region in July. If this is in fact the case, then aerial mapping of surface salinity might define the path of the Gulf Stream in this area in July, when surface temperature observations are inappropriate.

4.5.3.4.2 100-m Observations

At 100-m depths, temperature, and salinity were related directly and indirectly to sigma-t. Observations at this depth oscillated between coupling with surface and deeper (200 m) observations. They were coupled to the surface in January and to the bottom in July. A periodicity of two to three months was observed.

4.5.3.4.3 200-m Observations

At 200-m depth, temperature, and salinity were again related directly and indirectly to sigma-t. The lowest temperatures were observed from January through March and July through November; the highest from April through June and December. Related trends are apparent in the 200-m salinity and sigma-t plots (Figure 4.5-20b,c). When the 200-m data from the M/V Gill and authors'

Table 4.5-7. Locations of Stations 3 and 4 (Hazelworth, 1976).

Station	Location		Depth (m)
3	32°05'N	79°03'W	316
4	31°57'N	78°56'W	403

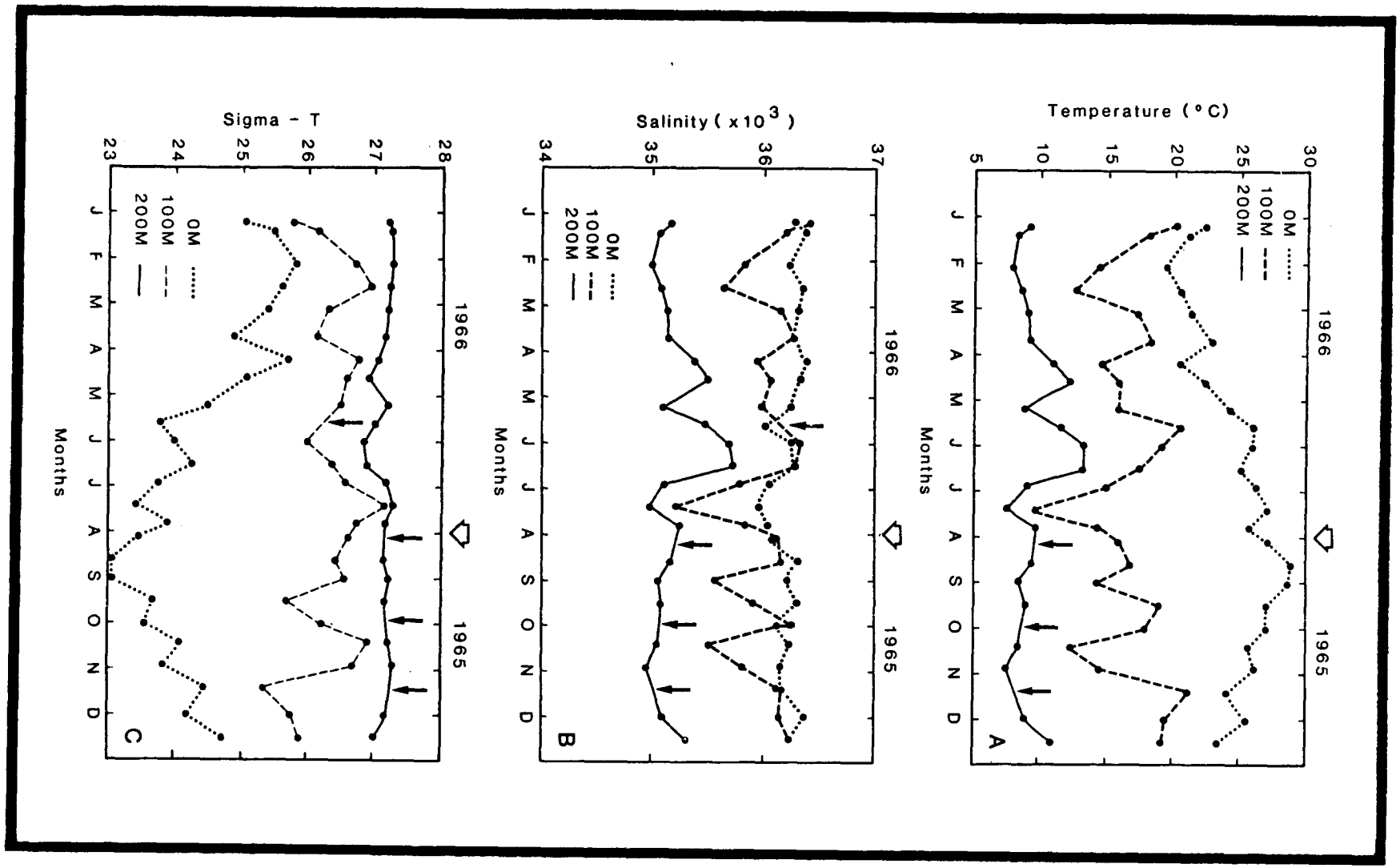

Figure 4.5-20. Seasonal variation in: (A) temperature, (B) corresponding salinity, and (C) corresponding sigma-t at NOAA Pierce cruise Stations 3 or 4 (see Figure 4.5-18) in the upwelling region. Small arrows indicate no data, and large unshaded arrow indicates beginning of the time series in August 1965.

Table 4.5-8 Extremes of temperature, salinity and sigma-t at 0, 100 and 200 m for Stations 3 and 4.

Depth	Temperature (°C)		Salinity ($x10^3$)		Sigma-t	
	Low	High	Low	High	Low	High
0	19.47	28.99	35.97	36.38	23.07	25.86
100	9.65	21.19	35.21	36.41	25.35	27.19
200	7.60	13.34	34.96	35.74	26.88	27.33

cruises along sections B and C (Figure 4.5-18) are included with the NOAA Peirce data, the lowest temperature periods are narrowed to January through February and July through October and the highest periods are lengthened to March through June and November through December (Figure 4.5-21). These results compare favorably with Iselin's (1940) observations of the seasonal variation in the depth of the main thermocline layer (12° to 6°C) of the Gulf Stream's northern and southern edges between Montauk Point and Bermuda. There, he noted that the isotherms of the main thermocline layer tended to be nearer the surface (cooler at 200 m) in January and in the June through August period. Also, he noted a deepening of isotherms (warmer at 200 m) in March or April and again in October or November. Subsequently, it appears that the 200-m observations are coupled to seasonal variations in the main thermocline. A possible explanation for this variation will be presented later.

4.5.3.4.4 Temperature-Salinity Correlation

Figure 4.5-22 presents temperature-salinity (T-S) correlations for seven recent cruises. The plots are from the same location off Cape Romain (32°20.0'N 78°00.0'W) in the doming region, in 305 m of water (station "TS", Figure 4.5-19, transect C). Table 4.5-9 identifies the cruise station numbers, and Figure 4.5-23 locates the position along the transect. These plots show seasonal warming of surface waters between March and August, and cooling between August and November. They also reveal that only in July did surface salinities fall significantly below 36°/oo (to as low as 35.62°/oo). This supports our earlier observations. In August, mid-depth waters (20-25°C) exhibited the highest salinities. These were due to the high salinity core of the Gulf Stream which had moved shoreward (see Figure 4.5-24). In October, low salinities were observed in the 13-19°C range, when a sharp thermocline (5.6°C over 5 m) may have caused CTD sensor mismatch. In May, a station 35 km further offshore (not shown) exhibited similar structure with a more gradual thermocline (5.6°C over 65-m), and Hazelworth (1976) has shown the occasional occurrence of similar structure at station 3 of the NOAA Peirce cruise data.

4.5.3.5 Repeated Hydrographic Sections off Cape Romain

Vertical plots of temperature, salinity, sigma-t, nitrate, and total chlorophyll are presented in Figures 4.5-23 through 4.5-27. These correspond to recent cruises off Cape Romain (Table 4.5-4; Figure 4.5-18, transect C).

Figures 4.5-23, through 4.5-25 show the greatest upward penetration of cold, low-salinity, high-density water occurring in March, July, August, and October 1979 and the least in March, April, and November 1978. These same observations (for temperature) are presented graphically in Figure 4.5-21 and have been discussed earlier as relating to an apparent variation in the seasonal thermocline. If such is the case, the fact that March exhibits both a maximum and minimum may indicate that it is a transitional month. May and September appear as intermediates.

4.5.3.5.1 Temperature

The temperature structure in Figure 4.5-23 reveals that doming (as defined earlier) may or may not be observed along this section. Also, there is a sharp structural contrast between March 1978 and March 1979. The 1978 observations were coincident with SW-SSW winds (5-25 knots), and the 1979

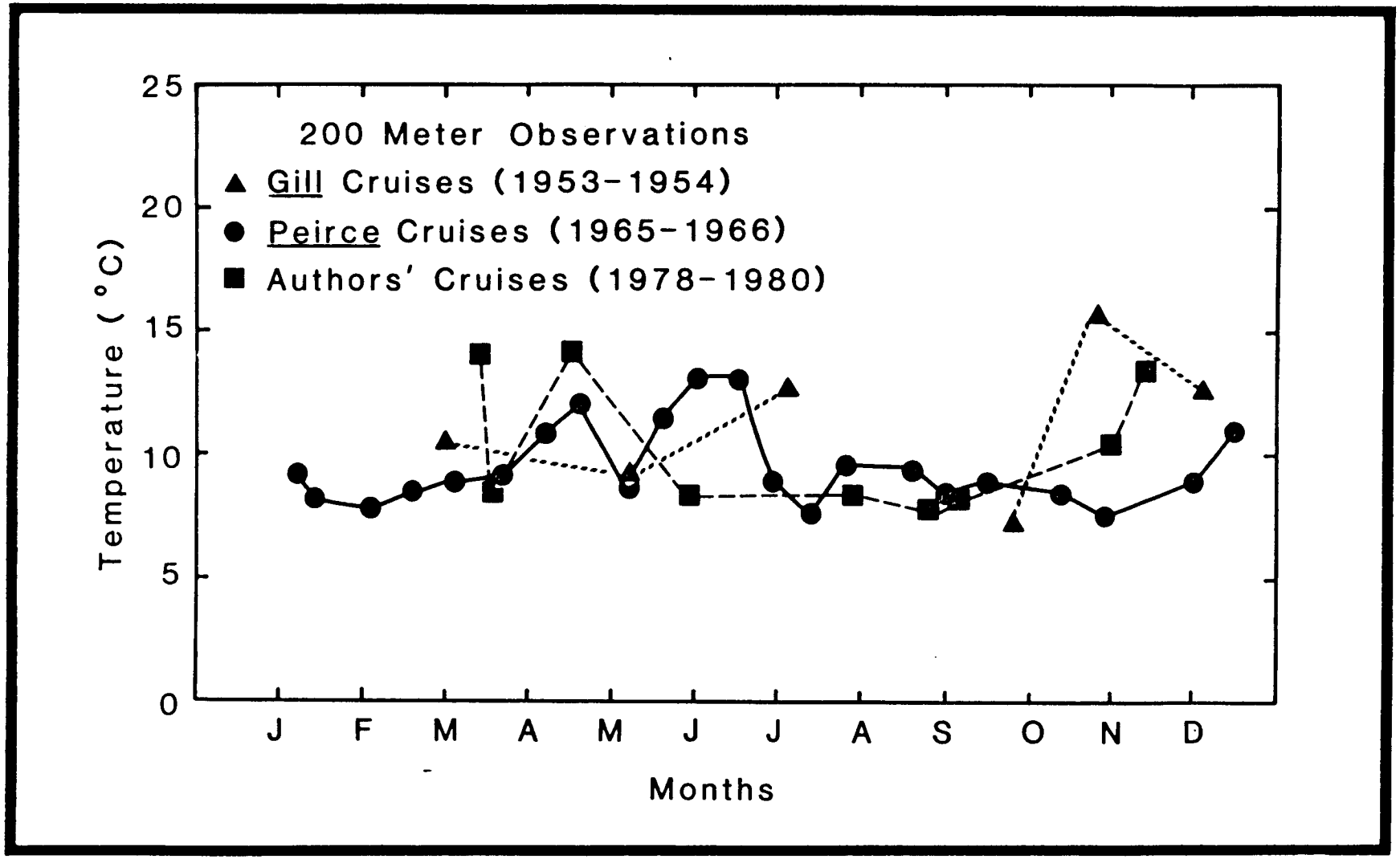

Figure 4.5-21. Seasonal observations of lowest temperature at 200 m off Cape Romain for three different time periods.

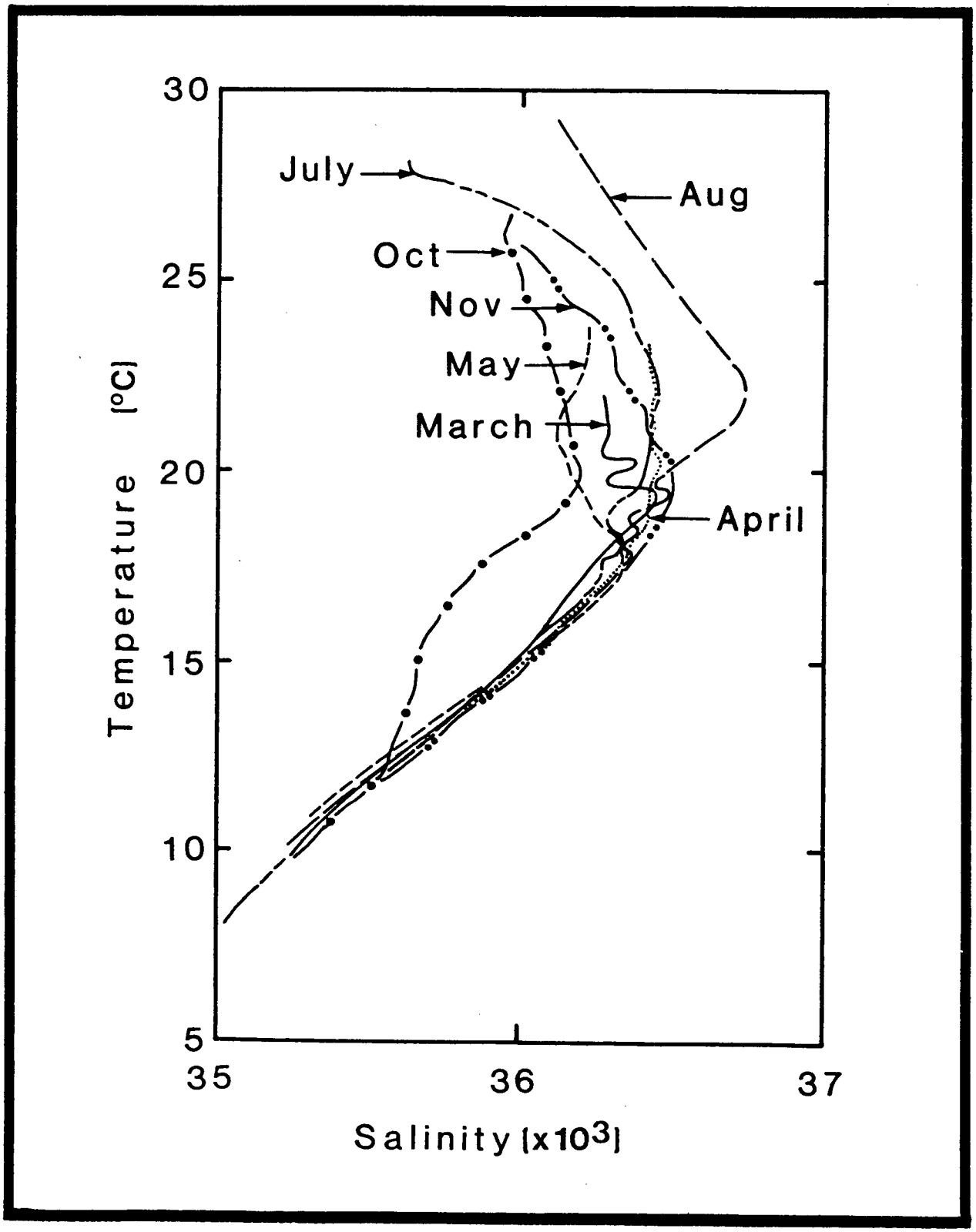

Figure 4.5-22. Seasonal T-S plots off Cape Romain at 32°20.0'N 78°25.0'W.

Table 4.5-9. Cruise identification of Station "TS".

Cruise	Actual Station
March 1979	90C
April 1978	3C
May 1979	8C
July 1978	77C
August 1979	92C
October 1979	100C
November 1978	89C

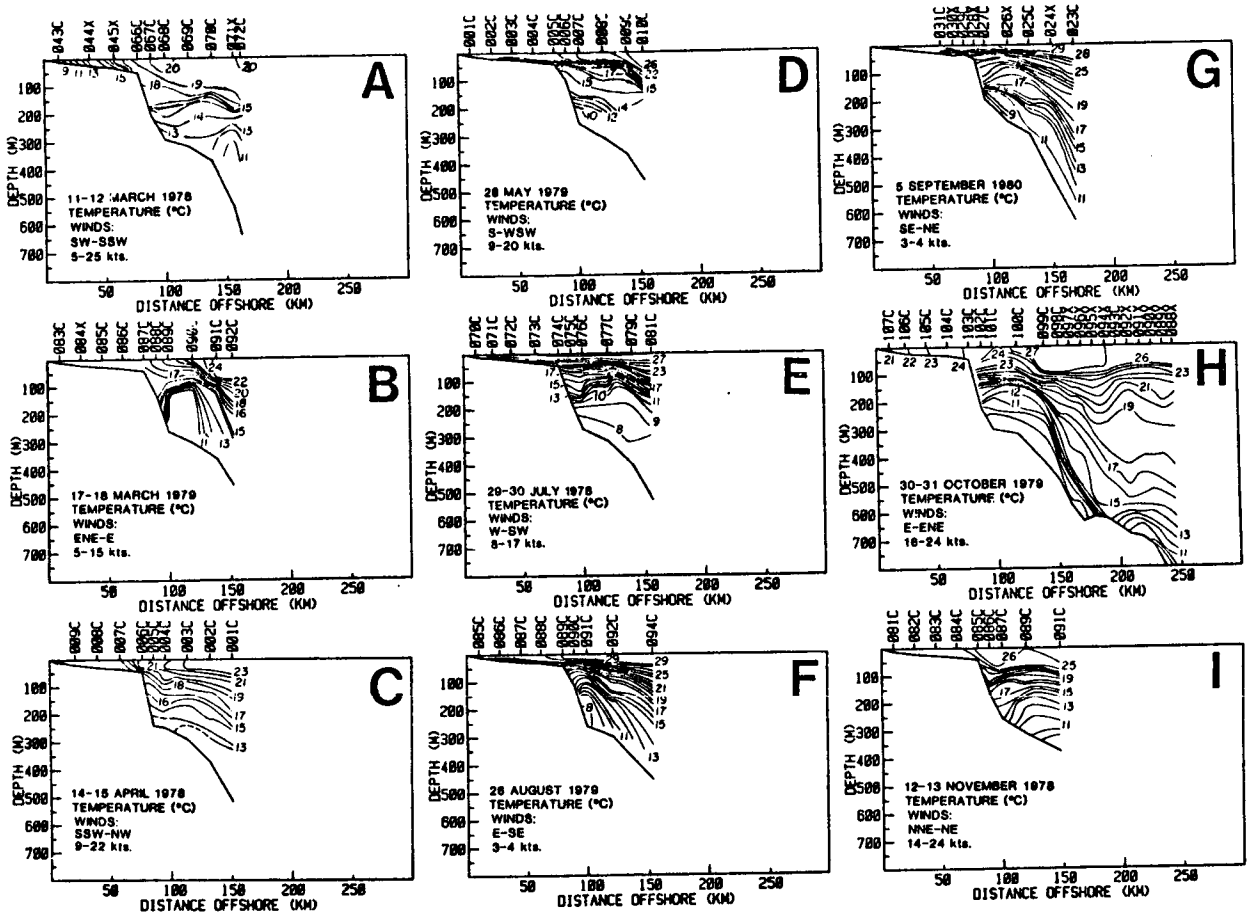

Figure 4.5-23. Seasonal vertical temperature data from nine cruises (Cape Romain section). "C" = CTD station; "X" = XBT station.

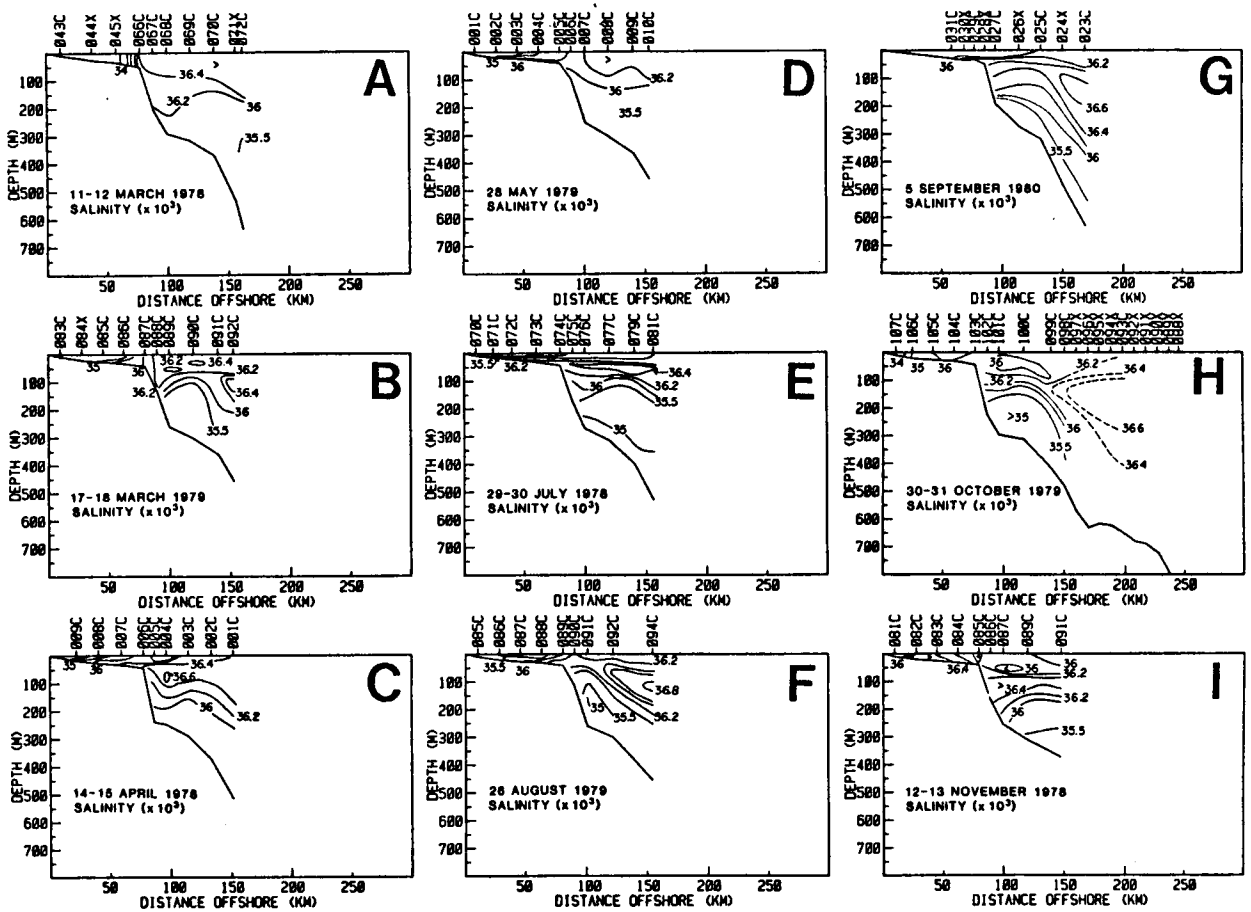

Figure 4.5-24. Seasonal vertical salinity data for nine cruises (Cape Romain section).

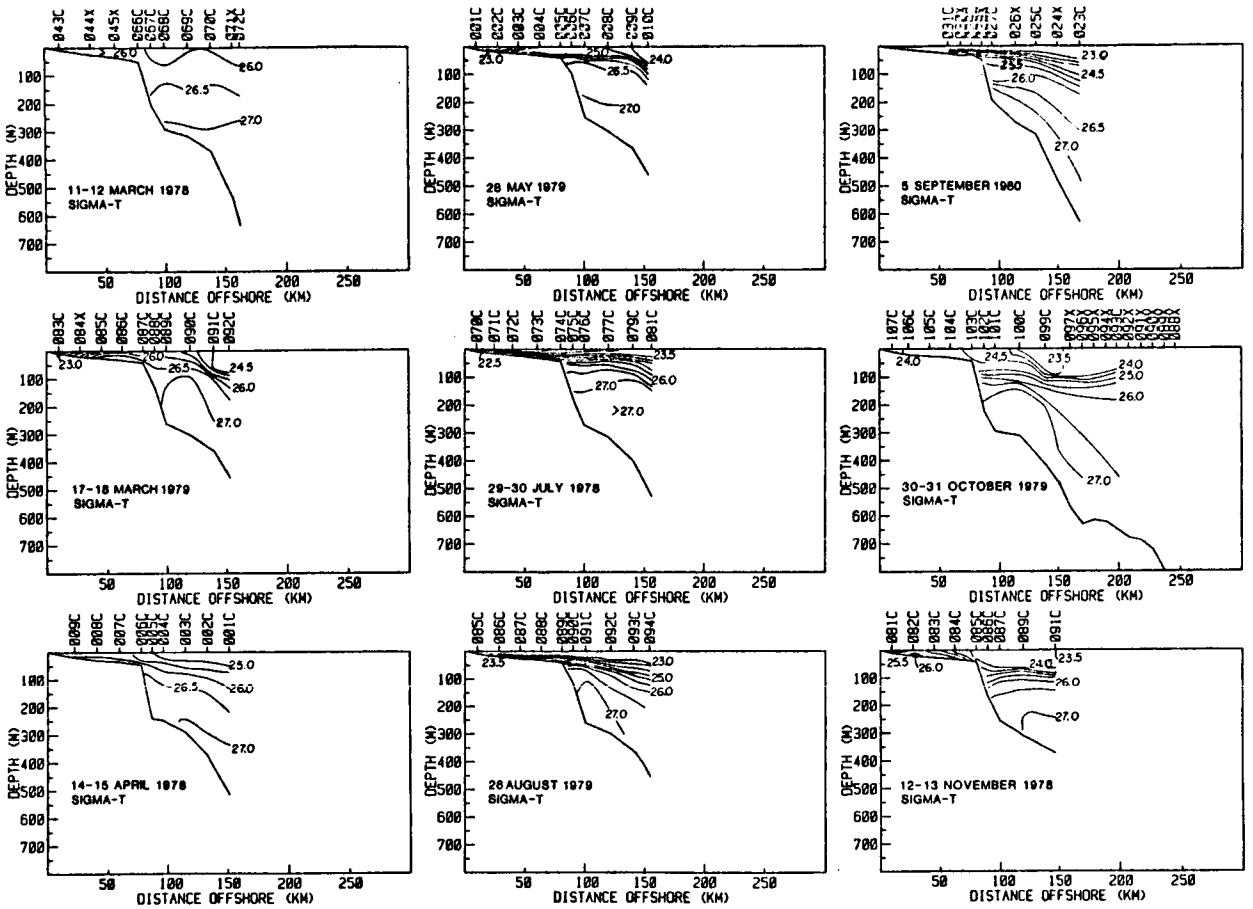

Figure 4.5-25. Seasonal vertical sigma-t data for nine cruises (Cape Romain section).

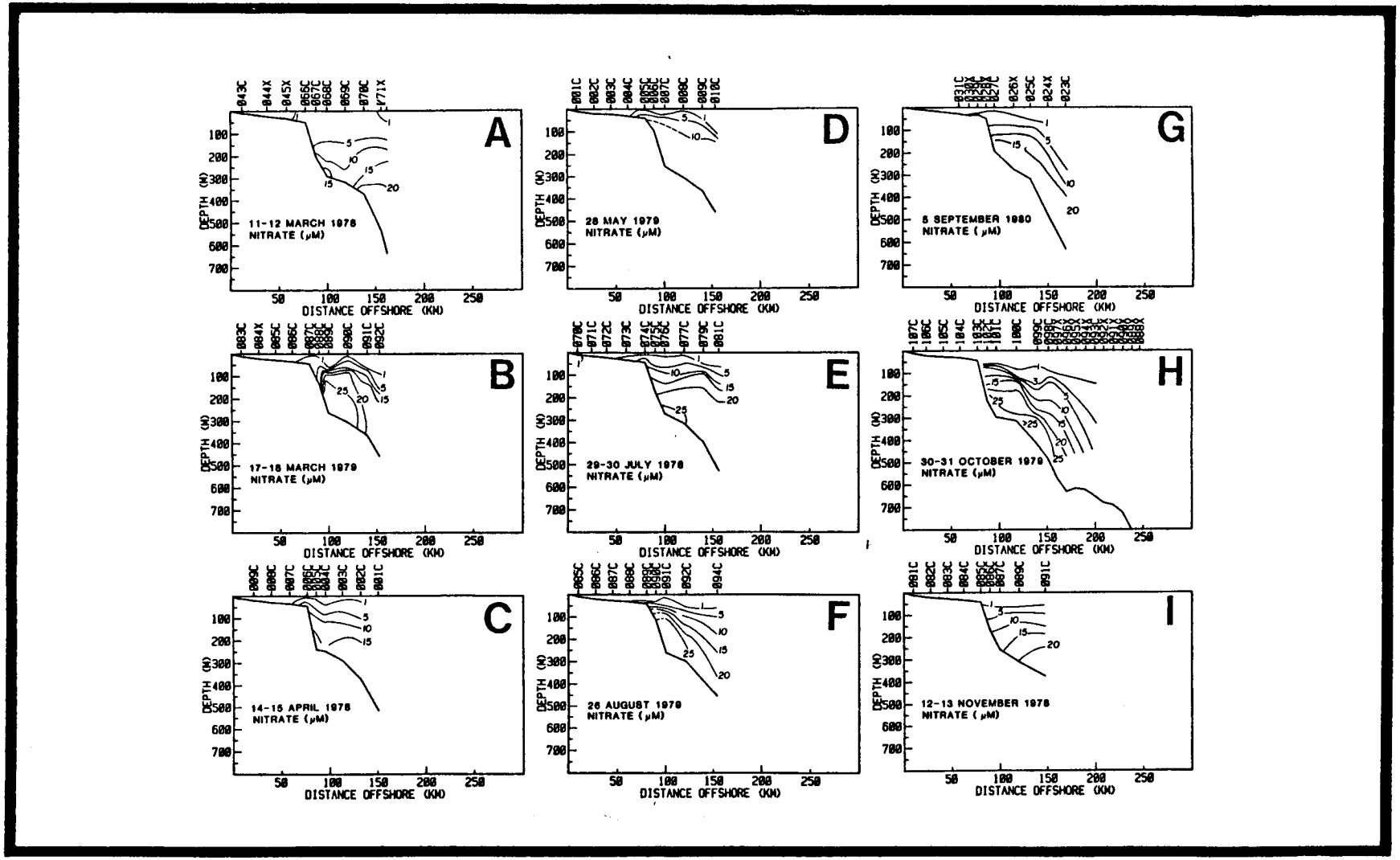

Figure 4.5-26. Seasonal vertical nitrate data for nine cruises (Cape Romain section).

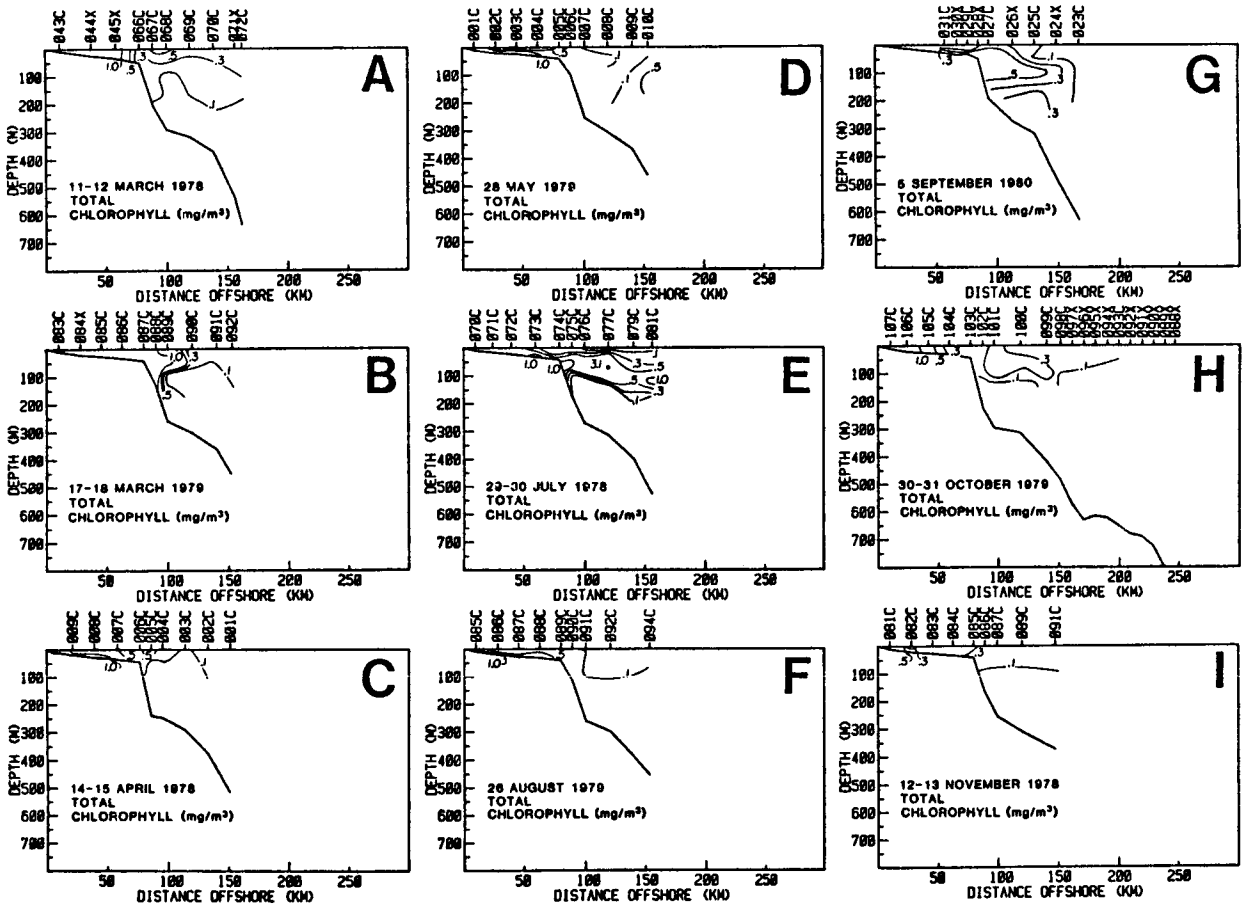

Figure 4.5-27. Seasonal vertical chlorophyll data for nine cruises (Cape Romain section).

observations corresponded to a period of ENE-E winds (5-15 knots). Since the Gulf Stream was approximately the same distance offshore for both periods (< 10 km difference), it is possible that the winds were in part responsible for the structural differences. Northerly winds could increase cyclonic flow and tighten the dome, whereas southwesterly winds should decrease cyclonic flow and broaden the dome. This relationship generally applies for all periods with wind speeds greater than 5 knots.

4.5.3.5.2 Nutrients

The greatest upward nitrate (and subsequent phosphate and silicate) penetration occurred for the same months that exhibited the greatest upwelling of cold, low salinity, high density waters (Figure 4.5-26). However, high near-surface nitrate levels (1-5 μM) were also observed in March, April, and May 1978, when surface waters were less than 22-23°C. This is probably explained by the nitrate-temperature relationship of Atkinson et al. (1978b), which suggests that high, surface nitrate levels can be sustained longer at such temperatures than at the higher surface temperatures of July and August. Subsequently, high springtime surface levels are probably of older upwelled origin than those observed in July and August.

4.5.3.5.3 Chlorophyll

Chlorophyll data were collected in the upper 200 m along this section. The highest total chlorophyll concentrations (chlorophyll-a plus phaeopigment-a) occurred during two of the four periods of strong upwelling: March and July 1979 (Figure 4.5-27). These observations were associated with the leading edge of strong thermal gradients at temperatures less than 17°C (Figure 4.5-23), with nitrate concentrations greater than 10 μM (Figure 4.5-26).

In the absence of upwelling offshore of the shelf break and in the Gulf Stream, one would expect total chlorophyll values less than 0.1-0.2 $mg.m^{-3}$ at the surface (Bishop et al., 1980). Here, however, offshore of the break, five of the nine sections exhibited higher values at the surface, and seven exhibited higher values in the upper 50 meters. The highest value observed was 3.1 $mg\ m^{-3}$ at 70 m in July. In contrast, surface values as high as 5.0 $mg\ m^{-3}$ have been observed further south in the SAB during upwelling events associated with meanders and frontal eddies (Bishop et al. 1980 and Yoder et al. 1981).

4.5.3.6 Gulf Stream Deflection off Long Bay

Temperature data from the M/V Gill and R/V Dolphin cruises and two additional cruises were examined in the horizontal at 150 m (Figure 4.5-28a-1). These cruises were selected because they provide sufficient data collected off Cape Romain, Long Bay, and Cape Fear to permit contouring of the region. The only other comprehensive data in the literature for this region are the AXBT data for November and February 1979 reported by Bane et al. (1980b) and Bane and Brooks (1981). One hundred fifty meters was selected, as fewer data are available at the 200-m level. Shallower depths (0,50 and 100 m) were ignored since they are more susceptible to seasonal warming and cooling. The 17 to 17.5°C isotherm is indicative of the Gulf Stream's western boundary at the 150-m level. The horizontal spacing of isotherms in Figure

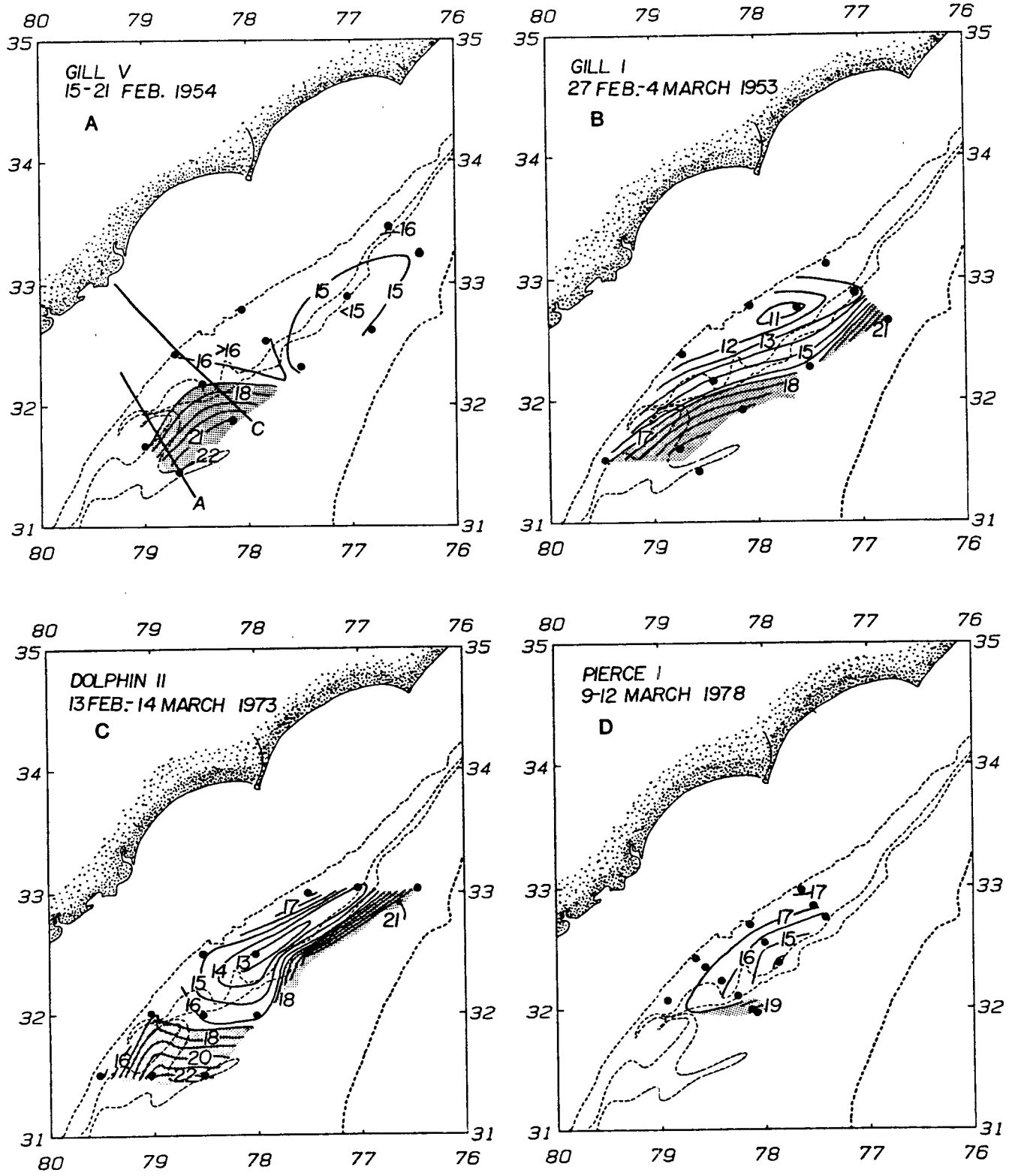

Figure 4.5-28. The 150-m horizontal temperature distribution opposite Long Bay for 12 different cruises.

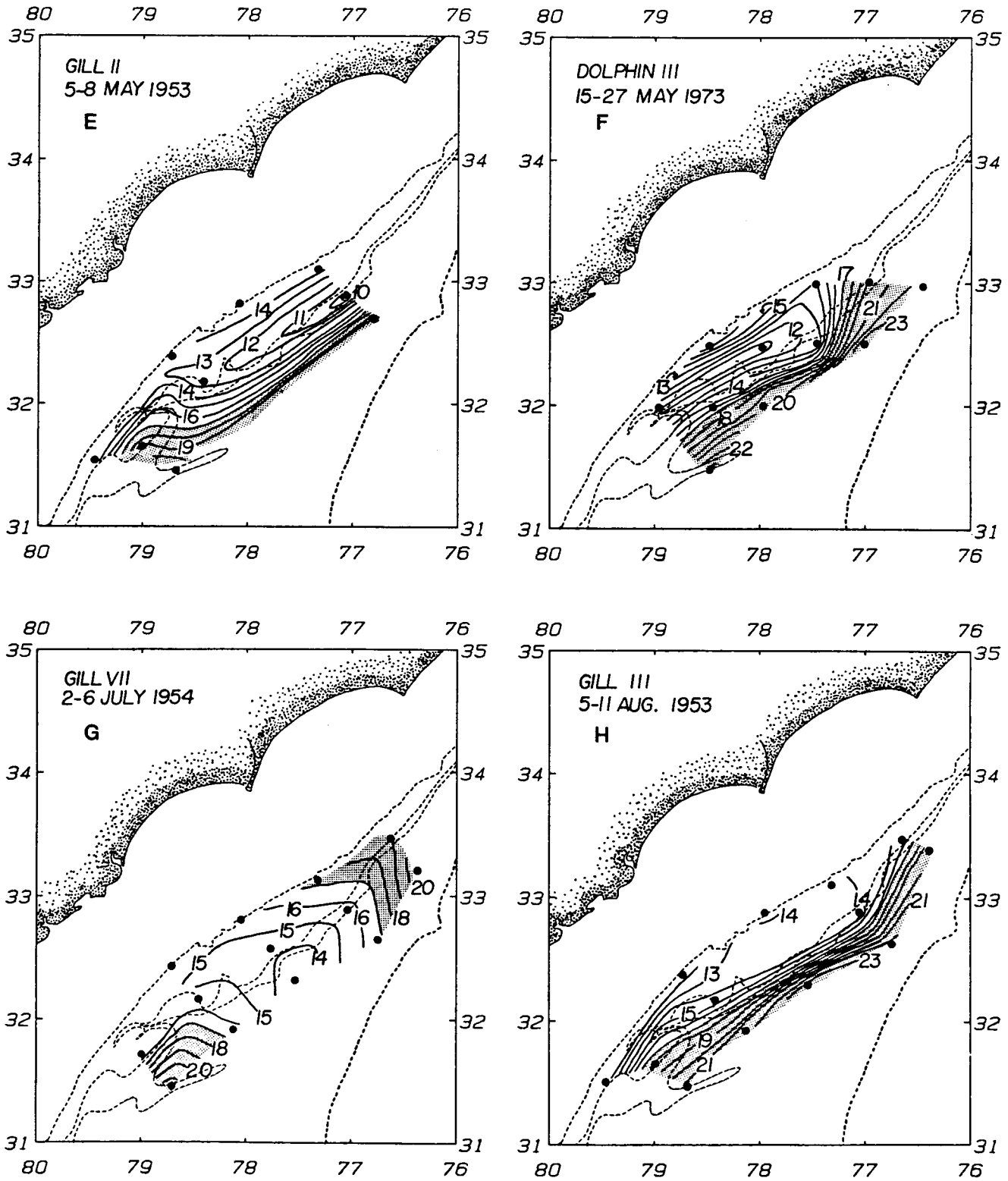

Figure 4.5-28 e-h. The 150-m horizontal temperature distribution opposite Long Bay for 12 different cruises.

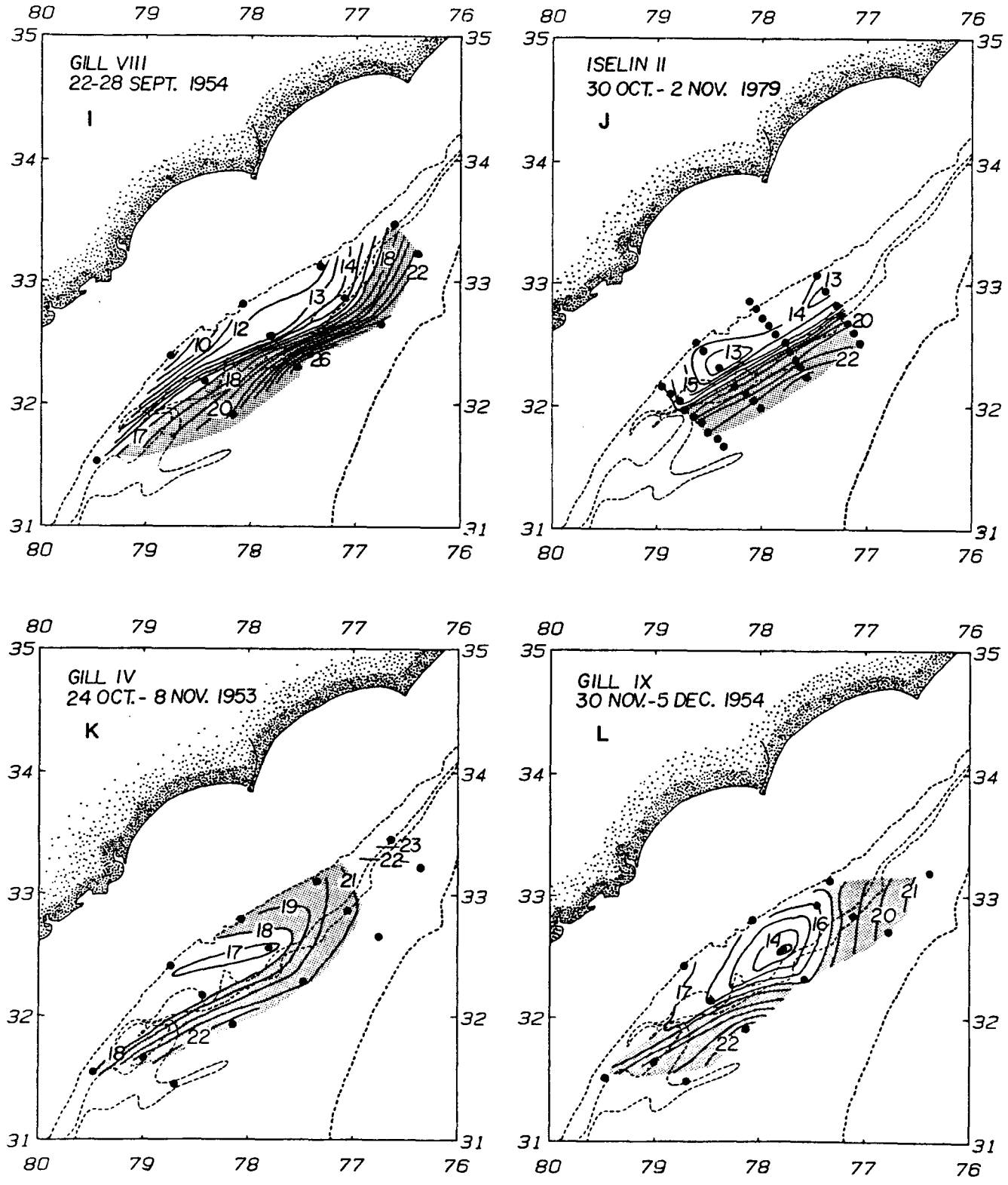

Figure 4.5-28 i-1. The 150 m horizontal temperature distribution opposite Long Bay for 12 different cruises.

4.5-28 should be representative of trends, but are not presumed to be absolutely accurate as to gradient width along the western edge of the Stream.

The total area short-term synopticity is in question for Figures 4.5-28c,f, and k, where sampling occurred over 12 to 30 days. Most of the data, however, were collected over a period of 3 to 6 days. The longer periods are satisfactory only if seasonal onshore-offshore trends exist and sampling is deep enough to remove the influence of short-term meander phenomena, or if meanders did not occur. However, since Bane et al. (1981) have observed the influence of meanders to as deep as 250 m (though significantly reduced), we cannot say that these data are independent of such influence.

It is pointed out that the deflection and meander processes are not necessarily inseparably related. If we define deflection as movement away from the 200-m isobath, there is always a deflection; but there is not always a meander. In addition, under identical flow conditions, the angle of incidence into the bathymetry of the region may in part influence the deflection response.

With this understanding, several interesting findings and trends are noted. First, the data indicate that throughout the year the Gulf Stream moves offshore and an upwelling region is formed off of Long Bay. Second, at times there is a gradual offshore-onshore movement roughly following the 400-m isobath (Figure 4.5-28h,i,j), and at other times, an abrupt easterly movement near 32°N (Figure 4.5-28a,c,e,g). This latter observation is highly correlated to a greater offshore movement of the Gulf Stream opposite Long Bay. Third, the least movement offshore opposite Long Bay occurred in the August through November period, and the greatest movement offshore occurred in the February through March, May, and July periods. The July deflection was particularly large. Interestingly, these same time frames are reproduced by repeated section off Cape Romain (Figure 4.5-23) for much shorter sampling intervals (< 12 h). There, the least deflection from the 200-m isobath occurred in April and August through October, and the greatest deflection occurred in March, May, July, and November 1978. Only the November observation is contradictory. Figure 4.5-28a shows this transect (line C) with respect to the horizontal field discussed. Clearly, this transect would have been a good indicator of the relative offshore deflection opposite Long Bay for nine of the twelve composites presented in Figure 4.5-28.

Further upstream, line A is shown in this same figure. It is the cruise track for the NOAA Peirce cruises. The deflection offshore from station 3 (see Figure 4.5-18, line A) along this transect has been determined relative to the mean for all the data. This information is presented in Figure 4.5-29. The Gulf Stream was defined as the 15°C isotherm at 200 m and the distances were obtained from the vertical plots of temperature presented by Hazelworth (1976). Examination of station locations reveals that the same transect line and stations were nearly identically (± 2 km across-shelf) reproduced through stations 4, 5, or 6 as applicable (the furthest offshore extent of the western wall of the Gulf Stream) for 16 repetitions. Four other repetitions showed SW or NE alongshore displacement between 4 and 9.5 nm (7.4 and 17.6 km) at the furthest applicable offshore extent, but had comparable across-shelf station spacing.

The range of deflection from station 3 was nearly 38 km, with maximum and minimum distances from station 3 of 56.4 and 18.5 km, respectively. The mean distance was 35.6 km. The short-term variability (two-week periods) was as much as 32 km (in August), but generally less than 21 km. The least offshore movement occurred in March, mid-August, and early December, and the greatest in May, June, early-August, and early-November. These observations contradict above stated observations for March, but also suggest a transitional period for November. In addition, by applying this section to the plots of Figure 4.5-28, the February through March period would exhibit both large and small deflections along this line, and the relative deflection opposite Long Bay would be predicted accurately 7 of 10 times.

Between April and August 1966, transport measurements were made corresponding to eight of the NOAA Peirce cruises. These values from Hazelworth (1976) are reported (in boxes) in Figure 4.5-29, and are the average of two values believed in error by no more than 10%. The first five of these values suggest a direct relationship between Gulf Stream transport and the relative distance offshore from station 3. However, the latter two observations, in particular, appear to contradict this trend.

Fuglister (1951) reported that the minimum and maximum currents for this region occur in November and July, respectively, and Montgomery (1938) has shown that sea-level data indicate minimum and maximum flow generally occur in October and July, respectively. There is also some indication that a secondary minimum occurs in April and a secondary maximum in January. Niiler and Richardson (1973) have presented evidence of an annual cycle to Gulf Stream transport for the Florida Straits. Their data suggest a similar time frame with minimums and maximums occurring in December and June, respectively. Interestingly, Brooks (1979) and Düing (1975) both have indicated that an eastward displacement of the Gulf Stream axis in the Florida Straits usually corresponds to an increase in transport. Consolidation of these findings with those above suggests that frequently there is a direct relationship between transport and deflection. In contrast, the latter three observations of the transport opposite station 3 of the NOAA Peirce cruise data tend to support the view of Rooney et al. (1978) that higher velocities would induce lesser deflection, and vice versa. Perhaps the differences between these and the other five observations are attributable to changes in the angle of incidence of the Gulf Stream into the region, or there is some other unidentified factor of influence. However, if the late June observation could be identified as an explainable anomally (which will not be attempted here) the latter two observations would remain consistent with the earlier arguments.

A direct relationship might be explained in part by adherence to Iselin's (1938) theory of the circulation of the North Atlantic. He proposed a large anti-cyclonic eddy that contracts as transport increases and presses closer to the coast as transport decreases. In the "Bump" region, the increasing current speed would deepen the Gulf Stream and increase its sensitivity to the bathymetry further offshore. On the other hand, a decreasing current speed would decrease its depth and sensitivity to the offshore bathymetry, and the Stream would move nearer shore but still be well offshore of the 200-m isobath.

As a corollary, one would expect the cyclonic velocity at the "Bump" to decrease with the Stream offshore particularly with southwest winds (creating

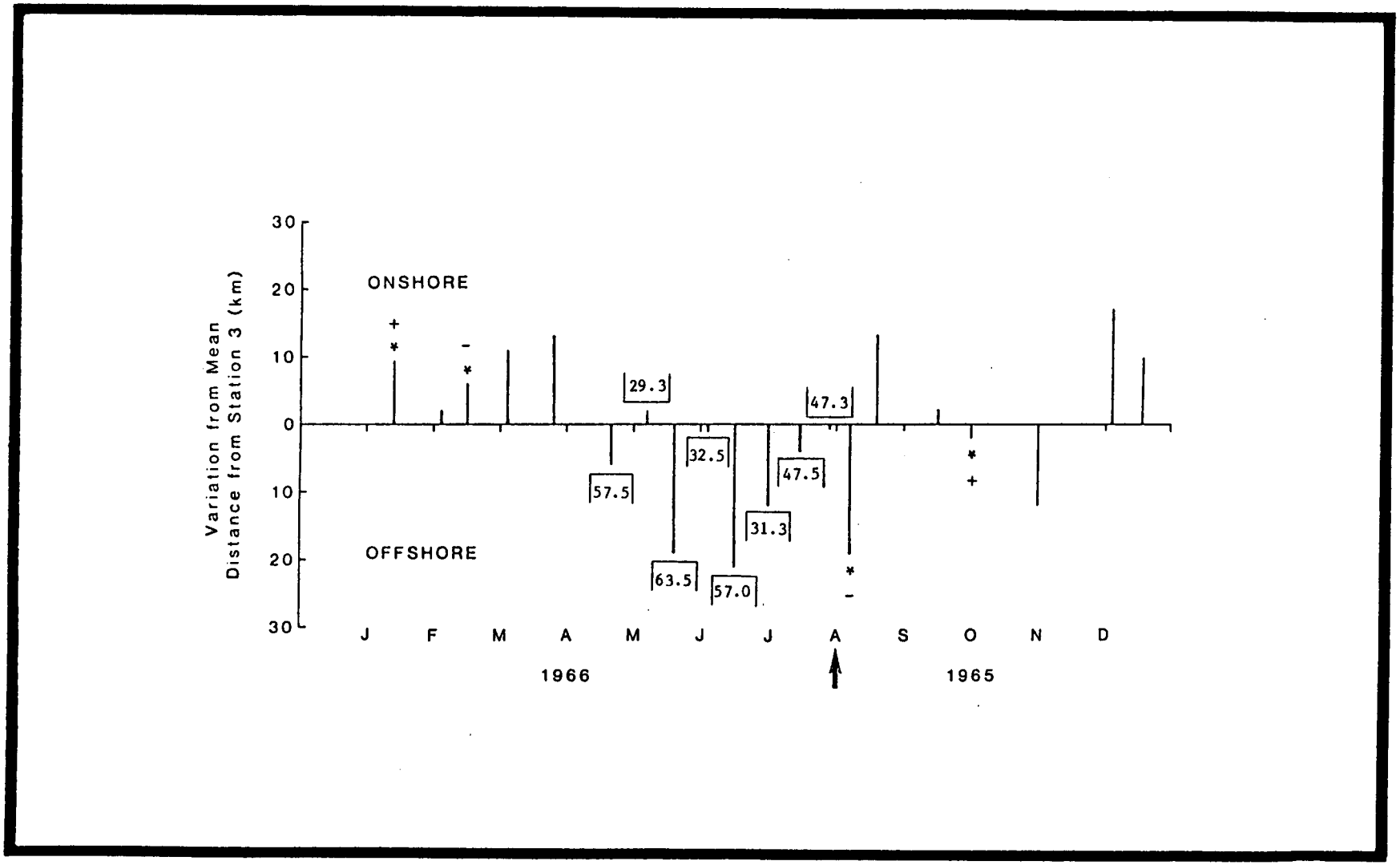

Figure 4.5-29. Onshore-offshore variation in distance of the Gulf Stream western wall from the mean from station 3 along line A (August 1965 - July 1966). Boxed numbers are estimated mean transport ($x10^6 m^3 s^{-1}$) (from Hazelworth 1976).

[* = As measured between 7.4 and 17.6 km from the standard stations in $\pm$ alongshore

a larger more diffuse cyclone), and to increase with the Stream onshore, particularly with northeast winds (creating a smaller tighter cyclone). Such seasonal onshore-offshore motion associated with current strength could explain much of the implied seasonal temperature structure in the doming region presented earlier in Figures 4.5-20 and 4.5-21. Hazelworth (1976) in fact, directly credited the thermocline fluctuations in this area to "meanderings of the Gulf Stream" and Iselin (1938) has noted in the deep ocean that ". . . As the current decreases in strength, bottom temperatures in the depths occupied by the main thermocline layer will rise, and vice versa." This could readily explain the low temperatures observed in July, but creates a problem for October. However, the seasonal occurrence of northeast winds in October may compensate for the onshore movement of the Stream, which would otherwise deepen the thermocline.

4.5.3.7 Summary and Conclusions

Doming was defined as an upward and then downward bending of the 15°C isotherm offshore of the 200-m isobath. A region satisfying this definition was identified, extending between 31.5 and 34.5°N. This is the same region over which the 400-m isobath goes offshore and then onshore with regard to the 200-m bathymetry. Nearly 75% of all doming observations occurred in the area between the 200- and 400-m isobaths. The incidence of doming for seasonal repeated sections in the SAB (from the M/V Gill cruises) was found to be highest off Long Bay (86%), Cape Fear (43%), and Cape Romain (25%). The higher incidence off Long Bay supports the view of Pietrafesa and Janowitz (1980) that a cyclonic circulation pattern persists throughout much of the year in the region.

Evidence was presented showing that lower salinity shelf waters move offshelf and collect in the doming region between late June and early August. This was attributed to the occurrence of sustained southerly to southwesterly winds, and is probably a seasonal occurrence. Aerial mapping of surface salinity was suggested as a means of quickly defining the path of the Gulf Stream in the area in July, since surface temperature observations are inappropriate that time of year.

Temperatures at 200 m suggest seasonal fluctuations in the depth on the main thermocline layer (12 - 6°C), and subsequent source nutrient levels in the doming region. The colder waters tended to be shallow for January through February and July through October, and deeper for March through June and November through December.

Along the Cape Romain section, the greatest upward nitrate penetration occurred for the same months as exhibited the greatest upwelling of cold, low salinity, high-density water (i.e., March 1979, and in summer and early fall). However, near-surface nitrate levels of 1-5 µM were observed in March, April, and May 1978, when weaker upwelling was observed. These high spring-time surface values were probably of older upwelled origin, being sustained by cooler (< 22-23°C) surface temperatures.

The highest total chlorophyll observations ($\leq$ 3.1 mg m^{-3}) were made in March and July 1979. These observations were associated with the leading edge of strong thermal gradients at temperatures less than 17°C, with nitrate concentrations greater than 10 µM. Such values are not as high as has been

observed further south in the SAB during studied upwelling events associated with meanders and frontal eddies (5.0 μM). However, since no special effort was made to sample the region in as much detail (tighter station density and more sampling depths), these total chlorphyll observations should be regarded as background for future work.

Throughout the year, the Gulf Stream moves offshore of the 200-m isobath, and an upwelling region is formed off Long Bay. At times there is a gradual offshore-onshore movement, roughly following the 400-m isobath, and at other times an abrupt easterly movement near 32°N. Much of the time, there appears to be a direct seasonal relationship between the historical seasonal velocity field and offshore deflection, with higher velocities corresponding to greater deflection, and vice versa. Iselin's (1938) theory of North Atlantic circulation may explain these observations. The large anti-cyclonic eddy of the North Atlantic contracts and deepens (moving the Gulf Stream offshore) as transport increases, and expands and shoals (moving the Gulf Stream onshore) as transport decreases.

This same theory predicts a larger more diffuse cyclonic circulation off Long Bay for high Gulf Stream transport, and a smaller tighter cyclonic circulation for lower Gulf Stream transport. In effect, a small eddy is driven by a larger one. Additionally, it has been noted that local winds might enhance or retard such cyclonic flow, and that the depth of the main thermocline layer in the doming region appears to respond to the relative transport of the Gulf Stream and the local wind.

4.6 CIRCULATION - GEORGIA EMBAYMENT

4.6.1 Introduction

The low-frequency current and temperature response to wind and Gulf Stream forcing in the southeast U.S. outer continental shelf is investigated, using moored current meter, hydrographic, wind, and satellite VHRR data collected as part of the Bureau of Land Management and Department of Energy supported interdisciplinary study of the region (GABEX-I experiment).

Shelf topography is particularly simple along the southeast U.S., consisting of a broad shallow shelf that slopes gently to a rather sharp shelf break at about the 75-m depth contour (Figure 4.6-1). Shelf widths vary from a minimum of about 50 km off Cape Canaveral to a maximum of 120 km off Brunswick and Savannah, Ga. Isobaths tend to follow the slight cuspate shape of the coast, with diverging isobaths north of Cape Canaveral and convergence at Cape Romain. A shallow shoal extending from Cape Fear forms the northern boundary of the region and has considerable influence over the flow in that region (Pietrafesa, unpublished report). East of Savannah, a topographic anomaly of the slope known as the "Charleston Bump" (Brooks and Bane 1978) protrudes into the Gulf Stream.

Previous investigations indicate that the shelf can be subdivided into three cross-shelf zones according to the physics controlling the low-frequency flow variability (Atkinson et al. in press). Waters in the inner shelf (0-20 m) are influenced by density effects from river run-off, which tend to form a band of low salinity, stratified waters near the coast (Blanton 1980). Bumpus (1973) found evidence of persistent southward flow from surface drifter

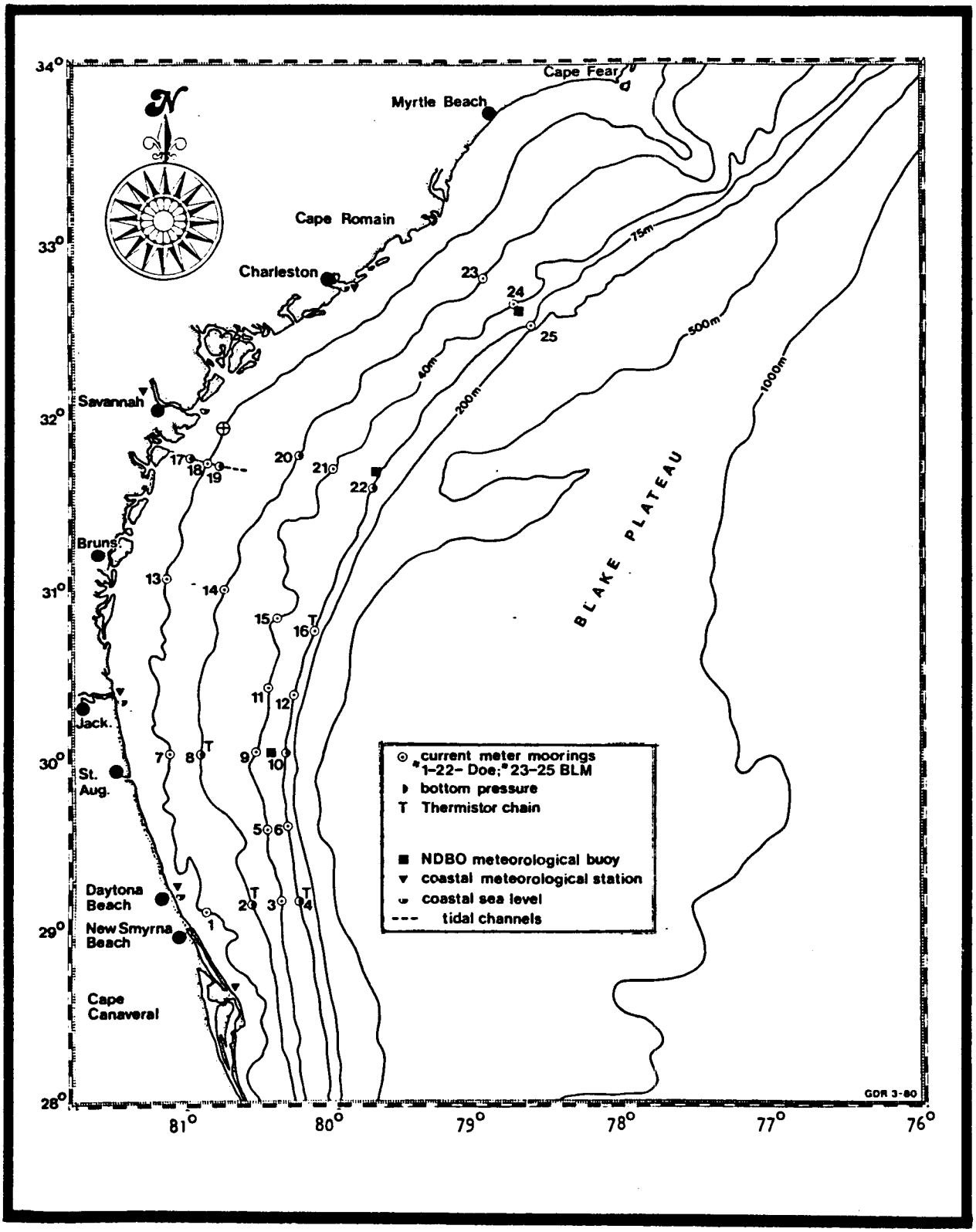

Figure 4.6-1. GABEX-I subsurface current meter array, 17 February to 26 June 1980.

trajectories in this band. Local wind forcing and seasonal atmospheric changes are also influential in this region.

In the mid-shelf zone (21-40 m), subtidal flow variability has been observed to be strongly related to local wind forcing in the 2-day to 2-week period band (Lee and Brooks 1979, Klinck et al. 1981) through a frictional equilibrium process similar to that observed in the Mid-Atlantic Bight (Beardsley and Butman 1974, Scott and Csanady 1976). This region undergoes a seasonal change in stratification, with vertically well-mixed conditions characteristic of fall and winter, and vertically stratified conditions occurring during spring and summer (Atkinson et al. in press).

Low-frequency flow variability and water exchange in the outer shelf (41-75 m) have been shown to be produced primarily by Gulf Stream frontal disturbances, such as northward propagating wave-like meanders and cold cyclonic frontal eddies, which occur on time scales of 2 days to 2 weeks (Lee and Brooks 1979, Lee et al. 1981). South of 32°N, the western edge of the Gulf Stream generally lies within ± 15 km of the shelf break (Bane and Brooks 1979). Frontal eddies have been shown to propagate along the outer shelf in this region, causing an exchange of water and momentum, and a net flux of nutrients to the shelf (Lee, et al. 1981). Yoder et al. (1981), found a significant phytoplankton response to upwelling in the cold core of frontal eddies. Between 32 and 33°N, the "Charleston Bump" appears to force an offshore meander of the Gulf Stream (Brooks and Bane 1978; Pietrafesa et al. 1978; Legeckis 1979). Downstream of the "Bump", enlarged wave-like meanders can displace the Gulf Stream front up to 100 km from the shelf break (Legeckis 1979, Bane and Brooks 1979). These enlarged "meanders" have similar kinematic properties (Brooks and Bane 1981, Bane et al. 1981), as observed in smaller frontal eddies off the Georgia shelf, and suggest a dynamic connection or correspondence.

During the winter/spring of 1980, a multi-institutional study of physical, chemical, and biological processes on the southeast U.S. shelf was undertaken (GABEX-I experiment). The University of Miami had responsibility for moored current meter measurements along the 40- and 75-m isobaths (outer shelf) from Savannah south. North Carolina State University was responsible for the mid- and inner-shelf moorings in this same region, and Science Applications, Inc., for the moorings off Cape Romain. In this report we present findings from the outer shelf, including synthesis and interpretation of its multiple BLM and DoE supported data sets.

4.6.2 Low-Frequency Current and Temperature Fluctuations

4.6.2.1 Time Domain

Low-frequency (40-HLP filtered) wind and upper layer currents along the outer shelf are shown in Figure 4.6-2. The influence of the Gulf Stream is clearly indicated at the shelf break, where current speeds were greater than 100 cm s^{-1}. South of 30°N, strong northward flows persisted for most of the measurement period, and current fluctuations were visibly coherent between stations. Only five flow reversals were observed at the St. Augustine transect (Mooring 10) during the 4-month study. The persistent northward flow was not observed at the shelf break off Savannah, Ga. (Mooring 22), and the number of flow reversals increased. At the Cape Romain transect, prolonged

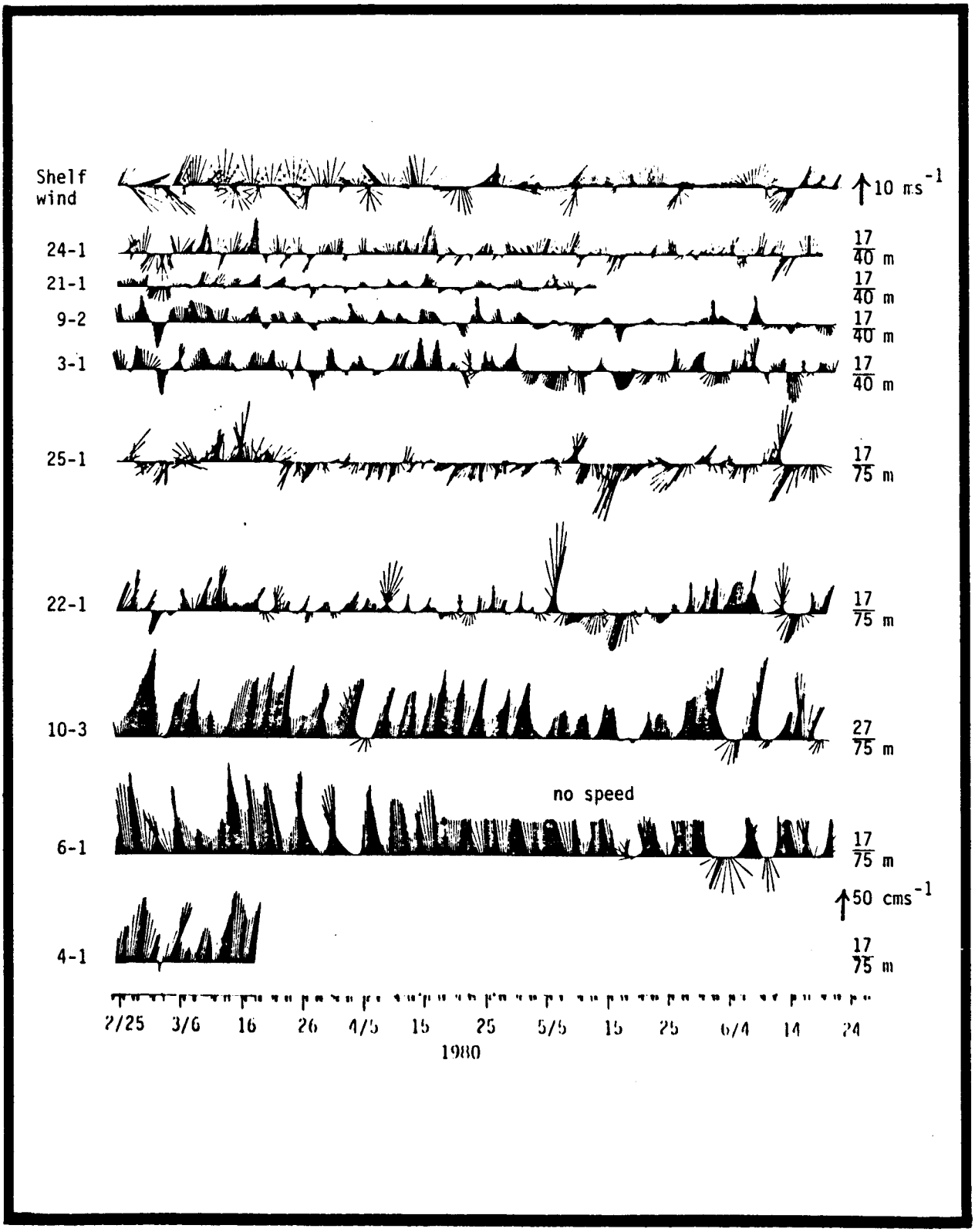

Figure 4.6-2. Time series of 6-hour rotated current and wind vectors from upper layer 40-HLP records for 25 February to 21 June 1980. Current meter identification is given on the left, and instrument and water depths on the right. Scale arrows are shown on the right.

southward flow events were observed at the shelf break showing little visual similarity to the currents off Savannah. Along the 40-m isobath, low-frequency currents in the upper layer show significant visual coherence between mooring sites and with shelf winds (Figure 4.6-2). Current amplitudes were also similar in magnitude between sites, with little indication of any seasonal trend.

The vertical distribution of subtidal currents and temperature at the St. Augustine transect is shown in Figures 4.6-3, -4, -5a and 5b. Current and temperature fluctuations were strongly coupled at the shelf break throughout the vertical array. Onshore flow events that occurred nearly simultaneously over the vertical array were shortly followed by decreasing along-shelf currents and decreasing temperatures. Thus, cold temperature anomalies occurred with cyclonic perturbations of the basic northward flow, and the effect was observed over the total water column. Over the total 4-month experiment, approximately 20 disturbances of this type were observed, giving an average period of about six days (Figures 4.6-5a and -b, Events 1-14). Vertical shears at the shelf break ranged from about $2 \times 10^{-3}\ s^{-1}$ in the fluctuations and $1 \times 10^{-2}\ s^{-1}$ in the mean, indicating a significant baroclinic component in both the fluctuating and mean parts of the flow. The baroclinicity was greatest at times of maximum northward currents, indicating periods when the Gulf Stream front was located near the shelf break.

Significant visual coherence is observed for wind stress events over the horizontal extent of the current meter array and between wind stress and current events at the 40-m isobath (Figure 4.6-4). Wind stress over the shelf at 30°N was approximately three to four times greater than wind stress at the coastal sites.

Current fluctuations at the 40-m isobath were highly correlated over the vertical array, as was temperature (Figures 4.6-3, -4, -5a and -5b), but the correlation between currents and temperature does not appear to be as strong as at the shelf break. Current perturbations at the 40-m isobath showed little change in amplitude with depth. The vertical shear of the mean flow was only $2 \times 10^{-4}\ s^{-1}$, indicating a strong baratropic character. Vertical shear in the fluctuations ranged from about 1 to $7 \times 10^{-3}\ s^{-1}$, with no significant difference between northward or southward flow events. The signature of the cold, cyclonic perturbations observed at the shelf break is not as clear at 40 m but is still recognizable for many of the Events (#5, 6, 7, 8 , 11, 12, 13 and 14 of Figure 4.6-5b).

Temperature fluctuations at the shelf break ranged from ± 2 to ± 8°C and were in-phase for all vertical positions. Temperature oscillations at 40 m had smaller amplitudes and less vertical correlation than at the shelf break. On several occasions, temperature jumps occurred as the water column suddenly warmed, which is indicative of advection of a warm front past the mooring. Northward current speeds also increased at these times.

A seasonal increase in stratification is apparent at both mooring locations, but is more pronounced at 40 m. Stratification generally extended to within 3 m of the bottom at the shelf break, except during periods of sharp temperature declines when near isothermal conditions occurred in the lower 15 to 30 m. Stratification was normally higher for increasing temperatures than

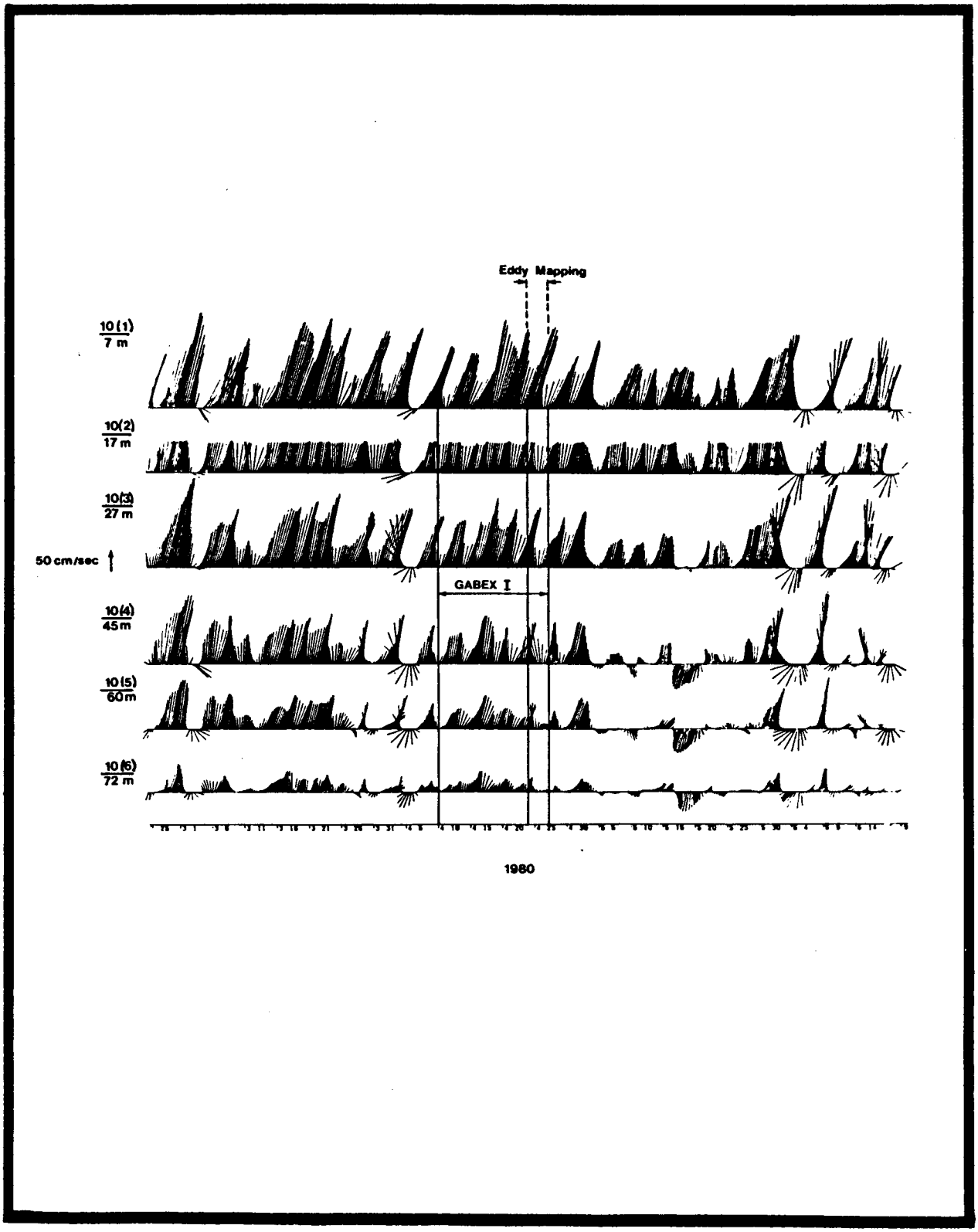

Figure 4.6-3. Time series 6-hour rotated, 40-HLP current vectors from Mooring 10 of the GABEX-I array. Mooring number, current meter identification and instrument depth are shown in the left of each time series. Vertical lines indicate shipboard measurement periods.

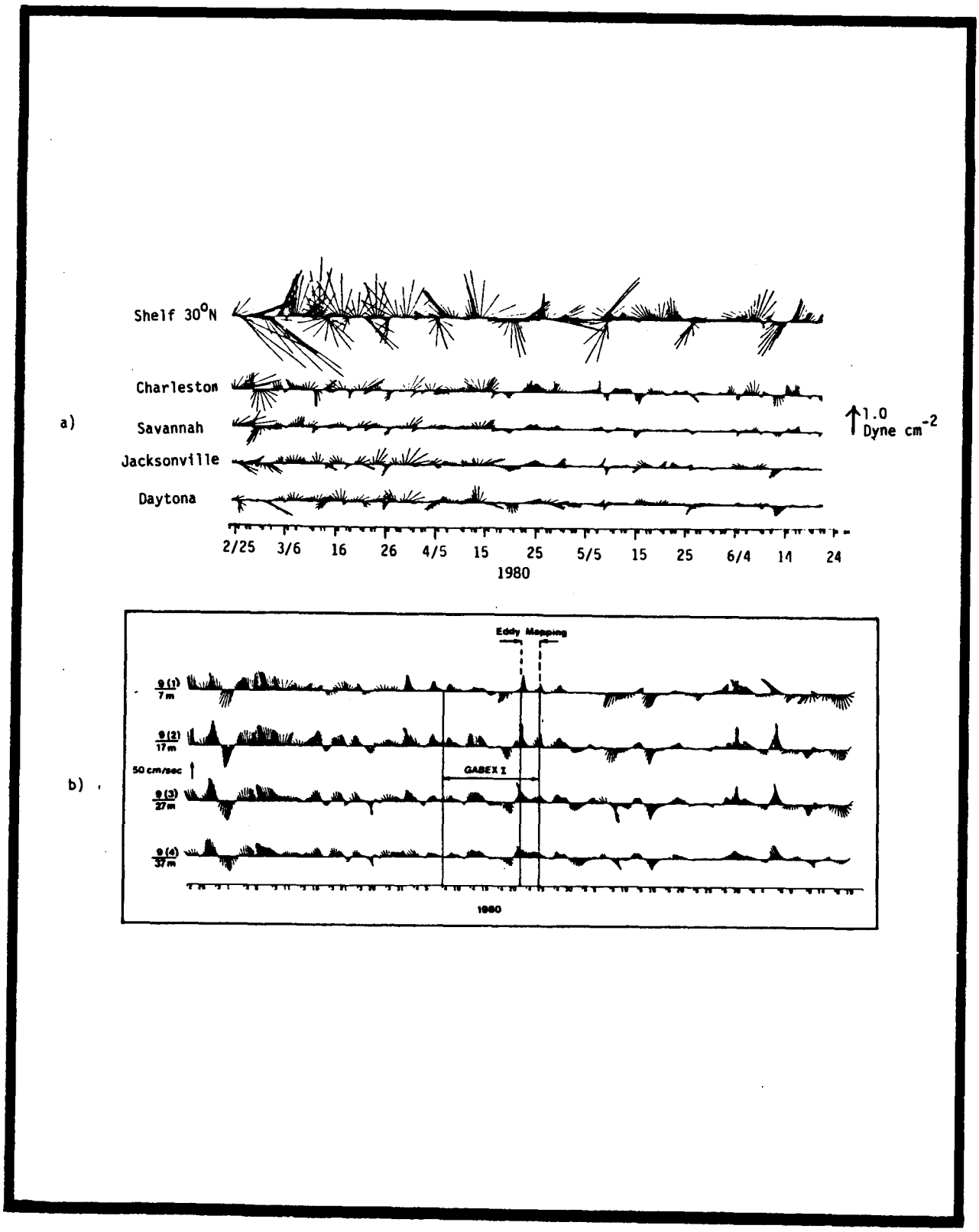

Figure 4.6-4. Time series of 6-hour rotated 40-HLP wind stress vectors (a) and current vectors (b) from Mooring 9 of GABEX-I array.

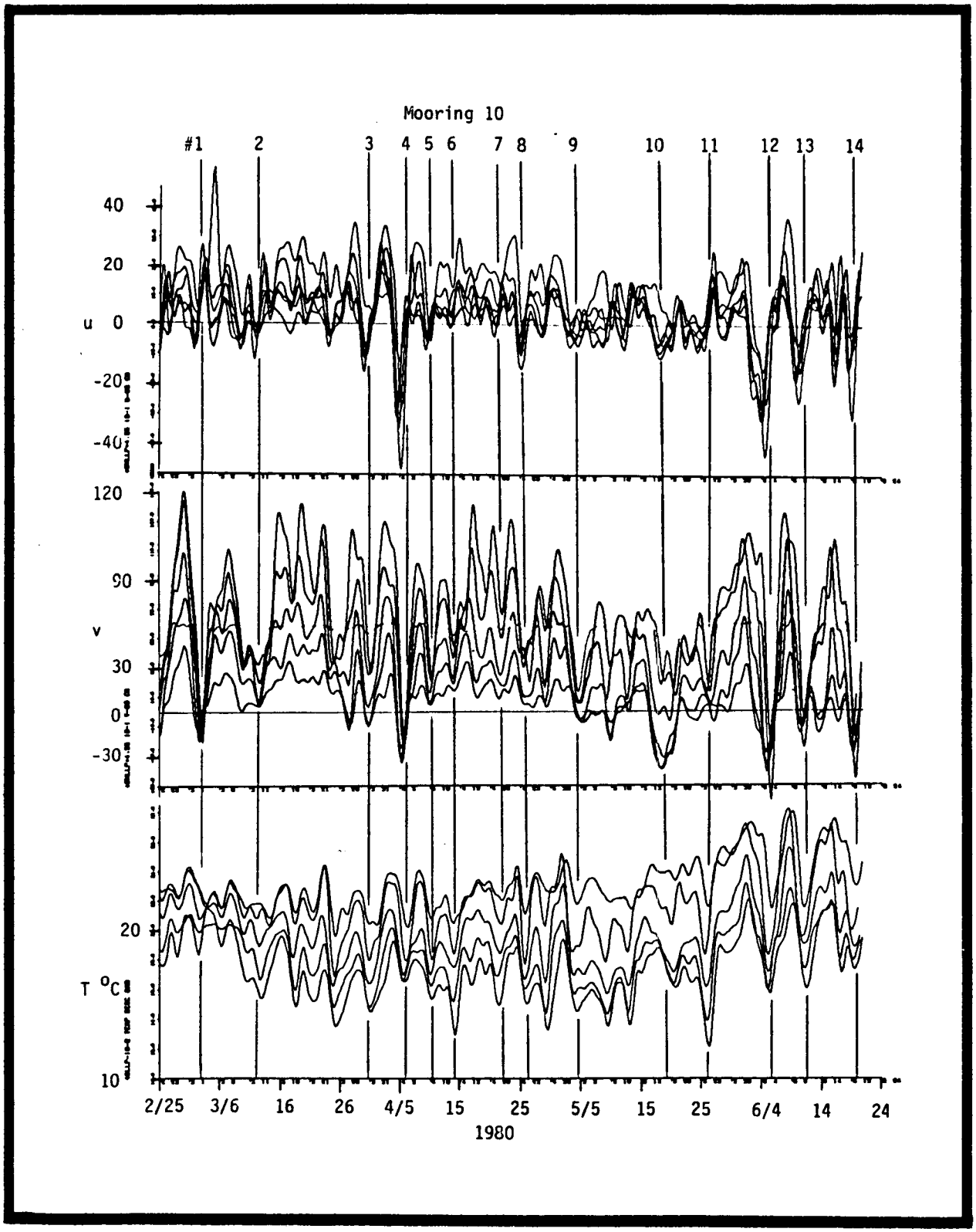

Figure 4.6-5a. Time series of 6-hour rotated 40-HLP U, V, and T from Mooring 10. Vertical lines are for event identification.

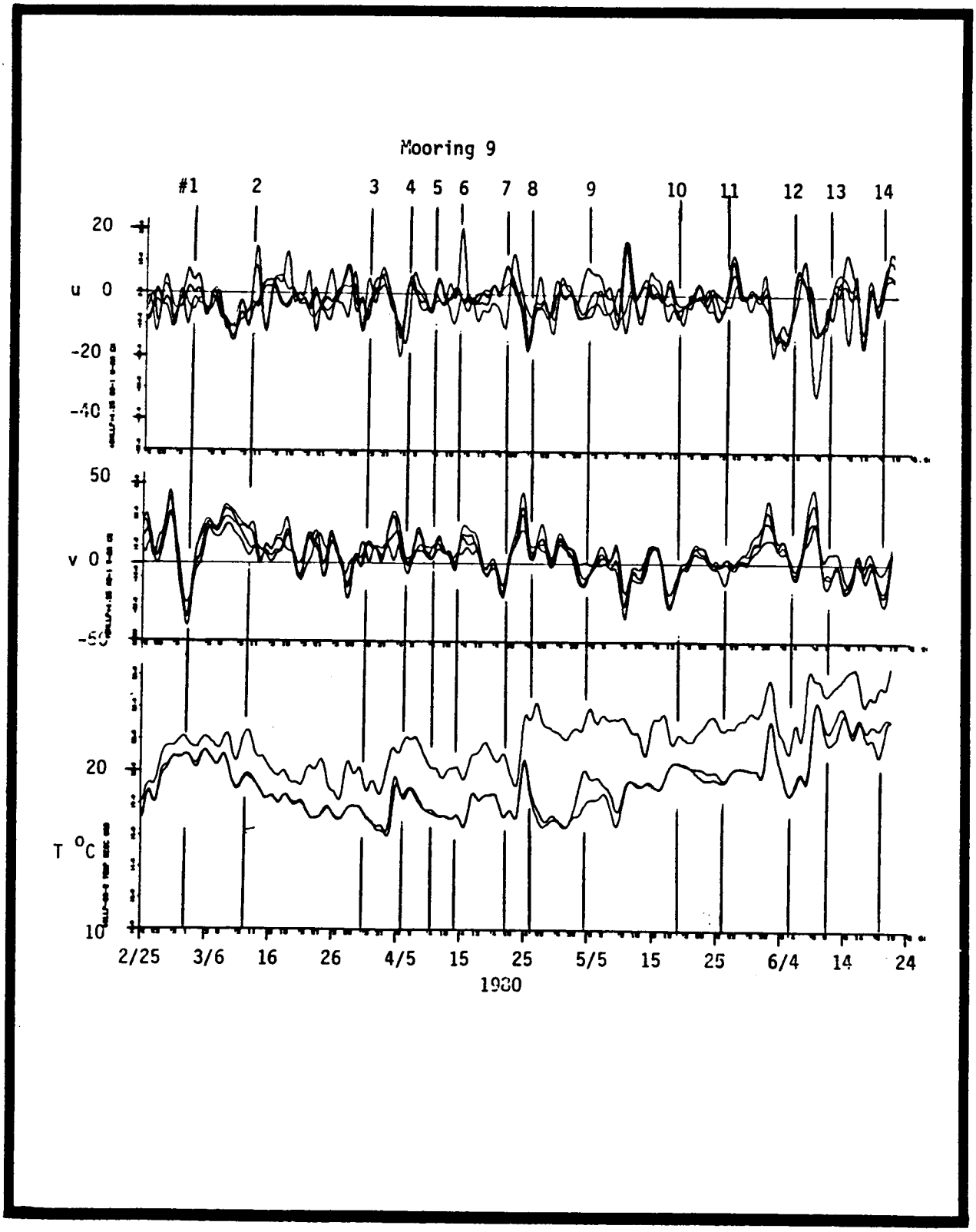

Figure 4.6-5b. Time series of 6-hour rotated 40-HLP U, V, and T from Mooring 9. Vertical lines are for event identification.

for decreasing. At the 40-m isobath, an isothermal bottom layer of at least 13 m thickness existed for most of the experiment.

Low-frequency current and temperature records indicate that the largest amplitude fluctuations occurred in a 2-day to 2-week period band. Therefore, the data were band-pass filtered about this band by smoothing the low-frequency time series with a 2-week high frequency cut-off, which removes fluctuations with periods less than 40 hours and greater than 2 weeks. The band-pass, cross-shelf (u), along-shelf (v), and temperature (T) time series from the upper and lower layers were compared to the band-pass shelf wind components, and coastal sea level measured at the mouth of the Savannah River for the period from 15 May to 17 June 1980 (Figure 4.6-6a and -6b).

Cold, cyclonic perturbations are observed to propagate northward along the shelf break at about 55 cm s^{-1}. The propagation is clearest in the lower layer, due to the greater number of available instruments, but is also readily apparent in the upper layer. Events #10-14 traveled to the north at nearly a constant speed and were clearly recognizable over along-shelf distances of up to 425 km (Event #12; Figure 4.6-6a and 6b). The signature of these perturbations appears more pronounced at the Cape Romain transect, especially the cross-shelf component, which was larger in magnitude than the along-shelf component in the upper layer at Mooring 25. Cold, cyclonic perturbations were observed to propagate northward along the shelf break at speeds of 5-70 cm s^{-1} throughout the 4-month study (Figure 4.6-5a; Events #1-14) and were not visually correlated to either wind or coastal sea level events.

Propagating disturbances were more difficult to identify at the 40-m isobath. At the 27- and 37-m levels, u and v appear to be 180° out of phase for a large part of the records and not significantly related to temperature fluctuations. At the 7- and 17-m levels, u and v were only occasionally out of phase and the correlation to temperature is not clear. Non-propagating events were observed many times at the 40-m isobath, when northward (southward) current fluctuations occurred simultaneously over the along-shelf extent of the array following northward (southward) winds and coastal sea level set-down (set-up) (Figure 4.6-6a, b), (Events a-d). Non-propagating events of this type are observed occasionally at the shelf break (Event a). Mixed responses also occur when propagating and stationary events interact. Large amplitude current fluctuations may occur when these events are in phase (Events c and d at Mooring 25). Non-propagating fluctuations were a major part of the current variability at the 40-m isobath, and a strong correlation with wind events is evident, especially in the lower layer (Figures 4.6-2, -4 and -6a, b). However, propagating disturbances were sometimes observed at 40 m and were visibly coherent with events at the shelf break (Events #11, 12, 13 and 14).

4.6.2.2 Frequency Domain

Cross-spectra of cross-shelf and along-shelf, low-frequency velocity components from the shelf break, 40-m isobaths, and shelf winds are presented in Figure 4.6-7. Spectra from records taken at the 45-m isobaths and shelf winds are presented in Figure 4.6-7. Spectra from records taken at the 45-m level at the shelf break off St. Augustine are shown as typical of the total water column at this location. Low-frequency currents at the shelf break show well-defined energy peaks at periods of 5 to 6 days for u, and 7 to 9 days for

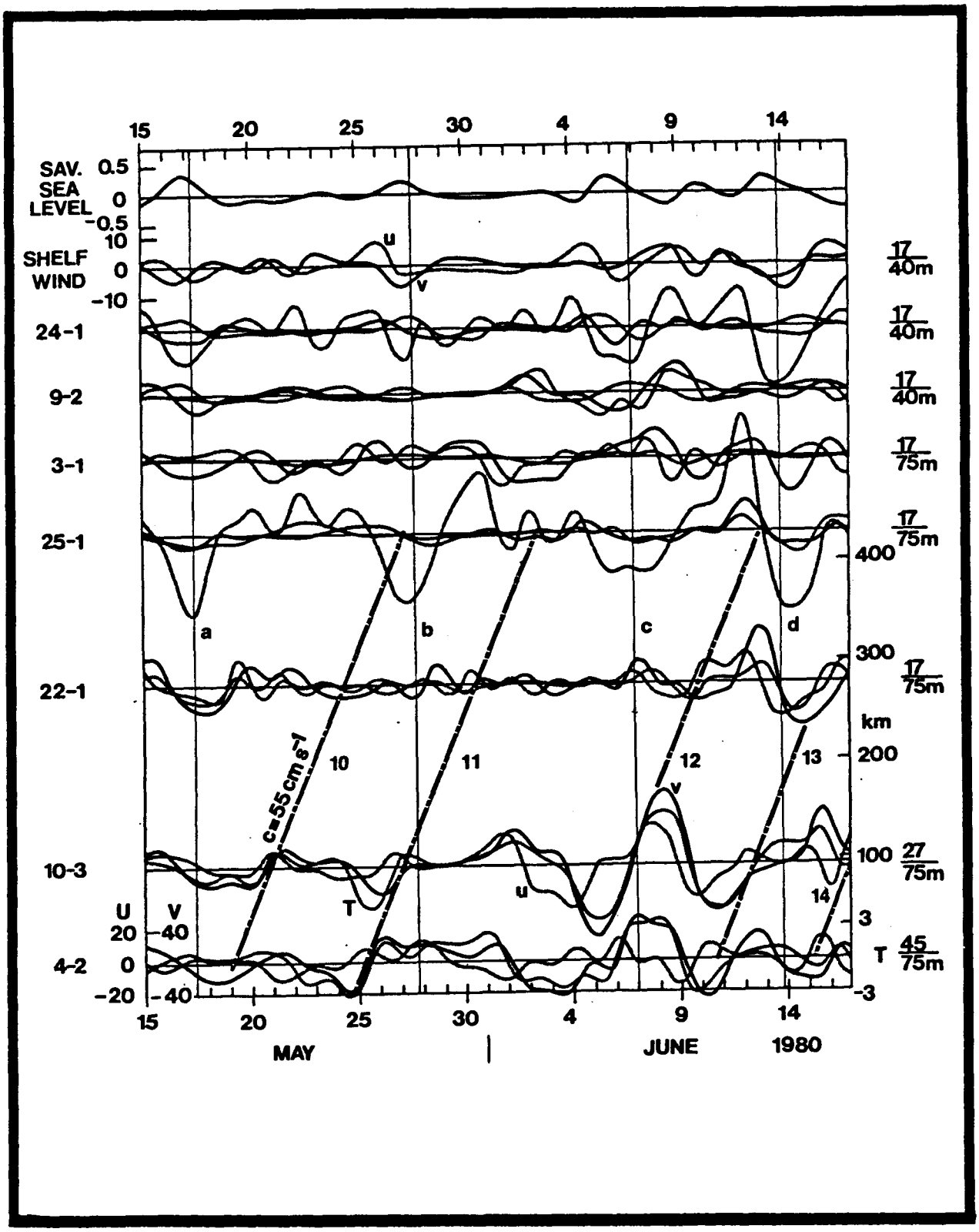

Figure 4.6-6a. Time series of 6-hour rotated band-pass U, V, and T from upper layer, shelf wind (U, V), and Savannah sea level. Propagating events shown by slanting lines with phase speed c = 55 cm s^{-1}. Nonpropagating events shown by vertical lines, V shown by solid lines, U by dashed lines, T by dotted lines. Sea level is also a solid line. Current (cm s^{-1}), wind (m s^{-1}), sea level (m).

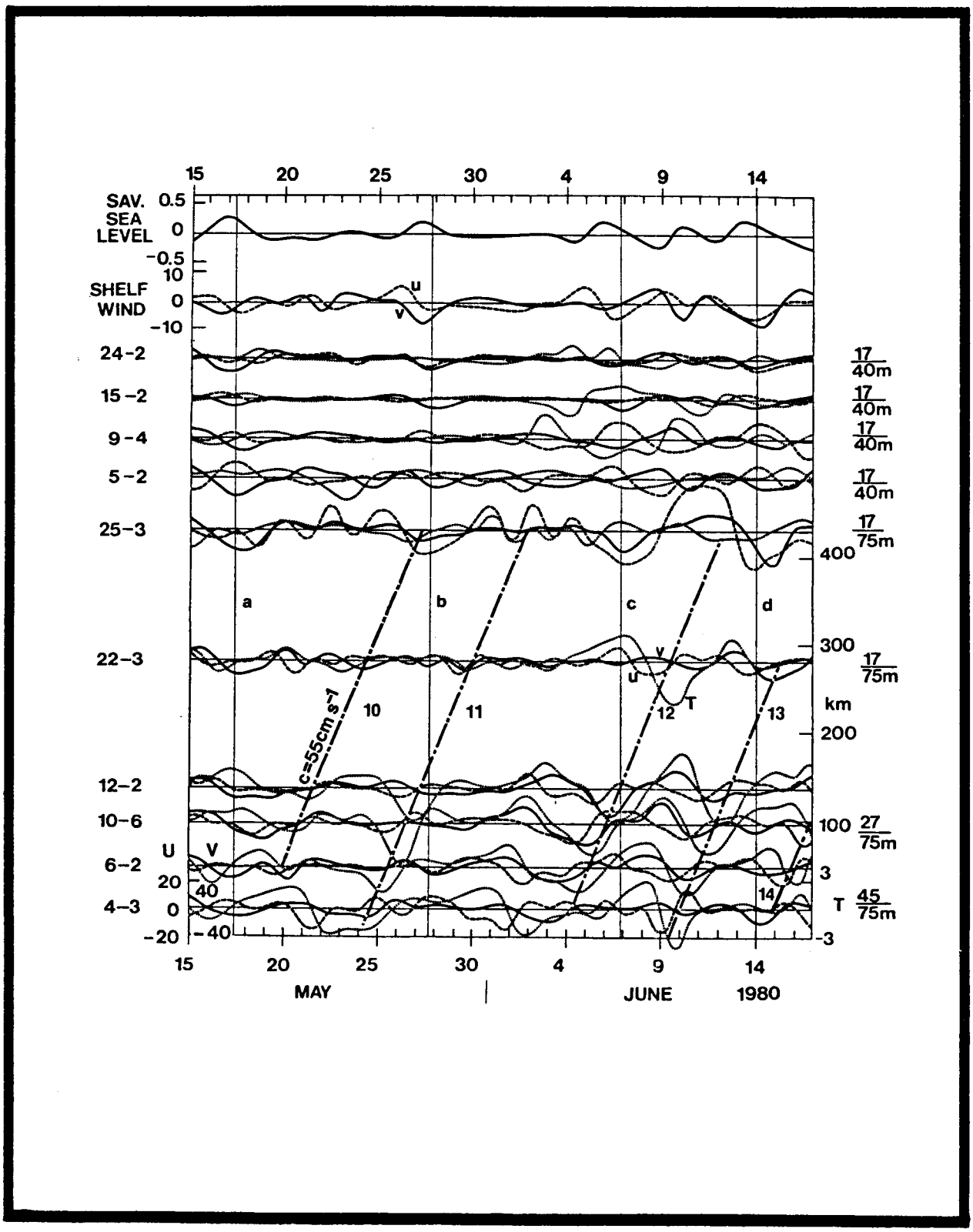

Figure 4.6-6b. Time series of 6-hour rotated band-pass U, V, and T from lower layer, shelf wind (U, V), and Savannah sea level. Propagating events shown by slanting lines with phase speed c = 55 cm s^{-1}. Nonpropagating events shown by vertical lines, V shown by solid lines, U by dashed lines, T by dotted lines. Sea level is also a solid line. Current (cm s^{-1}), wind (m s^{-1}), sea level (m).

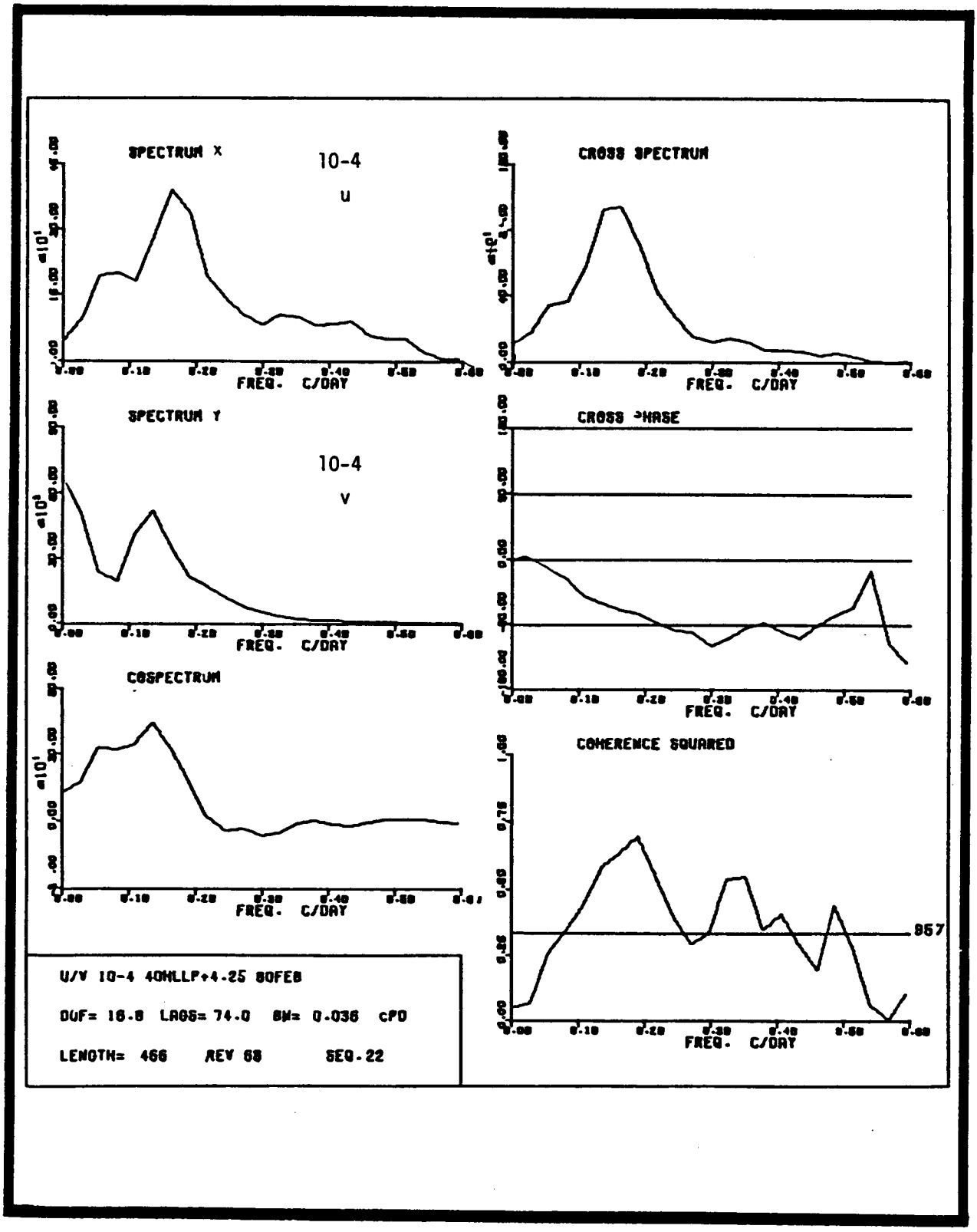

Figure 4.6-7a. Cross-spectra of U vs. V from current meter 10-4.

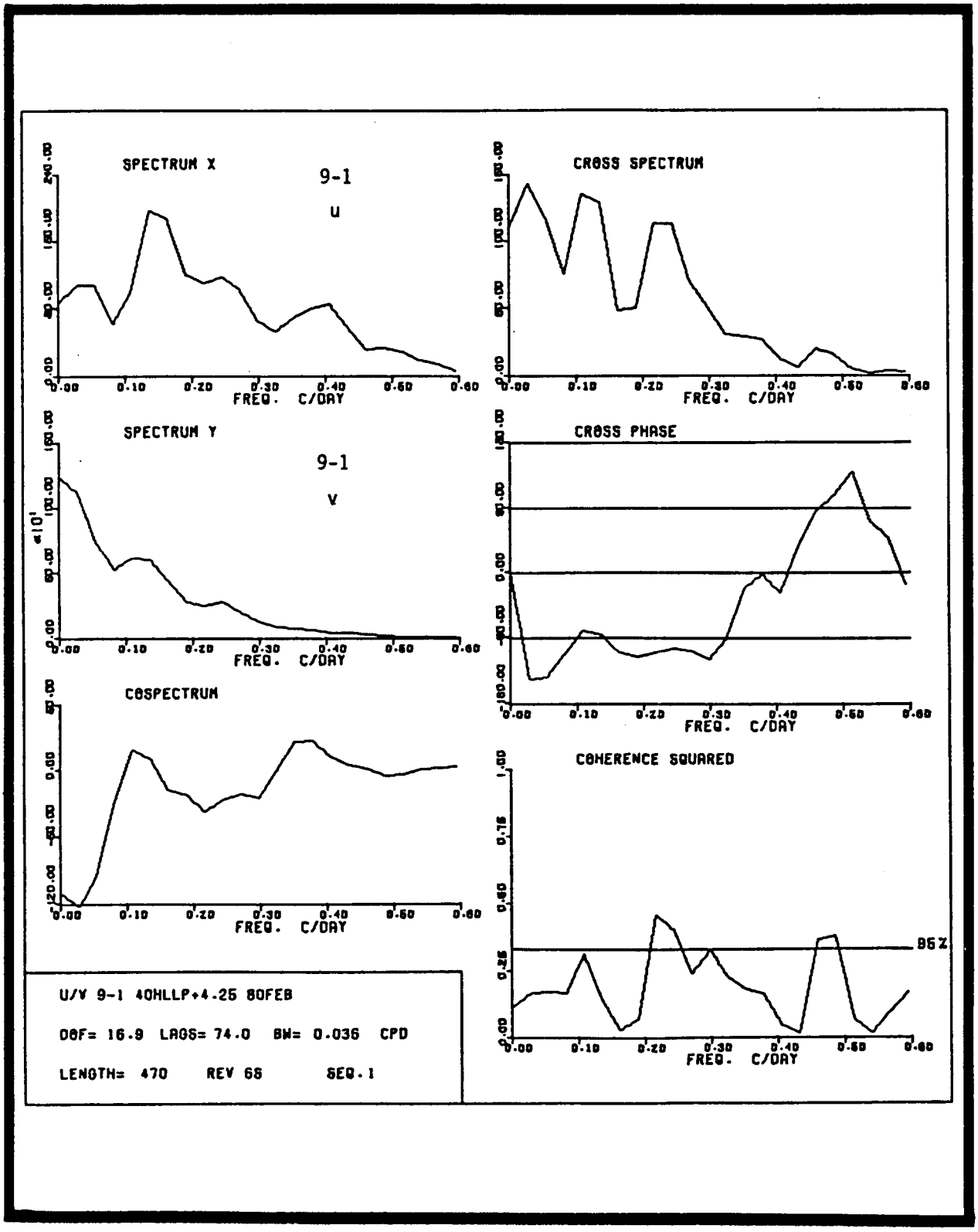

Figure 4.6-7b. Cross-spectra of U vs. V from current meter 9-1.

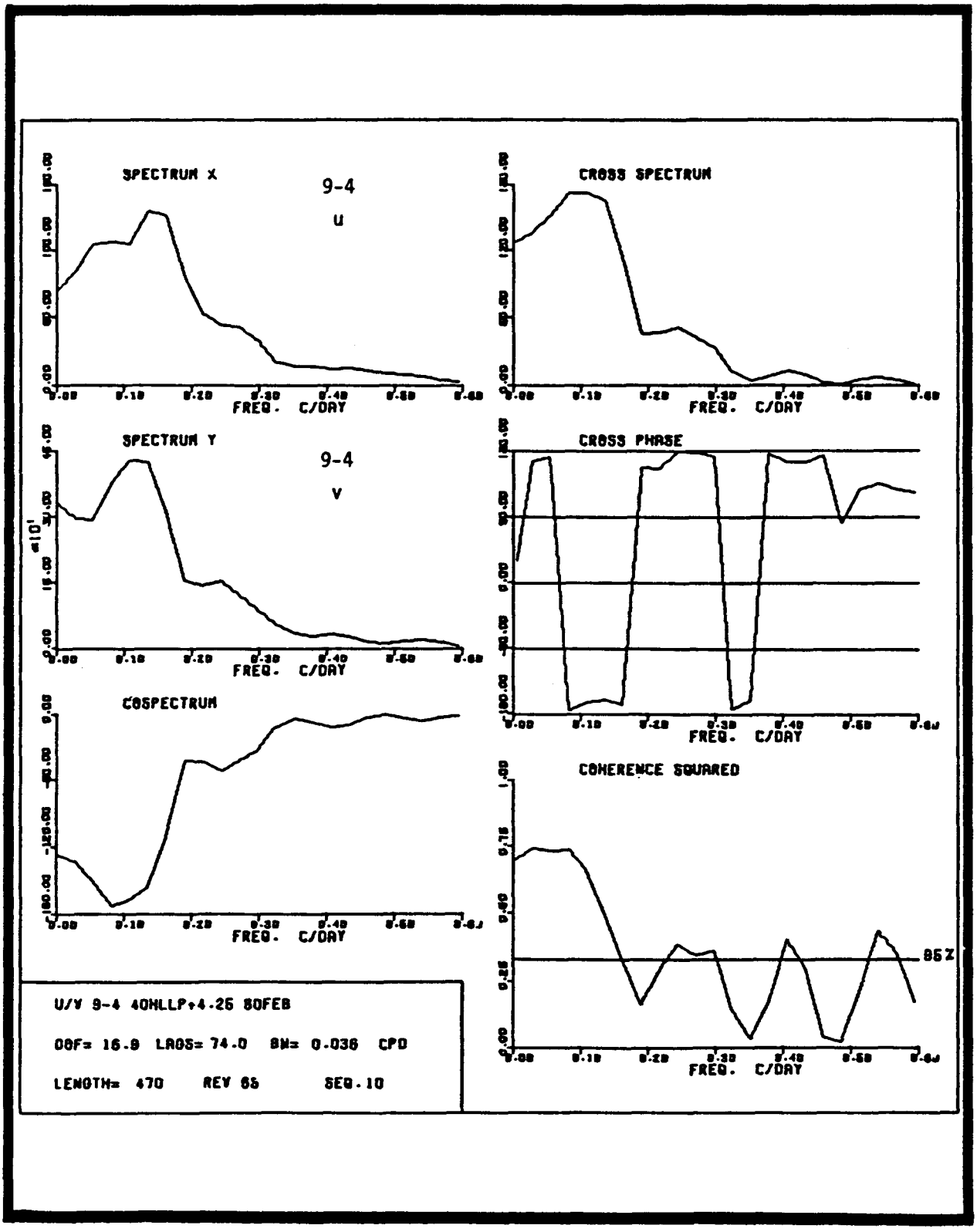

Figure 4.6-7c. Cross-spectra of U vs. V from current meter 9-4.

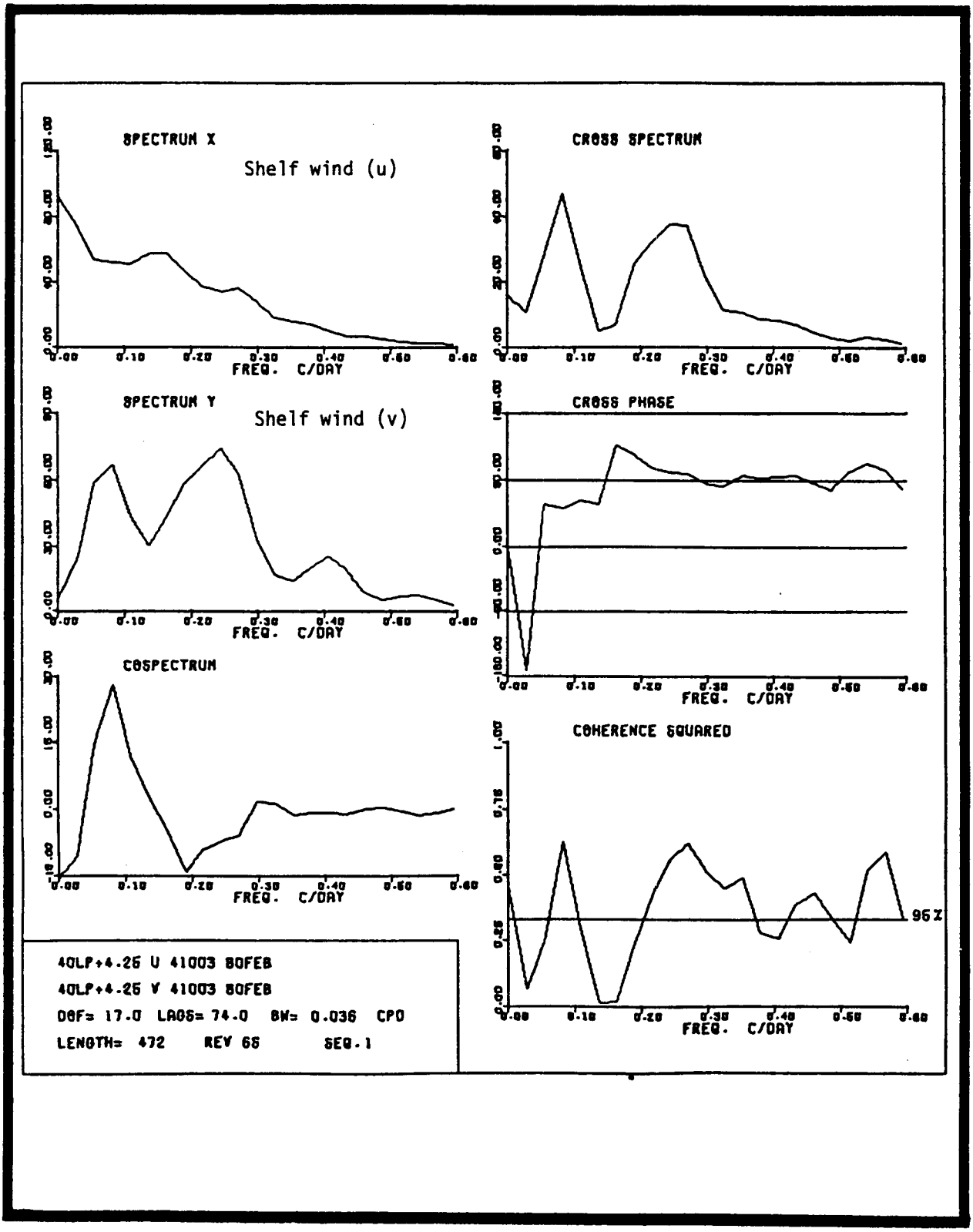

Figure 4.6-7d. Cross-spectra of U vs. V for shelf winds.

v. The velocity components were coherent at these periods, with u leading v by about 50 to 70°, which is indicative of propagating fluctuations. Coherence was also significant at periods of 3, 2.5, and 2 days but the energy levels were considerably reduced. Spectra of currents from the 40-m isobath also show energy peaks at 5 to 6-day periods for u and 7 to 9-day periods for v, but they are not as well resolved as at the shelf break and the coherence is weak. The only significant coherence between u and v in the upper layer (7 m) was at 2- and 4-day periods. In the lower layer, the velocity components were 190° out of phase for periods greater than two days. Coherence was high for periods greater than nine days but only marginally significant at periods of 1.8, 2.5, and 3.3 to 4 days. Shelf winds had energetic coherent fluctuations at the same period as the coherent lower layer motions at the 40-m isobath (1.8, 2.5, 3 to 4, and 12 days). Neither the currents at 40 m, nor the winds, showed significant coherence between u and v in the 5- to 9-day period band where the coherence was highest at the shelf break.

Coherence and phase relationships between along-shelf currents and along-shelf winds are shown in Figure 4.6-8; along-shelf currents vs. coastal sea level are shown in Figure 4.6-9. Currents at the shelf break were marginally correlated to wind and sea level at the 9-day period. This correlation was only apparent in the lower layer. Along-shelf flow in the upper layer at the 40-m isobath showed significant coherence with along-shelf winds at periods of 4 and 7-12 days, and high coherence with sea level at periods of 7-12 days. Currents were strongly correlated with wind and sea level in the lower layer at the period bands of 3-4 and 9-12 days. The coherence was generally higher between currents and sea level at these periods. Subtidal time series indicate that lower layer velocity fluctuations lag the wind by about 12-16 hours, and sea level by about 6 to 12 hours. Also, sea level was highly coherent with along-shelf winds at 10-day periods and with cross-shelf winds at 2- to 7-day periods, appearing to lag wind events by about 6 hours.

Velocity/temperature coherence and phase in the 7- to 9-day period band are plotted against along-shelf separation distance for different combinations of current meter pairs (Figures 4.6-10 through -13). The kinetic energy density in the upper and lower layer at each mooring site is also shown. Coherence falls off rapidly at the shelf break and defines an along-shelf coherent length scale of approximately 100 km for u, v, and T in the energetic 7- to 9-day period band. Phase indicates a near linear increase of negative phase, with separation for distances less than the coherent length scale. Negative phase lags occur for northward propagation, and the scatter of points tend to fall around a line equivalent to the constant phase speed of 55 cm s^{-1} ($\sim$48 km day^{-1}). The kinetic energy of along-shelf fluctuations in the 7- to 9-day period band was highest in the upper layer in the southern portion of the array and decreased northward. Minimum fluctuating energy occurred off Savannah (Mooring 22). No significant differences occurred between mooring sites for the along-shelf flow in the lower layer or the cross-shelf flow for upper and lower layers. The amplitudes of temperature fluctuations were larger over the southern portion of the array (Moorings 4-12) than the northern (Moorings 22 and 25), without any significant differences between upper and lower layers.

At the 40-m isobath, coherence of along-shelf distances is up to 425 km with small and nearly constant phase lags, which is indicative of

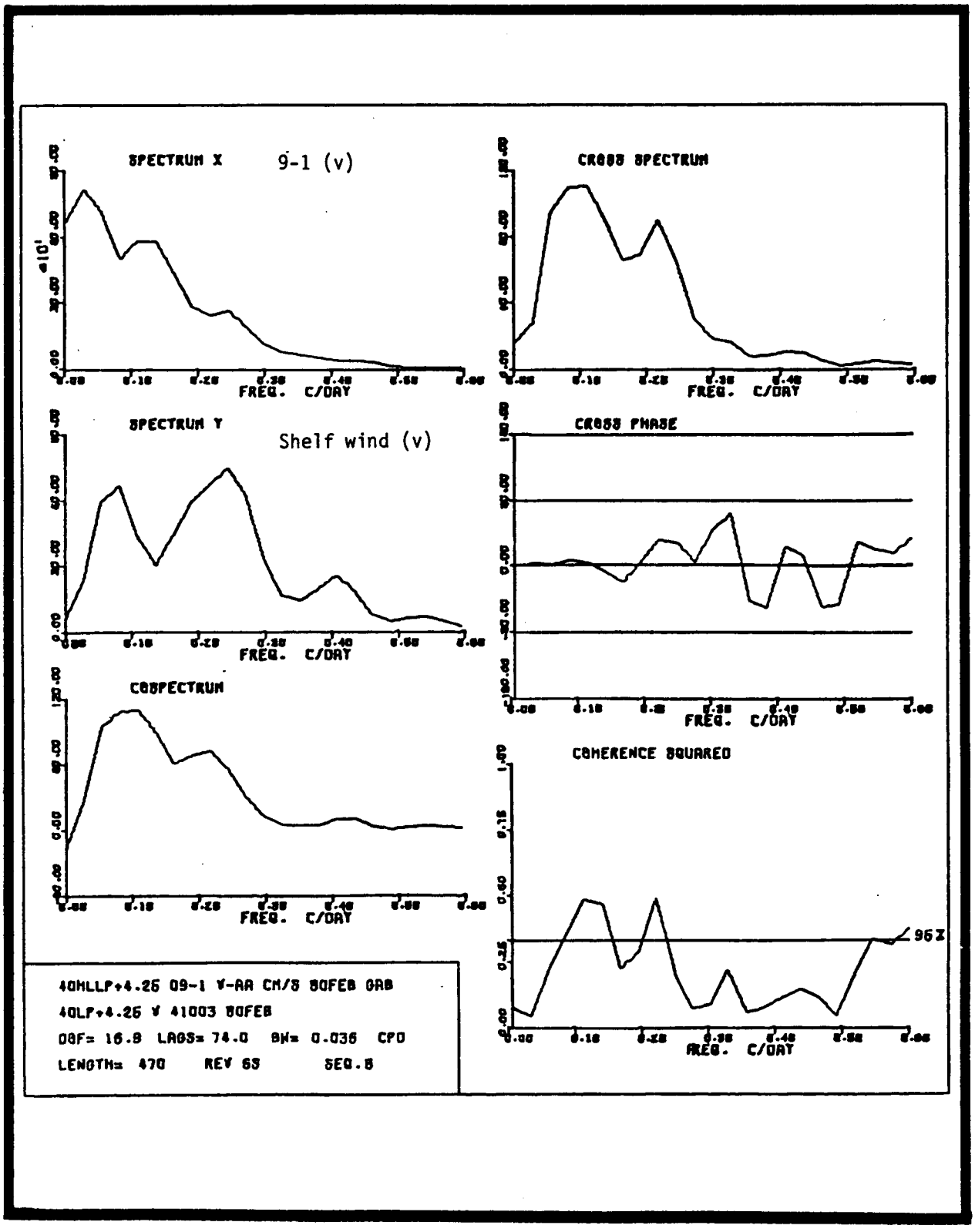

Figure 4.6-8a. Cross-spectra of 9-1 (V) vs. shelf wind (V).

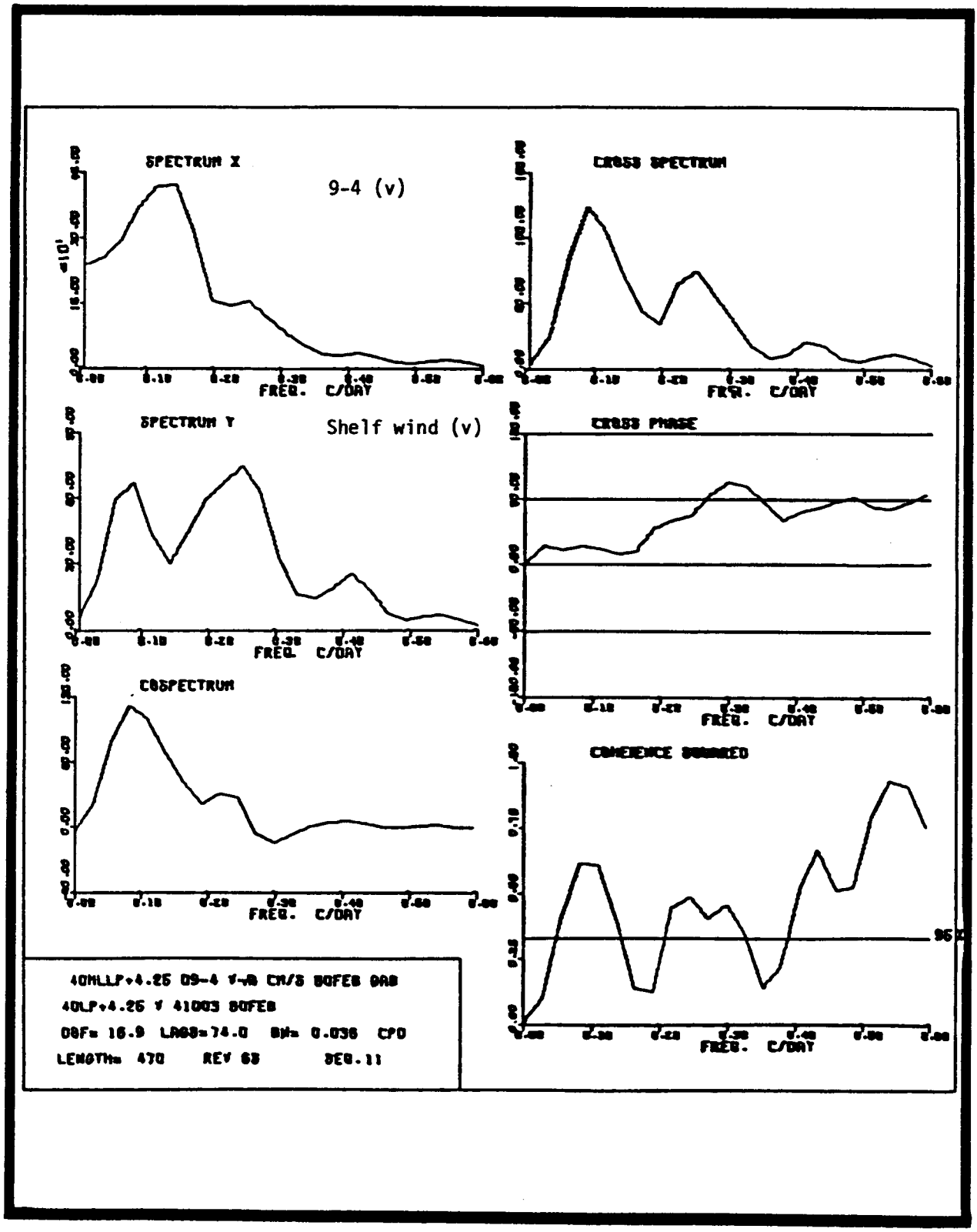

Figure 4.6-8b. Cross-spectra of 9-4 (V) vs. shelf wind (V).

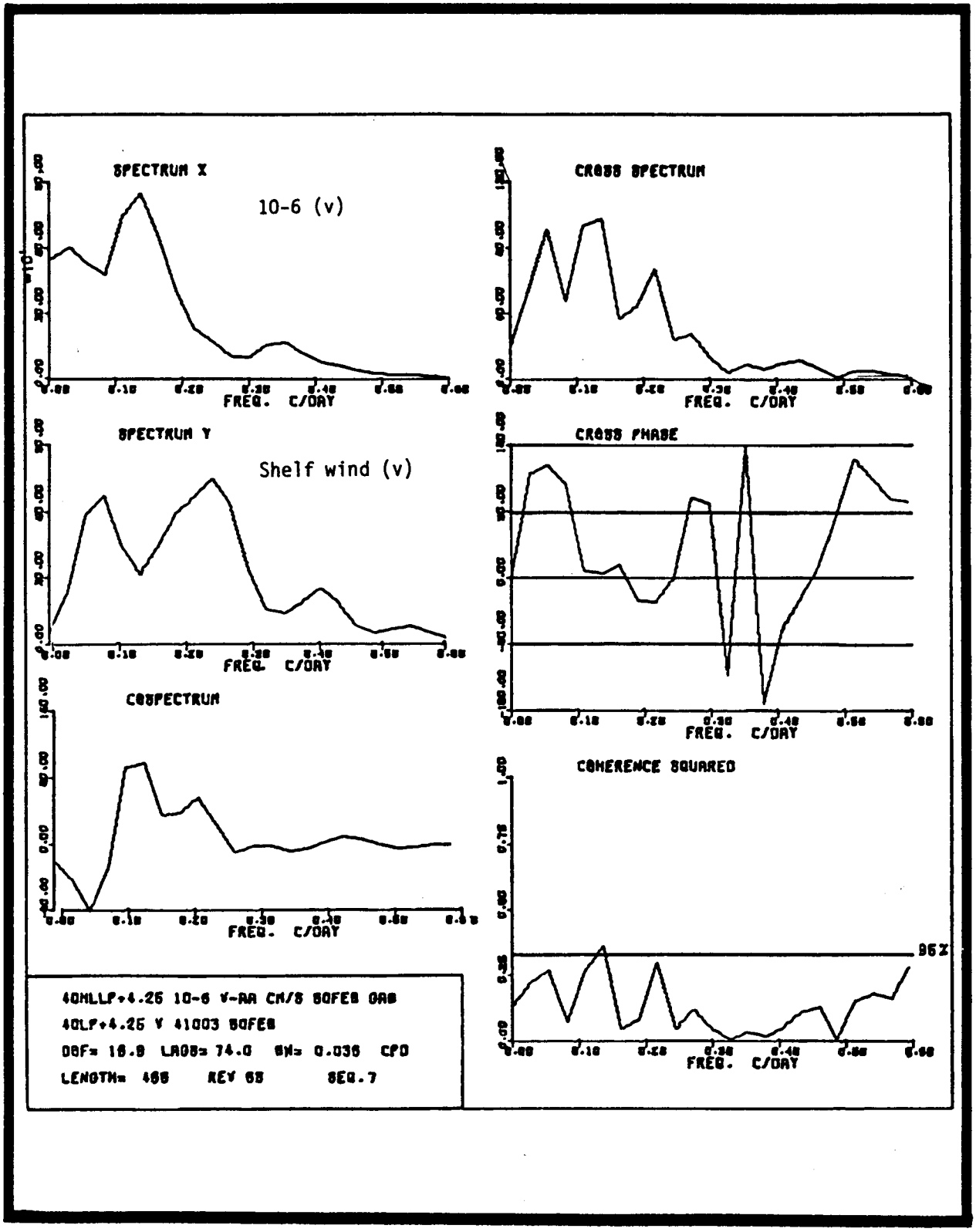

Figure 4.6-8c. Cross-spectra of 10-6 (V) vs. shelf wind (V).

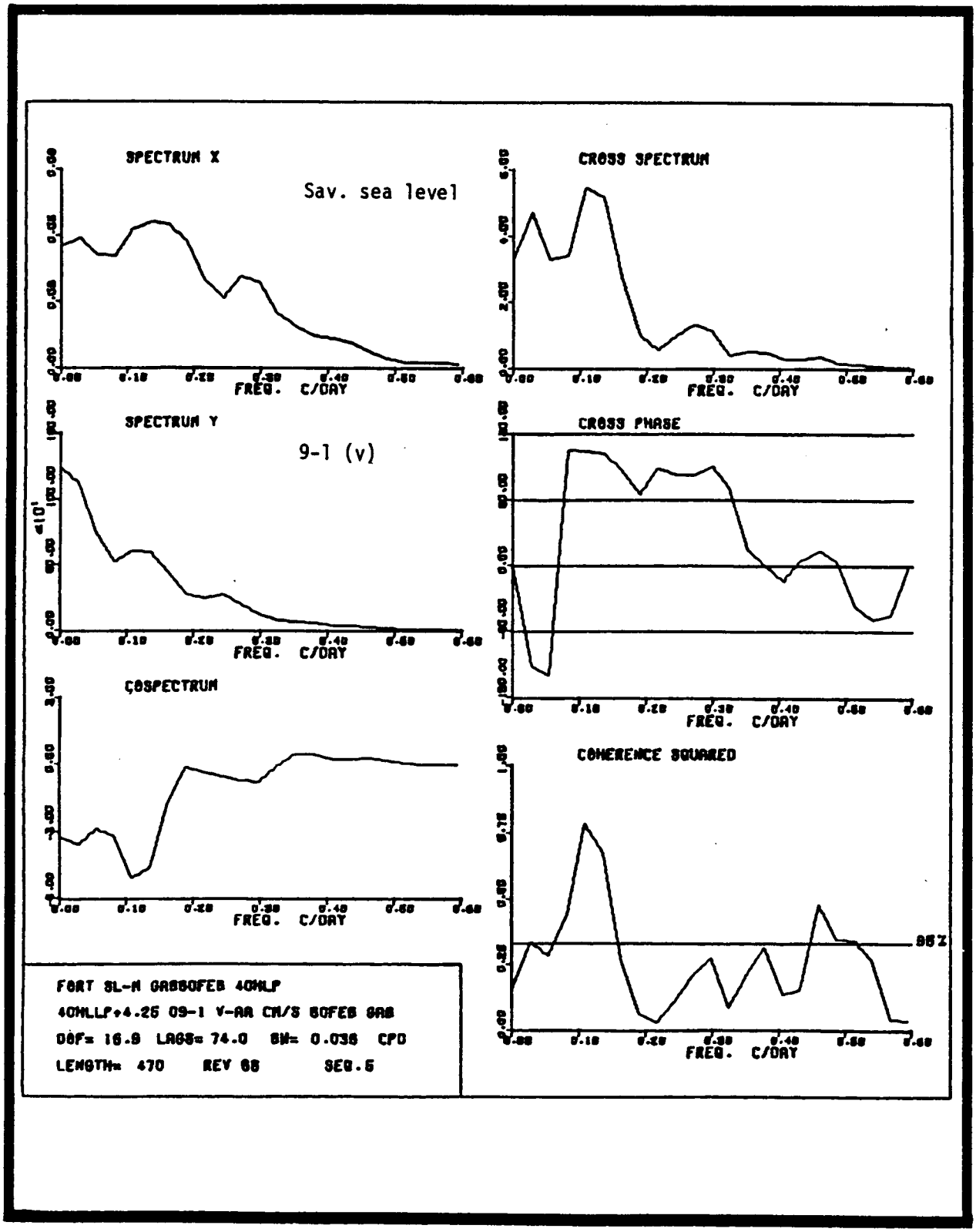

Figure 4.6-9a. Cross-spectra of Savannah sea level vs. 9-1 (V).

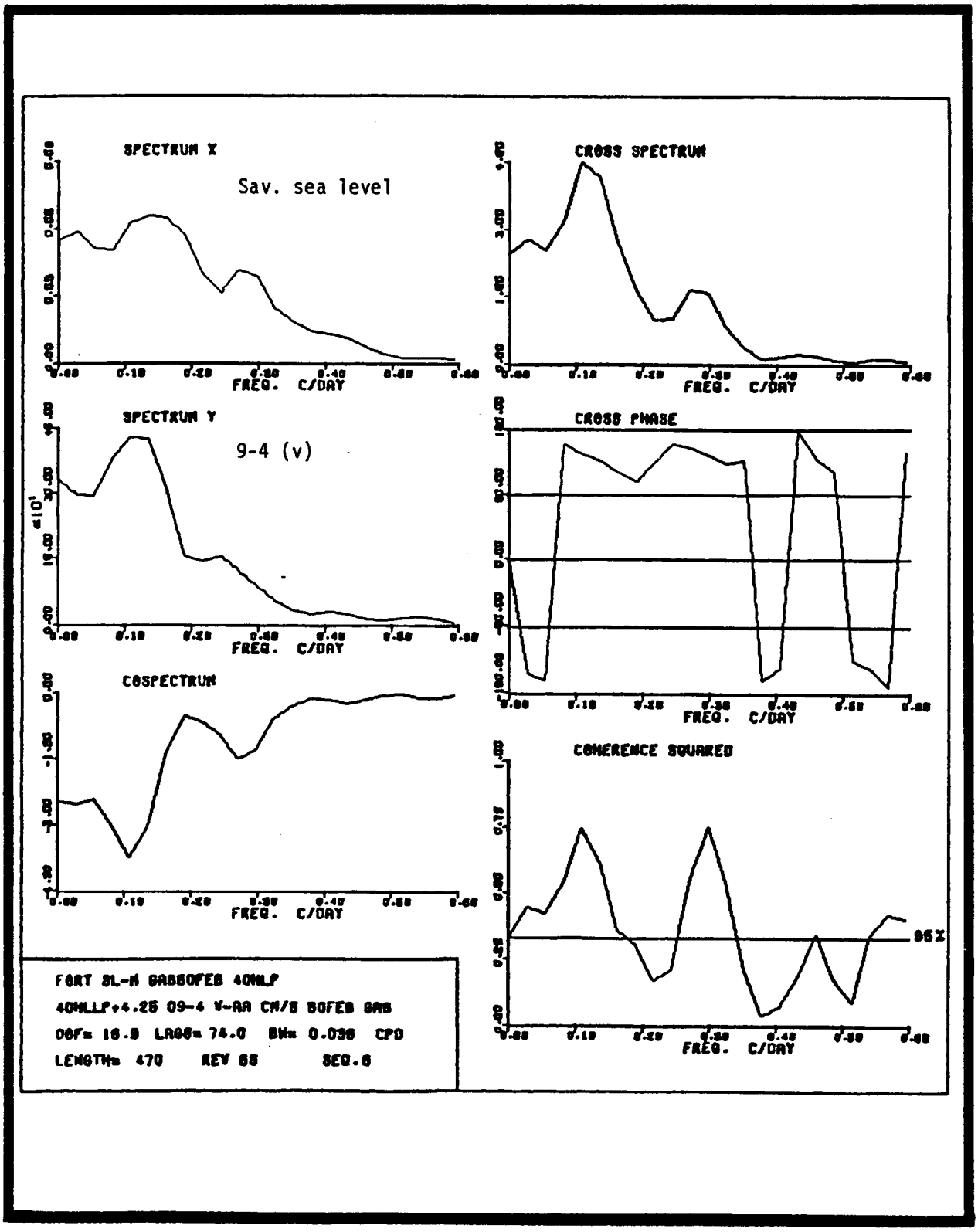

Figure 4.6-9b. Cross-spectra of Savannah sea level vs. 9-4 (V).

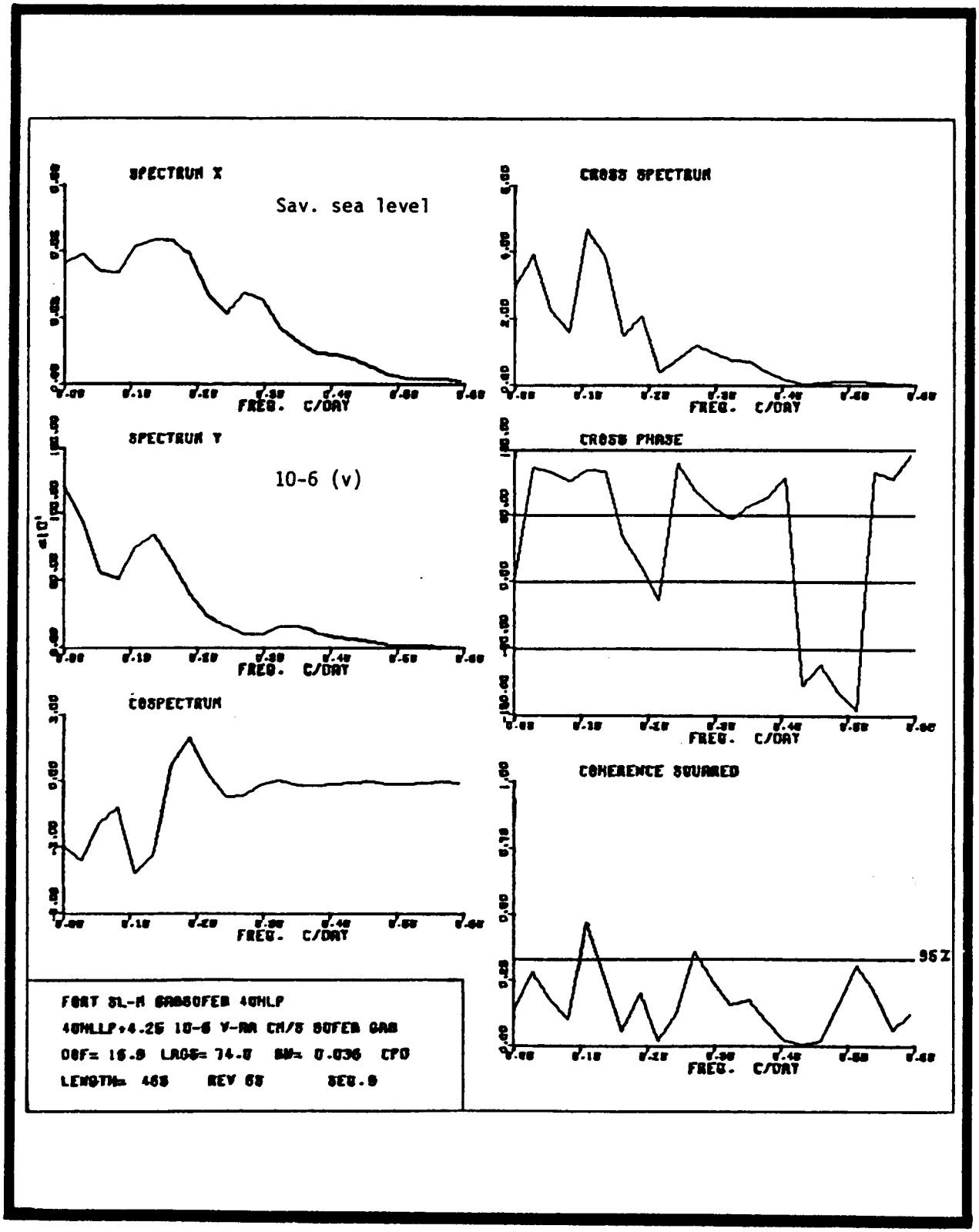

Figure 4.6-9c. Cross-spectra of Savannah sea level vs. 10-6 (V).

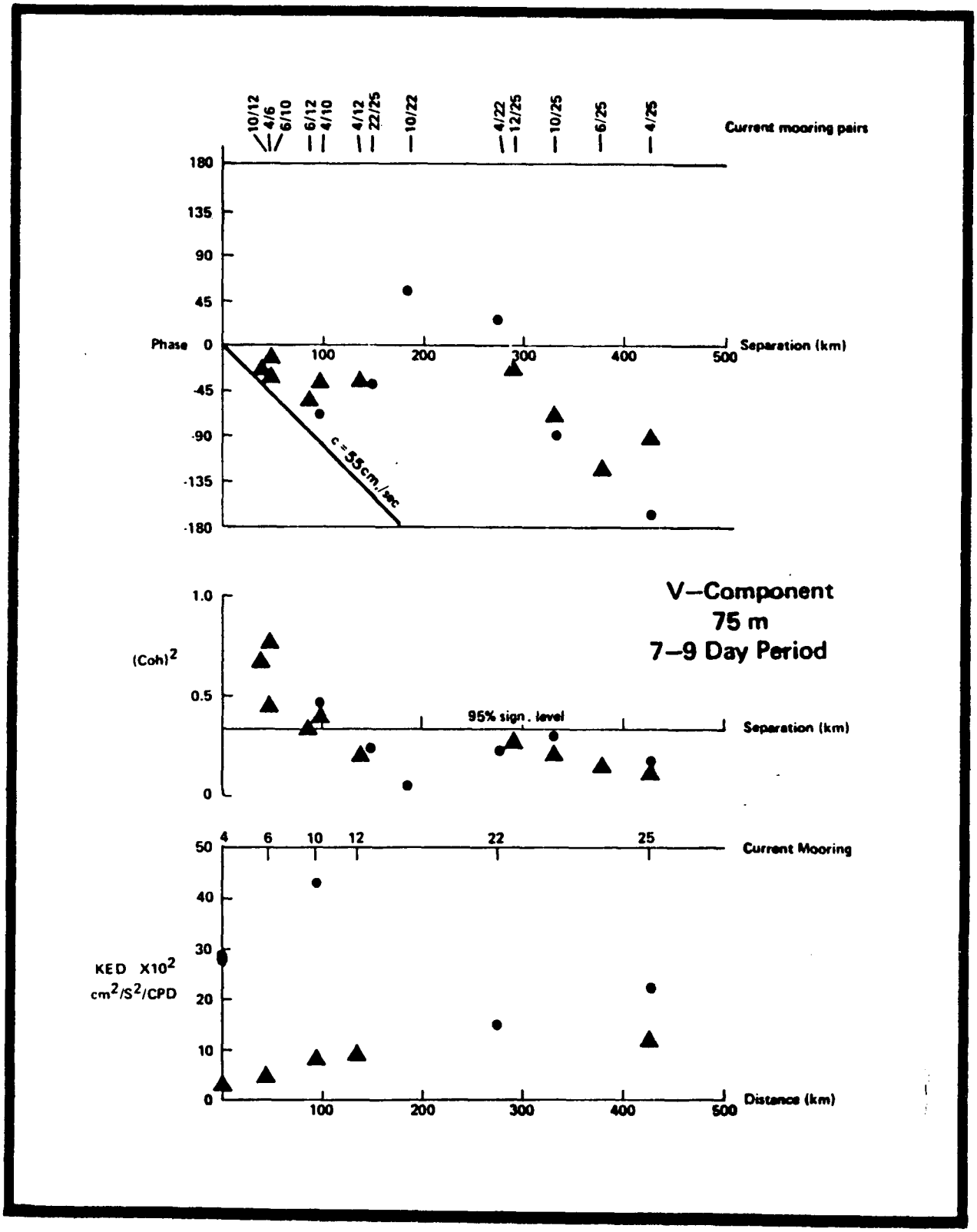

Figure 4.6-10. Along-shelf coherence squared, phase, and energy density for V component at shelf break in 7- to 9-day period band; dots are for upper layer, and triangles for lower layer.

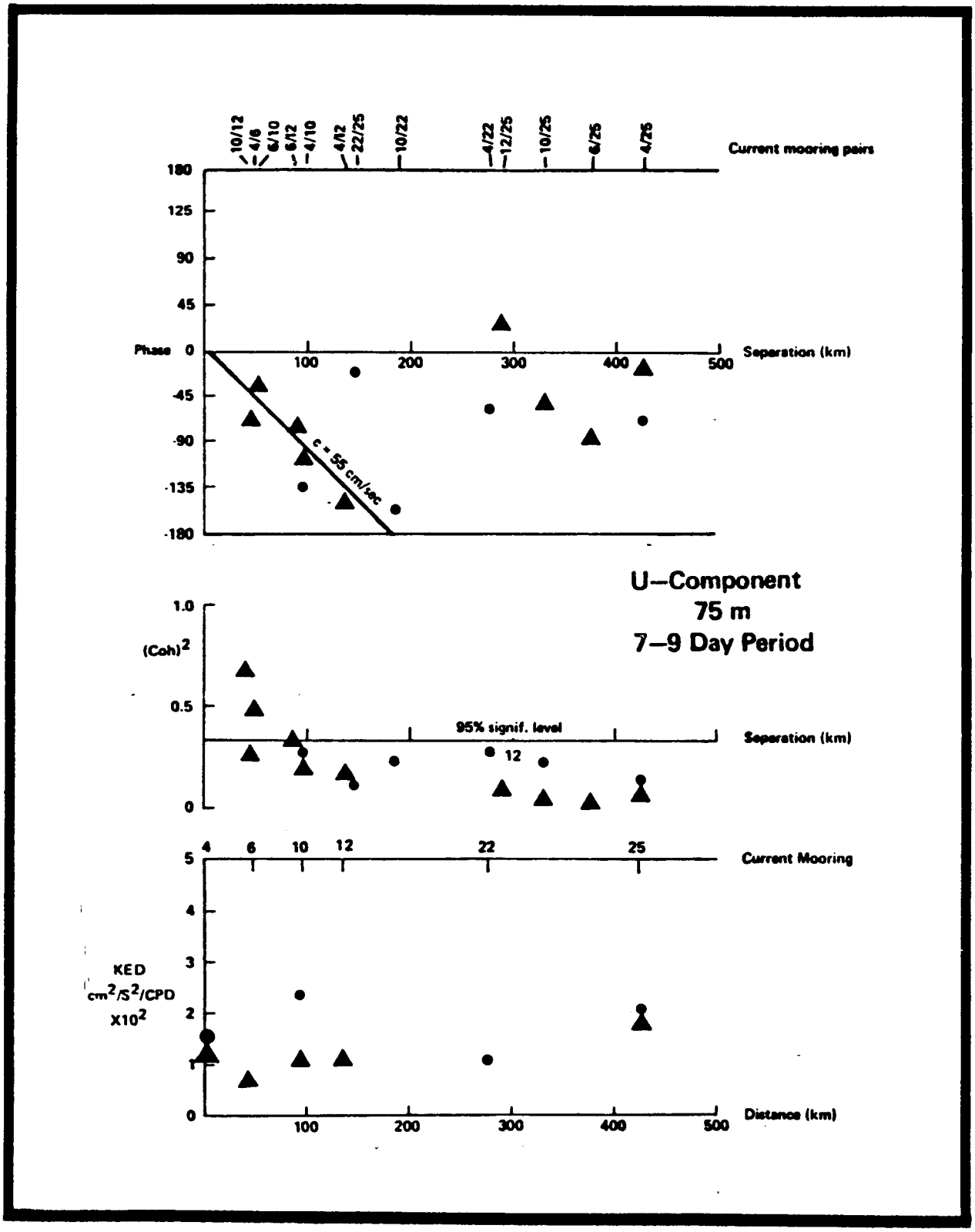

Figure 4.6-11. Along-shelf coherence squared, phase, and energy density for U component at shelf break in 7- to 9-day period band; dots are for upper layer, and triangles for lower layer.

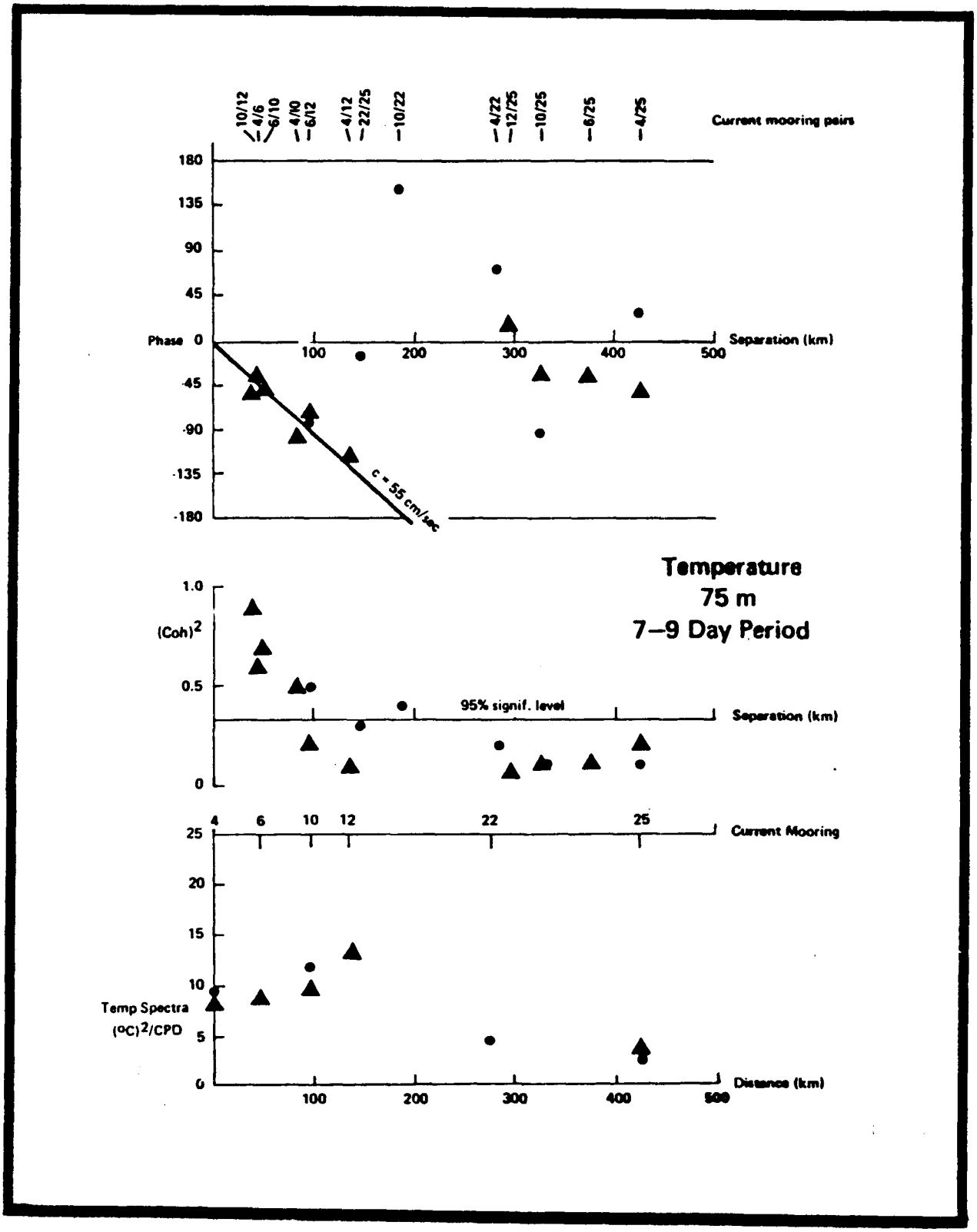

Figure 4.6-12. Along-shelf coherence squared, phase, and energy density for temperature at shelf break in 7- to 9-day period band; dots are for upper layer, and triangles for lower layer.

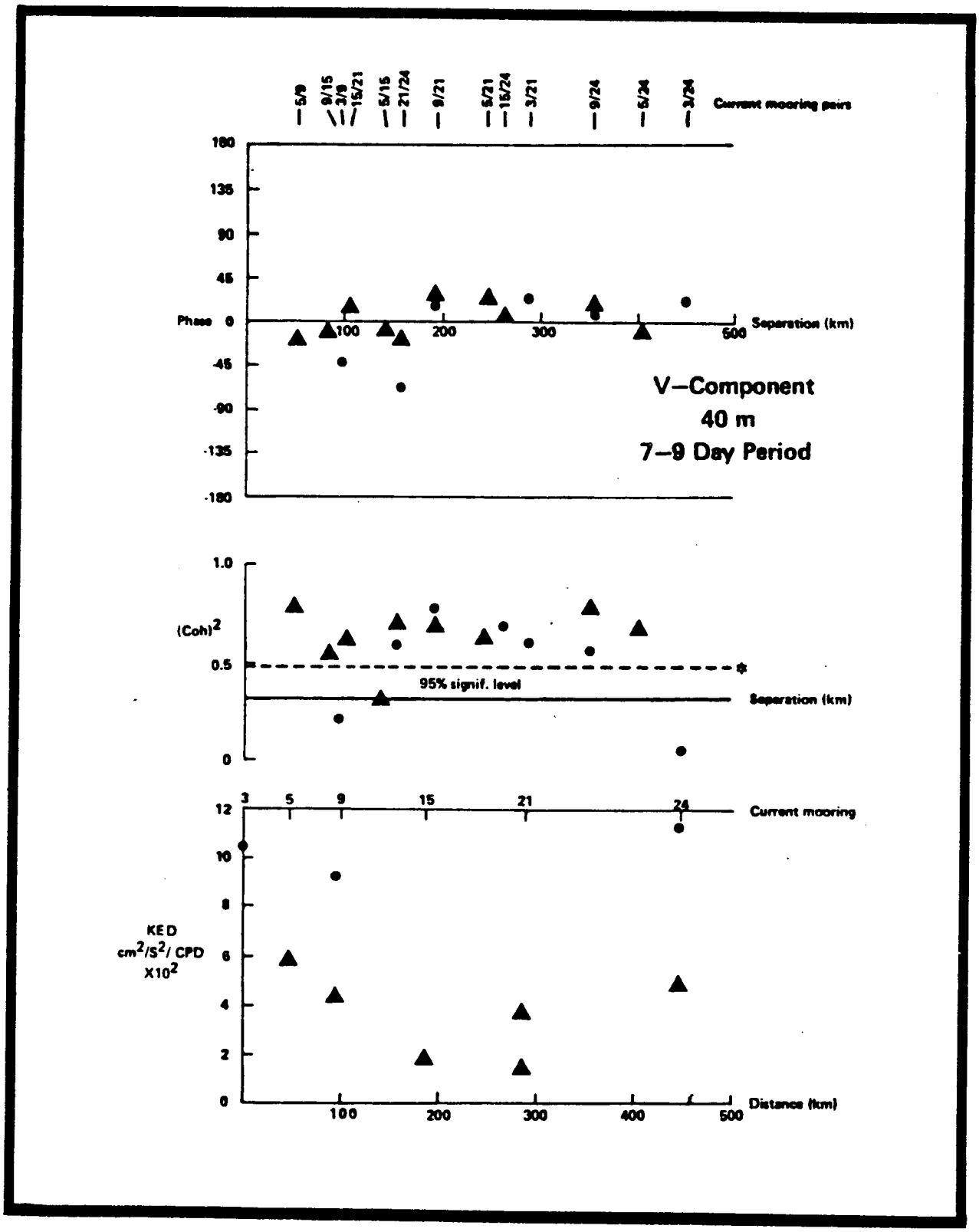

Figure 4.6-13. Along-shelf coherence squared, phase, and energy density for V component at 40-m isobath in 7- to 9-day period band; dots are for upper layer, and triangles for lower layer.

nonpropagating fluctuations. The cross-shelf velocity component and temperature did not show any consistent along-shelf coherent features so are not presented. Along-shelf coherence and phase estimates computed for fluctuations in the 5- to 6-day period band were similar to those shown for the 7- to 9-day band at both the 75- and 40-m isobaths so are not presented.

Cross-shelf estimates of coherence and phase between instrument pairs from Moorings 10 (shelf break) and 9 (40-m isobath) indicate significant coherence in the velocity components in the 5- to 9-day period band. The highest coherence in the cross-shelf component was centered at the 5-day period, with fluctuations at 40 m leading slightly in phase. The peak coherence in the along-shelf component was centered at the 7-day period with a near zero phase. Temperature was only coherent in the lower half of the water column at periods of about 4 and 7-12 days with fluctuations at the offshore mooring leading by about 90° in phase.

4.6.3 Mean Flows

Analysis of cumulative weekly means indicates that it normally took from 10 to 15 weeks for mean velocity components to stabilize. Mean temperature became stable in about 5 to 10 weeks. There was no obvious spatial dependency in the stability estimates, indicating that means began to stabilize after a sufficient number of random events occurred to average out individual event differences. Total record lengths were 16.5 weeks, except for current meters 21-1, 21-2, and 22-3 with lengths of about 11 weeks. Without longer record lengths it is impossible to know if the means would remain stable over longer periods. Most likely there will be seasonal effects on the shelf that may influence to 40-m isobath means. Seasonal changes at the shelf break were found to be small, compared to Gulf Stream influences on the 2-day to 2-week time scale (Lee et al. 1981), so the shelf-break means may be more representative of annual or longer averages, at least for the region south of Savannah.

Means and standard deviations of the low-frequency cross-shelf and along-shelf velocity components and temperature, together with the mean momentum and heat fluxes for all outer-shelf current meters of the array, are presented in Table 4.6-1. Mean velocity vectors in the upper and lower layers at each mooring site are plotted in Figure 4.6-14 for the total record period and for consecutive 2-weekly averages. South of the Savannah transect, mean flows are generally northward along the isobaths in the 4-month averages and most of the bi-weekly means. A strong Gulf Stream influence is indicated along the outer shelf, where 4-month mean flows in the upper layer were about 50 cm s^{-1}. Total record mean flows were also high near the bottom (4 to 10 cm s^{-1}) and at the 40-m isobath (3 to 8 cm s^{-1}). There was a mean onshore flow of about 3 cm s^{-1} near the bottom at the shelf break for the southernmost mooring site over the 4-month study and offshore flow at the four mooring sites to the north, with speeds ranging from 2 to 13 cm s^{-1}, indicating the possibility of a net water movement onto the shelf south of the array. Mean flows were generally weak at the Savannah transect for the 4-month and 2-weekly means, but the standard deviations were nearly as high as occurred at the sites to the south. The 4-month averages at the northernmost transect off Cape Romain indicate a strong southward mean flow at mid-depth for the shelf break, with along-shelf speeds ranging from 4 to 13 cm s^{-1}, with an onshore component of 2.6 cm s^{-1} in the upper layer and offshore at about 8 cm s^{-1} near

Table 4.6-1. Mean flow, temperature, momentum, and heat fluxes in the outer shelf for the period 25 February to 21 June 1980, from 40-HLP filtered data with sample interval of 6 hours (S.D. is standard deviation).

Current Meter	Inst. Depth (m)	Water Depth (m)	Record Lengths No. 6 h Data	$\bar{u}$ cm s^{-1}	± S.D.	$\bar{v}$ cm s^{-1}	± S.D.	$\bar{T}$ °C	± S.D.	$\overline{u'v'}$ cm^{2}s^{-2}	$\overline{u'T'}$ cm°cs^{-1}
3-1	17	40	471	-0.3	6.5	7.9	21.3	21.1	1.9	32.2	1.7
4-2	45	75	472	2.8	6.4	29.6	26.2	29.4	21.2	11.9	0.8
4-3	72	75	472	-2.8	6.2	10.7	11.0	16.9	2.3	-27.4	-1.3
5-2	37	40	471	-1.1	5.3	3.0	11.6	18.5	1.9	-40.8	-0.5
6-2	72	75	471	2.3	5.2	4.3	10.7	16.6	2.1	8.2	0.9
9-1	7	40	470	-2.6	7.0	4.3	13.2	-	-	-5.8	-
9-2	17	40	470	-2.9	5.1	7.2	15.3	22.0	1.9	-11.8	-0.8
9-3	27	40	470	-1.6	5.5	4.3	13.6	19.4	1.9	-35.1	-1.4
9-4	37	40	470	-1.4	5.4	4.0	9.4	19.1	1.8	-34.2	-1.3
10-1	7	75	467	13.0	12.0	67.3	37.7	-	-	257.6	-
10-2	17	75	468	-	-	-	-	23.1	1.7	-	-
10-3	27	75	465	6.4	10.3	53.7	34.6	21.9	2.2	194.3	6.6
10-4	45	75	466	1.3	9.2	32.0	31.0	19.8	2.0	86.3	3.8
10-5	60	75	466	3.0	8.4	17.0	24.0	18.3	1.9	80.5	2.0
10-6	72	75	468	2.4	5.8	7.7	13.6	17.3	2.0	13.0	-0.5
12-2	72	75	467	4.2	6.0	10.8	14.3	18.8	2.2	7.9	-0.6
15-1	17	40	466	-	-	-	-	21.1	2.1	-	-
15-2	37	40	466	-.88	2.5	3.3	7.3	20.4	1.6	-2.3	-0.2
*21-1	17	40	315	1.5	5.7	3.8	10.2	18.0	2.6	23.8	-8.1
*21-2	37	40	315	-0.9	3.9	1.0	7.8	17.4	2.3	-11.8	-3.9
22-1	17	75	465	2.9	10.2	14.1	29.8	21.8	2.4	158.0	-2.7
22-2	45	75	465	0.6	7.7	1.8	23.2	18.8	1.8	48.1	0.7
*22-3	72	75	338	-1.4	5.5	1.7	11.1	13.0	1.8	-1.4	-0.0
24-1	17	40	458	-0.8	8.3	8.3	17.9	21.4	2.8	79.2	-2.0
24-2	37	40	458	-0.3	5.4	1.2	12.0	20.1	1.9	-28.5	0.1
25-1	17	75	457	-2.6	16.0	-4.4	26.6	22.6	2.6	230.1	-6.9
25-2	45	75	457	0.3	9.9	-12.6	27.2	20.5	1.6	104.2	1.7
25-3	72	75	457	7.8	8.1	-9.4	18.8	19.1	1.3	-4.8	0.5

*Short record lengths

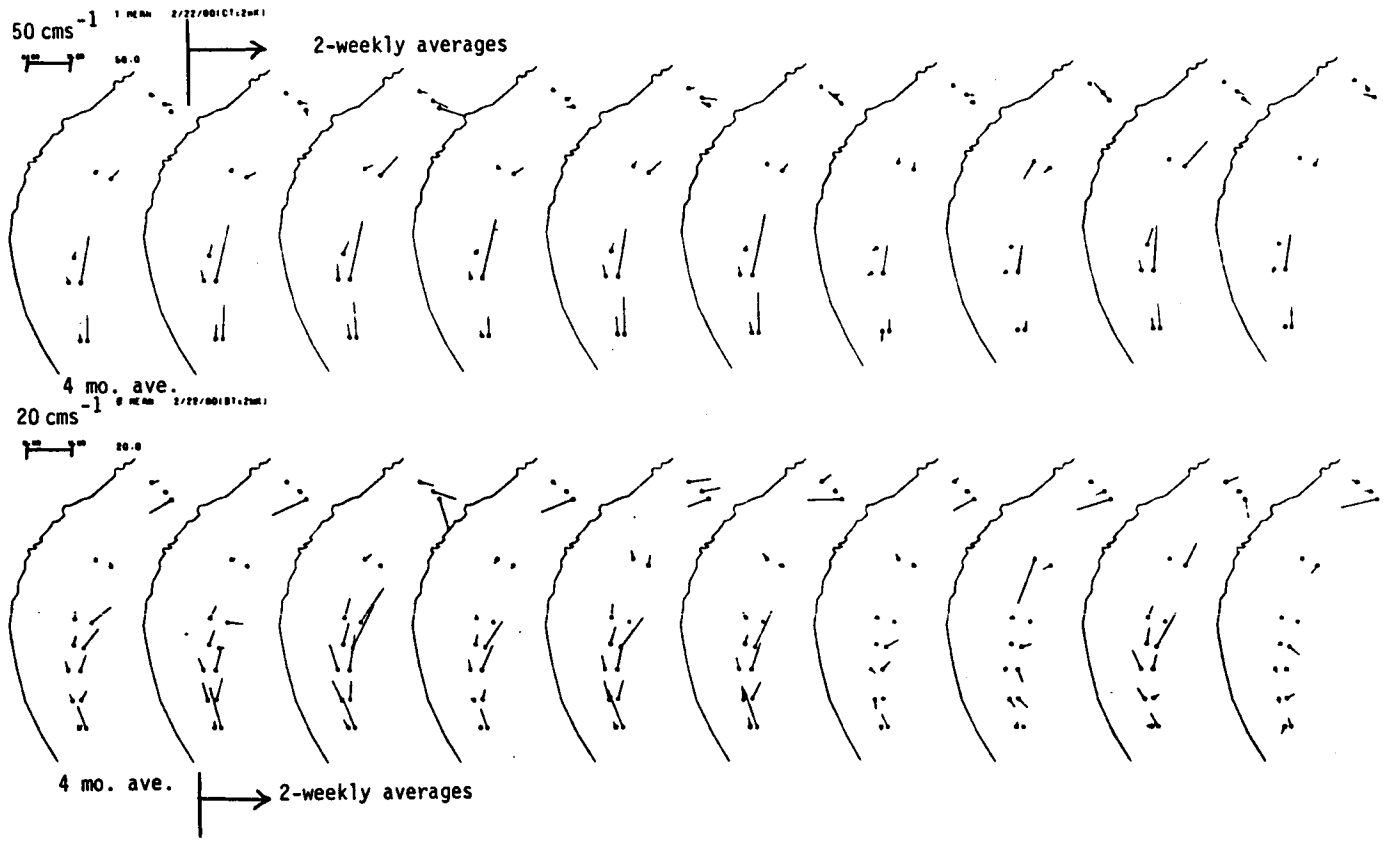

Figure 4.6-14. Mean flows at 40-and 75-m isobaths. Top panel is for upper layer, scale is 50 cm s^{-1}, and bottom panel is for lower layer, scale is 20 cm s^{-1}. First scene is for 4-month average, remaining scenes are for consecutive 2-weekly averages.

bottom. Standard deviations of the along-shelf and cross-shelf components were also high at ± 30 and ± 16 cm s^{-1}, respectively. Mean flows at the 40-m isobath were toward the north at about 8 cm s^{-1} in the upper layer, opposite to that found at the shelf break.

Mean flows in the outer shelf appear to be closely related to the position of the Gulf Stream. South of the Savannah transect, the Gulf Stream western edge lies close to the shelf break and strong northward currents result. Onshore/offshore displacements of the Gulf Stream front are generally less than 15 km in this region (Bane and Brooks 1979). Seaward of the Savannah transects, a topographic anomaly known at the "Charleston Bump" (Bane and Brooks 1979) protrudes onto the Blake Plateau and into the path of the Gulf Stream, apparently forcing a quasi-permanent offshore meander of the Stream on the lee side of the "Bump" (Brooks and Bane 1978, Pietrafesa et al. 1978, Legeckis 1979). Downstream of the Bump enlarged east-west meanders can displace the Gulf Stream front up to 100 km from the shelf break (Legeckis 1979, Bane and Brooks 1979). Thus, off Cape Romain the Gulf Stream front is normally located a considerable distance offshore of the moorings, and the observed mean southward flow must in some way be connected to this displacement; possibly due to the cumulative affect of the occurrence of filament shaped frontal disturbances that are known to enlarge and produce southward flow events downstream of the Bump (Legeckis 1979, Bane et al. 1981, Brooks and Bane 1981). The Savannah area appears to be a transition region between strong mean northerly and southerly flow regimes.

4.6.4 Cross-Shelf Flux of Momentum and Heat and Energy Conversion

The momentum flux, $(\overline{u'v'})$, averaged over the 4-month experiment was generally offshore (positive) along the shelf break (Table 4.6-1), indicating an average offshore transport of northward momentum. The only net onshore transport observed over the total period was near-bottom at the southern mooring (current meter 4-3). Cumulative weekly averages indicate that momentum flux estimates became reasonably stable for averaging periods of 12 to 15 weeks. The maximum offshore transport of about 260 $cm^2\ s^{-2}$ occurred in the upper layer at 30°N (10-1) and decreased rapidly with depth. The mean horizontal shear ($\partial\bar{v}/\partial x$) in the upper layer at this latitude was approximately $2.6 \times 10^{-5}\ s^{-1}$ which gives horizontal eddy viscosity of

$$A_H = \frac{-\rho\overline{u'v'}}{\frac{\partial \bar{v}}{\partial x}}$$

or $$A = -8 \times 10^6\ cm^2\ s^{-1}$$

The overbar (-) represents a time average over the record length, and the primes (') denote deviations from the average. Density, ρ, is taken as 1 g cm^{-3}, and x increases in the offshore direction. A negative viscosity was also found in the regions of the cyclonic Gulf Stream front off Onslow Bay, N.C. (Webster 1961a, Brooks and Bane 1981), and in the Florida Straits (Schmitz and Niiler 1969, Brooks and Niiler 1977) and is believed to indicate a baroclinic instability process where kinetic energy is transferred from the fluctuations to the mean flow (Orlanski 1969, Orlanski and Cox 1973).

Table 4.6-2. Net kinetic energy exchange rate at the shelf break from 25 February to 21 June 1980.

Quantity	Units	Net Value Upper Layer (27-45m depths)	Net Value Lower Layer (3m above bottom)
$\overline{u'^2}$	$cm^2 s^{-2}$	106	34
$\overline{v'^2}$	$cm^2 s^{-2}$	1198	184
$\overline{u'v'}$	$cm^2 s^{-2}$	194	13
$\frac{\partial \bar{u}}{\partial x}$	s^{-1}	4.2×10^{-6}	2.0×10^{-6}
$\frac{\partial \bar{v}}{\partial y}$	s^{-1}	2.5×10^{-7}	-3.1×10^{-7}
$\frac{\partial \bar{v}}{\partial x}$	s^{-1}	2.6×10^{-5}	2.0×10^{-6}
$\bar{\rho}\,\overline{u'^2}\,\frac{\partial \bar{u}}{\partial x}$	ergs $cm^{-3} s^{-1}$	4.4×10^{-4}	0.7×10^{-4}
$\bar{\rho}\,\overline{v'^2}\,\frac{\partial \bar{v}}{\partial y}$	ergs $cm^{-3} s^{-1}$	3.0×10^{-4}	-0.6×10^{-4}
$\bar{\rho}\,\overline{u'v'}\,\frac{\partial \bar{v}}{\partial x}$	ergs $cm^{-3} s^{-1}$	50.4×10^{-4}	0.3×10^{-4}
$\bar{\rho}\,\overline{u'^2}\,\frac{\partial u}{\partial x} + \bar{\rho}\,\overline{v'^2}\,\frac{\partial v}{\partial y} + \bar{\rho}\,\overline{u'v'}\,\frac{\partial v}{\partial x}$	ergs $cm^{-3} s^{-1}$	57.8×10^{-4}	0.4×10^{-4}

The rate of net energy transfer can be estimated with current meters at 30°N from $\{\overline{\rho u'v'}\ (\partial\bar{v}/\partial x)\}$ (Webster 1961b, Schmitz and Niiler 1969, Brooks and Niiler 1977). Brooks and Niiler (1977) found that the net conversion rate of peturbation kinetic energy can be estimated from:

$$\frac{d}{dt}\left\{\frac{1}{2}\left(\overline{u'^2} + \overline{v'^2}\right)\right\} = -\left\{\overline{u'^2}\,\frac{\partial\bar{u}}{\partial x} + \overline{v'^2}\,\frac{\partial\bar{v}}{\partial y} + \overline{u'v'}\,\frac{\partial\bar{v}}{\partial x}\right\} \qquad (1)$$

For a complete derivation of the perturbation energy equation, one is referred to Lumley and Panofsky (1964). Equation (1) relates to the rate of change of fluctuating kinetic energy to the total mechanical energy flux per unit volume, using the Boussinesq approximation and hydrostatic balance and assuming

$$\frac{\partial\bar{v}}{\partial x} >> \frac{\partial\bar{u}}{\partial y}$$

and ignoring the pressure fluctuation terms and vertical motion.

Brooks and Niiler estimated for the Florida Current between Miami, Fla. and Bimini, Bahamas, that total local kinetic energy conversion was dominated by the second term on the right hand side, but for the sectional area average, this term was small, and the first and third terms were larger and of similar magnitude.

At 30°N, net local perturbation kinetic energy at the shelf break can be estimated using current meter data from Moorings 4, 9, and 10. Results for the middle to upper water column and near-bottom layer are given in Table 4.6-2. In the upper layer, total local conversion of perturbation kinetic energy was dominated by $\{\overline{u'v'}\ (\partial\bar{v}/\partial x)\}$ which was about an order of magnitude larger than the first and second terms of Eq. (1). Near-bottom estimates are two orders of magnitude smaller and not significant. The positive net value indicates a net transfer of kinetic energy from the fluctuations to the mean flow at this location, consistent with similar findings in the Gulf Stream cyclonic frontal region off Onslow Bay in the surface layer (Webster 1961a) and middle to lower water column (Brooks and Bane 1981). Brooks and Niiler (1977) also found kinetic energy flux to the mean flow over the total water column in the cyclonic front of the Florida Current off Miami. However, the region of this transfer was displaced about 8 km east of the shelf break, and energy was transferred to the fluctuations at the shelf break. A similar result was found from current meters positioned at the shelf break in the Florida Straits (Lee 1975, Lee and Mayer 1977), indicating that the shelf-break strip was a region of mean energy removal. However, between Cape Canaveral and Savannah, the Gulf Stream front follows the shelf break closely, and the fluctuations release kinetic energy to the mean flow at about the same rate (58×10^{-4} ergs cm^{-3} s^{-1}) as was found off Onslow Bay and in the Florida Straits.

The co-spectrum of the u and v velocity components at the shelf-break (Figure 4.6-7) shows that the positive (offshore) momentum flux was selectively grouped in the 5- to 9-day period band where propagating cold cyclonic perturbations were found to produce coherent u and v fluctuations that were consistent at all levels. Thus, net conversion of perturbation to mean kinetic energy appears to occur throughout the water column at the shelf-

break and is being driven by fluctuations occurring in the 5- to 9-day period band.

Shelf-break heat flux $\overline{u'T'}$ averaged over the 4-month study period was positive within the water column and decreased to small negative values near the bottom (Table 4.6-1). A positive heat flux indicates a net offshore heat transport similar to that found in the Gulf Stream frontal region off Onslow Bay (Oort 1964, Brooks and Bane 1981) and in the Florida Straits (Brooks and Niiler, 1977). Following Brooks and Niiler (1977), the net conversion rate of potential energy can be estimated from:

$$\frac{d}{dt}\left\{\frac{g}{2}\overline{\rho'^2}\Big/\left|\frac{\partial\bar{\rho}}{\partial z}\right|\rho_o\right\} = -\left\{\overline{gu'\rho'}\,\frac{\partial\bar{\rho}}{\partial x}\Big/\rho_o\left|\frac{\partial\bar{\rho}}{\partial z}\right| + \overline{gv'\rho'}\,\frac{\partial\bar{\rho}}{\partial y}\Big/\rho_o\left|\frac{\partial\bar{\rho}}{\partial z}\right|\right\} \quad (2)$$

Equation (2) relates the rate of change of fluctuating potential energy to the total potential energy flux per unit volume of the perturbations. The name approximations and assumptions used in development of Equation (1) apply also to Equation (2).

Gulf Stream water present in the outer shelf produces a reasonably constant T-S relationship (Lee, Atkinson and Legeckis 1981) that is used with temperature from current meters on Moorings 4, 9, and 10 to evaluate rates of potential energy conversion in the same manner as kinetic energy conversion. There was a net transfer of perturbation potential energy from the fluctuations to the mean at the shelf break that can be almost entirely accounted for by $\{g\,\overline{u'\rho'}\,(\partial\rho/\partial x)/\rho_o\,|\partial\bar{\rho}/\partial z|\}$. Co-specturm of u and T are quite similar to u and v and indicates that coherent current and temperature fluctuations occurring in the 5- to 9-day period band were the cause of the local generation of mean potential energy at the shelf break.

4.6.5 Gulf Stream Frontal Eddies

4.6.5.1 General Patterns of Movement

Hydrographic and biological observations of shelf waters in the region of the current meter array and the adjacent Gulf Stream front were made during 10 to 26 April 1980. Two ships were involved: R/V Eastward and R/V Columbus Iselin. The Eastward was used to investigate shelf processes, while the Columbus Iselin was used to locate and track Gulf Stream frontal disturbances with the aid of a telefax system for receiving satellite SST images from the NOAA/NESS field station in Miami. The Iselin also received a detailed SST map every three days from a U.S. Coast Guard aircraft equipped with an airborne radiation thermometer. Current and temperature records from the outer shelf indicate that a succession of four cold cyclonic perturbations of the strong northward mean flow occurred during the shipboard sampling period (Figures 4.6-3, -4 and 4.6-5a, -5b; Events 5, 6, 7 and 8). These events were advected northward at a mean speed of about 60 cm s^{-1} which is close to the mean northward speed observed at the shelf break (Table 4.6-1) and close to the northward propagation speed determined for u, v, and T fluctuations in the 5- to 9-day period band (Figures 4.6-10 through -12). The onset of each disturbance produced onshore flow followed by decreasing temperature and northward current speeds throughout the water column and the shelf break. The end of the events produced offshore flow coupled with increasing temperature and northward speeds. A similar but less pronounced response occurred at the

40-m isobath. Shipboard observations indicate that the cold anomalous waters consisted of newly upwelled, nutrient rich Western Atlantic Central Water (Yoder et al., 1981).

The formation, growth, and northward movement of Event #8 was observed with shipboard hydrography and remote thermal imagery from 21 to 27 April. It was first observed with shipboard SST mapping as a small disturbance of the Gulf Stream surface thermal front off Cape Canaveral on 21 April (Lee, unpublished report). On 22 and 23 April, it was clearly observable as a well-defined frontal "shingle" (Von Arx et al. 1955) just north of Cape Canaveral in satellite thermal imagery (Figure 4.6-15). The shingle thermal pattern has been found to be the characteristic SST signature of cyclonic cold-core frontal eddies in this region (Lee et al. 1981). Detailed hydrographic sampling was obtained through the disturbance during a 20-hour period on 24 and 25 April, and again over a 37-hour period on 25 and 26 April (Figures 4.6-16 and -17). The northward speed of the event was estimated using remote imagery, shipboard mapping, and current meter records, all of which indicated a speed of about 55 cm s^{-1}. It took the combined effort of two ships to keep pace with this rapidly moving event. A warm filament of 23 to 24°C Gulf Stream water approximately 15 to 20 m in depth extended southward from the front around a cold-core with a minimum surface temperature of 22°C. The along-shelf dimension of the feature was approximately 130 km, and the cross-shelf length from the western edge of the filament to the center of the cold core was about 25 km. A typical temperature, density, salinity, and nitrate section through the center of the feature is shown in Figure 4.6-18a, b. Uplifted temperatures in the cold dome extended across the outer shelf beneath the warm filament in a cold subsurface intrusion of nutrient enriched waters. Euphotic zone nitrate concentrations of 5 μ moles ℓ^{-1} were observed beneath the warm filament and 20 μ moles ℓ^{-1} near the shelf break.

SST and hydrographic section data (Figures 4.6-16, -17 and -18) indicate that the cold core of Event #8 passed directly through Mooring 12, and the western edge of the warm filament passed through Mooring 9. The low-frequency temperature records from mooring Sites 9 and 10 further substantiate this movement (Figure 4.6-6a, b). At Mooring 10, temperature decreased then increased at all vertical positions between 24 and 27 April, which was the time the cold core passed the mooring. Temperature from mooring Site 9 first increased from 24 and 25 April at all levels then decreased in the lower 13 m and remained high in the upper 17 m. The initial temperature increase appears related to passage of the warm filament, which causes the temperature to remain high in the upper 17 m for the duration of the event. Below the level of the warm filament, temperatures decreased as the cold subsurface intrustion passed through the mooring.

The uplifted density structure in the cold core of the disturbance indicates a cyclonic circulation, with southward flow west of the core and northward flow east of the core. Previous investigations of Gulf Stream frontal eddies on the Georgia shelf (Lee et al. 1981) and in the Florida Straits (Lee 1975, Lee and Mayer 1977) have observed cyclonic current reversals in current meter records, as shingles with similar properties as found in Event 8 were encountered. However, low-frequency current records from Moorings 9 and 10 during April show a persistent northward flow that is perturbed by a succession of cyclonic cold anomalies, but no flow reversals (Figures 4.6-3, -4 and -5).

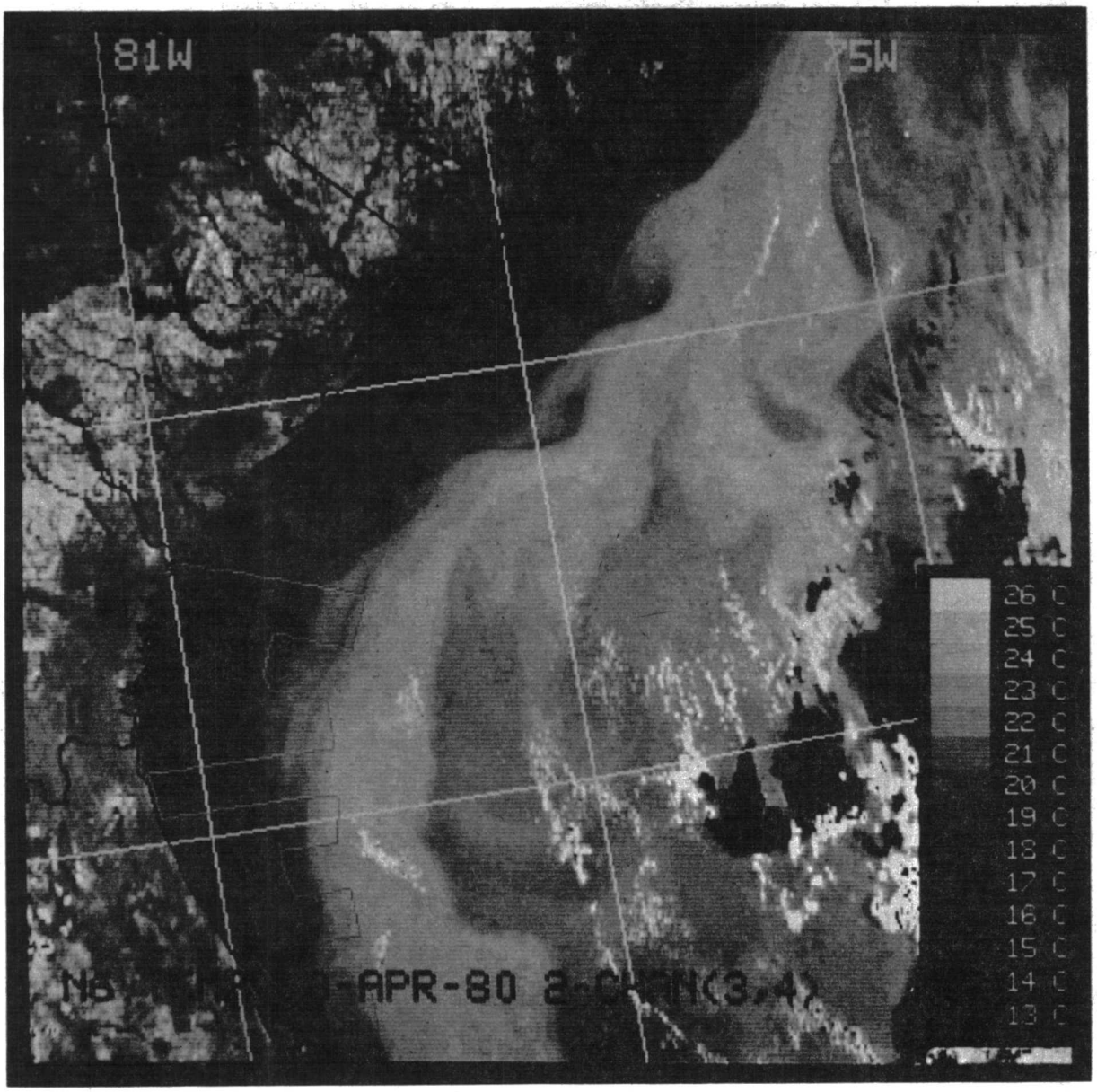

Fig. 4.6-15. Satellite VHRR thermal image of Gulf Stream at 0900 Z on April 22, 1980 (prepared by Otis Brown of University of Miami).

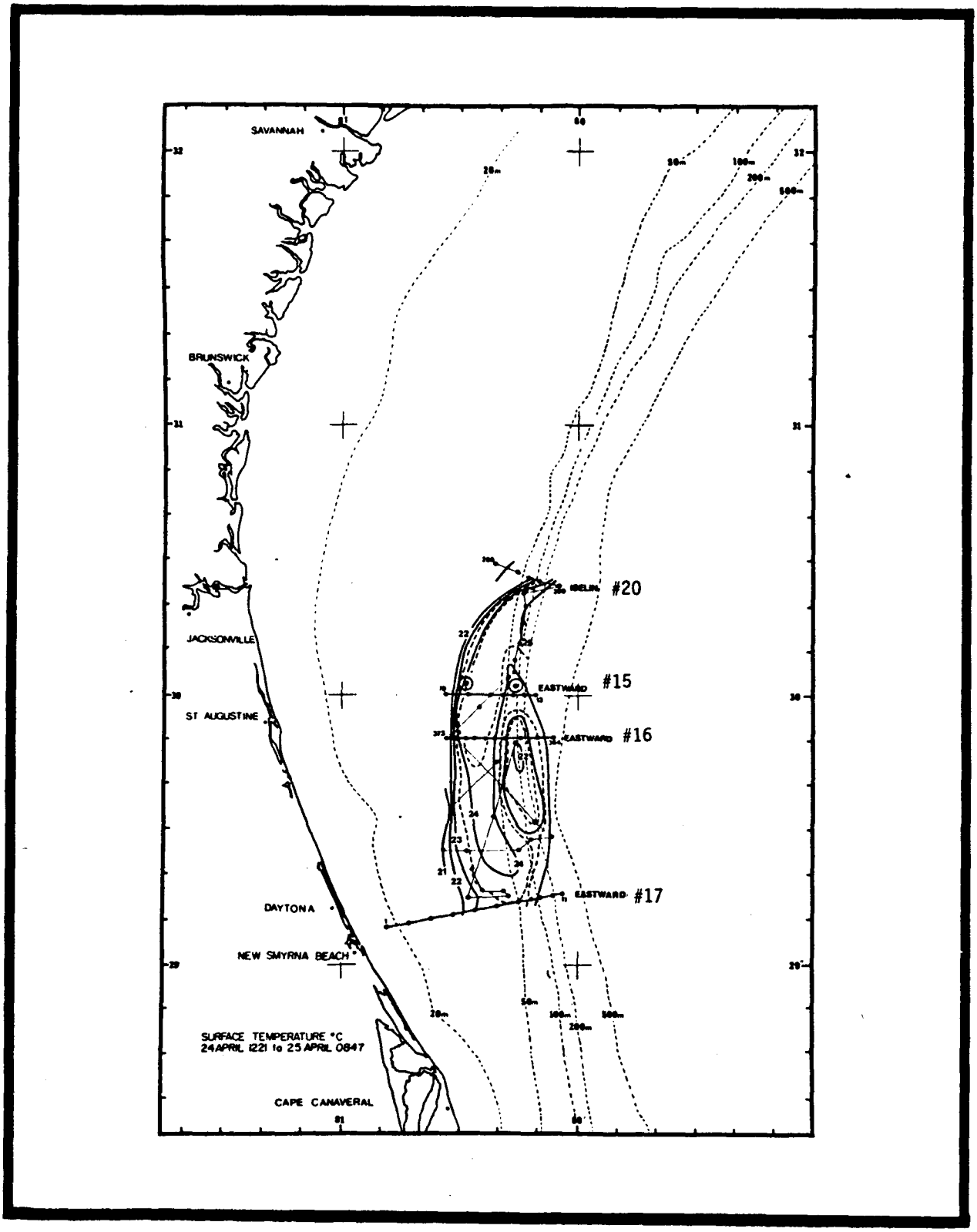

Figure 4.6-16. Surface temperature (°C) from thermosalinograph mapping 24 April (1221 hr) to 25 April (0847 hr). Straight lines with dots show Iselin ship track and stations. Wavy line and dots show Eastward track and stations. Hydrographic sections are labeled with ship name and end point station numbers. Moorings 9 and 10 are shown with circles and dots.

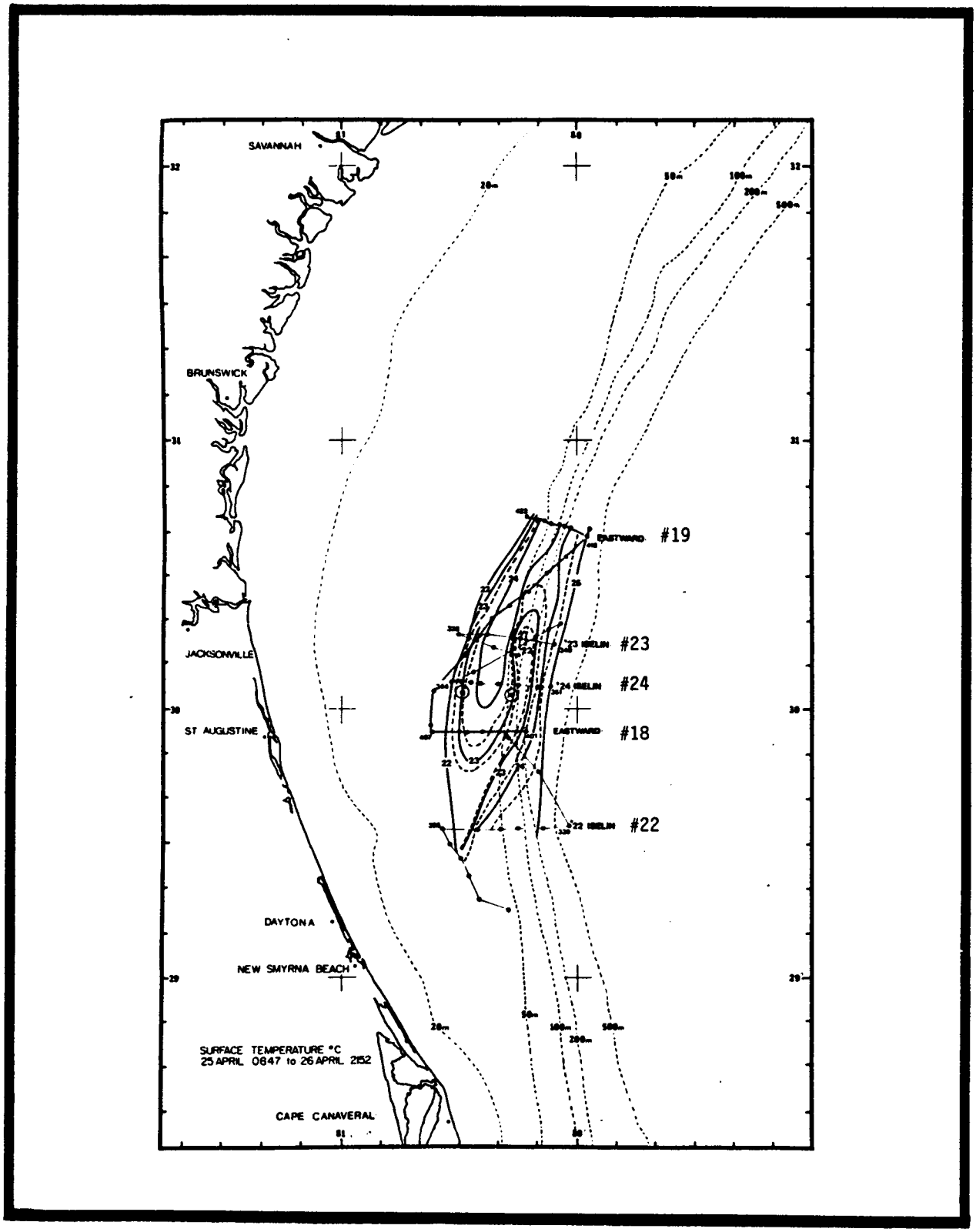

Figure 4.6-17. Surface temperature (°C) from thermosalinograph mapping 25 April (0847 hr) to 26 April (2152 hr). Straight lines with dots show Iselin ship track and stations. Wavy line and dots show Eastward track and stations. Hydrographic sections are labeled with ship name and end point station numbers. Moorings 9 and 10 are shown with circles and dots.

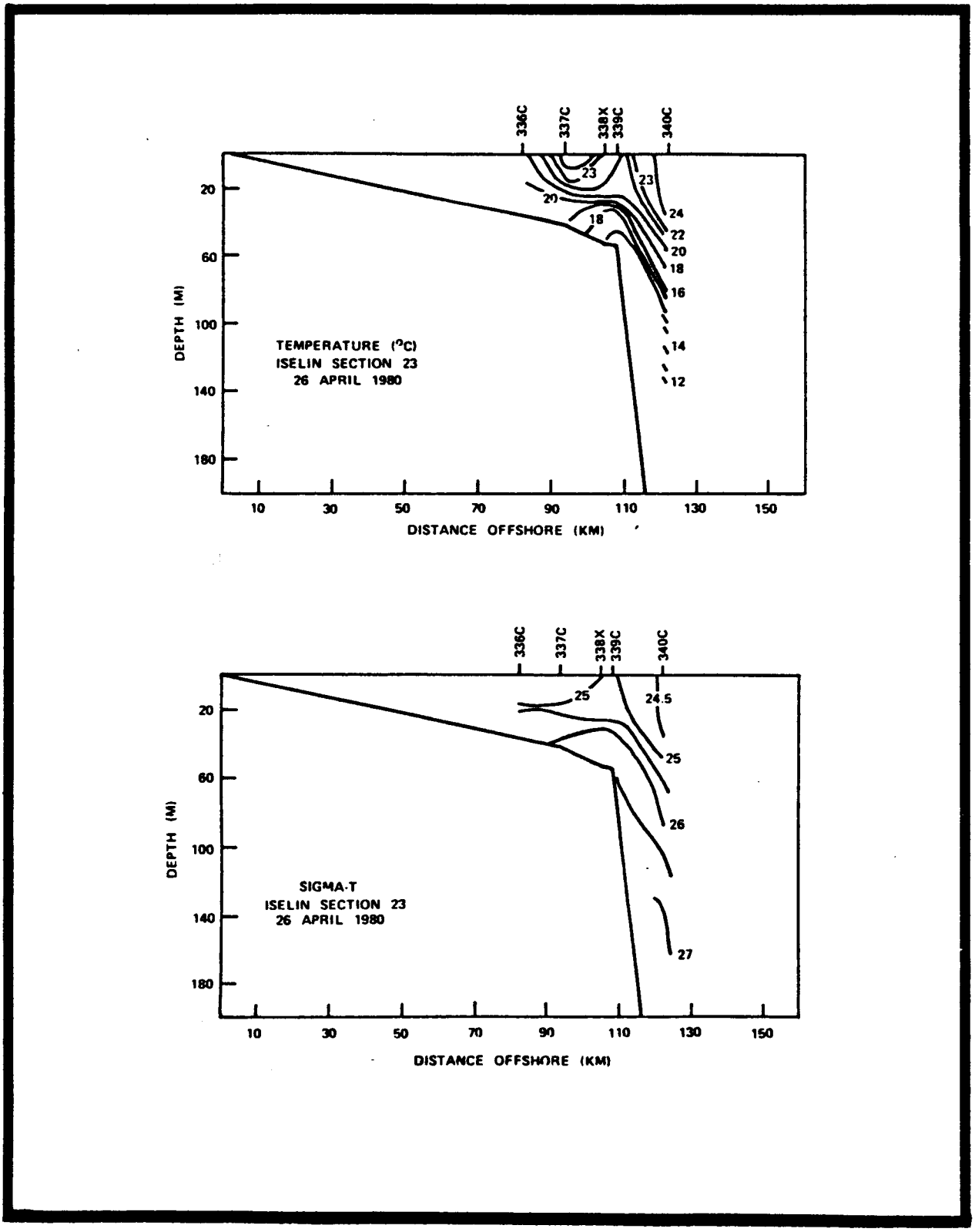

Figure 4.6-18a. Temperature (^{o}C) and density (σ_t) sections across Gulf Stream frontal eddy on 26 April (0028 to 0757 hr). Stations are numbers along the top. Iselin Section 23 of Figure 17.

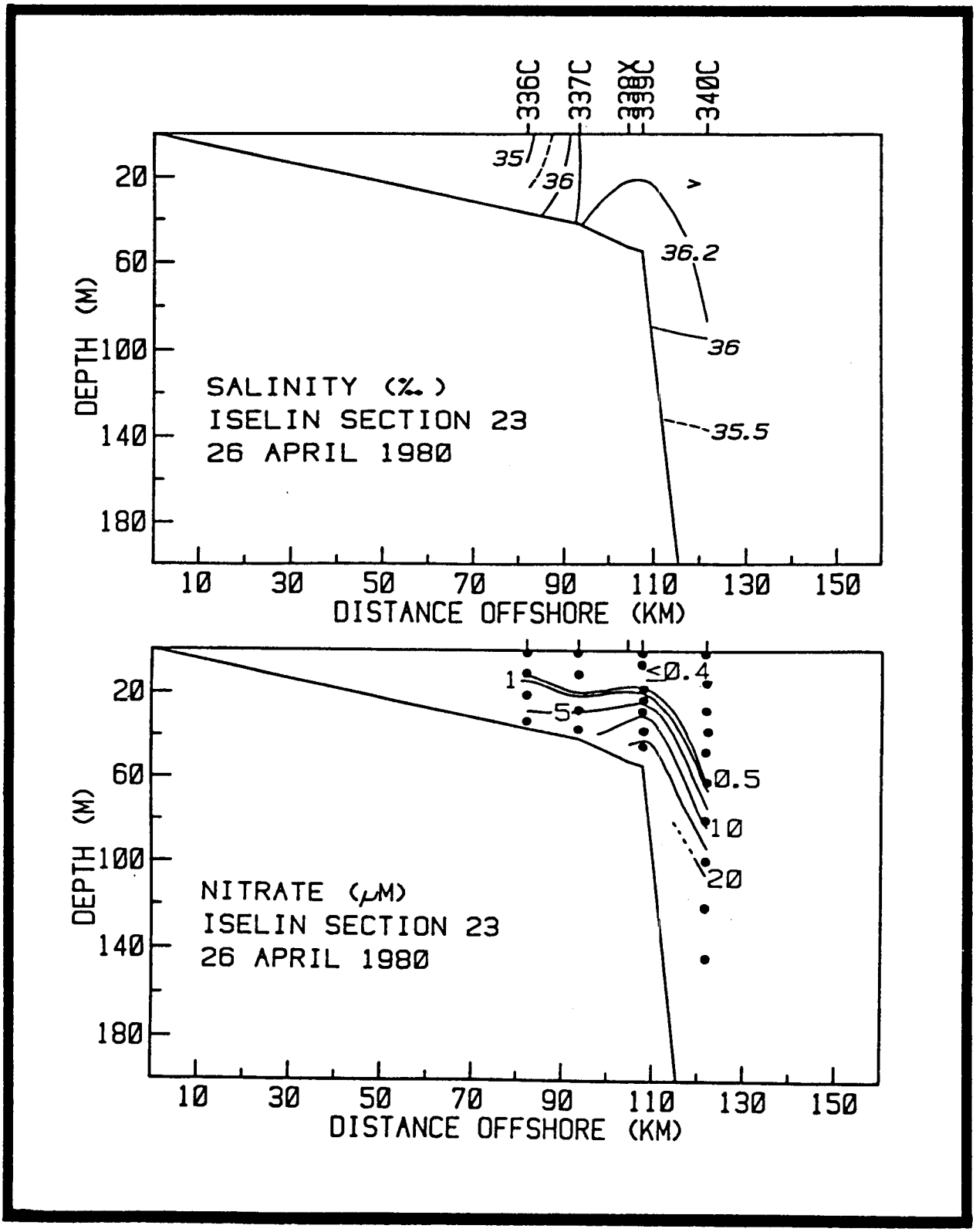

Figure 4.6-18b. Salinity (^{o}/oo) and nitrate (μM) sections 26 April (0028 to 0757 hr), Iselin Section 23.

A fixed current meter will record the mean flow (v) plus eddy motions (v') written as: $v = \bar{v} + v'$ for the along-shelf component. If the mean flow is larger than the eddy motion, a current reversal will not be observed at a fixed station. Band pass filtering the data from 40 hours to 2 weeks removes the effect of the mean and shows cold cyclonic perturbations propagating northward along the shelf break at about 55 cm s^{-1}, which was nearly the same speed as the mean (Figure 4.6-6a, b). When the effect of the mean flow is removed, cyclonic flow reversals are observed at all levels at Sites 9 and 10 during the passage of Event 8 (Figure 4.6-19).

Southward flows within Event #8 appear to be in approximate geostrophic balance with the uplifted density structure in the cold core, as determined from the thermal wind equation:

$$\frac{\partial \bar{v}}{\partial z} = \frac{g}{\rho f} \frac{\partial \rho}{\partial x} \qquad (3)$$

Daily averaged vertical shear measured at Mooring 9 during passage of Event #8 (26 April) was about 5×10^{-3} s^{-1} beneath the warm filament. The density gradient term on the right of (3) was about 4×10^{-3} s^{-1} at the 17-m level, and 3×10^{-3} s^{-1} at 37 m (from Stations 337 and 339 of Iselin Section 24). Within the filament, the relative shear between the 7- and 17-m levels was negative, indicating the possibility of a anticyclonic circulation within the filament. However, this was not observed in current meter data at the 7-m level (Figure 4.6-19), presumably due to the stronger cyclonic circulation within the larger cold anomaly. Station spacing was not small enough to resolve the relative density field of the warm filament. Thus, the propagating cold cyclonic pertubations described here appear to be the same type of frontal eddies as found previously (Lee et al. 1981). The only observable difference is that the northward propagation velocities were larger than the eddy velocities for most of the events.

4.6.5.2 Upwelling Velocity in Frontal Eddies

Upwelling velocities (w) in Event #8 can be estimated by comparing changing vertical isotherm positions in the cold core. The 17°C isotherm was uplifted 13 m in the core in a 37.8-hour period between Eastward Station #366 (Eastward Section #16, Figure 4.6-16) and Iselin Station #339 (Iselin Section 23, Figure 4.6-17), which gives a vertical veloctiy of 10^{-2} cm s^{-1}. Since subsurface temperature measurements can be aliased by internal tides it becomes useful to also estimate w from the conservation of relative vorticity (ζ) along a streamline. Following Arthur (1965) the conservation of relative vorticity in natural coordinates is:

$$f \frac{dw}{dz} = \frac{d\zeta}{dt} + \beta V \qquad (4)$$

where $\zeta = V/R - dV/dn$, and β is the change in planetary vorticity (f) with latitude; $\beta = 1.35 \times 10^{-13}$ cm^{-1} s^{-1}. Assuming a uniform flow V which tends to follow the temperature pattern shown in Figure 4.6-16, with cyclonic curvature of radius R around the cold core, the shear vorticity dV/dn in the filament is assumed zero, and the vertical velocity at depth h is given by:

$$w_h = -\frac{h}{f} \frac{d\zeta}{dt} - \frac{h\beta V}{f} . \qquad (5)$$

The tangential velocity V is assumed equal to the eddy velocity of Event #8 or approximately 40 cm s^{-1} (Figure 4.6-19) and has a radius of curvature R of 22 km north of the cold core and R = ∞ west of the core where the flow is southward in the warm filament. Therefore, $d\zeta/dt = -2.x10^{-10} s^{-2}$; $\beta V = 5.4x10^{-12} s^{-2}$; and at 40 m the vertical velocity is: $w = 1.4x10^{-2}$ cm s^{-1}, which is quite close to the estimate made following rising isotherms. The strength of the vertical velocity depends primarily on the change in curvature vorticity along a streamline. The curvature is cyclonic around the cold core of a frontal eddy which gives a positive (upwelling) vertical velocity. The strength of the upwelling velocity is about .01 cm s^{-1}, or 8.6 m day^{-1}, which is high compared to estimates of about 1 m day^{-1} in strong wind-driven upwelling areas (Smith, 1968).

4.6.5.3 Vorticity Conservation in Frontal Eddies

The conservation of potential vorticity as expressed by Woods (Personal Communication) is written:

$$\left(\frac{V}{R} - \frac{\partial V}{\partial n} + f \right) N^2 = \text{constant} \qquad (6)$$

where $\zeta = V/R - \partial V/\partial n$ is the same as (4) and the static stability $N^2 = (g/\rho)(\Delta\rho/\Delta z)$ depends on the strength of the pycnocline, with density difference $\Delta\rho$ between two isopycnals separated in the vertical by Δz. Considering a cyclonic cold-core eddy, both the curvature vorticity and shear vorticity will lead to an increase in potential vorticity, which must be compensated for by a decrease in static stability. The shear vorticity produces a positive effect, since in a natural coordinate system "n" increases to the left of the flow, making the shear term negative on the inside (east) of the warm tongue, and when combined with the minus sign gives a positive effect. On the outside (west) of the warm tongue, shear is positive and so can compensate for the cyclonic curvature by closing the streamlines. Thus, in the cold-core region, static stability must decrease to compensate for the increase in curvature and shear vorticity (changes in planetary vorticity are small). In the cold core of Event #8, N^2 was observed to decrease by about a factor of 2, compared to estimates in the frontal region north and south of the event. Similar results were found for the 1977 frontal eddy as reported by Lee et al. (1981).

4.6.5.4 Nitrate Flux and Biological Implications

Previous investigations on the Georgia shelf have shown that upwelling in the cold core of frontal eddies transports deeper Gulf Stream waters with high nutrient concentrations into the euphotic zone which is <50 m along the outer shelf (Lee et al. 1981, Yoder et al. 1981). In the absence of eddy-induced upwelling, nitrate concentrations in the outer shelf are usually less than 1.0 μ moles ℓ^{-1}. However in the cold core of Event #8, nitrate concentrations below 10 μ moles ℓ^{-1} were observed at a depth of 30 m, and at 25 km, shoreward of the shelf break, 5 μ moles ℓ^{-1} were observed in the subsurface intrusion at 30 m (Figure 4.6-18). Using an empirical linear relationship between temperature and nitrate for newly-upwelled Western Atlantic Central Water, Lee et al. (1981) found a net onshore nitrate flux during the passage of a frontal

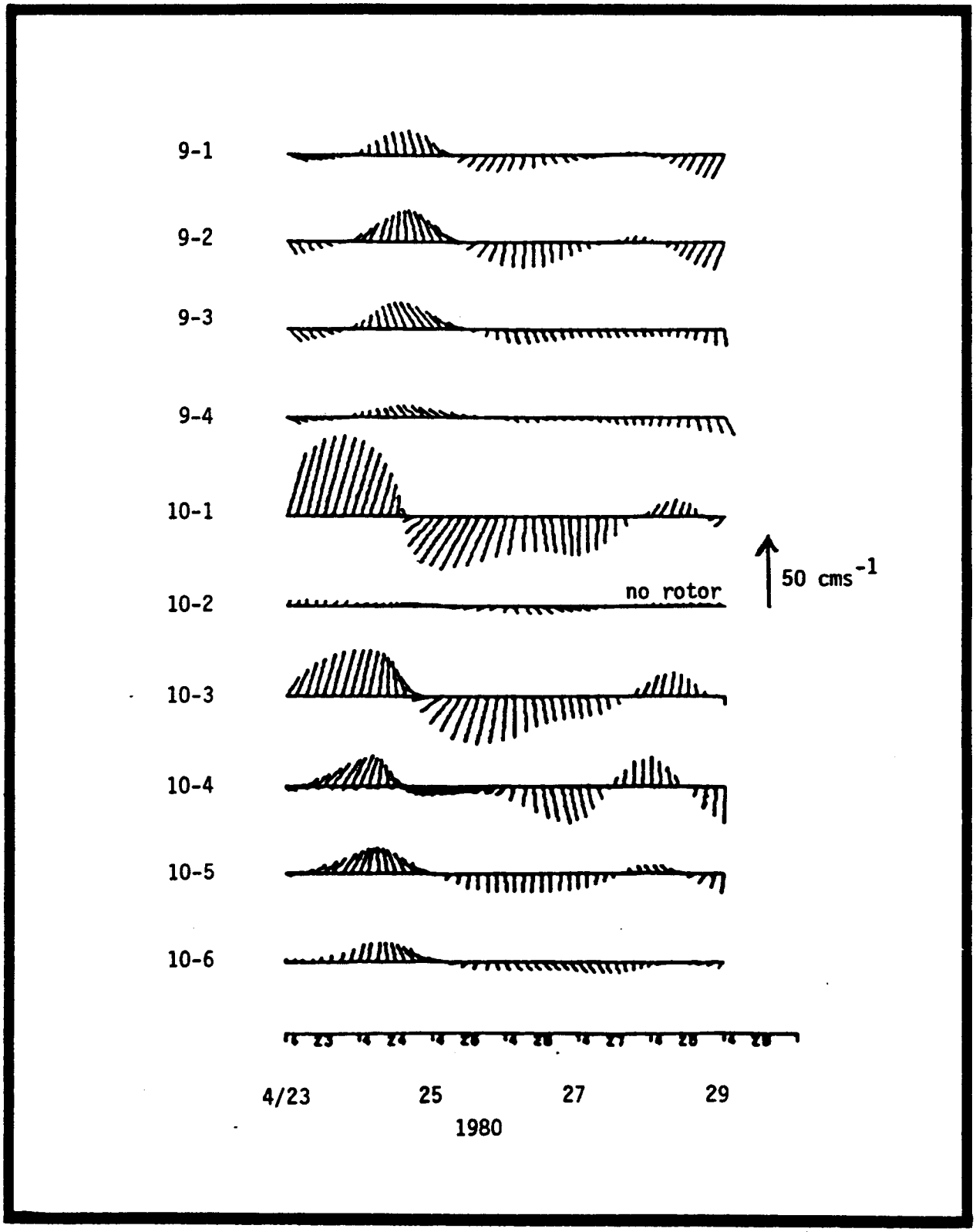

Figure 4.6-19. Time series of 3-hour demeaned 40-HLP current vectors from Moorings 9 and 10 during Event 8.

eddy at the shelf break of -18.6 μ moles $m^{-2}s^{-1}$. Their estimate was made using only two current meters at 72 and 17 m on the 75-m isobath. The increased resolution available on Mooring 10 makes it possible to determine the vertical structure of the nitrate flux and to make more accurate estimates of the vertically averaged flux.

A nitrate time series is computed from the low-frequency temperature (T) at each current meter from the empirical relation (O'Malley et al. 1978):

$$NO_3 = 53.0 - 2.6\ T \qquad (7)$$

where $NO_3 = 0$ for T > 20°C. The net nitrate flux is then computed from:

$$\overline{u'NO_3'} = \overline{(u - \bar{u})(NO_3 - \overline{NO_3})} \qquad (8)$$

where the over bar is a time average and $\bar{u}$ and $\overline{NO_3}$ are 4-month record long averages.

Vertical profiles of the nitrate flux averaged over the duration of Event #8 (23-27 April) and over the total record length (25 February - 21 June 1981) are shown in Figure 4.6-20. A strong onshore maximum is observed at 45 m in both the eddy averaged and total record average profiles. Due to poor vertical sampling resolution, Lee et al. (1981) missed the onshore maximum; as a result, their vertical average flux of -18.6 μ moles $m^{-2}s^{-1}$ may have greatly underestimated the nitrate transport. The vertical average net nitrate flux in Event #8 was -115 μ moles $m^{-2}s^{-1}$, and for the total record average it was -65 μ moles $m^{-2}s^{-1}$. Current and temperature records from the shelf break indicate that eddy-induced upwelling events occurred on the average of about 5 per month (Figures 4.6-5 and -6) and influenced the outer shelf for approximately half of the 4-month period. Since the vertically averaged net flux for the total record was approximately half of the eddy averaged value, and eddies appear to occur about half the time, it follows that frontal eddies were the dominant contributor to transport of nitrate across the shelf break.

Total nitrogen transported to the shelf by Event #8 can be determined by converting vertical eddy averaged nitrate flux to a nitrogen flux (Q_N) then finding the total nitrogen (N_T) transported to the shelf by the eddy from:

$$N_T = (Q_N)(H)(L)(T) \qquad (9)$$

where H is the height of the shelf break water column (75 m), L is the eddy length (130 km), and T is the time it takes the eddy to pass the mooring site or duration (5 days). Using these estimates in (9) with $Q_N = 1.6$ mg N m^{-2} s^{-1} gives $N_T = -68 \times 10^9$ g N per eddy, or about 7400 tons N per eddy, which is a factor of 3.5 larger than was found in 1977 (Lee et al. 1981). Assuming that on the annual average 2 eddies per month occur, this gives an annual net nitrogen transport to the shelf by the eddy process of approximately 190,000 tons N per year. This estimate is almost a factor of 7 greater than the estimate of the combined inputs of nitrogen from rivers, atmosphere, and the Gulf Stream made prior to 1977 by Haines (1974). Yoder et al. (1981) found the potential for carbon production, by phytoplankton in the outer shelf from the net onshore nitrogen transport of Event #8, was approximately 540 g C m^{-2} yr^{-1}; which is about a factor of 2 larger than estimates made for the inner

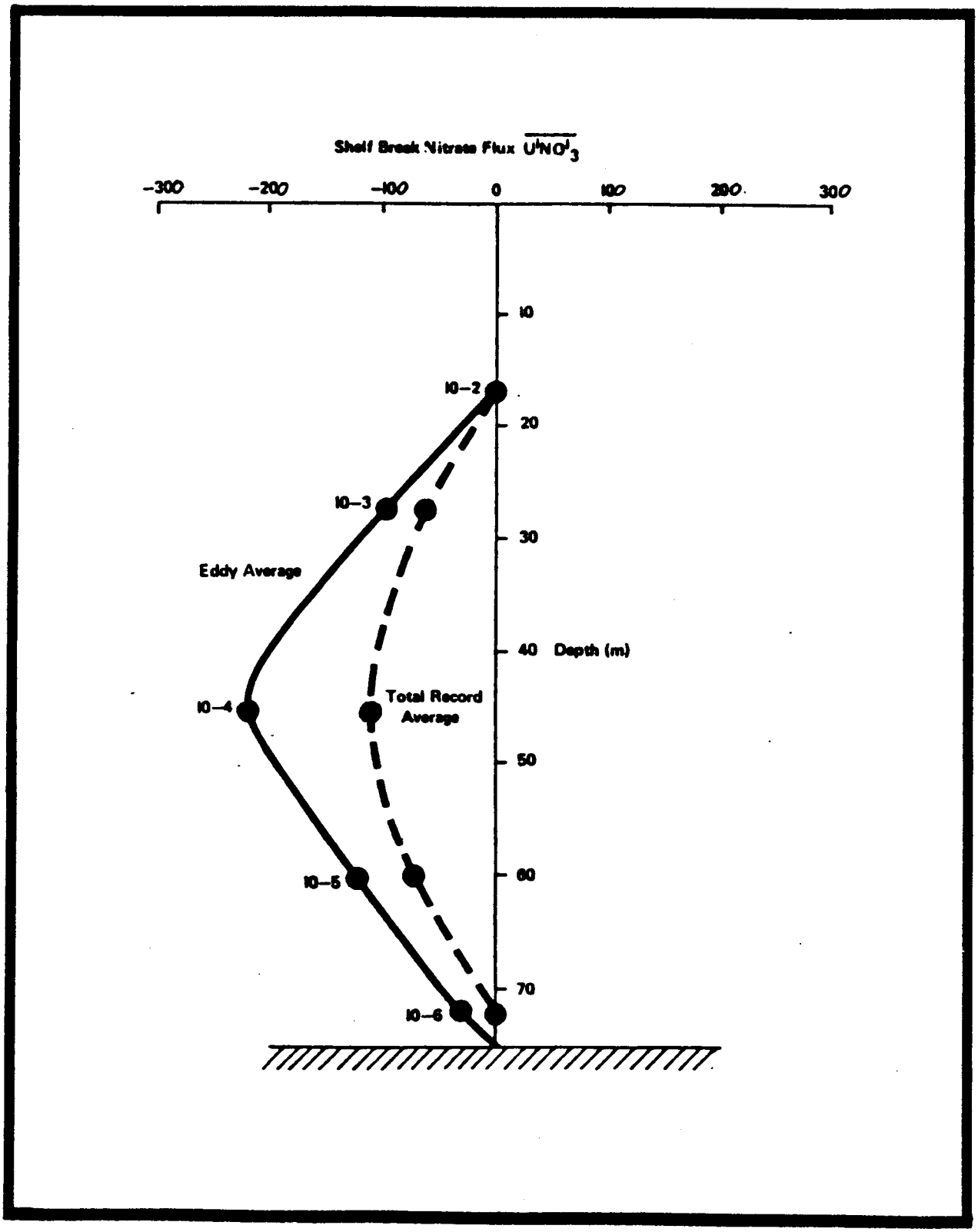

Figure 4.6-20. Shelf break nitrate flux $\overline{u'NO_3'}$ (μ moles $m^{-2}s^{-1}$) from Mooring 10.

shelf (depths <20 m) by Haines and Dunstan (1975) and equivalent to the primary production estimate for the mouth of the Altamaha River (Thomas 1966).

4.6.6 Summary

4.6.6.1 Introduction

Low-frequency current and temperature variability along the outer shelf of the southeastern U.S. continental shelf results from a combination of wind forcing and interaction with the Gulf Stream. Subtidal current and temperature fluctuations along the shelf break result primarily from propagating disturbances in the Gulf Stream front. Along the 40-m isobath which is about 10 to 30 km shoreward of the shelf break, the flow and temperature variability appear to be a mixed response to wind and Gulf Stream forcing, with non-propagating wind effects more clearly observable.

4.6.6.2 Wind Response

A significant part of the low-frequency variability at the 40-m isobath occurred as a non-propagating barotropic response to large-scale coherent wind forcing. Low-frequency along-shelf current fluctuations were nearly equal in magnitude and close in phase over the 425 km, along-shelf array spacing and 40-m water depth, indicating a non-propagating barotropic response to wind driven sea level fluctuations. Coastal sea-level elevations were highly responsive to both along-shelf and cross-shelf winds. Cross-shelf winds can drive coastal sea-level changes in the nearshore shallow-water zone due to bottom friction influences on the development of the surface Ekman layer. This in turn can cause transports to the right of the wind at angles less than 90°, as predicted for pure drift currents (Neumann and Pierson 1966). Assuming wind driven sea-level variations are small at the shelf break, a set-up (set-down) of sea level (η) at the coast will generate a surface slope and a cross-shelf pressure gradient that is in approximate geostrophic balance with a southward (northward) barotropic flow

$$v_g = (g/f)(\partial\eta/\partial x). \qquad (10)$$

The magnitude of the current response for observed coastal sea-level amplitudes of 20-30 cm ranges from approximately 20 to 45 cm s^{-1} for shelf widths of the array, assuming a linear slope to a constant mean sea level at the shelf break. The amplitudes of low-frequency currents at the 40-m isobath appear to fall within this range.

A similar frictional equilibrium response was observed in the Mid-Atlantic Bight (Beardsley and Butman 1974; Scott and Csanady 1976) and on the west coast (Hickey and Hamilton 1980) and appears to be a fundamental part of the dynamics of coastal wind driven flow. Southward propagating continental shelf waves were not observed in the coastal sea-level data or current meter data. Propagating disturbances are observed to travel north in this region due to advection by Gulf Stream and are restricted to the outer shelf. A large part of the variability at the 40-m isobath appears to have been caused by non-propagating, clockwise rotating frictional equilibrium responses to local wind driven sea level changes. This type of response was also observed occasionally at the shelf break but more often is masked by propagating disturbances.

4.6.6.3 Gulf Stream Frontal Eddies

Low-frequency current and temperature variability, and fluxes of momentum, heat, and nutrients at the shelf break were dominated by northward propagating Gulf Stream frontal disturbances. Current meter, hydrographic, and satellite observations indicate that these disturbances were cold cyclonic eddies embedded in the Gulf Stream front. The events were observed to propagate to the north at speeds of 50 to 70 cm s^{-1} and produce coherent fluctuations of cross-shelf and along-shelf velocity components and temperature throughout the water column in the 5- to 9-day period band over alongshelf coherence scales of 100 km. Frontal eddy signatures in alongshelf pairs of current meters at the shelf break consisted of propagating cyclonic perturbations of the northward mean flow coupled to a sharp drop in temperature. This response was observed throughout the water column with larger temperature fluctuations usually occurring in the lower layer. Cyclonic current reversals may occur if the eddy velocity is larger than the northward mean flow.

The eddy signature in SST data consists of the "shingle" pattern (Von Arx et al. 1955) which develops as a warm filament of near surface Gulf Stream water extends from the front and folds around the cold core. The eddies cyclonic circulation appears to be in quasi-geostrophic equilibrium with uplifted density surfaces in the cold core. The vertical shear of the perturbation velocity observed on the western side of a cold core was balanced by the horizontal density gradient, further substantiating the southward geostrophic flow on the west side of eddies.

The warm filaments or shingles appear to develop as near surface streamers (15 to 20 m in depth) of Gulf Stream water which are pulled out of the front are wrapped around the cold core in much the same manner as "streamers" associated with warm- and cold-core rings (Vukovich and Crissman 1978). There was no indication in current and temperature records of anticyclonic circulation in the warm filaments as was suggested by Chew (1981). However, the relative vertical shear within the warm filament did suggest anticyclonic circulation that may have been masked by the stronger cyclonic flow in the cold eddy. The movement of a warm filament with anticyclonic circulation should produce a propagating anticyclonic perturbation of the northward mean flow coupled to an increase in temperature, which was not observed at the outer-shelf current meter sites. Instead, clockwise rotating events were non-propagating and poorly correlated to temperature, and they appeared to occur in response to clockwise rotating wind events. Clockwise rotation was more observable at the 40-m isobath and the lower layer at the shelf break, where the wind response was more evident.

The formation process of frontal eddies is not well understood. The shingle signature observed in satellite imagery appears to be connected to growing wave-like meanders of the Gulf Stream (Legeckis 1975, Stumpf and Rao 1975, Legeckis 1979). (Theoretical investigations predict that both barotropic (Niiler and Mysak 1971) and baroclinic (Orlanski 1969, Orlanski and Cox 1973) instabilities can exist in the frontal region. Predicted wave properties of the fastest growing waves match reasonably well with satellite observations; i.e., wave lengths of 100 to 200 km and periods $\sim$ 10 days.) Our observations show that cyclonic eddies travel in conjunction with

the offshore meander portion of the waves. Similar findings were reported in the Florida Straits (Lee and Mayer 1977) and off Onslow Bay, N.C. (Bane et al. 1981). Frontal eddies do not appear to be directly or simply connected to wind forcing. However, wind events may act to trigger a frontal instability which could grow into an eddy.

Frontal eddies appear to be short-lived phenomena. They can form in only a few days and possibly dissipate just as fast. Satellite imagery suggests that the total cycle takes place in one to three weeks. The eddy process appears to be an important component in the Gulf Stream energy balance. Between New Smyrna Beach, Fla. and Savannah, Ga., current meter estimates indicate that frontal eddies transport momentum and heat to the Gulf Stream as part of the process of transferring both eddy kinetic and potential energy to the mean flow. Eddy production of mean energy in the area of the current meter array suggests an upstream formation region, possibly where the shelf widens north of Jupiter, Fla., as the Gulf Stream leaves the Florida Straits. Dissipation appears to occur through a rapid elongation process brought about by the large horizontal shear across the Gulf Stream front. Dissipation of this type is consistent with the estimated energy transfer and should cause a strengthening of the front.

As mentioned previously, eddy formation and dissipation processes are not well understood. Energy transfer estimates suggest an instability process, but we cannot differentiate clearly between barotropic and baroclinic instability with the available data. Both processes may, in fact, be occurring simultaneously. It is encouraging that our energy transfer estimates in the frontal zone are consistent with prior estimates from the Florida Straits and Onslow Bay. However, these estimates should be treated with caution. Energy transfer is a 3-dimensional process which may involve the total width of the Gulf Stream over some significant and unknown downstream length scale. Our estimates are only within a relatively small segment of the frontal zone and we were not able to evaluate the effects of pressure fluctuations and vertical motions on energy transfer.

A similar eddy formation process may occur off Onslow Bay, N.C. The kinematic and dynamic properties of the enlarged frontal disturbances that form downstream of the Charleston Bump appear to be consistent with the eddies we observed upstream of the "Bump" (Bane et al. 1981; Brooks and Bane 1981). Occasionally, shingles are observed in satellite imagery that maintain recognizable integrity as they propagate from the upstream to downstream region with considerable enlargement occurring downstream of the Bump (Lee et al. 1981). However, positive identification of events in satellite imagery requires about one week of consecutive cloud-free days, which rarely occur. Our shelf-break current meter records also indicate that frontal disturbances can maintain continuity between regions and produce larger fluctuations downstream of the Bump.

Frontal eddies are observed to have considerable influence on primary production in the outer shelf. Upwelling in the cold core, together with onshore flow in the cyclonic circulation, transports deeper nutrient enriched Gulf Stream waters into the euphotic zone for phytoplankton uptake. Upwelling velocities are estimated at 8.5 m day^{-1} which is high compared to estimates of 1 m day^{-1} for important wind induced upwelling regions. Rapid utilization of newly upwelled nutrients results in elongated patches of high chlorophyll that

propagate with the cold core and have similar dimensions (Yoder et al. 1981). Since the demise of frontal eddies appears to occur as a shear induced dissipation process rather than a collapse of isopycnal surfaces the upwelled nutrients should remain in the outer shelf, possibly causing chlorophyll bands in the Gulf Stream front. Estimates of nitrate flux from current meter records show a net onshore transport of -115 μ moles m^{-2} s^{-1} across the shelf break during the passage of a frontal eddy, which was approximately a factor of 2 larger than the 4-month average transport. Current meter records indicate that frontal eddies occurred at a frequency of about 5 per month and were the main contributor to the nitrate flux. The annual input of new nitrogen to the shelf by frontal eddies is estimated at 54.3 g N m^{-2} yr^{-1}. This new nitrogen has a potential for carbon production by primary producers of 540 g C m^{-2} yr^{-1}, which is about a factor of 2 higher than estimates for the inner shelf by Haines and Dunstan (1975) and equivalent to estimates by Thomas (1966) for the mouth of the Altamaha River.

4.7 CAROLINA CAPES AND CHARLESTON REGION

4.7.1 Introduction

The continental margin off Charleston, S.C. is of singular interest because physical oceanographic processes of the mid to outer shelf and upper slope differ from those in the rest of the SAB. The Gulf Stream is known to affect directly the outer shelf of Florida, Georgia, and North Carolina through the influence of frontal events. Alternatively, the Gulf Stream front (GSF) is known to be only occasionally present from the mid to outer shelf off Charleston.

Very High Resolution Radiometer (VHRR) data suggests that south of 32°N the GSF generally follows the 200-m isobath; however, at 32°N 79°W, a topographic feature of the continental slope and rise called the Charleston Bump (CB) deflects the Gulf Stream to the east causing a quasi-permanent "kink" in the GSF path (Figure 4.7-1). Many authors, including Pratt (1963), Pashinski and Maul (1973), Legeckis (1975), Pietrafesa et al. (1978), Brooks and Bane (1978) and Legeckis (1979) have presented VHRR imagery documenting this feature. Pietrafesa et al. (1978) estimated that the GSF was deflected 60-110 km offshore of the shelf break 70% of the time. Rooney et al. (1978) provided a theoretical basis to show that the bottom was the vorticity source necessary to induce the Gulf Stream to deflect eastward at the CB. These last authors also speculated that waves were generated in the deflection process and that these long frontal waves may be the meanders discussed by Webster (1961a,b). Other features frequently observed along the GSF are folded back tongues of warm water called "shingles" (Von Arx et al. 1955). These shingles are manifested as warm, southward oriented, filament shaped extrusions of GSF waters (Figure 4.7-1).

On the Charleston shelf, the signature of a filament passage is easily discernible since current vector rotation is almost always anticyclonic. Pietrafesa and Janowitz (1979b) showed that these filaments can appear to rotate either cyclonically or anti-cyclonically in the Eulerian sense relative to a current meter's location within the Lagrangian event. The GSF off Charleston and Cape Romain is typically well offshore of the shelf break since only the westernmost portion of a filament reaches the shelf proper.

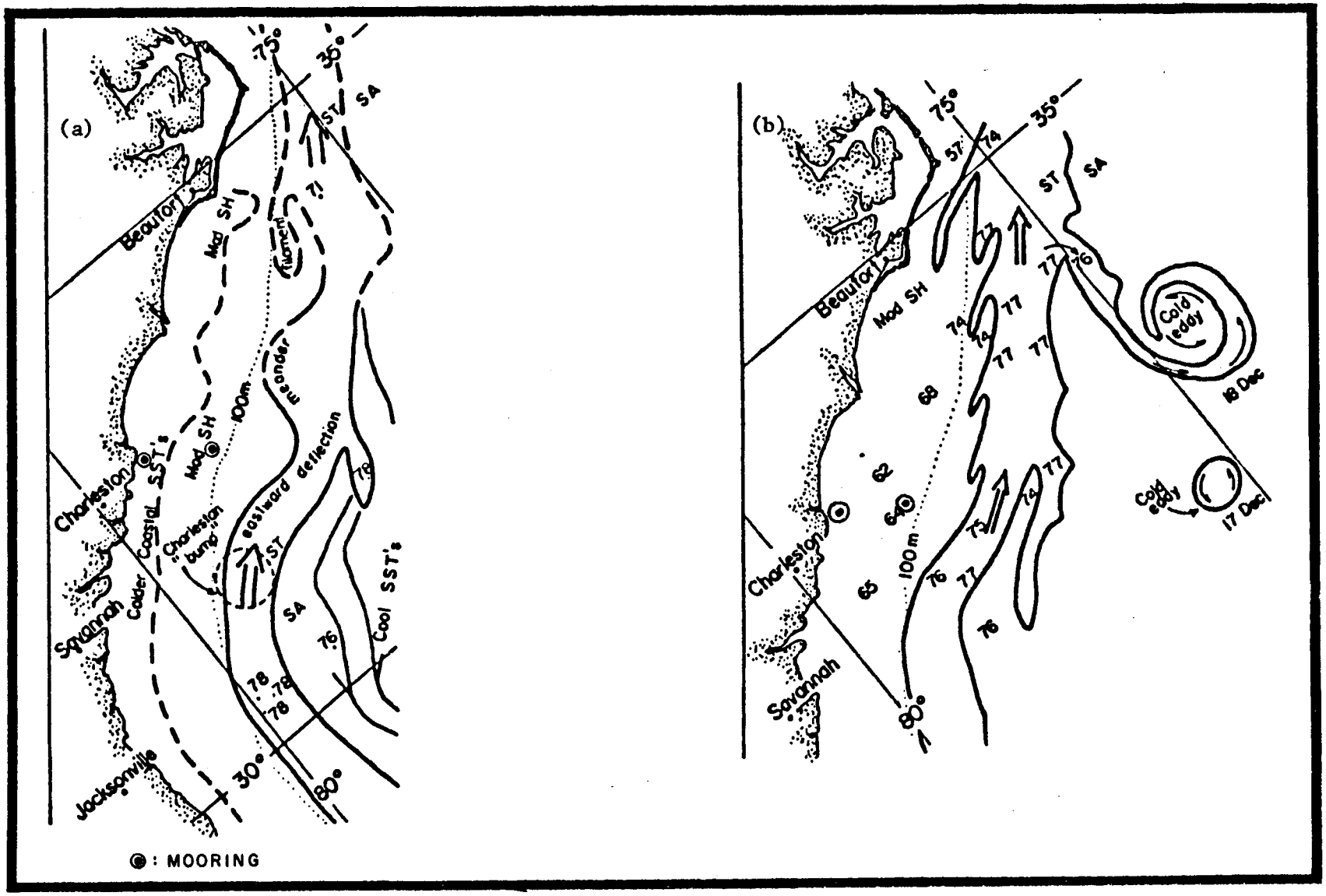

Figure 4.7-1 U.S. Naval Oceanographic Office Gulf Stream location maps derived principally from VHRR satellite imagery for (a) 12 December 1977 and (b) 22 December 1976. The ◉ represents the site of the Charleston Long Term Mooring (BLM) and NDBO Buoy.

Consequently the current vector rotation convention tends to be clockwise. Examples of such an event passage are shown in Figure 4.7-2.

Response of coastal currents to mechanical wind forcing is known to be important on the Charleston shelf. Janowitz and Pietrafesa (1980a) showed that coastal currents responded to winds in a time dependent, topographically influenced, coastal Ekman sense over time scales on the order of a day to a week. Moreover, Chao and Pietrafesa (1980) proved that coastal sea level also responds to the wind, nearly exclusively, over time scales of the order of a week in a seemingly predictable fashion. More recently, Janowitz and Pietrafesa (1982) showed that subinertial sea level variability at Charleston can be predicted from the time integral of the total wind vector.

Data products discussed in the following represent all or part of the interval from November 1977 through October 1979, a 24-month period when subsurface current meter, meteorological buoy, satellite imagery, and hydrographic data were being collected as part of SAPOS. The sequence of data presentation includes the following: atmospheric climatology, coastal sea level, Gulf Stream frontal variability, and climatology of observed currents and hydrography. The word climatology is used somewhat loosely here, but it is meant to encompass the weekly to seasonal variability of the system, as opposed to the 1- to 10-day event scale variability or "weather" of the system.

4.7.2 Atmospheric Winds

The Charleston meteorological regime was typified by Weber and Blanton (1980) as consisting of five subannual wind seasons including: winter, from November through February; spring, covering March through May; summer, encompassing June and July; fall, during August; and mariner's fall during September and October. There are, in general, preferred wind directions, magnitudes, and levels of variability during these five seasons. (See Section 4.5.2.3.2)

Wind stress vectors for 7-, 14-, 30-, and 90-day averages are shown in Figures 4.7-3 - 4.7-8 encompassing the period June 1978 to December 1979 at both the Charleston coastal and offshore NDBO sites (cf. Figure 4.7-2). From June through August wind vectors display slight clockwise turning but are essentially directed northward at an approximate mean of 2 m s^{-1} which corresponds to a mean stress of about 0.025 dynes cm^{-2}. August is shown to be a transitional month. September, October, and November are characterized by persistent northeasterly to northerly coastal winds with an associated mean stress of 0.5 dynes cm^{-2}. From December through February mean coastal winds are from the west-northwest and become southwesterly again by late March.

Mid-shelf winds are a little confusing, as suggested in Figures 4.7-6 to 4.7-8. While the 30- and 90-day stress vectors of shelf-break winds are typically 2 to 10 times larger than their coastal counterparts, they do tend to be aligned fairly closely to what is observed at the coast. Still, horizontal spatial gradients of the wind-stress vector are not negligible and may contribute to the mean circulation much as the wind-stress vector does directly. This possibility will be discussed below.

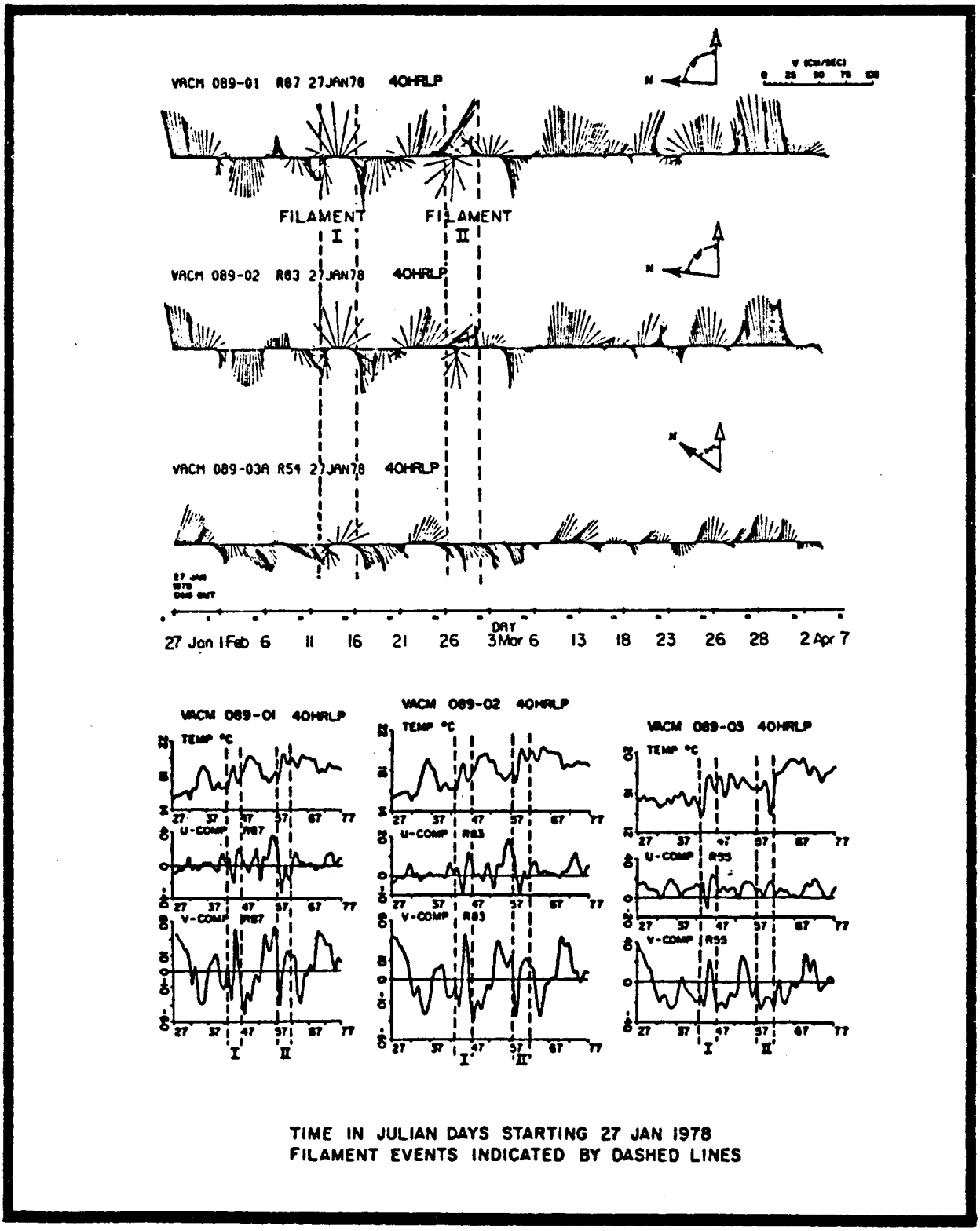

Figure 4.7-2. Forty-HLP stick plots and time series for Mooring 089 with the passage of a filament event indicated.

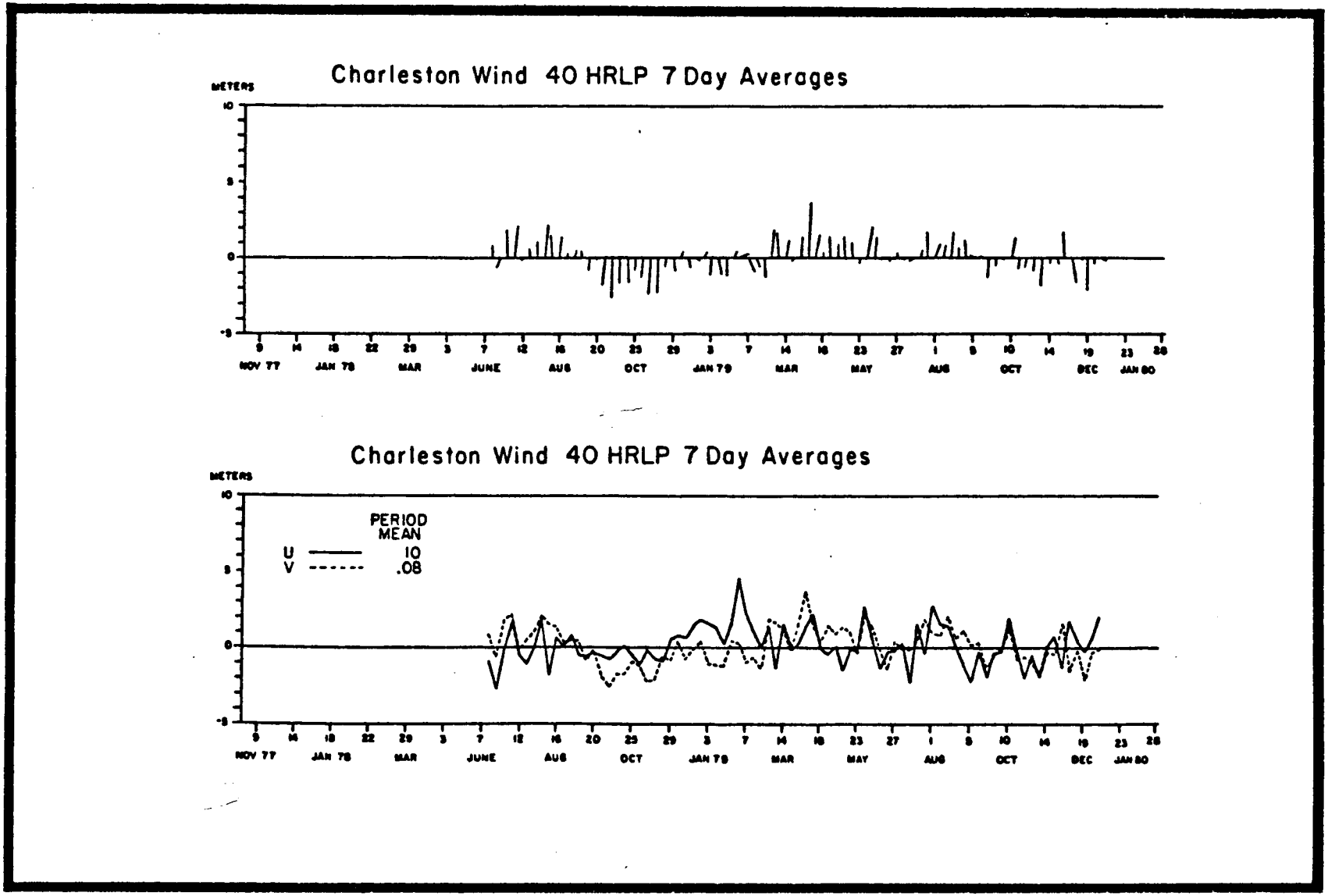

Figure 4.7-3. Seven-day averages for Charleston wind from June 1978 to December 1979.

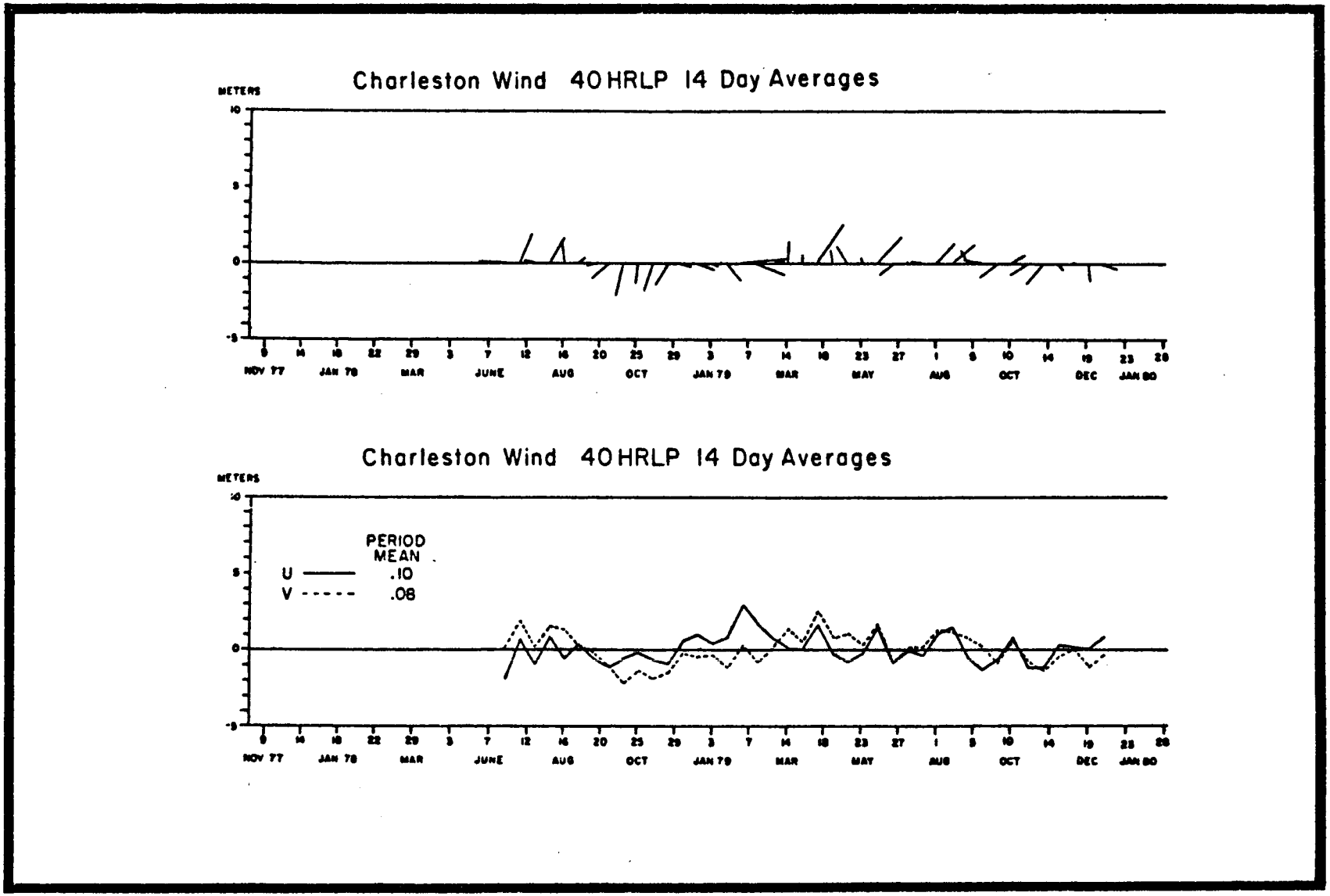

Figure 4.7-4. Fourteen-day averages for Charleston wind from June 1978 to December 1979.

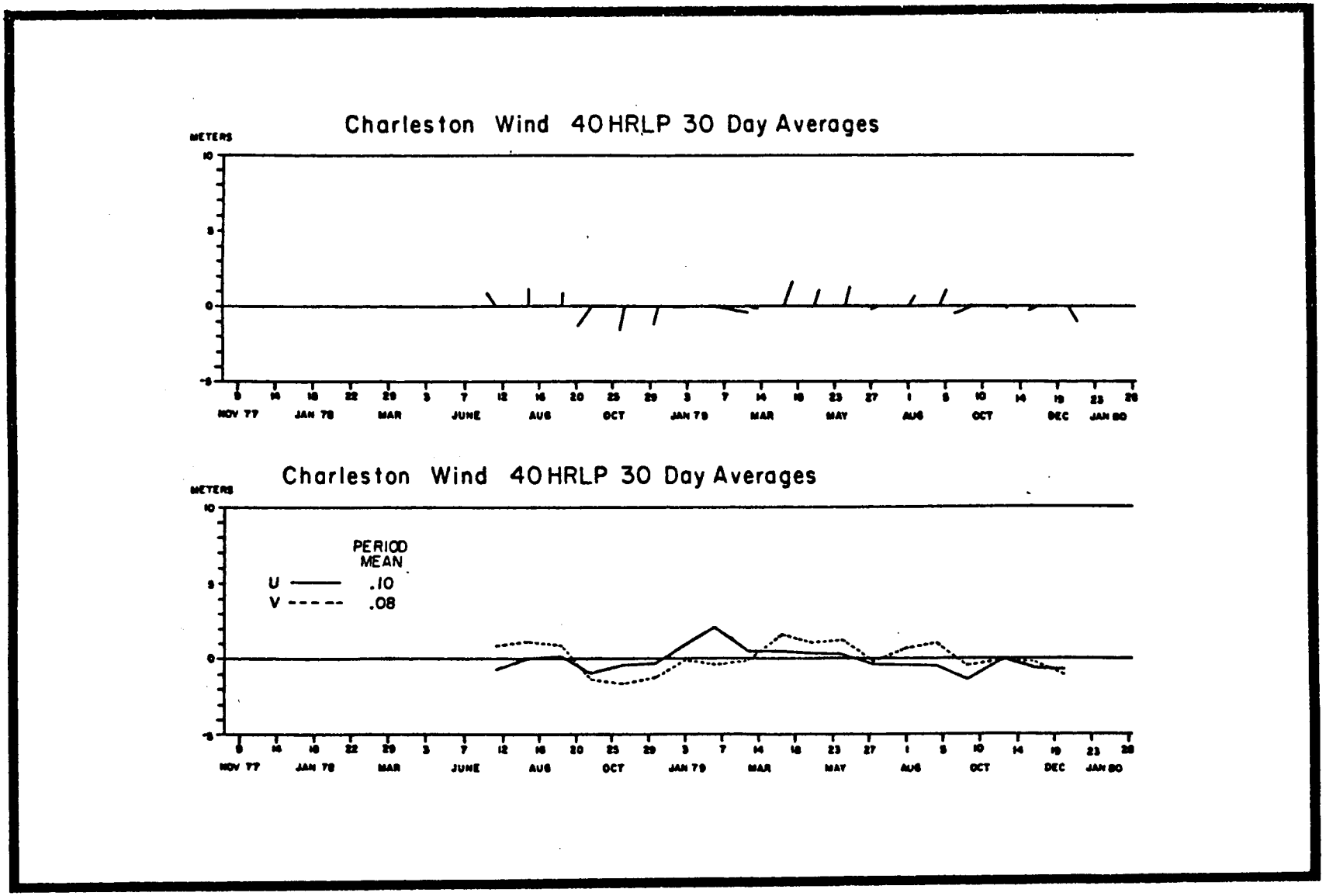

Figure 4.7-5. Thirty-day averages for Charleston wind from June 1978 to December 1979.

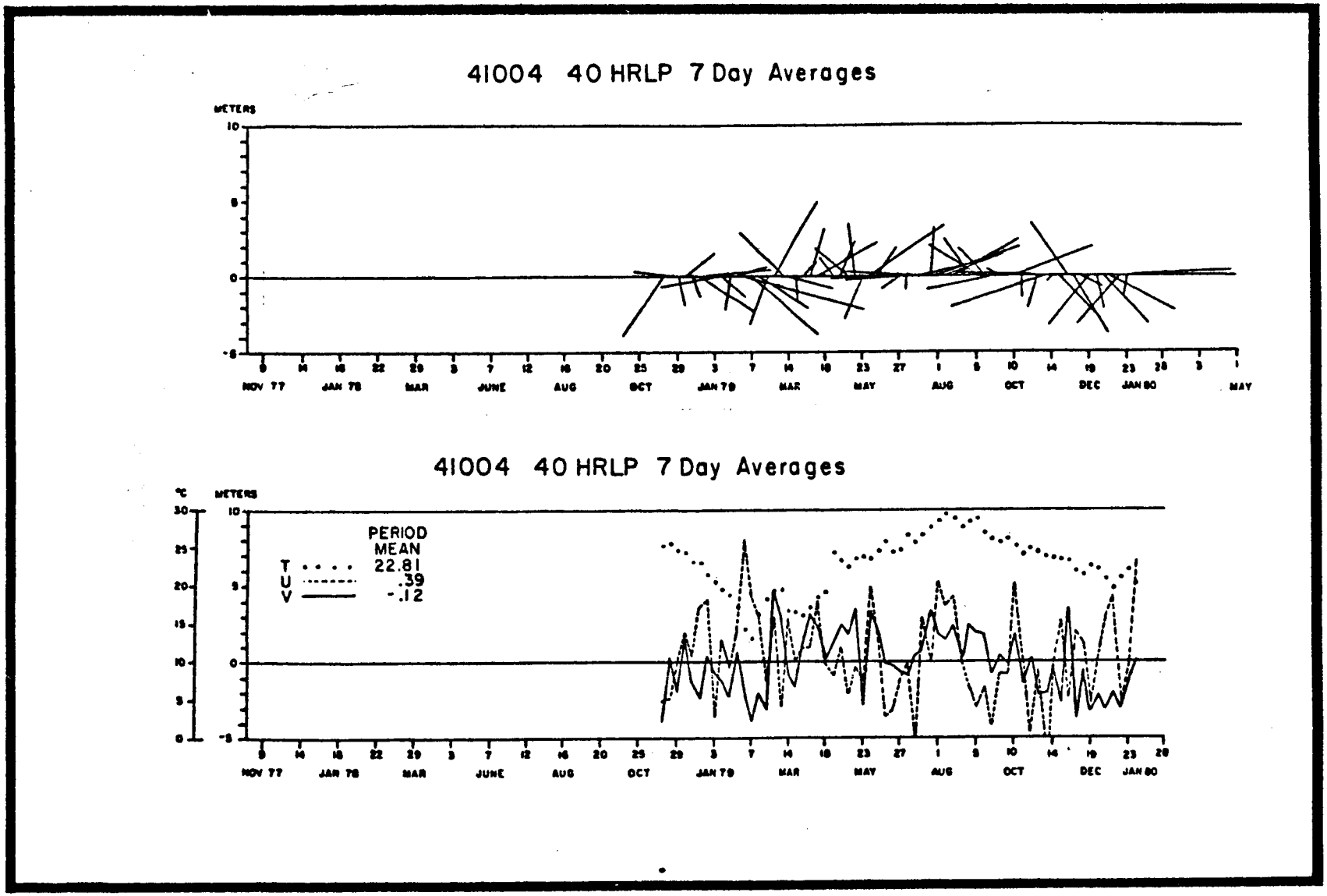

Figure 4.7-6. Seven-day averages from NDBO site 41004 from October 1978 to December 1979.

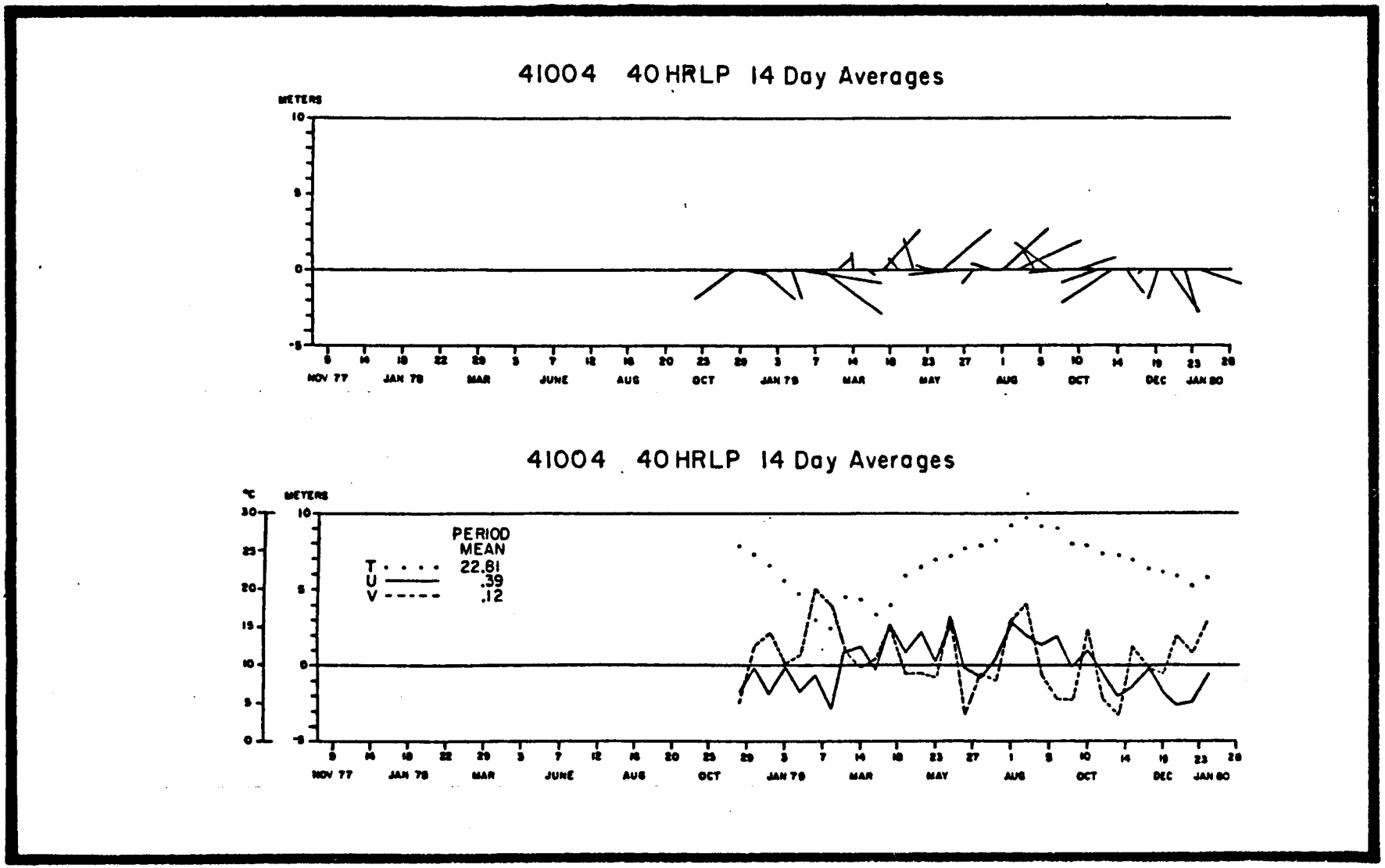

Figure 4.7-7. Fourteen-day averages from NDBO Site 41004 from October 1978 to December 1979.

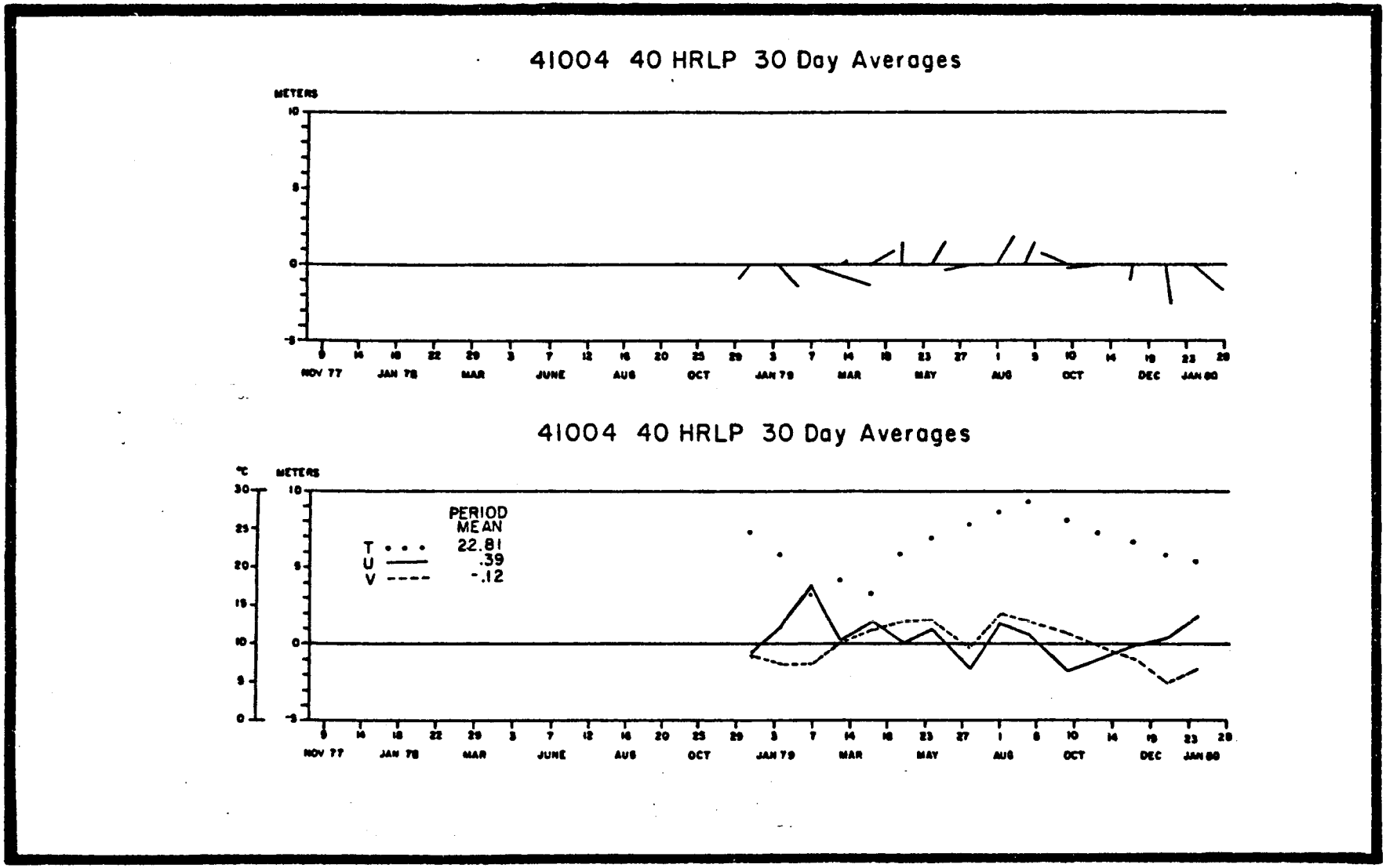

Figure 4.7-8. Thirty-day averages from NDBO Site 41004 from October 1978 to December 1979.

4.7.3 Coastal Sea Level

The 7-, 14-, 30-, and 90-day means of sea level at Charleston display a strong relationship to coastal wind direction and magnitude. In effect, northerly and easterly winds cause a rise in coastal sea level while southerly and westerly winds cause coastal sea level to fall. Bi-weekly, monthly, and seasonal sea level variations also can be attributed to the water column thermal structure and to longshore atmospheric pressure gradients. Examples of the variously de-meaned tide gauge data from Charleston Harbor for 1979 are shown in Figures 4.7-9 to 4.7-11. Interestingly, these data are not substantially different in their annual cycle from data collected during prior years from the same site or from other SAB sites, such as Beaufort an open ocean site, or from Wilmington, a site 45 km upstream from the mouth of an estuary (Figure 4.7-12).

During January and February, water temperatures are the lowest of the year, as shown in Figure 4.7-13. Due to atmospheric cooling, sea level is at its yearly minimum, standing 20-25 cm below mean annual datum. This process occurs sequentially during the fall with the regular passage of cold fronts and associated air masses. During late winter to early spring, when the heat content of North Atlantic Central Water (surface to 100m depth) is at its lowest, and toward March as the heat content begins to rise, the density structure changes and the sea level rises. Additionally, and at least for the 1979 period, the Gulf Stream itself was well offshore of the shelf break at Charleston (cf. Figure 4.7-13). This could also cause a drop in the mean sea level at the coastline. The opposite argument could also be made. That is, as the Gulf Stream moves offshore (onshore), sea level at the coast should rise (fall) to maintain geostrophic balance.

The closeness of the Gulf Stream to the coast off Charleston throughout the rest of 1979 (Figure 4.7-13) bears only an occasional and perhaps coincidental relation to the signature of sea level at the coast (Figures 4.7-9 - 4.7-13). For the most part, the 1- week to 1-month variability of sea level at Charleston is due to an accumulation of 2- to 10-day fluctuations superimposed on the large scale (seasonal to annual) low-frequency background fluctuations provided by increasing and/or decreasing heat content of North Atlantic Central Water. These 2- to 10-day fluctuations are caused by atmospheric cyclones and anticyclones propagating across the SAB on a regular 5 to 10 day basis, especially from October through February.

4.7.4 Very High Resolution Radiometer (VHRR) Imagery

Within the past decade a catalogue of VHRR impressions of Gulf Stream location, taken in a series of snapshots, has revealed the large spatial and temporal variability of the GS. It is now known that water masses frequently erupt from but remain attached to the westernmost boundary of the GS and move to the northeast (Figure 4.7-1). As discussed previously, the GSF takes an abrupt and persistent turn at 32°N 79°W. This phenomenon is evident in nearly all VHRR images collected since 1975. A summary of VHRR images collected from December 1978 to December 1979 is shown in Figure 4.7-13 in terms of the monthly maximum and minimum excursions of and monthly mean locations of the GSF relative to the 200-m isobath perpendicular to Charleston and Cape Romain.

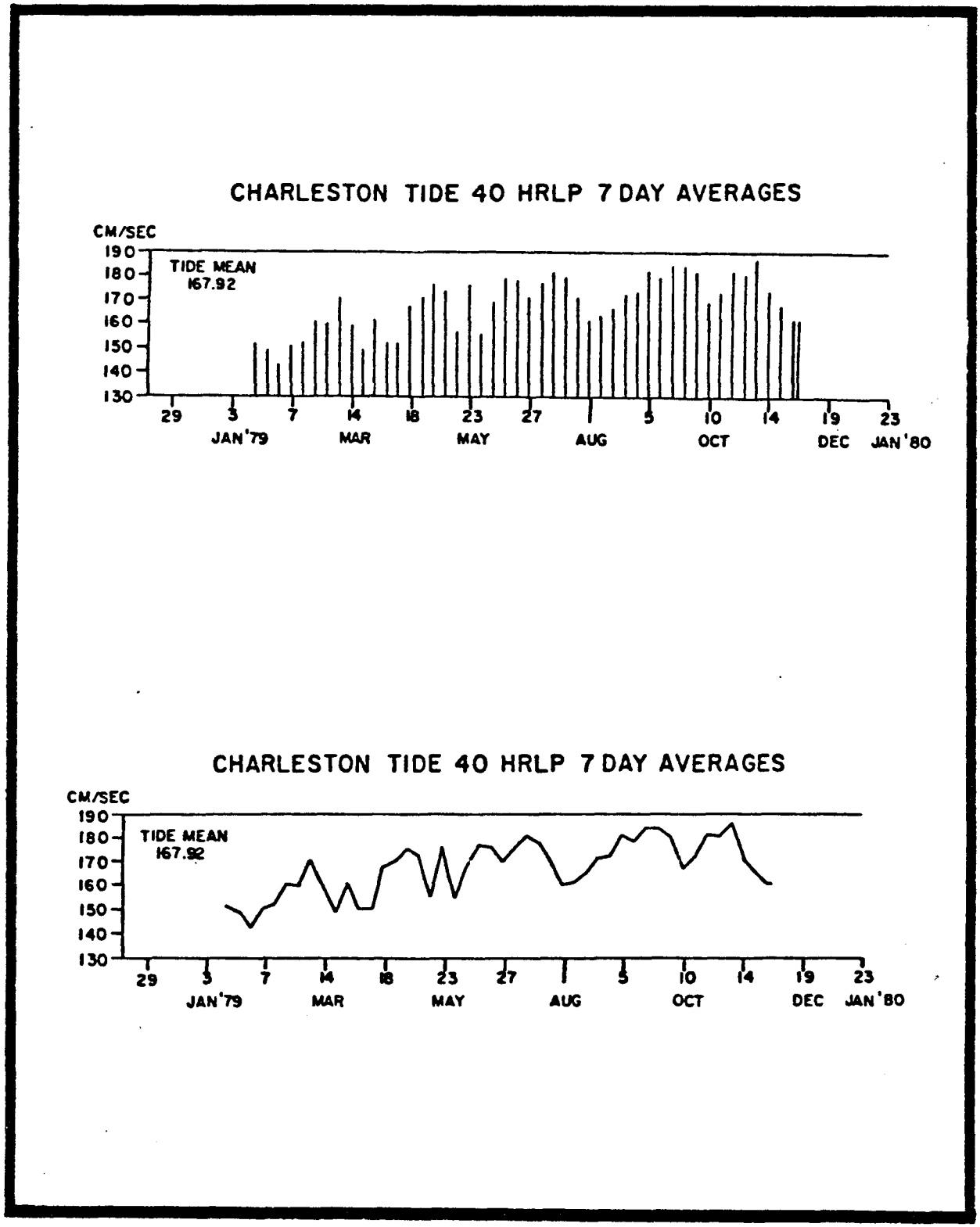

Figure 4.7-9. Seven-day averages for Charleston tide for 1979.

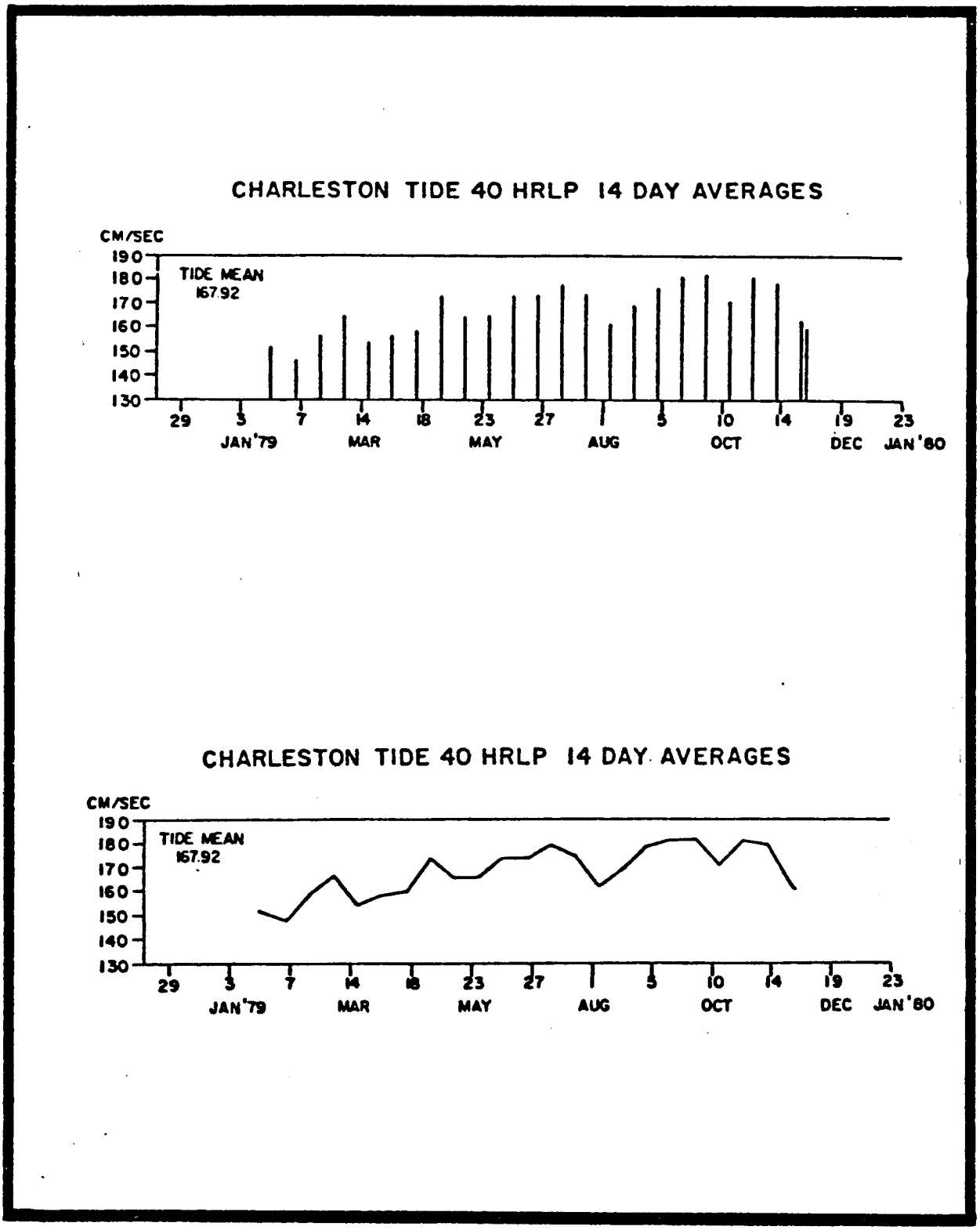

Figure 4.7-10. Fourteen-day averages for Charleston tide for 1979.

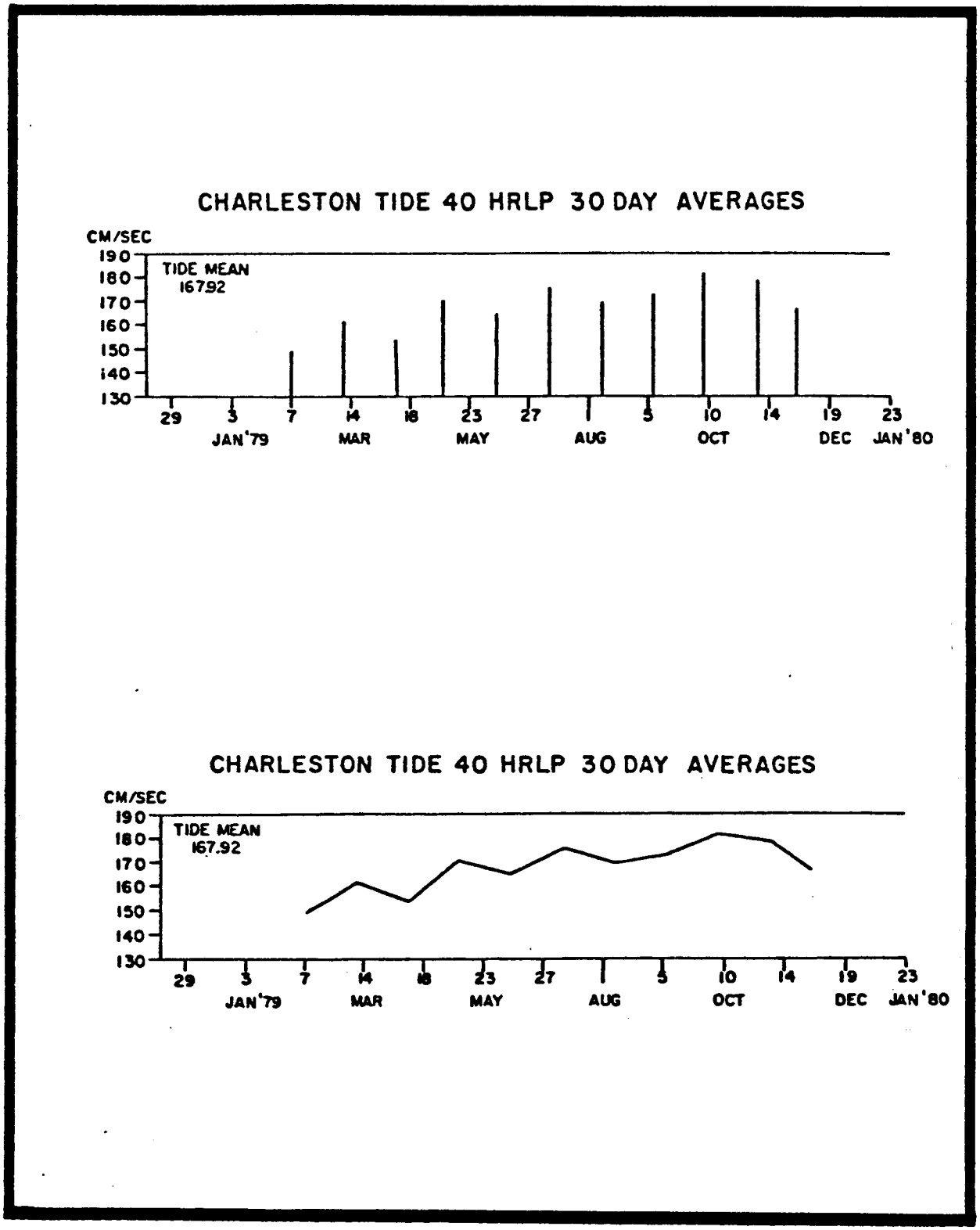

Figure 4.7-11. Thirty-day averages for Charleston tide for 1979.

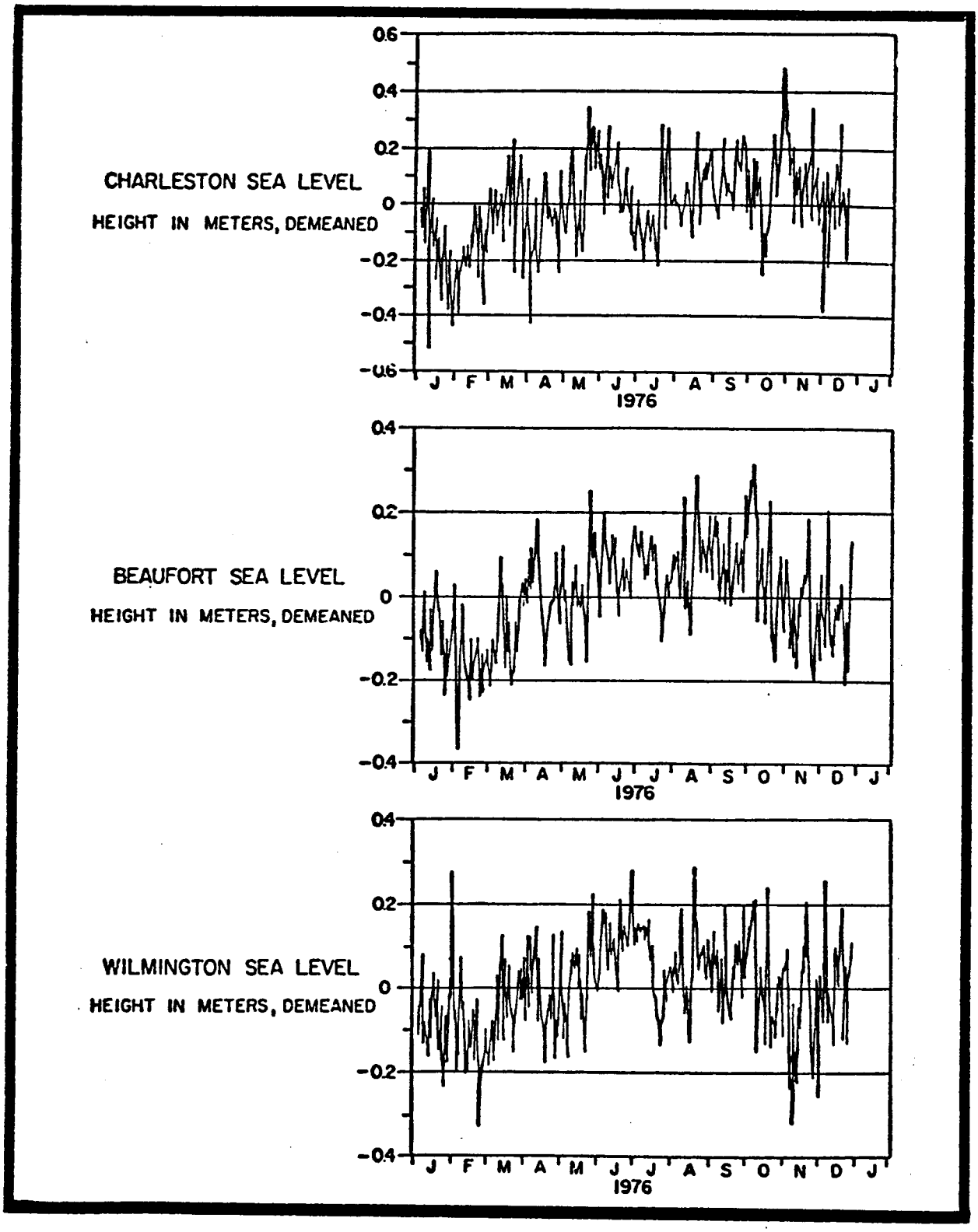

Figure 4.7-12 Time series of sea level at Charleston, S.C., Beaufort, N.C., and Wilmington, N.C., for 5 January to 27 December 1976.

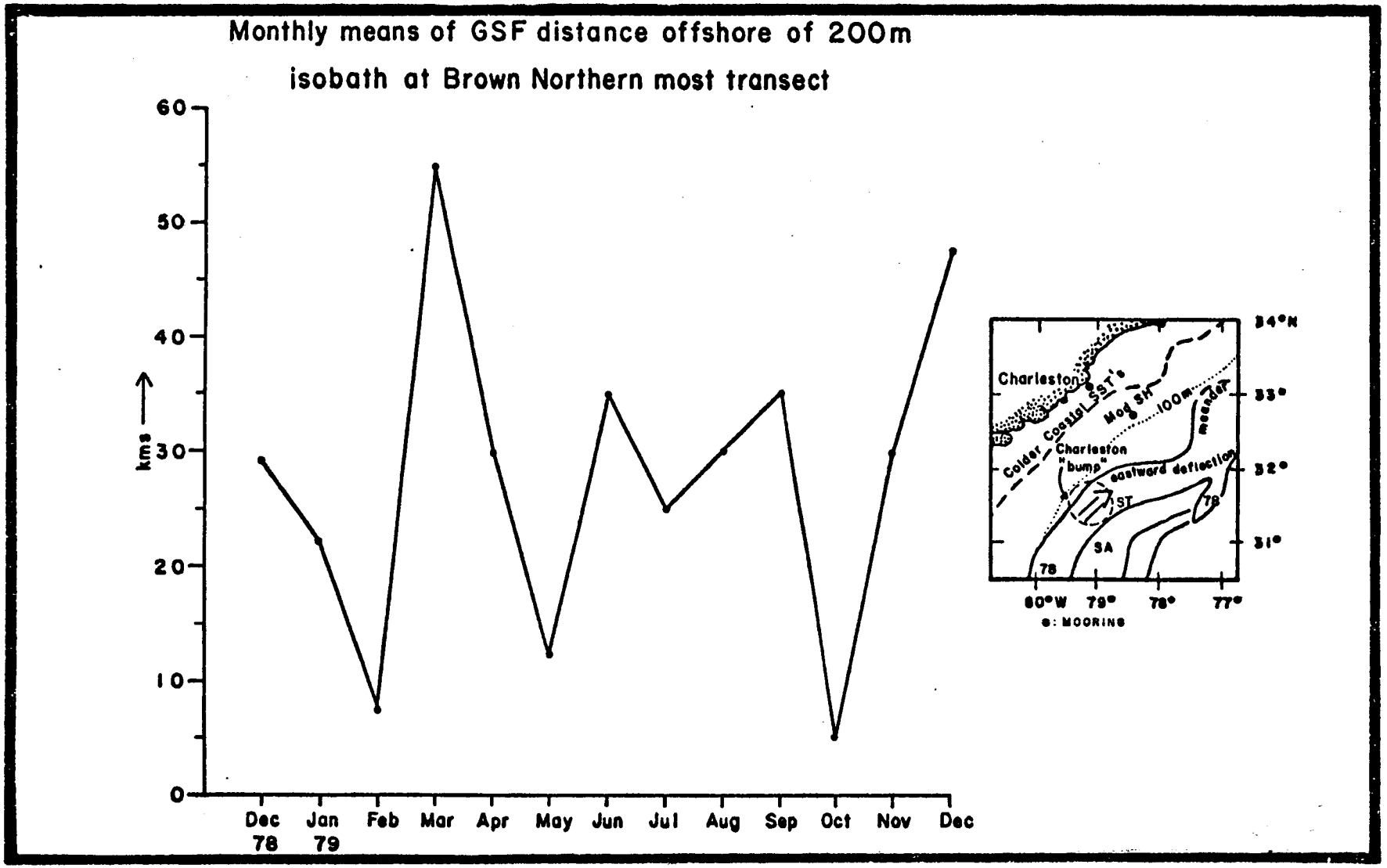

Figure 4.7-13. A summary of the culling of VHRR images collected from December 1978 to December 1979 in terms of monthly maximum and minimum diabathic excursions, and monthly mean locations of the Gulf Stream front relative to the 200-m isobath perpendicular to Charleston and Cape Romain.

Rooney et al. (1978) predicted that the Gulf Stream, and the GSF, would be deflected farther offshore of the Charleston Bump during periods when GS transport was reduced. These authors suggested an inverse relationship between deflection distance and transport. Unfortunately, the variability of transport and its periodicity have not been documented conclusively. While a number of investigators have made spatially intensive measurements at different times of the year, there is apparently no reliable report of the fluctuations at periods of months to seasons. Therefore the Rooney et al. (1978) theoretical prediction may be correct but there is no immediate way of checking it. The results shown in Figure 4.7-13, while curious, may simply reflect the norm of the so-called mean. Moreover, from year to year, these monthly means may not be repeatable. Culling of additional years of VHRR imagery may help to address these questions. The curve shown in Figure 4.7-13 bears a striking resemblance to averaged sea surface and subsurface temperatures collected in 45-m of water at a point on the transect line shown in Figure 4.7-13.

4.7.5 Air and Sea Surface Temperatures

Plots of 7-, 14-, and 30-day means (7-DM, 14-DM, and 30-DM) of the 40-HLP time series of temperatures as measured at both the sea surface and 10 m above the surface and their differences at Buoy 41004 (see Figure 4.7-1) and the coastal stations during the period November 1978 - January 1980 are shown in Figures 4.7-14 - 4.7-16. The most prominent features are the annual minimum at the end of January and the annual maximum in August. Thirty-DM buoy sea-surface temperature (SST) is always warmer than at-sea air temperature (buoy air temperature = BAT) and, except for a period in July, is also higher than Charleston (CAT) as well. The three curves track quite closely from late March through September. A 6-month period is essentially laterally isothermal, from coastal station to buoy station, and vertically isothermal across the air-sea boundary. Sea-surface temperatures are slightly higher than air temperatures except for July when the SST is briefly and slightly surpassed by land-based temperature.

Although the three 30-DM temperature curves shown in Figure 4.7-16 display general similarity in structure, there is a 6-month period of a substantial horizontal (CAT to BAT) temperature gradient extending from October into March. The maximum difference between CAT and BAT is about 6°C and occurs around 20 February. It is not known whether this maximum in horizontal temperature difference would repeat itself during the 1979/80 winter since the data ends in January 1980. By the last week in December 1979, CAT and BAT achieve a difference of 7°C which then appears to decrease. As shown in Figure 4.7-16, the sea surface appears to experience a brief warming period at the same time that there is an apparent maximum in the horizontal gradient. This can be explained by considering both Figure 4.7-15, which defines the 14 DM's at the three stations, and Figure 4.7-14, which describes the mean monthly location of the shoreward edge of the GSF, as determined from VHRR imagery.

The 14-DMs show that although both air and sea surface temperatures rose and fell during February and March, the rise and fall occurred first and had the largest amplitude in SST, then in BAT, and finally in CAT. It seems that there was a propagation of a sudden warming and cooling event from the ocean to the atmosphere and finally to the coast. The sudden warming of

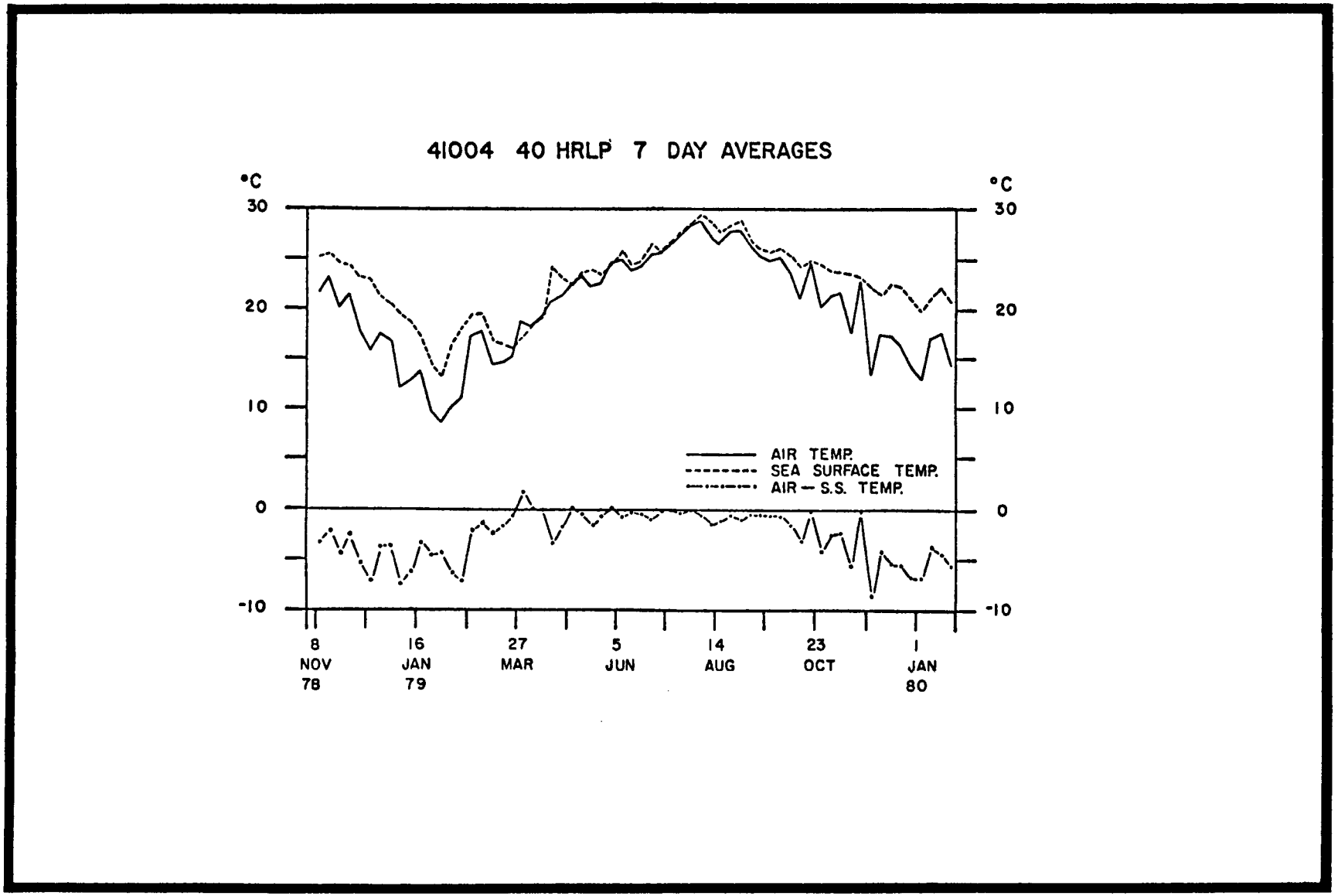

Figure 4.7-14. Seven-day averages of the 40-HLP time series of temperatures as measured at both the sea surface and 10 m above the surface, and their differences at NDBO Site 41004.

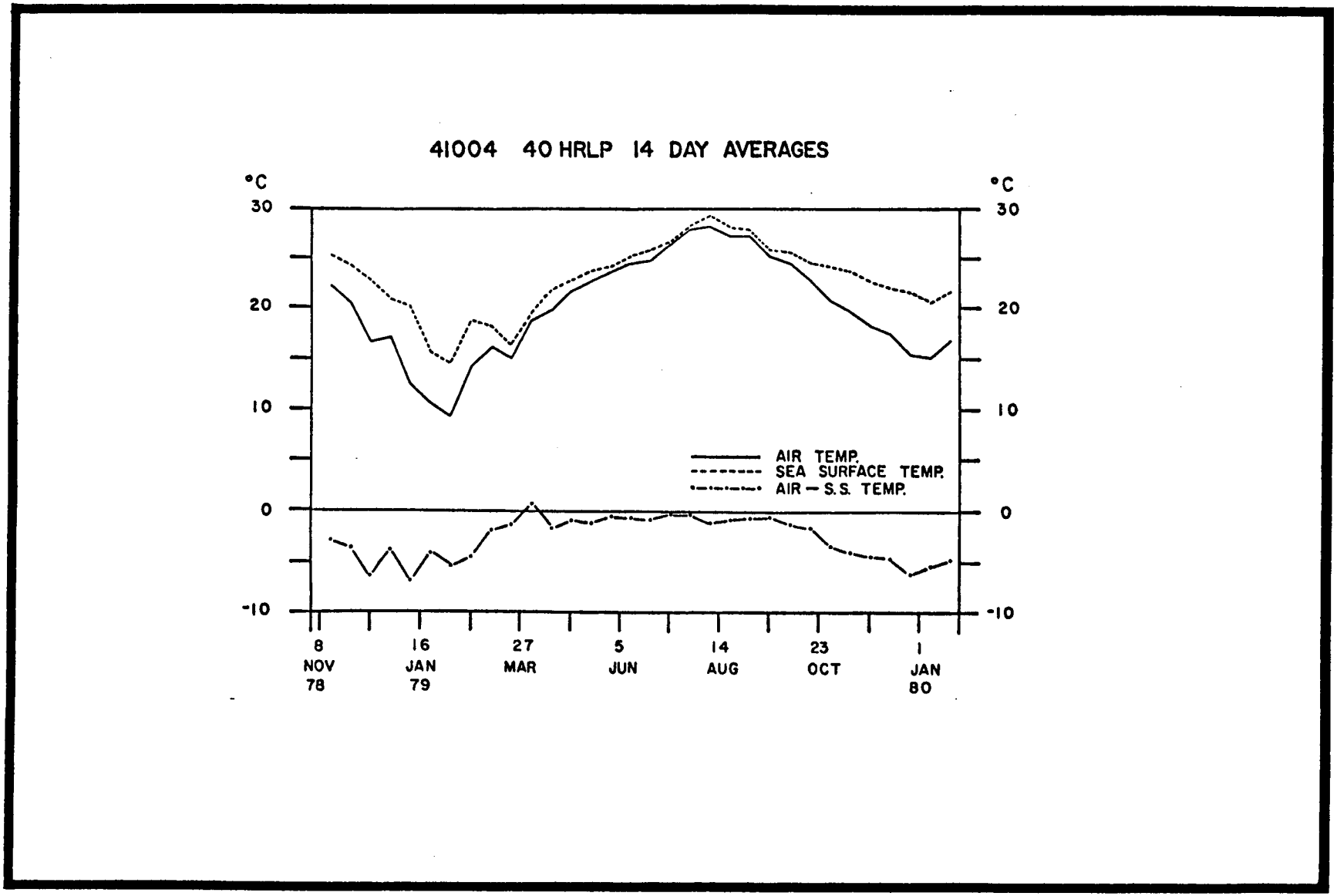

Figure 4.7-15. Fourteen-day averages of the 40-HLP time series of temperatures as measured at both the sea surface and 10 m above the surface, and their differences at NDBO Site 41004.

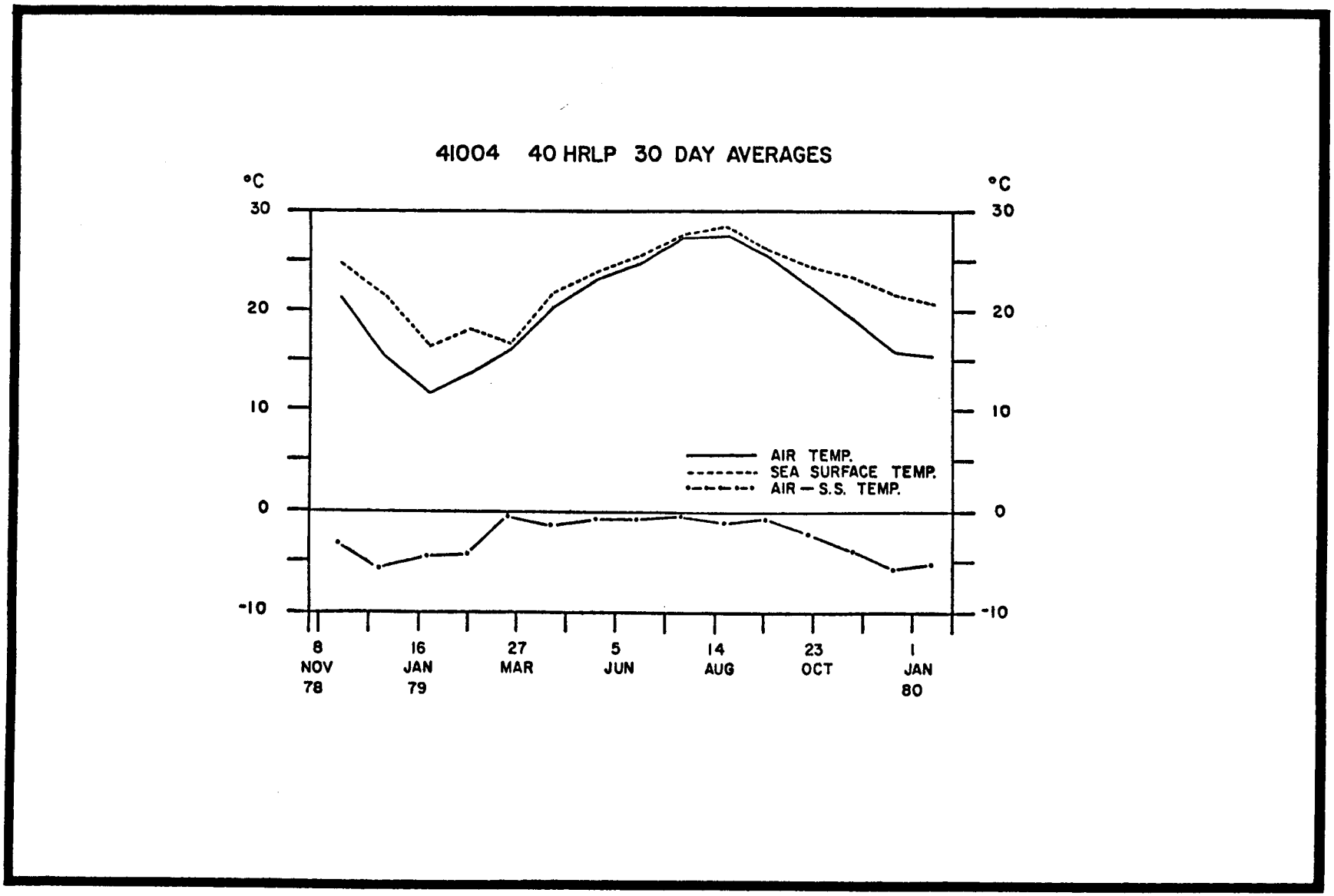

Figure 4.7-16. Thirty-day averages of the 40-HLP time series of temperatures as measured at both the sea surface and 10 m above the surface, and their differences at NDBO Site 41004.

the sea surface first occurred about 8 February, while the coastal warming pulse was delayed until 20 February. The three curves assumed the same slopes during late March. A combination of atmospheric and oceanic events could have caused these pulses of relatively warm air and water to appear at the offshore buoy but not at the coastal station until several days later. Consider Figure 4.7-13. During the period in question, the GSF was unusually close to the outer Charleston shelf. This proximity of the GSF to the 200-m isobath occurred during February. Curiously, the GSF then achieved a maximum offshore excursion during March. The two monthly extremes were 7.5 km in February and 55 km in March. It is of note that May and October were also similar months, while during December the GSF was distant from the coastal region. Although the closeness of warm Gulf Stream water to the outer shelf could and should have warmed the entire water column, it is difficult to say that this could account for the warming of CAT. This would require that the oceanic water heat the air mass above and that the air mass then move onshore, northwestward toward the coast. The time history of SST, BAT, and CAT during this period might also be explained as a response to atmospheric heating.

Considering the National Weather Service (NWS) 3-hourly weather maps for the month of February, there was little activity save for the period 5 to 9 February. At 0600 EST on 6 February, a high pressure system (HPS) was centered over Pennsylvania and extended well into the SAB. Flow around the eastward moving system resulted in moderate air flow from the east-northeast. By 0900 EST on the 6th, flow was onshore and from the southeast, bringing warm air toward the coast. By 2100 EST a low pressure system (LPS) centered over the Gulf of Mexico began to expand toward the SAB. Along the northern boundary of the low there was a coalesence of isobars with the southern boundary of the HPS. Additionally the counter-clockwise flow around the low and clockwise flow around the coupled high joined seaward of Charleston at about 30°N 77°W and resulted in strong southeasterly flow toward Charleston. By 0600 EST on the 7th the LPS had advanced past Charleston and warm air continued to move into the area.

The descriptions of the brief time histories of the HPS and LPS are important because these two events constituted the major atmospheric activity in the SAB during February 1979. Moreover, they resulted in the strong, sustained, northwest flow of warm air toward Charleston and thus encountered the buoy before the coast.

Still, it should not be forgotten that the GSF moved shoreward during February and then seaward during March. Additionally, minor upward blips occur in the buoy (BAT and SST) 14-DM temperature curves for both May and October when the GSF was relatively close to the coast. Presumably the observed negative air-sea temperature difference could cause a sea-surface buoyancy flux. This could provide for an effective surface stress, akin to, but apart from the wind, to mechanically drive circulation (Pietrafesa and Janowitz 1978). In addition, the negative difference might possibly modify atmospheric storms as well. The air-sea heat exchanges of both latent and sensible heat, at this time of year, may be substantial.

As is noted in Figures 4.7-14, 4.7-15, and 4.7-16, the coastal waters off Charleston generally act as a heat source for the local atmosphere since the buoyancy flux is upward, perhaps due to the presence of the GSF. From mid-spring to late summer the coastal waters and atmosphere do not exchange

much heat. During fall and winter, a great deal of heat is extracted from the ocean by the atmosphere, except for March and December when the GSF achieves its maxima in offshore excursion. The disappearance of the GSF from proximity to the outer shelf in December appears to result in a drop in the increasing upward heat exchange from fall to winter, and in a brief two-week reversal in the exchange in March and April as the temperature curves are beginning to coalesce. This is shown quite clearly in Figure 4.7-14. The general effect of a negative buoyancy flux at the surface is to create an effective stress in the northerly alongshore direction (Pietrafesa and Janowitz 1979a), with $\partial v/\partial z = 0$, v being the alongshore current, positive to the north and z being positive upward.

The primary effect of cooling could be to drive a northerly longshore upper water-column flow and possibly a southerly near-bottom flow. Since fluid parcels move onshore and offshore near the surface and bottom boundaries, respectively, several results could occur. First, the surface layer could bring warmer offshore waters onshore and the cooler bottom-layer waters offshore, so the surface (bottom) layer could act as a heat source (sink) for the rest of the water column, resulting in an increase in the vertical temperature difference. This assumes that there are warmer waters offshore. Alternatively, if there are cooler waters offshore, then the opposite would occur, i.e., the surface (bottom) would transport colder (warmer) waters onto (off) the shelf and the vertical temperature gradient would decrease. The current meter data will have to be culled for the answer to this question.

Recall that December was a month when the GSF reached an extreme in offshore migration (Figure 4.7-13) and that a cold temperature cell appeared at CAT, BAT, and SST (Figures 4.7-14 - 4.7-16). Additionally, BAT-SST values were more negative than at any other time in 1979. The departure of the GSF from the upper slope could have caused the temperature drops, but it is more likely that such a dramatic drop would result from a large, persistent mass of cold air suddenly moving into the region. Weather maps show that a large high pressure system covered the eastern seaboard for much of December and was most intense during the first several weeks. Once again, the combination of a large atmospheric event and movement of the GSF occurred in the right sense so as to reinforce one another. Since the temperature drops occurred nearly simultaneously and the flow of air was nearly perpendicular to the Charleston transect (our stations are positioned at either end), it could be concluded that the atmospheric event was principally responsible for the temperature drop. Note though that negative buoyancy flux processes are augmented at the surface and consequently along-shore currents can be driven by buoyancy stresses as well as by frictional wind stresses. They would work to drive upper water column currents to the north-northeast and near bottom currents to the southwest-southeast (Pietrafesa and Janowitz 1979a).

4.7.6 Mean Currents and Hydrography

The bases for the following discussion of weekly to seasonal means of currents and hydrography along the Charleston transect are observations at the Charleston Long Term Mooring site (CLTM) in Figure 4.7-1.

Examining 3-month averages of subsurface current speeds from November 1977 through October 1979 in Figure 4.7-17 shows that 3 m above the bottom in 40 m of water, the current always has southerly and usually easterly components. Over time scales of the order of a month, however, the long-term mooring bottom currents can be quite variable in both magnitude and direction. Of the nineteen months shown in Table 4.7-1 and Figure 4.7-18, thirteen months indicate a southerly component to the flow. It is of note that the monthly to seasonally averaged bottom flow is virtually never onshore at the CLTM site. Rather, flow is alongshore and to the south, thus slightly offshore, during the fall, more offshore during winter, offshore but alongshore to the north during March, and finally, very strongly to the south-southwest from mid-spring through summer.

Drifter study results of Bumpus (1973) suggest monthly current directions (not vectors) that agree 62.5% of the time with monthly means observed at the CLTM for near-bottom flow (Table 4.7-1), during the months of the year when Bumpus was willing to speculate on the monthly means. Over a full year period Bumpus' monthly drifter results were representative only 42% of the time. The same percentage applies for Bumpus' surface drifter data relative to the monthly averaged, near-surface current data. Of course, this comparison of drifter versus mooring data may be inappropriate, since the data were collected during different years and because the current meters are at neither the surface nor the bottom while the positively buoyant drifters were designed to float at the surface and slightly negatively buoyant to move along the bottom.

Three-monthly means (3MM), i.e., 90-day averaged, seasonal currents at the upper site, 10 m from the surface, show southerly flow during the period November 1977 through January 1978, then northeasterly flow from February through July 1978, and finally south-southwesterly flow from August to November 1978. The November 1978 through January 1979 mean flow was to the northeast, quite different from the mean for the same three months a year earlier. The difference is that from mid-December to mid-January 1979, there was no speed data available; consequently, that entire data set is biased toward the south by a large, persistent southerly current which occurred during the last week of November 1977.

Near bottom 3MM currents were either alongshore and to the southwest or slightly offshore, principally alongshore and to the south-southeast. In any case, the seasonal means were all southerly. Monthly means were southerly to southeasterly except for March to May and November in 1978 and February to March in 1979 when these currents were directed to the northeast.

In general the mid-depth currents, those measured 17 m from the surface, track the time series of near-surface currents almost identically (Figures 4.7-17 to 4.7-25). Current speeds and directions are virtually indistinguishable in the upper and middle water column, except for a 10-20% reduction in magnitude and a slight (1-10°) counterclockwise rotation of the mid-column vector relative to the near surface.

The previous discussion of sub-weekly sea level variability indicated that there is a strong correlation between coastal winds and coastal sea level. We now investigate the meaned-current time series with those of the coastal winds and coastal sea level.

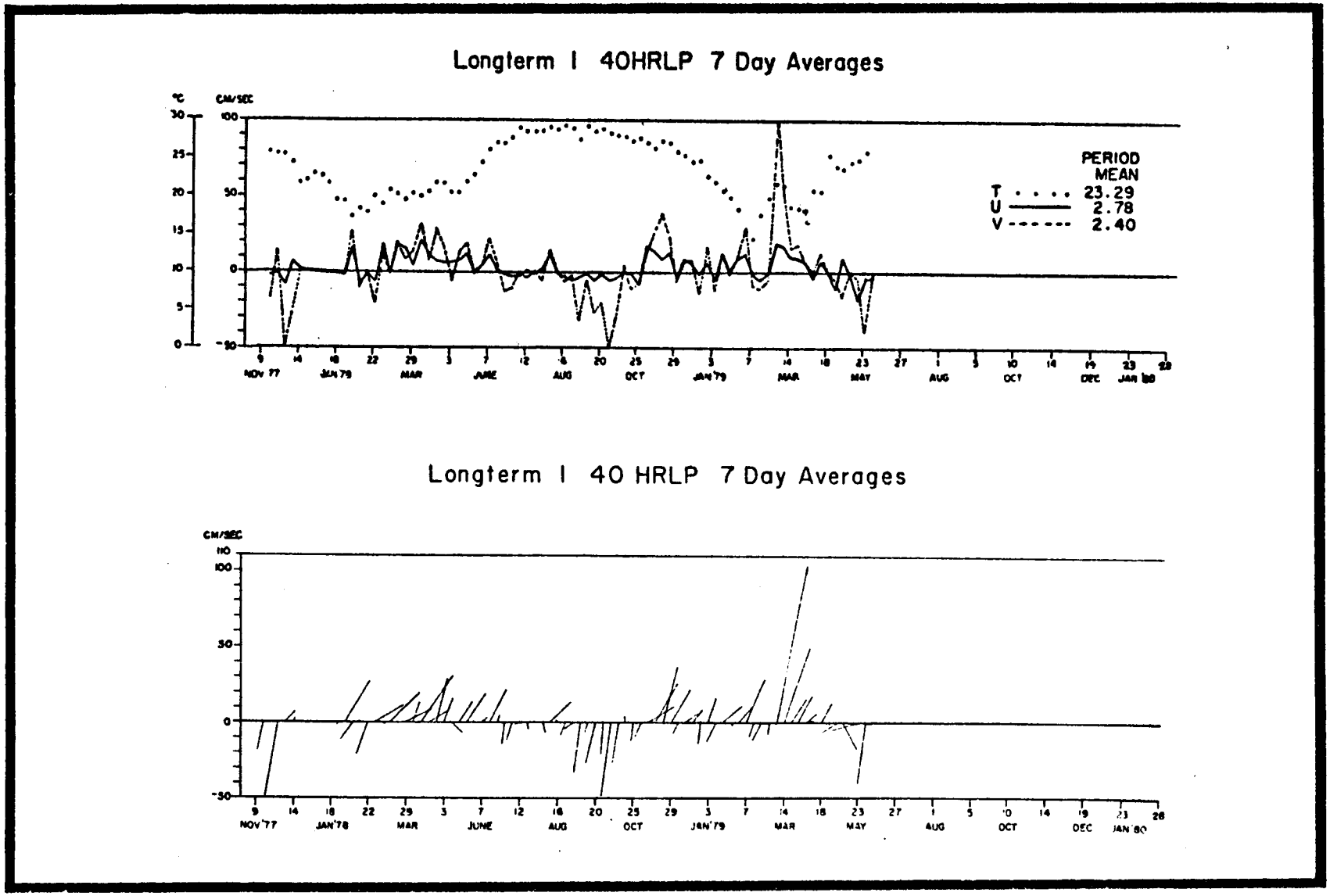

Figure 4.7-17. Long Term 1, 40-HLP, 7-day averages.

		Wind Direction Chas	Wind Direction Buoy	Bumpus Surface	Long Term Surface	Long Term Surface	Bumpus Bottom	Long Term Bottom	Long Term Bottom
1977	Nov	SW		---	S		---	S	
	Dec	ENE		---	NE	S	---	SSE	SE
1978	Jan	E		---	NE		SW	ESE	
	Feb	SE		---	S		NE	SE	
	Mar	NE		NE	NE	NE	NE	NE	ESE
	Apr	NE		NE	NNE		WNW	NE	
	May	NNE		SW	NE		N	NE	
	Jun	NW		NE	NE	NE	NW	SSE	SE
	Jul	NNE		___	S		SW	SSE	
	Aug	NNW		SW	SSW		___	S	
	Sept	SW		SW	S	SSW	WSW	SSE	SSE
	Oct	SSW		---	S		---	SE	
	Nov	S	SW	---	NE		---	NE	
	Dec	ESE	S	---	SE	NE	---	SSE	ESE
1979	Jan	E	SE	---	NE		SW	SE	
	Feb	ESE	ESE	---	E		NE	ENE	
	Mar	N	NE	NE	NE	NE	NE	NE	S
	Apr	NNE	NNE	NE	S		WNW	S	
	May	N	N	SW	SW		N	SSE	
	Jun	WSW	WSW	NE			NE		
	Jul	NE	NE	---			SW		
	Aug	NNE	NE	SW			---		
	Sept	WSW	NW	SW			WSW		
	Oct	WSW	SW	---			---		
	Nov	SSW	SSW	---			---		

Table 4.7-1. Direction of indicated measurements. All directions given in oceanographic sense; current flows and wind blows towards.

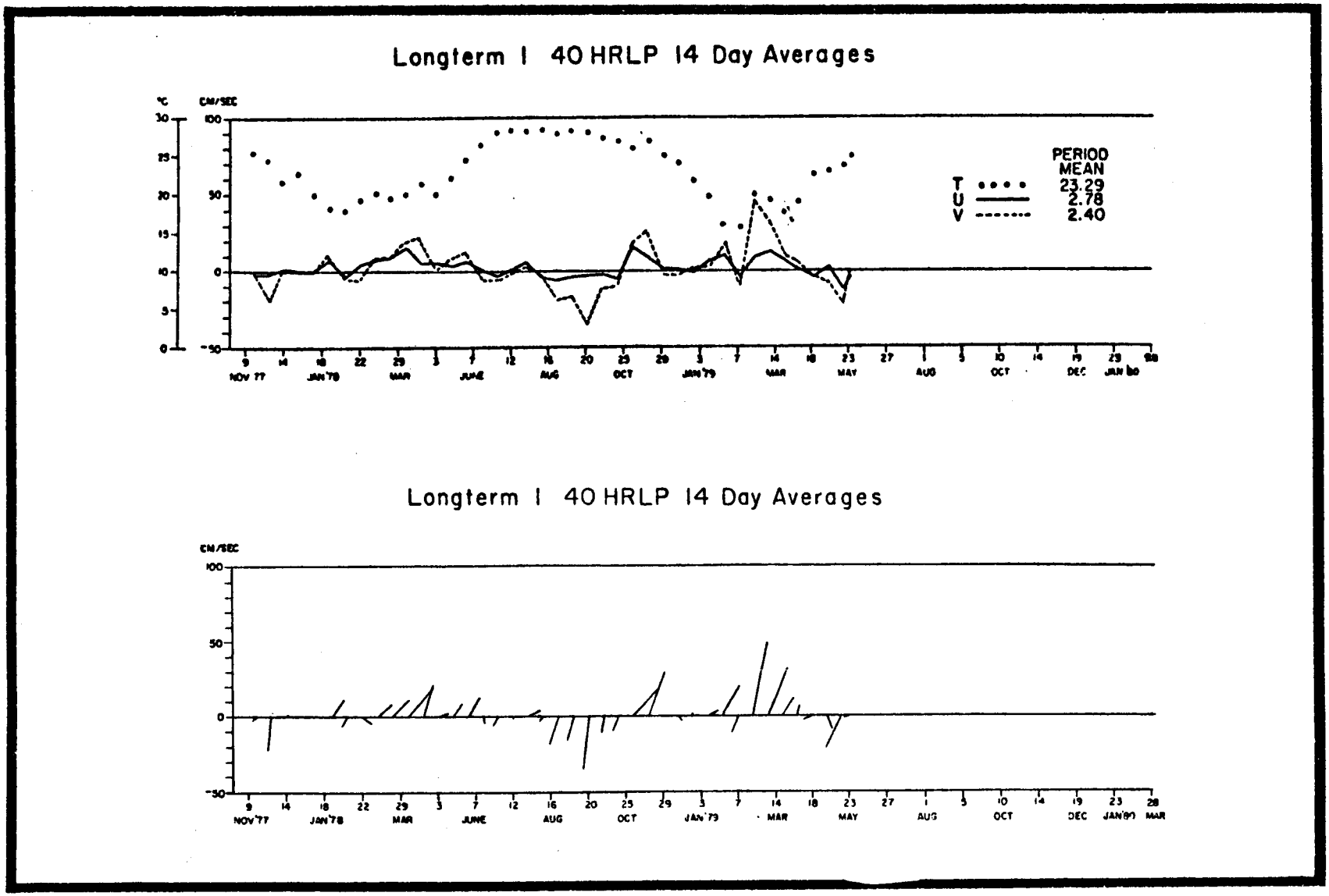

Figure 4.7-18. Long Term 1, 40-HLP, 14-day averages.

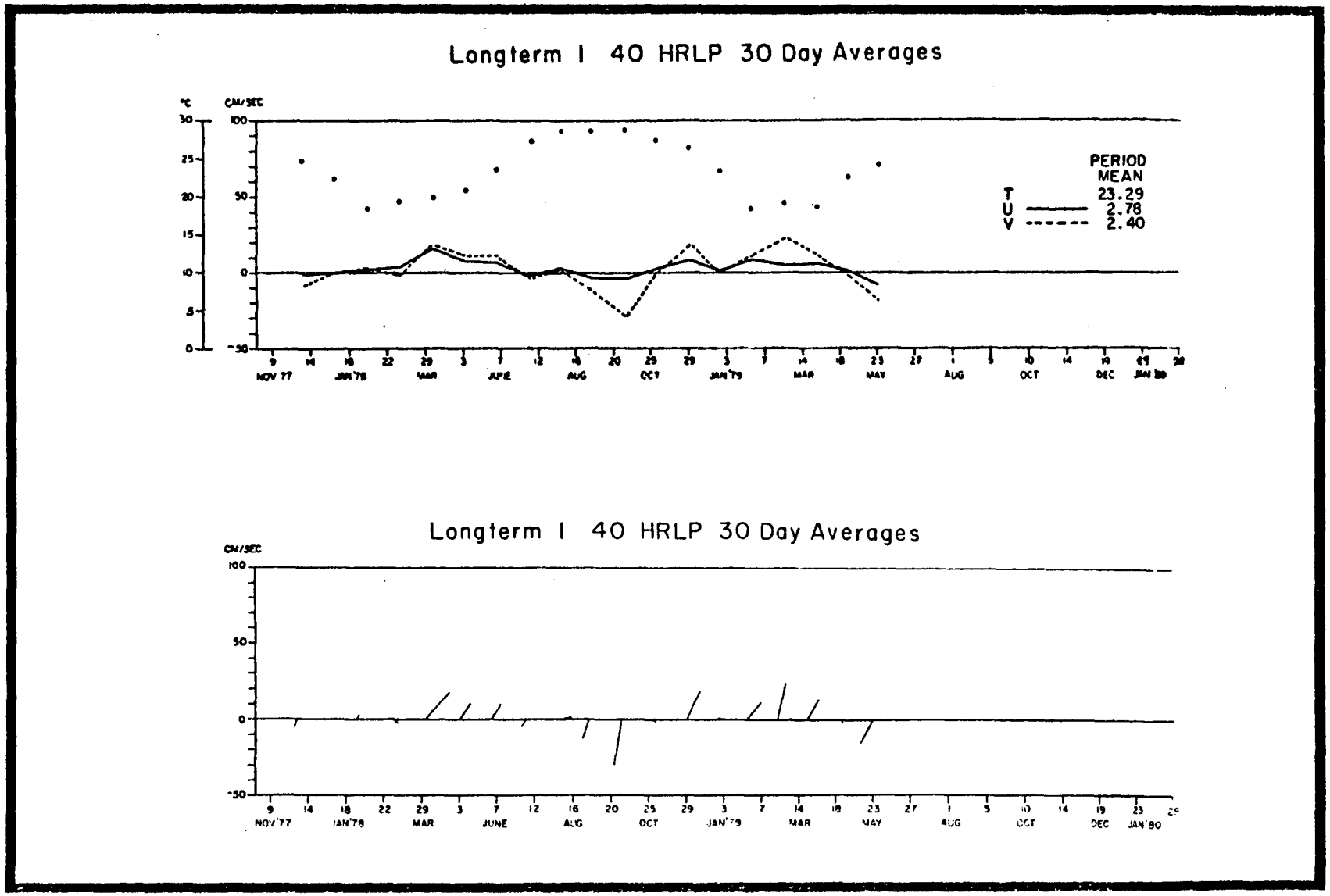

Figure 4.7-19. Long Term 1, 40-HLP, 30-day averages.

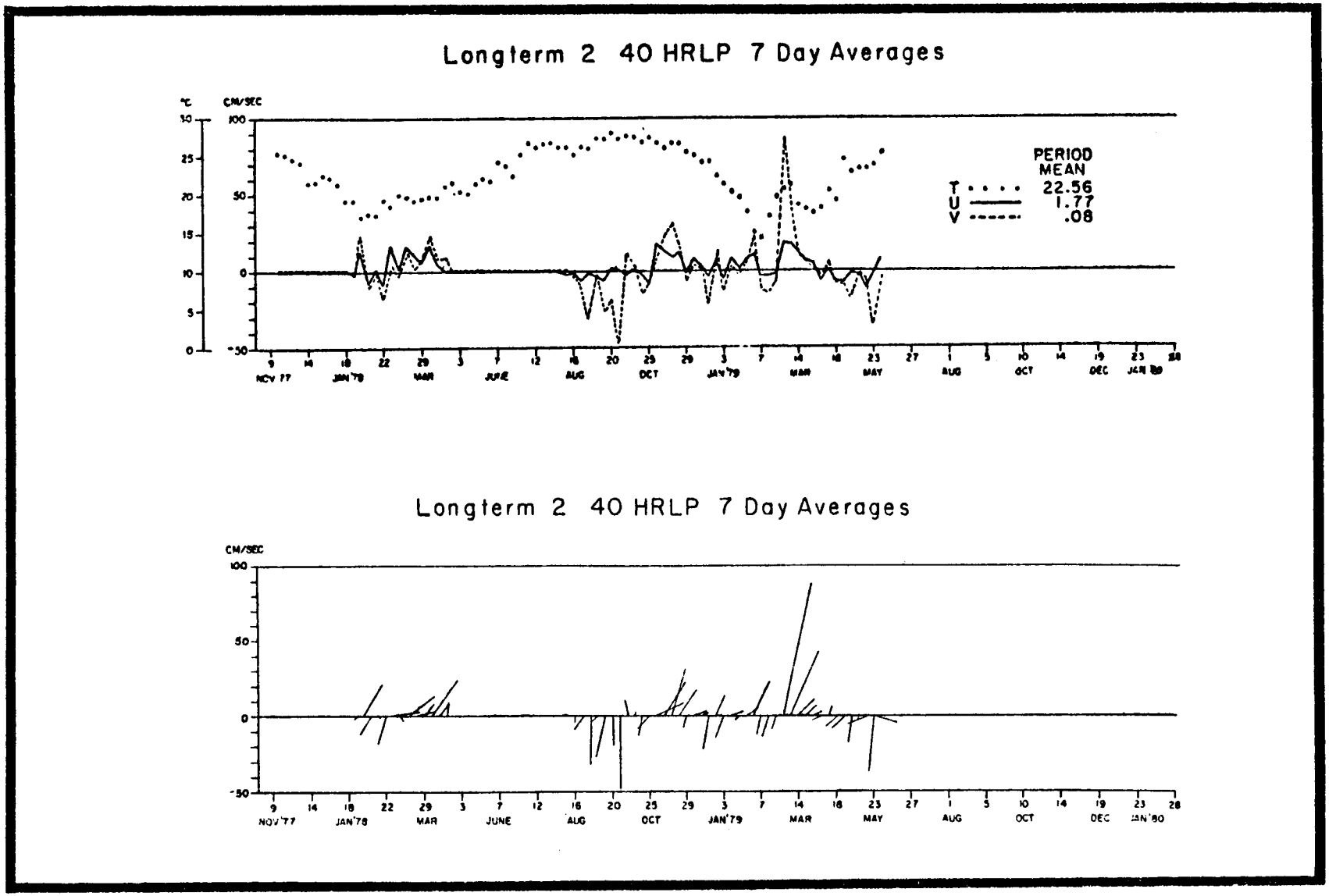

Figure 4.7-20. Long Term 2, 40-HLP, 7-day averages.

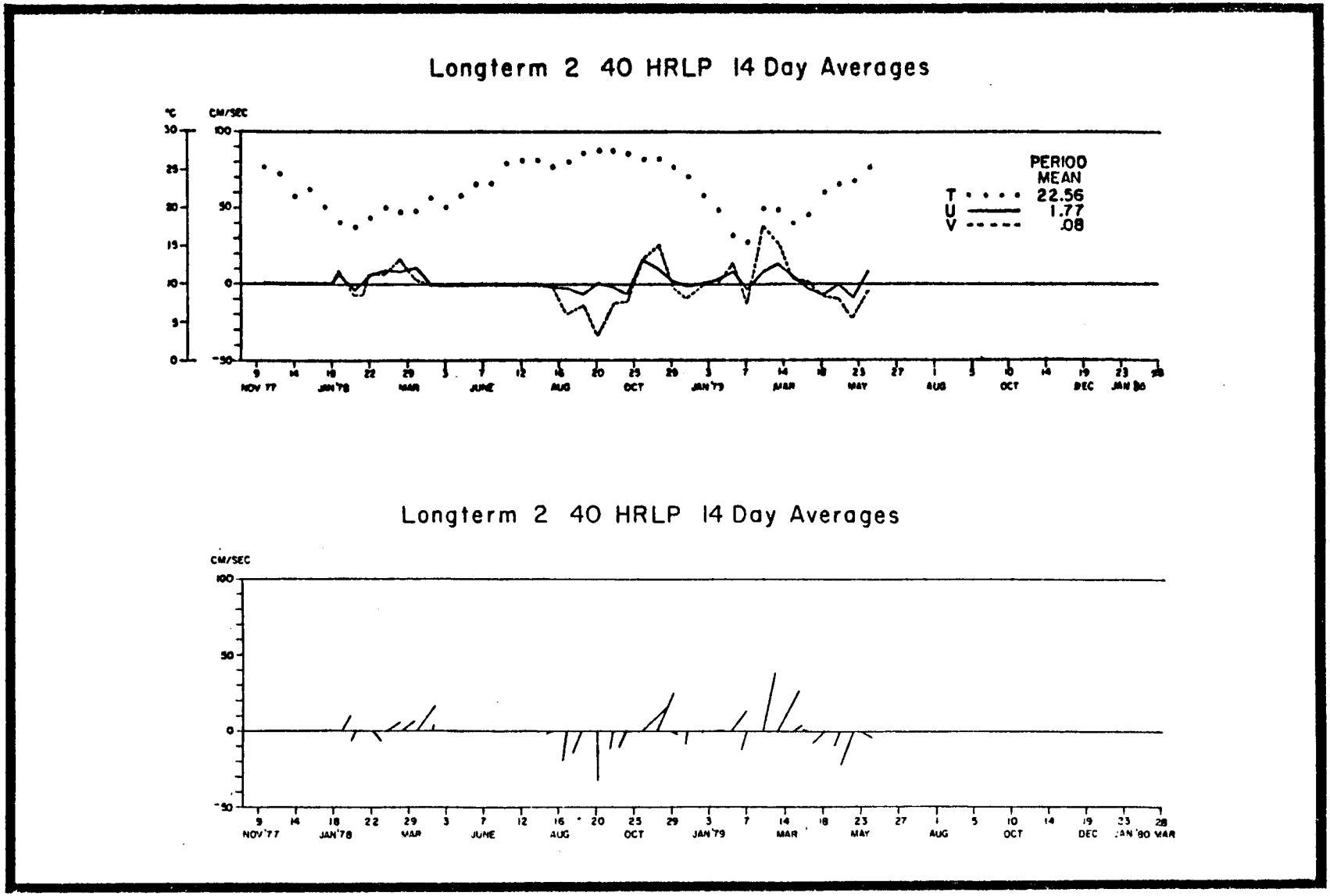

Figure 4.7-21. Long Term 2, 40-HLP, 14-day averages.

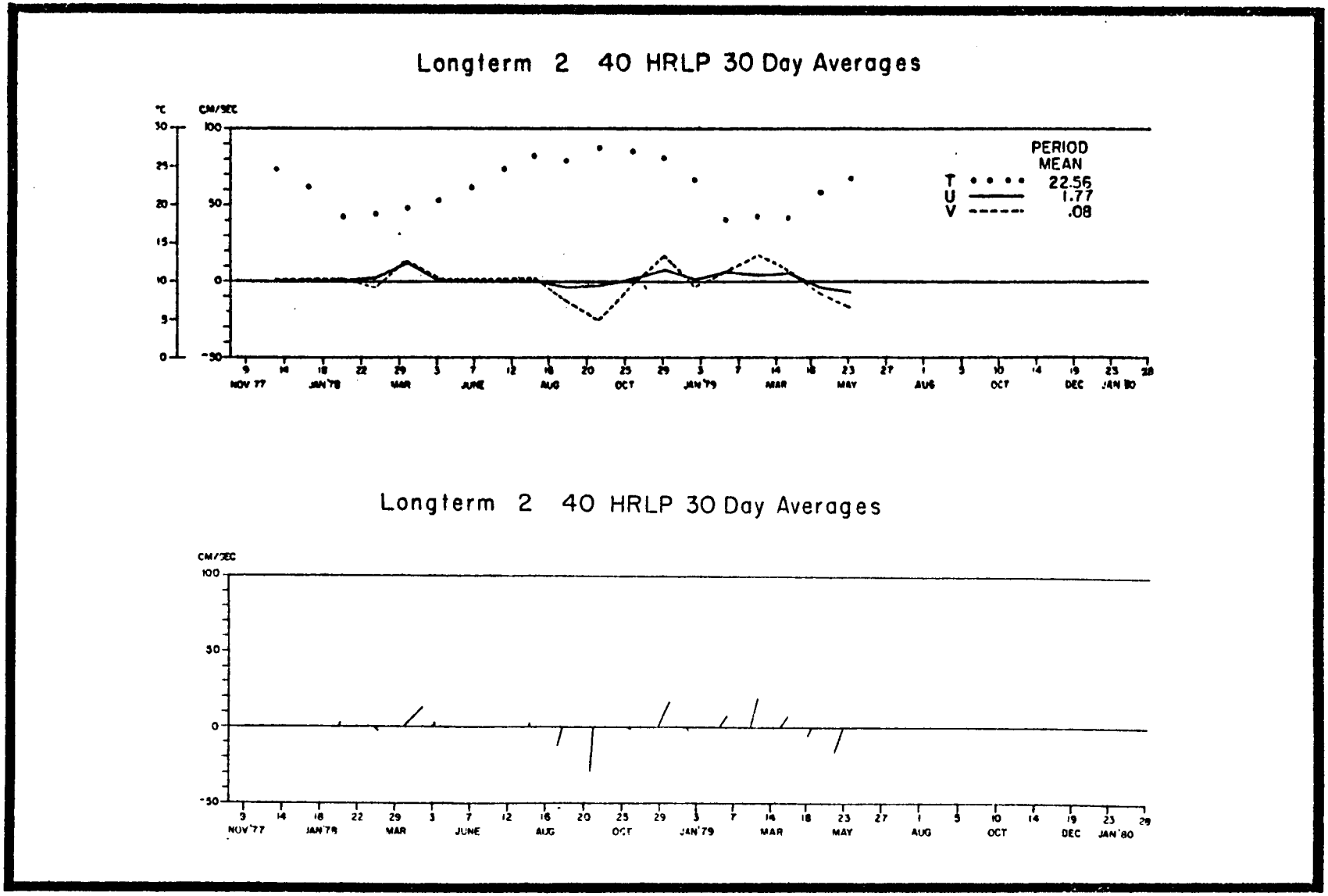

Figure 4.7-22. Long Term 2, 40-HLP, 30-day averages.

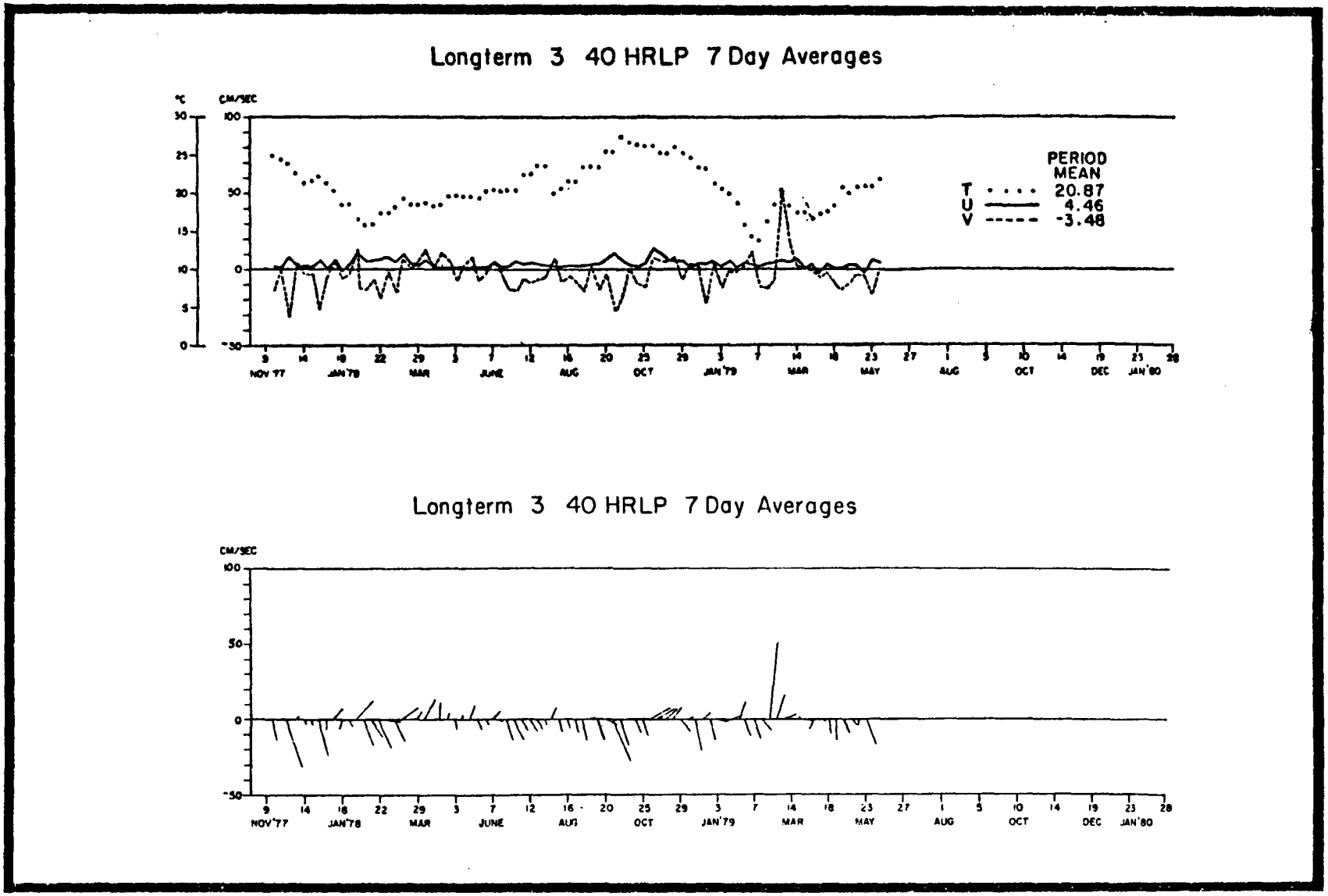

Figure 4.7-23. Long Term 3, 40-HLP, 7-day averages.

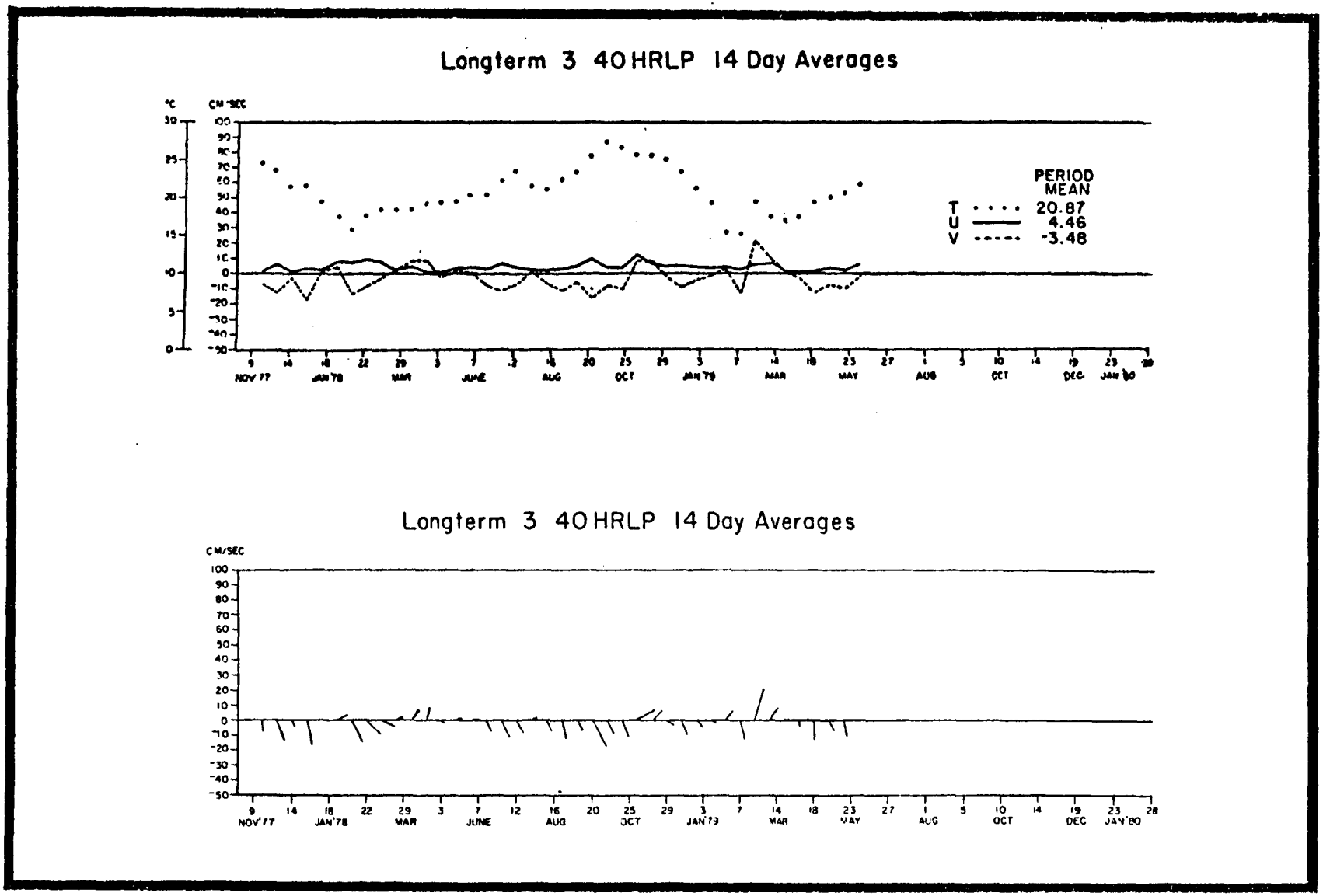

Figure 4.7-24. Long Term 3, 40-HLP, 14-day averages.

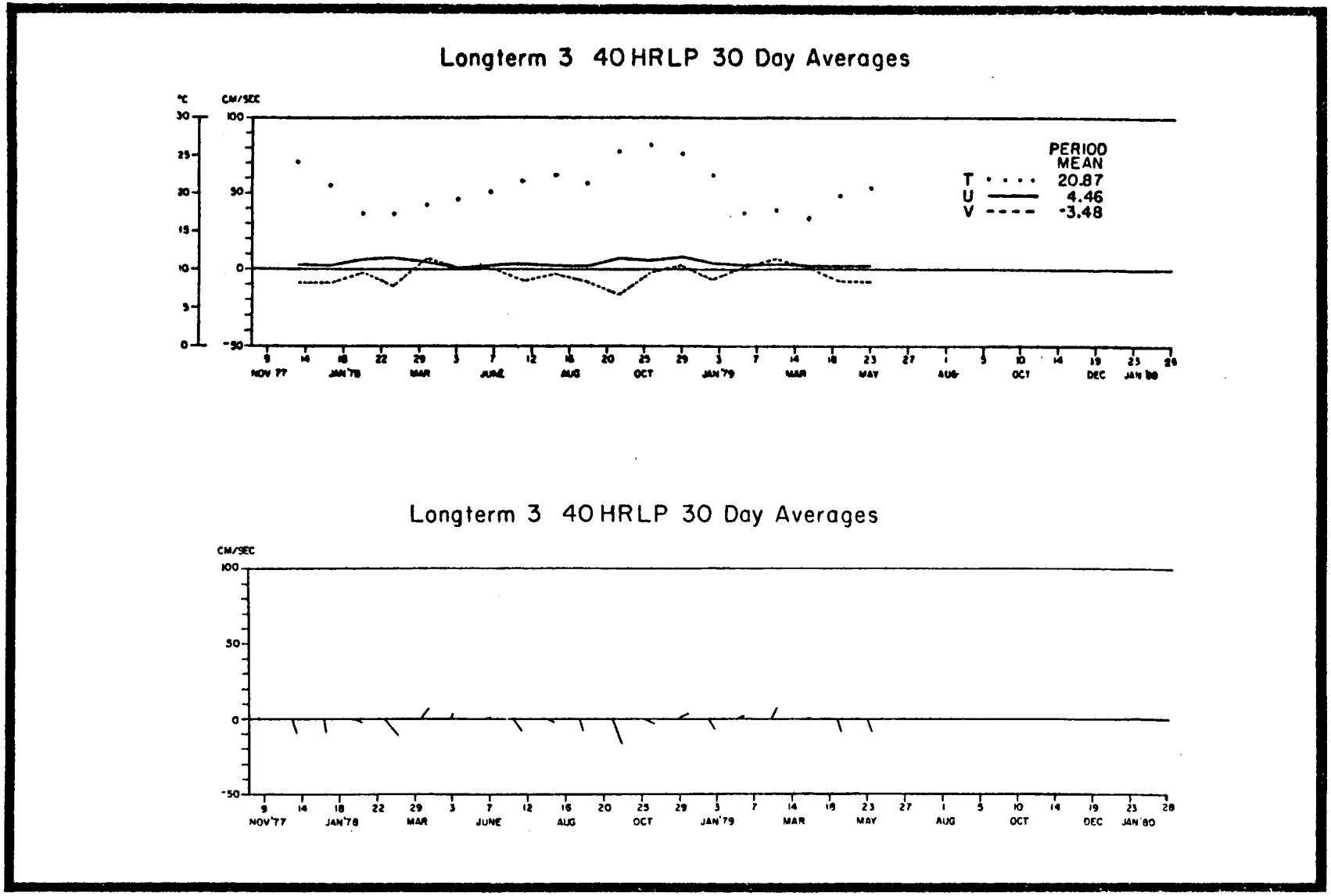

Figure 4.7.25. Long Term 3, 40-HLP, 30-day averages.

Currents at the upper and middle levels of the water column only occasionally seem to be related directly to either atmospheric wind conditions or coastal sea level adjustment (cf. Figures 4.7-17 to 4.7-27 and 4.7-3 to 4.7-11). For example during September to October 1978 and March to May 1979 the upper and interior currents appeared to be in geostrophic adjustment with the wind. These were periods when the winds were predominantly to the south in the fall, and predominantly to the north in the spring.

Next, it is necessary to consider thermohaline effects via a surface buoyancy stress condition as possible sources of current forcing for the May to August and November to February periods. Referring to Figures 4.7-14 - 4.7-16, maximum buoyancy flux occurred during November to February while minimum stress was exerted from April to September. Since the mean upper and middle water-column currents tended to be to the northeast during the winter period, it is entirely possible and most likely probable that buoyancy flux stresses were driving the upper to mid-depth flows to the north-northeast. This same stress mechanism would also serve to drive a southerly near-bottom flow.

By flow pattern and mechanism, it seems that there was a southerly flow throughout the column during September and October 1978 when the winds were predominantly to the south and surface buoyancy flux effects were at a minimum. There was a north-northeasterly mean flow, in opposition to the wind, in the middle to upper water column from late October 1978 to February 1979, when the negative buoyancy flux at the air-sea surface was at a maximum, and provided a north-northeastward directed surface stress. During the summertime, the winds tended to persist from the south but were relatively weak in magnitude and did not appear to influence the currents.

Pietrafesa (1980) speculated that the shelf-break region off Charleston may be part of a counterclockwise rotating gyre that has the inshore side of the GSF as its southern, eastern, and northern boundaries and is closed on its inshore side by a southerly flowing current. Figure 4.7-1 represents these basic conceptual notions. The bottom currents at the CLTM site are persistently southerly for the most part and may be a manifestation of the inshore side of the gyre (Figure 4.7-26).

Pietrafesa et al. (1978) presented observational evidence of an eastward, offshore deflection of the GSF at 32°N 79°W over the Charleston Bump, and Rooney et al. (1978) established a theoretical basis for the permanent deflection of the GSF at that site (cf. Figure 4.7-1). The essence of their theory is that the topographic feature causes an imbalance in the vorticity of the jet, which causes a movement of the jet offshore. As the GS moves to deeper water, the opposite scenario occurs, and the jet moves back toward the shelf-break slope. This offshore and subsequent onshore deflection of the Gulf Stream and the GSF is shown in VHRR imagery from 21 October - 3 November 1979 (Figures 4.7-27, 4.7-28). Note that a filament has wrapped itself around and essentially encircles the Charleston Bump. An additional satellite image, derived from the Nimbus Coastal Zone Color Scanner (CZCS), the visible 430 nm channel, on 28 October 1979, is shown in Figure 4.7-29. The blue channel has been enhanced and clearly shows that something has absorbed the blue part of the light spectrum on several occasions. One locale is near the coast, and this absorption could be due to organic material coming from the estuaries and coastal marshes. The second prominent locale is depicted as a dark ellipse

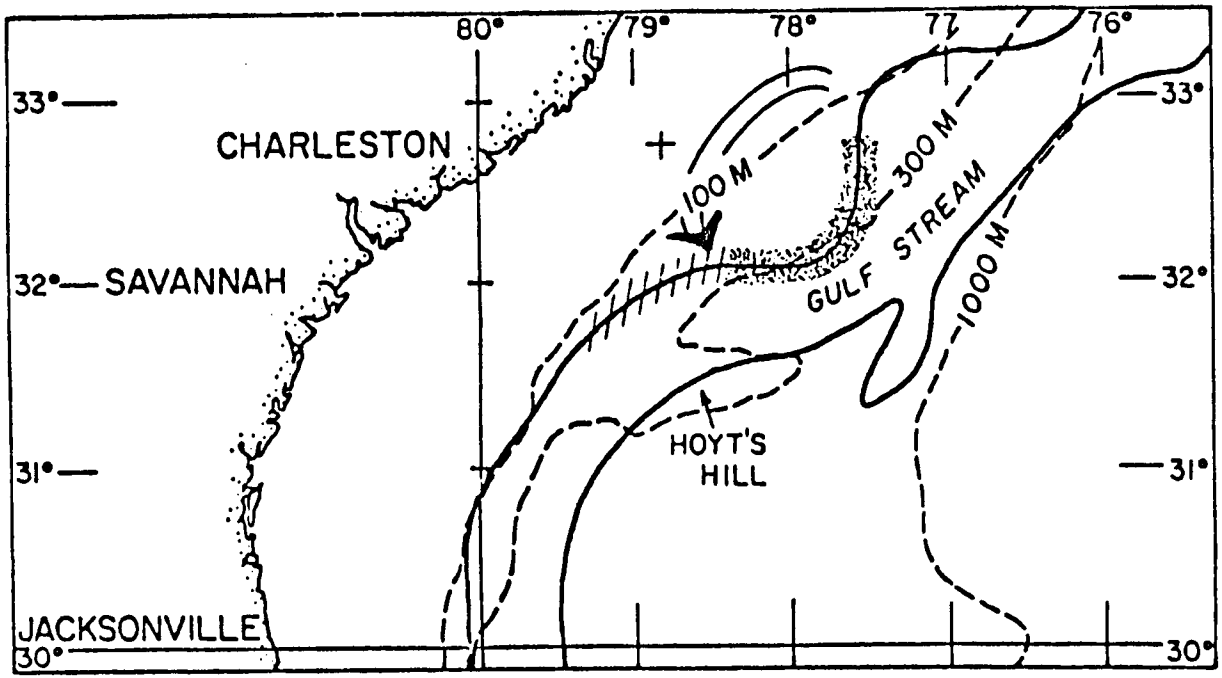

Figure 4.7-26. Flow in the region of the Charleston Bump (Hoyt's Hill). The region (/////) has C/R negative. The region ( ) has C/R positive with $-\partial C/\partial n$ positive in both regions implying ζ_z positive definite in the region ( ). The cross indicates the location of the Long Term Mooring.

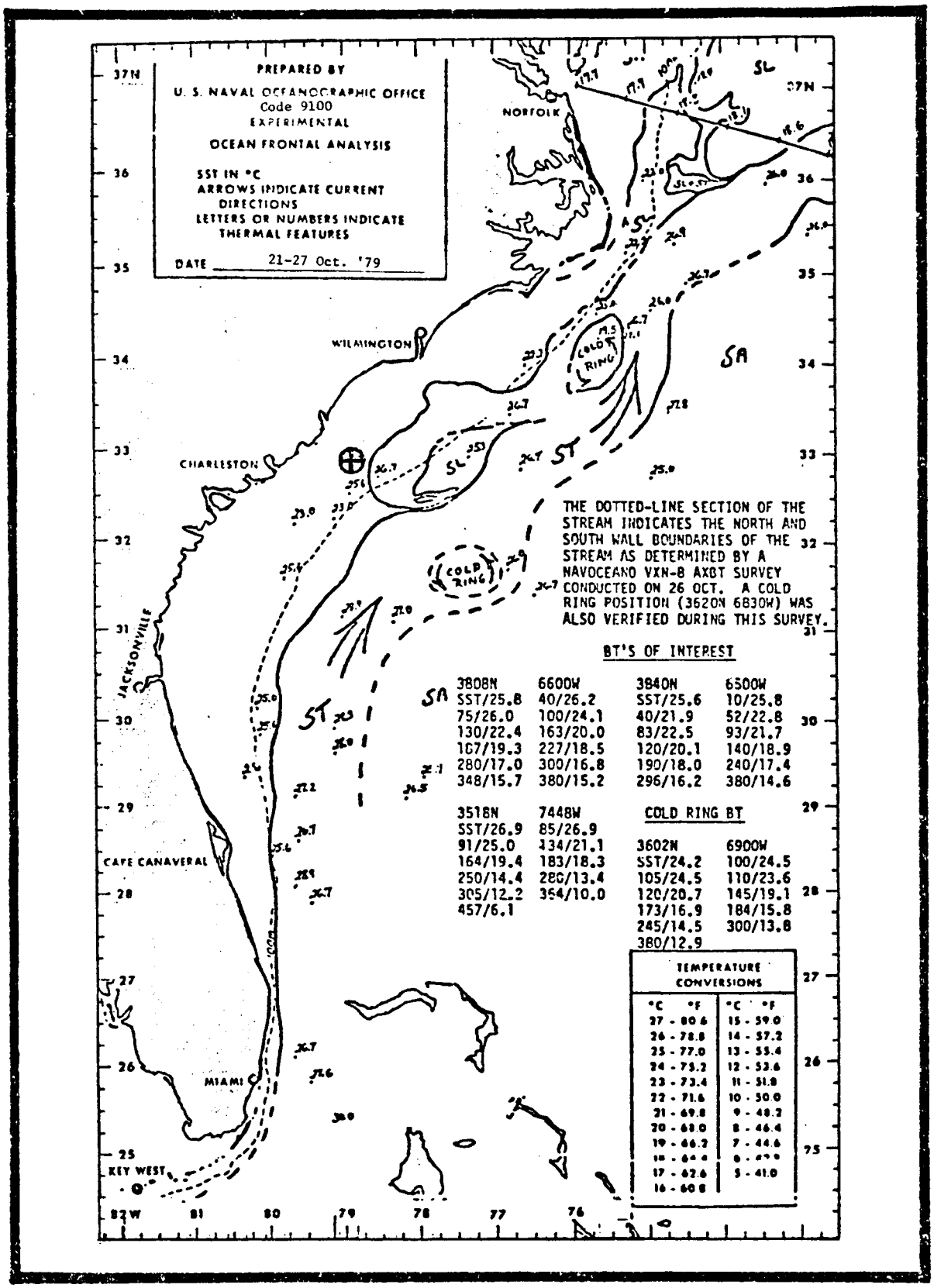

Figure 4.7-27. NOAA Experimental Ocean Frontal Analysis for 21-27 October 1979. The ⊕ indicates the location of the Charleston Long Term Mooring.

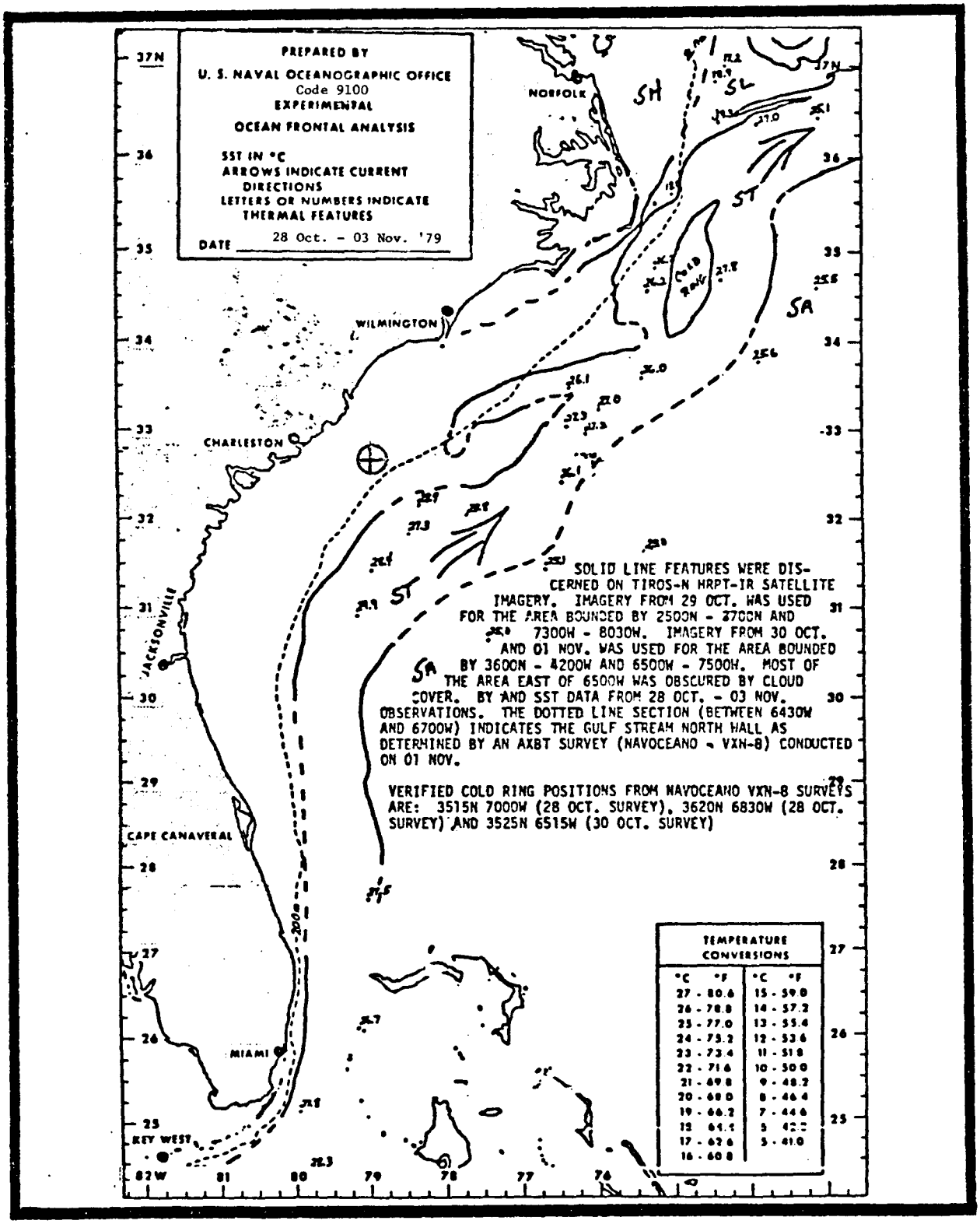

Figure 4.7-28. NOAA Experimental Ocean Frontal Analysis for 28 October to 3 November 1979. The ⊕ indicates the location of the Charleston Long Term Mooring.

Figure 4.7-29. Nimbus Coastal Zone Color Scanner (430 nm) enhanced blue visible image, 29 October 1979. Darker water indicates blue light absorption due to the presence of chlorophyll. The spot indicates the location of mooring Long Term 3, referred to in the text. Chlorophyll presence is heavy in the area of the Charleston Gyre over the "bump."

centered to the northwest of the Charleston Bump. It is postulated that chlorophyll is responsible for the blue absorption in this region.

The GSF moves offshore at 32°N 79°W and then back onshore, as discussed previously, and if the flow on the outer shelf is generally to the south, then a large counter-clockwise rotating cell is located in the area and we shall refer to this region henceforth as the Charleston Gyre. In fact, current meter data collected at the outer-shelf site on 28 October show flow to be southwesterly and accompanied by a drop in temperature. It appears that a Gulf Stream filament formed downstream of the "Bump" was superimposed on the background southerly flow and literally encompassed an elliptical dome within which upwelling occurred.

Pietrafesa (1980) speculated that the mechanism responsible for driving this current is likely to be an offshore drop in sea level coupled with an onshore rise in isopycnals. The net pressure gradient, which would be directed seaward, would then geostrophically drive a current to the south. Singer et al. (in press) and Atkinson et al. (in press) have separately provided evidence for a shoreward rise of isopycnals and for a doming up of the isopycnals to the northwest of the Bump. Unfortunately, pressure gradients associated with this isopycnal structure are not sufficient to drive a southerly current and may be, in fact, a consequence rather than an effect of the current. This leaves the sea surface and its diabathic structure as a possible source of the force responsible for driving a southerly flow.

Figure 4.7-30 depicts transect crossings 780, 823, and 866 made by the Seasat satellite during August 1978. Line 823 was crossed on 23 August and Line 866 on 26 August. These are the two lines of concern for the purpose of this report. Figures 4.7-31a,b represent the filtered and geoidally corrected residual heights of the surface of the ocean along those transects. These data also were then used to construct surface velocities related to the measured (residual) slopes of the ocean surface. Notice that the GS is a definite feature in both surface slope and associated current and that while the residual height plot of Transect 866 collapes to the left of the GSF, between latitudes 33 and 34°N, the residual height plot rises quite dramatically between latitudes 32.5 and 33.3°N along Line 823. The importance of this result is that Line 866 cuts through the southern part of Onslow Bay while Line 823 cuts across the Charleston Gyre. The transect across the southerly portion of Onslow Bay suggests no major sea-surface slope while the transect across the southerly portion of Long Bay, the proposed Charleston Gyre region, suggests a sea-surface rise of 45 cm, which translates to a south-southwesterly flow of magnitude 56 cm s^{-1} on 23 August. Amazingly the data collected at the CLTM site, mooring Number 092, show that the currents during the period 19-29 August 1978 were between 50-65 cm s^{-1} and to the southwest. This example of a diabathic pressure gradient force sufficient to drive a southerly jet on the outer Charleston shelf is not an isolated one. In fact all Seasat transects have been culled for sea-surface residuals and the story remains the same.

For completeness, it should be pointed out that the Charleston Gyre likely produces a dome of upwelling in its center. We conclude from observations that the region over and to the north of the Bump, which is not part of the Gulf Stream, has positive vorticity and is thus a likely candidate for Ekman induced upwelling. The vorticity in natural coordinates (Haltiner

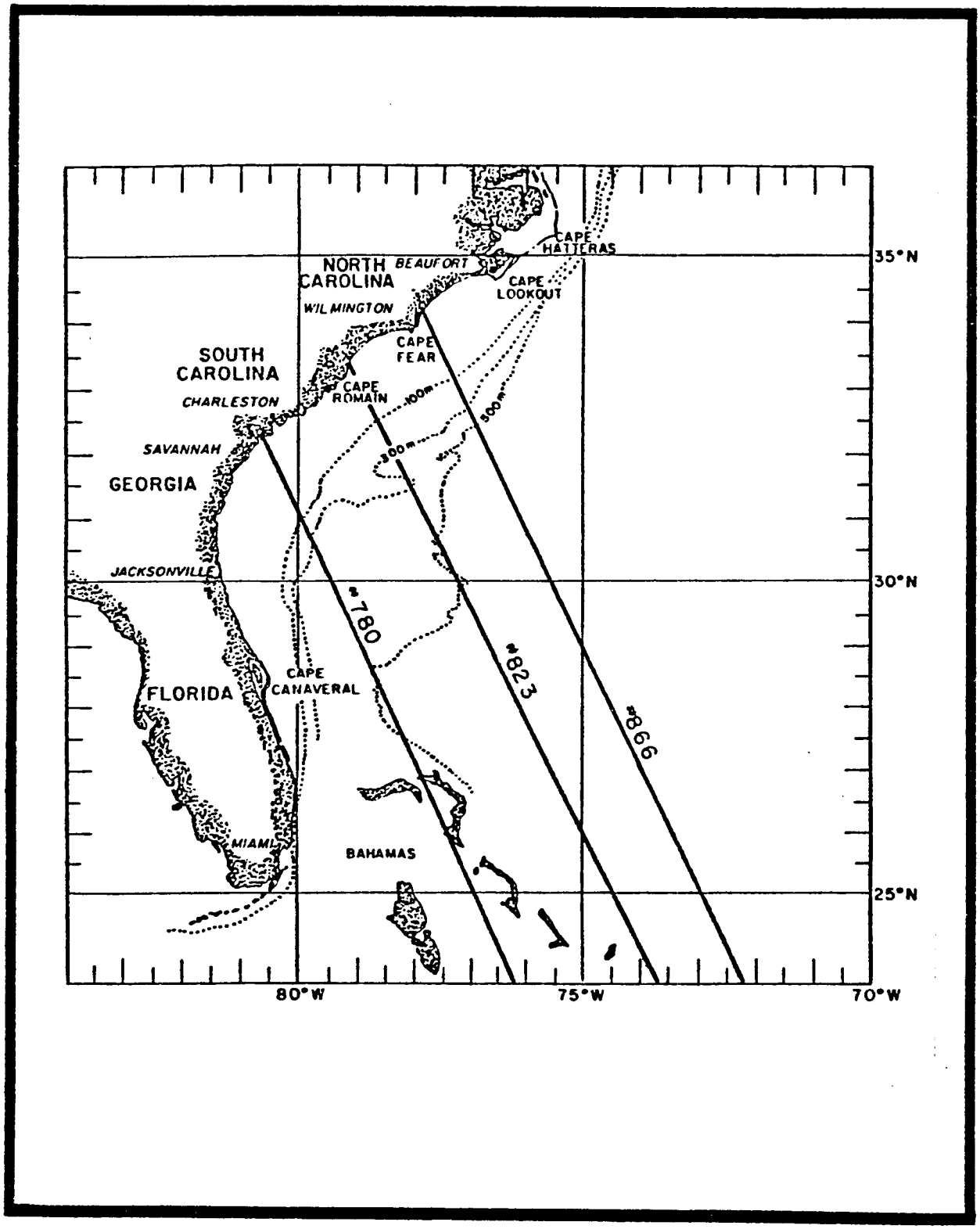

Figure 4.7-30. Transect crossings 780, 823 and 866 made by the Seasat satellite during August 1978.

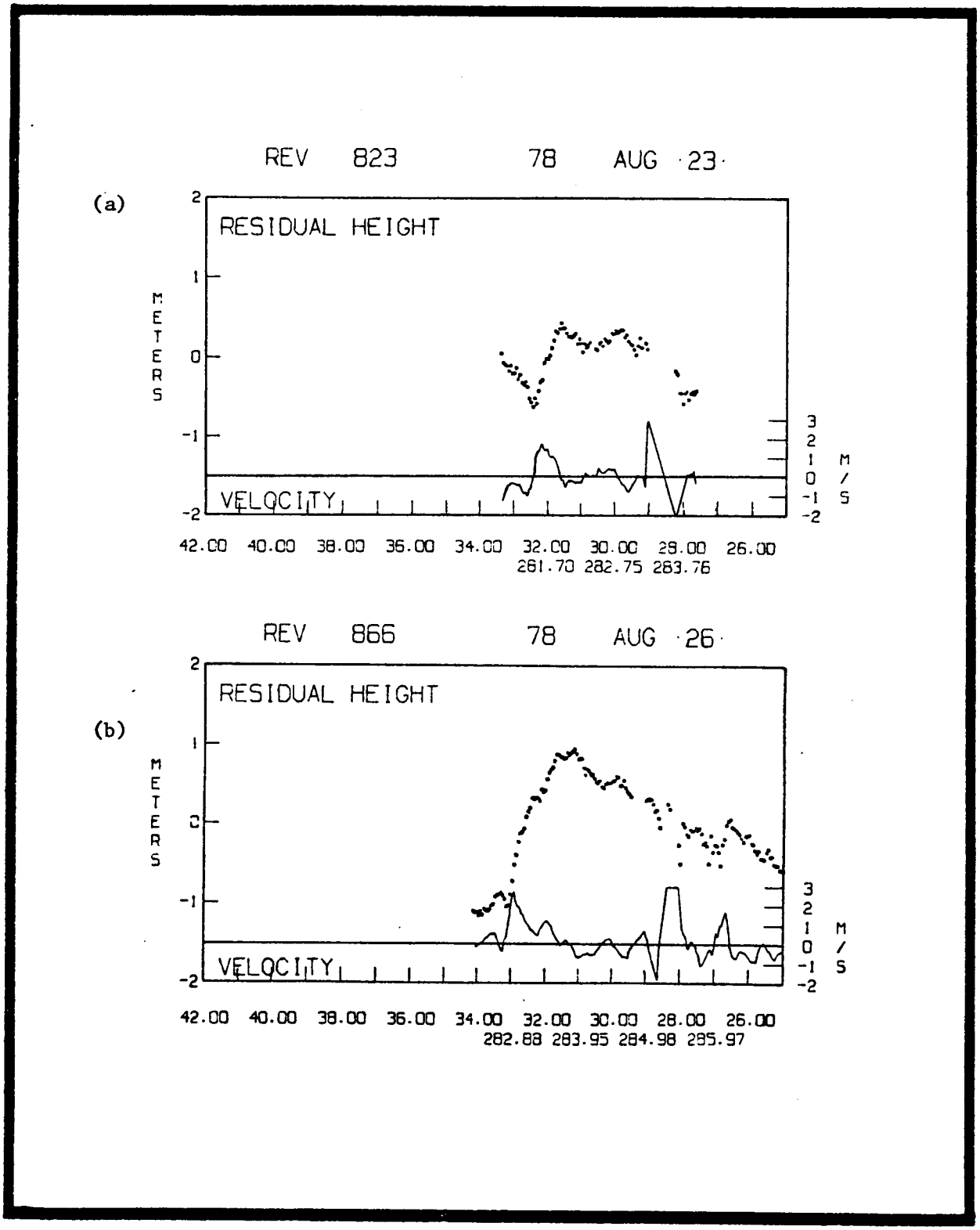

Figure 4.7-31. The filtered and geoidally corrected residual heights of the surface of the ocean along transects (a) 823 and (b) 866.

and Martin 1957) is C/R - $\partial C/\partial n$, where the radius of curvature, R, is positive (negative) for counterclockwise (clockwise) turning of a northward flowing jet and n increases in the onshore direction.

We first discuss the C/R term in the vorticity and then $\partial C/\partial n$. At 32°N 79°W the current turns in a clockwise direction and has (C/R) <0. Just downstream (north) of this point the GS then deflects in a counterclockwise direction and has (C/R) >0.

The velocity gradient in the jet in this region is not well-known but inshore of the maximum velocity of the jet $\partial C/\partial n$ <0 and - $\partial C/\partial n$ >0. The total vertical vorticity is then positive on the inshore side of the jet, which is the seaward boundary of the Charleston Bump region from 32 to 33°N. Since the deflection of the jet seems to be a permanent feature of the flow in this region, it is plausible to assume that, given the constant supply of positive vorticity to the seaward boundary, positive vorticity will diffuse into the waters that are treated over and to the north of the Charleston bump.

The order of magnitude of the bottom Ekman-layer-induced, positive upward, vertical velocity (see relation 1 below) can be estimated to be $h_e \zeta_z$, where ζ_z is the relative vorticity contained along the western edge of the GSF and h_e is a bottom frictional layer height scale, roughly equivalent to one-sixth that of a bottom Ekman layer. A minimal estimate of the bottom-layer thickness (cf. Janowitz and Pietrafesa 1980a) is one meter and an estimate of the relative vorticity across the GSF toward the axis of the Gulf Stream is of the minimum order of 10^{-5}, so that the persistent upward velocity is of lower order of 10^{-3}, in cgs units.

$$W = Av/2f\zeta_z \qquad (1)$$

This, we now consider the sense of curvature of the GSF and flow gradients normal to the Gulf Stream in the region of the Charleston Bump between Savannah, Ga. and Cape Fear, N.C. Through the mechanism of bottom layer suction, ζ_z can induce vertical velocities comparable to those associated with wind induced upwelling. Both the curvature and velocity gradient on the landward side of the Stream lead to positive vorticity, which should be diffused laterally into the region leading to upwelling by bottom suction.

This theory is general in formulation, and while we apply it to a region specific to the SAB, it is clear that there are regions in other parts of the world where it may have application. It is of final note that Figures 4.7-32 a, b indicate that the center of the Charleston Gyre region contains relatively high surface sediment concentrations of organic nitrogen (Figure 4.7-32a) and organic carbon (Figure 4.7-32b). This evidence lends further support to the notion that upwelling and high biological productivity are occurring there.

4.7.7 Continental Margin Low-Frequency Waves

There are a series of continental margin waves (CMWs) which can theoretically exist on the Charleston inner, middle, and outer continental shelves. The terminology CMWs is used, rather than continental shelf waves (CSWs) or topographic Rossby waves (TRWs), because it is more inclusive of the

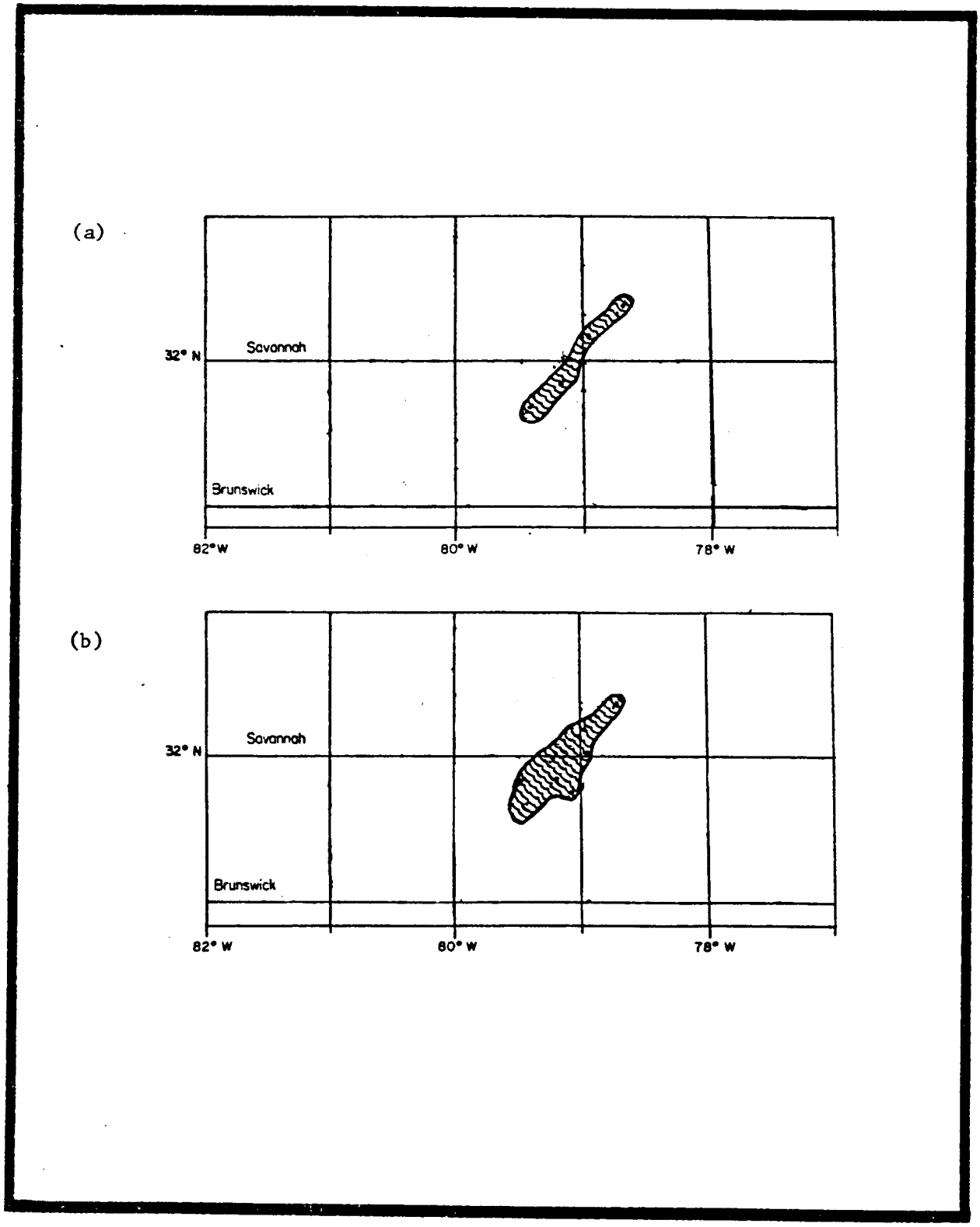

Figure 4.7-32. Organic (a) nitrogen and (b) carbon in the surface sediments in the region of the Charleston Gyre.

types of longwave phenomena that can be induced and supported across the entire continental margin surrounding Charleston. As an example, consider the current description shown in Figure 4.7-33.

Figure 4.7-33 is presented for instrument 08501, which measured currents during the period November 1977 to January 1978 at a depth of 12 m in 45 m of water at the Long Term Mooring site. Depicted in the figure are current principal axis orientations, current hodograph ellipse stabilities, ratios of semi-minor to semi-major ellipse axes, and maxima and minima of coherences squared between orthogonal velocity components in and relative to the principal axes directions as a function of frequency. Hodograph ellipse orientations and stability can be considered in tandem since the latter description is the coherence-squared between positive (+) and negative (-) rotating motions that linearly superpose to yield the resultant elliptical motions, with appropriate orientations, as indicated by the directionality of the ellipse semi-major axes. These axes are measured counterclockwise from zero (east) and normalized by 180° or pi radians. If we find regions in low-frequency space (less than 0.48 cycles per day) that reflect high ellipse stability, we have identified possible stable recurring motions that may be wavelike. Table 4.7-2 presents the mooring periods and instrument depths for the entire Charleston measurement program and Table 4.7-3 summarizes the hodograph description results for the measurement program extending from November 1977 to November 1979 and from February 1980 to June 1980.

From Table 4.7.3 one can reach the following conclusions:

(a) There are low frequency wavelike motions in the system.

(b) Most of the wavelike motions exhibit clockwise rotation in their horizontal plane particle paths, though this clearly is not the rule.

(c) There is a tendency toward east/west alignment of the major axis of motion.

(d) The counterclockwise rotating waves tend to occur in late spring, summer and early fall and not during winter.

The kinematical, hodograph descriptors of currents on the Florida-Georgia shelf during late winter and spring 1980 indicate that Gulf Stream frontal events do not generally penetrate to the 28 m-isobath and, in fact, are not totally prevalent at the 40-m sites. They tend to be clockwise polarized and are likely not GSF related since the frontal waves are counterclockwise polarized. At the 40-m isobath, cyclonically rotating wavelike motions with 2.5-, 4-, 5-, and 8 to 9-day periods are evident at 29°N latitude, 4- and 10-day periods at 30°N, 2.5-days at 31°N and 10-days at 32°N. It appears that the frontal events penetrate across the shelf in greater numbers off Florida than to the north off Georgia. The wavelike features in the GABEX-I region from February to June 1980 are summarized in Figure 4.7-34. The Florida/Georgia/South Carolina shelf has waves on the inner and mid-shelf, which are likely not Gulf Stream related, while the North Carolina region has no inner-shelf long waves (Pietrafesa, 1981). The North Carolina mid- to outer shelf shows waves existing across nearly the entire 2.7- to 12.4-day period band, while the Florida/Georgia/South Carolina middle (40 m) shelf is

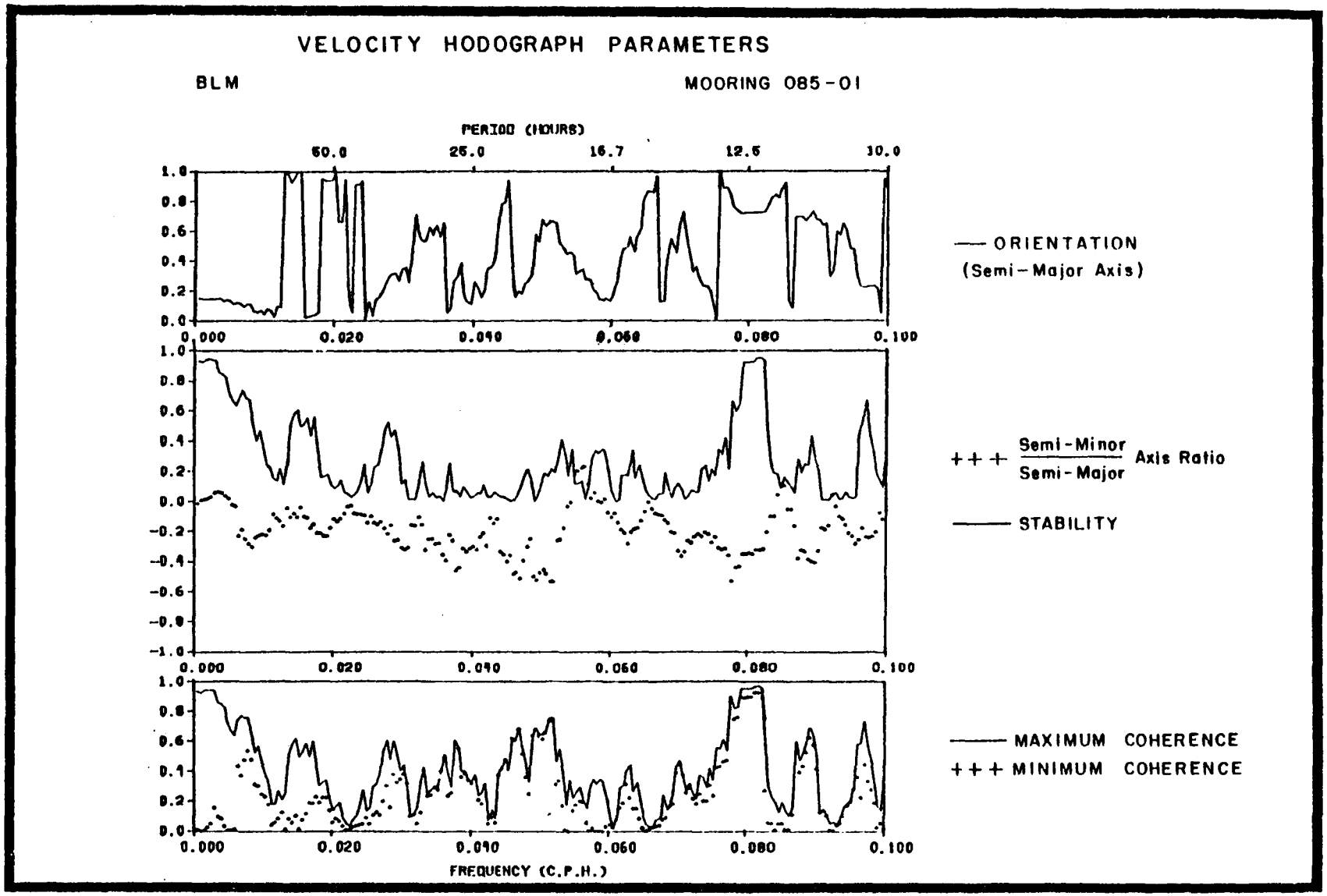

Figure 4.7-33. Hodograph plot for Mooring 085-1.

Table 4.7-2. Mooring Scenario

Mooring #	Mooring Depth, m	Instrument*	Instrument Depth, m	Data Dates, GMT	Δt, hrs	Comments
085	45	8501	10	0930 hrs 04 Nov 77-	.25	V, T all meters
		8502	22	1730 hrs 22 Jan 78	.25	
		8503	42		.25	
089	47	8901	12	2215 hrs 22 Jan 78-	.25	V, T all meters, also
		8902	24	1345 hrs 13 Apr 78	.25	P for 8901
		8903	44		.0625	
091	45	9101	10	1700 hrs 13 Apr 78-	.25	V for 9101 and 9103,
		9102	22	1700 hrs 01 Aug 78	.0625	P for 9101
		9103	42		.25	T for all meters
092	46	9201	11	2000 hrs 01 Aug 78	.25	V, T all meters, also
		9202	23	1245 hrs 15 Nov 78	.25	P for 9201
		9203	43		.0625	
094	30		Not Retrieved			
095	38	9501	10	1200 hrs 15 Nov 78-	.25	V, T all meters
		9502	19	2100 hrs 20 Mar 79	.25	(2 1-hr gaps plus 36 pt gaps
		9503	35		.0625	in 9503, interpolation f d)
096	47	9601	12	1430 hrs 15 Nov 78-	.25	V, T all meters
		9602	24	2245 hrs 20 Mar 79	.25	
		9603	45		.0625	
097	46	9701	11	0200 hrs 21 Mar 79-	.25	V, T all meters
		9702	23	0930 hrs 27 May 79	.25	(9702 T + spd/dir
		9703	43		.0625	only. u,v to be generated)
098	29	9801	9	0700 hrs 27 May 79-	.0625	9801-Rotor failed at 1652 hrs
		9803*	27	0452 hrs 30 Oct 79	.33	3 Jun 79. 9803-stopped recording 0540 hrs 5 Oct 79

continued.....

Table 4.7-2. Mooring Scenario con't.

Mooring #	Mooring Depth, m	Instrument*	Instrument Depth, m	Data Dates, GMT	ΔT, hrs	Comments
099	35	9901	8	0415 hrs 27 May 79–	.25	V, T all meters
		9902	17	2215 hrs 04 Nov 79	.25	9902 stop 2330 hrs 26 Sept 79
		9903	32		.0625	9903 stop 0430 hrs 30 Oct 79
100	44	10001	9	1315 hrs 27 May 79–	.25	V,T all meters
		10002	21	1930 hrs 04 Nov 79	.25	(10003 record ended 0455
		10003	41		.0625	hrs 30 Oct 79)
117	30	11701	17	2115 hrs 20 Feb 80–	.25	V, T all meters
		11702	27	2300 hrs 07 Apr 80	.25	
					.25	
118	40	11801	17	1630 hrs 20 Feb 80–	.25	V, T all meters
		11802	37		.25	
119	75	11901	17	1415 hrs 20 Feb 80–	.25	V, T all meters
		11902	45		.25	
		11903	72		.25	

	Location (~)
94, 98	32°47.8'N, 78°53.8'W
95, 99	32°40.6'N, 78°45.4'W
85, 89, 91, 92, 100	32°33.9'N, 78°36.7'W
117	32°48.5'N, 78°55.3'W
118	32°39.8'N, 78°43.7'W
119	32°32.4'N, 78°36.1'W

*All instruments are VACM's except 9803 which is an Aanderaa current meter with temperature sensor.

V = Velocity, T = Temperature, P = Pressure

Table 4.7-3. Wave-like motion

Mooring Period	Mooring Name	Mooring Depth in meters	Frequencies in cycles per day	Principal Axis Alignment	Current Vector Rotation
11/77-01/78	085	01 45	0.15-0.2	20°	clockwise
		02	0.15-0.2	20°	clockwise
		03	0.3	70°	clockwise
02/78-04/78	089	01 47	0.14	0°	clockwise
			0.38	0°	clockwise
			0.14	0°	clockwise
		02	0.29	0°	clockwise
			0.38	0°	clockwise
		03	0.27-0.38	35°	clockwise
04/78-07/78	091	01 45	0.14	0°	counterclockwise
			0.22	0°	clockwise
			0.42	0°	clockwise
		02 (lost)	----	---	------
			0.16	35°	clockwise
			0.22	35°	clockwise
		03	0.29	35°	counterclockwise
			0.42	35°	clockwise
08/78-11/78	092	01 46	0.39	18°	clockwise
		02	.36	90°	counterclockwise
		03	nothing		
	094 (lost)				
11/78-03/79	095	01 38	0.22	0°	clockwise
			0.38	35°	
			0.22		
		02	0.38	35°	clockwise
		03	0.39	20°	clockwise
11/78-03/79	096	01 47	weak		
		02	weak		
		03	0.27	35°	clockwise
03/79-05/79	097	01 46	0.27-0.3	20°	counterclockwise
		02	0.33	70°	counterclockwise
05/79-10/79	098	03 29	0.18	70°	counterclockwise
			0.36	70°	

Table 4.7-3. (continued)

05/79-11/79	099	01	35	0.14	30°	clockwise
				0.14	20°	
		02		0.2	20°	all clockwise
				0.26	20°	
				0.15	70°	
		03		0.19	70°	all clockwise
				0.26	70°	
				0.39	70°	
05/79-11/79	100	01	44	0.09	15°	all counterclockwise
				0.22	30°	
				0.09	15°	
		02		0.22	15°	all counterclockwise
				0.31	15°	
		03		0.44	15°	clockwise
03/80-05/80	023	01	28	0.38	35°	clockwise
				0.16		
		02		0.31	50°	clockwise
				0.38		
	024	01	40	0.28	15°	clockwise
				0.34		
				0.09		counterclockwise
				0.16		
		02		0.22	50°	
				0.32		all clockwise
				0.39		
	025	01	75	0.08		counterclockwise
				0.18	10°	counterclockwise
				0.38		clockwise
				0.44		counterclockwise
		02		nothing		
		03		nothing		

more finely tuned, with waves appearing at the selective periods listed in Table 4.7-3. The outer-shelf sites (75) display a more broad-banded wavelike signature much like that which appears across the entire mid- to outer North Carolina shelf.

Figure 4.7-34 characterizes the wave field measured along the Cape Romain transect of Moorings 23, 24, and 25. Although all sites except Moorings 1 and 2 sensed waves, those at 23 were peaked at 0.16, 0.31, and 0.38, cpd and rotated clockwise with u lagging v, while those at 25 peaked at 0.08, 0.18, 0.38 and 0.44 cpd and rotated cyclonically with u leading v at all frequencies but 0.38cpd. Site 24 displayed many peaks, but the particle rotation was always clockwise except for the peak at 0.09 cpd, which indicated cyclonic rotation. The area appears to be "littered" with continental shelf waves, but many of these wavelike features are not conventional CSW.

Using cross-spectra of along-shore currents at several locations on the 75-m isobath, the phase propagation of wavelike features can be assessed. Figure 4.7-35 depicts dispersion curves from Onslow Bay created using several phase differences. These waves propagate to the north along the 75-m isobath and are manifested as either filaments or meanders. Curves a(bottom) and b(top) are from the 75-m isobath mooring and curve c(top) is from the 40-m isobath mooring.

Considering cross-spectral products of alongshore currents at the 28-m isobath, there is no indication of waves propagating either north or south. In fact, the phase is nearly zero, suggesting simultaneous forcing.

As discussed in the SAPOS Year 3, Final Report and as further discussed by Pietrafesa and Janowitz (1979a) and Chao and Pietrafesa (1980), the contentions of southerly propagating, free CSWs made by Mysak and Hamon (1969) and Brooks (1978) are probably incorrect. These latter authors believed, from separate studies of tide gauge data in Onslow Bay, N.C. and from the Cape Fear River, N.C., that observed coastal sea level fluctuations were representative of CSWs that propagated along the Carolina coast. More recently, Schwing et al. (in press) surmised that low-frequency fluctuations in South Carolina estuaries might be caused non-locally by CSWs moving by the estuary mouths. Unfortunately, there has been no evidence presented to prove that southerly propagating CSWs exist on the Carolina coast. In fact, Chao and Pietrafesa (1980) present good evidence that sub-inertial fluctuations in sea level at the mouth of Charleston Harbor are due nearly entirely to the mechanical set-down and set-up produced by local wind stress.

The first thing of note in Figure 4.7-34 is that these purported waves break into two groups: a cyclonically rotating group at the 75-m isobath and a clockwise rotating group on the 28-m isobath. The 40-m isobath is a region of counterclockwise rotating features off Florida and of mostly clockwise rotating features off Charleston. The counterclockwise rotating features are called "meanders" and "filaments." Figure 4.7-36 provides a diabathic breakdown between the zones with and without direct Gulf Stream frontal event dominance.

In contrast to the Carolina Capes region, the shelf in the Georgia Embayment has "waves" on the inner and mid-shelf, which are not Gulf Stream related, while the North Carolina region has no inner-shelf long waves evident

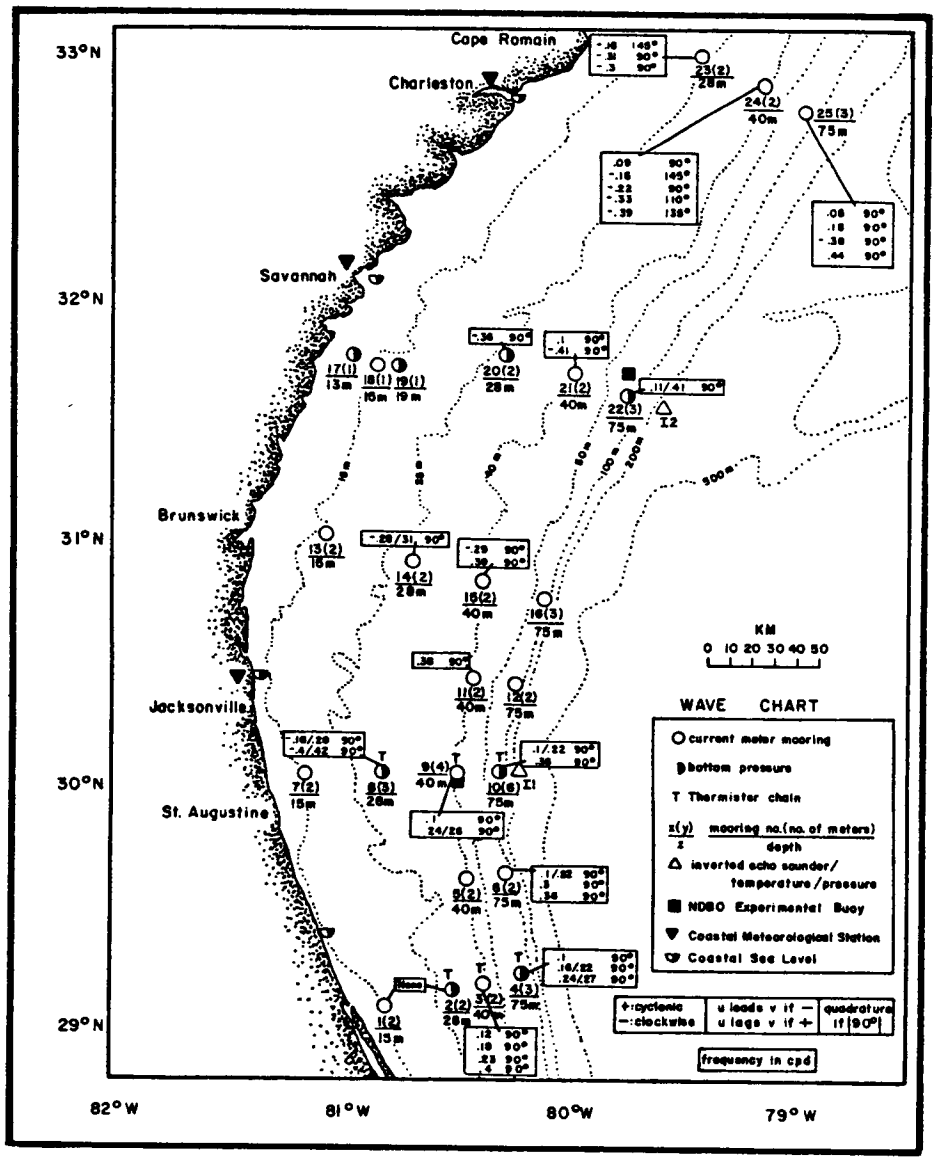

Figure 4.7-34. GABEX-I wave chart.

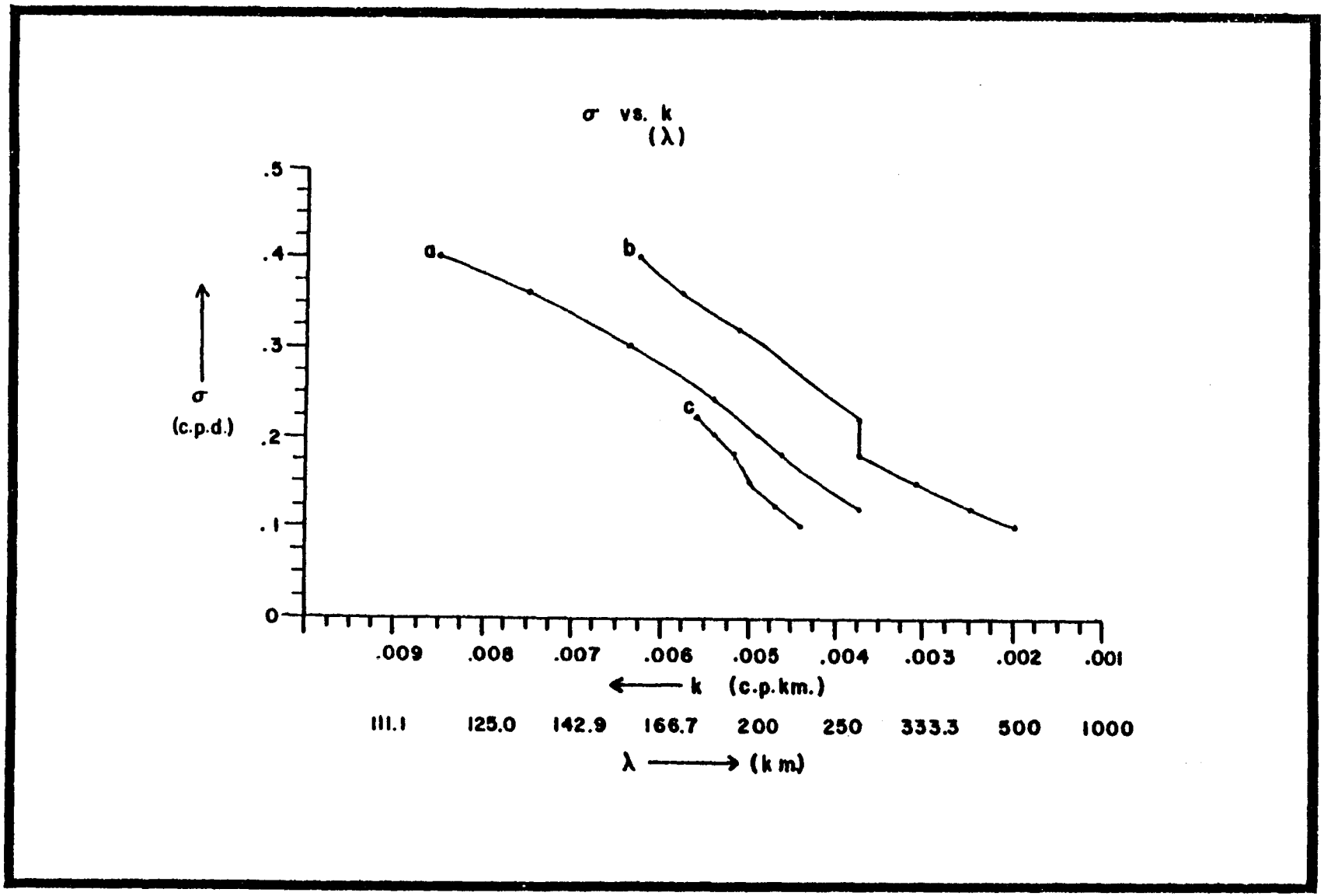

Figure 4.7-35. Dispersion curves for Gulf Stream frontal wave propagation in Onslow Bay (see text for discussion of curves a, b, and c).

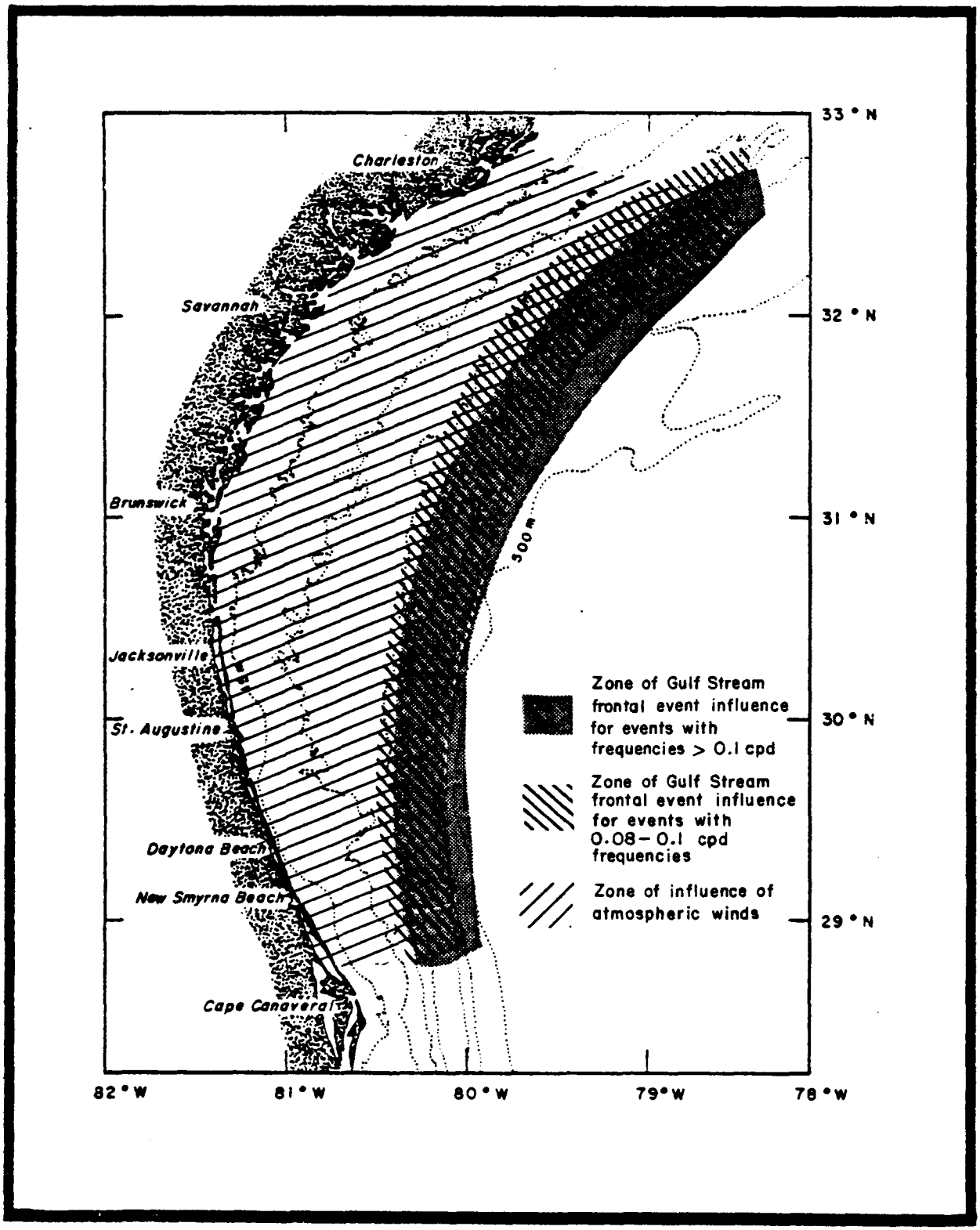

Figure 4.7-36. Cross- and along-shelf zonation of low-frequency currents in terms of principal forcing mechanisms: wind stress vs. the Gulf Stream front.

at all. The North Carolina mid- to outer shelf shows waves existing across nearly the entire 2.7- to 12.4-day period band, while the South Carolina to Florida middle (40 m) shelf is more finely tuned with waves appearing at the selective periods mentioned above. The outer-shelf sites (75m) display a more broad-banded wavelike signature much like that which appears across the entire mid- to outer North Carolina shelf.

Coastal sea-level data were obtained from the National Ocean Survey (NOS) for the GABEX-I period from Winyah Bay (WIN) near Georgetown, South Carolina, Charleston Harbor (CHS) and Fort Pulaski, Georgia at the mouth of the Savannah River (SAV). As seen in cross-spectral plots (Figure 4.7-37), there is no apparent phase lag of sub-inertial frequency (periods of approximately one day) fluctuations between any of the three combinations of station pairs. The time series at each of the stations are coherent and in-phase over a maximum station separation distance of approximately 200 kilometers between WIN and SAV. This result was suggested by Chao and Pietrafesa (1980) and further contradicts southerly propagating CSWs in this region.

4.7.8 Wind Driven Circulation

Comparing sea level and wind-stress components at Savannah and Charleston (Figure 4.7-38), it appears that the alongshore winds mechanically force sea level to rise and fall at the periods at which the wind component is energized. These periods are 10, 5, 3.3, and 2.2 days. The cross-spectra of Savannah alongshore winds versus sea level and of Charleston alongshore winds versus sea level had to be plotted separately since they are virtually identical. Clearly, the likely similarity holds when correlating cross-shelf wind-stress components to local sea level. As shown in Figure 4.7-38 (a and b), sea level is less finely tuned to cross-shelf wind components but is coherent everywhere for 0.06 to 0.2 cycle per day meteorological events. There is a phase lag between sea-level response to wind forcing of approximately 8 hours, as predicted by Chao and Pietrafesa (1980) for North Carolina and by SAI (1981) for the entire SAB.

We next consider frequency domain relationships between coastal winds and currents and sea level and currents. Figures 4.7-39 and 4.7-40 depict the relationships in the frequency domain between coastal winds and alongshore currents and coastal sea level and alongshore currents along the Savannah and Charleston mooring transects. Clearly, the winds and sea level all correlate well with alongshore current fluctuations at the 28- and 40-m isobaths off Savannah. Somewhere between the 40- and 75-m isobaths though, the coherence collapses. This is shown in Figure 4.7-41. Figure 4.7-42 is a plot of coherence versus distance offshore at the Charleston transect.

Coherence between alongshore winds and currents and alongshore currents off of Charleston tends to be higher than those to the south. The same is true for coherence between sea level and currents off Charleston versus those time and frequency domain relationships to the south. The Charleston shelf, while greatly influenced by Gulf Stream frontal events, is also more influenced by mechanical wind forcing. This is not startling since the Gulf Stream is further offshore of the shelf at Charleston than anywhere else in the SAB.

An alongshore wind to the northeast drives an alongshore surface flow with an offshore component. This pattern is initially balanced by an interior

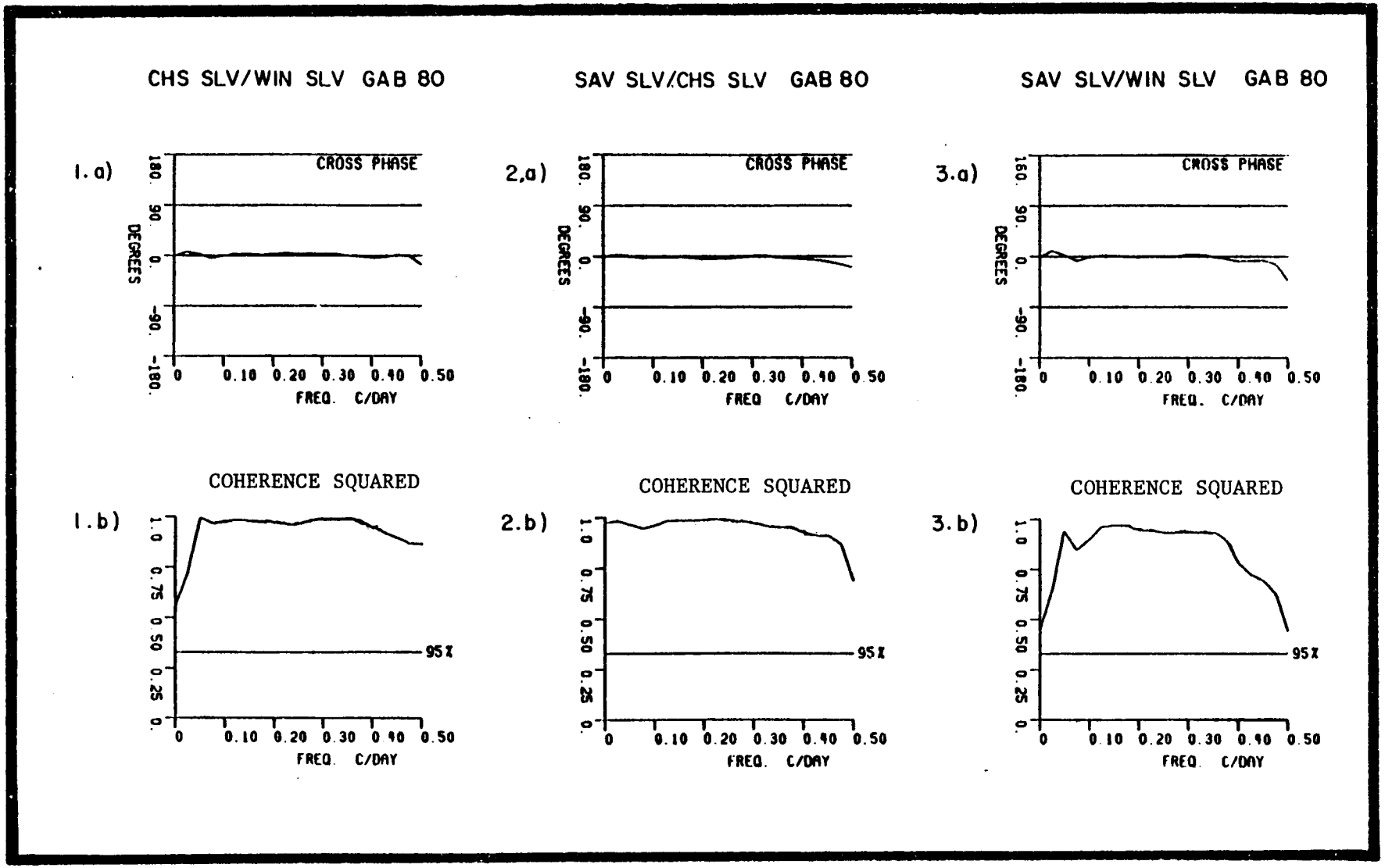

Figure 4.7-37. Cross spectra for GABEX-I period for Winyah Bay (WIN) Charleston Harbor (CHS) and Savannah (SAV).

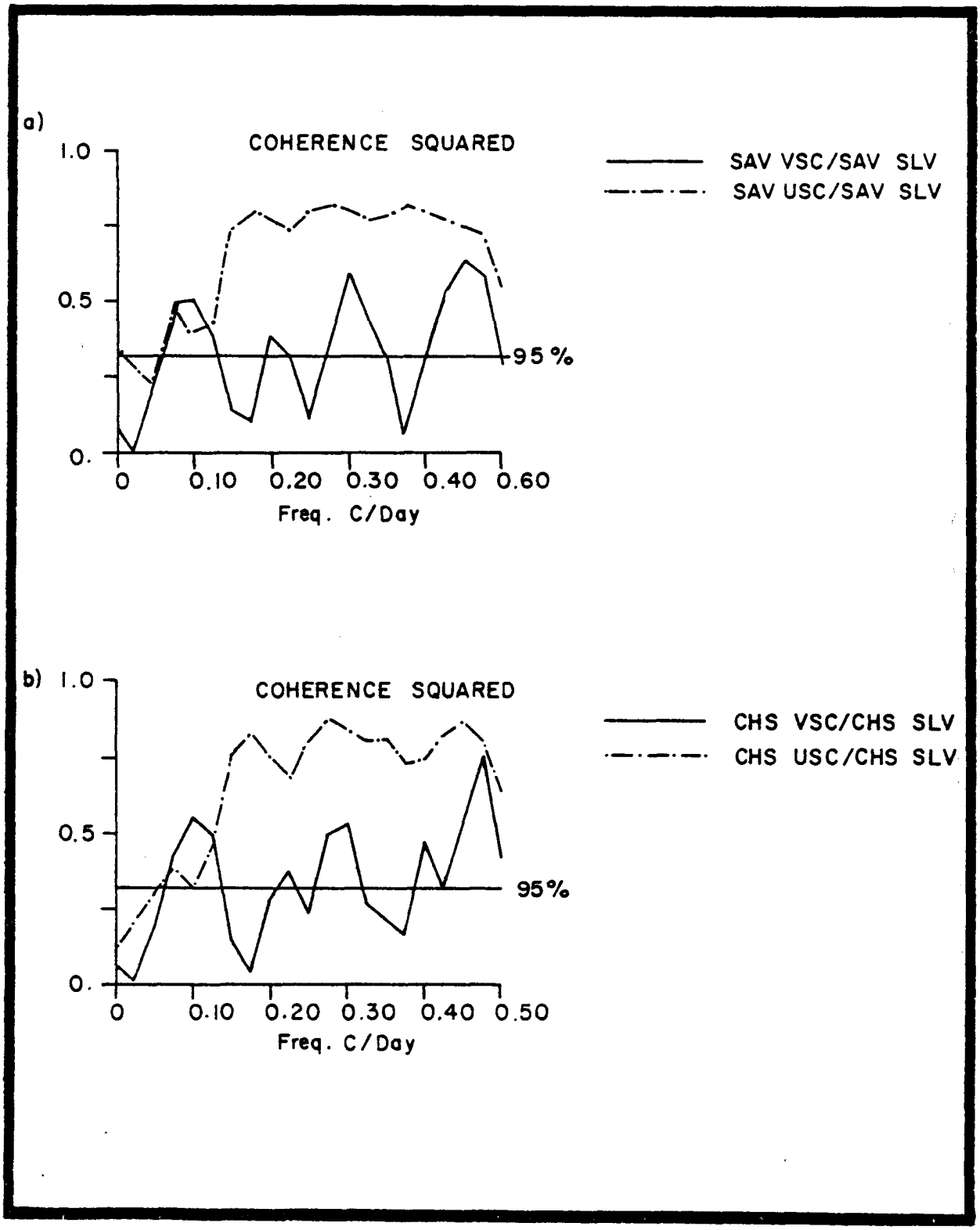

Figure 4.7-38. (a) Coherence squared for Savannah winds (u and v components) vs. sea level.
(b) Coherence squared for Charleston winds (u and v components) vs. sea level.

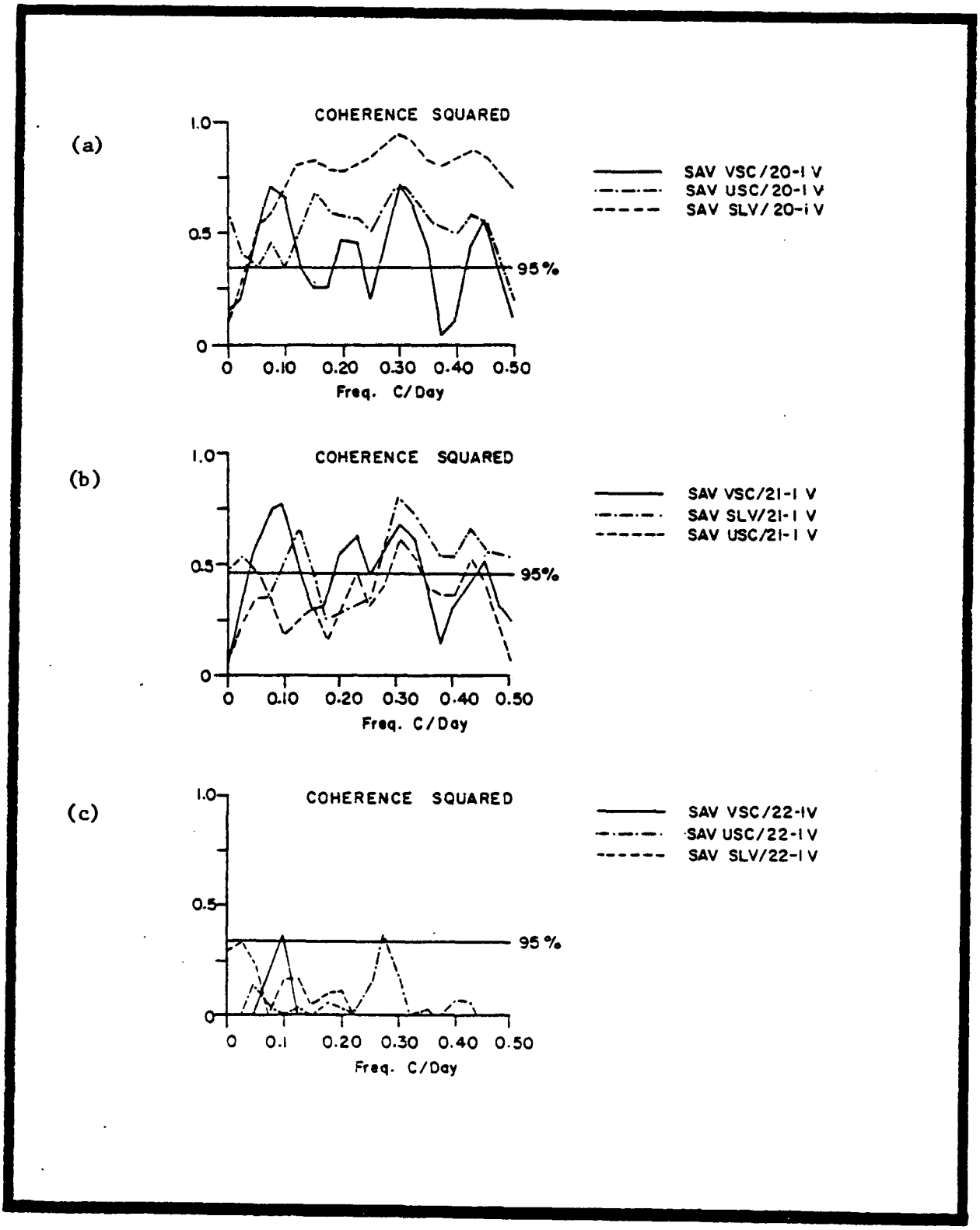

Figure 4.7-39.

(a) Coherence squared for current V component from Mooring 20-1 vs. Savannah winds (U and V components) and sea level.

(b) Coherence squared for current V component from Mooring 21-1 vs. Savannah winds (U and V components) and sea level.

(c) Coherence squared for current V component from Mooring 22-1 vs. Savannah winds (U and V components) and sea level.

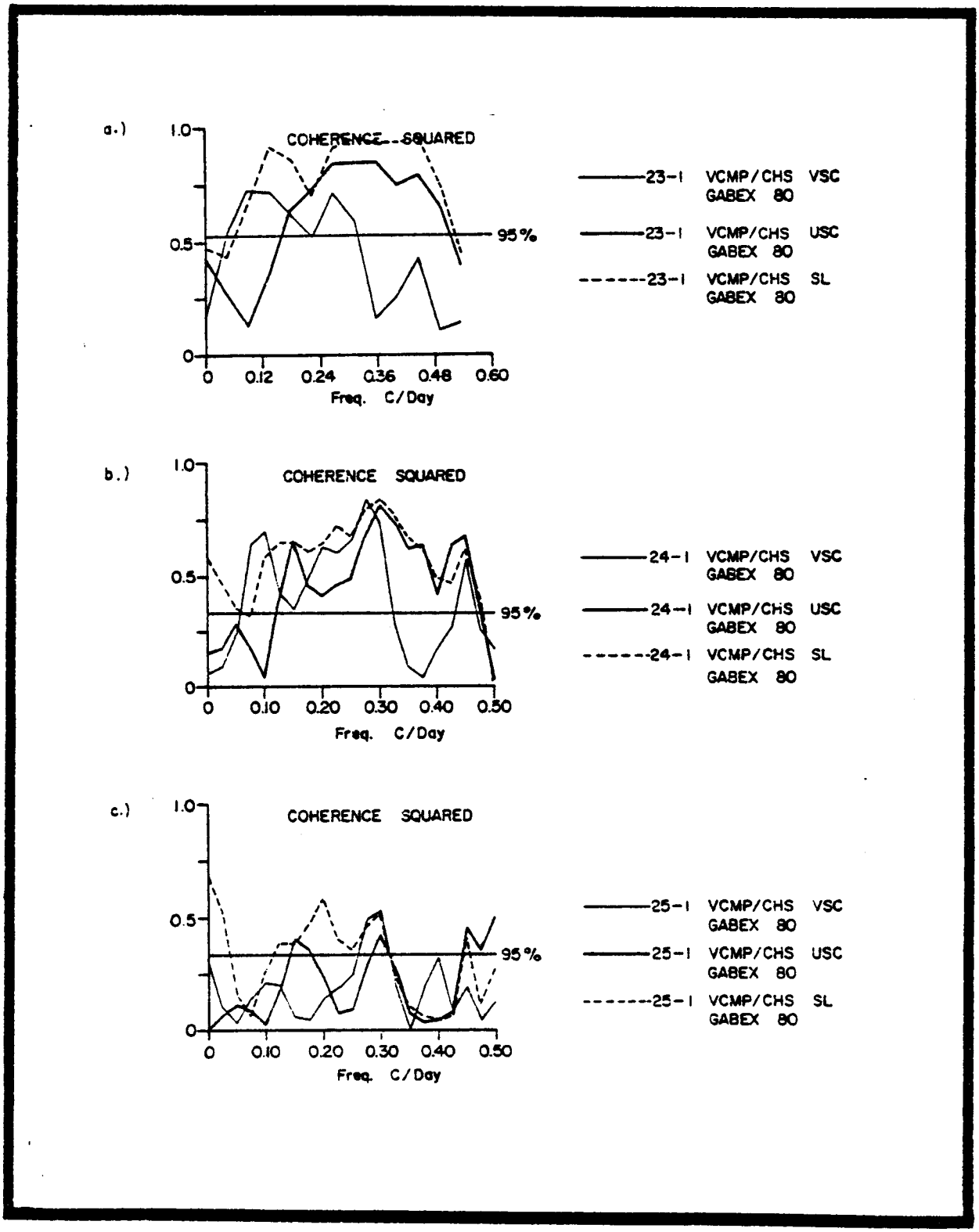

Figure 4.7-40.

(a) Coherence squared for current V component from Mooring 23-1 vs. Charleston winds (U and V components) and sea level.

(b) Coherence squared for current V component from Mooring 24-1 vs. Charleston winds (U and V components) and sea level.

(c) Coherence squared for current V component from Mooring 25-1 vs. Charleston winds (U and V components) and sea level.

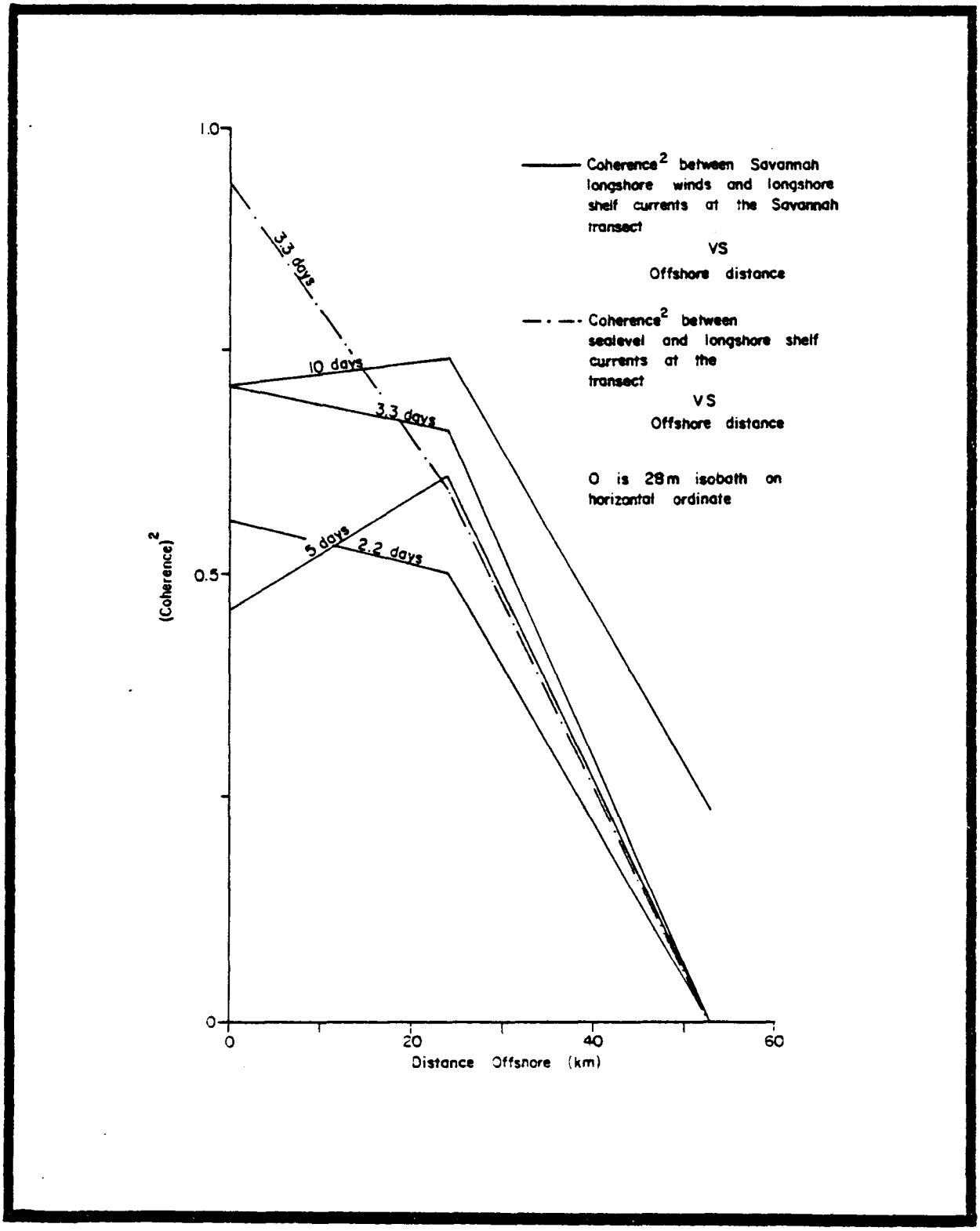

Figure 4.7-41. Coherence squared between Savannah longshore winds and longshore shelf currents at the Savannah transect (Moorings 20, 21, and 22) vs. offshore distance; and coherence squared between Savannah sea level and longshore shelf currents at the Savannah transect vs. offshore distance.

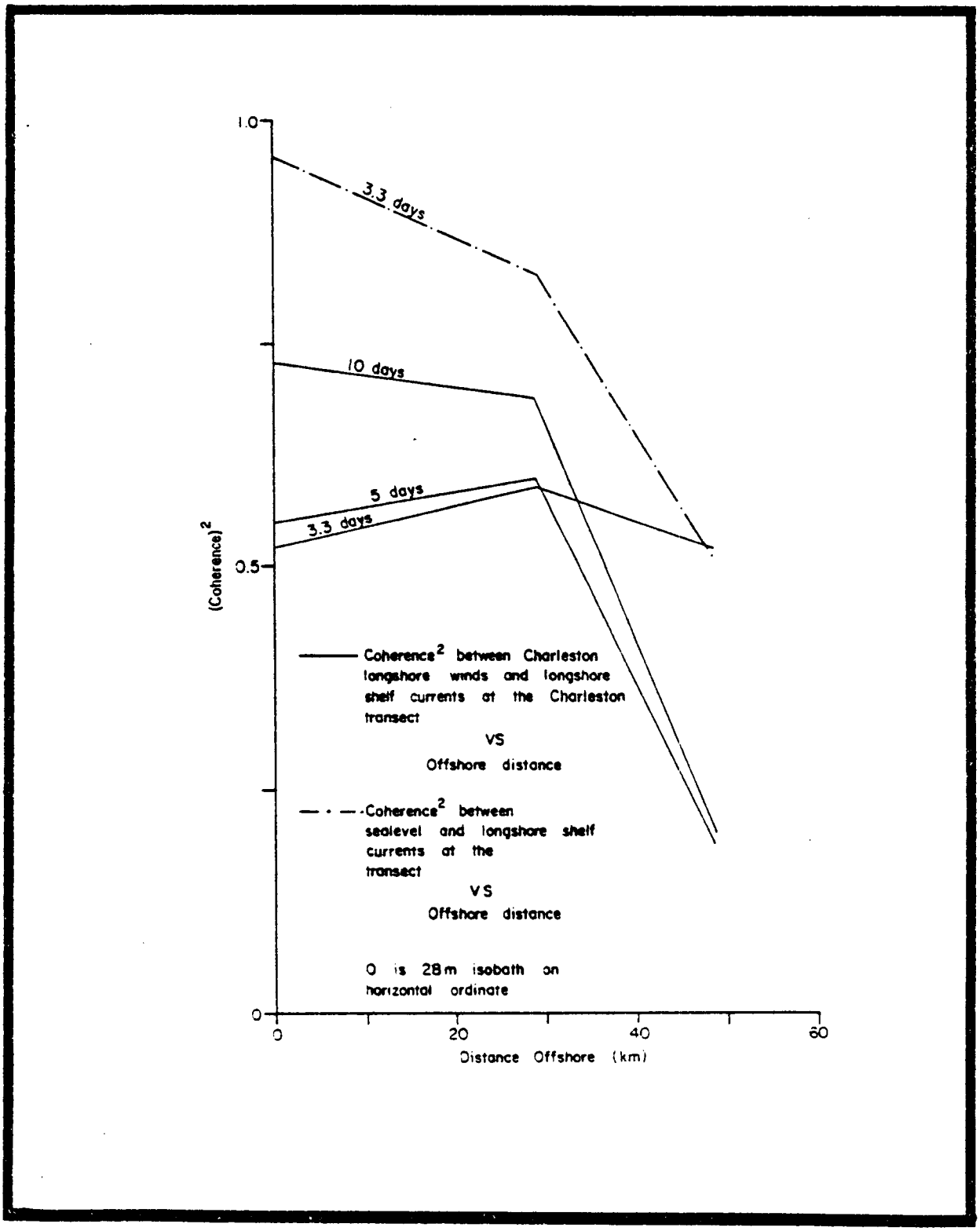

Figure 4.7-42. Coherence squared between Charleston longshore winds and longshore shelf currents at the Charleston transect (Moorings 23, 24, and 25) vs. offshore distance; and coherence squared between Charleston sea level and longshore shelf currents at the Charleston transect vs. offshore distance.

flow onshore and alongshore. Within a day, a bottom frictional layer becomes fully established and the flow within is directed onshore. Since this bottom layer is supplying mass, the interior flow drops off somewhat from its initial strength. An alongshore jet is set up during this process. Since the shallow waters spin-up more quickly than deeper regions, isopycnals appear to rise more quickly in shallow water. Actually, they simply have less distance to travel. The longshore jet has a negative cross-shelf gradient, out to the GSF, which occurs within a day. As a consequence of this, the isopycnal rise process is suppressed. Since the spin-up process occurs first in shallower waters, the suppression of the rise creates the impression of an isopycnal bulge moving from shallow to deeper waters.

With a negative longshore wind the process is reversed, the alongshore flow is southerly, downward mixing occurs, vertical thermohaline stratification is broken down, flow of bottom waters to the offshore results, and a drop of coastal sea level occurs.

4.7.9 Hurricane David

Hurricane David (HD) which existed between 25 August and 7 September 1979 is cataloged as a "Cape Verde" hurricane because it achieved hurricane intensity well east of the Lesser Antilles; it followed a parabolic path around the periphery of the Azores-Bermuda High, the Greater Antilles and the U. S. eastern seaboard; it maintained hurricane strength until landfall and it expanded in size as it moved north. Of the 1979 hurricanes, David achieved the lowest central pressure (924 millibars) and the highest sustained winds (approximately 150 knots). It is of note that only 6 other hurricanes on record have achieved a lower central pressure. Fortunately for the U. S., particularly Florida, David encountered the mountains of Hispaniola in the Dominican Republic and was somewhat diminished in strength. Moving over the GS, Hurricane David reintensifed and by Monday, 3 September, intruded upon the beaches stretching from Miami to Daytona. Hurricane David was near Savannah by the 4th, and by the 5th had become a weakened tropical storm as it moved through South and then North Carolina. It was out of the SAB region by the 6th.

Figures depicting David's pressure field and satellite, thermal imagery are shown in the sequence 4.7-43 through 4.7-47. The approximate path of the eye through the SAB is shown in Figure 4.7-48, with David's speed in knots noted. All times given are in Greenwich Mean Time (GMT).

At Savannah on the morning of 3 September at 0100 hours, the sky was clear and air temperature was 24°C, with an east-northeasterly wind of 3 knots. Hurricane David was centered over Miami. The ceiling, at this time, was unlimited. At Charleston, conditions were similar to those at Savannah except that the wind was north-northwesterly at 4 knots. At 0700 (1000) hours, the ceiling fell to 250 feet at Savannah (Charleston) and wind speeds had tripled (doubled). By 1300 (1600) hours the ceiling had reduced to several tens of feet at Savannah (Charleston) with winds of 10-12 knots now blowing from the east-southeast. Winds maintained sustained peaks of 20-40 (20-30) knots between 1000 (1300) hours, September 4, and 1900 (1900) hours on the 4th (5th) at Savannah (Charleston). The reason that the winds were not so intense at either of the two cities is that the eye passed directly over Savannah and within 30 kilometers to the west of Charleston. The winds at

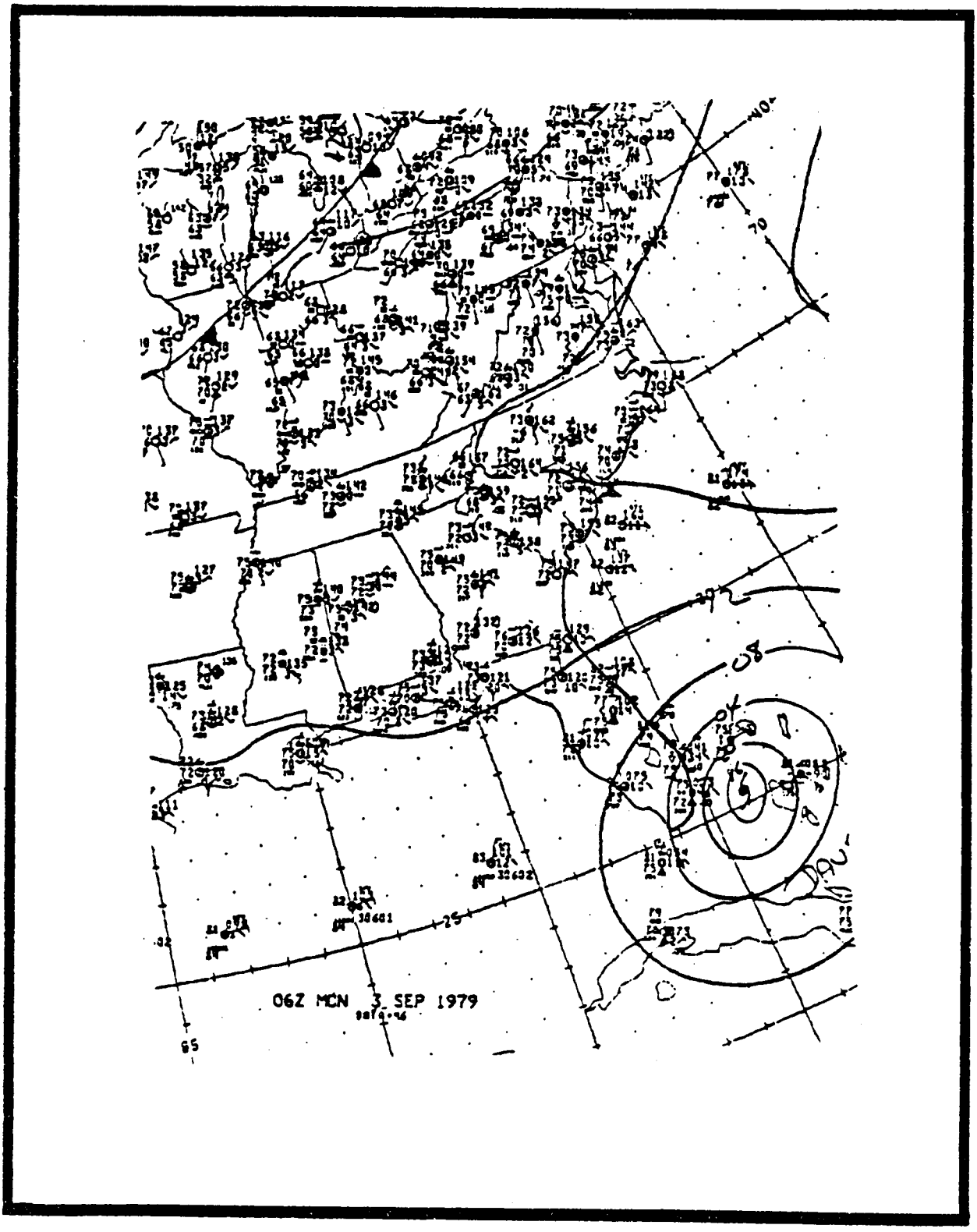

Figure 4.7-43. Weather map showing the position of Hurricane David at 06Z, Monday, 3 September 1979.

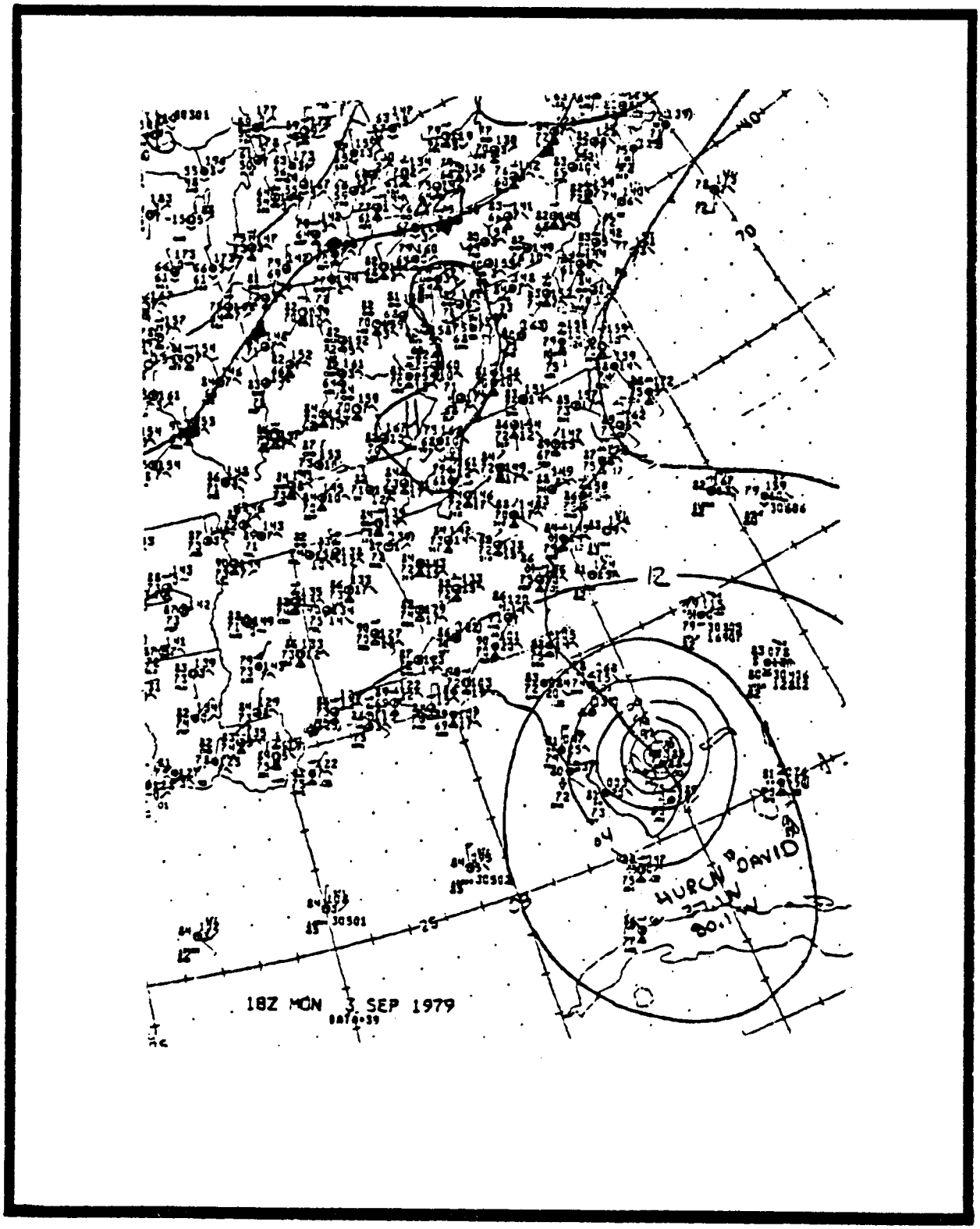

Figure 4.7-44. Weather map showing the position of Hurricane David at 18Z, Monday, 3 September 1979.

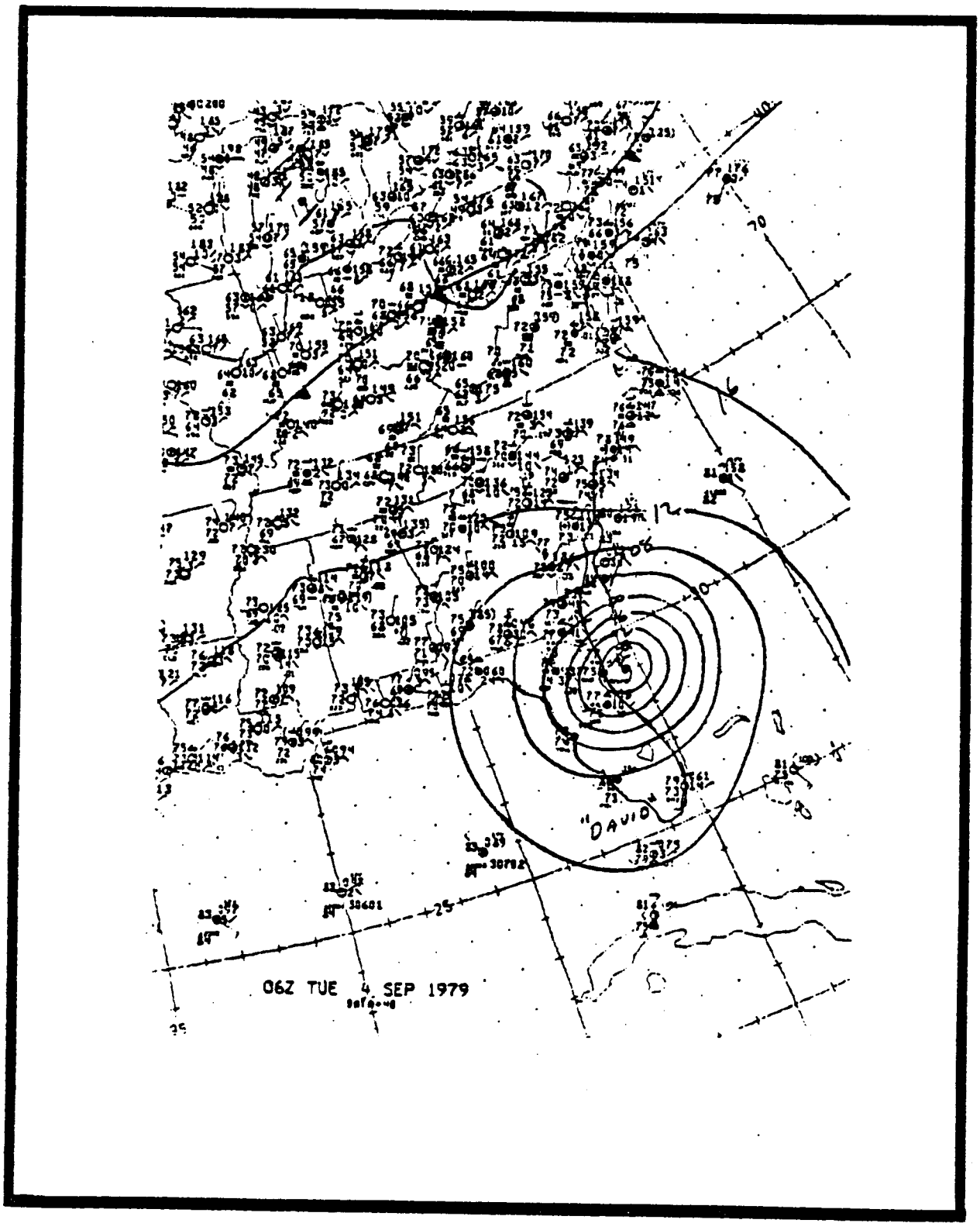

Figure 4.7-45. Weather map showing the position of Hurricane David at 06Z, Tuesday, 4 September 1979.

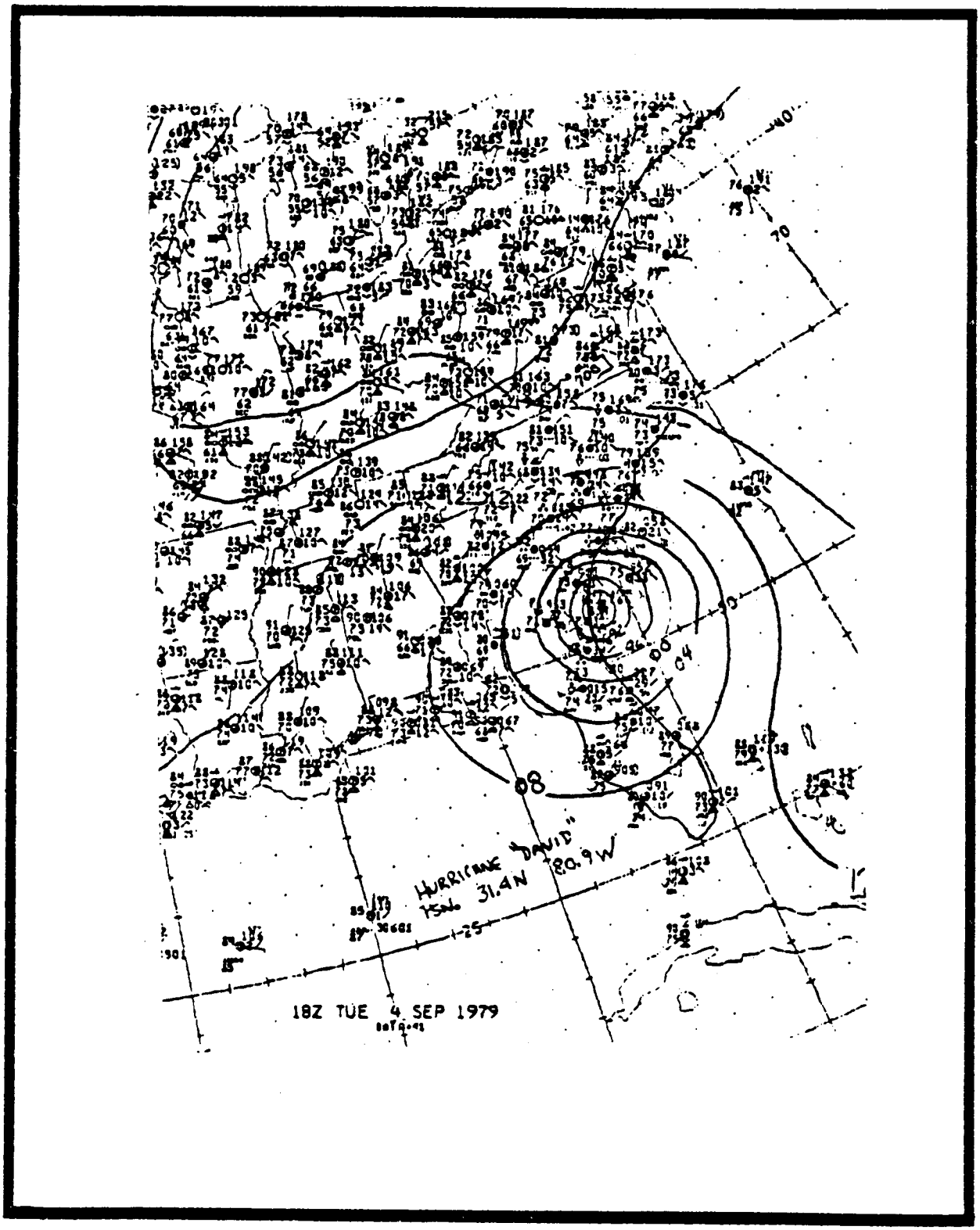

Figure 4.7-46. Weather map showing the position of Hurricane David at 18Z, Tuesday, 4 September 1979.

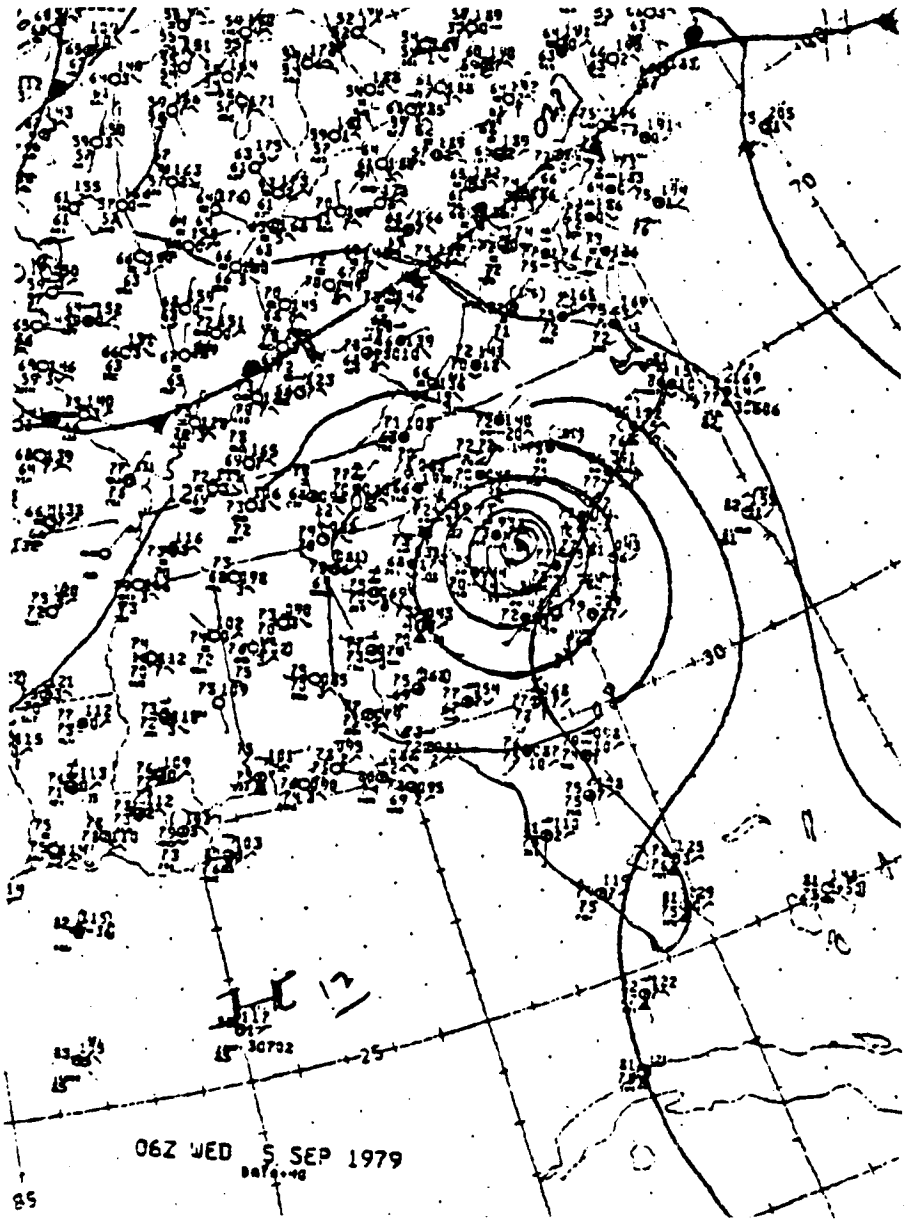

Figure 4.7-47. Weather map showing the position of Hurricane David at 06Z, Wednesday, 5 September 1979.

Savannah were southeasterly then northeasterly and finally southwesterly, on the 3rd, 4th and 5th. At Charleston the winds tended to be northeasterly, southeasterly and finally south-southwesterly over the three-day period.

During this period Moorings 098, 099, and 100 were in place in the BLM cross-shelf transect, as shown in Figure 4.7-48. Evident in all of the mooring data is an inertial loop through which the currents rotated about Day 247 (4 September). These singular loops are noted in Figures 4.7-49, 4.7-50, and 4.7-51 by a small black arrow. This response fits well with previous observational evidence and theoretical considerations for the inertial current response to impulsive wind forcing on the Charleston shelf (Klinck et al. 1981). In fact, that description defines the high frequency, i.e., frequencies greater than 0.5 cycles per day, for the oceanic response to the storm.

The center of the hurricane passed within 150 kilometers of the mooring array late on the 4th and 5th. About 5 days prior to the passage of the event, winds were blowing from the northeasterly to southeasterly quadrant and air-sea temperature differences at the mooring site were about zero. Currents at the outer two mooring sites were directly toward the southwest and increased from about 20 cm s^{-1} at Mooring 99 to about 50 cm s^{-1} at Mooring 100 at the upper levels. There was a small amount of shear in the vertical at both sites, so that the alongshore flow was a decreasing function of increasing depth. In fact, 3 meters from the bottom of middle Mooring 99, which was in 38 meters of water, the flow was reversed. As one moved to the 28-m isobath, one found a 20 cm s^{-1} flow to the northeast.

Between days 31 August and 3 September, there was a slight temperature drop of 2°C at the interior and bottom depth of Mooring 100, while Moorings 98 and 99 were witnessing temperature rises. In fact, the uppermost instrument at 99, which was 8 m from the surface, measured a 2°C temperature rise. It is entirely likely that a Gulf Stream frontal filament was present within the region. Unfortunately, the VHRR imagery needed to confirm this shows nothing but clouds. This current and temperature description is consistent with the filament concepts presented in Section 4.7-1 of this report.

With the approach of the northern boundary of David, the winds suddenly increased in magnitude. On 3 September the winds were easterly and of magnitude 30 m s^{-1} at the mooring array site. By 4 September the winds had rotated somewhat and were southeasterly. The magnitude was about 25 m s^{-1}. On the 5th, the eye at its closest to the Charleston array, but the central pressure had been reduced. Winds were southerly and about 16 m s^{-1}. On the 6th, 7th, and 8th the mooring array winds continued to rotate clockwise, since they were on the eastern edge of the hurricane and their magnitudes and directions were 20 m s^{-1} and southeasterly on the 6th, 15 m s^{-1} and southereasterly on the 7th, and 10 m s^{-1} and east-southeasterly on the 8th. At Charleston, winds were about double the offshore magnitude values given above, and directions were consistent with the buoy winds described above.

The pressure sensor at Site 9803, 27 m from the surface in 29+ of water indicated a rather dramatic drop of about 35 centimeters between 3 and 7 September. This was followed by a 33 cm rise, peaking on the 10th, and then another 33 cm drop, bottoming on the 16th. Pressure rose 15 cm and then vacillated thereafter. It is quite likely that the initial drop in pressure reflected the atmospheric depression. Herein it is of note that pressure

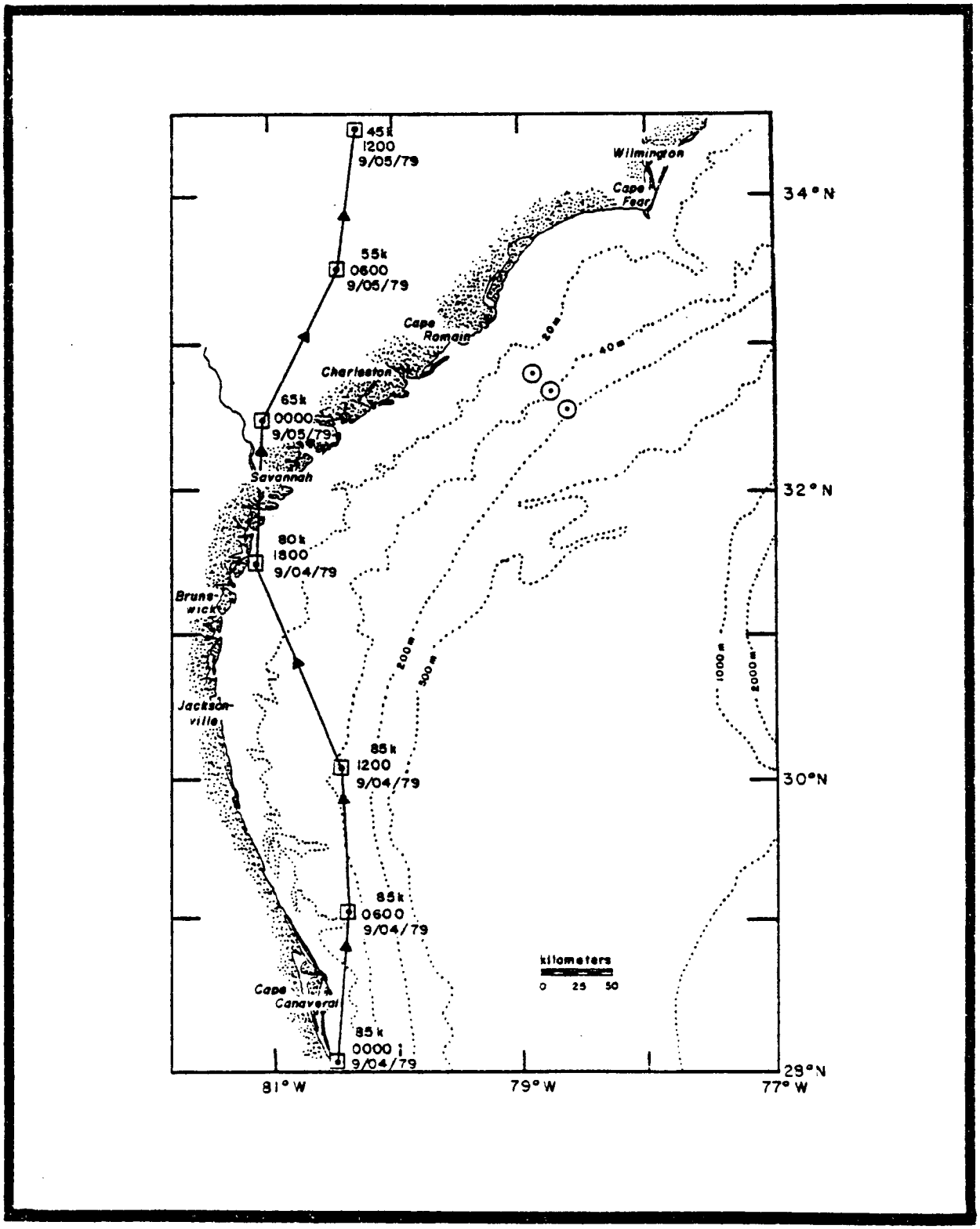

Figure 4.7-48. Map showing approximate path of David's eye through the South Atlantic Bight, with wind speed in knots noted. Note also the location of Moorings 098, 099, and 100 (⊙).

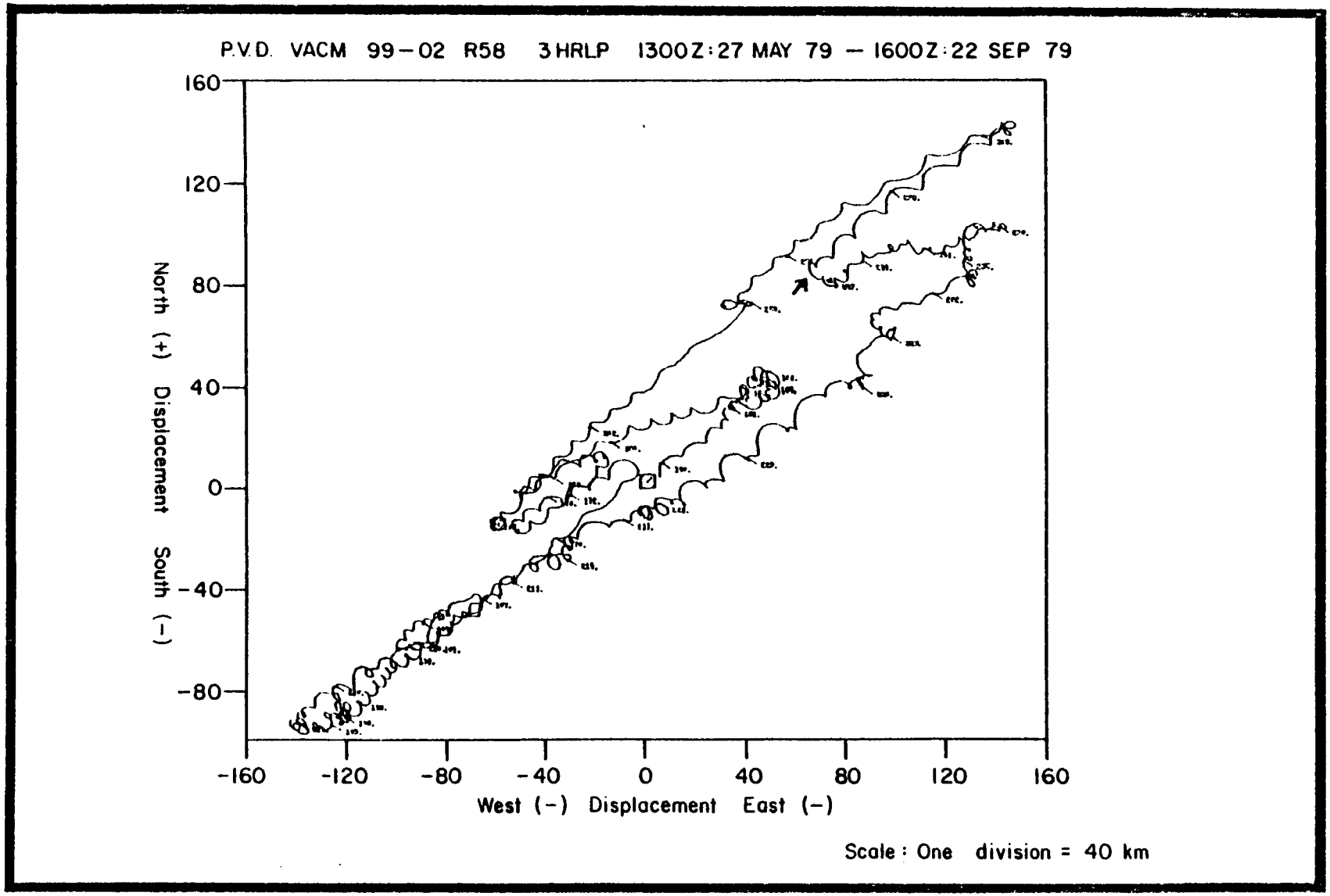

Figure 4.7-49. Progressive vector diagram for Mooring 099-02. Arrow indicates inertial loop through which currents rotated about 4 September 1979.

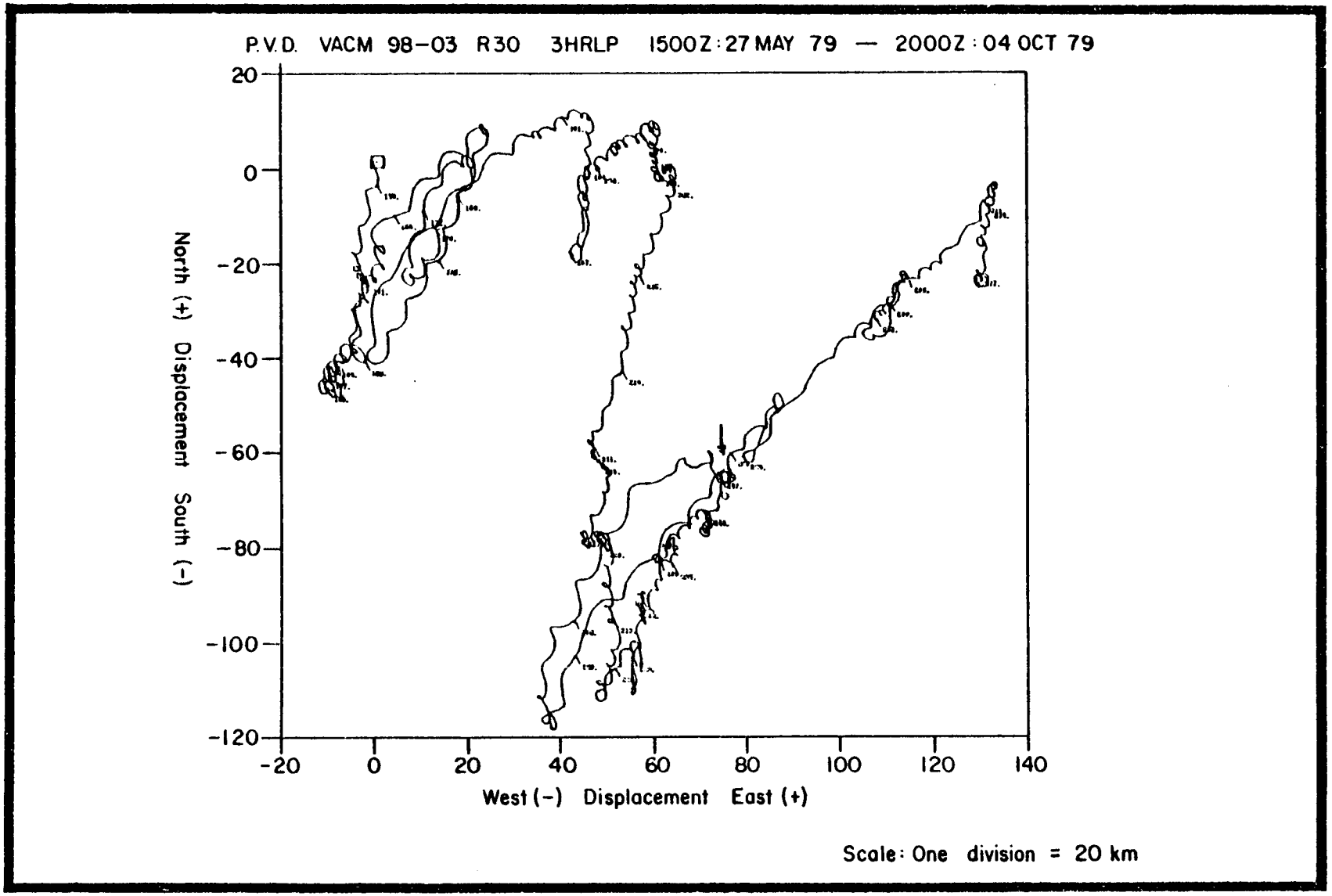

Figure 4.7-50. Progressive vector diagram for Mooring 099-02. Arrow indicates inertial loop through which currents rotated about 4 September 1979.

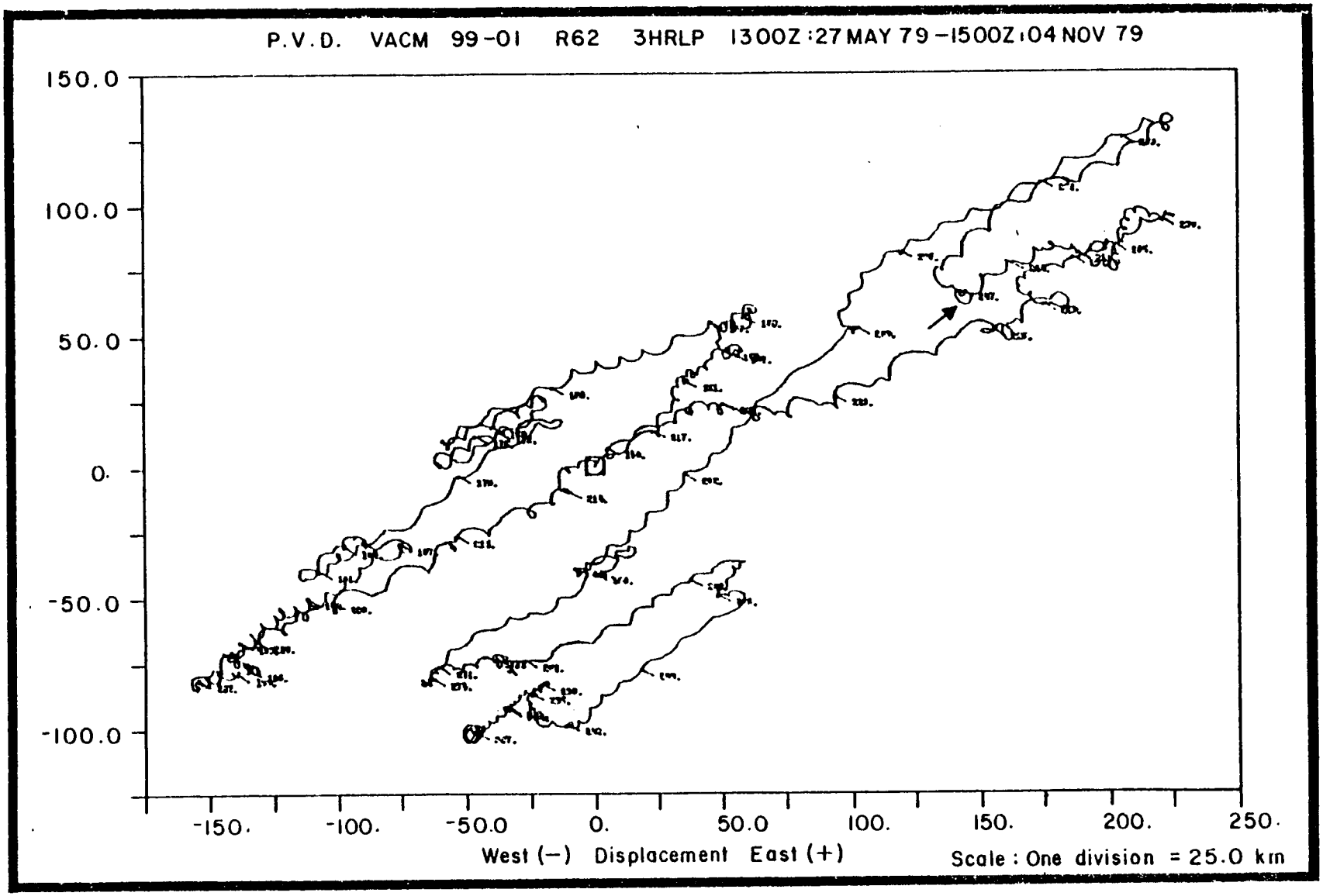

Figure 4.7-51. Progressive vector diagram for Mooring 099-01. Arrow indicates inertial loop through which currents rotated about 4 September 1979.

fluctuations, nearly as high as those observed during the storm, existed for nearly a week after the storm had passed.

The current meter records are presented in Figures 4.7-52 through 4.7-54. These are 40-HLP records. In Section 4.7-6 the mean circulation on the outer Charleston shelf was described as being southeasterly to southwesterly. Clearly that is the norm at Mooring 100 and more often the case at Mooring 99. Therefore, the passage of David caused one anomaly to the flow on the outer shelf; it caused the currents to flow to the northeast at the 35- and 44-m isobaths, throughout the entire water column. Given the previous description of the winds, this appears to have been a mechanical, time dependent response wherein the flow from top to bottom was in the direction of, with some clockwise turning from, the wind stress vector. Curiously, currents at Mooring 98 in 29+ m of water reflect a jet-like, 50 cm s^{-1} to the southwest to south-southeast. This data was collected 2 m from the bottom and likely does not reflect the net response in the interior or at the surface. What occurred was that the southeasterly winds, while driving outer-shelf waters away from the coast, actually piled water up at the coast. In addition, there was a surge of water up into the eye. The net result was a sea surface sloping downward from the coast out to about the 30-m isobath and an upward tilt of the surface out to beyond the 45-m isobath. In addition, the shelf was flooded with a layer of cold water, reaching lows of 16.5, 17.5, and 22.4°C at the 44-, 35-, and 29-m isobaths, respectively.

The sea-surface drop from the coast out to the 30-m isobath would barotropically-geostrophically drive a jet to the south, which is manifested at current meter element 9803. The 15 cm rise required at the coast relative to sea level at the 30-m isobath was substantiated by the actual rise of 24 cm at the coast, which was in excess of that required to drive the flow.

The time series of temperatures reflecting the flooding is shown in Figures 4.7-55 through 4.7-57. Because of the inner-shelf dynamics, this essentially became a one-sided divergence of outer-shelf water with massive self-break upwelling of cold nutrient rich water which subsequently spilled across the shelf.

Within several days of the event passage, the outer-shelf currents were southerly again, as is the norm, and the inner-shelf currents were adjusted to the conventional seasonal wind field.

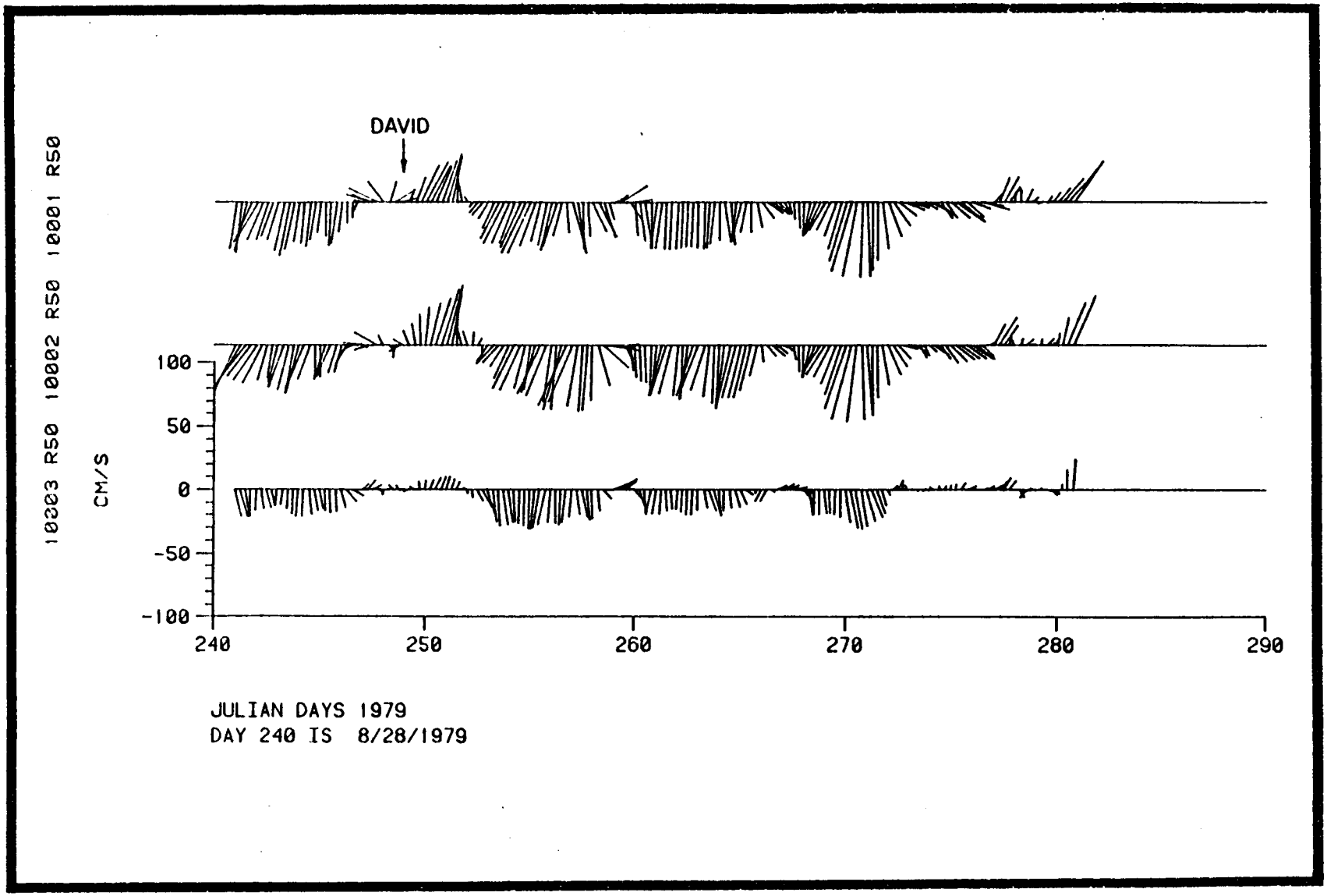

Figure 4.7-52. Forty-HLP current vectors for Mooring 100-03 with the passage of Hurricane David indicated.

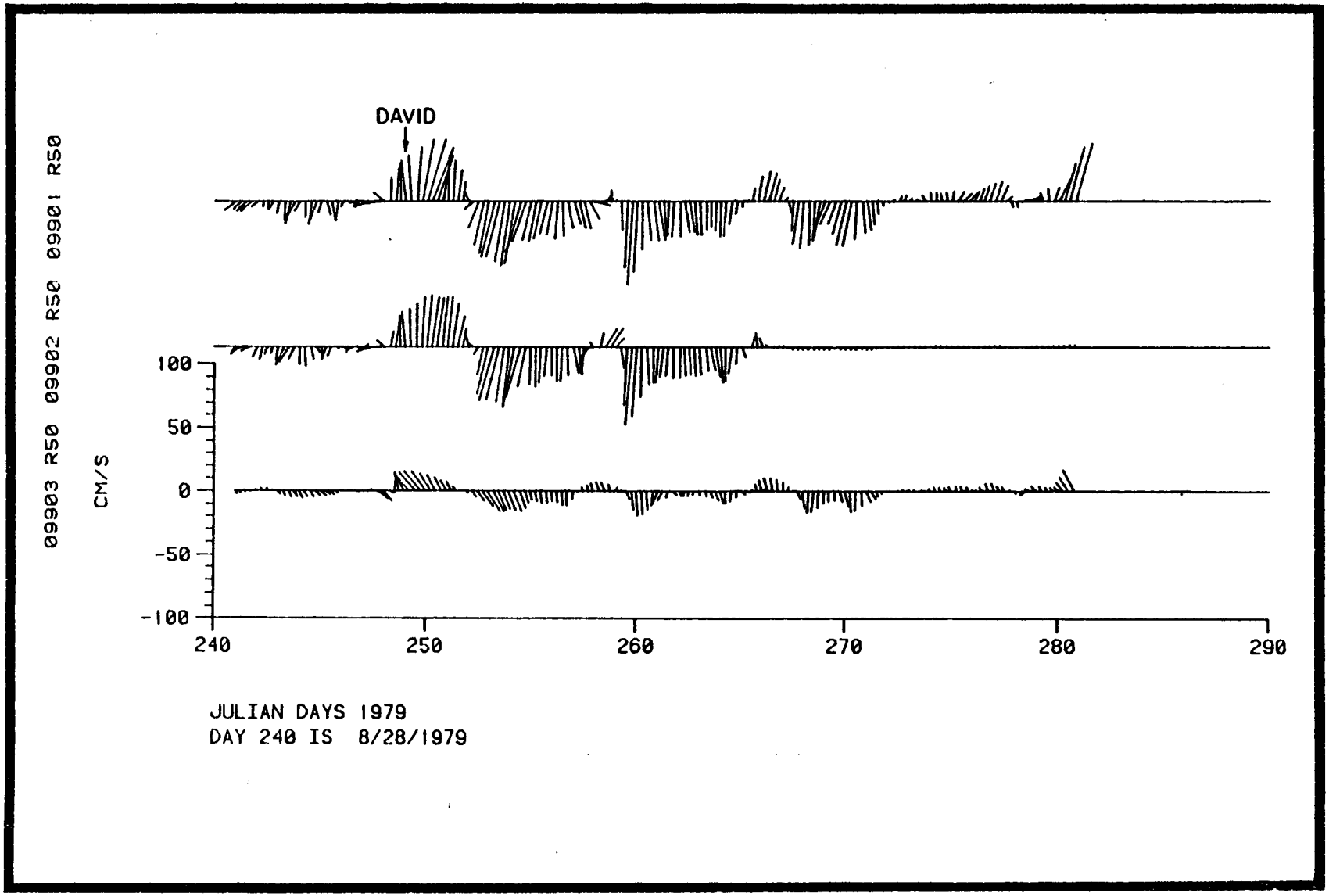

Figure 4.7-53. Forty-HLP current vectors for Mooring 099-03 with the passage of Hurricane David indicated.

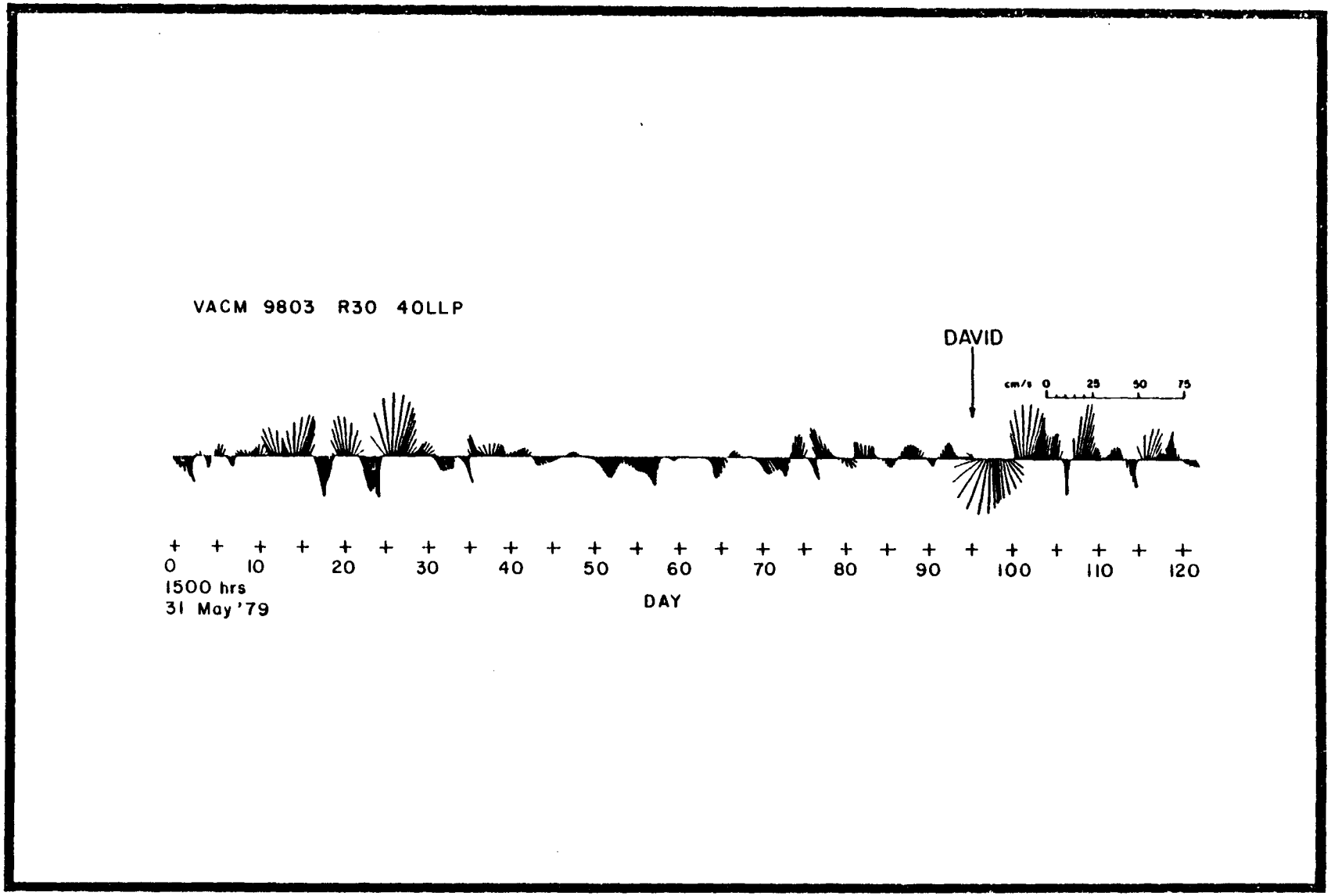

Figure 4.7-54. Forty-HLP current vectors for Mooring 098-03 with the passage of Hurricane David indicated.

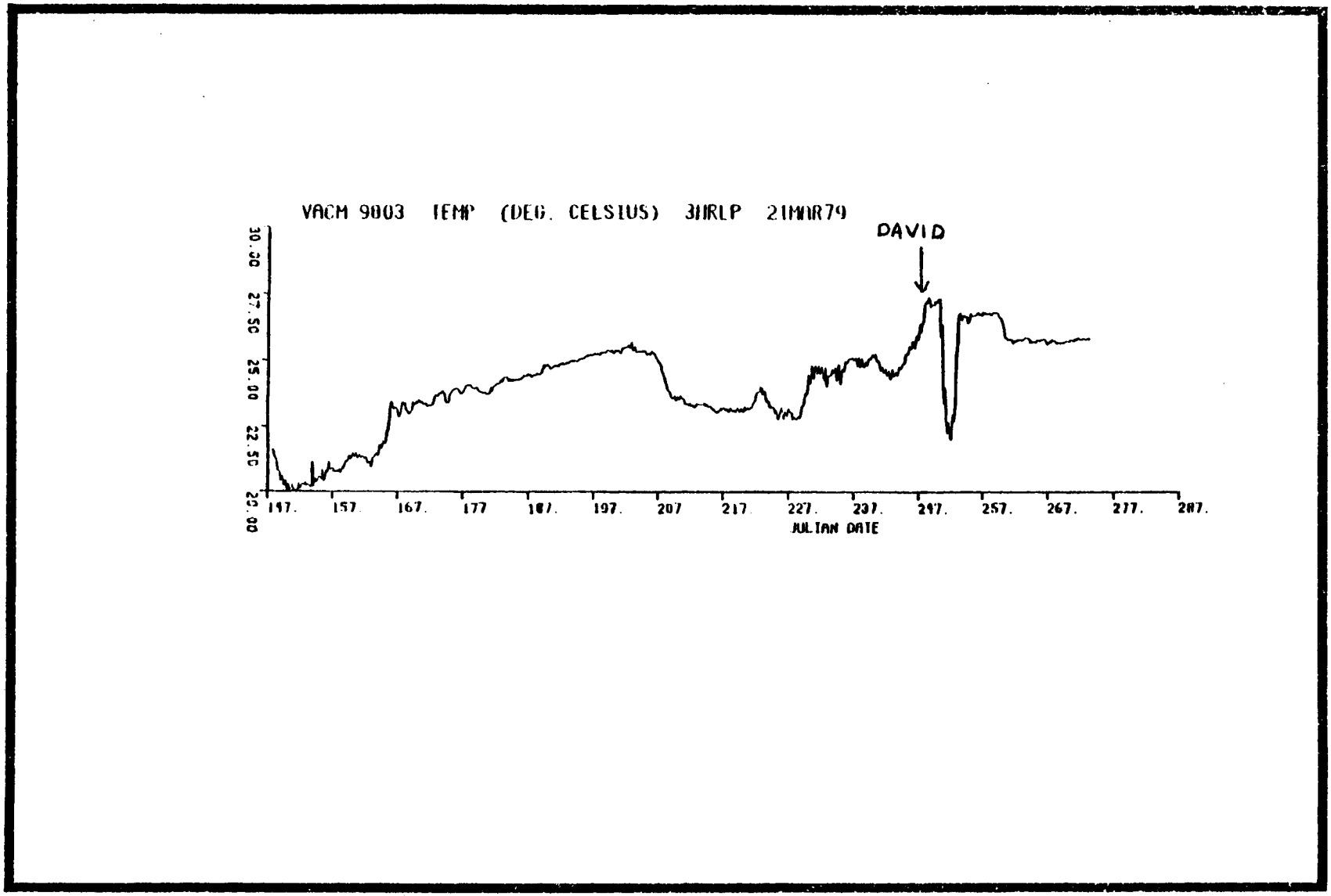

Figure 4.7-55. Three-HLP time series of temperature for Mooring 098-03 with the passage of Hurricane David indicated.

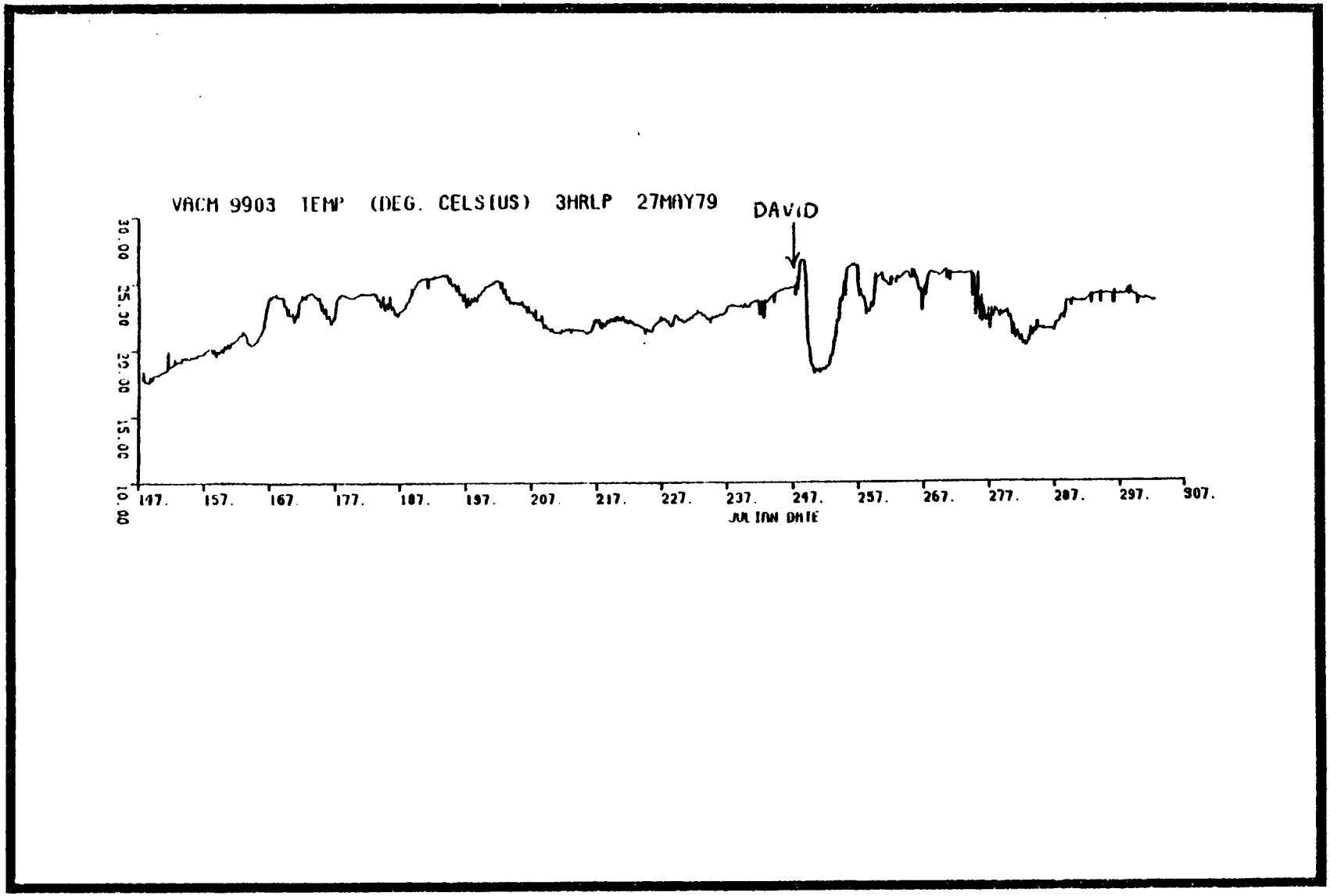

Figure 4.7-56. Three-HLP time series of temperature for Mooring 099-03 with the passage of Hurricane David indicated.

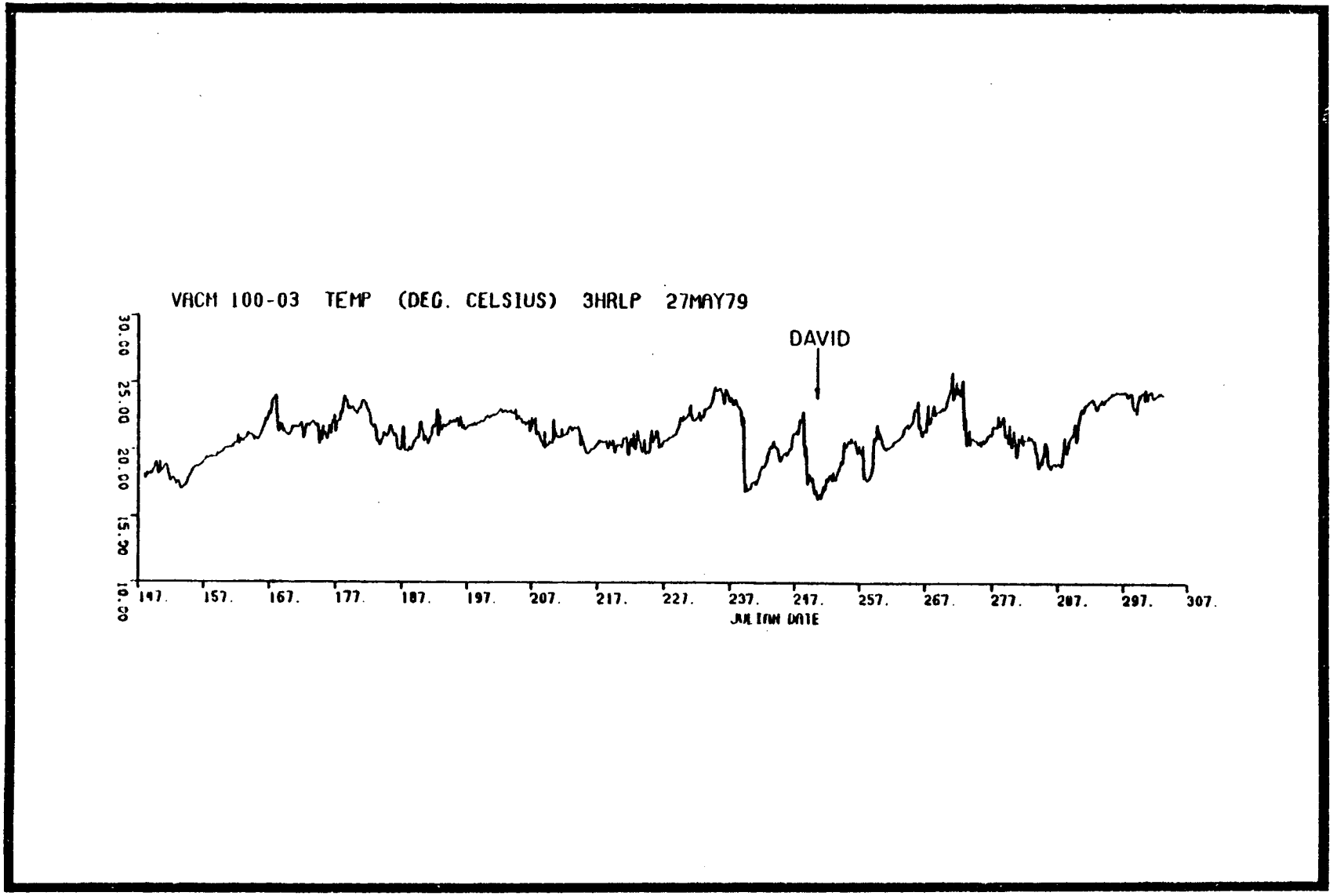

Figure 4.7-57. Three-HLP time series of temperature for Mooring 100-03 with the passage of Hurricane David indicated.

REFERENCES

American Association of Petroleum Geologists, 1970. Bathymetric Maps, Eastern Continental Margin, USA, Atlantic Ocean South of Cape Hatteras. Sheet 2 of 3.

Anderson, W. and J. Gehringer 1957a. Physical oceanographic, biological and chemical data: South Atlantic Coast of the United States, M/V Theodore N. Gill Cruise 3. U.S. Fish and Wildlife Serv., Spec. Sci. Rep. No. 210, 208 pp.

Anderson, W. and J. Gehringer, 1957b. Physical oceanographic, biological and chemical data: South Atlantic Coast of the United States, M/V Theodore N. Gill Cruise 4. U.S. Fish and Wildlife Serv., Spec. Sci. Rep. No. 234, 192 pp.

Anderson, W. and J. Gehringer, 1958. Physical oceanographic, biological and chemical data: South Atlantic Coast of the United States, M/V Theodore N. Gill Cruise 5. U.S. Fish and Wildlife Serv., Spec. Sci. Rep. No. 248, 220 pp.

Anderson, W. and J. Gehringer, 1959a. Physical oceanographic, biological and chemical data: South Atlantic Coast of the United States, M/V Theodore N. Gill Cruise 7. U.S. Fish and Wildlife Serv., Spec. Sci. Rep. No. 278, 277 pp.

Anderson, W. and J. Gehringer, 1959b. Physical oceanograpic, biological and chemical data: South Atlantic Coast of the United States, M/V Theodore N. Gill Cruise 8. U.S. Fish and Wildlife Serv., Spec. Sci. Rep. No. 303, 227 pp.

Anderson, W. and J. Gehringer, 1959c. Physical oceanographic, biological and chemical data: South Atlantic Coast of the United States, M/V Theodore N. Gill Cruise 9. U.S. Fish and Wildlife Serv., Spec. Sci. Rep. No. 313, 226 pp.

Anderson, W., J. Gehringer and E. Cohen, 1956a. Physical oceanographic, biological and chemical data: South Atlantic Coast of the United States, M/V Theodore N. Gill Cruise. U.S. Fish and Wildlife Serv., Spec. Sci. Rep. No. 178, 160 pp.

Anderson, W., J. Gehringer and E. Cohen, 1956b. Physical oceanographic, biological, and chemical data: South Atlantic Coast of the United States, M/V Theodore N. Gill Cruise 2. U.S. Fish and Wildlife Serv., Spec. Sci. Rep. No. 198, 270 pp.

Armstrong, F.A.J., C.R. Stearns and J.D.H. Strickland, 1967. The measurement of upwelling and subsequent biological processes by means of the Technicon Autoanalyzer and associated equipment. Deep-Sea Res. 14: 381-389.

Arthur, R.S., 1965. On the calculation of vertical motion in eastern boundary currents from determinations of horizontal motion. J. Geophys. Res. 70: 2799-2803.

Atkinson, L.P., 1978. The results of four oceanographic cruises in the Georgia Bight. Georgia Marine Science Center, Tech. Rep. 78-1, 77 pp.

Atkinson, L.P., J.O. Blanton and E.B. Haines, 1978a. Shelf flushing rates based on the distribution of salinity and freshwater in the Georgia Bight. Estuarine and Coastal Mar. Sci. 7: 467-472.

Atkinson, L.P., A.L. Edwards, J.J. Singer, W.S. Chandler and G.-A. Paffenhöfer, 1979. Hydrographic observations in the Georgia Bight (July 1977). Georgia Marine Science Center, Tech. Rep. 79-3, 126 pp.

Atkinson, L.P., T.N. Lee, J.O. Blanton and W.S. Chandler, in press. Climatology of the Southeastern United States continental shelf waters. J. Geophys. Res.

Atkinson, L.P., G.-A. Paffenhöfer and W.M. Dunstan, 1978b. The chemical and biological effect of a Gulf Stream intrusion off St. Augustine, Florida. Bull. Mar. Sci. 28: 667-679.

Atkinson, L.P. and T.E. Targett, in press. Upwelling along the 60-m isobath from Cape Canaveral to Cape Hatteras and its relationship to fish distribution. Deep-Sea Res.

Bane, J.M., Jr., in press. Initial observations of the subsurface structure and short term variability of the seaward deflection of the Gulf Stream off Charleston, South Carolina. J. Geophys. Res.

Bane, J.M., Jr. and D.A. Brooks, 1979. Gulf Stream meanders along the continental margin from the Florida Straits to Cape Hatteras. Geophys. Res. Lett. 6: 280-282.

Bane, J.M., Jr. and D.A. Brooks, 1981. The Gulf Stream meanders experiment: AXBT/PRT data report, R/A Project Seascan flights, 21-29 November 1979. University of North Carolina, Chapel Hill, Tech. Rep. CMS-81-1, 174 pp.

Bane, J.M., Jr., D.A. Brooks and M.J. Ignaszewski, 1980a. The Gulf Stream meanders experiment: hydrographic data report, R/V Endeavor cruises EN-040 (2-8 August 1979) and EN-045 (16-23 November 1979). Texas A&M University. Rep. 80-10T, 170 pp.

Bane, J.M., Jr., D.A. Brooks, and K.R. Lorenson, 1981. Synoptic observations of the three-dimensional structure and propagation of Gulf Stream meanders along the Carolina continental margin. J. Geophys. Res. 86: 6411-6425.

Bane J.M., Jr., D.A. Brooks, K.R. Lorenson and C.M. Seay, 1980b. The Gulf Stream meanders experiment: AXBT/PRT data report, R/A Project Birdseye flights 9-18 February 1979. University of North Carolina, Chapel Hill. Tech. Rep. CMS-80-2, 213 pp.

Bane, J.M., Jr., D.A. Brooks, K.R. Lorenson and C.M. Seay, 1980c. Three-dimensional view of a Gulf Stream meander between Savannah, Ga. and Cape Hatteras, N.C. Gulf Stream 6(5): 3-7.

Bartlett, J.R., 1883. Deep-sea soundings and temperatures in the Gulf Stream off the Atlantic coast. Proc. Amer. Assoc. Ad. Sci. 31:349-352.

Beardsley, R.C. and B. Butman, 1974. Circulation on the New England continental shelf: response to strong winter storms. Geophys. Res. Lett. 1: 181-184.

Beardsley, R.C. and W.C. Boicourt, 1981. On estuarine and continental shelf circulation in the middle Atlantic Bight. In: B.A. Warren and C. Wunsch (eds.), Evolution of Physical oceanography, Scientific Surveys in Honor of Henry Stommel. MIT Press, pp. 198-233.

Bishop, S.S., J.A. Yoder and G.-A. Paffenhöfer, 1980. Phytoplankton and nutrient variability along a cross-shelf transect off Savannah, Georgia, USA. Estuarine and Coastal Mar. Sci. 11: 359-368.

Blanton, J.O., 1980. The transport of freshwater off a multi-inlet coastline. In: P. Hamilton and K.B. Macdonald (eds.), Estuaries and Wetland Precesses with Emphasis on Modeling. Plenum Press, New York, pp. 49-64.

Blanton, J.O., 1981. Ocean currents along a nearshore frontal zone on the continental shelf of the southeastern U.S., J. Geophys. Res. 11: 1627-1637.

Blanton, J.O., L.P. Atkinson, L.J. Pietrafesa and T.N. Lee, 1981. The intrusion of Gulf Stream water across the continental shelf due to topographically induced upwelling. Deep-Sea Res. 28: 393-405.

Bradshaw, A. and K.E. Schleicher, 1965. The effect of pressure on the electrical conductance of sea water. Deep-Sea Res. 12: 151-162.

Brooks, D. A., 1978. Subtidal sea-level fluctuations and their relationship to atmospheric forcing along the North Carolina coast. J. Phys. Oceanogr. 8:481-493.

Brooks, D. A. and C.N.K. Mooers, 1977. Wind-forced continental shelf waves in the Florida Current. J. Geophys. Res. 82: 2569-2576.

Brooks, D.A. and J.M. Bane, Jr., 1978. Gulf Stream deflection by a bottom feature off Charleston, South Carolina. Science 201: 1225-1226.

Brooks, D.A. and J.M. Bane, Jr., 1981. Gulf Stream fluctuations and meanders over the Onslow Bay upper continental slope. J. Phys. Oceanogr. 6: 111-156.

Brooks, D.A., J.M. Bane, Jr. and M.J. Ignaszewski, 1980. The Gulf Stream meanders experiment: hydrographic data report, R/V Endeavor cruises EN-031 (12-19 January 1979) and EN-037 (23-29 May 1979). Rep. 80-1-T, Texas A&M University, 145 pp.

Brooks, I.H., 1979. Fluctuations in the transport of the Florida current at periods between tidal and two weeks. J. Phys. Oceanogr. 9: 1048-1053.

Brooks, I.H. and P.O. Niiler, 1977. Energetics of the Florida Current. J. Mar. Res. 35: 163-191.

Brown, N.L. and Allentroft, 1966. Salinity, conductivity and temperature relationship of sea water over the range 0-50 ppt. (ONR Contract No. 4290 (00) Final Report, MJO No. 2003).

Bumpus, D.F., 1955. The circulation over the continental shelf south of Cape Hatteras. Trans. Am. Geophys. Union. 36: 601-611.

Bumpus, D.F., 1973. A description of the circulation on the continental shelf of the East Coast of the United States. Prog. in Oceanogr., 6: York, , 111-156.

Bumpus, D.F. and J. Chase, 1965. Changes in the hydrography observed along the east coast of the United States. In: International Commision on Northwest Atlantic Fisheries, Spec. Pub. No. 6, WHOI Contribution 1467, pp 847-853.

Bumpus, D.F. and E.L. Pierce, 1955. The hydography and the distribution of chaetognaths over the continental shelf off North Carolina. Deep-Sea Res. 3, Supplement: 92-109.

Bunker, A.F., 1976. Computations of surface energy flux and annual air-sea interaction cycles of the North Atlantic Ocean. Monthly Weather Review 104: 112-1140.

Busby, R.F., 1969. The drift of the Ben Franklin. The Gulf Stream, 3(8): 2-3.

Cartwright, D.E. and R.J. Taylor, 1971. New Computations of the tide-generating potential. Geophys. J. of Roy. Astr. Soc. 23:45-74.

Chandler, W.S., L.P. Atkinson, J.J. Singer, P.G. O'Malley and C.V. Baker, 1978. A CTD system: description, operation, data acquisition and processing. Georgia Marine Science Center. Tech. Rep. 78-7, 84 pp.

Chao, S.Y. and G.S. Janowitz, 1979. The effect of a localized topographic irregularity on the flow of a boundary current along the continental margin. J. Phys. Oceanogr. 9: 900-910.

Chao, S.Y. and L.J. Pietrafesa, 1980. The subtidal response of sea level to atmospheric forcing in the Carolina Capes. J. Phys. Oceanogr. 10: 1246-1255.

Chase, J., 1969. Surface salinity along the east coast of the United States. Deep-Sea Res. 16, Supplement; 25-29.

Chase, J., 1971. Oceanographic observations along the east coast of the United States. Oceanogr. Rep. No. 38 (CG 373-38), U.S. Coast and Geodetic Survey, 149 pp.

Chew, F., 1974. The turning process in meandering currents: A case study. J. Phys. Oceanogr. 4: 27-57.

Chew, F., 1981. Spin-off eddies and a hypothesis. Deep-Sea Res. 28: 329-391.

Church, P., 1937. Temperatures of the western North Atlantic from thermograph records. In: Publication Scientifique No. 4., Association de'Oceanographie Physique, Union Geodesique et Geophysique Internationale, 36 pp.

Costin, J.M., 1969. Gulf Stream transits south of Cape Hatteras. The Gulf Stream, 4(9): 3-4.

Curtin, T.B., 1979a. Ocean outfall waste water disposal feasibility and planning study: oceanographic field observations off North Carolina, summer survey 2-12 August 1977. North Carolina State University, Rep. No. 79-2, 87 pp.

Curtin, T.B., 1979b. Ocean outfall waste water disposal feasibility and planning study: oceanographic field observations off North Carolina, winter survey 2-12 February 1978. North Carolina State University, Rep. No. 79-3, 29 pp.

Curtin, T.B., 1979c. Ocean outfall waste water disposal feasibility and planning study: oceanographic field observations off North Carolina, spring survey 12-22 May 1978. North Carolina State University, Rep. No. 79-4, 84 pp.

Curtin, T.B., 1979d. Ocean outfall waste water disposal feasibility and planning study: oceanographic field observations off North Carolina, fall survey 1-11 November 1977. North Carolina State University, Rep. No. 79-5, 81 pp.

DeRycke, R.J. and P.K. Rao, 1973. Eddies along a Gulf Stream boundary viewed from a Very High Resolution Radiometer. J. Phys. Oceanogr., 3: 490-492.

Deschamps, J.R., L.P. Atkinson, J.J. Singer, W.S. Chandler and T.N. Lee, 1979. Hydrographic observations in the Georgia Bight (December 1976). Georgia Marine Science Center, Tech. Rep. 79-1, 97 pp.

Doodson, A.T. and H.D. Warburg, 1941. Admiralty Manual of Tides. His Majesty's Stationary Office, London, 270 pp.

Düing, W., 1975. Synoptic studies of transients in the Florida Current. J. Mar. Res. 33: 53-73.

Ewing, H., M. Ewing and R. Leyden, 1966. Seismic-profiler survey of Blake Plateau. Bull. Amer. Assoc. Petr. Geolog. 50: 1948-1971.

Foreman, M.G.G., 1977. Manual for tidal heights analysis and prediction. Institute of Ocean Sciences, Pacific Marine Science Report 77-10, Patricia Bay, Victoria, B.C., 97 pp.

Friederich, G.E. and T.E. Whitledge, 1972. Autoanalyzer procedures for nutrients. In: S.P. Pavlou (ed.), Phytoplankton Growth Dynamics: Technical Series 1, Chemostat Methodology and Chemical Analyses, Spec. Rep. No. 52. Department of Oceanography, University of Washington, Seattle, Washington, pp. 38-60.

Fuglister, F.C., 1947. Average monthly sea surface temperatures of the western North Atlantic Ocean. Pap. Phys. Oceanogr. and Meteorol. 10(2): 1-25 pp.

Fuglister, F.C., 1951. Annual variations in current speeds in the Gulf Stream system. J. Mar. Res. 10: 119-127.

Fuglister, F.C. and A.D. Voorhis, 1965. A new method of tracking the Gulf Stream. Limnol. Oceanogr. 10: R115-R124.

Fuglister, F.C. and L.V. Worthington, 1951. Some results of a multiple ship survey of the Gulf Stream. Tellus 3(1): 1-14.

Fukuoka, J., 1961. An analysis of the mechanism of the cold and warm water masses in the seas adjacent to Japan: Records of Oceanographic Works in Japan 6(1): 63-100.

Galt, J.A., 1975. Development of a simplified diagnostic model for interpretation of oceanographic data. NOAA Tech. Rep. ERL 339-PMEL 25, 46 pp.

Gill and Schumann, 1974. The generation of long shelf-waves by the wind. J. Phys. Oceanogr. 4: 83-90.

Glibert, P.M. and T.C. Loder, 1977. Automated analysis of nutrients in seawater: a manual of techniques. Woods Hole Oceanographic Institute, Tech. Rep. 77-47, 46 pp.

Godin, G., 1972. The Analysis of Tides. University of Toronto Press, Toronto, 264 pp.

Green, C.K., 1944. Summer upwelling, northeast coast of Florida. Science 100: 546-547.

Haines, E.B., 1974. Processes affecting production in Georgia coastal waters. Ph.d. Dissertation, Duke University, 118 pp.

Haines, E.B. and W.M. Dunstan, 1975. The distribution and relation of particulate organic material and primary productivity in the Georgia Bight. Estuarine and Coastal Mar. Sci. 3: 431-441.

Haltiner, G.J. and F.L. Martin, 1957. Dynamical and Physical Meteorology. McGraw-Hill, New York, 470 pp.

Hazelworth, J.B., 1976. Oceanographic variations across the Gulf Stream off Charleston, South Carolina during 1965 and 1966. NOAA Tech. Rep. ERL 383-AOML 25, 73 pp.

Hickey, B.M. and P. Hamilton, 1980. A spin-up model as a diagnostic tool for interpretation of current and density measurements on the continental shelf of the Pacific Northwest. J. Phys. Oceanogr. 10: 12-24.

Iselin, C. O'D., 1938. A promising theory concerning the causes and results of long-period variations in the strength of the Gulf Stream system. Trans. Amer. Geophys. Union 19: 243-244. Meeting, 243-244.

Iselin, C. O'D., 1940. Preliminary report on long-period variations in the transport of the Gulf Stream system. Papers Phys. Oceanogr. and Meteorol. (8)1: 1-40.

Jacobson, J.P., 1974. A socio-economical environmental baseline summary for the South Atlantic region between Cape Hatteras, North Carolina and Cape Canaveral, Florida, Phys. Oceanogr., Vol. 1. Virginia Institute of Marine Science, Gloucester Point, Virginia. (BLM Contract No. EQ4AC007, Final Report, NTIS Access. No. PB80-216187), 247 pp.

Janowitz, G.S. and L.J. Pietrafesa, 1980a. A model and observations of time-dependent upwelling over the mid-shelf and slope. J. Phys. Oceanogr. 10: 1574-1583.

Janowitz, G.S. and L.J. Pietrafesa, 1980b. Verification of a time dependent upwelling model. EOS, Trans., AGU 61 (46): 986.

Janowitz, G.S. and L.J. Pietrafesa, 1982. The effects of alongshore variation in bottom topography on a boundary current (topographically induced upwelling). Continental Shelf Res. 1(2): 123-141.

Kantha, L.H., A.F. Blumberg, H.J. Herring and G.L. Mellor, 1981. The physical oceanographic and sea-surface flux climatology of the South Atlantic Bight. Dynalysis of Princeton Report No. 70 (BLM Contract No. AA551-CT9-32), 142 pp.

Klinck, J.M., L.J. Pietrafesa, and G.S. Janowitz, 1981. Continental shelf circulation induced by a moving localized wind stress. J. Phys. Oceanogr. 11: 836-848.

Knauss, J.A., 1969. A note on the transport of the Gulf Stream. Deep-Sea Res. 16: 117-123.

Lasley, S.R., L.P. Atkinson, J.J. Singer and W.S. Chandler, 1979. Hydrographic observations in the Georgia Bight (April 1978). Georgia Marine Science Center, Tech. Rep. 79-5, 94 pp.

Lasley, S.R., L.P. Atkinson, J.J. Singer and W.S. Chandler, 1981. Hydrographic observations in the Georgia Bight (April 1979). Georgia Marine Science Center, Tech. Rep. 81-1, 210 pp.

Leaman, K.D., T.N. Lee and R.D. Finley, in press. Performance of an experimental Aanderaa current meter modified for near-surface measurements. Marine Technical Society.

Lee, T.N., 1975. Florida current spin-off eddies. Deep-Sea Res. 22: 753-765.

Lee, T.N., and L.P. Atkinson, in press. Low frequency current and temperature variability from Gulf Stream frontal eddies and atmospheric forcing along the southeast U.S. outer continental shelf. J. Geophys. Res.

Lee, T.N. and D.A. Brooks, 1979. Initial observations of current, temperature and coastal sea-level response to atmospheric and Gulf Stream forcing on the Georgia shelf. Geophys. Res. Lett. 6: 321-324.

Lee, T.N. and D. Mayer, 1977. Low-frequency current variability and spin-off eddies on the shelf off southeast Florida. J. Mar. Res. 35: 193-220.

Lee, T.N., E. Daddio and G.C. Han, 1982. Steady-state diagnostic model of summer mean circulation on the Georgia shelf. J. Phys. Oceanogr. 12: 820-838.

Lee, T.N., L.P. Atkinson and R. Legeckis, 1981. Observations of a Gulf Stream frontal eddy on the Georgia continental shelf, April 1977. Deep-Sea Res. 28: 347-378.

Legeckis, R., 1975. Application of synchronous meteorological satellite data to the study of time-dependent, sea-surface temperature changes along the boundary of the Gulf Stream. Geophys. Res. Lett. 2: 435-438.

Legeckis, R., 1979. Satellite observations of the influence of bottom topography on the seaward deflection of the Gulf Stream off Charleston, South Carolina. J. Phys. Oceanogr. 9: 483-497.

Lumley, J.L. and H.A. Panofsky, 1964. The structure of atmospheric turbulence. In: Monographs and Texts in Physics and Astronomy. New York, Interscience.

Mathews, T.D. and O. Pashuk, 1977. A description of oceanographic conditions off the Southeastern United States during 1973. South Carolina Marine Resources Center, Tech. Rep. No. 19, 105 pp.

Matsukawa, Y., 1979. A consideration on the mechanism of generation, stagnation and disappearance of the Kuroshio Meander. J. Oceanogr. Soc. Japan. 35(2): 118-125 (in Japanese).

Maul, G.A., P.W. DeWitt, A. Yanaway and S.R. Baig, 1978. Geostationary satellite observations of Gulf Stream meanders: Infrared measurements and time series analysis. J. Geophys. Res. 83: 6123-6135.

McCreary, J.P., Jr. and W.B. White, 1979. On a theory of the Kuroshio meander. Deep-Sea Res. 26A: 317-320.

Montgomery, R.B., 1938. Fluctuations in monthly mean sea level on eastern U.S. coast as related to dynamics of western North Atlantic Ocean. J. Mar. Res. 1: 165-185.

Moriyasu, S., 1959. Supplementary note on the dynamical property of the cold water region. The Oceanographical Magazine 2(1): 13-19.

Moriyasu, S., 1961. An example of the conditions at the occurrence of the cold water region. The Oceanographic Magazine 12(1): 67-76.

Murphy, J. and J.P. Riley, 1962. A modified single solution method for the determination of phosphate in natural waters. Anal. Chim. Acta 27: 31-36.

Mysak, L. A. and B.V. Hamon, 1969. Low-frequency, sea-level behavior and continental shelf waves. J. Geophys. Res. 74:1397-1405.

Nan-niti, T., 1958. A theory of the mechanism of the generation of the Cold Water Region in the offing of Enshûnada. Papers Meteorol. and Geophys. 8: 317-331.

Neumann, G. and W.J. Pierson, Jr., 1966. Principles of Physical Oceanography. Prentice-Hall, Inc., New Jersey, 545 pp.

Niiler, P.P. and L.A. Mysak, 1971. Barotropic waves along an eastern continental shelf. Geophys. Fluid Dynamics 2: 273-278.

Niiler, P.P. and W.S. Richardson, 1973. Seasonal variability of the Florida Current. J. Mar. Res. 31: 144-167.

O'Malley, P.G., L.P. Atkinson, J.J. Singer, W.S. Chandler and T.N. Lee, 1978. Hydrographic observations in the Georgia Bight (April 1977). Georgia Marine Science Center, Tech. Rep. 78-5, 208 pp.

Oort, A.H., 1964. Computations of eddy heat and density transport across the Gulf Stream. Tellus 16: 55-63.

Orlanski, I., 1969. The influence of bottom topography on the stability of jets in a baroclinic fluid. J. Atmos. Sci. 26: 1216-1232.

Orlanski, I. and M.D. Cox, 1973. Baroclinic instability in ocean currents. Geophys. Fluid Dynamics 4: 287-332.

Parr, A.E., 1933. A geographical-ecology analysis of the seasonal changes in temperature conditions in shallow water along the Atlantic coast of the United States. Bull. Bingham Oceanog. Coll., 4(3): 1-90.

Pashinski, D. J. and G.A. Maul, 1973. Use of ocean temperature while coasting between the straits of Florida and Cape Hatteras." Mariners Weather Log 17(1): 1-3.

Pierce, E.L., 1953. The chaetognatha over the continental shelf of North Carolina with attention to their relation to the hydrography of the area. J. Mar. Res. 12: 75-91.

Pietrafesa, L. J., 1980. Upwelling in the region of the Charleston Bump and areas of the outer continental shelf. EOS, Trans. AGU 61(46): 986.

Pietrafesa, L. J., 1981. Continental shelf processes affecting the oceanography of the South Atlantic Bight. N.C. State University, Raleigh, N.C. (DoE - Contract No. AS09-76-EY00902, Final Report), 765 pp.

Pietrafesa, L.J., 1983. Shelf-break circulation, fronts and physical oceanography: east and west coast perspectives. In: D.J. Stanley and G.J. Moore (eds.), Shelf-slope Boundary, a Critical Interface on Continental Margins. Society of Economic Paleontologists and Mineralogists, Spec. Pub. No. 33, Tulsa, Oklahoma.

Pietrafesa, L.J. and G.S. Janowitz, 1979a. On the effects of buoyancy flux on continental shelf circulation. J. Phys. Oceanogr. 9: 911-918.

Pietrafesa, L.J. and G.S. Janowitz, 1979b. A note on the identification of a Gulf Stream spin-off eddy from Eulerian data." Geophys. Res. Lett. 6: 549-552.

Pietrafesa, L.J. and G.S. Janowitz, 1980. Dynamics of Carolina Capes and implications for sediment transport. Proceedings of Twenty-sixth International Geological Congress, Paris, France, 2-17 July 1980.

Pietrafesa, L.J., J.O. Blanton and L.P. Atkinston, 1978. Evidence for deflection of the Gulf Stream at the Charleston Rise. Gulf Stream 4(9): 3-7.

Pillsbury, J.E., 1891. The Gulf Stream: A description of methods employed in the investigation and the results of the research. Report, U.S. Coast and Geodetic Survey for 1890, Appendix No. 10, pp. 461-620.

Pratt, R.M., 1963. Bottom currents on the Blake Plateau. Deep-Sea Res. 10: 245-249.

Pratt, R.M., 1966. The Gulf Stream as a graded river. Limnol. Oceanogr. 11: 60-67.

Pritchard, D.W., 1960. Salt balance and exchange rate for Chincoteague Bay. Chesapeake Sci. 1: 48-57.

Roa, P.K., A.E. Strong and R. Koffler, 1971. Gulf Stream meanders and eddies as seen in satellite infrared imagery. J. Phys. Oceanogr. 2: 237-239.

Richardson, W.S., W.J. Schmitz, Jr. and P.P. Niiler, 1969. The velocity structure of the Florida current from the Straits of Florida to Cape Fear. Deep-Sea Res. 16, Supplement: 225-231.

Robinson, A.R. and B.A. Taft, 1972. A numerical experiment for the path of the Kuroshio. J. Mar. Res. 30: 65-101.

Rooney, D.M., G.S. Janowitz and L.J. Pietrafesa, 1978. A simple model of deflection of the Gulf Stream by the Charleston Rise. Gulf Stream 4(11): 3-7.

Ruzecki, E.P., 1974. A socio-economic environmetal baseline summary for the South Atlantic region between Cape Hatteras, North Carolina and Cape Canaveral, Florida." Climatology, Vol. 1. Virginia Institute of Marine Science, Gloucester Point, Virginia (BLM Contract No. EQ4AC007, Final Report, NTIS Access. No. PB80-216286), 211 pp.

Science Applications, Inc., 1979. South Atlantic OCS Physical Oceanography, Final Progress Report (First Year), Vol. II: Technical Report. (BLM Contract No. AA550-CT7-29, NTIS Access No. PB80-181555), 326 pp.

Science Applications, Inc., 1981. South Atlantic OCS Physical Oceanography, Final Progress Report (Second Year), Vol. II: Technical Report. (BLM Contract No. AA551-CT8-52), 354 pp.

Science Applications, Inc., 1982. South Atlantic OCS Physical Oceanography, Final Progress Report (Third Year), Vol. II: Technical Report. (BLM Contract No. AA851-CTO-12, NTIS Access No. PB83-144394), 515 pp.

Saunders, P.M., 1977. Wind stress on the ocean over the eastern continental shelf of North America. J. Phys. Oceanogr. 7: 555-556.

Schmitz, W.J., Jr. and P.P. Niiler, 1969. A note on the kinetic energy exchange between fluctuations and mean flow in the surface layer of the Florida current. Tellus 21: 814-819.

Schmitz, W.J., Jr. and W.S. Richardson, 1968. On the transport of the Florida Current. Deep-Sea Res. 15: 679-693.

Schroeder, E.H., 1963. North Atlantic temperatures at a depth of 200 meters. Serial atlas of the marine environment, Folio 2, American Geographical Society.

Schwing, F.B., B. Kjerfve and J.E. Sneed, in press. Scales of estuarine sea level oscillations. Estuarine, Coastal and Shelf Science.

Scott, J.T. and G.T. Csanady, 1976. Nearshore currents off Long Island. J. Geophys. Res. 81: 5401-5409.

Singer, J. J., L.P. Atkinson, J.O. Blanton and J.A. Yoder, in press. Cape Romain and the Charleston Bump: historical and recent hydrographic observations. J. Geophys. Res.

Singer, J.J., L.P. Atkinson, W.S. Chandler and S.S. Bishop, 1980. Hydrographic observations off Savannah and Brunswick, Georgia (March, May and September 1977 and January 1978). Georgia Marine Science Center, Tech. Rep. 80-1, 105 pp.

Smith, R.L., 1968. Upwelling. In: H. Barnes (ed.), Oceanography, George Allen and Unwin Ltd., London, pp. 11-46.

Stefánsson, U., L.P. Atkinson and D.F. Bumpus, 1971. Hydrographic properties and circulation of the North Carolina shelf and slope waters. Deep-Sea Res. 18: 383-420.

Strack, S.L., 1953. Surface temperature gradients as indicators of the position of the Gulf Stream. Woods Hole Oceanographic Institute, Tech. Rep. 53-53, 25 pp.

Strickland, J.D. and T.R. Parsons, 1972. A practical handbook of seawater analysis. Bull. Fish. Res. Board Can. 167: 1-310.

Stumpf, H.G. and P.K. Rao, 1975. Evolution of Gulf Stream eddies as seen in satellite infrared imagery. J. Phys. Oceanogr. 5: 388-393.

Sturges, W., 1974. Sea-level slope along continental boundaries. J. Geophys. Res. 79: 825-830.

Swallow, T.C. and L.V. Worthington, 1961. An observation of a deep countercurrent in the Western North Atlantic. Deep-Sea Res. 8: 1-19.

Taylor, C.B. and H.B. Stewart, 1959. Summer upwelling along the east coast of Florida. J. Geophys. Res 64: 33-40.

Thomas, J.P., 1966. Influence of the Altamaha River on primary production beyond the mouth of the river. M.S. Thesis, University of Georgia, 88pp.

Uda, M., 1964. On the nature of the Kuroshio, its origin and meanders. In: Studies on Oceanography. K. Yoshida (ed.), University of Tokyo Press, pp. 89-107.

Von Arx, W.S., D. Bumpus and W.S. Richardson, 1955. On the fine structure of the Gulf Stream front. Deep-Sea Res. 3, 46-65.

Vukovich, F.M. and B.W. Crissman, 1978. Further studies of a cold eddy on the eastern side of the Gulf Stream using satellite data and ship data. J. Phys. Oceanogr., 8: 838-845.

Vukovich, F.M. and B.W. Crissman, 1980. Some aspects of Gulf Stream western boundary eddies from satellite and in situ data. J. Phys. Oceanogr. 10: 1792-1813.

Wang, D.P., 1979. Low-frequency, sea-level variability on the Middle Atlantic Bight. J. Mar. Res. 37: 683-697.

Weber, A.H. and J.O. Blanton, 1980. Monthly mean wind fields for the South Atlantic Bight. J. Phys. Oceangr. 10: 1256-1263.

Webster, F., 1961a. A description of Gulf Stream meanders off Onslow Bay. Deep-Sea Res. 8: 130-143.

Webster, F., 1961b. The effects of meanders on the kinetic energy balance of the Gulf Stream. Tellus 13: 392-401.

Weisberg, R.H. and L.J. Pietrafesa, in press. Meteorological parameters of the South Atlantic Bight. J. Phys. Oceanogr.

Yentsch, C. and D.W. Menzel, 1963. A method for the determination of phytoplankton chlorophyll and phaephytin by fluorescence. Deep-Sea Res. 10: 221-231.

Yoder, J.A., L.P. Atkinson, S.S. Bishop, E. Hofmann and T.N. Lee, in press. Effect of upwelling on phytoplankton productivity on the outer souteastern U.S. Continental Shelf Research.

Yoder, J.A., L.P. Atkinson, T.N. Lee, H.H. Kim and C.K. McClain, 1981. Role of Gulf Stream frontal eddies in forming phytoplankton patches on the outer southeastern shelf. Limnol. Oceanogr. 26: 1103-1110.